NASA CONFERENCE PUBLICATION

NASA CP-2062

(NASA-CP-2062) SEVENTH NASTRAN USER'S COLLOQUIUM (NASA) 499 p HC A21/MF A01 CSCL 20K G3/39

N78-32466 THRU N78-32491 Unclas 33249

SEVENTH NASTRAN USER'S COLLOQUIUM

Papers to be presented at NASA, Marshall Space Flight Center,
October 4 - 6, 1978

October 1978

Prepared by

NASA - GEORGE C. MARSHALL SPACE FLIGHT CENTER
Marshall Space Flight Center, Alabama 35812

FOREWORD

NASTRAN (NASA STRUCTURAL ANALYSIS) is a large, comprehensive, nonproprietary, general purpose finite element computer code for structural analysis which was developed under NASA sponsorship and became available to the public in late 1970. It can be obtained through COSMIC (Computer Software Management and Information Center), Athens, Georgia, and is widely used by NASA, other government agencies, and industry.

NASA currently provides continuing maintenance and improvement of NASTRAN through a NASTRAN Systems Management Office (NSMO) located at Langley Research Center. Because of the widespread interest in NASTRAN, and finite element methods in general, NSMO organized the Seventh NASTRAN Users' Colloquium held at Marshall Space Flight Center, October 4-6, 1978. (Papers from previous colloquia held in 1971, 1972, 1973, 1975, 1976, and 1977 are published in NASA Technical Memorandums X-2378, X-2637, X-2893, X-3278, X-3428, and X-2018, respectively.) The Seventh Colloquium provides some comprehensive general papers on the application of finite element methods in engineering, comparisons with other approaches, unique applications, pre- and post-processing or auxiliary programs, and new methods of analysis with NASTRAN.

Individuals actively engaged in the use of finite elements or NASTRAN were invited to prepare papers for presentation at the colloquium. These papers are included in this volume. No editorial review was provided by NASA, but detailed instructions were provided each author to achieve reasonably consistent paper format and content. The opinions and data presented are the sole responsibility of the authors and their respective organizations.

Cochairmen:

Deene J. Weidman, Manager
NASTRAN Systems Management Office
Langley Research Center
Hampton, Virginia

and

Robert L. McComas
Marshall Space Flight Center
Huntsville, Alabama

CONTENTS

Page

N78-32467

DYNAMIC STORAGE EXPANSION IN NASTRAN

Edwin N. Hess
Lockheed Electronics Co., Inc.

SUMMARY

Some functions of NASTRAN require a large block of working storage to execute. The method of meeting this requirement, because of insufficient data, has been to specify in advance an excessive amount to avoid a fatal exit. A method has been developed at the Lyndon B. Johnson Space Center (JSC) to calculate the amount of working space needed for the analysis and to inform the analyst of this data or, in the case of UNIVAC computers, to acquire this extra storage and continue the analysis.

INTRODUCTION

The design philosophy of NASTRAN dictated a completely open-ended design whenever possible. The use of a fixed dimension for large arrays was outlawed since this limited the size of the analysis that could be solved. Instead, modules were programmed to allocate space as required and to use spill logic to transfer data to scratch file if working space was limited.

The first public release of NASTRAN for the UNIVAC 1100 computers (level 11) assumed a limitation of direct addressing of 65,535 words. The HICORE system, which allowed indirect addressing of up to 262,143 words, was developed on level 12 NASTRAN at JSC. The UNIVAC computers were then competitive. As structures became larger and more complex, larger amounts of storage are required. The amount of working space for a particular analysis has been left to the analyst, with disastrous results. Either there was "insufficient core", leading to system fatal message 3008, or more working space than that required was attached and computer throughput and turnaround time suffered.

At JSC, fatal message 3008 has been changed to reflect the amount of working space required by the offending subroutine. Going beyond this, the branch to message 3008 was changed to branch to increase the space dynamically, and continue processing. The extra working storage required by a particular analysis is not necessarily that required to eliminate spill logic. We have found that spill may be economically advantageous in regards to extra time as opposed to an outrageous amount of working storage.

The subroutines mentioned will be either matrix subroutines which may be used by more than one module or module subroutines which are an exclusive part of the module. Utility and executive subroutines are not included except for changes necessary for the analyst's information. The term "working storage" is

used instead of core, and the word "problem" to mean analysis is avoided. A problem is encountered when an analysis fails.

FATAL MESSAGE 3008 (ref. 1)

System fatal messages usually consist of three parameters:

1. The message number
2. The data block name
3. The subroutine name

In the case of message 3008, the second parameter is not used, but is always set to zero, and the message reads:

SYSTEM FATAL MESSAGE 3008 - INSUFFICIENT CORE FOR SUBROUTINE NNN

Subroutine MSGWRT was altered to skip the FNAME call, which recovers the data block name, and the message rewritten to read:

SYSTEM FATAL MESSAGE 3008 - MMM ADDITIONAL CORE NEEDED FOR SUBROUTINE NNN

MODULE MODIFICATIONS

Most module and matrix subroutines have at least one branch to message 3008, but the majority of these are only safety valves and will not be taken if the working storage length is in the range of 20,000-25,000 words, which is the case when the UNIVAC is operating at the default core size of 65,536 words.

McCormick and Redner (ref. 2) studied the module core requirements and arrived at the following categories:

Group 0 - Modules which have no requirements of open core

Group 1 - Modules which require space for vectors or tables which do not exceed eight times the number of grid points in the model and do not provide spill.

Group 2 - Modules which require space for tables or matrices of variable size. Spill logic may be provided.

Group 3 - Modules for which the working space requirements are established by one or more matrix routines. Spill logic is usually present.

This information was used to determine which subroutines were likely to need additional working space. The decomposition subroutines real symmetric,

real unsymmetric, and complex require the largest space. The group 2 modules were also studied as to the working storage required.

Most subroutines have a preface section where file assignments and working space are calculated from table and matrix trailers. A calculation of working space is made with the result of a fatal message when insufficient. A simple change in these subroutines to add the second parameter in the call to subroutine message will give the analyst additional information of core requirements for subsequent analysis. Most of the matrix subroutines in group 3 were modified to state the amount of additional working space required.

Another method of calculating working storage is to read a record into working storage where the full record must be in core. If the number of words available is filled before the end of record is reached, the call to fatal message 3008 is taken. The following branch was added:

1. Reset the address of storage

2. Read the remainder of the record

3. The number of words read on the subsequent call(s) to read is the amount of insufficiency

This is necessary in modules such as TA1 (subroutine TA1A). This method is also used in subroutine XSORT as it prepares the continuation card dictionary. A correction was made by inserting a count, from which the space requirements could be calculated, of the continuation cards as they were read on the first pass through the bulk data cards.

Some care must be taken when using the results given by this message. On a large static analysis we found the following storage requirements:

TA1	80,000
RBMG2	90,000
SSG3	103,000

TYPICAL SUBROUTINE (SDCOMP)

Decomposition of a symmetric matrix is performed in steps by rows. The row under consideration is called a pivotal row. The contribution of the pivot row into each row of the resulting matrix is dependent upon the active (nonzero) column elements of that row and are combined with the corresponding column positions of the other rows. All computations can occur without spill if sufficient space is available to contain a triangular matrix whose row dimension is equal to the maximum number of active columns. When sufficient space is not available, the spill logic divides the triangular matrix into spill groups containing consecutive rows which will fit into the available space. It is expected that a reasonable compromise between time and space can

be realized by requesting sufficient working storage to contain a triangular matrix with a dimension equal to the average number of active columns. This scheme would allow for the majority of processing to be contained in core and allow spill for the larger pivotal rows (see fig. 1).

Current preface processing of SDCOMP involves the organization of working storage and the determination of spill groups. Before beginning computational processing, statistics gathered during the preface are printed for the user's information. The statistics reported include:

- o Maximum number of active columns
- o Space required to eliminate spill
- o Number of spill groups
- o Average number of rows in each spill group

Tests on a Space Shuttle analysis were made to determine the costs of spill to conform to available core, as shown in the following table. A decreasing benefit was derived after a certain point which shows eliminating spill is not beneficial. The figure for additional core should be that needed for the average column.

Storage size total (K)	Percent increase	Time in SDCOMP	Percent decrease
65		1520	
80	22	992	53
137*	71	657	50

*Required to eliminate spill.

The choice of subroutine SDCOMP as being typical was made because of the completeness of calculating optimum working space. This same method is used in subroutine GENVEC, which is a slave of both real unsymmetric and complex decompositions. Spill has not been calculated into requirements of any other subroutines at this time.

DYNAMIC CORE ALLOCATION

The ability to dynamically extend main storage without terminating an execution is available on the UNIVAC 1100 computers. This function has been successfully implemented at JSC.

The calls to message 3008 were changed to call a computer dependent subroutine EXPAND, reset necessary parameters, and return to the beginning of the

subroutine. Figure 2 shows the subroutine SDCOMP flow as regards dynamic expansion.

The design requirements of subroutine EXPAND were as follows:

- Provide for levels of expansion
- Access the UNIVAC 1100 function MCORE$
- Place a limit on expansion
- Provide for moving the contents of reserved storage
- Restore the contents of reserved storage
- Inform the user of the expansion

Levels of expansion were provided in case a matrix subroutine (SDCOMP) needed additional working storage after a module subroutine (INVPWR) had requested additional working storage and, as in these cases, the module subroutine reserves a section of storage not available to the matrix subroutine. Figure 3 shows a typical map of working storage area.

The limit on main storage is required by the addressable limit of 262,143 or by the computer facility.

The subroutine that requires additional working space calls EXPAND with the following parameters:

- Address of working storage
- Additional storage required
- Length of working space currently available
- The calling subroutine name

An additional entry into subroutine EXPAND (SHRINK) is called before exiting to provide for the restoration of the contents of the reserved area to its original position and to reduce the level index.

A new call to the 1100 executive (LCORE$) was made on each reentry into the main Module driver subroutines XSEMii. This provided for the release of core to its default value following each module.

MODIFICATION TECHNIQUES

Executive and Utility Modifications

The use of the system data block (ref. 3, section 2.4.1.8) was expanded to store the following data:

31 Current length of main storage

35 Maximum length of main storage

36 Default length of main storage

57 First level length of assigned main storage

58-61 Subsequent level lengths of assigned main storage

Two functions were added to the computer dependent subroutine MAPFNS (ref. 3, section 5.4.7) to execute the executive requests to MCORE$ and LCORE$. These were labeled GETCOR and RELCOR, respectively.

Subroutine MSGWRT was modified to skip the call to subroutine FNAME for message 3008 and to write the modified message. This change is computer independent.

An additional line was placed in subroutines XSEMii to call subroutine RELCOR on each return from a module execution.

Matrix and Module Subroutine Modifications

When a call to subroutine EXPAND is necessary, all files must be closed before returning to the beginning of the subroutine to reexecute the preface. The GINO buffers will be reassigned. Care must be taken that files opened previously be closed without rewind and reopened without rewind. This is the case of the PG file in module SSG1 (Static Solution Generator, Phase 1). This load vector file is opened in subroutine SSG1 and the load vectors written by subroutine EXTERN for the external load vectors and by subroutine EDTL for the element deformation and temperature load vectors. Either EDTL or EXTERN may require extra storage.

If a matrix subroutine is denied the use of a section of upper storage, the additional storage requested must be at least as large as the total length of the GINO buffers to prevent GINO error 1151 (buffer overlaps a previously assigned buffer). GINO will remember the address of the buffer in the reserved area and prohibit this area to be used as a buffer again.

RESULTS

Dynamic expansion has been successfully demonstrated in static and normal modes analysis from the following modules and/or subroutines. These subroutines reflect the size required by the analysis by their varying needs and hence are calls to the prime candidates for calculating the required working storage and the improved message 3008:

Module	Subroutines
READ	INVPWR
SDR2	SDR2C
	SDR2D
SSG1	EDTL
RBMG2	DECOMP
SSG3	MPYAD
XSORT	XSORT

The following subroutines have had the call to subroutine MESAGE changed but have not called for increased storage and are therefore untested.

RCOVB	TRDIA2
AMG	TRHT
PARTN	FCNTL
TRD	TRNSP
TRDIA	INVP3

GENVEC (preface for both DECOMP and CDCOMP)

All of the above subroutines should calculate the storage requirements and relay this information to the analyst on all computers.

CONCLUDING REMARKS

The improvement in user fatal message 3008 is a useful tool to the analyst and is a guide to total main storage requirements of an analysis. After this improvement to the message, a zero value of additional storage is an alert to the system programmer that the minor change in the offending subroutine is desirable.

For the sake of keeping the computer independence, it is recommended that a call to the computer dependent subroutine EXPAND be made in all cases of insufficient main storage. This subroutine would then directly make the call to subroutine MESAGE for those computers where the insufficiency is fatal.

All of the areas of storage insufficiency have not been discussed; others are anticipated as the structural models get larger and other paths through NASTRAN, particularly dynamic analysis, are explored.

Further work on the storage requirements should include earlier detection of insufficient size. Table trailers are sparsely used and could, in some cases, be used to cause an earlier demise of an analysis that has insufficient main storage.

REFERENCES

1. The NASTRAN User's Manual. NASA SP 222(03), July 1978, Section 6.2.2.

2. McCormick, C. W., and Redner, K. H.: Study of Modifications Needed for Effective Operation of NASTRAN on IBM Virtual Storage Computers. NASA CR-2527, April 1975.

3. The NASTRAN Programmer's Manual. NASA SP 223(03), July 1978.

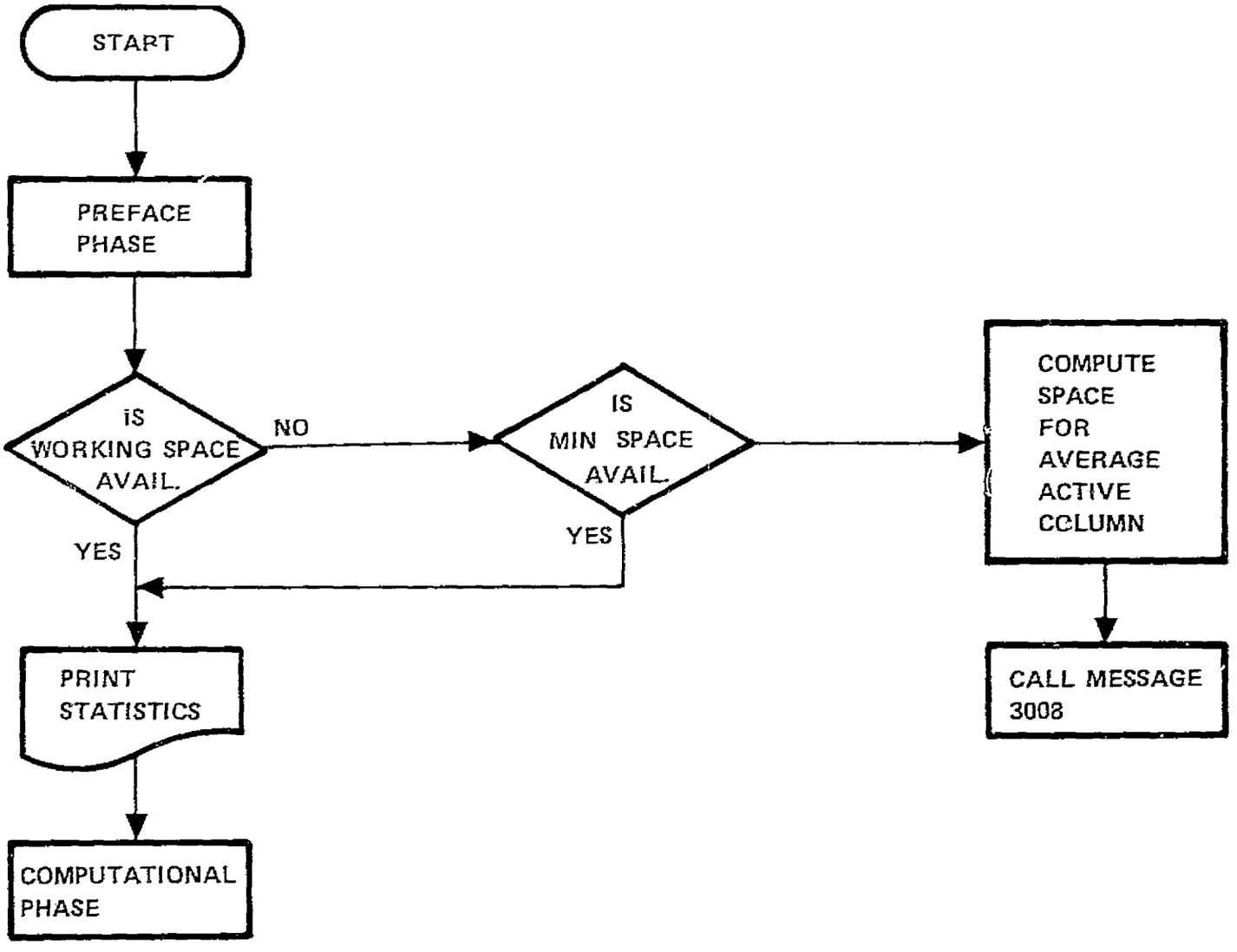

Figure 1. — Storage Calculation With Spill Optimization (SDCOMP).

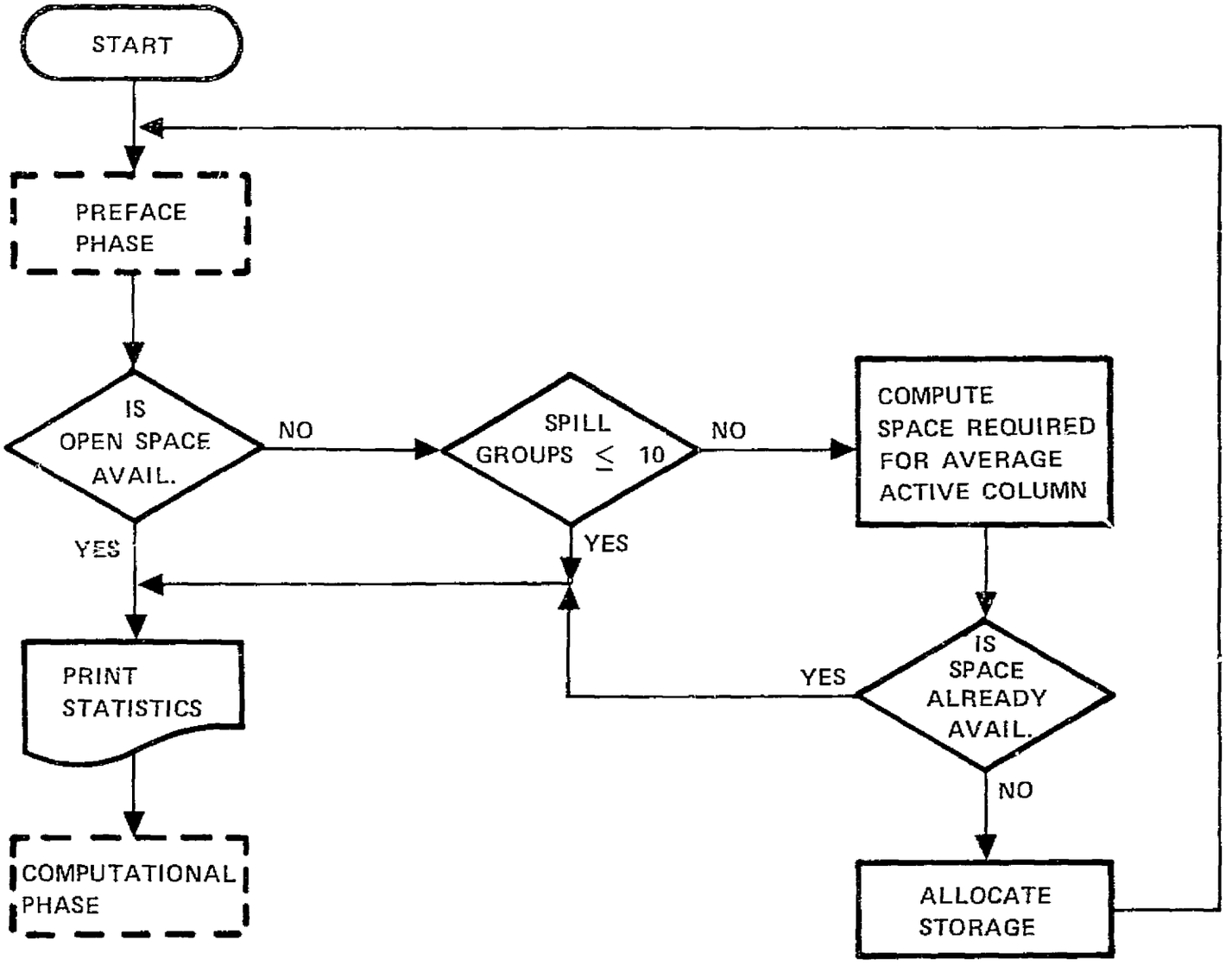

Figure 2. — Dynamic Expansion With Spill Optimia Optimization (SDCOMP).

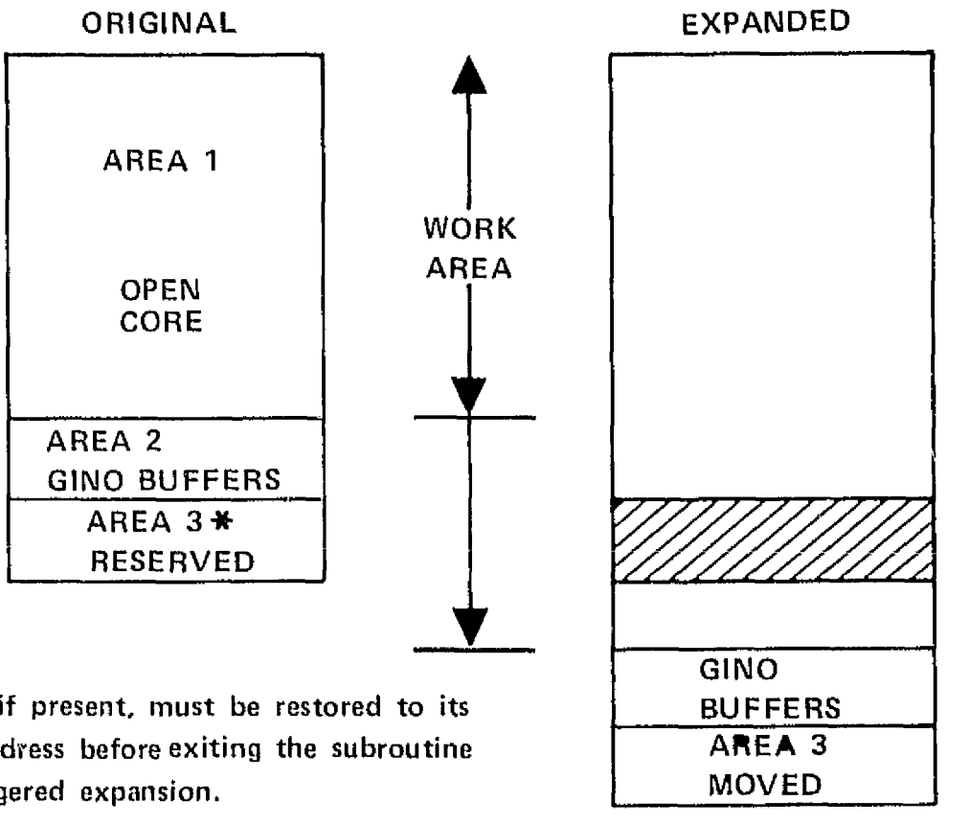

*This area, if present, must be restored to its original address before exiting the subroutine which triggered expansion.

Figure 3. – Open Core Allocation Subroutine Any.

THIS PAGE INTENTIONALLY LEFT BLANK.

D2

N78-32468

NASTRAN COMPUTER RESOURCE MANAGEMENT FOR THE MATRIX DECOMPOSITION MODULES

Charles W. Bolz
Computer Sciences Corporation

SUMMARY

Detailed computer resource measurements of the NASTRAN matrix decomposition spill logic were made using a software input/output monitor. These measurements showed that, in general, job cost can be reduced by avoiding spill. The results indicated that job cost can be minimized by using dynamic memory management. A prototype memory management system is being implemented and evaluated for the CDC CYBER computer.

INTRODUCTION

The early large structural analysis programs were designed for second-generation computer systems that were severely core-limited, requiring structural programmers to develop ingenious strategies for using mass storage to extend the range of solvable problems. It was for such a computer that NASTRAN was initially developed, and the matrix decomposition code with its efficient spill logic was a singular achievement in numerical analysis software. As NASTRAN was implemented on third generation computers which allowed multiprogramming, such as the UNIVAC 1108 and the CDC 6000 series, it remained expedient to use as little central memory as possible in order to maximize overall system efficiency. However, present day computers such as the CDC CYBER 175 and the UNIVAC 1110 have very large, fast, low-cost semiconductor memories, and excessive mass storage usage can rapidly degrade overall system efficiency and increase job cost. It therefore becomes important for the user to select an optimum memory region size for his problem.

In order to accurately assess the effects of memory region size on I/Ø utilization and job cost, a software monitor was developed to measure I/Ø volumes by file on CDC CYBER computers. Spill volume statistics were accumulated for the SDCØMP and CDCØMP matrix decomposition modules using NASTRAN Level 17.0.0 on the CDC CYBER 175 under the NØS 1.2 operating system. These statistics were interpreted using job cost accounting relations typical of CDC and UNIVAC systems. The results suggested that a dynamic memory management system designed to avoid spill would be cost effective, and a prototype system is being implemented on the CDC CYBER.

SPILL

Matrices to be decomposed by NASTRAN are normally sparse banded matrices with relatively few terms away from the band. During the decomposition, it is desirable to have all the non-zero terms of a row, and all the non-zero terms of the triangular factor generated by reduction of that row, in main memory. If this is possible for each row, then the matrix need be read in from secondary storage only once during the decomposition, and the factorized matrix written out. If insufficient memory is allocated, however, intermediate results must be stored on spill files. Numerous passes through the spill files may be required to perform the decomposition.

The matrix decomposition and spill logic is described in detail in references 1 and 2.

JOB COST ACCOUNTING ALGORITHMS

The astute NASTRAN user interprets computer resource utilization guidelines in terms of job cost, as assessed by his installation accounting algorithm. Results presented in this study are interpreted in terms of two accounting algorithms: one used commonly at CDC installations, and the second at UNIVAC sites.

Many factors go into an accounting algorithm, but for NASTRAN execution only central memory used (CM), central processor-unit time (CPU), and mass storage input/output transfers (I/Ø) are important. In terms of these resources, the CDC accounting formula may be generalized as

$$\text{Cost} = (1 + C_1\ \text{CM})\ (C_2\ \text{CPU} + C_3\ \text{I/Ø})C_4$$

and the UNIVAC relation as

$$\text{Cost} = \text{CM}\ (C_2\ \text{CPU} + C_3\ \text{I/Ø})C_4$$

where C_2 and C_3 are functions of the CPU and mass transfer device speeds. The constant C_1 is set by the CDC NØS operating system at 0.007 per 512-word block. The dollar multiplier, C_4, is installation dependent, so all matrix decomposition costs presented in this study are normalized to the no-spill case.

IBM accounting formulas vary with installation and operating system, so the IBM user should interpret the results presented in terms of his particular system.

THE I/Ø MONITOR

The basic utility for this study is a software monitor which was originally developed by the author for analyzing the I/Ø usage of programs running under the CDC SCØPE operating system. The monitor decodes all I/Ø requests and records, by data block, the type of request and the number of physical records transferred between central memory and mass storage. The record is printed at the end of each module, as shown in Figure 1.

As adapted for the CDC version of NASTRAN, the I/Ø monitor is called from XIØRTNS, which is the interface between GINØ (General input/output) and the operating system (ref. 3). The monitor was validated by checking the total I/Ø volume printed out against accounting log (dayfile) statistics for each NASTRAN run. Since the monitor itself occupies only 350 words of CYBER 175 memory, and uses about 20 microseconds of central processor time per I/Ø request, it has negligible impact on the job environment.

THE COMPUTER RESOURCE UTILIZATION STUDY

Complex Decomposition

Two problems were chosen for study. The first is a complex eigenvalue analysis of a gas-filled, thin elastic cylinder (NASTRAN Demonstration Problem 7-2-1 of reference 4). This case requires decomposition of an order 390 complex matrix, and can be solved by NASTRAN in a reasonable memory region only by using the determinant method. This particular problem was the impetus of the present study. When it was run on an IBM S/360-95 under the Multiple Variable Tasking (MVT) operating system with a memory region of 410000 bytes, an I/Ø timeout resulted after twenty minutes I/Ø time. When the region size was increased to 500000 bytes, the I/Ø time was less than five minutes.

Computer resource requirements for this problem are shown in figure 2, and dramatically illustrate the effect of spill on resource utilization. As long as memory region size is small enough to require spill, I/Ø volume and CPU time are steep inverse functions of open core (scratch memory) size and job cost (as measured by the CDC accounting algorithm) is decreased by increasing core. But once sufficient open core is provided to avoid spill, CPU and I/Ø utilization remain constant, and job cost increases with increasing memory size.

Real Symmetric Decomposition

The second problem chosen is the static analysis of a long, narrow orthotropic plate, based on NASTRAN Demonstration Problem 1-4-1 of reference 4. This problem is useful for study because data can be readily generated for a broad range of grid sizes. Problem sizes ranging from 128 to 1100 active

columns were studied. (For a given memory region, spill is closely related to the number of active columns.) These were produced by grids of from 300 to 2100 points, generating matrices of order 760 to 4990, respectively.

A problem size of 277 average active columns, generated by a grid of 660 points, resulting in a matrix of order 1660 was selected for detailed investigation. This problem has spill characteristics typical of large user problems commonly analyzed using NASTRAN. The grid is comparatively small; however for problems of similar spill behavior, CPU and I/Ø resource utilization are linearly proportional to matrix order for a constant memory region.

Results for this case are shown in figure 3 in non-dimensional form, normalized to the conditions at the open core size where spill is no longer required. The outstanding feature of figure 3 is the I/Ø required by spill. At an open core size of 50% of that required for in-core reduction, I/Ø volume is seven times that required for in-core reduction. The CPU time curve illustrates that, refined as the symmetric decomposition spill logic is, considerable computer time is used processing spill I/Ø. And the cost curve shows that the cost penalty incurred by using more open core is more than compensated for by the reduced I/Ø and CPU resource requirements.

To lend perspective, a cost curve was developed for a typical UNIVAC 1110 system, where cost is directly proportional to memory used, and I/Ø is relatively less expensive. This curve is not as dramatic as the CDC curve, but still shows the importance of increasing open core to minimize spill.

DYNAMIC MEMORY MANAGEMENT

When matrix decomposition dominates a NASTRAN problem, the foregoing discussion indicates that computer resource utilization can be minimized by requesting sufficient core to avoid spill, if possible. For typical problems, however, matrix decomposition is only part of the solution procedure. This is illustrated by the problem described in Table 1. The decomposition of the order 7000 matrix without spill would require a memory region of 160,000 decimal words on a CYBER 175, which is 30,000 words more than is available to a single program. But the decomposition step is only about 40% of the computational effort. Another 50% of the computation can be performed in 50,000 words core, and the remainder in 70,000.

This suggests that an ideal strategem to reduce computer costs would be to dynamically manage memory to give each module only the core it needs. Direct implementation of this idea would present a formidable task - 160 NASTRAN modules to be modified. However, the results presented in Table 1 indicate that most of these modules - input, sort, geometry processing, element matrix assembler and generator, etc; require a small memory region, and suggest the following three-phase memory management scheme.

(1) Execution of each module is attempted in a small memory region.

(2) Modules which can be expected to have large memory requirements compute and request the needed core.

(3) Any other module which runs out of core while executing has its memory region expanded to a predetermined intermediate size.

CDC IMPLEMENTATION OF DYNAMIC MEMORY MANAGEMENT

The dynamic memory management scheme described above is being implemented on the CDC CYBER 175 as follows.

(1) The user specifies to NASTRAN an initial and a nominal memory region size.

(2) Before invoking each module, the link driver (XSEM) routine calls a subroutine MEMMGR (memory manager) to reset the memory region to its initial value.

(3) The matrix decomposition routines call MEMMGR to obtain the open core needed to execute without spill. If insufficient memory exists, all available memory is obtained.

(4) Modules that run out of open core normally issue an error abort call to subroutine MESAGE. This call is intercepted by MEMMGR, the nominal memory region is assigned, and control returned to the calling module. (Note that this requires that the call to MESAGE be an in-line call).

This scheme is being tested using the cases of figures 1 and 2 and Table 1. The predicted cost savings are shown in figure 2. These cases indicate that dynamic memory management to avoid spill can reduce job costs significantly.

CONCLUSION

An input/outout monitor was developed for the CDC version of NASTRAN which allows detailed analysis of computer resource utilization of the matrix decomposition modules. This analysis shows that for typical accounting algorithms, job costs can be reduced by avoiding spill in the decomposition. Analysis of a typical problem indicates that dynamic memory management could further reduce overall job cost.

REFERENCES

1. The NASTRAN Programmer's Manual, NASA SP-222(03), July, 1976.

2. The NASTRAN Theoretical Manual, NASA SP-221(03), March, 1976.

3. Brown, W. K., and Schoellmann, W. F., "Study of the NASTRAN Input/Output Subsystems," Sixth NASTRAN Users' Colloquium, NASA CP-2018, October, 1977.

4. The NASTRAN Demonstration Problem Manual, NASA SP-224(03), July 1976.

TABLE 1

THERMAL STABILITY STUDY

Order of Matrix = 7215
Average Active Columns = 238
Maximum Active Columns = 505
Three Spill Groups

Operation	CPU, seconds	I/O, 10^3PRU(1)	Memory Region (60 bit words)
Input Processing	49	16	52000
Geometry Processing	14	20	52000
Element Matrix Processing	140	81	52000
Constraint Elimination	183	25	52000
Decomposition	307	157	98000(2)
Static Solution Generation	70	81	66000
Totals	736	380	

(1) One PRU = Sixty-four 60 bit words

(2) The decomposition would require 160000 words without spill

TABLE 2

NASTRAN DYNAMIC MEMORY MANAGEMENT ON THE CYBER 175

EXPECTED RESOURCE UTILIZATION AND COST SAVINGS

Problem	Memory Region (10^3 word)	CPU (seconds)	I/Ø (10^3PRU)(1)	Cost Savings (Percent)
Demo Problem 7-2-1	52	45.3	12.4	
	74	242.8	49.2	2.5%
Demo Problem 1-4-1	52	49.6	34.7	
	94	66.3	26.9	12.7%
Thermal Stability Study	52	386	142	
	66	70	81	
	98(2)	307	157	14.3%

(1) One PRU = sixty-four 60 bit words

(2) The decomposition would require 160,000 words without spill

```
 105 RBMG2   END

   CALL 21                    PRUS          AVERAGE
FILE          PPCALLS      TRANSFERRED   DATA TRANSFER   READ/WRITES   OPEN/CLOSE   FILE POSITION
POOL               14              140              10            14            0               0
NTRAN               6              323              53             6            0               0
KFF                49              819              16            49            0               0
SCRATCH4          999            16395              16           998            0               1
SCRATCH1            5               38               9             4            0               1
                  472             7496              15           472            0               0
KGGX             5793            94741              16          5786            0               7
SCRATCH3         6513           106537              16          6506            0               7
MOD. TOTAL      13851           226449              16

 GRAND SUM      15167           248131              16


 111 SSG1    END

   CALL 22                    PRUS          AVERAGE
FILE          PPCALLS      TRANSFERRED   DATA TRANSFER   READ/WRITES   OPEN/CLOSE   FILE POSITION
POOL               11              131              11            11            0               0
MPYAD              19             1154              60            19            0               0
KGGX                9               54               9             6            0               3
SLT                 6               60              10             6            0               0
CASECC              4               40              10             4            0               0
SCRATCH1            5               38               9             4            0               1
SCRATCH3            5               38               9             4            0               1
BGPDT               4               54              13             4            0               0
SIL                 2               20              10             2            0               0
PG                  2               18               9             2            0               0
MOD. TOTAL         67             1607              23

 GRAND SUM      15234           249738              16
                                MPYAD--NULL MATRIX PRODUCT

   CALL 28                    PRUS          AVERAGE
FILE          PPCALLS      TRANSFERRED   DATA TRANSFER   READ/WRITES   OPEN/CLOSE   FILE POSITION
POOL               4               40              10             4            0               0
NTRAN              8              898             112             8            0               0
KELM               3               18               9             2            0               1
KSS                3               18               9             2            0               1
SCRATCH6           3               18               9             2            0               1
PG                 3               18               9             2            0               1
KDICT              3               18               9             2            0               1
KGGX               3               18               9             2            0               1
PS                 3               18               9             2            0               1
ULV                3               18               9             2            0               1
YS                 3               18               9             2            0               1
USET               3               18               9             2            0               1
KFS                3               18               9             2            0               1
MOD. TOTAL        49             1130              25

 GRAND SUM      16523           271898              16


 137 SDR2    END

   CALL 29                    PRUS          AVERAGE
FILE          PPCALLS      TRANSFERRED   DATA TRANSFER   READ/WRITES   OPEN/CLOSE   FILE POSITION
POOL               4               40              10             4            0               0
NTRAN             15             1152              76            15            0               0
KELM               3               18               9             2            0               1
KSS                3               18               9             2            0               1
SCRATCH6           3               18               9             2            0               1
PG                 3               18               9             2            0               1
KDICT              7               52              10             5            0               2
KGGX             196             3191              16           196            0               2
PS                11              116              12             9            0               2
ULV                3               18               9             2            0               1
YS                 9               84              12             7            0               2
USET               3               18               9             2            0               1
KFS                3               18               9             2            0               1
CASECC             8               80              10             8            0               0
MPT                2               20              10             2            0               0
LST               19              309              16            19            0               0
EQEXIN             7               91              13             7            0               0
KLL                2               20              10             2            0               0
UGV                8              108              13             8            0               0
MOD. TOTAL       311             5389              17

 GRAND SUM      16834           277207              16
```

Figure 1. Output from the NASTRAN I/Ø Monitor (typical).

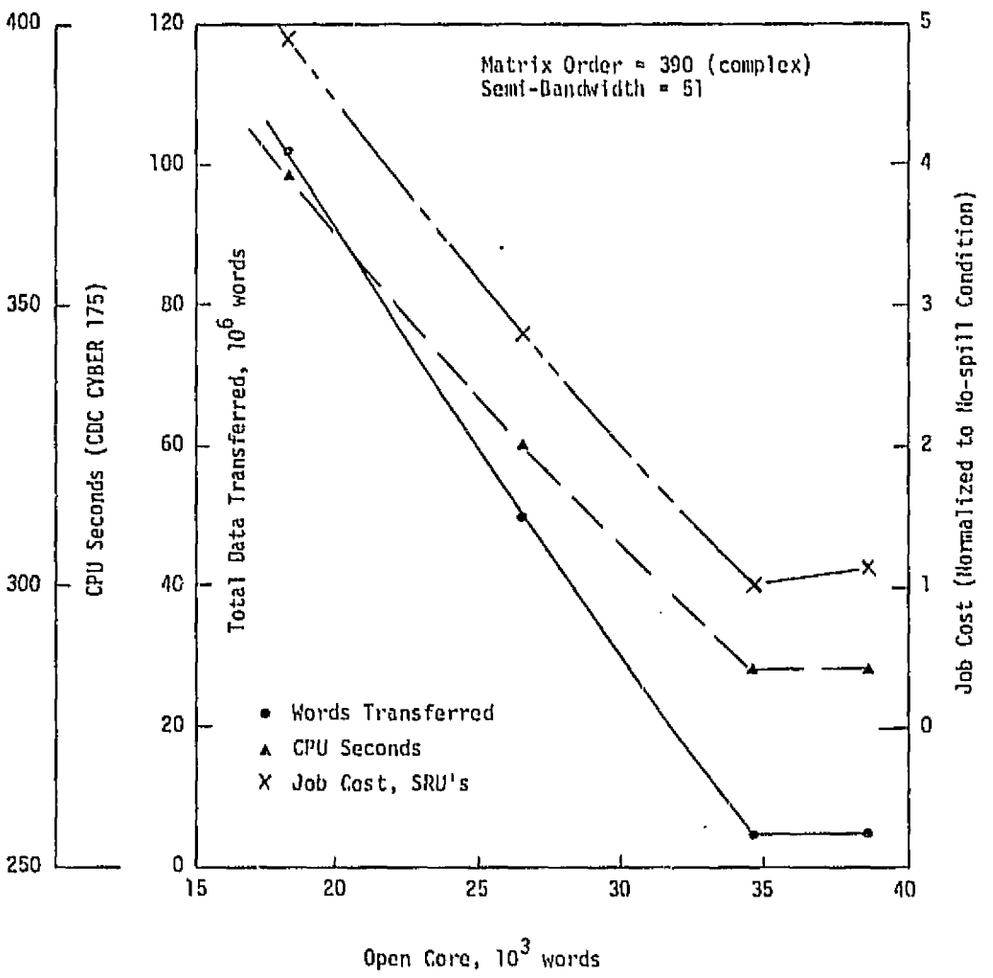

Figure 2. Resource Analysis vs. Open Core
Eigenvalue Analysis of a Thin Elastic Cylinder.

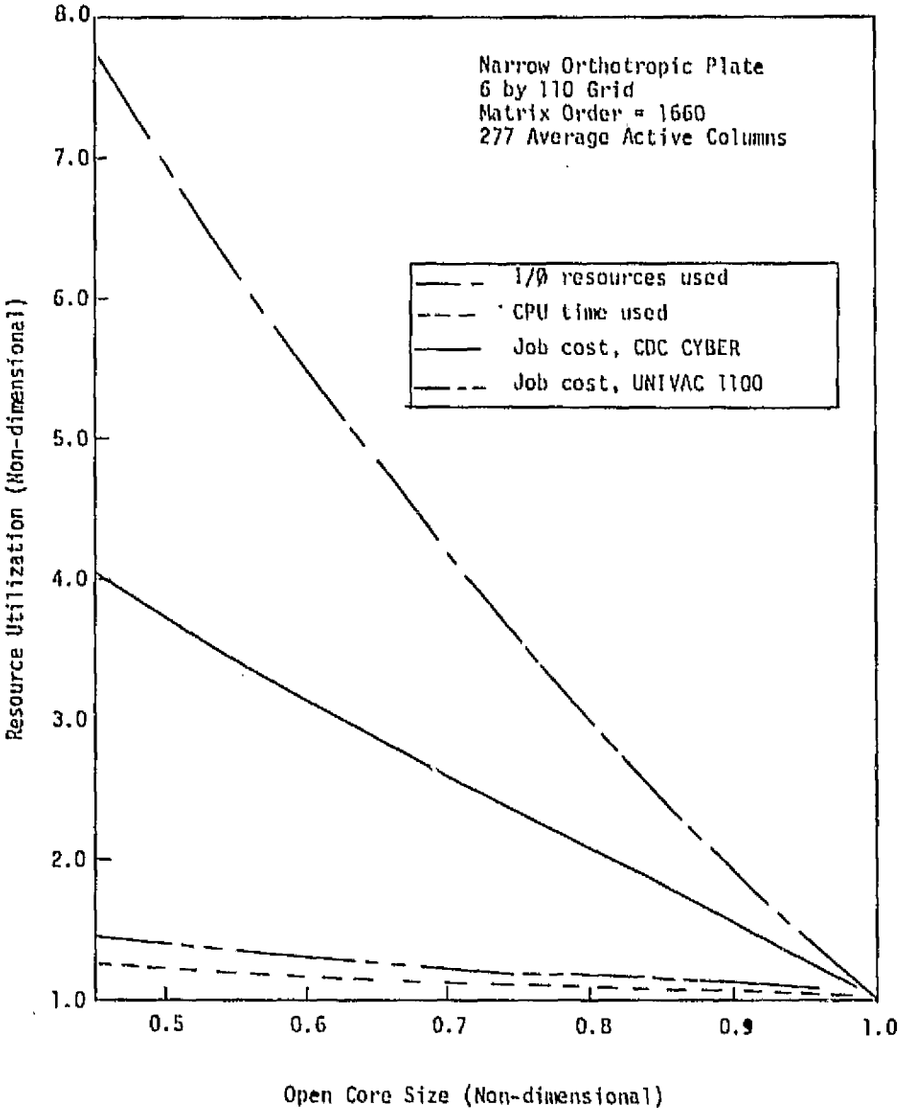

Figure 3. Resource Utilization for Symmetric Decomposition Normalized to No-spill Values.

THIS PAGE INTENTIONALLY LEFT BLANK.

N78-32469

ADDING STRESS PLOT FUNCTION TO NASTRAN

Shunichi Katoh
IBM-Japan

ABSTRACT

Stress plot function was developed and added to the NASTRAN level 15.5, the latest level available at IBM-Japan. Computed stress distribution can be displayed by this function, with vectors showing the principal stresses of the finite elements over the specified portions of the structure.

First, NASTRAN is reviewed in the aspect of plotting capabilities. Stress tensor field is examined in preparation of stress display. Then the stress plot function as added to the NASTRAN is described. A sample plotout by this function is shown.

PLOTTING CAPABILITIES OF NASTRAN

There is no question that plotouts are much more effective than printouts for the users to grasp global state of computed results. Plotted outputs are often included in analysis reports.

NASTRAN has extensive plotting capabilities. The level 15.5 can generate the following kinds of plot (ref. 1):

1. Undeformed geometric projections of the structural model.

2. Static deformations of the structural model by either displaying the deformed shape (alone or superimposed on the undeformed shape), or displaying the displacement vectors at the grid points (superimposed on either the deformed or undeformed shape).

3. Modal deformations resulting from real eigenvalue analysis by the same options stated in the above item.

4. Transient deformations of the structural model by displaying either vectors or the deformed shape for specified points of time.

5. X-Y graphs of transient response or frequency response.

6. Topological displays of matrices.

Structure plots (items 1-4) are available by either orthographic, perspective, or stereoscopic projections. Users can specify portions of structure to be plotted by SET definition cards. Various parameters can be specified or de-

faulted.

Examining the above list, we notice that, in spite of versatility of the NASTRAN plotting capabilities, we cannot get stress distribution display, which is often more necessary than deformation display and is desired by many NASTRAN users.

Contour plot function is reported to have been added to the current level NASTRAN, to which the author doesn't have access. It is useful for displaying a scalar field (a single-valued function over a field) such as temperature distribution, but seems to be insufficient for a vector or tensor field such as stress distribution. After some study, the author developed the stress plot function as will be introduced.

STRESS TENSOR FIELD

Stress distribution is a tensor field over a structure. And distribution of principal stress is a complete expression of the field. Numerically, a stress tensor at any point of a structure is described with a real symmetric matrix in reference to an orthogonal coordinate system. The eigenvalues and the unit eigenvectors of the matrix are the magnitudes and the unit direction vectors of the principal stresses at the point. Let the expression "principal stress vector" mean the unit eigenvector multiplied by the corresponding eigenvalue. Because the original matrix is completely represented by the eigenvalues and eigenvectors, the stress tensor is completely expressed by the principal stress vectors as defined above.

Therefore, stress distribution can be displayed with principal stress vectors at a number of points well scattered over the structure. Solution of a finite element structural program like NASTRAN gives us ready material for such display with the principal stresses at each structural element.

THE STRESS PLOT FUNCTION

Overview

In order to assist NASTRAN users in the interpretation of output, the stress plot function was developed and added locally to the NASTRAN level 15.5 at IBM-Japan. It was not designed as a postprocessor but was incorporated into the structure plotter of the NASTRAN in order to utilize the versatile capabilities of the existing structure plotting routines and to make the expanded usage simple and natural extension keeping uniformity. Any of the original capabilities were not deleted.

By this function, computed stress distribution is displayed with principal stress vectors of the specified finite elements. The portion of the structure is drawn underlying. Computed principal stress vectors are drawn on each structural element.

Stresses to be Displayed

For the one-dimensional elements ROD, CONROD, TUBE and BAR, the average axial stresses are displayed. For the two-dimensional elements TRMEM, TRPLT, TRIA1, TRIA2, QDMEM, QDMEM1, QDMEM2, QDPLT, QUAD1 and QUAD2, the principal fiber stresses are displayed. Z1 or Z2 can be specified to calculate the stress at the corresponding fiber distance from the mid plane for each two-dimensional element that has bending stiffness. It makes possible to take the stress due to the bending moment as well as the membrane stress into consideration.

It is difficult for viewers to grasp the directions of the three principal stress vectors of a three-dimensional stress tensor by means of the two-dimensional display. The condition that they are mutually perpendicular is a helpful but insufficient information to restore the three directions uniquely. For three-dimensional elements TETRA, WEDGE, HEXA1 and HEXA2, a convenient method is recommended instead. Users attach two-dimensional elements on appropriate sides of three-dimensional elements, and specify the two-dimensional elements rather than the three-dimensional elements for plotout of stresses. If the two-dimensional elements are thin enough, their stiffness is completely neglected in the computation of accumulated stiffness because of the finite precision of computer arithmetic. By this technique, stresses are obtained on sides rather than at the centroids of the three-dimensional elements.

Implementation

The functional module PLOT was modified: five existing subroutines DPLOT, PARAM, PLOT, HEAD and DRAW in the module were modified, and two GETSTR and DRWSTR were added. The number of input data blocks for the module was increased by one. The Module Property List (MPL) and the Rigid Formats were modified accordingly (ref. 2). The modification of Rigid Format 1 could have been expressed in the following form of ALTER packet in Executive Control Deck (ref. 1):

```
ALTER  15,15
PLOT   PLTPAR,GPSETS,ELSETS,CASECC,BGPDT,EQEXIN,SIL,,,/
       PLOTX1/V,N,NSIL/V,N,LUSET/V,N,JUMPPLOT/V,N,PLTFLG/V,N,PFILE $
ALTER  123,123
PLOT   PLTPAR,GPSETS,ELSETS,CASECC,BGPDT,EQEXIN,SIL,PUGV1,,OES1/
       PLOTX2/V,N,NSIL/V,N,LUSET/V,N,JUMPPLOT/V,N,PLTFLG/V,N,PFILE $
ENDALTER
```

In the new tenth position of input data block section, substituted is the data block OES1, which corresponds to user's request for element stress output. This is the source which supply computed stresses to the functional module.

New Parameters

Several parameters were added for use in plot request packet. They are listed and explained subsequently, in the same way as the existing plot parameters are in reference 1.

MAXIMUM STRESS s

PLOT [{STATIC / MODAL / TRANSIENT} {DEFORMATION / STRESS} i1,i2...] ... [MAXIMUM STRESS s] ... ,

... [PENS t,c] ... [Z1 / Z2] ...

MAXIMUM STRESS card is interpreted by the modified PARAM subroutine. It must always be included if stress is to be plotted. The value of s represents the length to which the maximum absolute principal stress is scaled in each subcase. It must be specified in units of structure. This card for stress plot corresponds to the MAXIMUM DEFORMATION card for deformation plot.

New parameters in expanded PLOT logical card are interpreted by the modified PLOT subroutine.

Non-zero integers following the new keyword STRESS refer to subcases that are to be plotted. Zero to request underlying drawings is not used in stress plot request because stress plot always includes underlying drawings.

Real number following the keywords MAXIMUM STRESS is used as the maximum principal stress value in scaling the stress vectors for all subcases. Each subcase is separately scaled according its own maximum if this item is absent. This parameter in PLOT card for stress plot corresponds to the MAXIMUM DEFORMATION parameter in PLOT card for deformation plot.

Two integers following the keyword PENS identify pens to be used to draw tensile and compressive principal stress vectors respectively. Pen selection had been activated for our plotter routine before. Pen 1 is always used for underlying drawings.

Z1 and Z2 select fiber distances from the mid planes of two-dimensional elements that have bending stiffness, where stresses are to be calculated.

Headings

For a frame of stress plot, in the bottom line "STATIC STRESS ... " is written instead of "STATIC DEFOR. ... ". In the top line "MAX-STR." with the maximum absolute principal stress value is written instead of "MAX-DEF." with the maximum absolute component of deformation. These are done by the modified HEAD subroutine.

Underlying Drawings

Underlying drawings of structures for stress plots are written by the modified DRAW subroutine like those for deformation plots. Therefore, parameters applicable to underlying drawings are common.

Plot of Principal Stress Vectors

Computed principal stresses are fetched and plotted by the added subroutines GETSTR and DRWSTR under control of the modified PLOT subroutine. A principal stress vector is plotted in the shape of an arrow having heads at both ends. The arrow is located so that the middle point of the shaft expediently coincides with the gravity center of the vertices of the finite element. The direction of the arrow is that of the principal stress. The length of the shaft is proportionate to the magnitude of the principal stress. The size of the heads is also proportionate.

The heads are outward if the principal stress is tensile, and inward if compressive. Heads are drawn not as triangles but as trapezoids in order to avoid indistinctness of positions of the apexes of triangles when plotted. It is well known that a shaft looks to have different length if triangular heads are attached in two ways, outward and inward for comparison. To avoid this optical illusion, outward heads are drawn slender, and inward ones flat. When the absolute values of tension and compression are equal, the outward and the inward heads with equal areas have their centroids equally apart from the connecting points with the shafts.

Projection

Stress arrows are projected orthographically or perspectively along with underlying drawings.

Upon request, projected sizes of arrows can be retained to be proportionate to the magnitudes of principal stresses as before projection. Then users can compare magnitudes of principal stresses by measuring the projected sizes. For natural appearances viewing parameters should be so specified as the projection plane does not make large angles against significant principal stresses.

SAMPLE

Figure 1 was drawn by the stress plot function. Related part of the plot request packet was as follows:

```
OUTPUT(PLOT)
SET 1 ALL
...
PERSPECTIVE PROJECTION
MAXIMUM STRESS 10.0
VIEW 0.0 45.0 0.0
FIND SCALE SET 1 ORIG 1
PLOT STATIC STRESS 3 SET 1 Z1 ORIG 1 PENS 2,3
```

Pen 1 (black) was used for headings and underlying drawings, Pen 2 (blue) for tensile principal stresses, and Pen 3 (red) for compressive ones.

CONCLUDING REMARKS

Utilizing existing capabilities of the NASTRAN structure plotter, stress plot function was developed and incorporated into the NASTRAN level 15.5 with relatively little effort. But it provides effective means for us to grasp global state of computed results.

REFERENCES

1. McCormick, C. W. (Ed.): The NASTRAN User's Manual, NASA SP-222(01), with Level 15.5 Supplement, May 1973.

2. The NASTRAN Programmer's Manual, NASA SP-223(01), with Level 15.5 Supplement, May 1973.

6/28/78 MAX-STR. 6.18534240

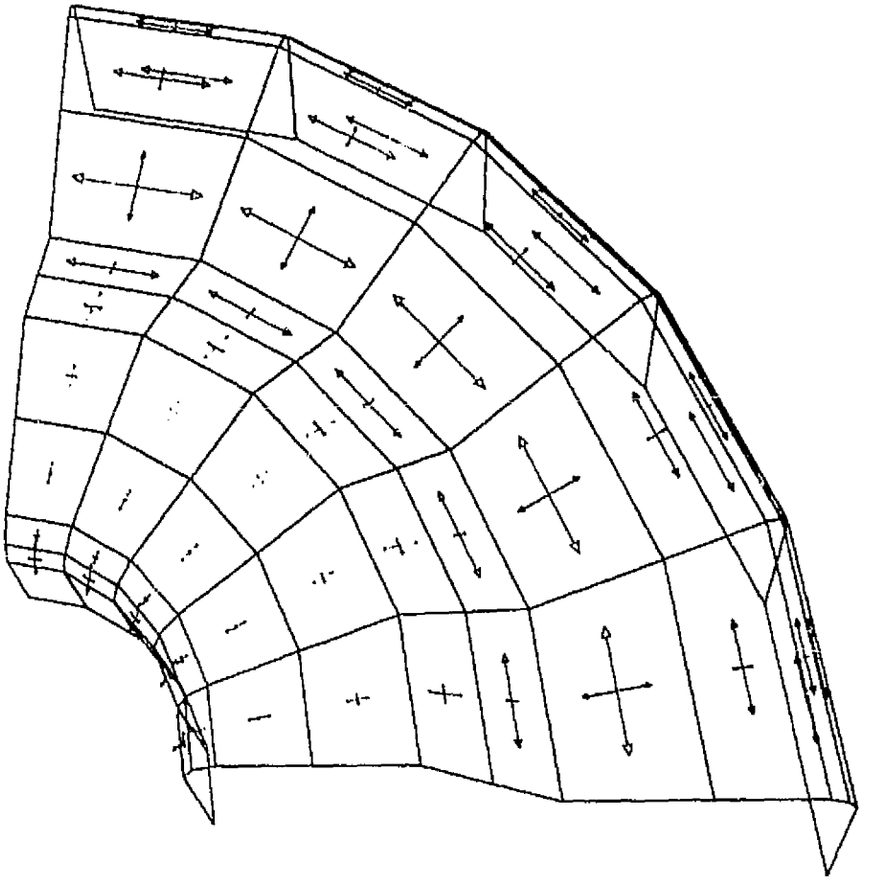

TEST
CENTRIFUGAL FORCE

STATIC STRESS SUBCASE 3 LOAD 300

Figure 1. SAMPLE PLOTOUT

THIS PAGE INTENTIONALLY LEFT BLANK.

TYPICAL USES OF NASTRAN IN A PETROCHEMICAL INDUSTRY

J. Ronald Winter
Tennessee Eastman Company

OBJECTIVE

The two major objectives of this report are (1) to present a summary of the typical uses of NASTRAN in a petrochemical industry and (2) to describe the unique environment in which the program is used at the Tennessee Eastman Company (TEC).

BACKGROUND

NASTRAN is principally used at TEC to perform failure analysis and redesign process equipment. In addition, it is employed in the evaluation of vendor designs and proposed design modifications to existing process equipment. Its direct usage as a design tool is quite limited at this time, but I feel confident that this area of usage will grow in the future.

NASTRAN usage as a failure analysis tool is not unique, but its usage for this purpose in a production environment with primary emphasis on minimizing lost production due to mechanical/structural failures is probably unique. Its use in this way means that solutions to sometimes quite difficult problems must be obtained in relatively short periods of time. This often entails the use of models with much coarser mesh networks than would normally be desired if more time was available. However, we have found that even with the use of relatively coarse models one can obtain satisfactory results in a minimal length of time. In any event, the results obtained are generally superior to those obtained by hasty, error prone hand calculations that usually require numerous simplifying assumptions if a solution is to be obtained in the desired time frame.

We also use NASTRAN on some relatively small problems simply because the rigid formats available in NASTRAN allow one to perform several different types of analyses using essentially the same model. For instance, there are numerous cases where a stress analysis (Rigid Formats 1 or 2), a heat transfer analysis (Rigid Formats 1, 3 or 9) and a dynamic analysis (Rigid Formats 3, 8, 9, or 11) are required to insure the complete structural adequacy of a redesigned component. In these cases we find this procedure more efficient and more economical than performing the associated solutions via classical mechanics methods.

DISCUSSION

In this paper there will be no attempt to give "detailed" descriptions of any particular model or the results. In general, there will be a brief description of several problems and the associated models, the type analyses performed on the models, a summary of the results and conclusions, and typical undeformed and deformed plots. Photos of some failures will also be included. Some typical process equipment that has been analyzed via NASTRAN are listed below.

Table 1: Analyses Discussed in This Paper

	Description	Type Analyses	Rigid Formats
(1)	Large Forced Draft Fan	Static, Inertial Relief	1,2
(2)	Distillation Trays (Orthogonally Stiffened Plates)	Static, Normal Mode	1
(3)	Steel Stacks (Chimneys)	Static, Normal Mode, Frequency Response, Buckling	1,3,5,8
(4)	Large Jacketed Pipe Systems	Static	1
(5)	Heat Exchangers (Shell & Tube with Single and Double Tube Sheets)	Static, Heat Transfer	1
(6)	Large Centrifugal Fans	Static, Normal Mode	1,3
(7)	Agitator Support Structures	Static	1

Table 2: Analyses Not Discussed in This Paper

	Description	Type Analyses	Rigid Formats
(1)	Bimetallic Junctions	Static	1
(2)	Fan-Motor Shaft Failures	Normal Mode	3
(3)	Sigma Blade Mixers	Static	1

(4)	Orthogonally Stiffened Flat Heads	Static	1
(5)	Analysis of Pipe Systems	Static, Normal Mode, Forced Response, Frequency Response	1,3,8,9
(6)	Frames and Trusses	Static, Buckling	1,5
(7)	Storage Silos	Static, Buckling	1,5
(8)	Large Dryers/Blenders	Static	1
(9)	Pressure Vessels	Static	1
(10)	Shells Associated With Combustion Chambers	Static	1
(11)	Plastic Vessels	Static	1
(12)	Cyclones	Static, Normal Mode	1,3
(13)	Extruders	Static	1

Discussion of Analysis Listed in Table 1

(1) Forced Draft Fan Failure

During attempts to balance a large forced draft fan, the unit disintegrated at a rotational speed of ≈ 900 rpm (15 Hz). The normal operating speed for this unit is 1200 rpm (20 Hz). See Figures 1, 2, and 3 for photos of a typical forced draft fan and the debris from this failure.

Initially it was impossible to determine from the resulting debris what caused the failure. Several theories were postulated, but there was insufficient proof to substantiate any particular theory. This led to a NASTRAN analysis in an effort to prove or disprove several postulated sequences of events that could have resulted in the same failure. The NASTRAN model is shown in Figure 4. Rigid formats 1 (static analysis) and 2 (static analysis with inertial relief) were employed. The results indicated that the highest stress levels were at the ends of each blade and not in the outer rings. But the levels were not sufficiently high to cause failure in the absence of a defect (crack, poor weld, etc.). This led to a careful reexamination of the blades (see Figure 2). This inspection revealed that blades made by two different manufacturers were employed.* The inspection also revealed that only the blades of a welded construction had broken while the formed blades had not.

*Although the use of two different blade designs on the same fan is not desirable, this was found to be a common practice.

Detailed inspection of the ends of the broken blades revealed extremely poor welding (see Figure 3). The major weld defect was classified as lack of penetration. Of course, other weld defects such as porosity, undercutting, etc., were also present but were not of such a severe nature. When the resulting NASTRAN stress levels at the ends of the blades were multiplied by the applicable stress concentration factor, the stress levels were more than sufficient to cause failure. Subsequently, several runs were made to investigate the loads assuming one or more blades had broken. These results indicated that the failure pattern would be similar to that indicated by the debris.

(2) Distillation Trays (Orthogonally Stiffened Plates)

A distillation tray essentially consists of a thin plate supported by beams. A typical distillation tray is shown in Figure 5. Numerous failures have been encountered with such trays. The failures have been attributed to:

(1) Fatigue associated with normal process pulsations (Figure 6).
(2) Resonant or near resonant conditions.
(3) Large pressure pulses due to process upsets, start-ups, etc. Flashing is a common problem (Figures 7 and 8).
(4) Corrosion (general attack and specific types of attack, e.g., stress corrosion).

NASTRAN analyses have essentially eliminated the first two failure mechanisms and has aided us in designing/specifying trays that are more resistant to minor pressure pulses. NASTRAN is also used to evaluate vendor tray designs especially if an unusual design is submitted or if the particular design is used in a critical application.

Typical tray models are shown in Figures 9 and 10. Typical plots of the first and second modes are shown in Figures 11 and 12.

(3) Metal Stack Analysis

Due to potential pollution problems, it was desired to add a 15.24 meter (50 ft.) extension to an existing 30.48 meter (100 ft.) stack. The existing oil fired boiler stack is shown in Figures 13 and 14. Due to potential vortex shedding problems, an analysis was requested. The resulting NASTRAN model is shown in Figure 15. A NASTRAN modal analysis showed that a resonant condition would occur due to vortex shedding at moderate to high wind velocities which were typical in the particular region. See Figure 16 for the first bending mode. A static analysis also revealed that the foundation loads were far too large. Additional analyses revealed that the stack would encounter an ovaling resonant condition at high wind velocities. Thus, it was shown that the desired corrective action would require the installation of new stacks.

(4) Jacketed Pipe Analysis

In many situations in a petrochemical plant it is necessary to maintain the temperature of a product in a pipeline to prevent solidification. The use of jacketed pipe (steam in the external pipe, process material in the inner pipe) is often used to achieve this result. In these cases the internal pipe is typically a 300 series stainless steel while the outer pipe (steam jacket) is carbon steel. Due to the temperature difference between the inner and outer pipes and the fact that their thermal coefficients of expansions are quite different one can encounter large differential thermal expansions. As a result of these conditions, we have encountered numerous failures with this type of pipeline in the past. NASTRAN, with the MPC/rigid element capability, is ideally suited for "rapid" analysis of these type pipelines. A typical pipeline model is shown in Figure 17. The results of a NASTRAN analysis of a vendor's design before and after the implementation of modifications based on NASTRAN analyses is shown in Figures 18 and 19. The NASTRAN analyses of several lines led to the development of a set of general jacketed pipe design guidelines to be used by engineers and draftsmen. These layout guidelines have virtually eliminated failures in this type pipeline.

(5) Heat Exchangers

The failure of the tube sheet/flange assembly of several vendor designed heat exchangers led to a NASTRAN analysis. The typical failures encountered in this case are shown in Figures 20 and 21. The associated finite element models are shown in Figures 22 and 23. The NASTRAN analysis readily showed that differential radial thermal expansion was the major cause of failure (see Figure 24). However, differential thermal expansion between the tubes and shell wall also contributed to the problem. The units were redesigned based on the NASTRAN results.

(6) Large Centrifugal Fan

The development of cracks in the large centrifugal fan shown in Figure 25 led to the development of a NASTRAN model of a portion of the fan. The basic model is shown in Figure 26. As expected, the static analysis showed that the highest stress levels were in the region where the cracks had appeared. However, the stress levels were not sufficiently high to cause fatigue cracks to develop in the applicable time frame. This led to a modal (real eigenvalue) analysis. These results revealed the true culprit. A panel natural frequency existed relatively close to a normal operating frequency. The applicable mode shape is shown in Figure 27. Since the panel frequency was just below the normal operating frequency, it was established that the fan was being seriously damaged during each start-up and shutdown. Until a new fan could be built, it was recommended that the fan be allowed to run continuously if possible. It was later established that due to process problems and bearing problems the unit had been started and stopped numerous times during the period before the cracks were discovered.

The NASTRAN analysis established the cause of the failure and served as the basis for designing a new fan. The model was also used to modify the original fan which now serves as a back-up.

(7) Agitator Support Structures

Inadequate structural supports for large agitators have been diagnosed via NASTRAN analysis to be the cause of severe shaft wear, premature bearing failures and cracking of the agitator housings. This problem was resulting in unusually high maintenance costs. As a result of these analyses, a new design procedure which accounts for dynamic effects has been developed. A typical model of an agitator support system is shown in Figure 28.

CLOSING COMMENTS

From the previously discussed typical uses of NASTRAN, it should be evident that our use of the program is quite broad. We have found NASTRAN to be the only diversified tool presently available which allows the user to deal with a very wide variety of difficult problems in a relatively short period of time. Needless to say, we are very dependent on the capabilities available in this program.

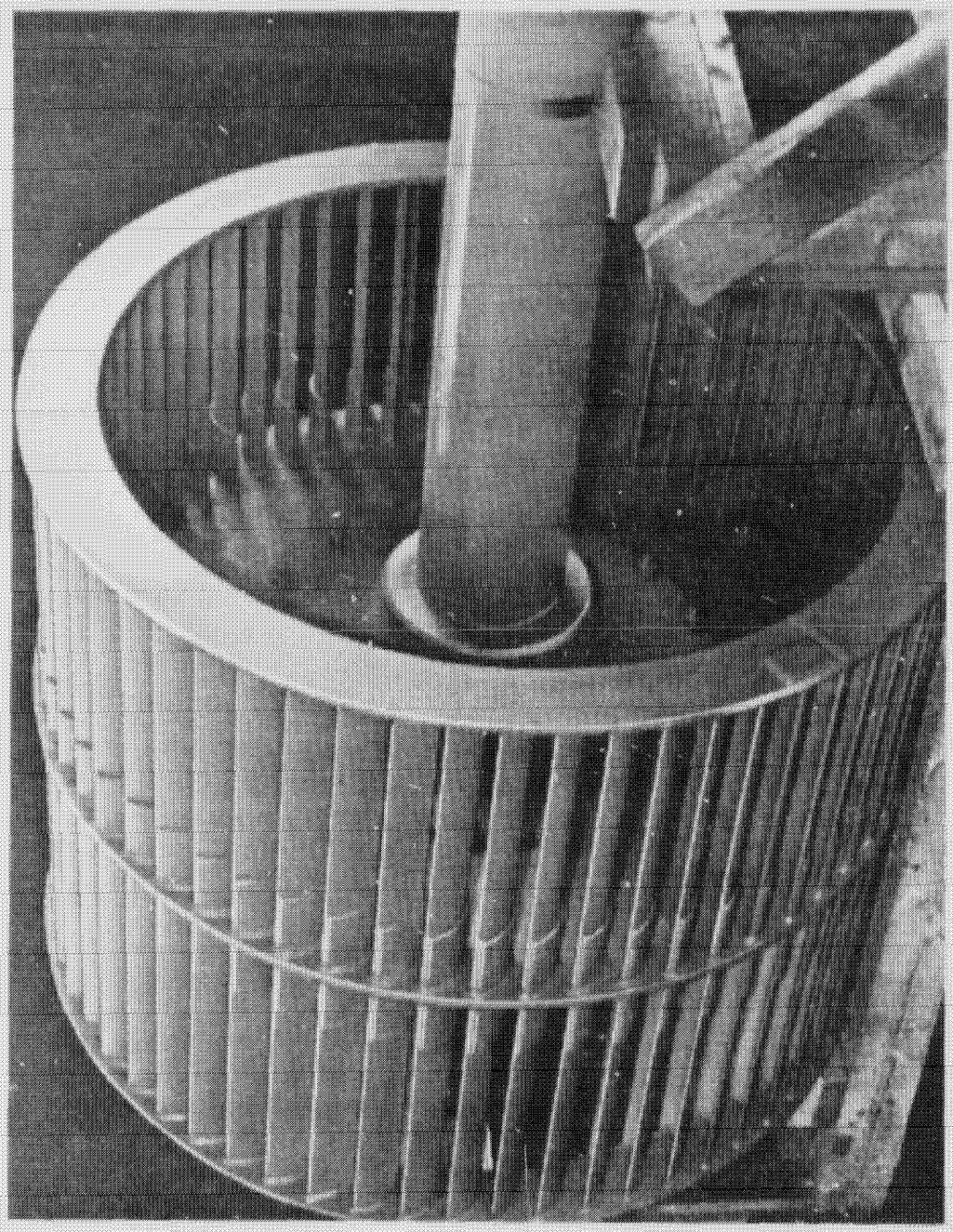

FIGURE 1: TYPICAL FORCED DRAFT FAN

FIGURE 2: DAMAGED BLADES (FORMED BLADE AT TOP, WELDED BLADE AT BOTTOM)

ORIGINAL PAGE IS
OF POOR QUALITY

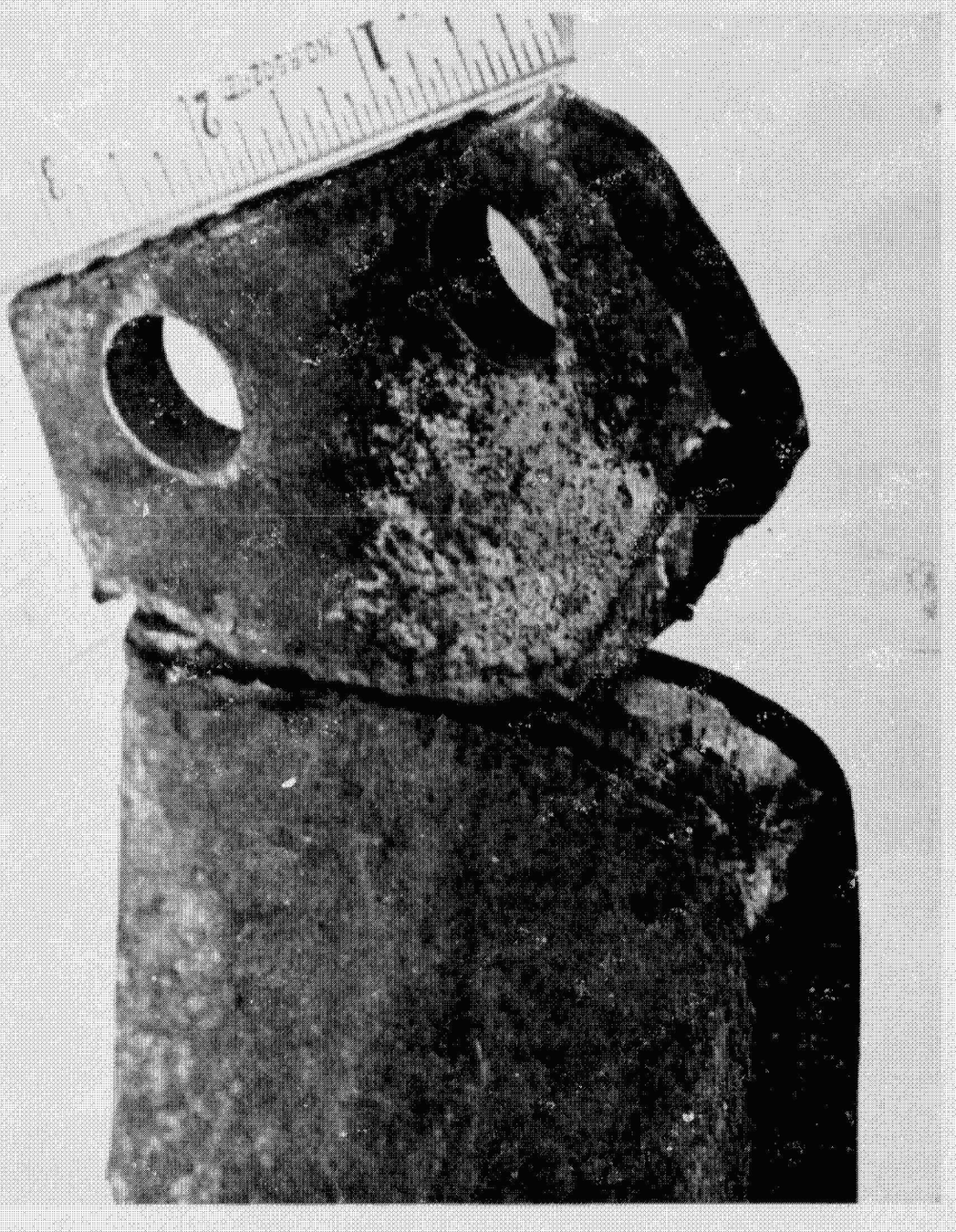

FIGURE 3: FAILURE OF A WELDED BLADE

FIGURE 4: MODEL OF FORCED DRAFT FAN

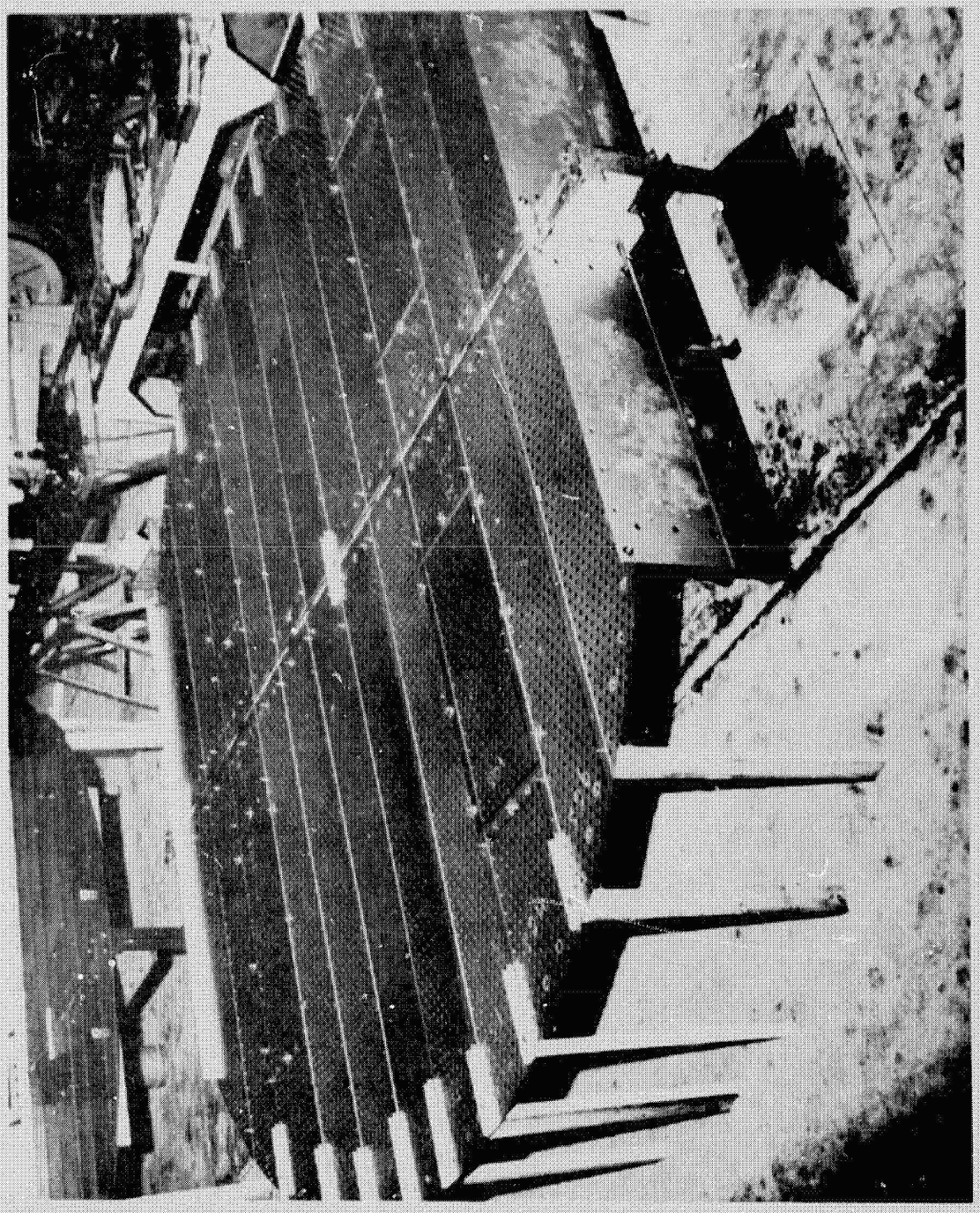

FIGURE 5: TYPICAL DISTILLATION TRAY

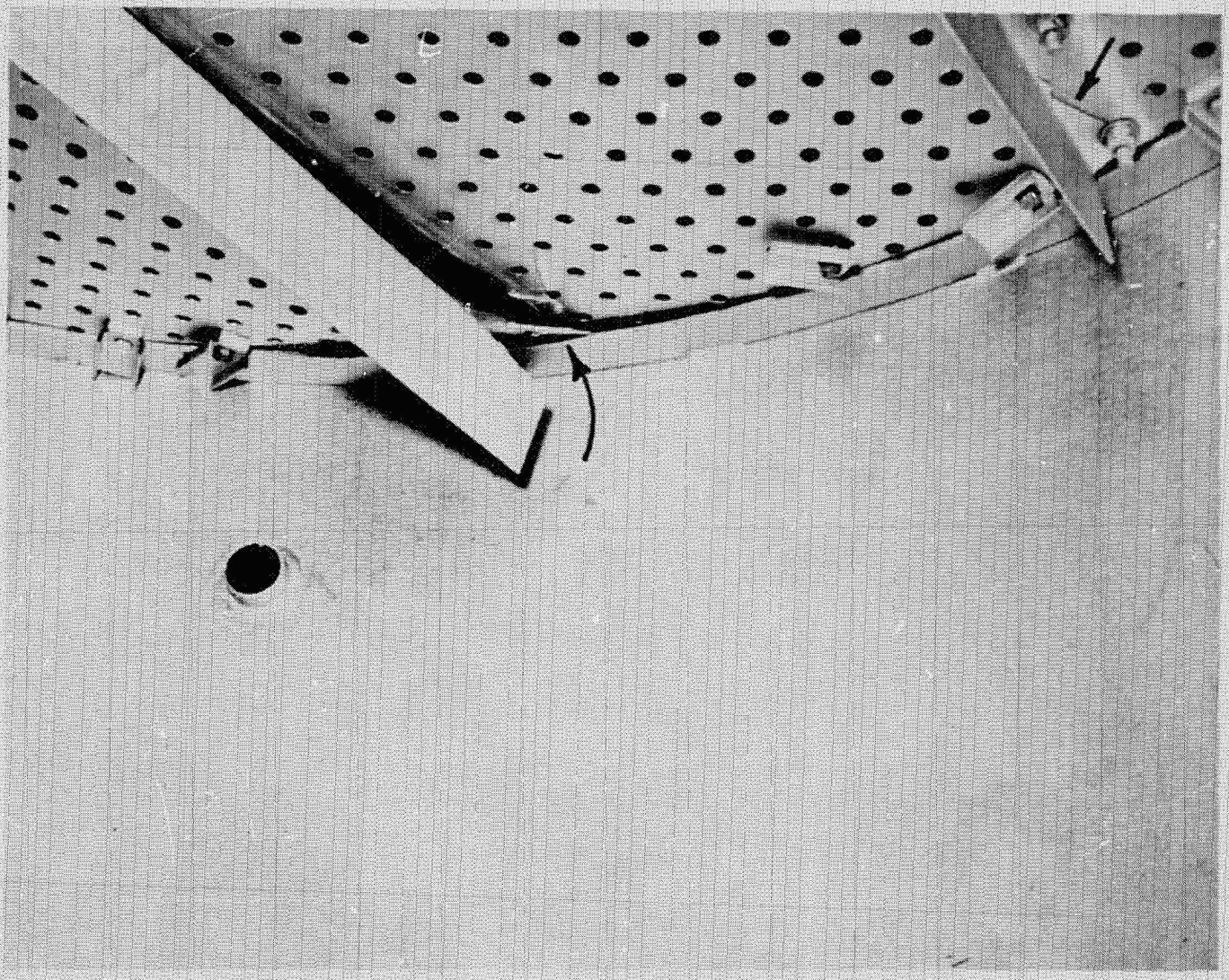

FIGURE 6: FATIGUE FAILURE OF A DISTILLATION TRAY DUE TO NORMAL PROCESS PULSATIONS

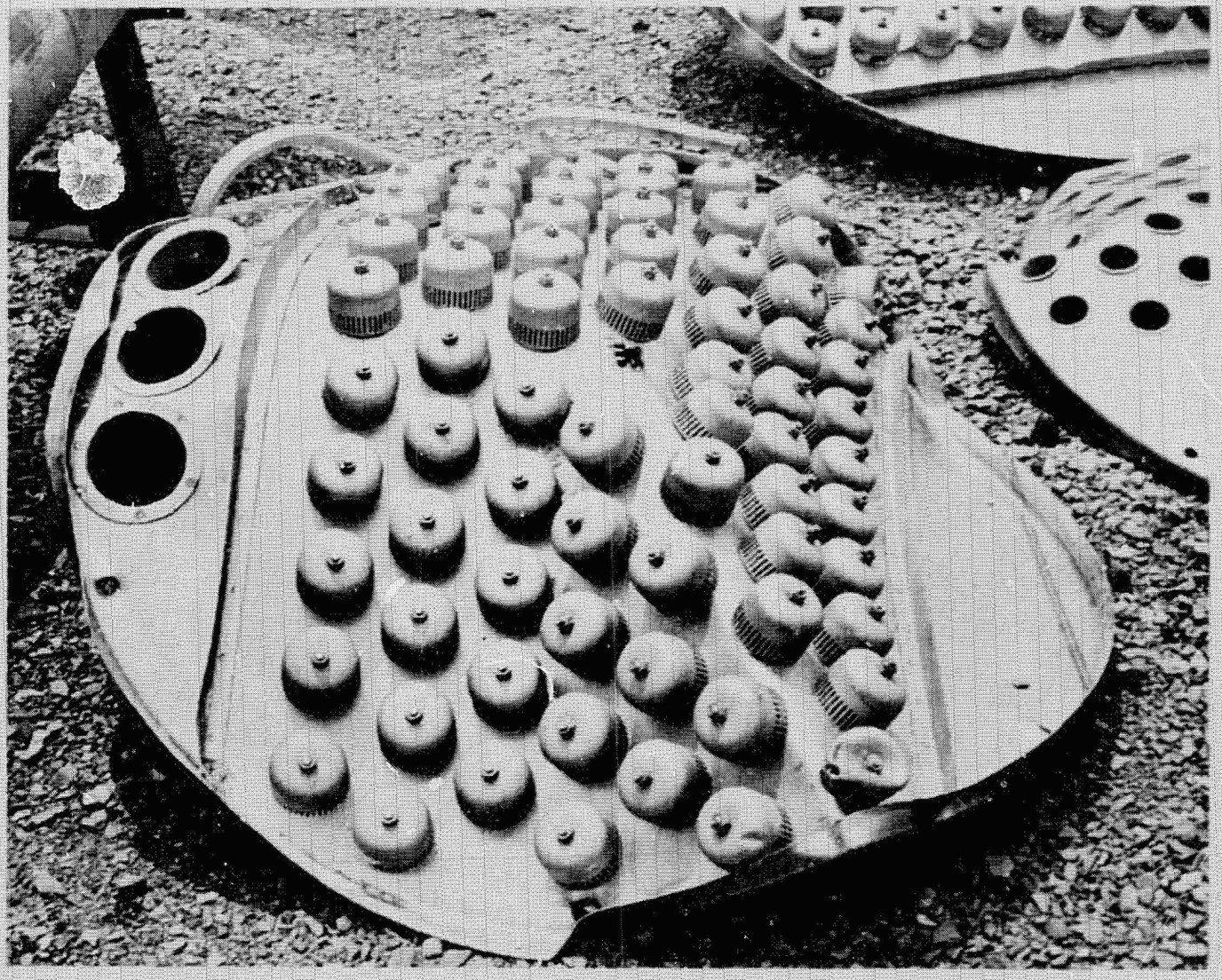

FIGURE 7: FAILURE OF A SMALL DIAMETER DISTILLATION TRAY DUE TO A LARGE PRESSURE PULSE

FIGURE 8: FAILURE OF A LARGE DIAMETER DISTILLATION TRAY DUE TO A LARGE PRESSURE DIFFERENTIAL

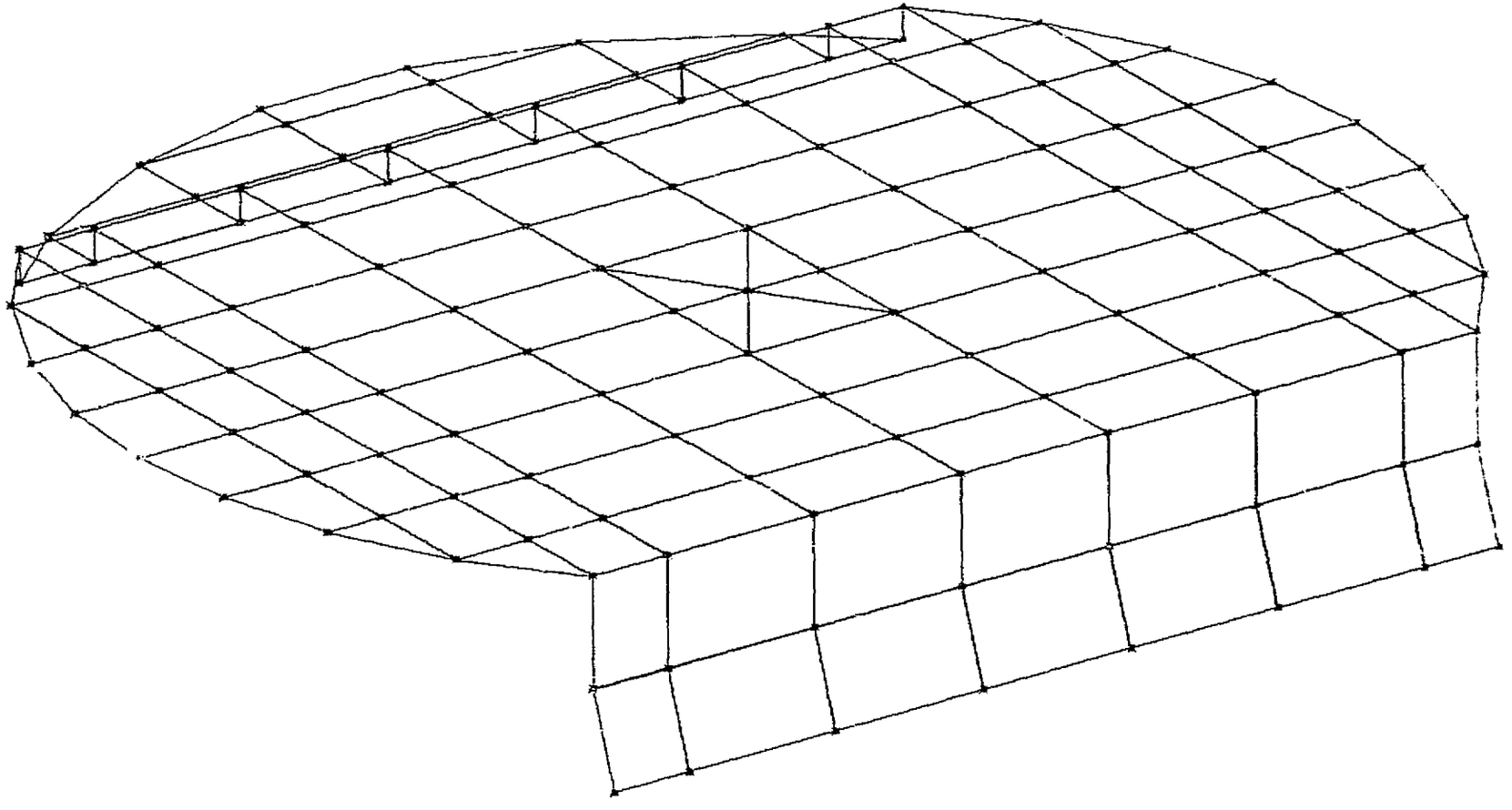

FIGURE 9: TYPICAL MODEL OF A LARGE DIAMETER DISTILLATION TRAY

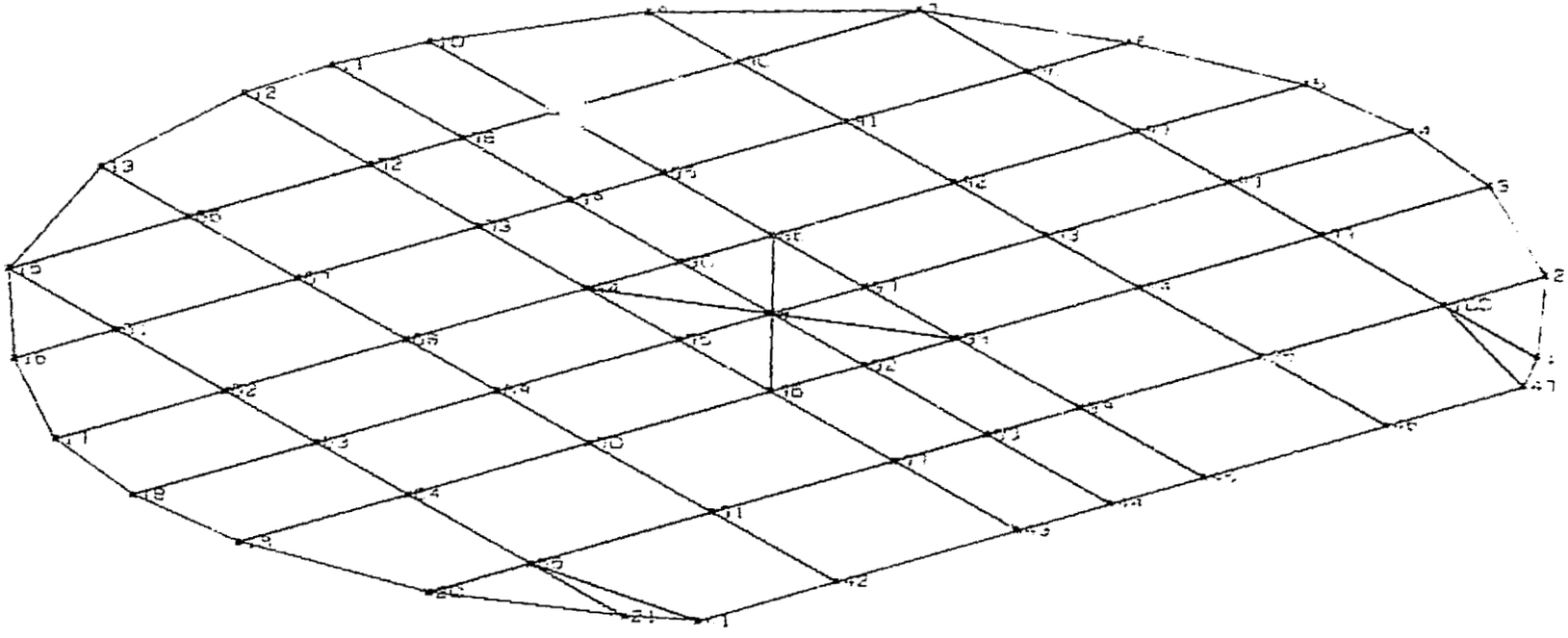

FIGURE 10: TYPICAL MODEL OF A SMALLER DISTILLATION TRAY

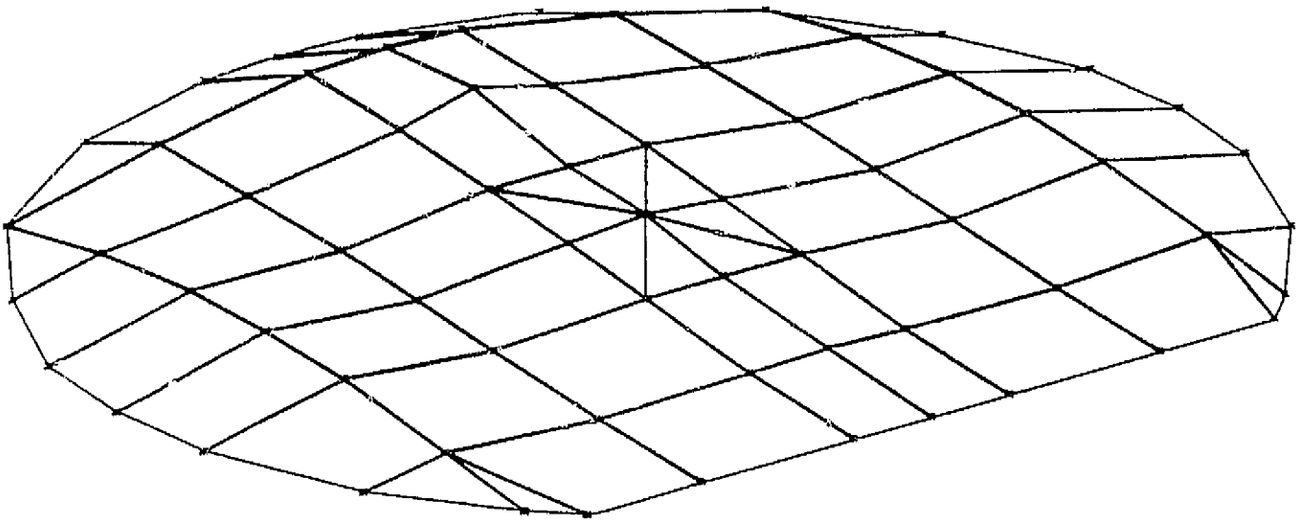

FIGURE 11: FIRST MODE OF A DISTILLATION TRAY

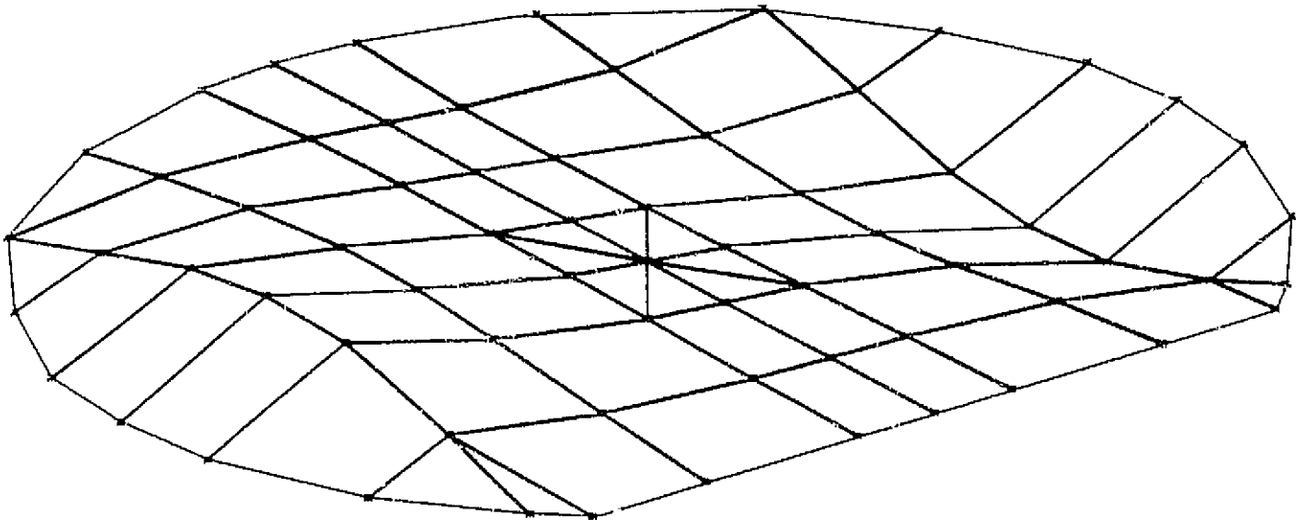

FIGURE 12: SECOND MODE OF A DISTILLATION TRAY

FIGURE 13: DISTANT VIEW OF ORIGINAL STACKS

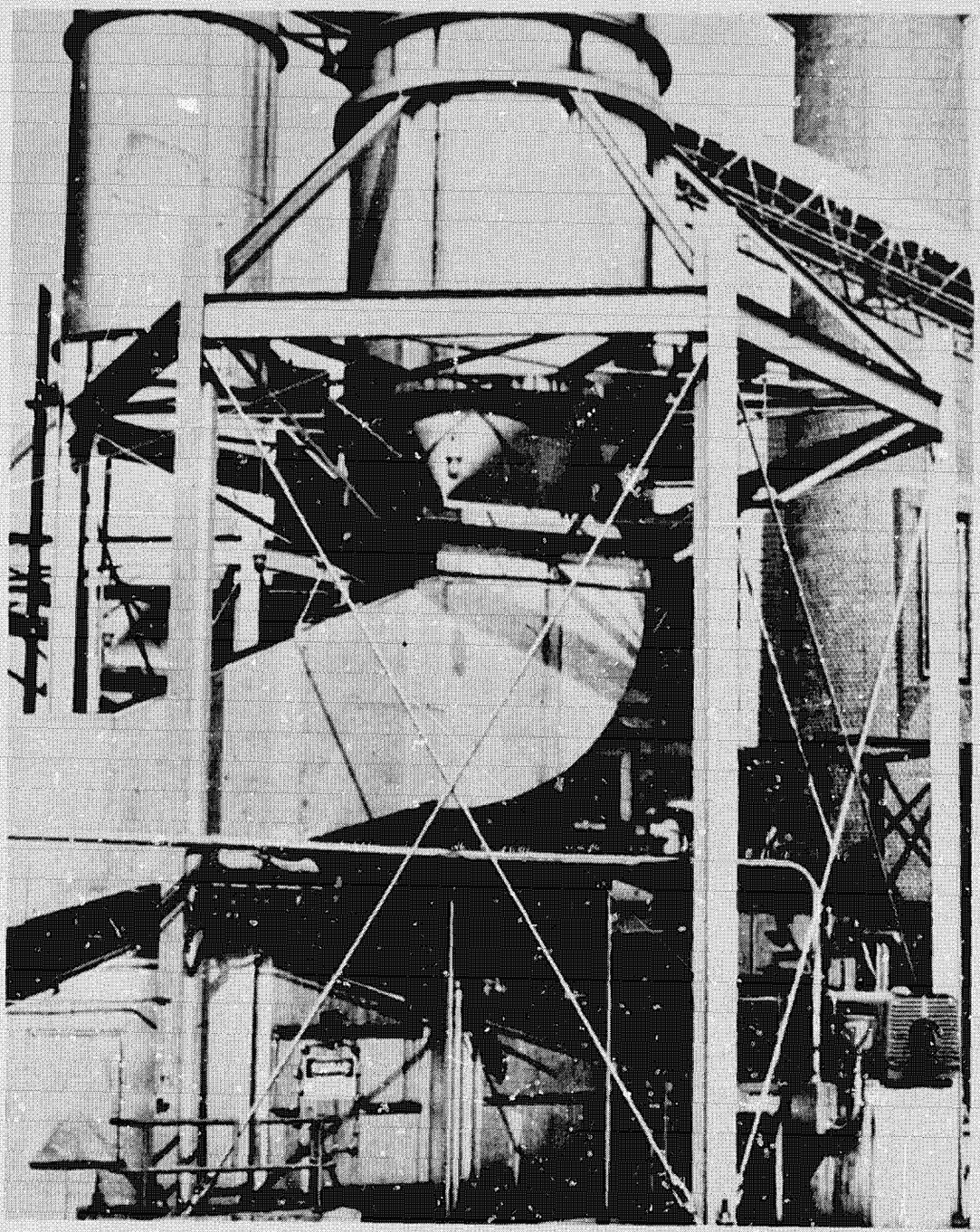

FIGURE 14: VIEW OF THE STACK SUPPORT STRUCTURE

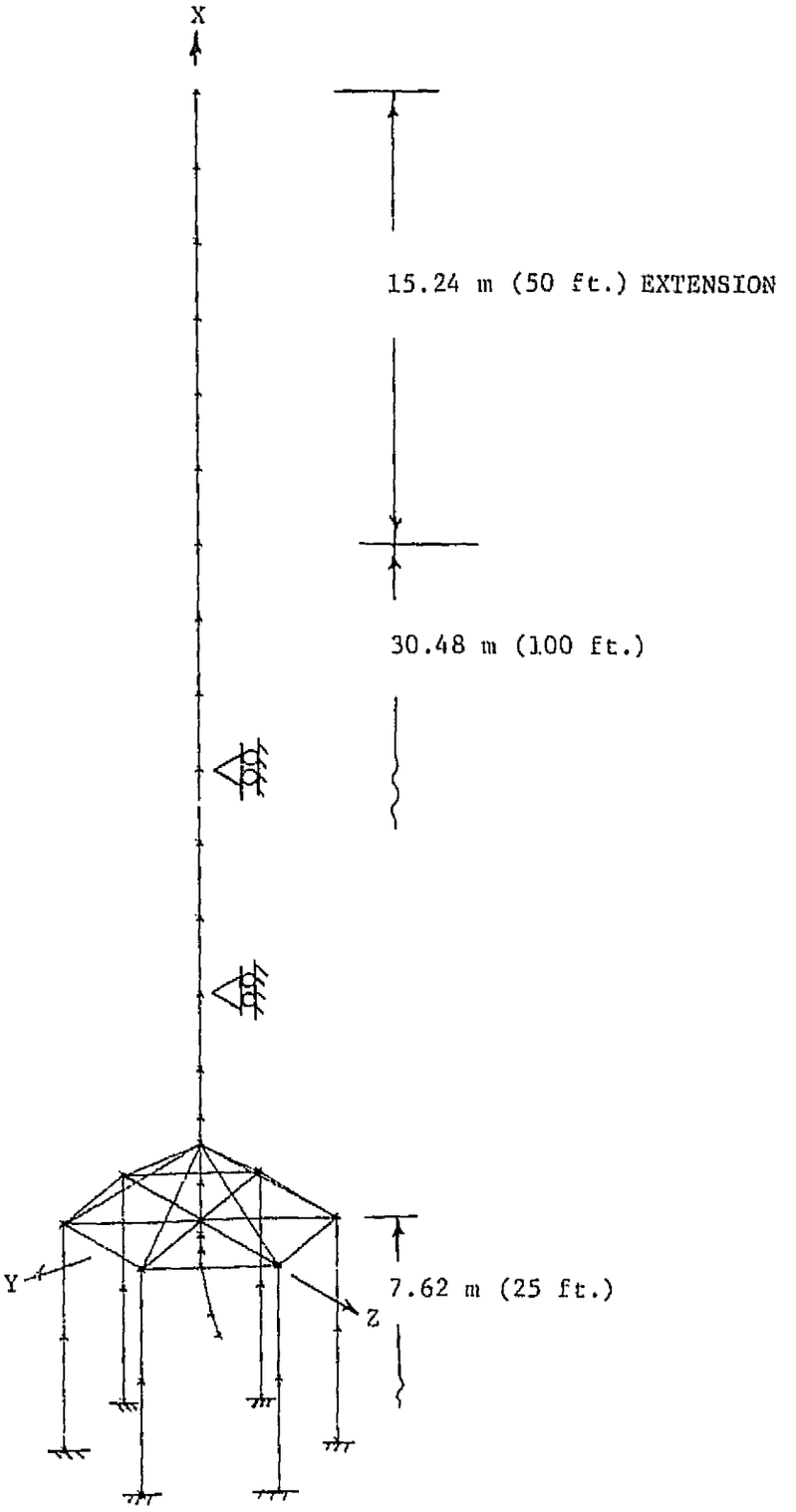

FIGURE 15: BASIC NASTRAN STACK MODEL

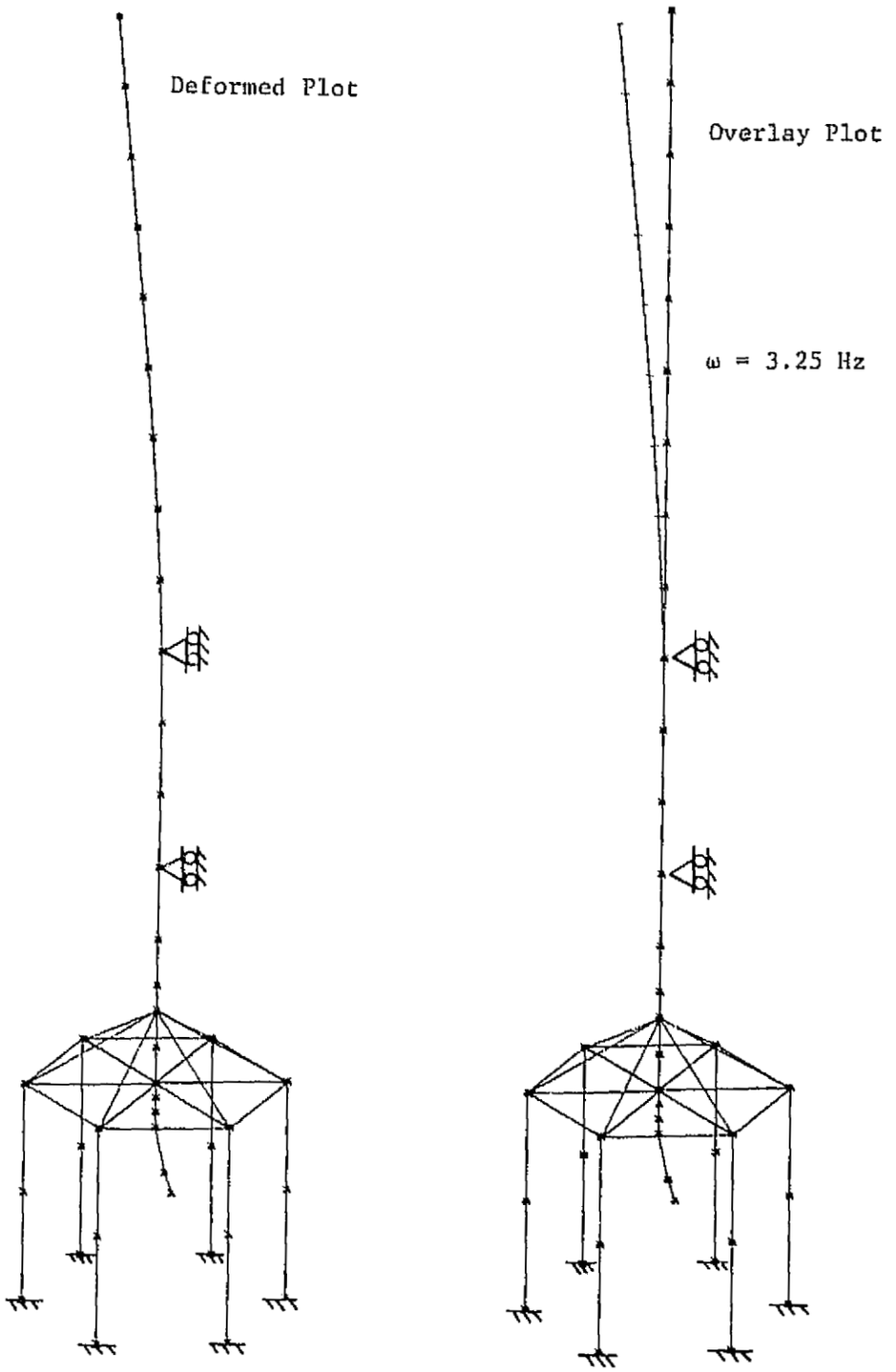

FIGURE 16: FIRST STACK BENDING MODE

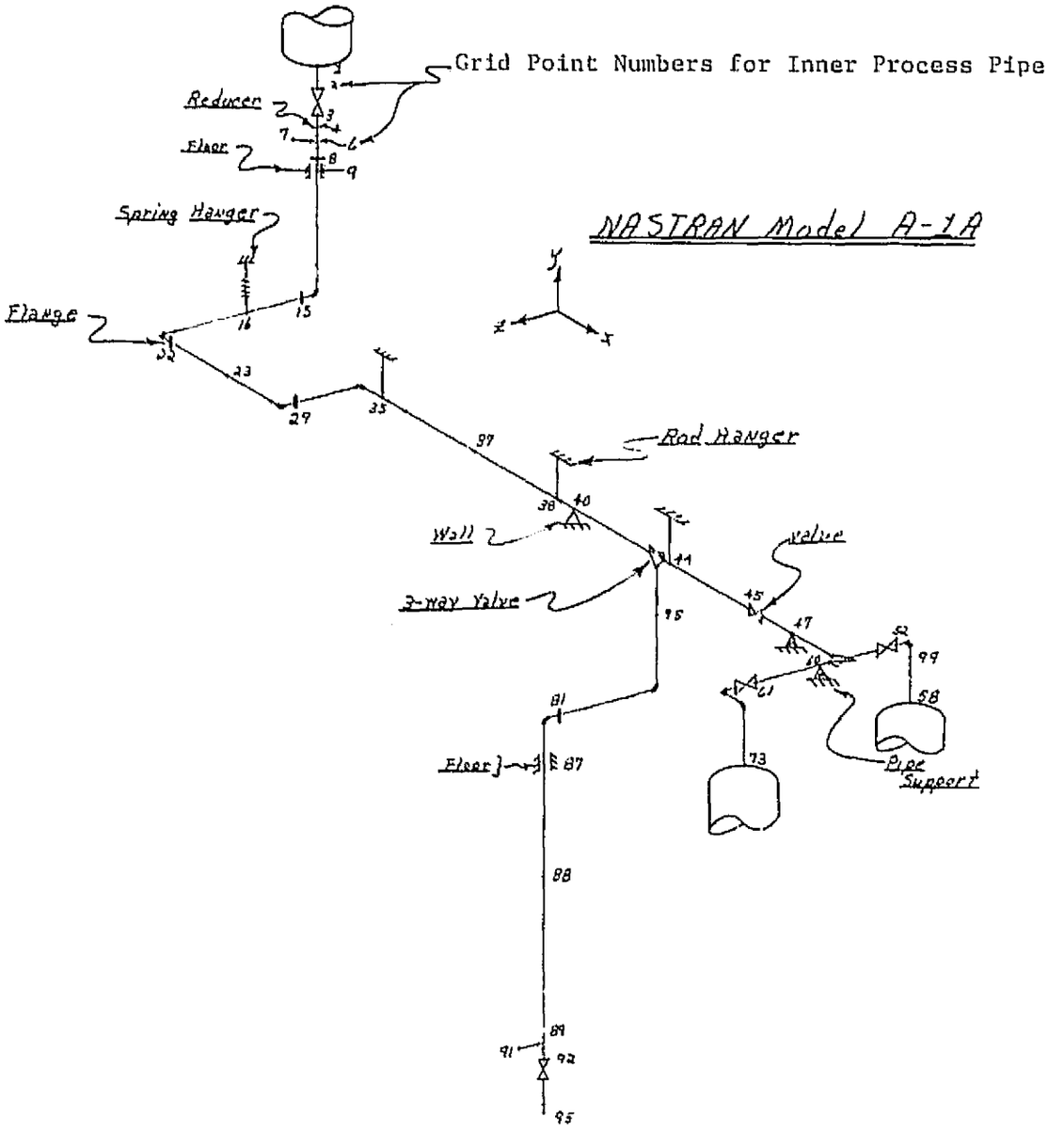

FIGURE 17: TYPICAL MODEL OF JACKETED PIPE SYSTEM

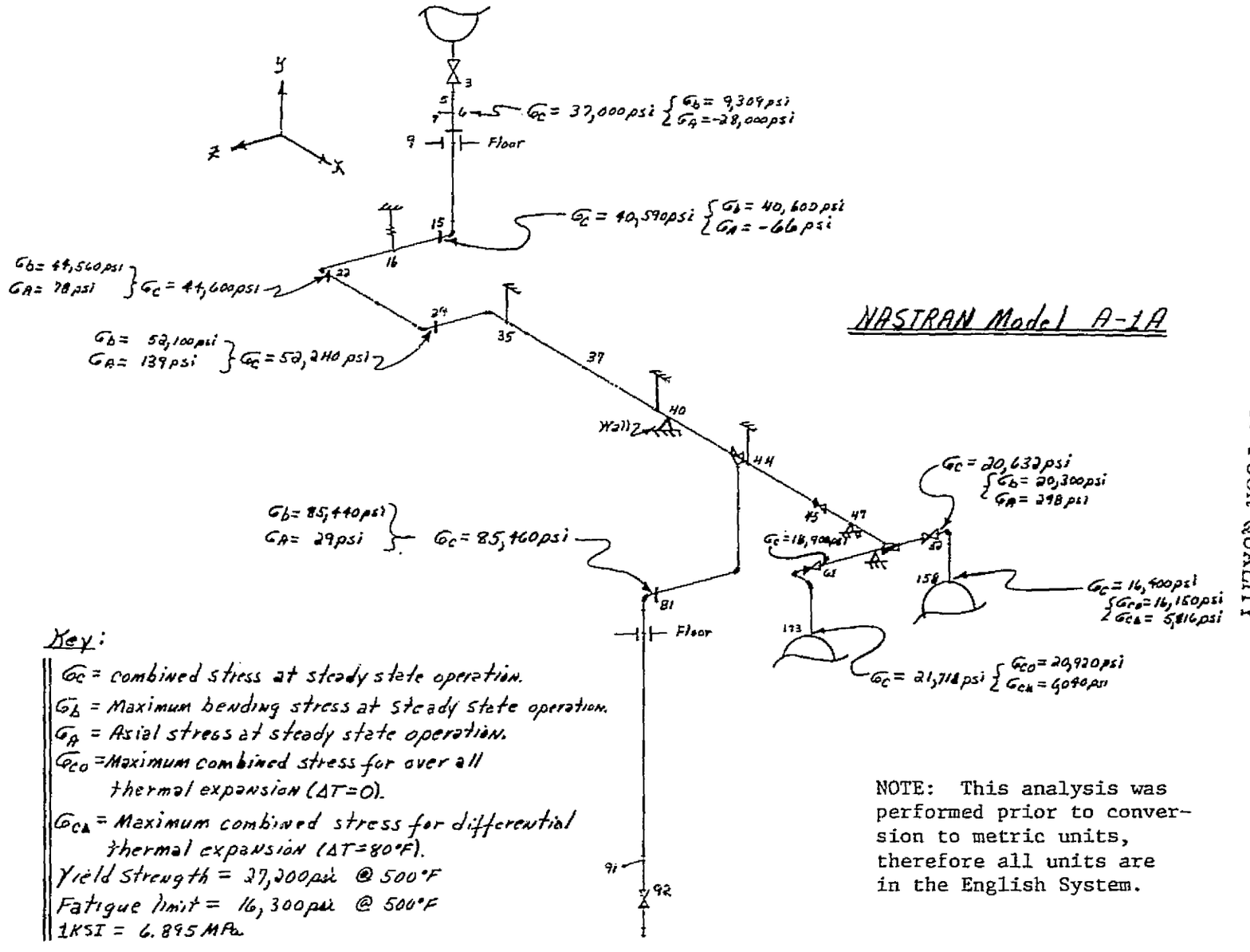

FIGURE 18: RESULTS FROM ANALYSIS OF DESIGN SUBMITTED BY VENDOR

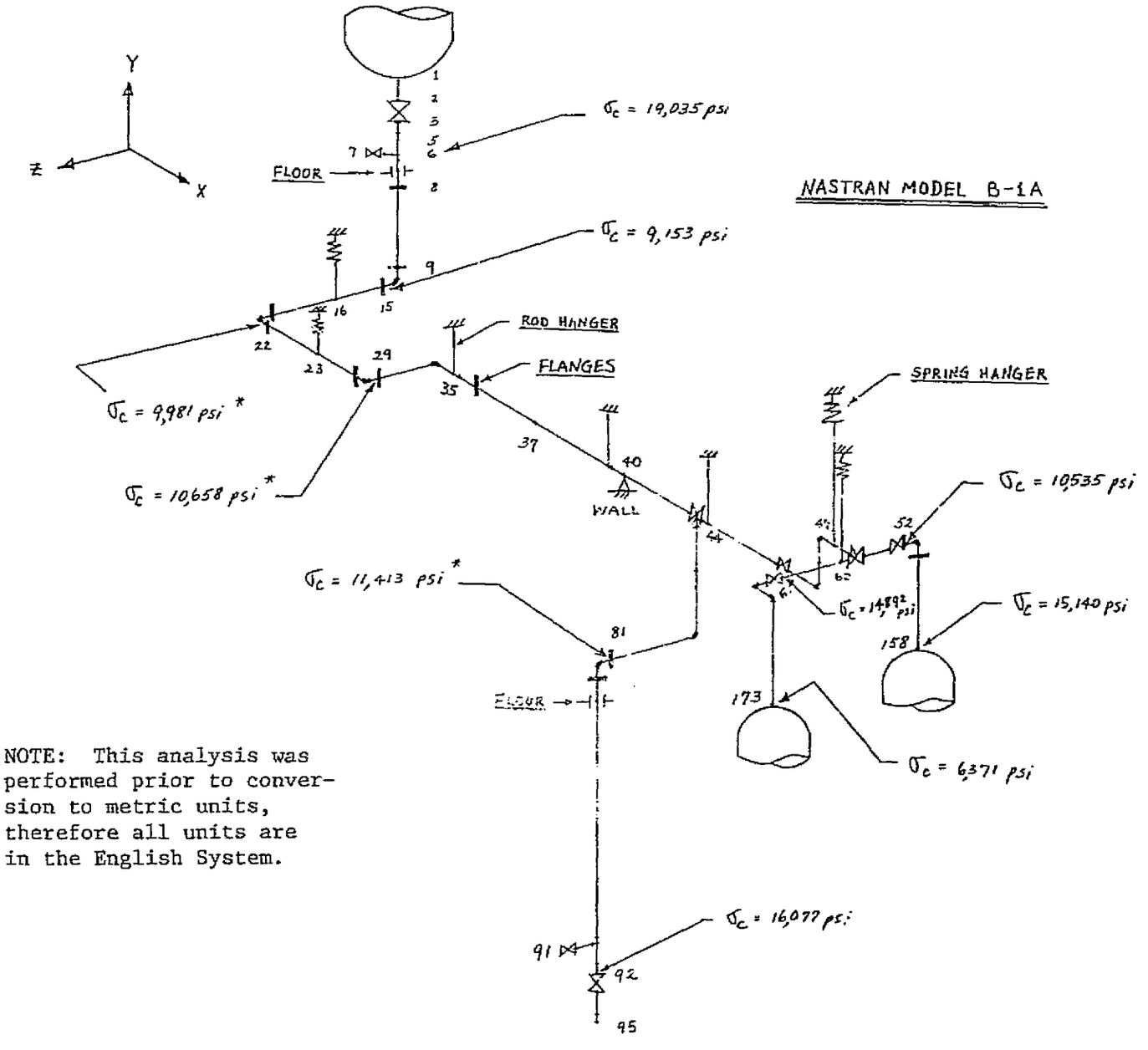

NOTE: This analysis was performed prior to conversion to metric units, therefore all units are in the English System.

FIGURE 19: RESULTS AFTER MAKING REVISIONS BASED ON NASTRAN ANALYSIS

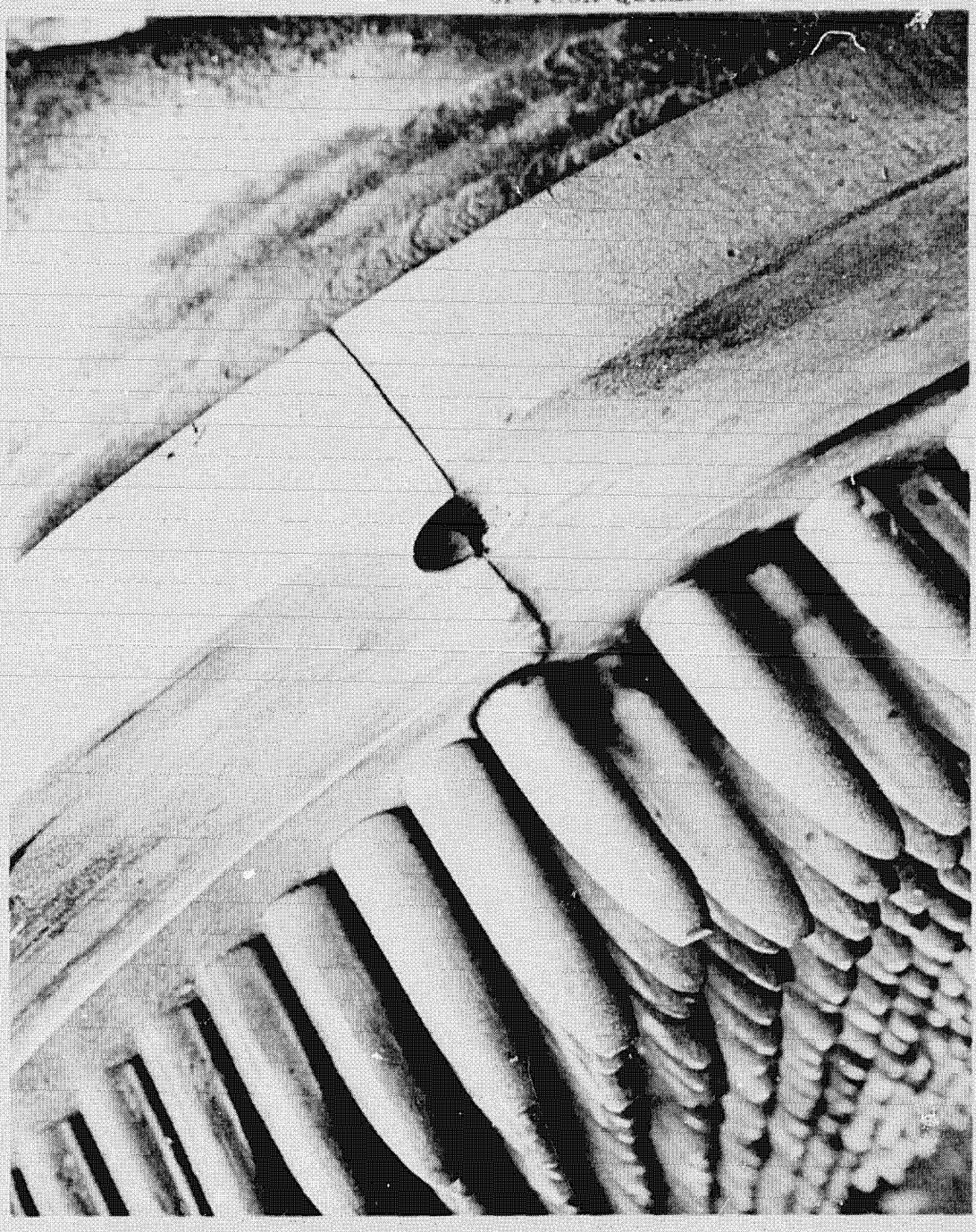

FIGURE 20: TYPICAL FAILURE IN A HEAT EXCHANGER TUBE SHEET/FLANGE ASSEMBLY
(NOTE: CRACK HAS PROGRESSED INTO THE TUBES)

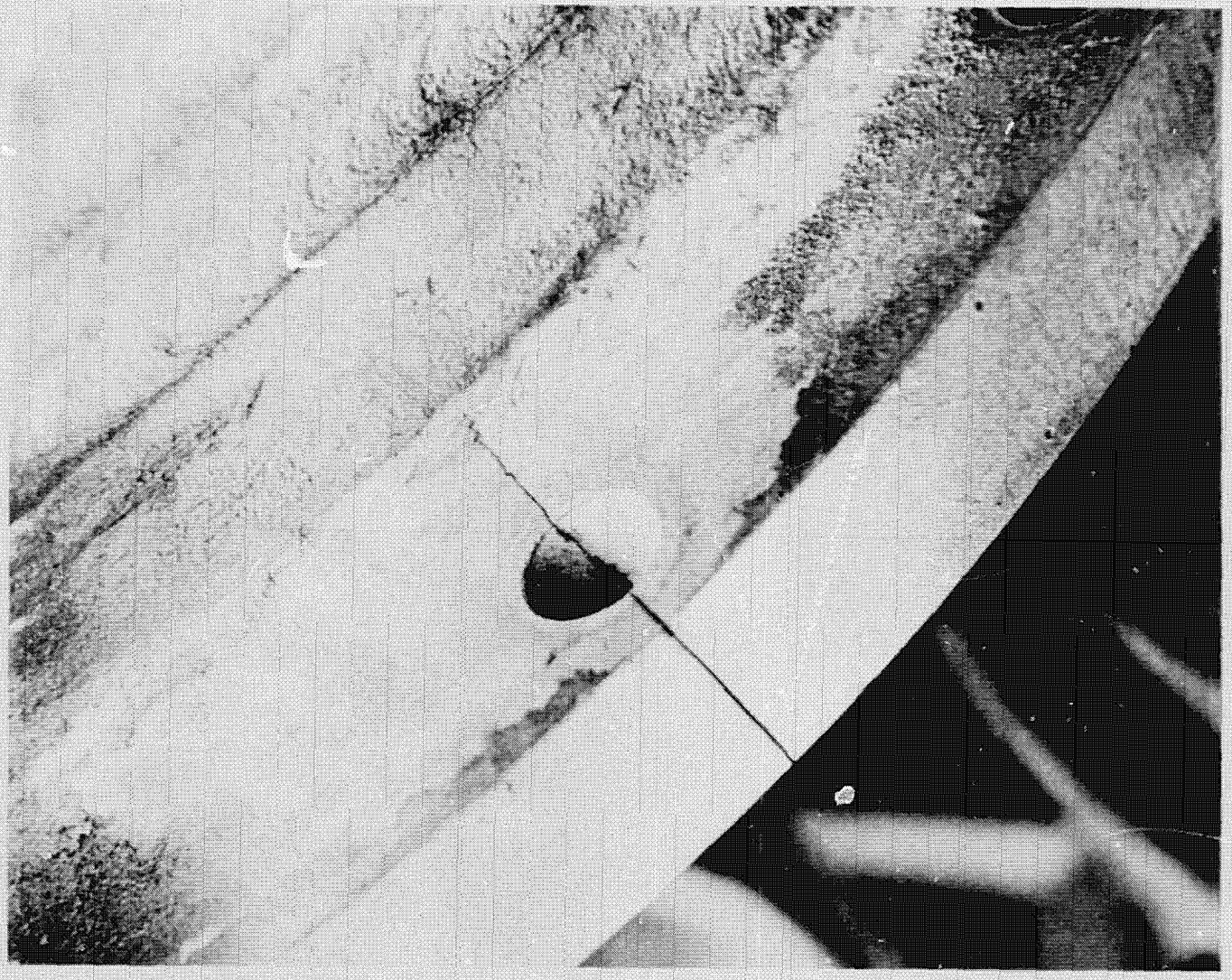

FIGURE 21: TYPICAL FAILURE OF A HEAT EXCHANGER TUBE SHEET/FLANGE ASSEMBLY
(NOTE: CRACK HAS PROGRESSED INTO VESSEL WALL)

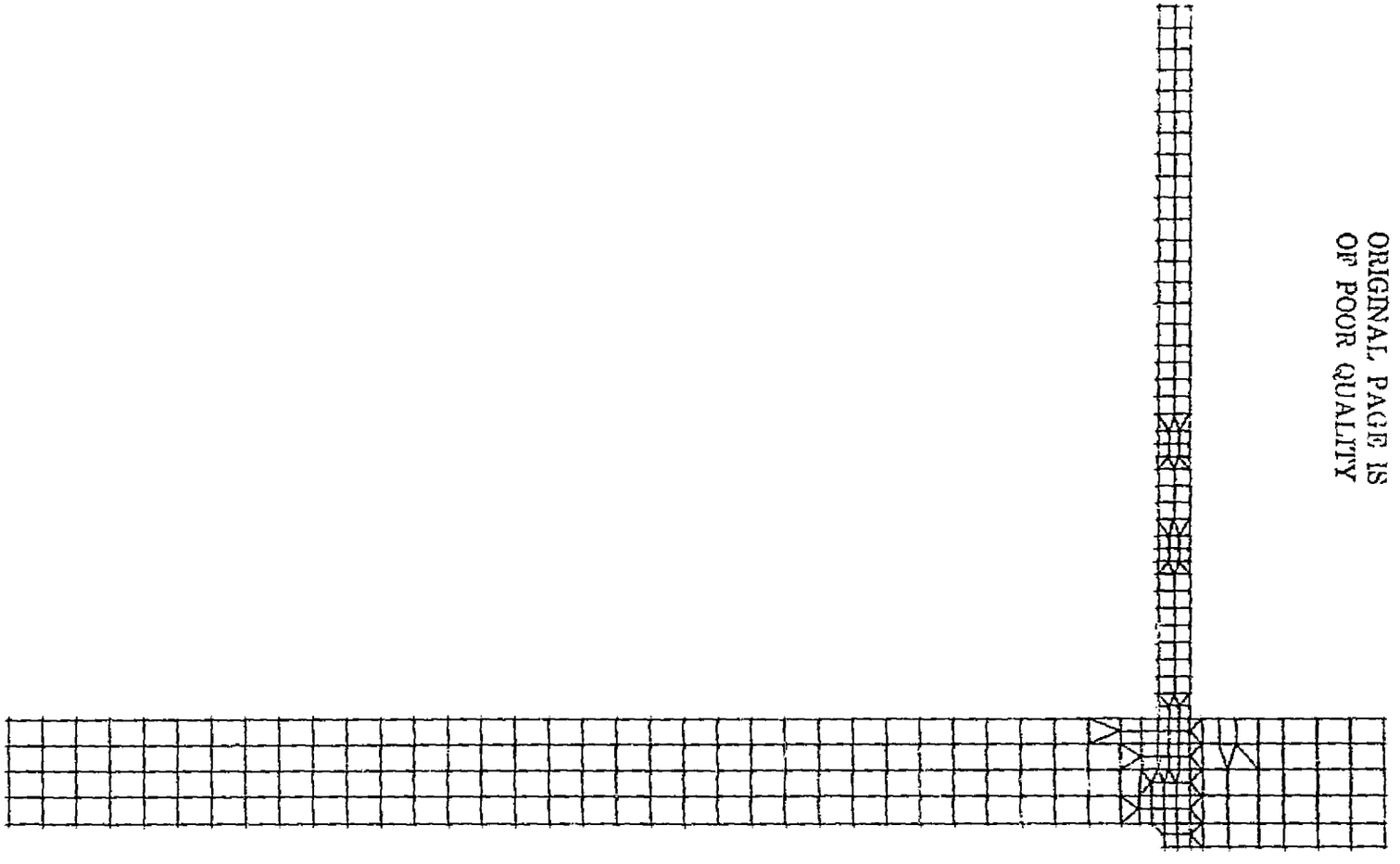

FIGURE 22: TYPICAL MODEL OF A SINGLE TUBE SHEET ASSEMBLY

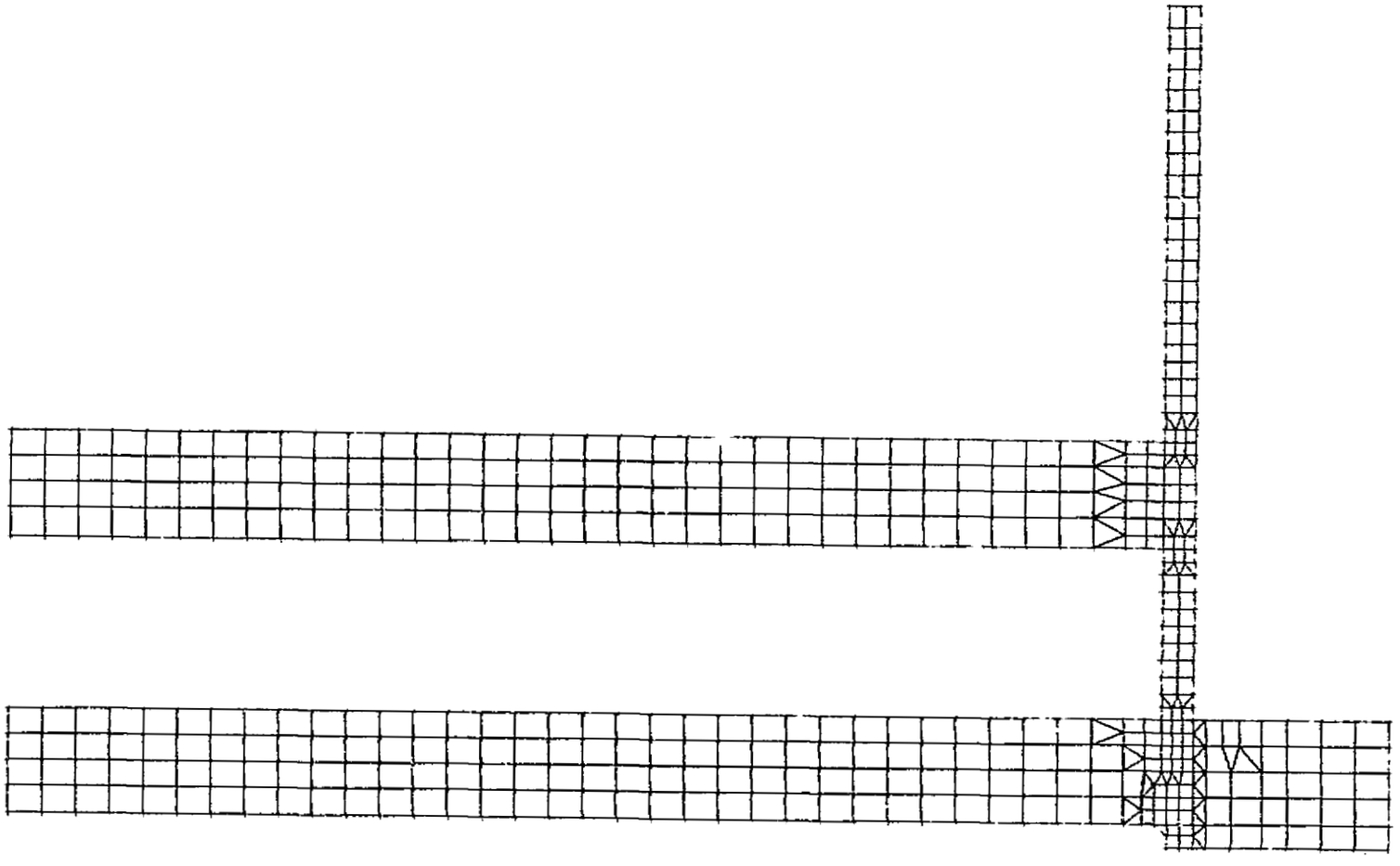

FIGURE 23: TYPICAL MODEL OF A DOUBLE TUBE SHEET ASSEMBLY

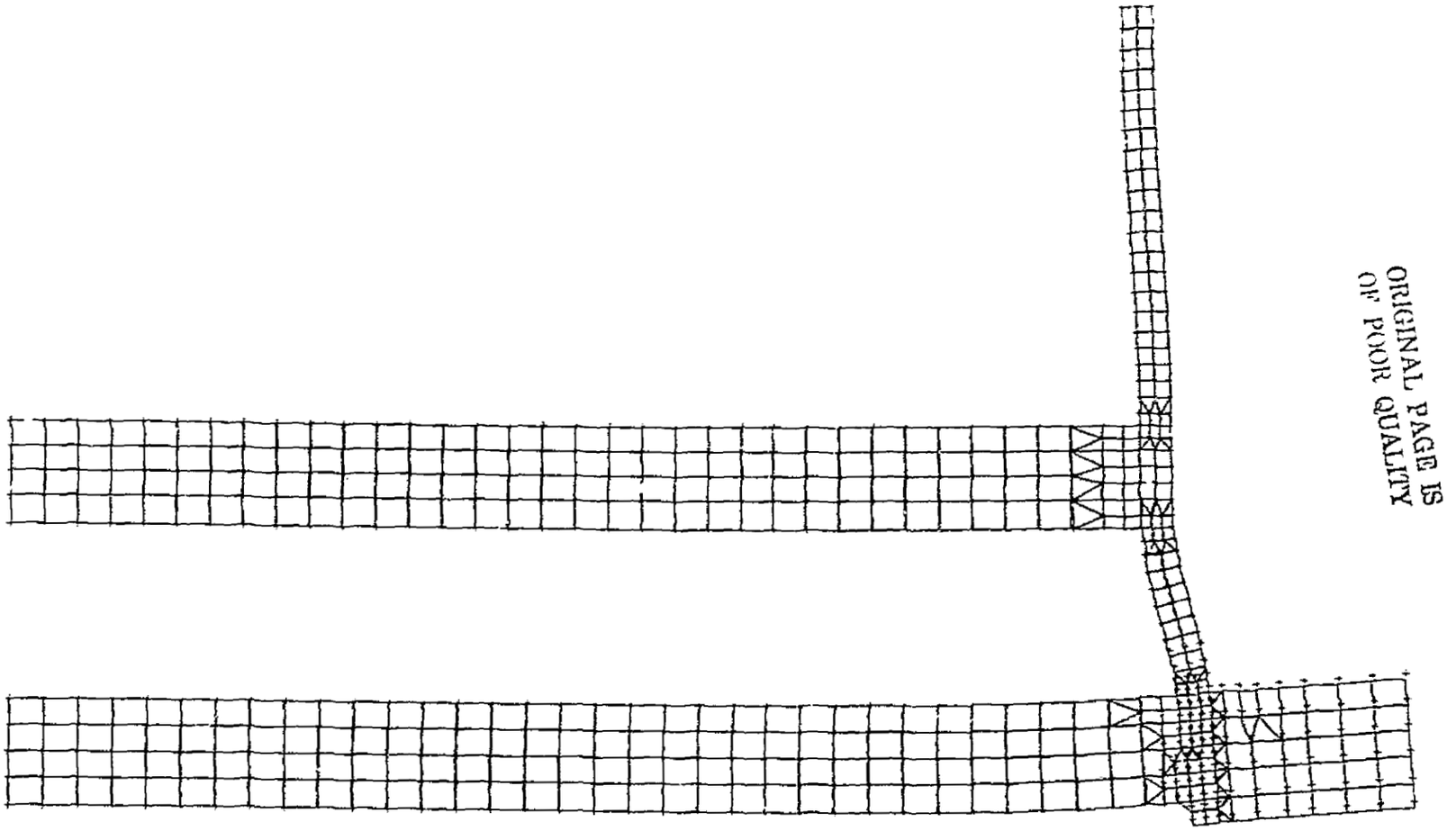

FIGURE 24: THERMALLY INDUCED DEFORMATIONS OF A DOUBLE TUBE SHEET ASSEMBLY

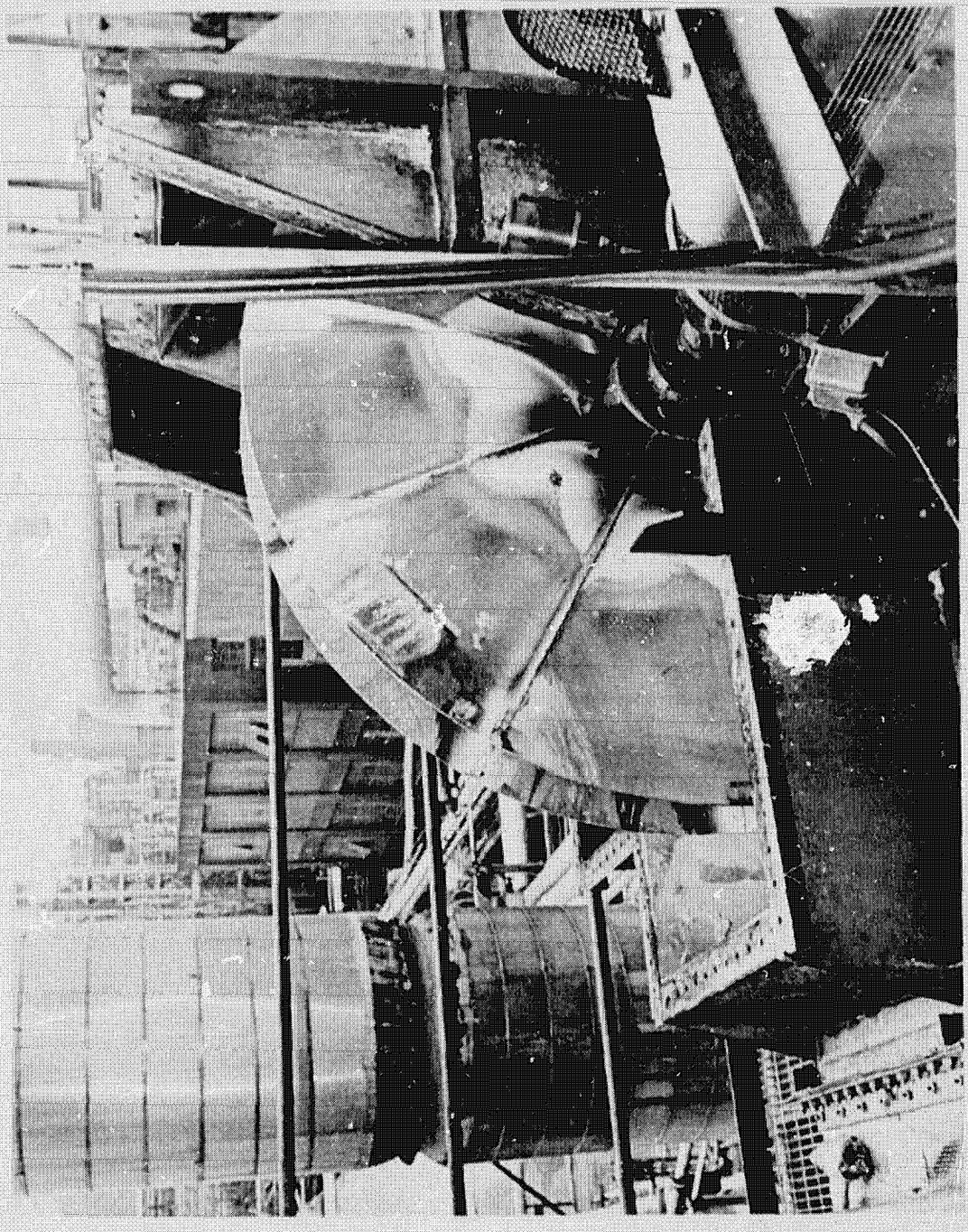

FIGURE 25: LARGE CENTRIFUGAL FAN

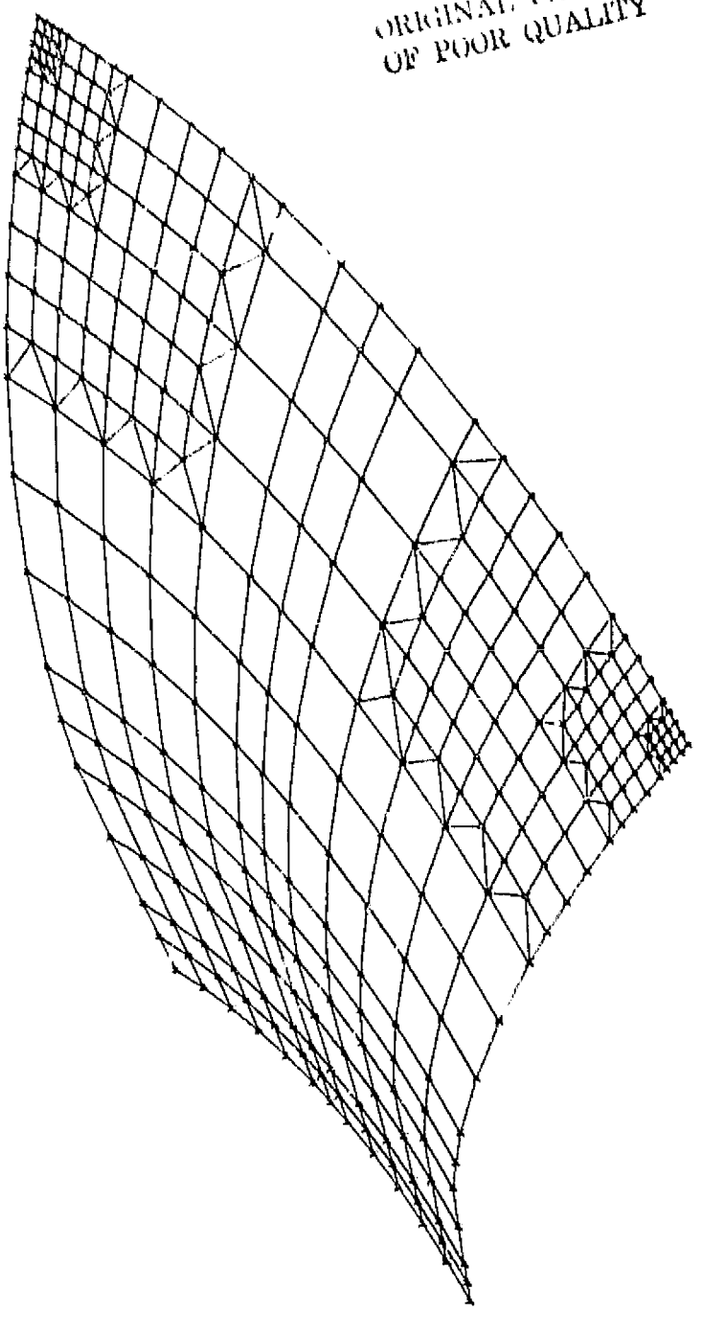

FIGURE 26: MODEL OF ONE PANEL OF THE CENTRIFUGAL FAN

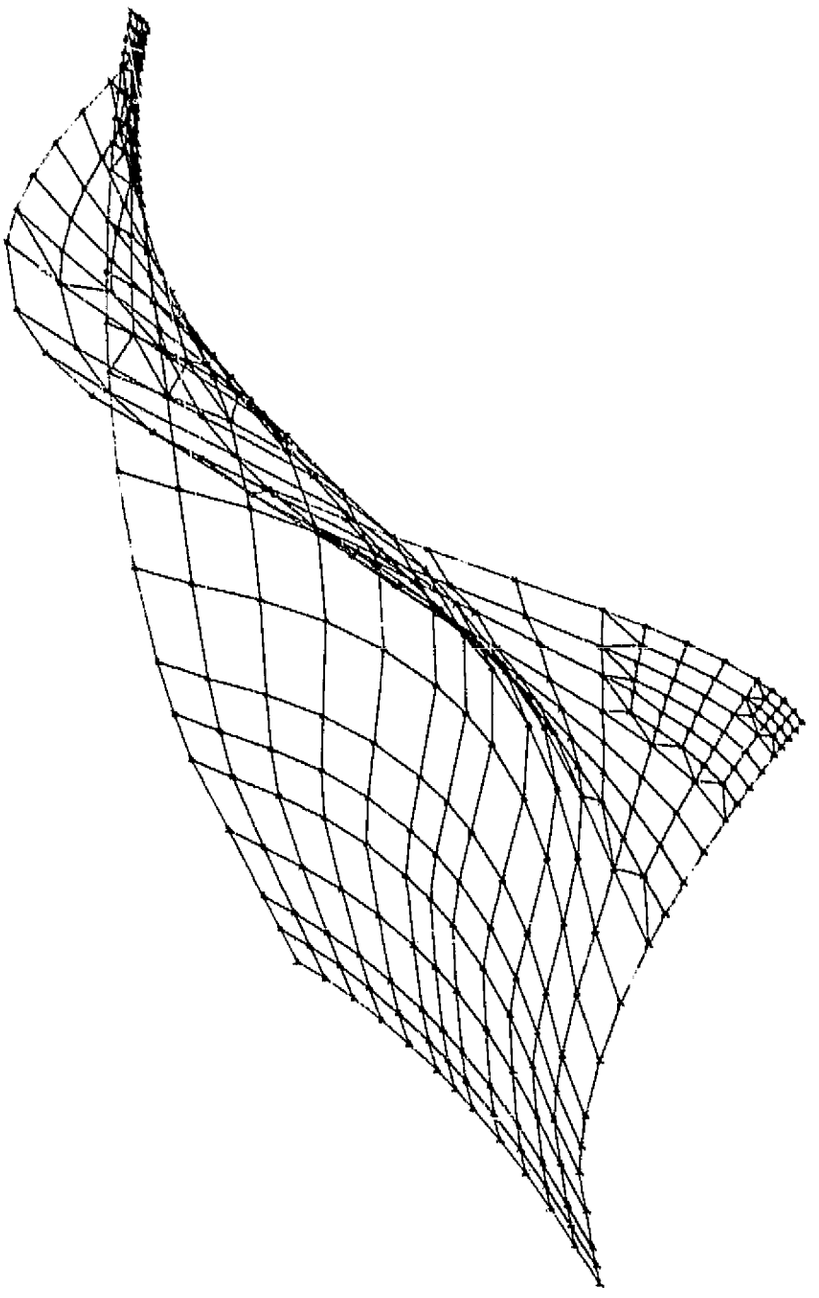

FIGURE 27: FIRST PANEL MODE

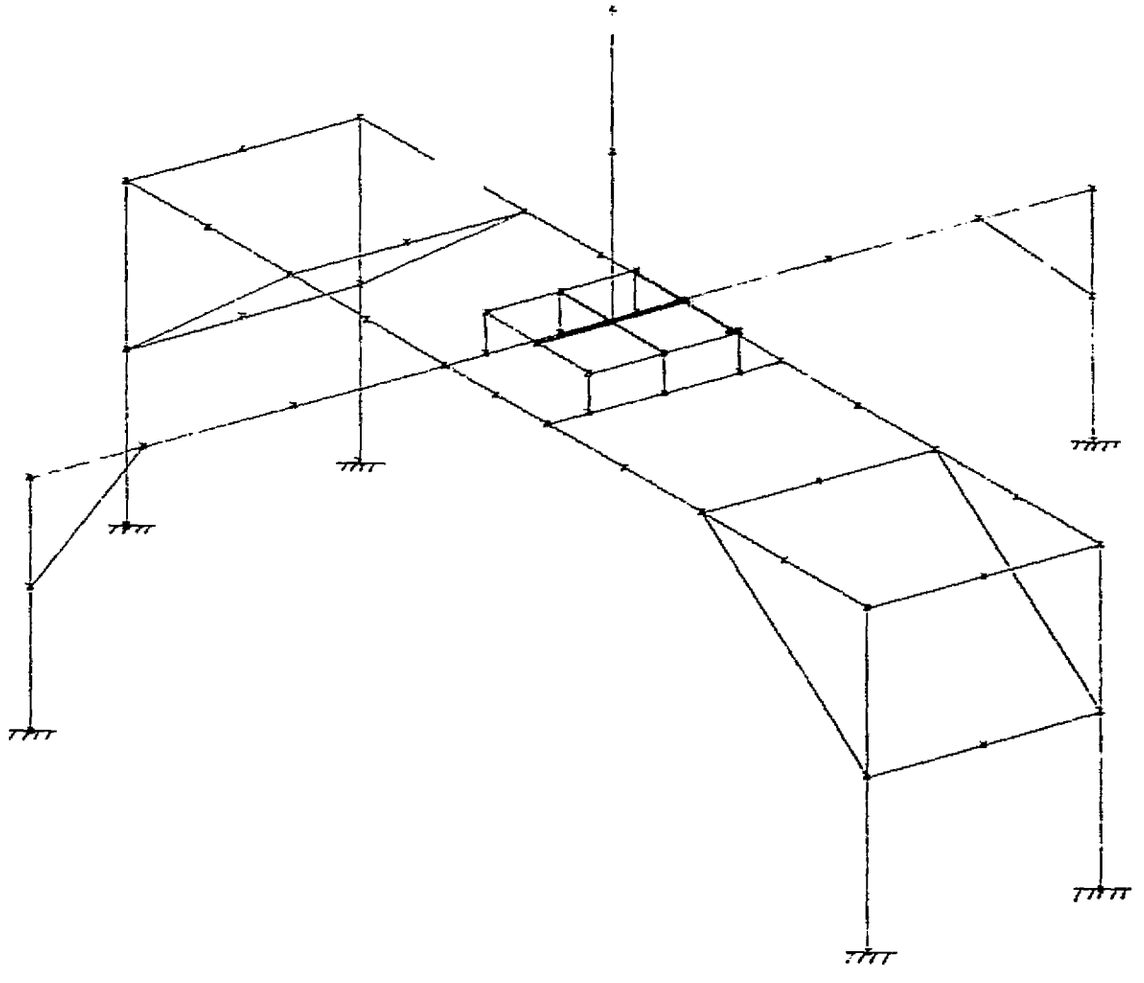

FIGURE 28: MODEL OF A TYPICAL AGITATOR SUPPORT SYSTEM

THIS PAGE INTENTIONALLY LEFT BLANK.

D5

N78-32471

USE OF NASTRAN IN A UNIVERSITY ENVIRONMENT

Chuh Mei
University of Missouri - Rolla

SUMMARY

The heavy use of NASTRAN here and abroad has demonstrated its value as a resource for structural and heat transfer analyses. This paper brings another view of NASTRAN as an educational and research tool in a university. A survey was conducted in the middle of the 1977-78 school year. Each faculty member of the civil engineering, engineering mechanics, and mechanical and aerospace engineering departments was asked to give information on the present (Level 15.5) and future projected (Level 17) usage of NASTRAN program. Results from the survey study are summarized in this paper.

WIDE ACCEPTANCE FROM INDUSTRIES

The NASTRAN systems management office surveyed the user group in May 1974. At that time 2300 users and 5200 CPU hours per month computer time on various NASTRAN activities were reported (ref. 1). These numbers are probably conservative, since not all users responded and not all users got the questionnaire. Besides, many small engineering companies run their NASTRAN jobs through the CDC/CYBERNET or Sperry UNIVAC systems. They find that it is more economical and also more convenient. Wide acceptance of the program from the industry has been observed, and the user community is steadily growing.

IN AN EDUCATIONAL INSTITUTE

One interesting result from the 1974 survey was the large number of non-aerospace users. They account for more than 75 percent of the total computer use. This specific non-aerospace group consists of computer and engineering consulting companies, automobile and manufacturing industries, universities, etc. However, very little information on NASTRAN use was reported from academic institutions. Wilkinson discussed his experiences with incorporation NASTRAN as a teaching tool in undergraduate courses at Louisiana Tech University (ref. 2). He found that most students tend to be overwhelmed by the magnitude and bulk of the NASTRAN user's manual. He proposed that a "Mini-Manual" be made available which describes the essential steps for setting up a NASTRAN job. This has been accomplished by the release of a "Condensed Form of NASTRAN" (ref. 3). It is specifically designed for university instructions and short courses. A more general view of NASTRAN in several of the university's educational and research programs at Rolla campus is presented in this paper.

THE SURVEY

A survey was conducted in several departments of the school of engineering at the end of Fall semester 1977. A questionnaire was sent to each faculty member of the civil engineering, engineering mechanics, and mechanical and aerospace engineering departments. The purpose was to gather information on the usage of NASTRAN programs (Level 15.5) in the school of engineering so that a conclusion could be reached on whether or not to recommend to the office of computing activities the leasing of Level 17 NASTRAN. Responses were obtained from 27 faculty members. The questions being asked were:

1) Courses presently using NASTRAN.

2) Number of graduate students using the program in their theses.

3) Research projects using NASTRAN.

4) Will use Level 17 in courses and/or research work.

The results are presented in the following section.

FINDINGS

NASTRAN program has been incorporated in twelve undergraduate and graduate courses as a supplemental teaching tool. Those courses are:

AE	253	Aerospace Structures
AE	351	Intermediate Aerospace Structures
CE	425	Finite Element Application in Structural Design
CE	428	Matrix Methods of Structural Analysis
EMe	300	Vibration Experiments
EMe	361	Theory of Vibrations
EMe	401	Advanced Topics in Engineering Mechanics
EMe	405	Numerical Methods of Mechanics
EMe	431	Theory of Plates
EMe	432	Theory of Shells
MeAE	300	Special Problems
MeAE	407	Advanced Mechanical Vibrations

Course numbers 399 and below are basically designated for undergraduates, and, 400 and above for graduate courses. Instructors have learned from experience that students with very little computerized structures background are able to readily grasp the program's logic and begin solving realistic problems. This is due to the fact that the program is user oriented with easy input and extensive error checks. Faculty members also indicated interest in using

NASTRAN in thirteen other courses.

The program is also being used as a research tool for graduate students on their thesis work, and for faculty members on various research projects. Thirteen M.S. and Ph.D. theses have used NASTRAN for some part of their analysis. The research problems covered a broad range of engineering areas. Following are examples of research topics:

Interactive Graphics

Analysis of Power Plant Piping Systems

Nonlinear Analysis of Reinforced Concrete Beams

Vibrations of an Airplane Wing

Stress Concentration Factors in Gears

Fracture Analysis of Rocks

Buckling of Cold-Rolled Steel Thin-Wall Structures

Research grants utilizing NASTRAN computations, totaling in excess of $250 K, are currently pending. Faculty members were unanimously in favor of the acquisition of Level 17 NASTRAN instead of the "Condensed Version". Considering the extensive use of NASTRAN by both faculty and students, the choice is obvious. Also, those students with experience using finite element methods and NASTRAN are enjoying a high level of interest from interviewers.

CONCLUDING REMARKS

NASTRAN program has a significant effect on several of the university's education and research programs. They have been described and can be summed up with the following observations:

1. Supplemental teaching tool in many mechanics and structural courses.

2. Graduate students use NASTRAN in their theses.

3. Use in research contracts and projects involving NASTRAN computation.

4. Faculty in favor of Level 17 instead of the "Condensed Version".

5. Some experience with NASTRAN is a definite plus for students seeking employment.

REFERENCES

1. Weidman, Deene J.: NASTRAN Status and Plans. NASTRAN: Users' Experiences. NASA TM X-3278, 1975, pp. 1-10.

2. Wilkinson, Michael T.: Use of NASTRAN as a Teaching Aid. NASTRAN: Users' Experiences. NASA TM X-2637, 1972, pp. 415-419.

3. Rogers, James L. Jr.; Mei, Chuh; and Brown, W. Keith: A Condensed Form of NASTRAN. NASTRAN: Users' Experiences. NASA CP-2018, 1977, pp. 299-303.

D6

N78-32472

NASTRAN
FINITE ELEMENT ANALYSIS ACTIVITY AT NORTHROP

Sveinn Thordarson
Northrop Corporation

SUMMARY

This paper briefly summarizes the NASTRAN-related internal loads support activity at the Aircraft Group of the Northrop Corporation. Finite Element Analysis, in the present form, started at the Aircraft Group in the late sixties. NASTRAN was selected as the primary finite element tool for static analysis in 1972. Extensive pre- and postprocessing programs have been brought on-line since then to facilitate handling of the massive input and output data for the program.

In-house evaluation of the various analytical capabilities of the MSC version of NASTRAN, prior to production release, is a continuous effort. The NASTRAN superelement and subsonic aero features are presently being tested and brought on-line for production use.

Two examples of recent NASTRAN structural solutions are also presented in this paper.

INTRODUCTION

Finite Element Analysis in the structural analyses groups at Northrop started in the late nineteen sixties with the in-house developed NORAN Program. This program, although offering a good element library and relatively fast solution time, suffered from a lack of user-oriented features. Consequently, a changeover to Level 15 of COSMIC NASTRAN was made in 1972.

The MacNeal-Schwendler Corporation (MSC) version of NASTRAN was adopted as the standard finite element program of the Aircraft Division in 1974. It has yielded significant improvements in accuracy, user-oriented features, increased capability for larger more complex solutions, and reduced modeling and running times.

The responsibility for NASTRAN within the Aircraft Group resides in the Advanced Structural Computer Methods group (ASCM). The core of the effort involves the NASTRAN Utilization Improvement effort initiated in 1975 to provide interactive graphics programs in support of production analyses.

The ASCM group, in addition, provides program assistance, in-house training and documentation for the NASTRAN users at Northrop. Key members of the Group also reside in the major stress groups to ensure timely interaction between the NASTRAN production and development effort.

COMPUTER GRAPHICS

Northrop embarked on an extensive pre- and postprocessor interactive graphics development in 1975 in support of the NASTRAN analyses. This task is being performed in three phases.

Phase I - Geometry

A series of programs was written to define the geometry of major airplane structural components using parametric cubics (P.C.'s), splines and Coon's patches (fig. 1). These components are then cut at the required stations and the contours interfaced with programs in Phase II and Phase III. Digitizing programs were also developed which allow grid points to be directly digitized from blueprints and curve-fitted into loft lines (fig. 2).

Phase II - Preprocessors

The loft lines, P.C. cross-section cuts or GRID points are passed into the GEN3D program in Phase II for NASTRAN grid and element generation. This program is flexible enough to give the user complete control of very complex models and to take advantage of repeated sets of geometry patterns. The models thus generated may then be plotted on a Tektronix 4014 using such features as ZOOM, LABEL (element and grids), 3D rotation MOVE, SLICE, THICKNESS and AREA of elements for verification (fig. 3 and 4). A limited capability for generating property cards for the elements is also available. An added feature is the ability to use the 3D P.C. geometry from Phase I to calculate the area and volume of a fuel tank and also automatically generate pressure load cards for various fuel heads and acceleration vectors (fig. 5).

Phase III - Postprocessors

The analytical results from NASTRAN are stored for postprocessing. Stresses and strains can be recovered at any arbitrary angle, running loads computed, and a min-max search performed. Selected results are then printed in report format. The postprocessed data can also be plotted, superimposed on the structural plots, by the POSTPLOT Program. These plots can be displayed in either vector or alphanumeric form (fig. 6).

NASTRAN TESTING

All major analysis features of NASTRAN are tested by the ASCM group prior to their introduction into the analysis process.

Extensive evaluation of the MSC NASTRAN Superelement Analysis features has been concluded recently. This evaluation, in preparation for new major inter-

nal loads analysis work, shows substantial savings in computer costs and reduced turnaround time for analysis of large structures.

The evaluation of subsonic aeroelastic analyses using NASTRAN was initiated in 1978. Results to date indicate a very good correlation with previous flutter analyses conducted using in-house programs. Again, significant time savings are indicated, both within NASTRAN and from using structural models common to the static analyses.

PRODUCTION SUPPORT ACTIVITY

The Advanced Structural Computer Methods group serves as a pool of specialized NASTRAN talent in support of the production effort, in addition to the development work. Key Group engineers are also assigned to the major production programs, where they are responsible for the NASTRAN model development and internal loads generation in support of stress analyses.

FUTURE DEVELOPMENT EFFORT

In conjunction with other groups at Northrop, the ASCM group is studying a data base system which will provide a basis for an integrated computerized structural analysis system. A greatly enhanced geometry handling capability is evolving around parametric cubics. Other finite element methods in and outside of NASTRAN are also being reviewed. These include nonlinear approaches, optimization through fully-stressed design, and aeroelastic/flutter analysis.

NASTRAN ANALYSIS EXAMPLES

T-38 Local Model

A detailed (fine mesh) model of a T-38 wing lower skin was incorporated into a three substructure wing model in the vicinity of the root rib, rear spar intersection. This detail was generated to obtain very accurate stress levels and gradients for fracture and fatigue analyses (fig. 7 and 8).

Flutter Analysis

Flutter analysis using a vertical stabilizer supported by a general element was conducted using the NASTRAN Subsonic Aeroelastic package. The results compare well with the previous flutter analyses using in-house programs. The single submittal NASTRAN process provided significant improvements in calendar time and computer CPU time (fig. 9).

CONCLUSIONS

The dedicated NASTRAN support at Northrop has effectively moved the structural analysis groups along the NASTRAN learning curve. Significant reductions in internal loads analysis time have been demonstrated as the result of the pre- and postprocessor development and NASTRAN user support (fig. 10).

The increasingly tighter development schedules for new aircraft projects dictate still faster and more efficient analysis processes in the future. Greater details in modeling and new analysis techniques yielding more accurate solutions are also required to satisfy future design criteria in the field of static, fracture, and dynamic analyses.

ADVANCED STRUCTURAL COMPUTER METHODS

NASTRAN SUPPORT ACTIVITY

SYSTEM SUPPORT BY NORTHROP DATA PROCESSING

NASTRAN UTILIZATION IMPROVEMENT GROUP

- o PROVIDES EFFECTIVE NASTRAN PRODUCTION SUPPORT
- o IS RESPONSIBLE FOR PRODUCTION MODELS
- o PROVIDES INTERACTIVE GRAPHICS SUPPORT
  - PRE PROCESSORS
  - POST PROCESSORS
- o TESTS AND EVALUATES NASTRAN FEATURES
- o GENERATES NASTRAN IN-HOUSE DOCUMENTATION
- o PROVIDES NASTRAN IN-HOUSE TRAINING
- o PROVIDES NASTRAN ASSISTANCE TO PRODUCTION STRESS GROUP ON COMPLEX NASTRAN SOLUTIONS
- o PLANS FOR INTEGRATED STRUCTURAL ANALYSIS

ADVANCED STRUCTURAL COMPUTER METHODS

NORTHROP CORPORATION

AIRCRAFT GROUP

FINITE ELEMENT ANALYSIS ACTIVITY

HISTORY

- PRE FINITE ELEMENT PROGRAMS
- 1969 - NORAN IN-HOUSE FINITE ELEMENT PROGRAM
- 1972 - NASTRAN COSMIC LEVEL 15
- 1973 - NASTRAN COSMIC LEVEL 15.5
- 1974 - MSC NASTRAN
- 1978 - MSC NASTRAN 38 TO 46
- UP TO 1000 JOB SUBMITTALS PER MONTH

WHY MSC NASTRAN?

- CPU TIME IMPROVEMENT
- IMPROVED FEATURES
- FREQUENT UPDATES
- PROXIMITY OF MSC

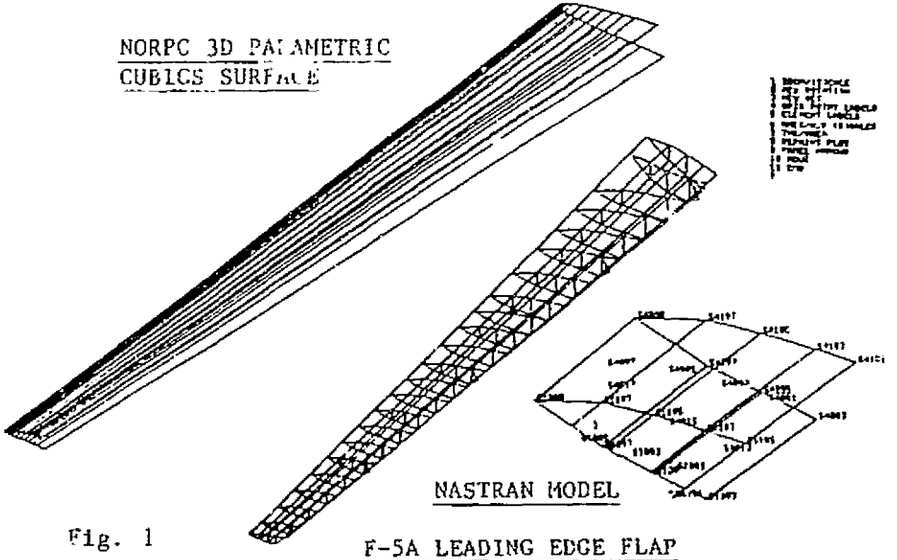

Fig. 1

F-5A LEADING EDGE FLAP

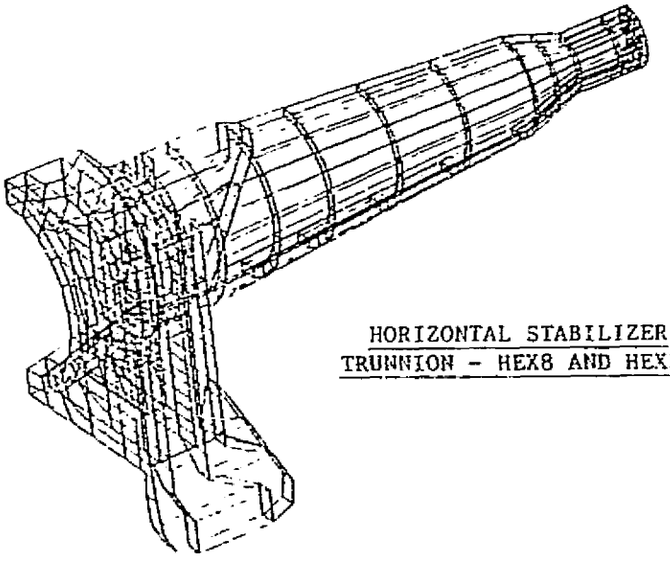

HORIZONTAL STABILIZER
TRUNNION - HEX8 AND HEX20

YF-17

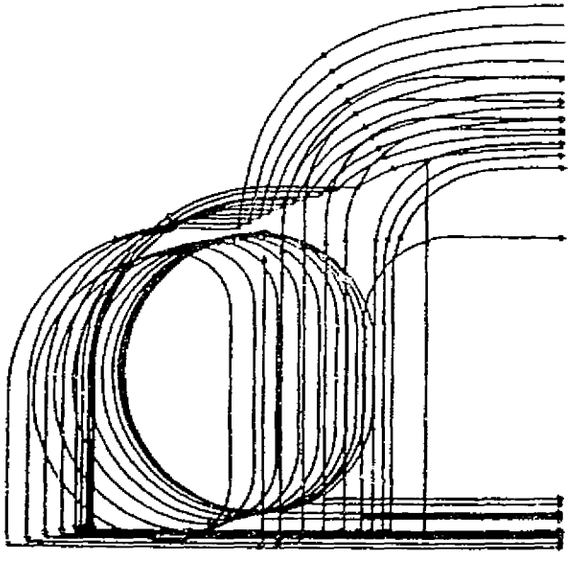

LOFTLINES FROM TABLOFT

Fig. 2

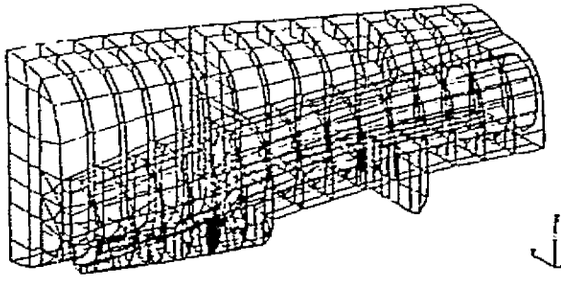

T-38 CENTER FUSELAGE

Fig. 3

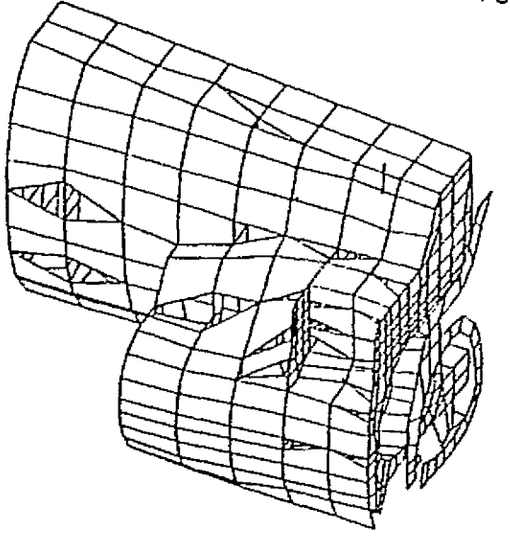

HIDDEN LINES

Fig. 4

MODEL GENERATION

PARAMETRIC CUBICS (P.C.) LOADS APPLICATIONS

FUEL TANK LOADS

EXAMPLE: F-18 FUEL TANK

- o VERY COMPLEX NASTRAN MODEL INPUT
- o EXTERNALLY SURFACED BY P.C.'s
- o APPLIED LOAD FACTOR IN ANY DIRECTION
- o DETERMINES FREE FUEL SURFACE
- o COMPLETE NASTRAN LOAD CARDS OUTPUT

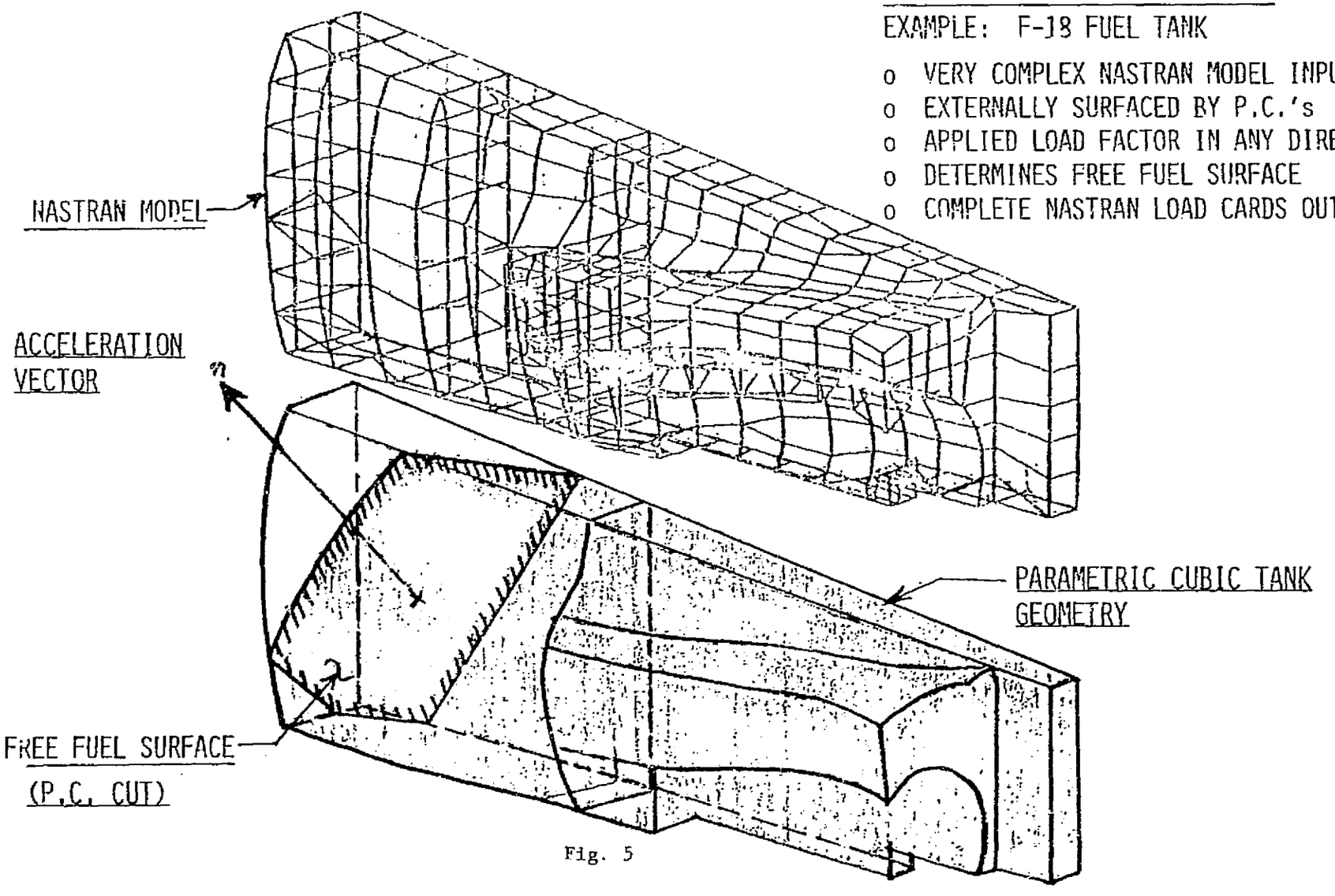

Fig. 5

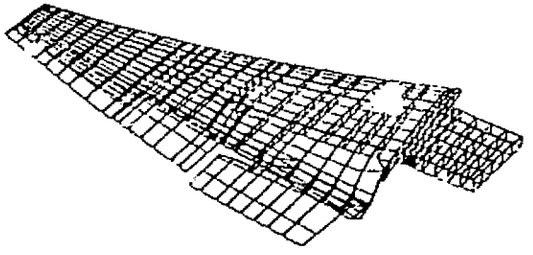

DEFORMED PLOTS

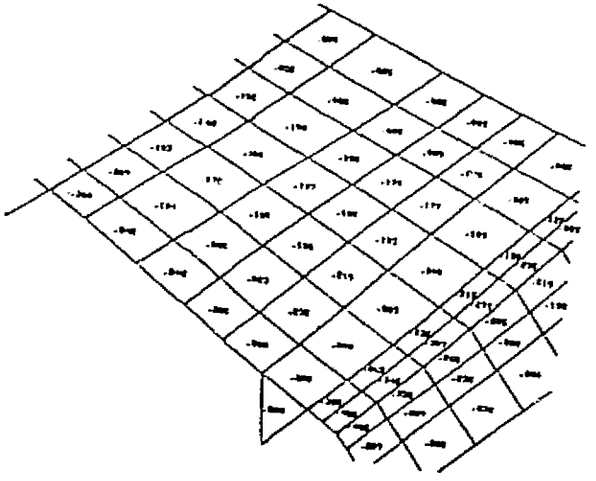

PROPERTY DISPLAY

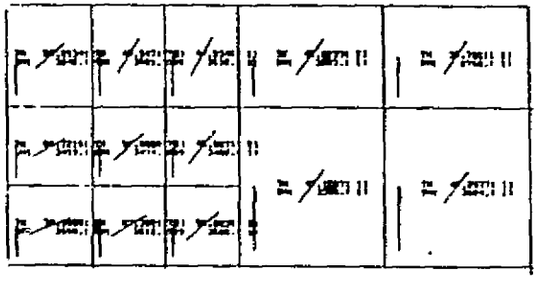

STRESS/STRAIN PLOTS WITH VECTORS

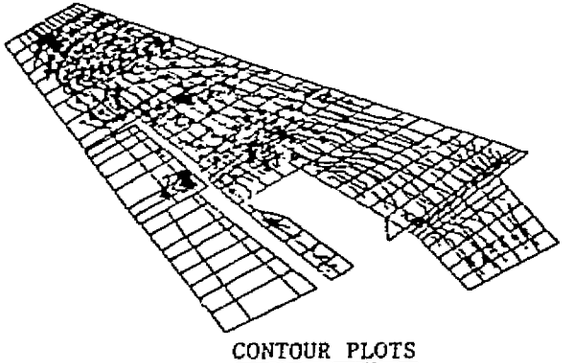

CONTOUR PLOTS

ORIGINAL PAGE IS
OF POOR QUALITY

NASTRAN DATA VISIBILITY

Fig. 6

T-38 WING SUBSTRUCTURE ANALYSIS

Model Generation

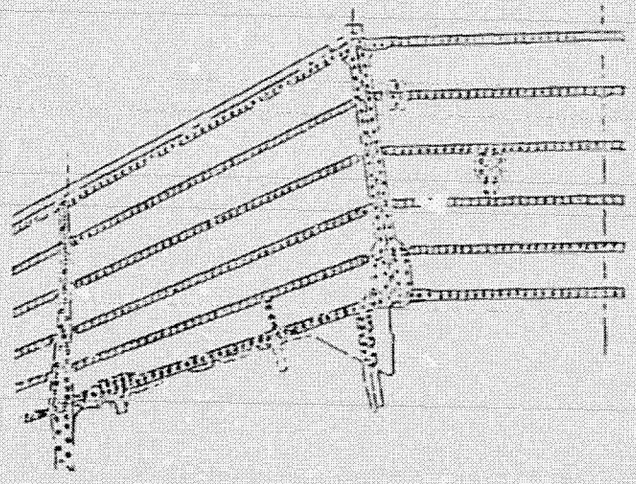

WING LOWER SKIN

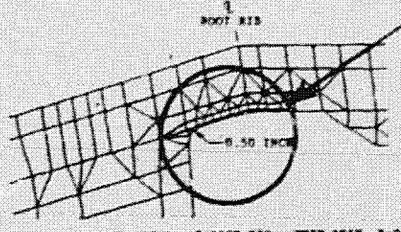

MODEL DETAIL AT ROOT RIB - THIN SKIN, R=0.50 INCH

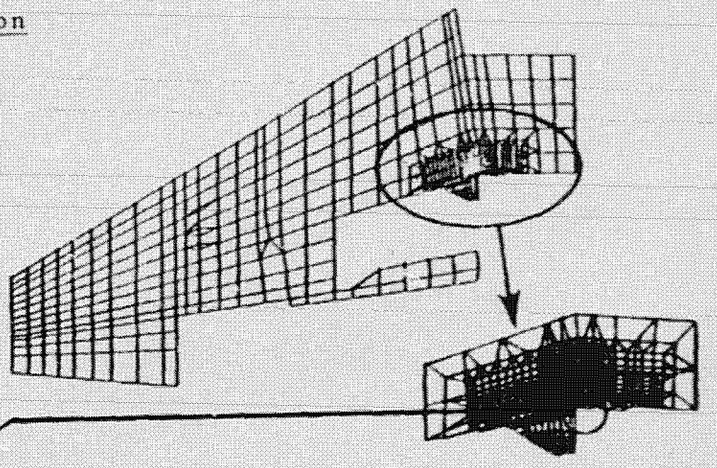

LOWER SKIN WITH FINE MESH LOCAL AREA

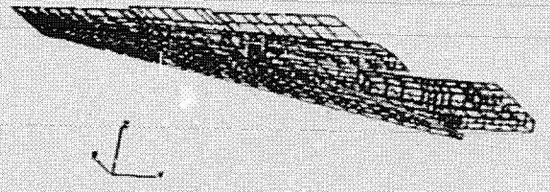

WING SUBSTRUCTURE

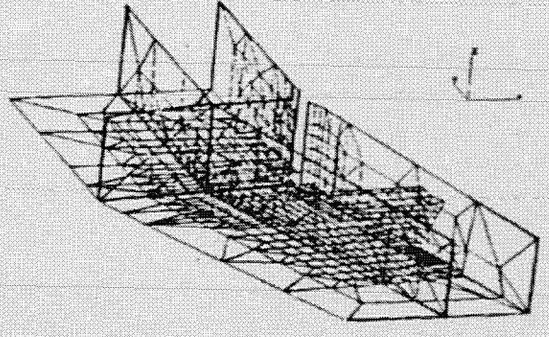

LOCAL MODEL SUBSTRUCTURE

Fig. 7

T-38 WING SUBSTRUCTURE ANALYSIS

NASTRAN STRESSES AND MODEL VALIDATION

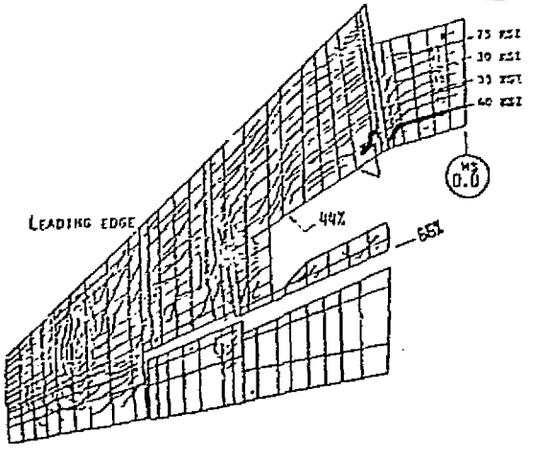

CONTOUR PLOT - GROSS WING MODEL
LOWER SKIN

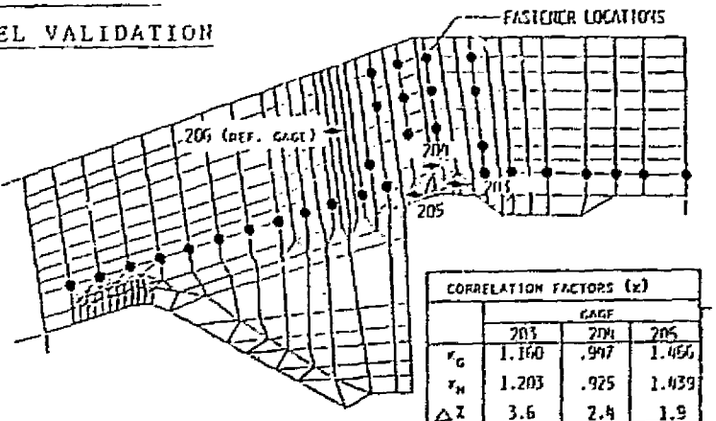

CORRELATION FACTORS (x)			
	GAGE		
	203	204	205
F_G	1.160	.997	1.466
F_H	1.203	.925	1.439
ΔZ	3.6	2.4	1.9

$F_G = \frac{\epsilon_{GAGE}}{\epsilon_{GAGE\ 205}}$

$F_H = \frac{\epsilon_H}{\epsilon_{N\ PANEL\ 221008}}$

LOCAL MODEL VALIDATION
STRESS GRADIENTS

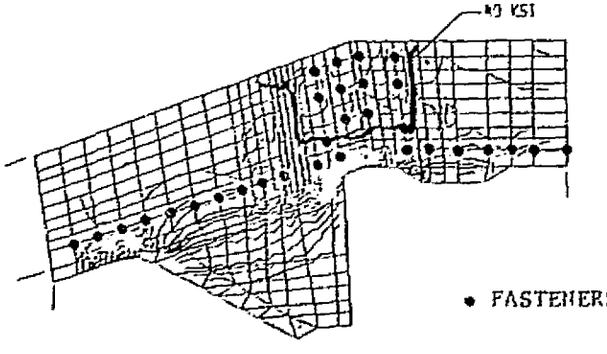

CONTOUR PLOT - LOCAL MODEL

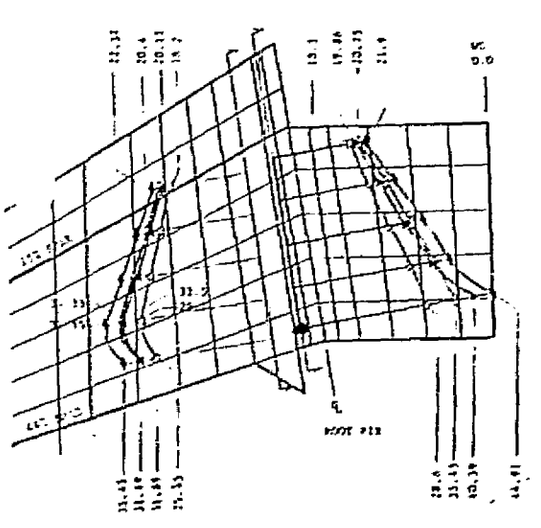

GROSS MODEL CHORDWISE STRESS DISTIRBUTION
Fig. 8

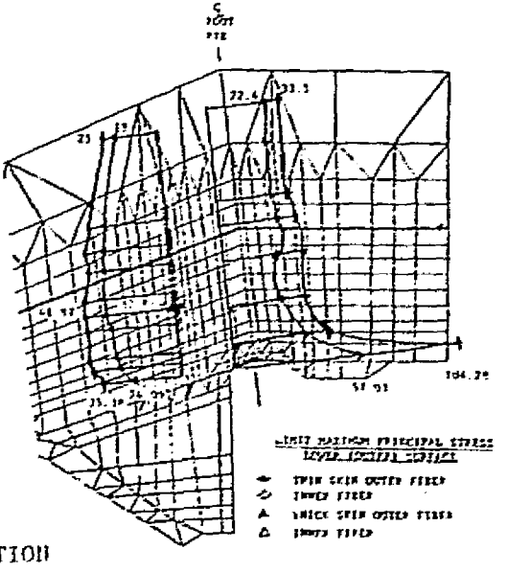

LOCAL MODEL STRESS DISTRIBUTION

NASTRAN FLUTTER ANALYSIS

VERTICAL STABILIZER & RUDDER

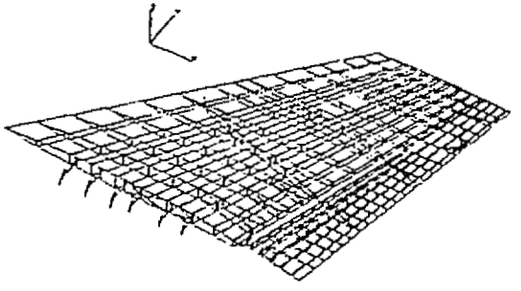

NASTRAN STRUCTURAL MODEL

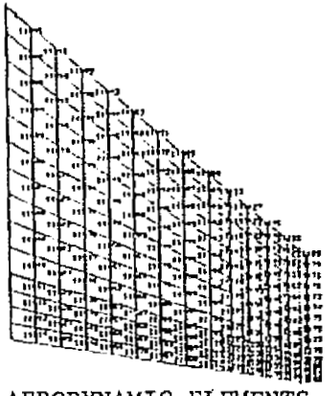

AERODYNAMIC ELEMENTS

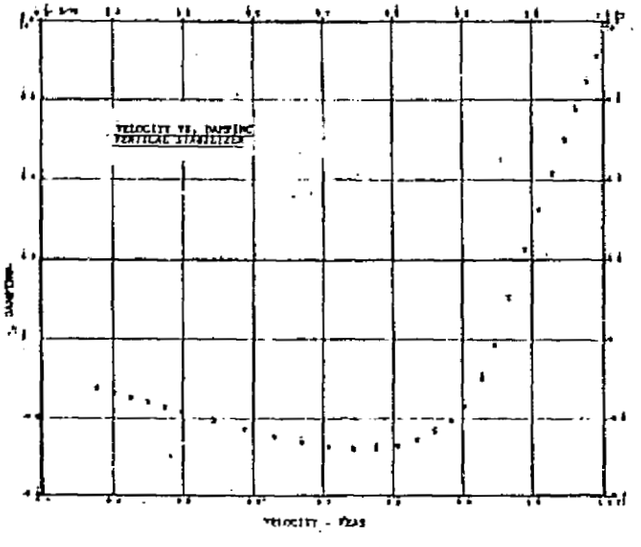

V-g PLOT

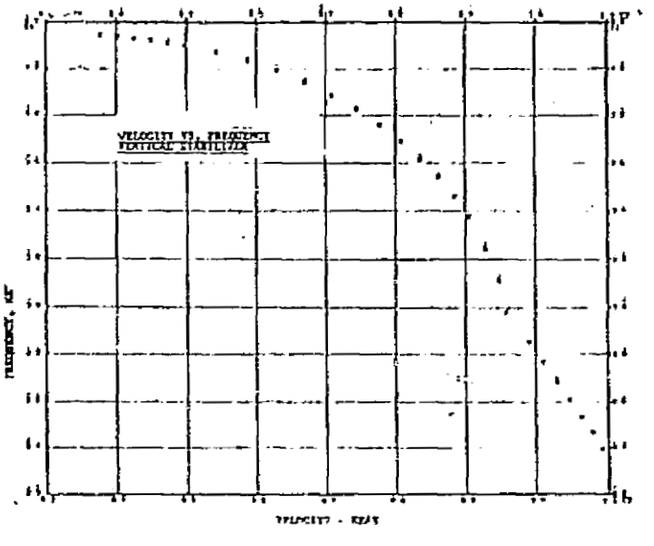

FREQUENCY PLOT

Fig. 9

NASTRAN EFFICIENCY IMPROVEMENTS

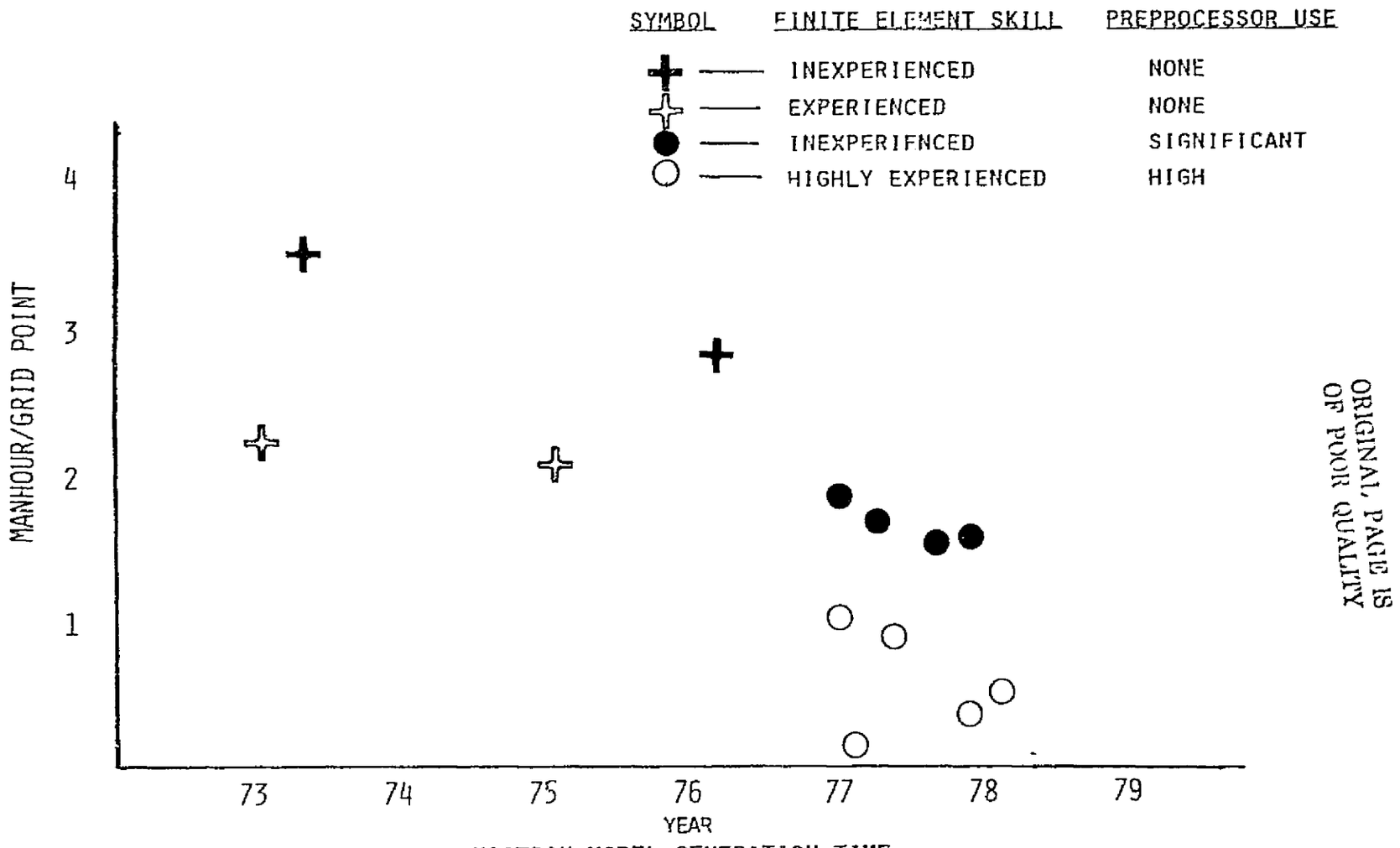

NASTRAN MODEL GENERATION TIME

Fig. 10

D7

N78-32473

DEVELOPMENT OF STRUCTURAL DYNAMIC TEST ENVIRONMENTS FOR SUBSYSTEMS AND COMPONENTS

Robert J. Coladonato
Goddard Space Flight Center

SUMMARY

Structural dynamic environmental test levels were developed for the Thematic Mapper instrument, components of the Tandberg-Hanssen instrument, and components of the International Ultraviolet Explorer (IUE) spacecraft using NASTRAN structural models and test data. Both static and dynamic NASTRAN analyses were used. The model size required could be as small as 300 degrees of freedom for the static analysis and as large as 1000 degrees of freedom or more for the high frequency dynamic analysis. An important step in the development of the levels is model verification by test. The launch environments that generally dictate many important features of the design of an instrument or component are steady state acceleration, sinusoidal vibration, and random vibration. These are the environments that the analyst should examine closely when determining the appropriate test levels.

INTRODUCTION

Instruments and components that are designed for aerospace applications must function satisfactorily after being exposed to the launch environment. In order to gain a high level of confidence that the instrument will function satisfactorily after launch, the instrument is subjected to testing which attempts to simulate the conditions produced by the launch. The principal types of structural/dynamic testing used are sinusoidal vibration, random vibration, acoustic noise, shock, and steady state acceleration. These environments are normally defined or specified at the spacecraft level and the environmental test levels for the instrument typically have to be determined through test and/or analysis. These levels are influenced by the dynamic characteristics of the spacecraft. Once the test levels for the instrument are established, one

can proceed one more step and generate the test levels for components mounted within the instrument. The test levels for the components are then a function of the dynamic characteristics of the instrument. Figure 1 provides a typical environmental test and analysis plan.

The test levels for the instrument or components can be determined by performing the appropriate analysis using NASTRAN structural models. Alternately, test levels can also be established from actual test data obtained during spacecraft system testing of the hardware. However, in most cases, testing of the spacecraft hardware does not occur until sometime after the design levels have been established for the instrument or component. When test data are available, however, they are used to evaluate the test levels that have been previously determined through analysis and these levels are updated or modified as deemed necessary. The test data should also be used to examine the veracity of the NASTRAN model. An attempt should always be made to achieve good correlation between model predictions and actual test data.

NASTRAN MODELS

Model Size

The size of the NASTRAN model that is required in terms of degrees of freedom is dependent upon the type of analysis that one is performing. The analysis can be divided into two general types, static analysis and dynamic analysis. Static analysis is used to simulate the steady state acceleration condition while dynamic analysis is used to simulate sinusoidal vibration, random vibration, acoustic noise and shock. For static analysis a NASTRAN model size of between 300 and 500 degrees of freedom is normally adequate for determining critical loads for most instruments. However, if one wishes to determine stresses in sensitive areas of the instrument, a more detailed model may be required. The problem with a detailed model is that it takes a long time to generate and then it takes a long time to run on the computer. A preferred technique for static analysis is to determine the critical loads from the smaller 300 to 500 degree of freedom model and then perform a detailed hand calculated stress analysis of the parts that are most sensitive.

For dynamic analysis the size of the model required depends upon the particular environment that is being simulated. Sinusoidal vibration test specifications cover frequencies up to 200 Hertz (Hz), and a model of between 300 and 500 degrees of freedom for an instrument is usually adequate. Random vibration specifications contain frequencies up to 2000 Hz and shock contains frequencies up to 4000 Hz. For these environments, a much more detailed model is necessary, possibly 2000 to 3000 degrees of freedom or more. The larger detail is necessary to provide confidence that the high frequency modes are realistically represented.

Acoustic noise contains frequencies up to 10,000 Hz and would require an extremely detailed model for accurate predictions. Acoustic noise is also a very complex environment to represent analytically and this type analysis is rarely performed. Part of the reason for not doing acoustic noise analysis is that historically it has been observed that it does not produce significant structural loads except on thin filmed windows or items that have large areas and low masses such as solar arrays. For these items an acoustic test is recommended. The foregoing discussion demonstrates that before the analyst generates a NASTRAN model, he should determine what the use of the model is really going to be and then decide upon an appropriate size. Perhaps it may be advantageous or even necessary to produce models of different sizes.

Model Verification by Test

The predictions from the model should be checked against actual test data as early in a program as possible. One needs to run an analysis using the model which represents the test configuration of the hardware. The test does not have to be a very severe high level test. Preferrably, it should be a low level test. A static load test where loads are applied at particular points on the instrument and deflections are measured can be used for model verification. To verify the dynamic characteristics of the model, a low level sinusoidal sweep can be done on the instrument with response data recorded on magnetic tape. The data can then be analyzed by plotting acceleration levels versus frequency and comparing these to predictions from the model. Also, coincident and quadrature plots versus frequency can be made to determine mode shapes and modal damping. Another test that can be used for dynamic verification is the modal survey test. In this test the instrument is excited by a low level input, generally random vibration. There are several automated modal survey test

packages which store data from the test and then compute the mode frequency, mode shape, and modal damping automatically as well as display the mode shape on a screen.

Regardless of the testing technique used to verify the model, the knowledge that the model agrees well with test data is very reassuring. Once good correlation is obtained between model predictions and test data, the model can be used with confidence to evaluate the effect of design changes or to predict responses to various types of inputs. With the advent of the Space Shuttle the trend seems to be a deemphasis on qualification type structural testing with more reliance placed on predictions by analysis. However, this trend should not be interpreted to mean that no testing need be done. Testing to provide assurance of model veracity is still very important.

NASTRAN ANALYSIS METHODS

Steady State Acceleration

The steady state acceleration levels are defined in terms of gravitational acceleration units (g's) for the thrust and lateral directions. For example, 16.8 g's thrust and 3.0 g's lateral are typical for a Delta launched payload. The static analysis, Rigid Format 1, is used for steady state acceleration analysis. The most flexible way to run the analysis is to apply a 1.0 g load in each of the three orthogonal axes and then use subcase combinations (SUBCOM) to obtain the desired combination of loads.

Sinusoidal Vibration

The sinusoidal vibration analysis is normally performed using frequency response analysis. Either the direct formulation, Rigid Format 8, or the modal formulation, Rigid Format 11, can be used. The modal formulation is preferred because an eigenvalue analysis can first be performed and the modes saved on tape. This information, after checking, is used in a restart for the frequency response analysis.

The sinusoidal vibration test levels are defined as g's versus frequency and the frequency range is usually 5 Hz to 200

Hz. To run the analysis one can input the sinusoidal levels as defined in the specification and observe the response levels at points of interest. However, a more informative method is to input a constant unit acceleration and observe the response at the points of interest because using a constant input draws a much cleaner picture of the response characteristics.

The magnitude of the responses depends upon the value that is chosen for structural damping and hence modal amplification (Q) since modal Q equals the reciprocal of structural damping. Previous testing of instruments and components has shown that a modal Q of 15 is generally a conservative assumption for analysis. Assuming modal Q's greater than 15 quite frequently results in very high response levels and consequently unnecessary design changes. As a general rule of thumb, response levels greater than 20 g's would not be expected due to the dynamics of the launch environment. Therefore, unless there is substantiating evidence available, one should not assume Q's too high in the analysis.

Another variable in the frequency response analysis is the frequency at which response calculations are made. The frequency can be defined by a tabular listing of discrete frequencies, a linear spacing where a frequency increment is chosen, or a logarithmic spacing where the number of logarithmic intervals between the first and last frequency is chosen. It is important for one to pick the proper frequencies for the response calculations so as not to miss any peaks that occur. Using the modal formulation one can accomplish this by first doing an eigenvalue analysis, restarting, and then including all of the modal frequencies, as well as frequencies on either side, in a tabular listing of frequencies to be used for the response calculations. For the case of linear or logarithmic spacing the required frequency increment or the number of logarithmic intervals can be determined analytically. For example, assuming a Q of 15, in order to be sure that the calculated response is at least 90% of the peak response a frequency increment of 0.032 times the lowest frequency of interest is required and 114 logarithmic intervals are required for analysis between 5 Hz and 200 Hz (see Appendix).

Random Vibration

Random Vibration analysis is performed using Rigid Formats 8 or 11 as an extension of the frequency response analysis. One must run the frequency response analysis to get the random

response analysis. The only additional requirement is the inclusion of the power spectral density (g^2/Hz) loading description, the TABRNDl card, which defines g^2/Hz versus frequency.

Shock

Shock analysis can be performed in NASTRAN but the uncertainty of the definition of the input makes the results questionable. The shock level is described as a shock response spectrum which is a shock response level (response g's) as a function of frequency. In order to perform a shock analysis, this shock response spectrum must be converted to a transient pulse. The problem is that a given shock response spectrum does not correspond to a unique transient input pulse. There could be several different types of transients that give the same shock response spectrum. If one does convert the shock response spectrum to a transient pulse, either the direct transient response, Rigid Format 9, or the modal transient response, Rigid Format 12, can be used for the analysis.

The transmission of a shock pulse through a structure is susceptible to the number of joints and the fixity of these joints in the path of the pulse. This characteristic is difficult to model. Therefore, caution should be used when interpreting the results of a shock analysis.

TEST LEVEL DEVELOPMENT

The paths for test level development for instruments or components can proceed in several different directions. Three examples will be given. The first is a review of methods employed for the development of levels for the components on the presently orbiting International Ultraviolet Explorer (IUE) spacecraft. The second is a description of the development of the test levels for components of the Tandberg-Hanssen instrument. This is an instrument that will be flown on the Solar Maximum Mission (SMM) spacecraft during 1979. The third is the development of test levels for the Thematic Mapper instrument. This instrument will be part of the LANDSAT-D mission and is scheduled for launch in 1981. The three situations are different as will be explained.

IUE Components

The system test levels for the IUE spacecraft (reference 1) were defined and known. Based on this information, test levels for the components were developed for sinusoidal vibration, random vibration, acoustic noise, shock, and steady state acceleration (reference 2). Since the input to the spacecraft was known, the problem became one of determining the response of the spacecraft at various locations which would describe the environment seen by a component mounted at that location. A graphical representation of the IUE spacecraft is shown in figure 2 and the NASTRAN models are shown in figures 3 and 4. For steady state acceleration and acoustic noise the levels for the components are the same as the levels for the spacecraft. For the other environments the levels for the components are dependent upon the dynamic response of the spacecraft.

The IUE Project was fortunate in that a structural model of the spacecraft was available very early in the program for testing. Consequently, the component test levels for sinusoidal vibration, random vibration, and shock were derived directly from test data. However, before the testing started, frequency response runs were made with the NASTRAN model to provide predictions of the responses at particular locations. These predictions agreed well with the test data. Although the NASTRAN model of the IUE spacecraft was not used to develop component test levels, it was used extensively in performing coupled launch vehicle/spacecraft launch loads analyses and also to predict occurrences during the sinusoidal vibration test of the spacecraft.

The technique for developing the sinusoidal vibration test levels for instruments or components is fairly straightforward. The method is to envelop the peak responses into a smooth spectrum as shown in figure 5. The same applies for shock response spectrum test levels as shown in figure 6.

The random vibration test levels were also developed from test data. However, one should not use the method of enveloping the peak responses because this results in a subsystem test specification that is much more severe than it should be. For the IUE components, the test data were divided into appropriate groups and a statistical analysis (reference 3) was performed to establish the random vibration specification for each group. More refined methods (reference 4 and reference 5) also consider the damaging effects of the environment when developing the subsystem test levels.

Tandberg-Hanssen Components

The test levels for the Tandberg-Hanssen instrument were established (reference 6) and two NASTRAN models of the instrument were generated. One was a small simple 400 degree of freedom beam model and the other was a very detailed 4000 degree of freedom model. The small model is shown in figure 7 and the large model in figure 8. The main purpose of the small model was to provide the SMM Project with an adequate dynamic representation of the instrument to be used in the coupled launch vehicle/spacecraft launch loads analysis. The large model was used to develop sinusoidal and random vibration test levels for selected components and also to examine critical loads for both the static and dynamic environments.

The sinusoidal vibration levels for one component, the polarimeter, were developed by first using the NASTRAN modal frequency response analysis. The model was excited in each axis according to the input levels described for the instrument (reference 6) and response plots were made at a point corresponding to the mounting location of the polarimeter. The response plots representing the thrust direction were examined as well as the response plots representing the lateral directions. The peaks of the responses were enveloped to develop a corresponding thrust axis specification and a corresponding lateral axis specification.

A critical component in the instrument is the circular flex pivot. The secondary mirror/two axis gimbal assembly is supported by four of these pivots and the pivots are particularly susceptible to failure due to random vibration. Even the large model did not have the flex pivot - secondary mirror/two axis gimbal assembly modelled. Therefore, the plan was to run a random response analysis using the large model and pick a response point that would represent the input to the secondary mirror/two axis gimbal assembly. Then, using the calculated response, a random vibration specification would be generated for the secondary mirror and gimbal assembly. The analysis was run, the responses were plotted, and the random vibration specification was determined using the methods previously cited (reference 4).

Development of a random vibration specification, whether it be from test data or from analytical predictions, is a subjective procedure. The more refined methods (reference 4 and reference 5) are a step in the direction of removing some of the subjectiveness. However, even these methods are not universally accepted. Without going through the refined techniques, a suggested method is to manually smooth out the response so that

the reuslting specification has an overall level that is no more than approximately two times the overall level of the response. An example of this technique is shown in figure 9.

Thematic Mapper

The Thematic Mapper is a large and complex earth viewing instrument that will be flown on the LANDSAT-D spacecraft. Because it represents an advanced long-lead time item, the instrument is being designed and built prior to the spacecraft. Consequently, the test and design levels for the instrument have had to be developed before the dynamic characteristics of the spacecraft become known. Also, the test levels have been made compatible with both the launch environment of the Delta launch vehicle and the launch and recovery environments of the Space Shuttle. The test levels developed for the Thematic Mapper are sinusoidal vibration, random vibration, shock, acoustic noise, and steady state acceleration.

The steady state acceleration levels used for the Thematic Mapper covered Delta launch (reference 1) and Shuttle launch, landing, and crash (reference 7 and reference 8). The acoustic noise specification was based on the worst case combination of the Delta and Shuttle environment. The predicted acoustic environment for the Shuttle below 200 Hz is significantly higher than the environments of any of the expendable launch vehicles. To cover this condition, a low frequency random vibration test was specified from 20 Hz to 200 Hz. The determination of the random vibration levels was based on a procedure outlined for Shuttle payloads (reference 8). This procedure requires knowledge of the mass distribution of the payload from which reaction loads are calculated. For the Thematic Mapper the payload is the LANDSAT-D spacecraft mounted in a cradle. Since this information was not known, some assumptions were made which would yield a worst case condition and the random vibration levels were derived from this condition. The shock levels were based on the recommendations for component vibration (reference 1).

The sinusoidal vibration levels were derived using a NASTRAN model of a "characterized" LANDSAT-D spacecraft. Since, as indicated, the LANDSAT-D spacecraft has yet to be designed, the NASTRAN model was based on conceptual design information. Also, stiffness parameters for the conceptualized spacecraft and the instrument support module were varied to try to bound the best and worst case conditions that could be expected from the final design. The NASTRAN model used in the analysis was a

simple beam and is shown in figure 10. The frequency range of the analysis was from 5 Hz to 100 Hz and the beam representation was considered satisfactory for the analysis.

Two types of analyses were performed using the beam model. One was a modal transient response of the combined spacecraft and Delta launch vehicle. This was used in the simulation of the lateral liftoff event. The output from this analysis was the acceleration levels at all the indicated points on the LANDSAT-D spacecraft model and also the bending moment at the Delta attach fitting/spacecraft interface. The bending moment was of interest because it is the load that is traditionally used as a limitng factor during lateral sinusoidal vibration tests of spacecraft.

Using the bending moment predicted from the lateral liftoff analysis as a limiting factor, a frequency response analysis was run which simulated the lateral sinusoidal vibration test of the spacecraaft. A modal Q of 15 was assumed and the predicted response at the mounting location of the Thematic Mapper was output. The responses indicated that the Thematic Mapper would be exposed to levels during the spacecraft lateral sinusoidal vibration test that would be higher than the levels predicted to occur due to the liftoff event. Therefore, in order not to overtest the instrument, it was decided to base the lateral sinusoidal levels on the responses predicted from the lateral liftoff analysis. This, in turn, will probably impose some restrictions during the lateral sinusoidal vibration test of the total spacecraft system to ensure that overtesting of the instrument does not occur.

For the Delta launch vehicle the maximum thrust axis dynamic response occurs as a result of POGO. POGO is a longitudinal oscillation resulting from closed-loop coupling of the engine system and the vehicle longitudinal mode and is the major thrust axis dynamic loading. A thrust axis frequency response analysis simulating the thrust axis vibration test of the spacecraft was run. The predicted response at the mounting location of the Thematic Mapper resulting from the POGO event was used as the maximum thrust axis sinusoidal vibration test level for the instrument.

As can be seen, sinusoidal vibration levels for the Thematic Mapper were derived from predicted responses due to launch events. This departs from the traditional approach which required instruments or components to survive not only the levels predicted for flight but also the levels that would occur during sinusoidal vibration testing of the spacecraft to which the instrument was mounted. This often times resulted in considerable overtesting and overdesign of instruments. The

approach used for developing the sinusoidal test levels for the Thematic Mapper does not contradict existing test philosophy but it does impose restrictions on spacecraft testing to ensure that instruments and components are not overtested.

CONCLUDING REMARKS

The three examples given demonstrate variations in the development of test levels for instruments and components. For the IUE components, the test levels were developed primarily from test data. For the Tandberg-Hanssen instrument, the levels were defined and the instrument component levels were derived from analysis. For the Thematic Mapper instrument, the levels were developed based on launch environment analysis, statistical information, and mutual spacecraft environments such as steady state acceleration and acoustic noise. Of the three, the preferred approach is that used for the Thematic Mapper instrument. This approach provides the levels that are the most consistent with the occurrences due to the launch.

The analyst must determine the environment that is most critical for the instrument and therefore the priority to place in the analysis plan. The first priority should be the steady state acceleration analysis because this is the environment that generally produces the highest load on the primary structure of the instrument. The next step should be the sinusoidal vibration analysis. This analysis frequently indicates high dynamic loads on some parts of the instrument. If this is the case, one should pursue the possibility of doing a launch loads analysis to determine if the loads predicted from the sinusoidal vibration analysis are realistic. However, typically a launch loads analysis is not a readily available option. Therefore, one should keep in mind that response levels on the order of 20 g's, assuming a modal Q of 15, probably will not be exceeded during launch. Some engineering judgment should be exercised before making design changes because of high loads predicted from sinusoidal vibration analysis. The random vibration analysis is one that should not be overlooked. Generally, random vibration is a high frequency environment that causes problems with electronic components or boards and also picks up workmanship problems. However, there are times when random vibration does cause structural problems. The analyst will have to use his own judgment when determining whether or not a random vibration analysis is warranted. The analytical shock analysis is questionable because the response is dependent upon the input and the definition of the input is not unique. Acoustic noise analysis is not done as a matter of course

basically because the analytical definition of the input is difficult and the analysis is too complex to spend the time to do it. If an instrument is designed to withstand steady state acceleration loads, sinusoidal vibration loads, and random vibration loads the chances are that a failure will not occur due to shock or acoustic noise.

REFERENCES

1. General Environmental Test Specification for Spacecraft and Components (Expendable Launch Vehicles). GETS(ELV)-1, NASA/Goddard Space Flight Center, May, 1977.

2. Environmental Test Specification for IUE Subsystems. IUE-320-74-008 Revision 1, NASA/Goddard Space Flight Center, December, 1975.

3. Keegan, W. Brian: A Statistical Approach to Establishing Subsystem Environmental Test Specifications. X-321-74-174, NASA/Goddard Space Flight Center, June, 1974.

4. Stahle, C. W.; and Gongloff, H. R.: Interim Report Study on Component Environmental Specification Development and Test Techniques. G. E. Document No. 75SDS4254, General Electric Space Systems Organization, October, 1975.

5. Keegan, W. B.; Stahle, C. E.; and Gongloff, H. R.: Development of Component Random Vibration Requirements Considering Response Spectra. The Shock and Vibration Bulletin, The Shock and Vibration Information Center, August, 1976.

6. SMM/Experiment General Interface Specification. SMM-670-01 Revision 1, NASA/Goddard Space Flight Center, September, 1976.

7. Space Shuttle System Payload Accomodations. JSC 07700 Volume XIV Revision E, NASA/Lyndon B. Johnson Space Center, June, 1977.

8. Shuttle Orbiter/Cargo Standard Interfaces. ICD No. 2-19001, NASA/Lyndon B. Johnson Space Center, October, 1977.

APPENDIX

Determination of the minimum number of points required for a frequency response analysis to assure that the calculated response is at least 90% of the peak response.

Nomenclature

f - frequency

f_H - high root of equation

f_L - low root of equation

f_n - natural frequency

HF - high frequency

LF - low frequency

N - number of points

Q - modal amplification

X_I - imaginary response

X_R - real response

Δf_{max} - maximum increment; $(f_H - f_L)\ f_n$

Assume a single degree of freedom system

$$X_R = \frac{1-\left(\frac{f}{f_n}\right)^2}{\left[1-\left(\frac{f}{f_n}\right)^2\right]^2 + \left(\frac{f}{Q f_n}\right)^2} \qquad \text{and} \qquad X_I = \frac{-\frac{f}{Q f_n}}{\left[1-\left(\frac{f}{f_n}\right)^2\right]^2 + \left(\frac{f}{Q f_n}\right)^2}$$

let $f_n=1$ then

$$X_R = \frac{1-f^2}{(1-f^2)^2 + \left(\frac{f}{Q}\right)^2} \qquad \text{and} \qquad X_I = \frac{-\frac{f}{Q}}{(1-f^2)^2 + \left(\frac{f}{Q}\right)^2}$$

$$\text{Response Magnitude} = \sqrt{X_R^2 + X_I^2}$$

$$= \frac{1}{\sqrt{(1-f^2)^2 + \left(\frac{f}{Q}\right)^2}}$$

for $f=1$ Response Magnitude = Q

Let Response Magnitude = $0.9Q$

then

$$0.9Q = \frac{1}{\sqrt{(1-f^2)^2 + \left(\frac{f}{Q}\right)^2}}$$

and

$$f^4 - \left(2 - \frac{1}{Q^2}\right) f^2 + 1 - \frac{1}{0.81\,Q^2} = 0$$

from the equation above

Q	f_L	f_H	f_H/f_L	$f_H - f_L$
5	.939	1.039	1.106	.100
10	.973	1.022	1.050	.049
15	.983	1.015	1.033	.032
20	.987	1.011	1.024	024

A. For a logarithmic sweep

$$N = \frac{\log\left(\frac{HF}{LF}\right)}{\log\left(\frac{f_H}{f_L}\right)}$$

B. For a linear sweep

$$\Delta f_{max} = (f_H - f_L)\ f_n$$

Figure 1.
TYPICAL ENVIRONMENTAL TEST AND ANALYSIS PLAN

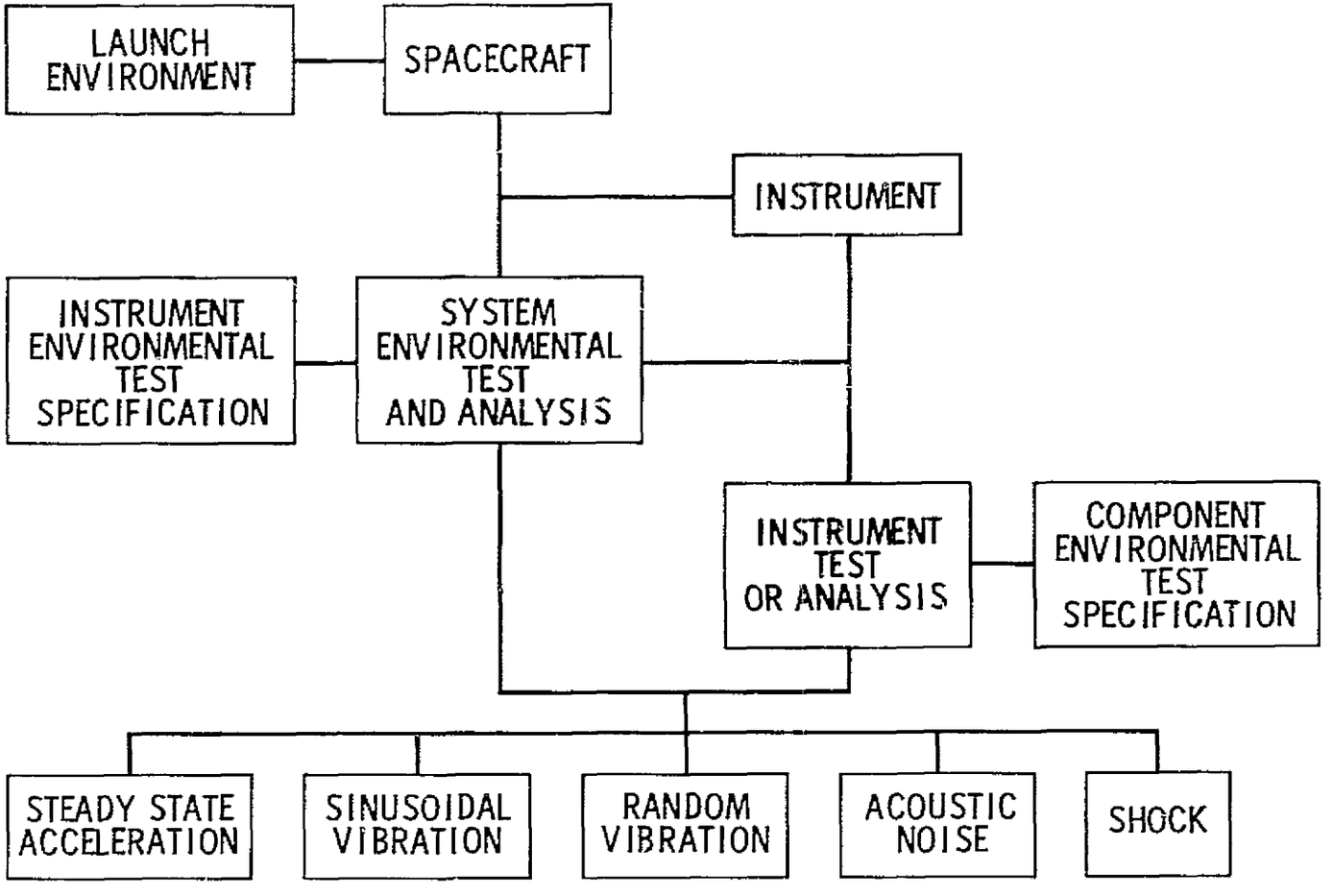

Figure 2.
IUE EXPLODED VIEW

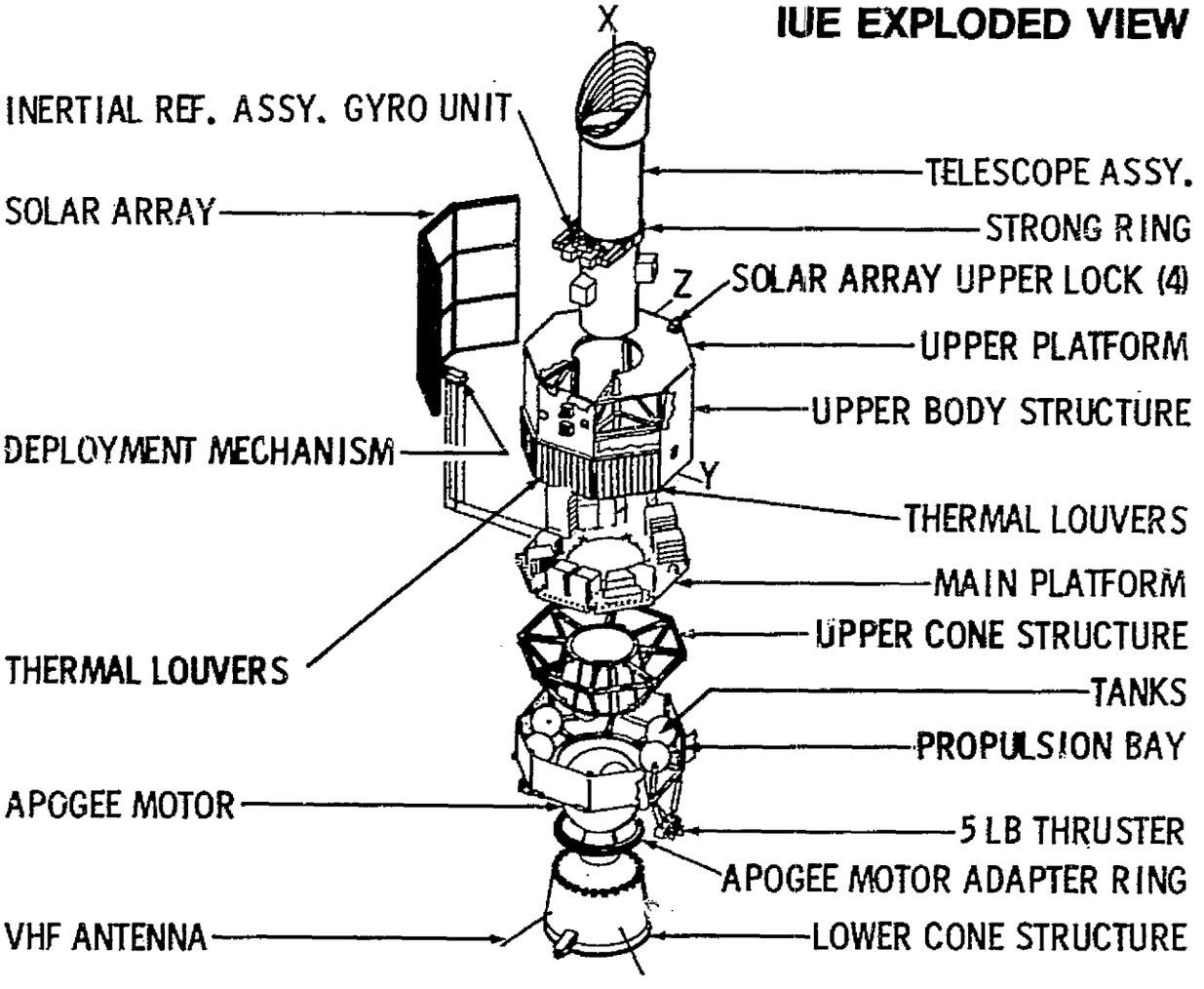

Figure 3.
FINITE ELEMENT MODEL OF IUE SPACECRAFT STRUCTURE

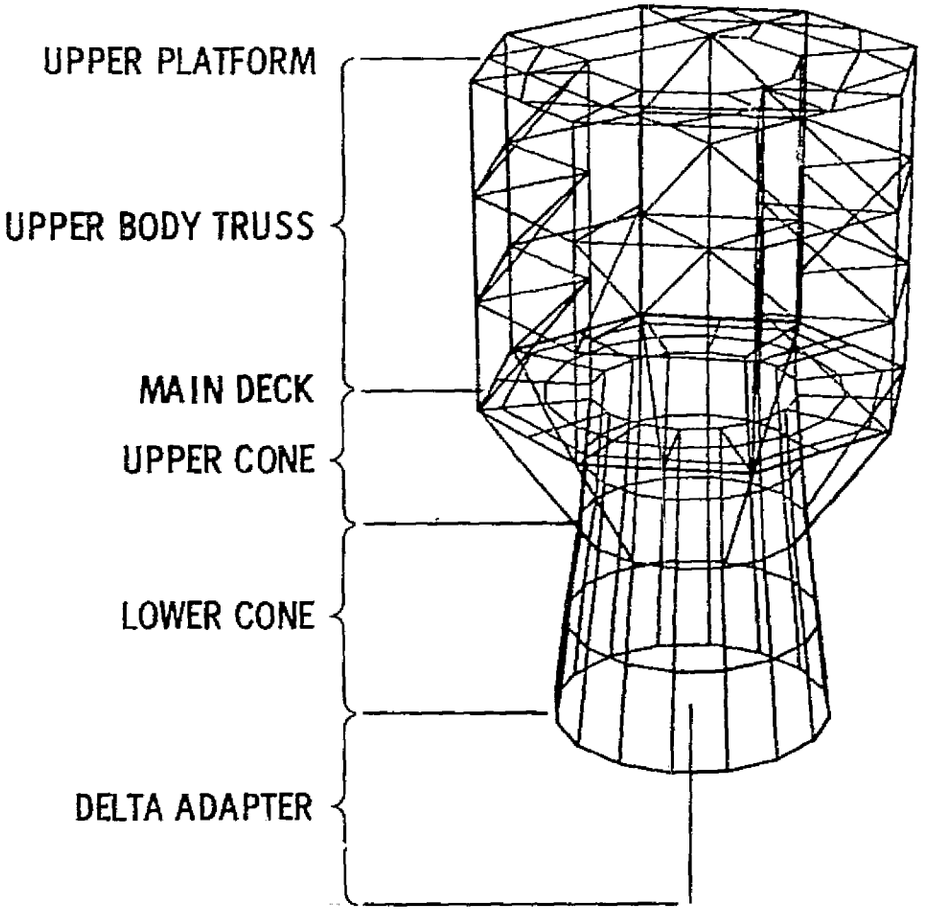

Figure 4.
FINITE ELEMENT MODEL OF IUE SCIENTIFIC INSTRUMENT

Figure 5.
EXAMPLE OF SINUSOIDAL SPECIFICATION

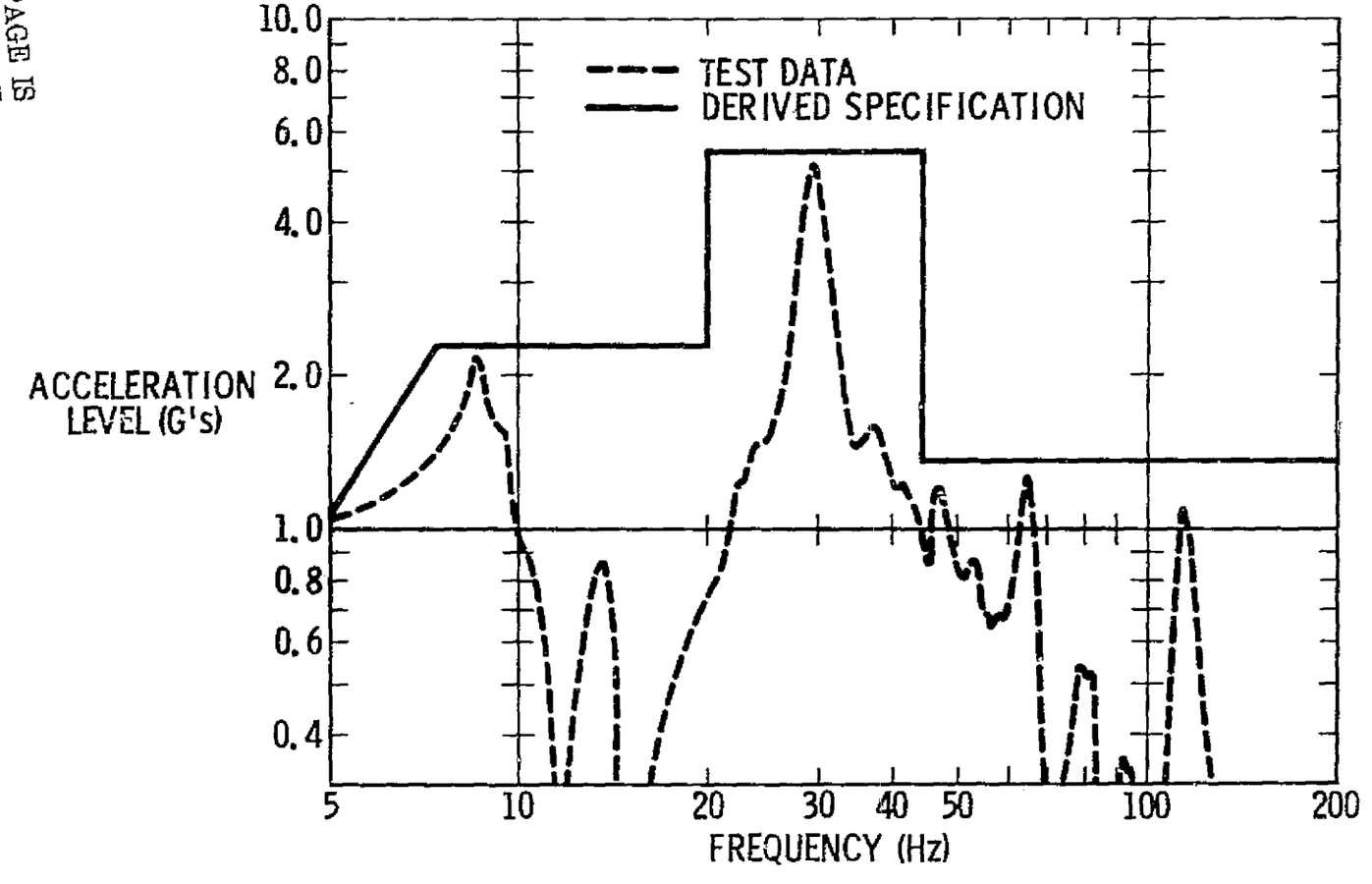

Figure 6.
EXAMPLE OF SHOCK RESPONSE SPECTRUM SPECIFICATION

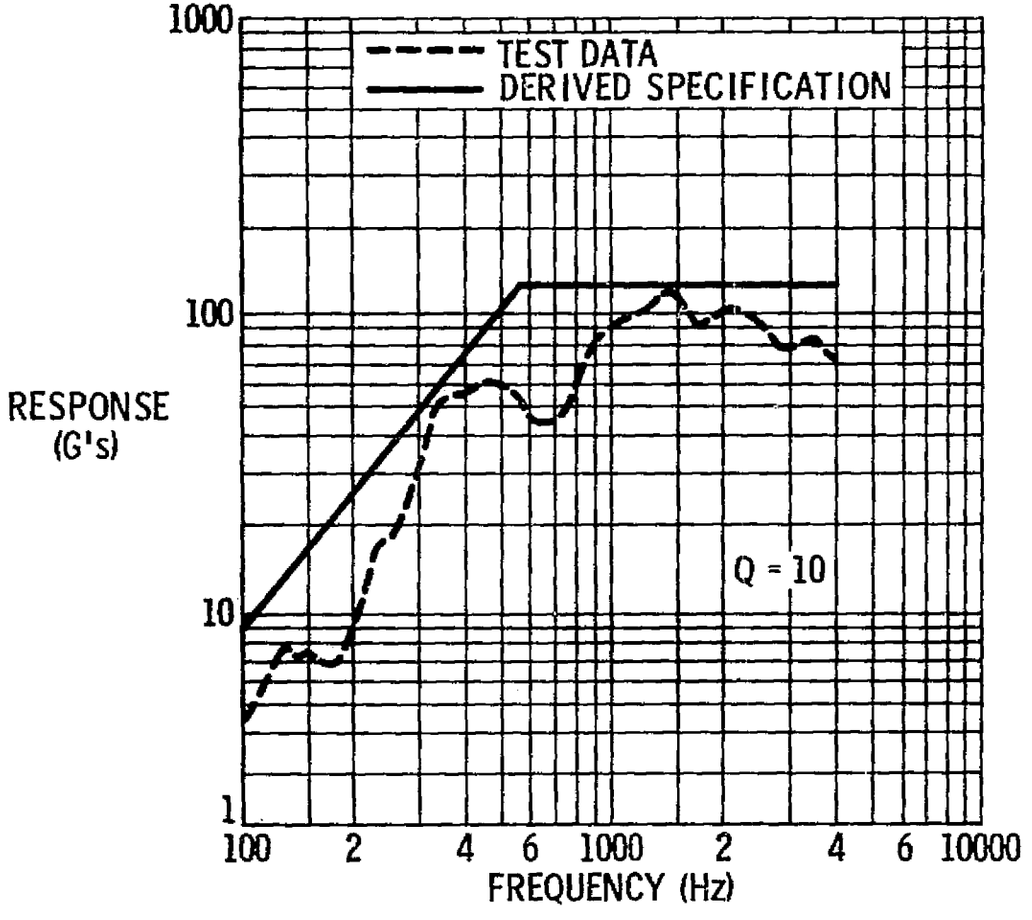

Figure 7.
TANDBERG HANSSEN SIMPLE BEAM MODEL

Figure 8.
TANDBERG HANSSEN DETAILED MODEL

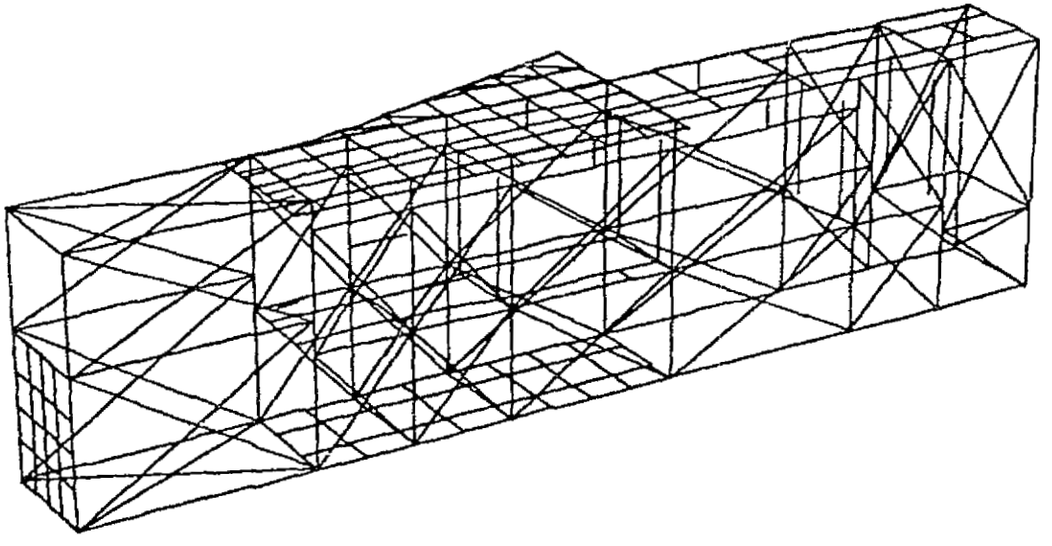

Figure 9.
EXAMPLE OF RANDOM VIBRATION SPECIFICATION

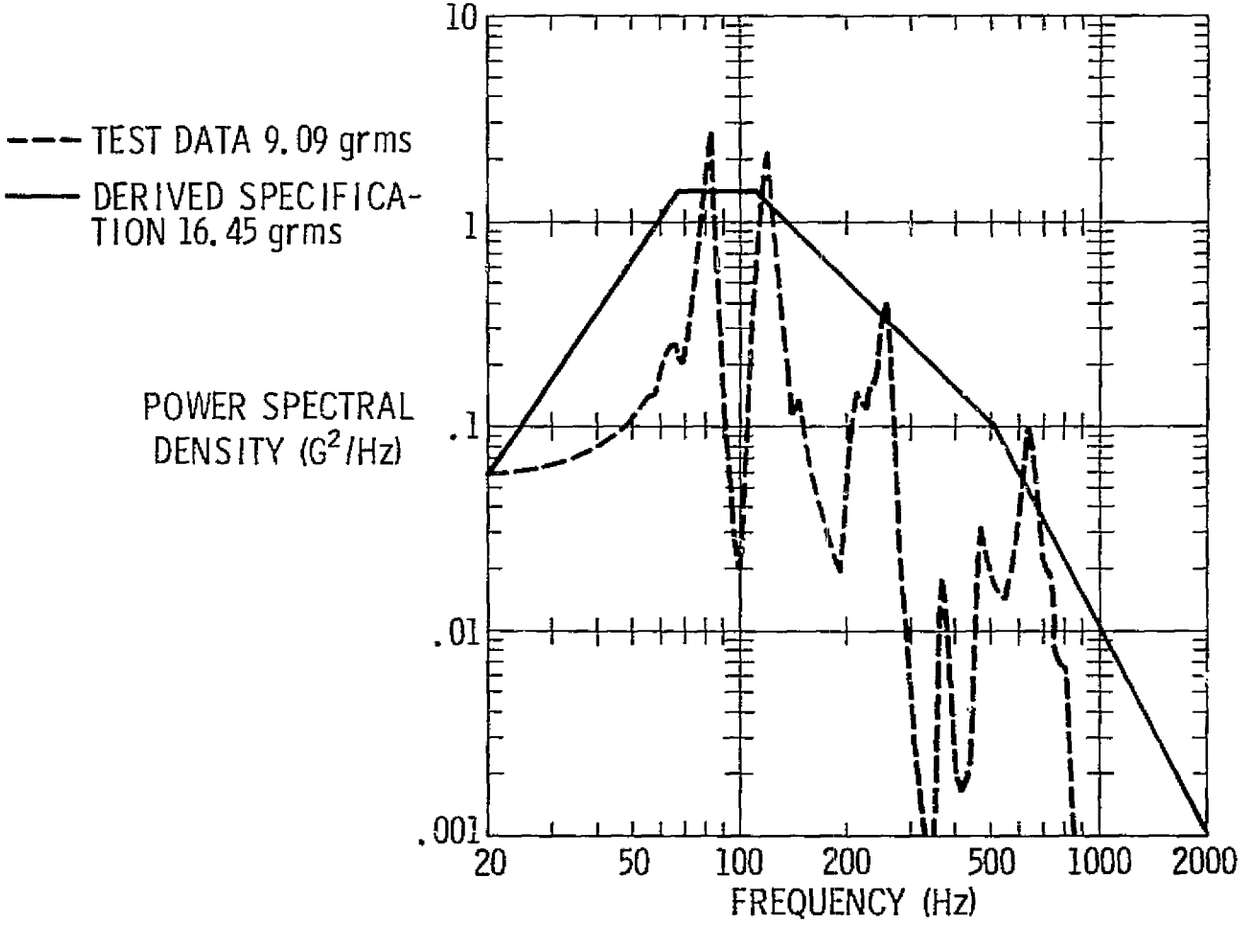

Figure 10.
LANDSAT-D SIMPLE BEAM MODEL

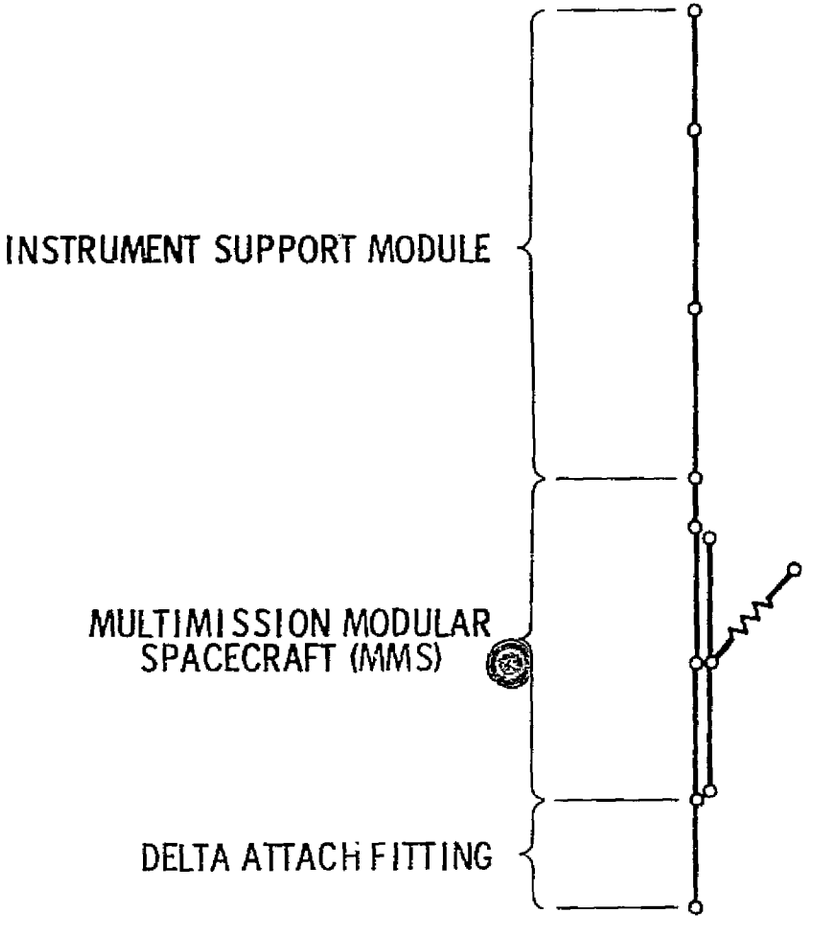

D8

N78-32474

REDUCTION OF MATRIX WAVEFRONT FOR NASTRAN

Gordon C. Everstine
David W. Taylor Naval Ship Research and Development Center

SUMMARY

The three grid point resequencing algorithms most often run by NASTRAN users are compared for their ability to reduce matrix root-mean-square (rms) wavefront, which is the most critical parameter in determining matrix decomposition time in NASTRAN. The three algorithms are Cuthill-McKee (CM), Gibbs-Poole-Stockmeyer (GPS), and Levy. The first two (CM and GPS) are in the BANDIT program, and the Levy algorithm is in WAVEFRONT. Results are presented for a diversified collection of 30 test problems ranging in size from 59 to 2680 nodes. It is concluded that GPS is exceptionally fast and, for the conditions under which the test was made, the algorithm best able to reduce rms wavefront consistently well.

INTRODUCTION

A central feature of structural analysis with NASTRAN is the factoring (or decomposition) of a matrix into upper and lower triangular forms. NASTRAN's current triangular decomposition algorithm is an active column routine similar to a variable band or wavefront approach. As such, the computer time required to perform a matrix decomposition depends strongly on the sequence assigned to the grid point labels.

For real, symmetric decomposition, for example, the time T required can be estimated from the relation (ref. 1)

$$T = \frac{1}{2} T_m \sum_{i=1}^{N} c_i^2 \qquad (1)$$

where N = matrix order,
c_i = number of active columns in matrix row i, and
T_m = time for multiply-add operation (an experimentally determined machine time constant).

The time T is sequence-dependent since the c_i's are sequence-dependent.

Since c_i is sometimes referred to as the row wavefront for row i, equation (1) can alternatively be written in terms of the root-mean-square (rms) wavefront, W_{rms}:

$$T = \frac{1}{2} T_m N W_{rms}^2 \qquad (2)$$

Because of the large size of Σc_i^2 in equation (1) for many problems, this latter form of the timing equation is often the more convenient one to use in practice. For reference purposes, typical values for the machine constant T_m are listed in Table 1 for several computers.

Core storage requirements for matrix decomposition are also dependent on the nodal sequence, the most critical parameter being the maximum matrix wavefront W_{max}, which is the maximum value of any c_i.

Thus, for most efficient matrix decomposition, the user would like to assign grid point labels so as to minimize both W_{rms} and W_{max}, with the former probably the more important. Unfortunately, it is often difficult for users to know how to sequence the nodes to effect a good numbering, particularly for large complicated meshes or those generated automatically on a computer. As a result, many users turn to NASTRAN preprocessors which automate the labeling process. The two most often run by NASTRAN users are BANDIT (refs. 2-4), which contains the Cuthill-McKee (CM) (ref. 5) and Gibbs-Poole-Stockmeyer (GPS) (refs. 6-7) schemes, and WAVEFRONT (ref. 8), which contains the Levy resequencing algorithm (refs. 9-10). Both preprocessors read NASTRAN data decks as input, resequence the nodes, and generate NASTRAN SEQGP bulk data cards (which tell NASTRAN what the new internal sequence should be).

The questions which then naturally arise are: How do these three resequencing algorithms (CM, GPS, and Levy) compare for their ability to reduce rms wavefront? What are the time and core requirements of the three algorithms?

These questions were addressed recently in another paper (ref. 11), in which the algorithms were also compared for matrix profile reduction. Complete descriptions of the test problems used for the comparison were presented. The purpose of this paper, which is adapted from reference 11, is to summarize for the NASTRAN user community the rms wavefront results obtained.

Subsequent sections of this paper present precise definitions of the relevant terms, a brief description of the three algorithms to be tested, the ground rules of the test, and the test results.

DEFINITIONS

Although the definitions given here are reasonably standard (at least in finite element circles), uniformity of definitions and notation among the various workers in the field does not yet exist.

Given a symmetric square matrix A of order N, we define a "row bandwidth" b_i for row i as the number of columns from the first nonzero in the row to the

diagonal, inclusive. Numerically, b_i exceeds by unity the difference between i and the column index of the first nonzero entry of row i of A. Then the matrix bandwidth B and profile P are defined as

$$B = \max_{i \le N} b_i \tag{3}$$

$$P = \sum_{i=1}^{N} b_i \tag{4}$$

Let c_i denote the number of active columns in row i. By definition, a column j is active in row i if $j \ge i$ and there is a nonzero entry in that column in any row with index $k \le i$. The matrix wavefront W is then defined as

$$W = \max_{i \le N} c_i \tag{5}$$

Sometimes c_i is referred to as the row wavefront for row i. Since the matrix A is symmetric,

$$P = \sum_{i=1}^{N} b_i = \sum_{i=1}^{N} c_i \tag{6}$$

The wavefront W is sometimes called the maximum wavefront W_{max} to distinguish it from the average wavefront W_{avg} and root-mean-square wavefront W_{rms} defined as

$$W_{avg} = \frac{1}{N} \sum_{i=1}^{N} c_i = \frac{P}{N} \tag{7}$$

$$W_{rms} = \sqrt{\frac{1}{N} \sum_{i=1}^{N} c_i^2} \tag{8}$$

From these definitions, it follows that, for a given matrix,

$$W_{avg} \le W_{rms} \le W_{max} \le B \le N \tag{9}$$

The first two inequalities would be equalities only for uninteresting special cases such as diagonal matrices.

We define the degree d_i of node i as the number of other nodes to which it is connected; i.e., more precisely, d_i is the number of nonzero off-diagonal terms in row i of the matrix A. (This implies, for example, that all nodes in the same finite element are "connected" to each other.) Hence, the maximum nodal degree M is

$$M = \max_{i \le N} d_i \tag{10}$$

The number of unique edges E is defined as the number of nonzero off-diagonal terms above the diagonal. Hence, for a symmetric matrix,

$$E = \frac{1}{2} \sum_{i=1}^{N} d_i \tag{11}$$

Thus the total number of nonzeros in A is 2E+N, and the density ρ of the matrix A is

$$\rho = (2E+N)/N^2 \tag{12}$$

Note that, in these definitions, the diagonal entries of the matrix A are included in b_i and c_i (and hence in B, P, W_{max}, W_{avg}, and W_{rms}). These definitions make it easy to convert the various parameters from one convention (including the diagonal) to the other (not including the diagonal).

Also note that, in this context, the order N of the matrix A is sometimes taken to be the same as the number of nodes. In general finite element usage, however, each node (grid point) has several degrees of freedom (DOF), not just one. For structures having, say, six DOF per node, the actual DOF values of B, W_{max}, W_{avg}, or W_{rms} would be (in the absence of constraints) six times their corresponding grid point values.

Example

Definitions (3)-(12) can be illustrated by the following simple example. Consider the matrix shown below, in which nonzeros are indicated by X's.

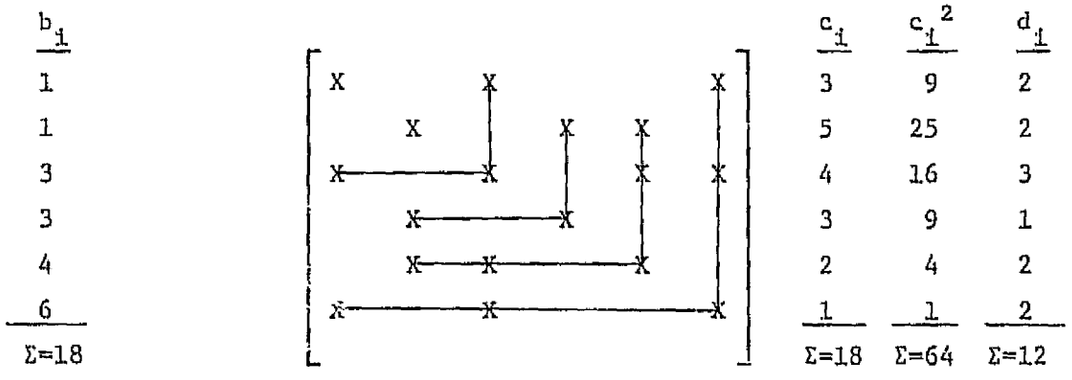

In each row and column a line is drawn from the first nonzero to the diagonal. Thus b_i is the number of columns traversed by the solid line in row i. Similarly, the number of active columns c_i in row i is the number of vertical lines in row i to the right of and including the diagonal. Thus, from the definitions, B=6, W_{max}=5, P=18, W_{avg}=3.0, W_{rms}=3.3, M=3, E=6, and ρ= 50.0%.

THE RESEQUENCING ALGORITHMS TESTED

The three algorithms tested are Cuthill-McKee (CM) (ref. 5), Gibbs-Poole-Stockmeyer (GPS) (refs. 6-7), and Levy (refs. 9-10). In this section each algorithm is described briefly, with details concerning the specific implementation used. It is recognized that one cannot really evaluate algorithms per se, but only specific implementations of algorithms.

Cuthill-McKee (CM) (ref. 5)

The original version of CM operated generally according to the following procedure: Among the nodes of low degree, select as potential starting nodes those which can root a graph of minimal width. (The term "starting node" refers to a node which is assigned the label 1 in the new sequence.) For each potential starting node, assign the labels 2 through N by numbering those adjacent to new label I (and unnumbered) in order of increasing degree, starting with I=1 and continuing with increasing I until all nodes are sequenced. Of the sequences attempted, select the one having the smallest bandwidth.

The implementation of CM used in these tests is that appearing in the BANDIT computer program, version 8 (refs. 2-4), which contains a version of CM differing from the original algorithm in two ways. First, the new sequence obtained is reversed (by setting I to N+1-I for each I), since it was observed by George (ref. 12) and proved by Liu and Sherman (ref. 13) that such a reversal (which preserves matrix bandwidth) will often reduce the matrix profile and never increase it. Second, of all sequences attempted, the one with the smallest rms wavefront is the one selected. Except for these two changes, the CM computer code is that originally written by Cuthill and McKee.

The data structure originally used by CM required about (M+8)N words of core storage for the problem-dependent arrays, where N is the number of grid points and M is the maximum nodal degree. In the BANDIT implementation of CM, word packing is used to reduce the storage requirements to (M/L+8)N, where L, the packing density, is an integer (between 2 and 6, inclusive) which depends on the problem size and the computer being used. On a CDC 6400, for example, the CP time penalty for packing is about 80 μsec per pack or unpack.

Gibbs-Poole-Stockmeyer (GPS) (refs. 6-7)

The GPS algorithm differs from CM primarily in the selection of starting nodes. In GPS, only one starting node is selected, and it is an endpoint of a pseudo-diameter of the graph associated with the matrix. Thus, the structure need be numbered only once, using a procedure which is similar to the CM numbering algorithm.

The storage requirements of GPS are identical to those of CM, including the use of integer packing in the BANDIT (version 8) implementation, which is the form of GPS used for the testing. The original GPS code was written by the developers (ref. 7).

Levy (refs. 9-10)

Unlike CM and GPS, which were developed to reduce matrix bandwidth and profile, the Levy algorithm was designed specifically to reduce the maximum matrix wavefront, W_{max}. The algorithm operates generally according to the following recursive procedure: Given the first I nodes of a new sequence, the node selected as I+1 is the one for which the increase in the row wavefront between rows I and I+1 will be minimum. Levy calls this a "minimum growth" method.

This procedure is followed for one or more trial starting nodes, and the sequence yielding the smallest wavefront W_{max} is selected. The first sequence attempted uses as the starting node either a user-selected node or a node of minimum degree. The latter option was chosen for these tests since it was felt that, for a production mode program, the user ought to be relieved of the burden of specifying a starting node. The second and succeeding sequences attempted by the Levy algorithm select starting nodes randomly. The number of new sequences to be attempted must be specified by the user. After some preliminary experimentation to estimate the speed of the algorithm, it was decided to request ten sequencing attempts for each test problem. Clearly a different number would yield different results.

The implementation used for the tests was that obtained by the author from Levy in 1973, the only change being that the sequence selected as best is the one yielding the smallest rms wavefront W_{rms}. Since the Levy algorithm aborts any resequencing attempt in progress once it determines that it cannot reduce the previous best W_{max}, the sequence finally selected will be the one among those carried to completion yielding the smallest W_{rms}.

The Levy data structure requires about 6N+10E words of core storage for the problem-dependent arrays, where N is the number of grid points and E is the number of unique edges. The code was not rewritten to use word packing for the tests.

TEST RESULTS AND DISCUSSION

The three grid point resequencing algorithms described in the preceding section were tested on a collection of 30 finite element meshes. These problems were collected over a period of several years from NASTRAN users representing various U.S. Navy, Army, Air Force, and NASA laboratories. Since these meshes are described in detail and plotted elsewhere (ref. 11), that information need not be repeated here. In general, however, the collection is probably large enough and diversified enough to provide a good test of nodal resequencing algorithms.

The nodes for the 30 test problems were resequenced using the three algorithms, the objective being to reduce rms wavefront. All computer runs were made on a CDC 6400 computer under the NOS/BE operating system. The source code

was compiled using the FTN compiler, OPT=1. For reference purposes, a CDC 6400 is about one-third as fast as a CDC 6600.

The results of the tests appear in Table 2. In addition to the rms wavefront obtained by each algorithm, Table 2 also lists, for each algorithm, the CP time expended and the storage requirements for the problem-dependent arrays. In the case of CM and GPS, which use word packing, the worst-case of half-word packing is assumed. The CP times listed do not include basic setup of the arrays.

The first conclusion to be drawn from Table 2 is that, for most problems, all three algorithms achieve about the same reduction in rms wavefront. This is, perhaps, somewhat unexpected since CM and GPS were designed primarily to reduce matrix bandwidth, whereas the Levy scheme was designed to reduce matrix wavefront. For the 30 problems, Levy achieved the best reduction in rms wavefront 13 times, GPS 11 times, and CM 5 times. However, on four occasions (N=503, N=607, N=878, and N=918) Levy did significantly worse than the best achieved; on three occasions (N=209, N=245, and N=1242) GPS did significantly worse; and on two occasions (N=245 and N=592) CM did significantly worse.

The second, and perhaps most striking, conclusion to be drawn from Table 2 is that GPS is exceptionally fast. In all cases, CM is second fastest, the Levy algorithm slowest. The user, of course, has some control over the running time of the Levy program (but not of CM and GPS) through his specification of the number of resequencing attempts.

The third conclusion to be drawn from Table 2 is that the Levy algorithm, as is, requires considerably more array storage than either CM or GPS, which use the same data structure. In fact, for the Levy program, one problem (N=2680) was too big for a CDC 6400 and could not be run. Clearly, the program could be rewritten to use word packing (as CM and GPS do), but this may be a nontrivial task, since the programmer has to decide which arrays to pack to yield the best compromise between storage and CP time. (Word packing, of course, saves core at the expense of CP time.)

Table 2 indicates that Levy's wavefront reduction performance was generally best for the smaller problems and GPS's was generally best for the larger problems. This is probably due to the author's choice of ten sequencing attempts for the Levy algorithm. As the problems get larger, the probability of Levy's selecting a good starting node at random goes down. One can infer that the algorithm's performance would improve if the program were allowed to run longer. However, whether the expenditure of more computer time is justified would be a matter for each user to decide. One issue that enters into such a decision is the number of times a given matrix problem is to be solved. If a given problem is to be solved many times (as, for example, in nonlinear analysis), or if many right-hand sides are involved (as, for example, in time-dependent problems), the time spent in sequencing becomes less important.

One might also infer that the performance of the Levy algorithm would improve if trial starting nodes were selected using a strategy such as that used in CM or GPS, rather than at random. While this may be true sometimes, it

was not true for the test problem on which Levy performed the worst (N=918), because for this problem the first trial starting node selected by Levy (which uses a node of minimum degree for the first attempt) was the same starting node selected by GPS. This same problem (N=918) was also run by Gibbs with his profile algorithm (ref. 14) (which is a hybrid of GPS and King (ref. 15), the latter being similar to Levy) with good results. This would indicate that Gibbs' modification to the King numbering approach (given a starting node) has a significant effect for some problems.

Overall, GPS's combination of speed and consistency probably rate it the best algorithm of the three for rms wavefront reduction. Previous testing (ref. 3) has already shown it to be an excellent algorithm for matrix bandwidth reduction, for which it was designed.

Finally, the three algorithms tested were selected because of their heavy use by NASTRAN users. However, it would be interesting to see how other strategies, including Gibbs-King (ref. 14) and Snay (ref. 16), would perform on the same data. Both give good results for profile reduction and hence would probably also do well in rms wavefront reduction.

REFERENCES

1. The NASTRAN Theoretical Manual. NASA SP-221 (04), Washington, D.C., December 1977.

2. Everstine, G.C.: The BANDIT Computer Program for the Reduction of Matrix Bandwidth for NASTRAN. NSRDC Report 3827, Naval Ship Research and Development Center, Bethesda, MD, March 1972.

3. Everstine, G.C.: Recent Improvements to BANDIT. NASTRAN: Users' Experiences, NASA TM X-3278, Sept. 1975, pp. 511-521.

4. Everstine, G.C.: BANDIT User's Guide. TM-184-77-03, David W. Taylor Naval Ship Research and Development Center, Bethesda, MD, 1977.

5. Cuthill, E.H.; and McKee, J.M.: Reducing the Bandwidth of Sparse Symmetric Matrices. Proc. 24th Nat. Conf., Assn. for Computing Machinery, ACM Pub. P69, New York, 1969, pp. 157-172.

6. Gibbs, N.E.; Poole, W.G., Jr.; and Stockmeyer, P.K.: An Algorithm for Reducing the Bandwidth and Profile of a Sparse Matrix. SIAM J. Numer. Anal., vol. 13, no. 2, April 1976, pp. 236-250.

7. Crane, H.L., Jr.; Gibbs, N.E.; Poole, W.G., Jr.,; and Stockmeyer, P.K.: Algorithm 508: Matrix Bandwidth and Profile Reduction. ACM Trans. Math. Software, vol. 2, no. 4, Dec. 1976, pp. 375-377.

8. Levy, R.: Structural Stiffness Matrix Wavefront Resequencing Program (WAVEFRONT). JPL Tech. Rep. 32-1526, vol. XIV, 1972, pp. 50-55.

9. Levy R.: Resequencing of the Structural Stiffness Matrix to Improve Computational Efficiency. JPL Quart. Tech. Review, vol. 1, no. 2, July 1971, pp. 61-70.

10. Levy, R.; and Wall, S.: Savings in NASTRAN Decomposition Time by Sequencing to Reduce Active Columns. NASTRAN: Users' Experiences, NASA TM X-2378, Sept. 1971, pp. 627-631.

11. Everstine, G.C.: A Comparison of Three Resequencing Algorithms for the Reduction of Matrix Profile and Wavefront. To appear.

12. George, A.: Computer Implementation of the Finite Element Method. Ph.D. Dissertation, Tech. Rep. STAN-CS-71-208, Computer Sci. Dept., Stanford Univ., Stanford, CA, 1971.

13. Liu, W.-H.; and Sherman, A.H.: Comparative Analysis of the Cuthill-McKee and the Reverse Cuthill-McKee Ordering Algorithms for Sparse Matrices. SIAM J. Numer. Anal., vol. 13, no. 2, April 1976, pp. 198-213.

14. Gibbs, N.E.: Algorithm 509: A Hybrid Profile Reduction Algorithm. ACM Trans. Math. Software, vol. 2, no. 4, Dec. 1976, pp. 378-387.

15. King, I.P.: An Automatic Reordering Scheme for Simultaneous Equations Derived from Network Systems. Intl. J. Numer. Meth. in Engr., vol. 2, no. 4, 1970, pp. 523-533.

16. Snay, R.A.: Reducing the Profile of Sparse Symmetric Matrices. Bulletin Géodésique, vol. 50, no. 4, 1976, pp. 341-352.

TABLE 1.-MULTIPLY-ADD TIME CONSTANTS (T_m)

(Double precision for IBM and Univac, single precision for CDC)

Computer	T_m (microseconds)
CDC 6400	16
6600	4.5
7600	0.6
Cyber 173	8.2
174	8.2
175	1.1
176	0.7
IBM 360/370 - 50	100
65	20
75	12
85	2
91,95	1.7
155	25
165	2
195	0.5
Univac 1108	14
1110	4

Source: NASTRAN level 17 block data deck NTMXBD

TABLE 2 - RMS WAVEFRONT TEST RESULTS

NO. OF GRID POINTS (N)	RMS WAVEFRONT				CP TIME (SEC.)			STORAGE (WORDS)	
	BEFORE	AFTER CM	AFTER GPS	AFTER LEVY	CM	GPS	LEVY	CM&GPS (M/2+8)N	LEVY 6N+10E
59	8.2	* 5.5	6.0	6.1	0.5	0.2	2.7	620	1394
66	11.0	3.2	* 2.9	3.0	0.6	0.2	1.5	693	1566
72	3.5	NI	NI	NI	0.3	0.2	1.2	720	1182
87	29.4	* 8.3	8.9	8.9	1.5	0.4	6.1	1218	2792
152	19.0	10.3	10.6	* 8.6	2.8	0.8	13.4	1944	6072
193	43.8	26.0	27.1	* 24.7	11.9	6.6	36.2	4343	17558
198	30.9	7.3	* 7.1	7.2	2.7	1.6	23.1	2673	7158
209	50.3	19.9	24.5	* 18.4	6.0	1.3	37.6	3344	8926
221	50.4	* 10.2	10.4	13.3	5.7	1.5	38.0	2984	8366
234	9.4	7.3	7.1	* 5.1	1.5	0.9	14.9	2925	4404
245	18.5	17.5	18.4	* 13.5	4.5	1.4	26.4	3430	7550
307	27.4	NI	NI	* 25.7	10.7	1.9	73.7	3684	12922
310	9.9	NI	NI	* 9.7	16.2	2.2	32.0	4030	12550
346	27.1	22.8	24.3	* 21.8	18.0	2.7	61.5	5882	16476
361	15.4	14.3	* 14.2	14.3	11.3	1.8	38.7	4332	15126
419	107.1	22.5	22.2	* 19.8	19.5	2.5	155.1	5866	18234
492	79.5	14.5	13.0	* 10.6	13.3	2.9	145.7	6396	16272
503	78.6	* 33.1	34.6	41.9	43.3	4.2	294.3	10060	30538
512	14.5	12.7	12.5	* 12.4	10.1	4.5	161.0	7680	18022
592	55.2	25.6	* 20.5	21.3	56.3	5.2	133.1	8880	26112
607	55.4	29.2	* 28.9	38.0	37.6	4.0	362.5	8802	26262
758	37.9	15.9	* 12.1	15.2	93.4	6.2	306.7	9854	30728
869	25.0	20.4	20.7	* 19.8	132.2	10.4	450.2	12601	37294
878	31.9	23.7	* 22.9	NI	46.0	12.2	311.2	10975	38118
918	131.1	25.7	* 24.3	51.1	95.2	9.7	745.7	12852	37838
992	302.0	35.9	* 34.7	38.8	141.2	34.8	801.8	16368	84712
1005	137.7	* 43.5	49.3	44.5	252.6	7.0	1010.0	21105	44110
1007	26.9	24.5	* 22.9	NI	42.6	14.6	300.3	12588	43882
1242	105.2	42.9	48.6	* 38.7	124.2	16.9	1270.9	16767	53372
2680	234.4	40.4	* 39.9	#	342.3	23.5	#	45560	127810

* = GREATEST REDUCTION, NI = NO IMPROVEMENT, # = NOT RUN

D9

N78-32475

PRE AND POST PROCESSING USING THE IBM 3277 DISPLAY STATION GRAPHICS ATTACHMENT (RPQ7H0284)

S. H. Burroughs, M. B. Lawlor and Dr. I. M. Miller*

IBM General Technology Division
Essex Junction, Vermont

SUMMARY

A graphical interactive procedure operating under TSO and utilizing two CRT display terminals is shown to be an effective means of accomplishing mesh generation, establishing boundary conditions and reviewing graphic output for finite element analysis activity.

INTRODUCTION

This paper is written to show how a graphical interactive procedure may be utilized in a time sharing environment to create input data for the NASTRAN program. In particular the software was motivated to assist input to the NASTRAN Thermal Analyzer portion of the program. In addition the software was designed to run on the IBM 3277 Display Station Graphics Attachment shown in figure 1. This hardware takes advantage of the benefits derived from having two display heads coupled in a work station concept. The A/N processing is accomplished on the IBM 3277 display terminal and the vector graphics information displayed on any other vector graphic display terminal. For this work a Tektronix 619 terminal was connected to the IBM 3277 display terminal. However, the graphics attachment RPQ provides a standard RS-232 interface for attachment of any user selected vector graphics CRT terminal.

Two display heads are better than one for pre and post processing activities since the A/N communication with the program does not interfere with the picture being presented. By directing all menu related information to the A/N terminal or any standard print out information to this terminal, the graphics picture is preserved. The graphics attachment offers a performance improvement over conventional dial up systems. The graphics terminal is controlled entirely by the A/N terminal and receives data at the same rate data is transferred to the IBM 3277. Therefore the vector graphics terminal is local to the IBM 3277 and unknown to the host system. The work station is completed with a suitable hard copy unit.

* Dr. Miller is at IBM, Poughkeepsie, New York

The graphics attachment also has a FORTRAN and an APL software RPQ support. This work makes use of the FORTRAN software to generate the graphic orders.

PHASE 1 MESH GENERATION

A procedure has been developed which is named QT. This procedure is designed to provide an interactive mesh generation capability for two dimensional models. However a companion procedure has been written which uses an imaging technique to create three dimensional brick and wedge elements from a two dimensional mesh.

The mesh generation is accomplished using the hardware described above as shown in the following steps:

1. Create mesh generation algorithm input data using standard TSO editing procedures. Save the file.

2. Invoke the mesh generation algorithm using TSO.

3. The QT procedure will then display the mesh generated on the graphics CRT for review.

4. Review the mesh for errors.

5. If the mesh is accepted go on to set boundary conditions.

6. If the mesh is rejected return to Step 1 and modify input data for redisplay until model is satisfactorily completed.

Figure 2-A shows the general flow for interactive processing using the QT procedure.

PHASE 2 BOUNDARY CONDITIONS

Establishing boundary conditions is a task that requires great care. The exact grid point number or element number, for example, must be known in order to establish a constraint or loading condition. Since this is the case a program was written which displayed the results of mesh generation so that the analyst could interact with the design for the purpose of setting boundary condition information in a manner that did not require the key punching of data in the fields required by the NASTRAN program. In this application of interactive graphics the use of the dual headed work station greatly simplifies the task.

The procedure is really quite simple in concept; that is, one wants to point at a particular grid point or element and (fix

certain degrees of freedom or establish values of load) communicate constraints or loads to be applied through bulk data cards.

In the interest of speed, it was decided that a correspondence table should be established between a grid point or element number and a text string. This correspondence table would be decoded and the NASTRAN bulk data cards prepared at a later time through the execution of a batch program. (This program is a batch program and is designed to run at the same time as NASTRAN.)

The method incorporated for pointing at the display of the mesh makes use of the cross-hair cursor. A detection is made on a grid point or element and control is returned to the program through the A/N keyboard. The grid point or element number is then written on the A/N terminal for confirmation by the display operator, at which time the keyboard is unlocked for input. If the match is correct, a full 80 bytes of information can be entered. This procedure permits several data items to be entered at one time, separated by blanks. Obviously, the first data item should be the mnemonic associated with the type of B.C. information required. Therefore, SPC, SPC1, OVOL, etc., would be the first data item followed by a blank and the related information to be included on that bulk data card when the bulk data card is formed at a later time in batch mode. A null response indicates an incorrect match. After each detection, new data is keyed in and the enter key depressed. When the picture must be redisplayed to show a different section of the model or to magnify a section, the word END is entered so that a new window may be selected and further work done on the constraints, etc., in that section of the model. A null response on window selection terminates the procedure. When the procedure is terminated, the data is saved on the file initially allocated upon invoking the procedure.

TRANSLATION OF DATA TO NASTRAN FORMAT

The mesh and B.C. information must be translated from the graphic structures to the rigid format required for NASTRAN or another finite element analysis program. This is accomplished using the QTNAST (Quadrilaterals or Triangles/NASTRAN) program and files are created as shown in fig. 2b. This program can be run as a pre-NASTRAN step or as a stand-alone batch job. As a pre-NASTRAN step, the data sets (files) can be temporarily allocated and therefore a very compact form of the model data saved in lieu of the fully expanded card formatted data which can typically become thousands of card images.

The pre NASTRAN or pre FEM program step, therefore, has obvious advantages where space is costly or difficult to obtain on a permanent basis.

The QTNAST translation program will not be described in detail here as documentation exists on the program. Nevertheless, this program is a companion program in the procedure described which provides a very necessary function. The input data to this program provides substantial flexibility for the analyst to create, merge and modify models. The creation of three dimensional brick or wedge shaped elements from the two dimensional mesh is just one example.

PHASE 3 POST PROCESSING

An interface routine has been written to read the PLT2 plot data which is created by selecting to use the NASTRAN general purpose plotter interface. The Lvl 15.5 PLT2 data set may be written to disk instead of tape by making the following declaration on the NASTRAN card: SYSTEM(45) = 96. Then the PLT2 DD card should have a direct access data set specified in the NASTRAN procedure. This data set may be a partitioned data set for saving plotting data for more than one model in each member of the data set.

Once the data has been saved as described above the post processing (translation) routine can be invoked in the foreground using TSO (time sharing option) and the various frames can be drawn on the display terminal as shown in figure 3. The frame can then be manipulated through a windowing technique which permits the data to be redisplayed over and over again until the desired magnification is obtained. (Examples of this for the frame shown in figure 3 may be found in figures 4a & b. Note that the size of the numbers change also which can be of assistance for frames with very dense displays. In fact the grid point numbers can be suppressed to mere dots on the terminal if required for clarity.

Using this program, frames can either be displayed individually or over laid if desired.

The program has the ability to incline the alphanumeric data and the character size may be easily varied; however, normally standard upright characters have been used.

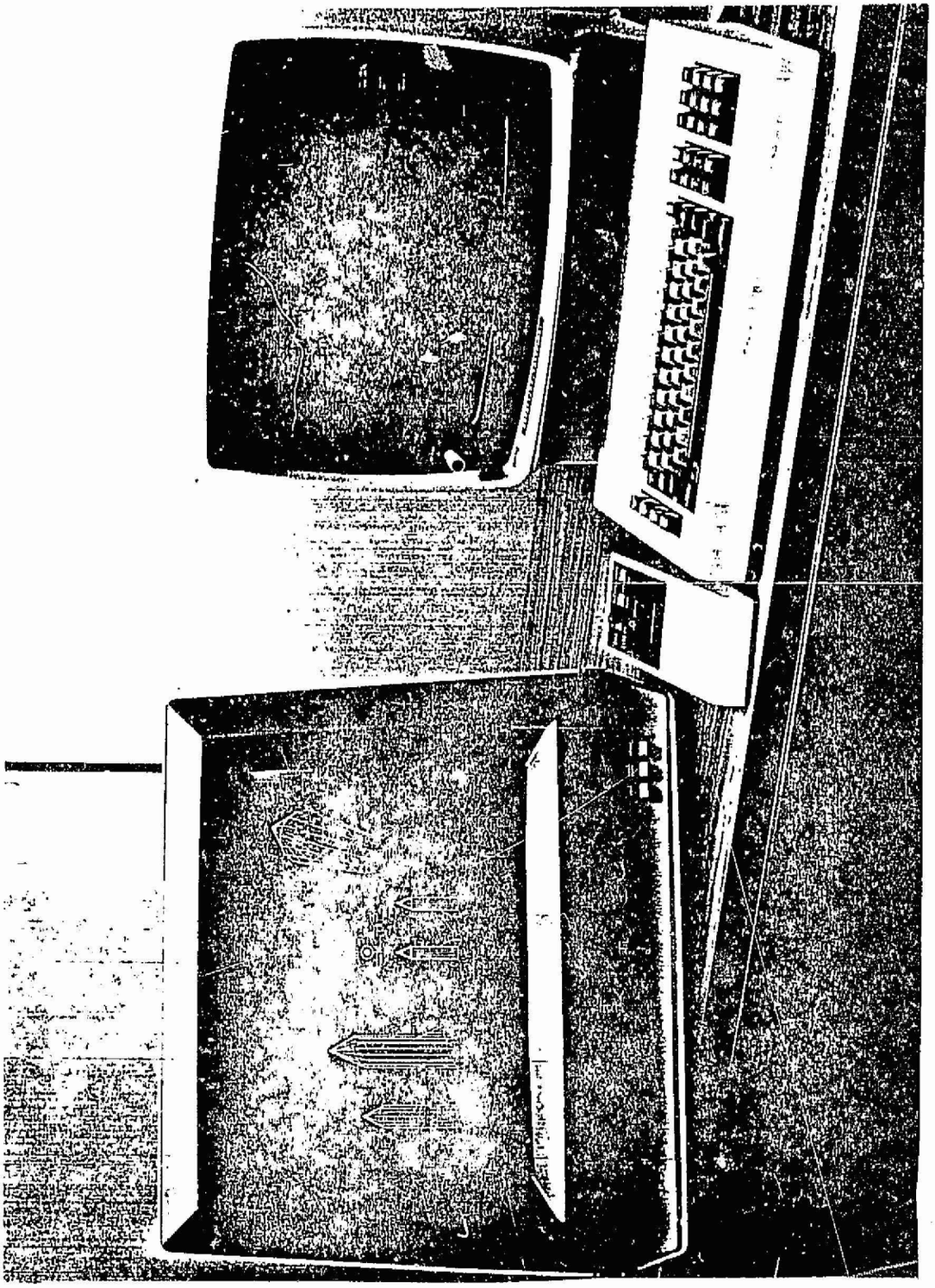

Fig. 1. A Configuration of the IBM 3277 Display Terminal Graphics Attachment.

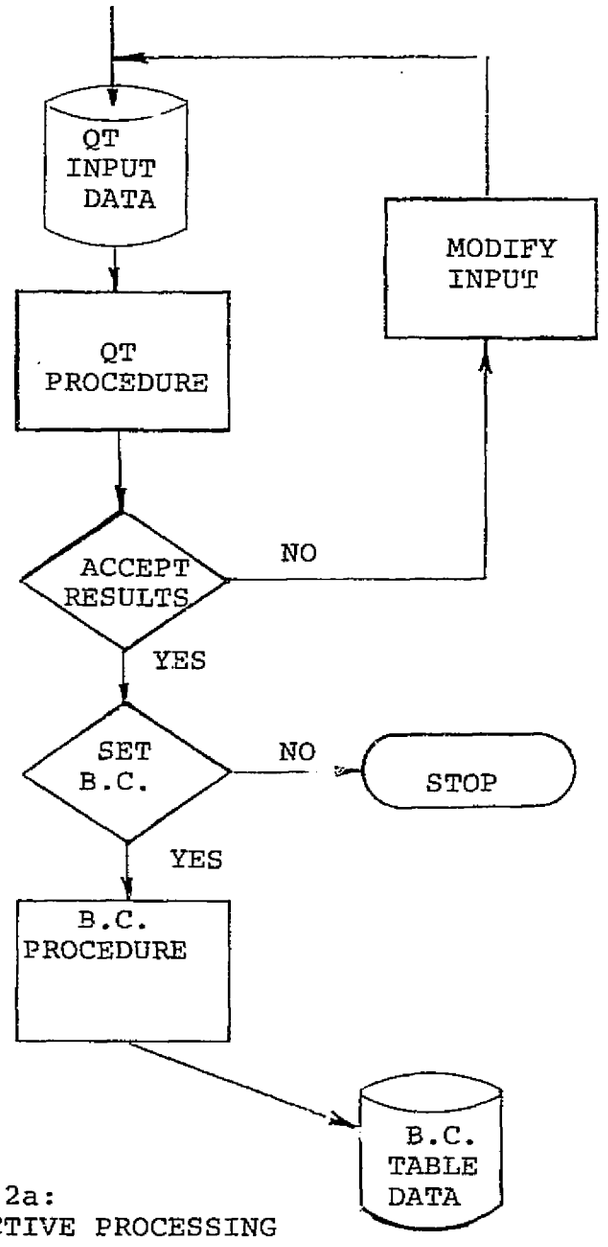

Figure 2a:
INTERACTIVE PROCESSING

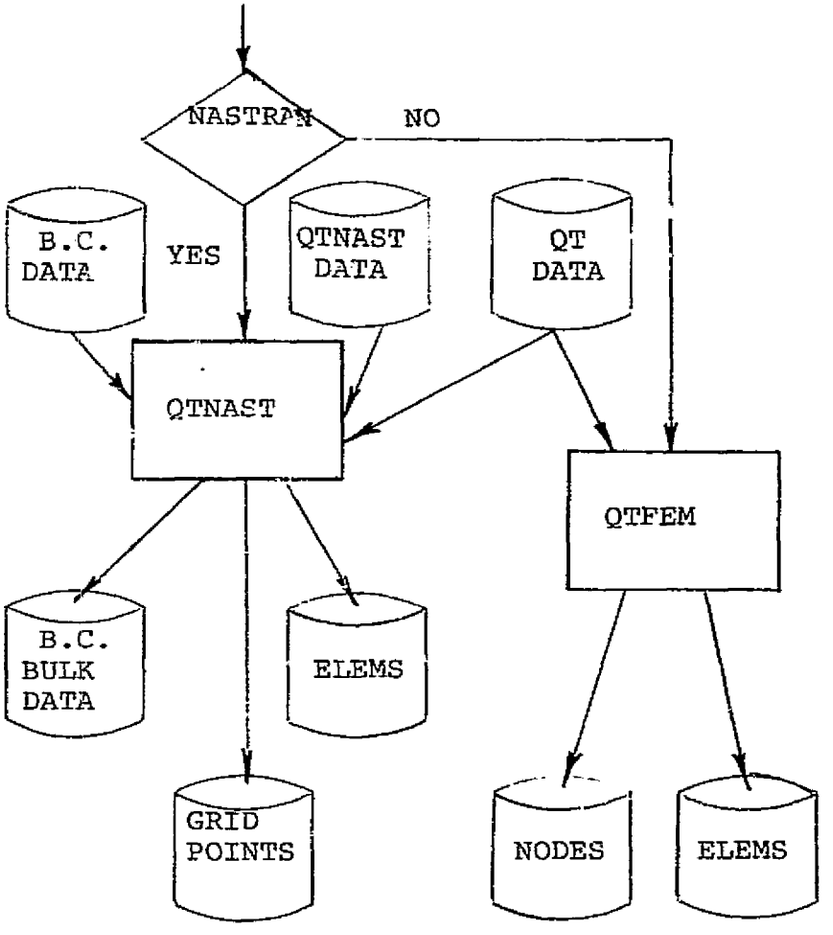

Figure 2b:
PRE PROCESSING OF FEM DATA

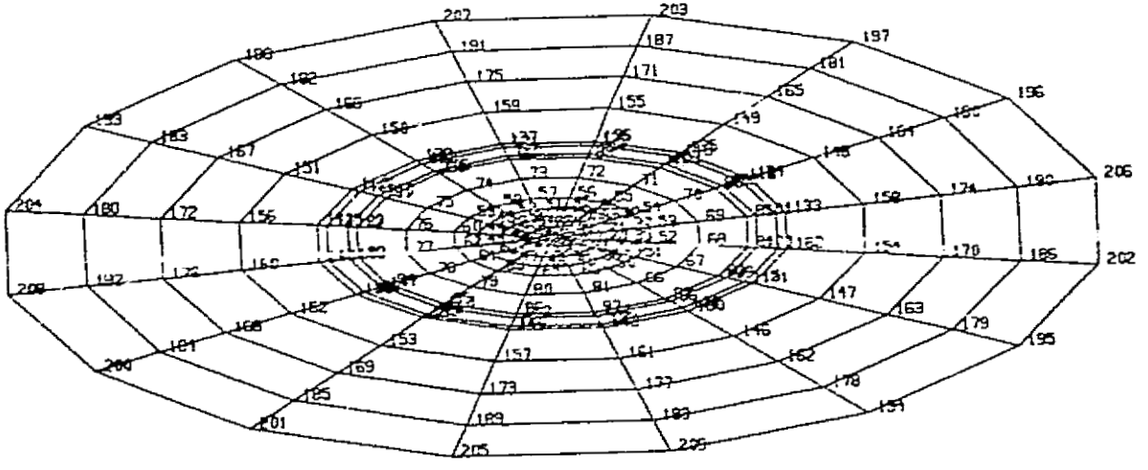

Fig. 3. NASTRAN Plot Output for Sample Problem.
Window Size: Full Frame (0, 0, 100, 100).
Character Size: 1.

A GRAPHICS TEST PROBLEM
IN POLAR COORDINATES

UNDEFORMED SHAPE

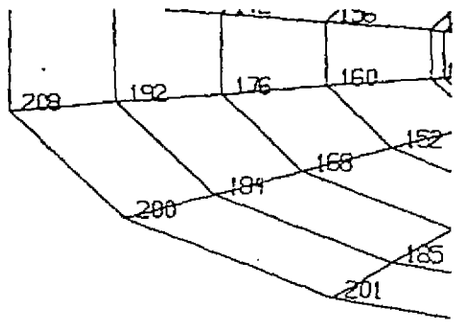

A GRAPHICS TEST PROBLEM
IN POLAR COORDINATES

UNDEFORMED SHAPE

Fig. 4a.

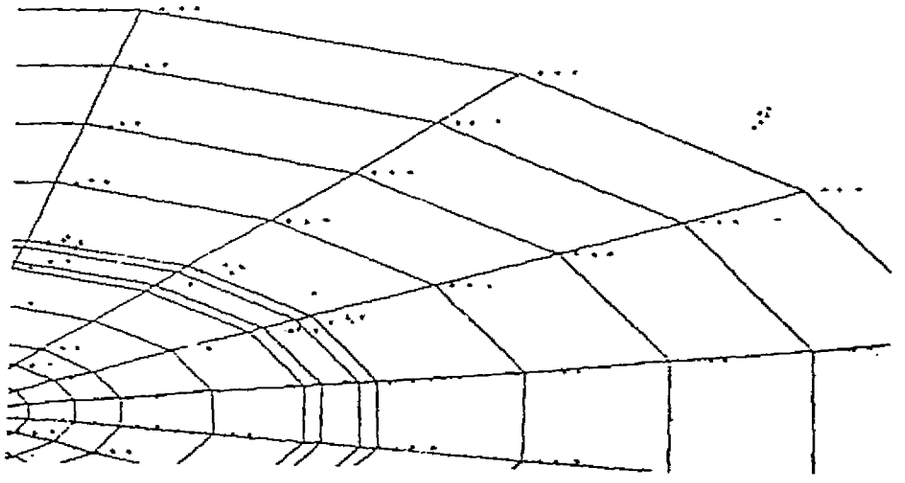

Fig. 4b.

Fig. 4a. Window Size: XL=YL=0, XH=28, YH=55.
Character Size: 0.6.

Fig. 4b. Window Size: XL=YL=50, XH=YH=90.
Character Size: 0.01.

Fig. 4. Examples of Window Clipping and Character Scaling for Output Shown in Fig. 3.
(Figs. 4a and 4b are formatted so as to be placed on this one page.)

D10

N78-32476

IG/OG PROGRAM FOR GENERATING AND DISPLAYING NASTRAN INPUT AND OUTPUT DATA

By Ryoichi Mishima
and Akinori Myojin

Hitachi, Ltd. Japan

SUMMARY

Hitachi,Ltd. has developed a software system in structural analysis fields using NASTRAN, and now HITAC users in Japan can use IG/OG (Input Generator/Output Generator) program for NASTRAN. IG/OG saves much time required to make a structure analysis data to interpret the result from an analysis by NASTRAN.

INTRODUCTION

Generally, large-scale calculations in structure analysis require more than 1000 elements and nodal points even in the analysis of plane structure. In addition, thousands of input data cards must be prepared. In the case of three-dimensional structure having various arbitary shapes, a numerous amount of input data more than these must be prepared. This operation is extremely difficult to be done by hand and also requires much time. On the other hand, the analytical results such as the node displacement outputted for each nodal point, and the elementary stress and force outoutted for each element reaches several times the input data. These bring about the fact that prodigious labor and time must be shared for rearranging and retrieving the resultant outputs and preparing all necessary reports.

The IG divides a structural model set by the user into elements, and generates the user communication file used as an input data file to NASTRAN. The IG incorporated in NASTRAN helps to simplify the aforementioned troublesome preparation of input data extremely.

The OG rearranges a numerous amount of output data and plot them graphically or in figures to facilitate the retrieval of analytical results. By writing the file-names used in the OG into the user communication file at the time of NASTRAN execution, the user enables the OG to draw various figures while changing the parameters provided for figure construction, after the completion of NASTRAN execution.

INPUT GENERATOR

Many excellent automatic mesh generation programs for specific structures such as aircraft and ship have been developed and introduced. For general structures, however,few of those programs are usable. The automatic mesh generation program (IG) of IG/OG inroduced in this paper has been developed for universal applications, for which various new concepts were incorporated.

A whole structure cannot be divided completely at a time . In this system, it is divided into sub-structures called parts which are then inputted. The part is formed by a relatively simple shape such as triangle, quadrilateral, or the like. In the IG the respective parts are mesh-generated and then combined with each other to complete dividing a whole structure in mesh. The number of processings necessary for dividing a structure into parts is only a fraction(several ten times less) of that needed for dividing into structural elements, although it depends on the shape. This brings about the fact that the number of processings needed for data preparation can be reduced greatly. In addition, special data are not required when combining the respective parts with each other, since the combining operation is performed based on the distance between the coordinates of grid points.

The data which can be obtained by automatic mesh generation are limited to some extent, but load and constraint conditions can be created in addition to grid point data and element combination data.

Part

Ten different kinds of parts are usable in the IG, each having its own divide method. The list of divide methods is as shown below.

(1) Quadratic shape function method
(2) Cubic shape function method
(3) Rotational quadratic plane method
(4) Coon's blending function method
(5) Plane parallelogram method
(6) Rotational parallelogram method
(7) Cylindrical parallelogram method
(8) Rotational plane curve method
(9) Similar translation method
(10)Orthogonally branched pipe method

Different kinds of parts may coexist within the same structure. A part is defined by specifying boundary lines. Straight line, quadratic curve, cubic curve, and arc are used as boundary lines. The boundary lines usable for each part differ according to the kind of part or divide method. A boundary line is defined by specifying 2 or more points on it. The points used to define boundary line are called characteristic points. For example, straight line is defined by specifying characteristic points at its both ends, and quadratic curve is by 3 points -- 2 at

its both ends and 1 at the intermediate portion of it.

The quadratic shape function method is one in which the plane structure consisting of triangle or quadrilateral is to be divided. The boundary line used in this method is represented by any one of straight line, quadratic curve, and cubic curve.

As shown in Fig. 1, the structure represented by A,E,B,F,C,G,D,H in the coordinate system XY is correlated with the square of abcd in the coordinat system $\alpha\beta$. Shape function is used to correlate the points in the coordinate system $\alpha\beta$ with the points in the coordinate system XY. The shape function is the same as those often used in the finite element method. Dividing operation is performed on the square in the coordinate system $\alpha\beta$. By obtaining the points corresponding to the grid points generated the aforementioned dividing operation, the structure of A,E,B,F,C,G,D,H is substanaially divided.

The cubic shape function method is the same as the quadratic shape function method, except that part shape is 3-dimensional.

The rotational quadratic plane method is an application of the quadratic shape function method. The section of thick-wall shell generated by rotating a plane around an axis is divided by using the quadratic shape function method. In the circumferential direction, the shell is divided evenly at the specified angle.

The Cooh's blending function method is one in which the method of creating a free curve used in numerical control is applied to automatic mesh generation.

In the plane parallelogram method, a structure approximating a quadrilateral, whose opposing edges run almost in parallel, is divided into parts. Each edge is defined as an aggregate of straight line, quadratic curve, and arc. If the opposing edges are not in parallel, an additional line can be specified at the intermediate portion of them, whereby the shapes of divided elements can be improved considerably.

The rotational parallelogram method is one in which the plane parallelogram method is utilized for a thick-wall shell generated by rotating a parallelogram around an axis, like in the rotational quadratic plane method. The section of the shell is divided by using the plane parallelogram method. In the circumferential direction, the shell is divided evenly at the specified angle.

In the cylindrical parallelogram method, the section of a cylinder is divided by using the plane parallelogram method. In the axial direction, the cylinder is divided evenly at the specified length.

The rotational plane curve method is one in which a thin-wall shell generated by rotating a curve defined on XZ plane is divided. The curve is defined as an aggregate of straight line, quadratic curve, and arc.

The similar translation method is one in which the surface generated by translating a straight line along acurve is divided. The curve is defined as an aggregate ofstraight line and arc.

The orthogonally branched pipe method is one which can be applied only to orthogonally branched pipe. However, such pipe can be combined with other parts.

Mesh Pattern

Fifteen different kinds of mesh patterns are available, whereby the normal dividing operations are satisfied. For example, the follwing patterns are included; a quadrilateral is divided into triangles by using shorter diagonal line instead of longer one, or the number of divisions is increased or decreased as dividing operation moves in a certain direction.

Each pattern has the corresponding code, thus a pattern to be used is selected by specifying the code corresponding to the part.

Load Generation

Loads such as grid point force and pressure can be generated. The amount of each component contained in grid point force and the amount of pressure must be represented by the linear function of grid point coordinate values. Pressure is assumed to be applied in the direction parpendicular to plane element. Grid point force is given for each component.

Constraint

A special part can be used for defining only the constraint condition of grid point. This part is linear, being represented by straight line, quadratic curve, or cubic curve. The boundary condition along the contour of structure can be generated easily by using the part.

Three-Views

In the analysis of complex structure, it is troublesome to input the coordinate values of characteristic points for defining the boundary lines. The IG is capable of inputting the coordinate values by using three-views in addition to inputting them directly This greatly helps to simplify the analysis of complex structure.

Command

The data incorporated in the IG are classified into the data used to define a structure and those necessary for activating the actual mesh generation. The data needed for activating the generation are called commands. The following commands are available.

(1) AUTOMESH

Activates the automatic mesh generation of part.

(2) TRANS
Tranlates automaically-mesh- generated parts similarly; i.e., the specified values are added respectively toeach grid point coordinate.
(3) ROTATE
Rotates automatically-mesh- generated part. This command is capable of placing the part at any desired position in combination with TRANS.
(4) SCALE
Contracts and expands part.
(5) REFLECT
Reflects part. For example, when a part is reflected on X axis, the sign representing the X value of grid point coordinate is reflected.
(6) ERASE
Eliminates part of grid points or elements within a part.
(7) COMBINE
combines the respective parts which have been mesh-generated by AUTOMESH command and operated by other commands.
(8) PLOT
Plots the data obtained by automatic mesh generation on the XY plotter.
(9) PRINT
Lists up the results of automatic mesh generation.
(10) ADD
Adds the data which cannot be created by the IG such as shape data or material data in the format of NASTRAN
(11) ADDEND
Indicates the end of additional data beginning with ADD command.

Output of IG

The output of IG is available as shown below.
(1) NASTRAN input user communication file
This file serves as an input to NASTRAN.
(2) Mesh-generated structure projection
The results of automatic mesh generation are plotted on the XY plotter.
(3) List of created data
The results of automatic mesh generation are listed up.

OUTPUT GENERATOR

The OG edits the results of NASTRAN. Attempts are being made to support the following functions in the feature; the aforementioned results are to be drawn on the XY plotter and graphic display, and the specified contents are to be listed up in the specified format. Currently, the OG supports the plotter function which is the same as that of NASTRAN and the function capable of drawing principal stress

diagram.
The input of OG is the output user communication file of NASTRAN. This file is prepared while execution is carried out in NASTRAN. The module for creating the file has been developed newly.

Principal Stress Diagram

Principal stresses occurring in the elements of a plane can be drawn on the XY plotter in which their amounts and directions are shown by arrows. The principal stresses calculated in NASTRAN are read and displayed via the output user communication file. The pen drawing the diagram can be changed automatically according to whether the stress is compressive or tensile.

User Communication File

Some of rigid formats supported by NASTRAN are looped. By writing the files created in the looped portions by the OUTPUT module, the data blocks having the same name are written as many times as the number of loops. These data blocks cause a confusion when they are referred to.
In the OUTPUT2 module currently supported, only the first and last data blocks are referred to although a number of data blocks having the same name exist. To cope with this, OUTPUT5 module has been developed newly. IN the OUTPUT5 module, data blocks are outputted separately for each loop, and loop number can be affixed to each data block. Therefore, any desired data block can be referred to by specifying the loop name or loop number or data block name. In addition, the OUTPUT5 module is capable of taking out not only data blocks but parameters.
The following is an example of alteration card in rigid format 8 used to create the user communication file.

```
1. ALTER 2
2. PARAM
     .
     .
     .
   ALTER 103
   PARAM//C,N,ADD/C,N,0/C,N,0/$
   ALTER 106
   PARAM//C,N,ADD/V,N,LOOP/V,N,LOOP/C,N,1/$
   OUTPUT5,,,,//C,N,0/V,N,UCF/C,N,X/C,N,B/V,N,LOOP/$
     .
     .
     .
```

In ALTER 106, 1 is added to parameter LOOP, and the LOOP value is written in OUTPUT5 next to ALTER 106.

EXAMPLES

The first example is one to divide a structure like a rocket shown in Fig.12. The fuselage which is axisymmetric is divided in the rotational plane curve method, and the wing is divided in the quadratic shape function method. 664 elements and 616 grid points are generated. The number of input cards to IG is 30.

The second example is a holed plate. A quarter of it is divided in the plane parallelogram method and the quadratic shape function method. It is easy to divide the part near the hole into smaller elements. 88 elements and 195 grid points are generated from 61 input cards.

The third example is a solid structure with the shape of L shown in Fig.14. The characteristic points of this example are inputted using three-views. For a simple structure like this it is not necessary to use three-views. 228 elements and 488 grid points are generated from 84 input cards.

The fourth example is also a solid structure as shown in Fig.15. The cylindrical parallelogram method is used. The input cards are shown in Fig.16 and the result which is drawn on XY plotter is shown in Fig.17.

CONCLUDING REMARKS

An automatic mesh generation program was developed for universal applications, in which the structure of arbitrary shape is divided into simple-shape sub-structures which are further divided into elements, and then the sub-structures are combined with each other to complete dividing the whole structure in mesh. The number of processings necessary for data preparation is reduced to several ten times less. The characteristic points defining the sub-structures can be defined by inputting the coordinate values directly and by using three-views. In the analysis of complex structure, characteristic points can be defined easily by using three-views.

A new output module was developed to support the function of editing outputs, by which the data blocks prepared in DMAP loop can be assigned accurately to addresses.

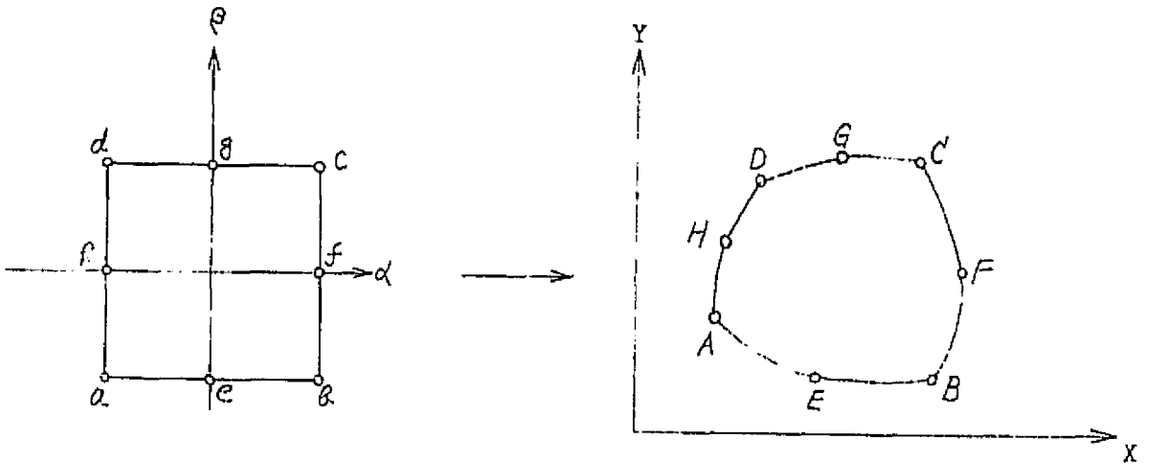

Fig.1 Quadratic shape function method

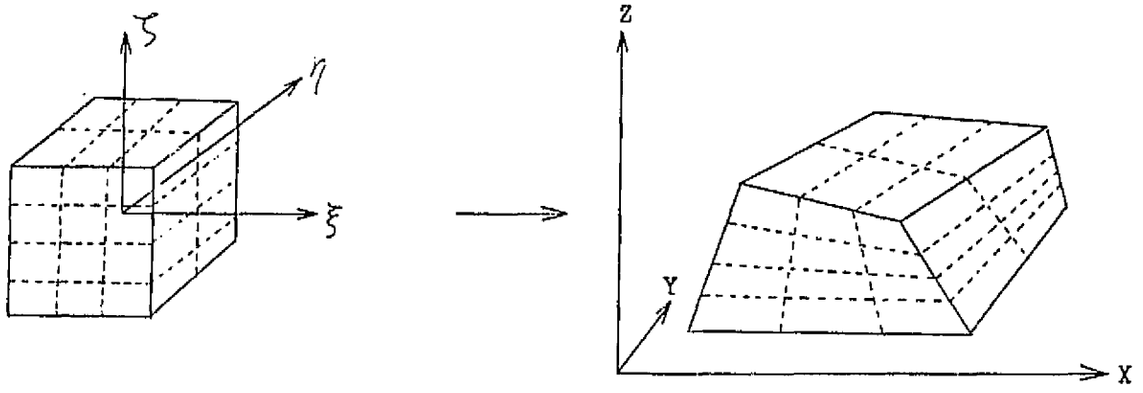

Fig.2 Cubic shape function method

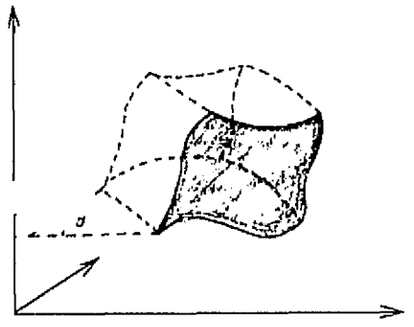

Fig.3 Rotational quadratic plane method

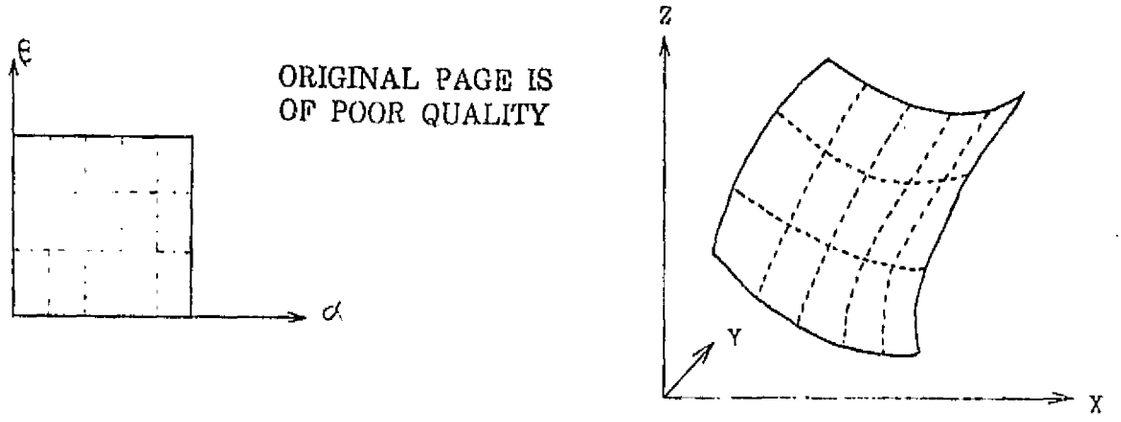

Fig.4 Coon's blending function method

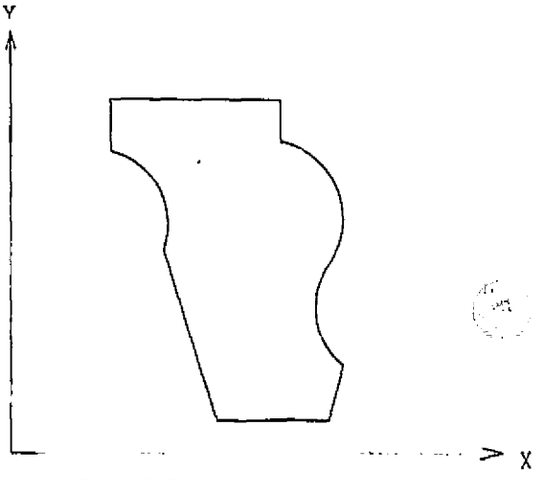

Fig.5 Plane parallelogram method

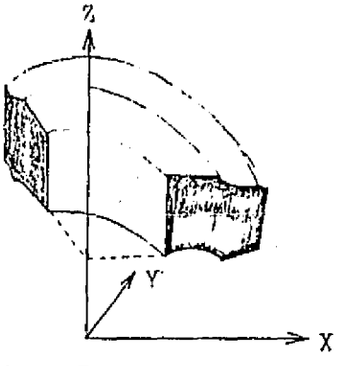

Fig.6 Rotational parallelogram method

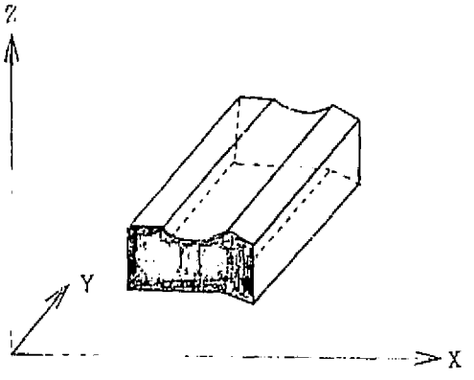

Fig.7 Cylindrical parallelogram method

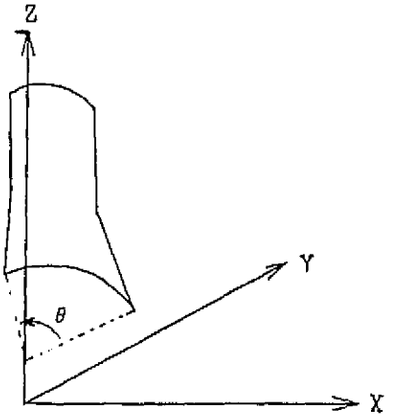

Fig.8 Rotational plane curve method

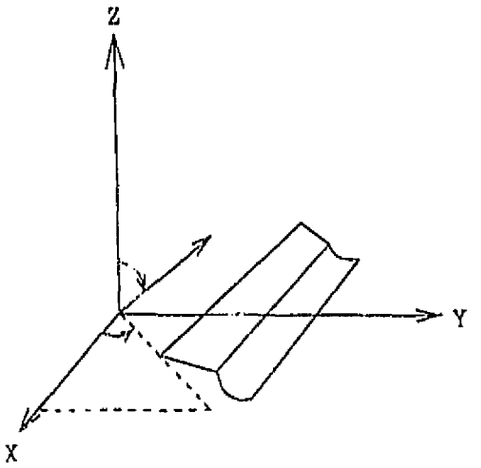

Fig.9 Similar translation method

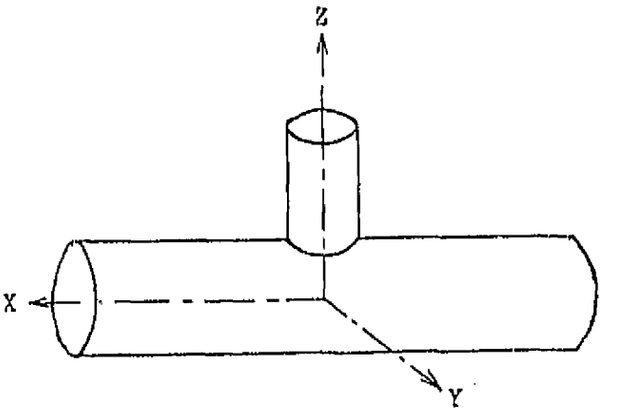

Fig.10 Orthogonally branched pipe method

Code	1000	2000	2100	2200	2300
Pattern					
Code	2400	2500	2600	2700	2800
Pattern					
Code	2900	3000	3100	3200	3300
Pattern					

Fig.11 Mesh Pattern and Code

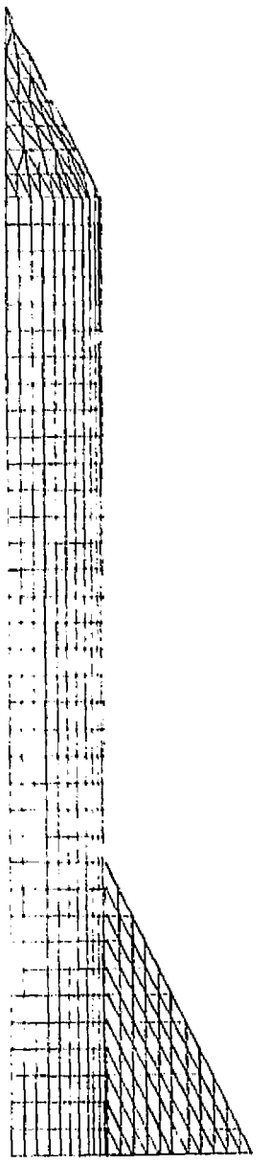

Fig.12 Example 1

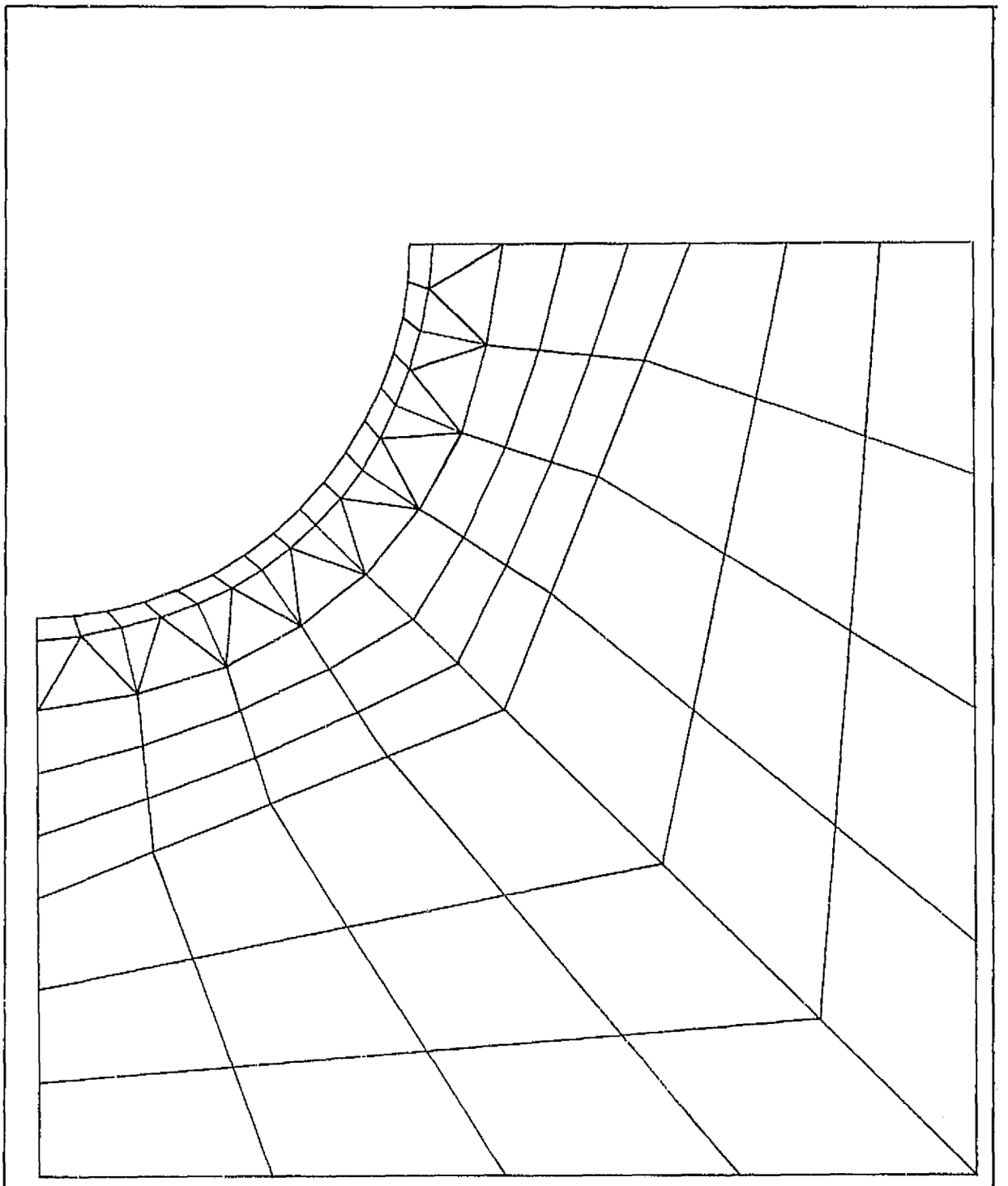

Fig.17 Example 2 A quarter holed plate

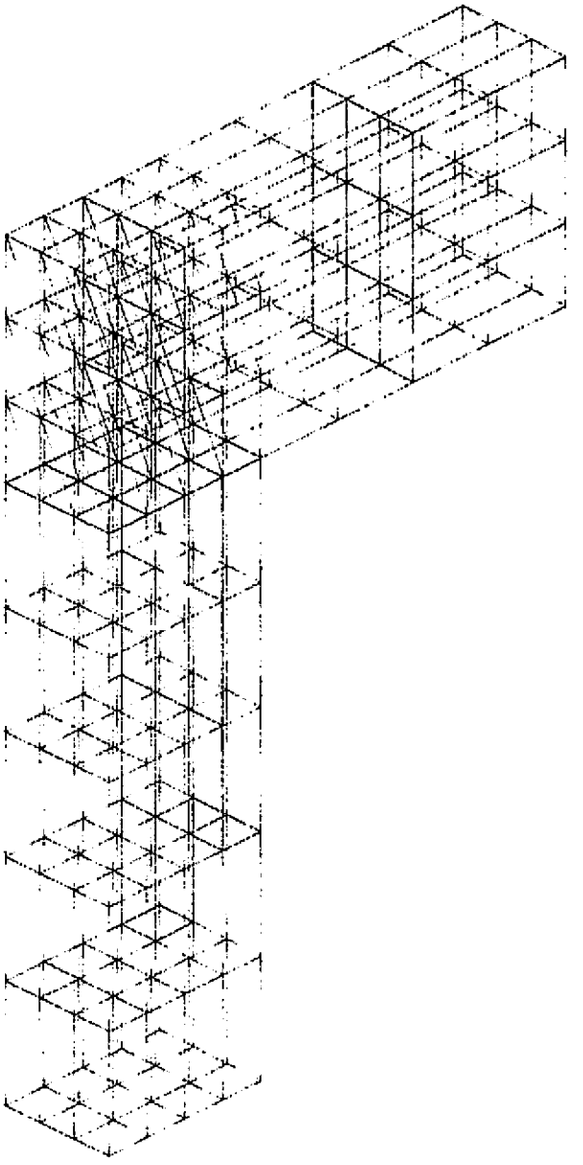

Fig.14 Example 3

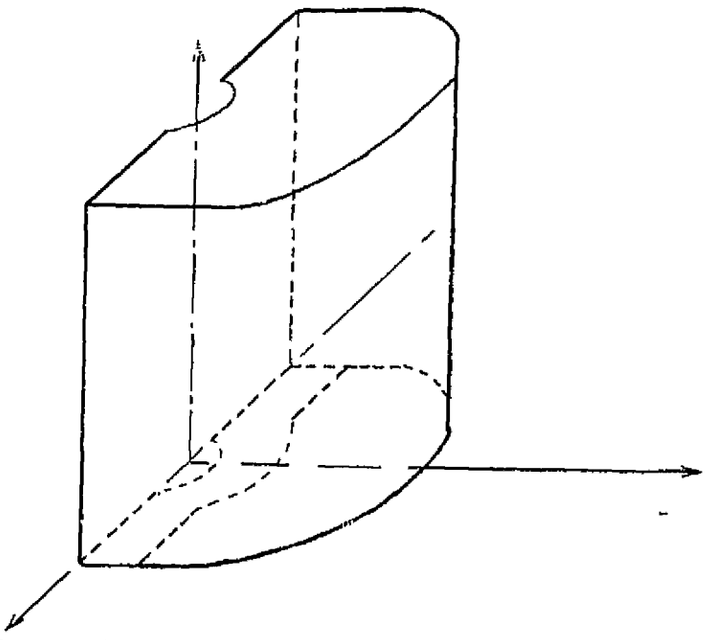

Fig.15 Example 4,A solid column

```
*****                    I N P U T  D A T A  L I S T                    *****

(CARD NO )     .....1.....2.....3.....4.....5.....6.....7.....8.....9.....0

(    1)     TITLE   MODEL(6)
(    2)     CONTROL NONE    1
(    3)     BLOCK   D       R
(    4)     POINT   1       0.0             400.0
(    5)     POINT   2       0.0             100.0
(    6)     POINT   3       100.0           0.0
(    7)     POINT   4       0.0             -100.0
(    8)     POINT   5       0.0             -400.0
(    9)     POINT   6       150.0           400.0
(   10)     POINT   7       150.0           200.0
(   11)     POINT   8       250.0           0.0
(   12)     POINT   9       150.0           -200.0
(   13)     POINT   10      150.0           -400.0
(   14)     POINT   11      300.0           400.0
(   15)     POINT   12      640.0           0.0
(   16)     POINT   13      300.0           -400.0
(   17)     LINEAR  1                       1       2
(   18)     ARC     2                       2       3       4
(   19)     LINEAR  3                       4       5
(   20)     ARC     4                       11      12      13
(   21)     LINEAR  5                       6       7
(   22)     ARC     6                       7       8       9
(   23)     LINEAR  7                       9       10
(   24)     PART    100     CLPL    3000    3       8       5
(   25)             HEXA1   1       1                               1000.0
(   26)     LINE    4       8
(   27)     LINE    1       2       2       4       3       2
(   28)     LINE    5       2       6       4       7       2
(   29)     AUTOMESH100
(   30)     COMBINE MODEL06 1       0.1
(   31)     PRINT
(   32)     PLOT    ORTH    A3      2
(   33)             60.0    30.0    0.0
```

Fig.16 Input data of Example 4

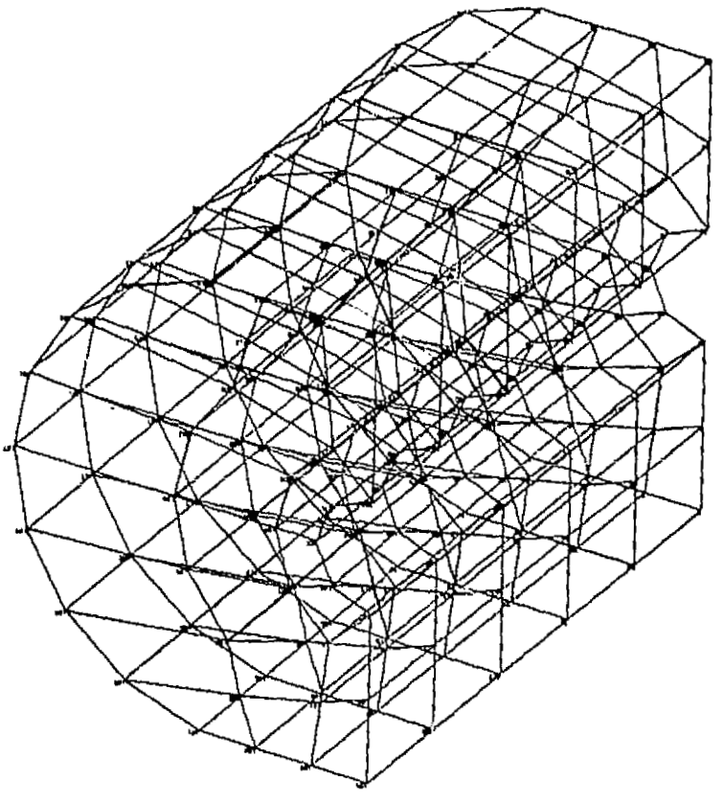

Fig.17 Result of Example 4

D11

NASTRAN IMPLEMENTATION OF AN ISOPARAMETRIC DOUBLY-CURVED QUADRILATERAL SHELL ELEMENT

By

A. B. Potvin and R. D. Leick
Exxon Production Research Company; Houston, Texas

SUMMARY

A quadrilateral shell element, CQUAD4*, has been added to level 15.5 and subsequently to level 16.0 of NASTRAN. The element exhibits doubly-curved surfaces and uses bi-quadratic interpolation functions. Reduced integration techniques are used to improve the performance of the element in thin-shell problems. Several details of previous authors' (ref. 1) work are clarified with respect to the present NASTRAN implementation. The creation of several new bulk data items is discussed along with a special module, GPNORM, to process SHLNORM bulk data cards. In addition to the theoretical basis for the element stiffness matrix, consistent mass and load matrices are presented.

Several potential sources of degenerate behavior of the element are investigated. Guidelines for proper use of the element are suggested. Performance of the element on several widely-published classical examples is demonstrated. The results show a significant improvement over presently available NASTRAN shell elements for even the coarsest meshes. Potential applications to two classes of practical problems are discussed.

INTRODUCTION

Until recently, only the CQUAD2 and its analog CTRIA2 were available in NASTRAN for analyzing shells of arbitrary geometry. Compared to current shell element technology, these elements are subject to the following limitations:

- o Faceted (flat) surface geometry is poorly adapted to model curved shapes.

* After the initial implementation of the new element was completed, the authors became aware of a similar proprietary element under development by the MacNeal-Schwendler Corporation which used the name CQUAD4. The reader should take care not to confuse these two identically named elements, since it is our understanding that the formulation and performance are quite different.

- Lower order polynomials used in membrane formulation cause element to be excessively stiff for in-plane deformation.

- While the enforced linear variation of the normal slope along the sides of the element guarantees interelement compatibility, it causes the bending behavior of the element to be quite stiff as well.

- In problems exhibiting thick shell and/or three-dimensional behavior over certain regions, the CQUAD2 element is an inadequate model and is difficult to interface with three dimensional elements.

To alleviate these problems development work on the present (CQUAD4) element was begun with the intention of implementing it in NASTRAN Level 15.5. The efforts were partially successful but full implementation was not achieved until NASTRAN Level 16.0 became available last year. The choice of the element was primarily influenced by the need to accurately represent curved surfaces as well as thick shell/3-D behavior. Such extremely accurate elements as Cowper's (ref. 2) and Dupuis' (ref. 3) were rejected due to the present authors' preference to adhere to the standard six degrees of freedom (dof) preferred by the majority of the user community. Although the theoretical development has often been presented elsewhere (refs. 1, 4, 5, 6, 7, and 8), we choose to repeat enough of the development to clarify certain issues which caused difficulty in the present implementation.

SYMBOLS (Scalars)

Values are given in both SI and U.S. Customary Units. The measurements and calculations were made in U.S. Customary Units.

a, b	Plate edge dimensions
D	Shell flexural rigidity $[Et^3/12(1-\nu^2)]$
E	Elastic modulus
g_{1i}, g_{2i}, g_{3i}, h_{3i}	Components of interpolation derivative arrays
k	Shear correction factor
L	Structure length dimension
$N_i(\xi, \eta, \zeta)$	Interpolation function for node i
p	Constant pressure load on element
P	Concentrated load magnitude
q	Displacement value
R	Mean (midsurface) radius
t_i	Thickness at node i
u, v, w	Translational displacements at a point in basic coordinate system
u', v', w'	Translational displacements at a point in local coordinate system
u_i, v_i, w_i	Translational displacements at node i
v_{1x}^i, v_{1y}^i, v_{1z}^i	Components of unit vector defining local x axis at node i
v_{2x}^i, v_{2y}^i, v_{2z}^i	Components of unit vector defining local y axis at node i
V_{3x}^i, V_{3y}^i, V_{3z}^i	Components of the shell normal at node i

x, y, z	Basic cartesian coordinate variables
x', y', z'	Local cartesian coordinate variables
x_i, y_i, z_i	Basic cartesian coordinates at node i
α_i, β_i	Rotational displacements at node i
$\gamma_{x'y'}, \gamma_{x'z'}, \gamma_{y'z'}$	Shearing strain components in local coordinate system
$\varepsilon_{x'x'}, \varepsilon_{y'y'}, \varepsilon_{z'z'}$	Direct strain components in local coordinate system
ν	Poisson's ratio
ω	Natural frequency of structure
ξ, η, ζ	Curvilinear coordinate variables
ξ_i, η_i, ζ_i	Curvilinear coordinate at node i
$\sigma_{x'x'}, \sigma_{y'y'}, \sigma_{z'z'}$	Direct stress components in local coordinate system
$\tau_{x'y'}, \tau_{x'z'}, \tau_{y'z'}$	Shearing stress components in local coordinate system
ϕ_{ij}	Component of transformation matrix
ρ	Mass density per unit volume

SYMBOLS (Matrices and Vectors)

[ALPHAT]	Diagonal matrix of nodal thicknesses times local x rotation
[BETAT]	Diagonal matrix of nodal thicknesses times local y rotation
[B']	Strain-displacement relation referenced to local coordinates
$[B_i']$	Strain-displacement relation pertaining to node i
[DELTAT]	Array of translational displacements at nodes
[D']	Constitutive relation in local coordinate system
$\vec{F}$	Consistent load vector for element
$[G_i]$	Derivative array transformed to local coordinates
$[H_i]$	Derivative array transformed to local coordinates pertaining to $\partial/\partial\zeta$ operator
[J]	Jacobian matrix relating (x, y, z) and (ξ, η, ζ) systems
[K]	Element stiffness matrix referenced to basic coordinates
[M]	Element mass matrix referenced to basic coordinates
$\vec{n}$	Third row of Jacobian - Interpolated value of nodal normals
$\vec{N}$	Vector of nodal interpolation functions
$[\bar{N}]$	Array of nodal interpolation functions
$\vec{s}$	First row of Jacobian - vector tangent to surface ζ = const
$\vec{t}$	Second row of Jacobian - vector tangent to surface ζ = const
$\vec{v}_s$	Unit vector tangent to surface ζ = const, defining local x' axis
$\vec{v}_t$	Unit vector tangent to surface ζ = const, defining local y' axis
$\vec{v}_n$	Unit vector normal to surface ζ = const, defining local z' axis
$\vec{v}_{1i}$, $\vec{v}_{2i}$, $\vec{v}_{3i}$	Unit vectors defining local tangent coordinates at node i

$\vec{V}_1, \vec{V}_2, \vec{V}_3$	Vectors defining the coordinate system for nodal rotations
[V1TAN]	Array of local x direction vectors at nodes
[V2TAN]	Array of local y direction vectors at nodes
[V3NORM]	Array of shell normals at nodes
[XCOORD]	Array of nodal coordinates
$\vec{\delta}_i$	Displacement dof at node i
$\vec{\delta}$	Collection of nodal displacement vectors
$\vec{\varepsilon}'$	Strain components in local coordinates
$[\theta]$	Local/global transformation matrix (direction cosines)
$\vec{\sigma}'$	Stress components in local coordinates
$[\phi]$	Transformation from (x', y', z') system to (ξ, η, ζ) system
$[\Omega]$	Differential operator matrix for computing strains

THE STIFFNESS MATRIX

Basic Assumptions

Figure 1 shows the geometry of a typical element. The curvilinear coordinate system (ξ, η, ζ) is used where ξ and η lie in the middle surface of the element while ζ is directed through the thickness. Each of these coordinates is allowed to vary from -1 to +1 on opposite faces of the element. We adopt the customary assumption of shell theory that the strain component ($\varepsilon_{z'z'}$) in the thickness direction is neglected compared to the other strains. The input items describing the element geometry include the basic coordinates at each of the eight mid-surface nodes (GRID cards) plus the vectors normal to that surface at each node (SHLNORM cards). The length of each normal vector is taken to be the thickness at that node. The thickness is interpolated quadratically over the element. At present only homogeneous, isotropic, materials (MAT1 cards) are allowed. The element is not available for heat transfer problems nor are thermal load vectors calculated.

Interpolation Functions

The nodal coordinates are related to the basic coordinates by the equation:

$$\begin{Bmatrix} x \\ y \\ z \end{Bmatrix} = [\text{XCOORD}] \cdot \vec{N} + \frac{\zeta}{2} \cdot [\text{V3NORM}] \cdot \vec{N} \qquad (1)$$

where

$$[\text{XCOORD}] = \begin{bmatrix} x_1 & x_2 & \cdots & x_8 \\ y_1 & y_2 & \cdots & y_8 \\ z_1 & z_2 & \cdots & z_8 \end{bmatrix}$$

$$[\text{V3NORM}] = \begin{bmatrix} v_{3x}^1 & v_{3x}^2 & \cdots & v_{3x}^8 \\ v_{3y}^1 & v_{3y}^2 & \cdots & v_{3y}^8 \\ v_{3z}^1 & v_{3z}^2 & \cdots & v_{3z}^8 \end{bmatrix}$$

$$\vec{N} = \langle N_1 \quad N_2 \quad \cdots \quad N_8 \rangle^T$$

Details of the biquadratic interpolation functions (Ni) and their derivatives are given in Appendix A.

The translational displacements are chosen as u, v, and w in the x, y, and z directions respectively. Two rotations, α_i and β_i, are defined about the local axes, $\vec{v}_{1i}$ and $\vec{v}_{2i}$, tangent to the mid-surface at each node (i). The choice of these two local axes is discussed in Appendix B.

We may relate the nodal displacements to the continuous displacement representation in a manner analagous to equation (1).

$$\begin{Bmatrix} u \\ v \\ w \end{Bmatrix} = [DELTAT] \cdot \vec{N} + \frac{\zeta}{2} \cdot [V1TAN] \cdot [ALPHAT] \cdot \vec{N} - \frac{\zeta}{2} \cdot [V2TAN] \cdot [BETAT] \cdot \vec{N} \quad (2)$$

where

$$[DELTAT] = \begin{bmatrix} u_1 & u_2 & \cdots & u_8 \\ v_1 & v_2 & \cdots & v_8 \\ w_1 & w_2 & \cdots & w_8 \end{bmatrix}$$

$$[V1TAN] = \begin{bmatrix} v^1_{1x} & v^2_{1x} & \cdots & v^8_{1x} \\ v^1_{1y} & v^2_{1y} & \cdots & v^8_{1y} \\ v^1_{1z} & v^2_{1z} & \cdots & v^8_{1z} \end{bmatrix}$$

$$[V2TAN] = \begin{bmatrix} v^1_{2x} & v^2_{2x} & \cdots & v^8_{2x} \\ v^1_{2y} & v^2_{2y} & \cdots & v^8_{2y} \\ v^1_{2z} & v^2_{2z} & \cdots & v^8_{2z} \end{bmatrix}$$

$$[ALPHAT] = \begin{bmatrix} \alpha_1 t_1 & 0 & \cdots & 0 \\ 0 & \alpha_2 t_2 & \cdots & 0 \\ \vdots & \vdots & & \vdots \\ 0 & 0 & \cdots & \alpha_8 t_8 \end{bmatrix}$$

$$[BETAT] = \begin{bmatrix} \beta_1 t_1 & 0 & \cdots & 0 \\ 0 & \beta_2 t_2 & \cdots & 0 \\ \vdots & \vdots & & \vdots \\ 0 & 0 & \cdots & \beta_8 t_8 \end{bmatrix}$$

Coordinate Transformations

The relation between the curvilinear coordinates (ξ, η, ζ) and the basic coordinates (x, y, z) is commonly called the Jacobian, [J], defined as:

$$[J] = \begin{bmatrix} \partial x/\partial\xi & \partial y/\partial\xi & \partial z/\partial\xi \\ \partial x/\partial\eta & \partial y/\partial\eta & \partial z/\partial\eta \\ \partial x/\partial\zeta & \partial y/\partial\zeta & \partial z/\partial\zeta \end{bmatrix} = \begin{Bmatrix} \vec{s}^T \\ \vec{t}^T \\ \vec{n}^T \end{Bmatrix} \qquad (3)$$

Using equation (1) we can write out these expressions as:

$$\vec{s} = \begin{Bmatrix} \partial x/\partial\xi \\ \partial y/\partial\xi \\ \partial z/\partial\xi \end{Bmatrix} = [XCOORD] \cdot \partial\vec{N}/\partial\xi + \frac{\zeta}{2} \cdot [V3NORM] \cdot \partial\vec{N}/\partial\xi \qquad (4)$$

$$\vec{t} = \begin{Bmatrix} \partial x/\partial\eta \\ \partial y/\partial\eta \\ \partial z/\partial\eta \end{Bmatrix} = [XCOORD] \cdot \partial\vec{N}/\partial\eta + \frac{\zeta}{2} \cdot [V3NORM] \cdot \partial\vec{N}/\partial\eta \qquad (5)$$

$$\vec{n} = \begin{Bmatrix} \partial x/\partial\zeta \\ \partial y/\partial\zeta \\ \partial z/\partial\zeta \end{Bmatrix} = \frac{1}{2} \cdot [V3NORM] \cdot \vec{N} \qquad (6)$$

where $\partial\vec{N}/\partial\xi = < \partial N_1/\partial\xi \quad \partial N_2/\partial\xi \quad \ldots \quad \partial N_8/\partial\xi >^T$

$\partial\vec{N}/\partial\eta = < \partial N_1/\partial\eta \quad \partial N_2/\partial\eta \quad \ldots \quad \partial N_8/\partial\eta >^T$

The explicit forms of $\partial Ni/\partial\xi$ and $\partial Ni/\partial\eta$ are given in Appendix A. Physically the $\vec{s}$ and $\vec{t}$ vectors may be considered tangent to the surface ζ = constant, while the $\vec{n}$ vector is merely the interpolated value of the node normals and may not be exactly normal to that surface at the position (ξ, η, ζ).

Perhaps the most confusing point of the cited references is the use of still another local coordinate system for definition of the stresses and strains. The need for this additional (x', y', z') system arises from the definition of the basic shell assumptions (particularly the neglect of the through-the-thickness direct strain, $\varepsilon_{z'z'}$). We wish to define, at any point in the element, a local (z') axis which is normal to the surface ζ = constant along with two other orthogonal axes (x', y') which are tangent to that surface. Since we have previously determined that $\vec{s}$ and $\vec{t}$ are tangents to the surface, we can determine a normal vector as:

$$\vec{V}_n = \vec{s} \times \vec{t} \tag{7}$$

and

$$\vec{v}_n = \vec{V}_n / |\vec{V}_n| \tag{8}$$

The other two unit vectors defining the local axes ($\vec{v}_s$ and $\vec{v}_t$) are computed in a manner analagous to that given in Appendix B. Thus, x' is measured along the $\vec{v}_s$ vector, y' is measured along the $\vec{v}_t$ vector, and z' is measured along the $\vec{v}_n$ vector. We can define the transformation [θ] as:

$$[\theta] = [\vec{v}_s \quad \vec{v}_t \quad \vec{v}_n] \tag{9}$$

So

$$\begin{Bmatrix} x \\ y \\ z \end{Bmatrix} = [\theta] \begin{Bmatrix} x' \\ y' \\ z' \end{Bmatrix} \tag{10}$$

and

$$\begin{Bmatrix} u \\ v \\ w \end{Bmatrix} = [\theta] \begin{Bmatrix} u' \\ v' \\ w' \end{Bmatrix} \tag{11}$$

The Strain-Displacement Relation

Using the newly developed local system and noting that $\varepsilon_{z'z'}$ is neglected, we write the basic definition:

$$\vec{\varepsilon}' = \begin{Bmatrix} \varepsilon_{x'x'} \\ \varepsilon_{y'y'} \\ \gamma_{x'y'} \\ \gamma_{x'z'} \\ \gamma_{y'z'} \end{Bmatrix} = \begin{bmatrix} \partial/\partial x' & 0 & 0 \\ 0 & \partial/\partial y' & 0 \\ \partial/\partial y' & \partial/\partial x' & 0 \\ \partial/\partial z' & 0 & \partial/\partial x' \\ 0 & \partial/\partial z' & \partial/\partial y' \end{bmatrix} \begin{Bmatrix} u' \\ v' \\ w' \end{Bmatrix} \tag{12}$$

We make use of equations (10) and (3) to develop the relation

$$\begin{Bmatrix} \partial/\partial x' \\ \partial/\partial y' \\ \partial/\partial z' \end{Bmatrix} = [\theta]^{-1} \begin{Bmatrix} \partial/\partial x \\ \partial/\partial y \\ \partial/\partial z \end{Bmatrix} = [\theta]^{-1} [J]^{-1} \begin{Bmatrix} \partial/\partial \xi \\ \partial/\partial \eta \\ \partial/\partial \zeta \end{Bmatrix} \qquad (13)$$

Define

$$[\phi] = [\theta]^{T} [J]^{-1} \qquad (14)$$

Where $[\theta]^{-1}$ is equal to $[\theta]^{T}$, since $[\theta]$ is defined to be an orthonormal matrix. Then $[\phi]$ will have the form:

$$\begin{bmatrix} \phi_{11} & \phi_{12} & 0 \\ \phi_{21} & \phi_{22} & 0 \\ \phi_{31} & \phi_{32} & \phi_{33} \end{bmatrix} \qquad (15)$$

A complete derivation of the terms in $[\phi]$ is given in Appendix C. However, $[J]^{-1}$ is best evaluated numerically at each integration point and cannot be written out explicitly. We combine equations (13), (14), and (15) with (12) to arrive at:

$$\vec{\varepsilon}' = \begin{bmatrix} \phi_{11}\,\partial/\partial\xi + \phi_{12}\,\partial/\partial\eta & 0 & 0 \\ 0 & \phi_{21}\,\partial/\partial\xi + \phi_{22}\,\partial/\partial\eta & 0 \\ \phi_{21}\,\partial/\partial\xi + \phi_{22}\,\partial/\partial\eta & \phi_{11}\,\partial/\partial\xi + \phi_{12}\,\partial/\partial\eta & 0 \\ \phi_{31}\,\partial/\partial\xi + \phi_{32}\,\partial/\partial\eta + \phi_{33}\,\partial/\partial\zeta & 0 & \phi_{11}\,\partial/\partial\xi + \phi_{12}\,\partial/\partial\eta \\ 0 & \phi_{31}\,\partial/\partial\xi + \phi_{32}\,\partial/\partial\eta + \phi_{33}\,\partial/\partial\zeta & \phi_{21}\,\partial/\partial\xi + \phi_{22}\,\partial/\partial\eta \end{bmatrix} \begin{Bmatrix} u' \\ v' \\ w' \end{Bmatrix}$$

$$= [\Omega] \begin{Bmatrix} u' \\ v' \\ w' \end{Bmatrix} \qquad (16)$$

Finally we use (11) along with (2) to substitute the appropriate expression for the displacements $< u' \quad v' \quad w' >$

$$\vec{\varepsilon}' = [\Omega]\,[\theta]^{T}[DELTAT] \cdot \vec{N} + [\Omega] \cdot [\theta]^{T} \cdot [V1TAN] \cdot [ALPHAT] \cdot \vec{N} \cdot \frac{\zeta}{2}$$

$$- [\Omega] \cdot [\theta]^{T} \cdot [V2TAN] \cdot [BETAT] \cdot \vec{N} \cdot \frac{\zeta}{2} \qquad (17)$$

By carrying out the indicated operations to allow the differential operator [Ω] to appropriately interact with ζ and $\vec{N}$ and by rearranging terms, we arrive at the relation:

$$\vec{\varepsilon}' = [B'] \vec{\delta} \tag{18}$$

where $\vec{\delta} = < \vec{\delta}_1 \quad \vec{\delta}_2 \quad . \; . \; . \quad \vec{\delta}_8 >^T$

and $\vec{\delta}_i = < u_i \quad v_i \quad w_i \quad \alpha_i \quad \beta_i >^T$

The explicit form of [B'] is shown in Appendix D.

The Stress-Strain Relation

Again referring to the primed local coordinates, the constitutive law is:

$$\vec{\sigma}' = [D'] \vec{\varepsilon}' \tag{19}$$

where $\vec{\sigma}' = < \sigma_{x'x'} \quad \sigma_{y'y'} \quad \tau_{x'y'} \quad \tau_{x'z'} \quad \tau_{y'z'} >^T$

and (for a homogeneous isotropic material):

$$[D'] = \frac{E}{1-\nu^2} \begin{bmatrix} 1 & \nu & 0 & 0 & 0 \\ \nu & 1 & 0 & 0 & 0 \\ 0 & 0 & \frac{1-\nu}{2} & 0 & 0 \\ 0 & 0 & 0 & \frac{1-\nu}{2k} & 0 \\ 0 & 0 & 0 & 0 & \frac{1-\nu}{2k} \end{bmatrix} \tag{20}$$

Here k is used to improve the shear representation. The displacement assumption causes the shear to be constant through the thickness, whereas the proper distribution is closer to parabolic. The ratio of the strain energies of the two distributions (parabolic/constant) is 1.2 which is substituted for k.

The Element Stiffness Matrix (Subroutine KQUAD4)

The standard virtual work arguments lead to the stiffness computation as follows:

$$[K] = \int_{Vol} [B']^T [D'] [B'] \; dVol \tag{21}$$

The usual volumetric measure is dx dy dz. Here the variables of integration are ξ, η, and ζ. The conversion of the cartesian volume to the curvilinear volume is via the Jacobian. Thus,

$$dVol = dx\ dy\ dz = \det [J]\ d\xi\ d\eta\ d\zeta \tag{22}$$

$$\text{So} \qquad [K] = \int_{-1}^{1}\int_{-1}^{1}\int_{-1}^{1} [B']^T [D'] [B'] \det [J]\ d\xi\ d\eta\ d\zeta \tag{23}$$

The integration is carried out numerically using two Gauss points in each direction. While capable of properly integrating the element's volume, this "reduced" integration is not sufficient to exactly evaluate the complex polynomials produced by equation (23). This implies that, while ultimate convergence is assured, the behavior will not be either bounded or monotonic. However, several authors (ref. 4 and 9) have shown that, by purposely underestimating the energy, the performance of the element is enhanced. By taking [J] and [0] to be invariant through the thickness, it is possible to explicitly carry out the integration in ζ. We choose not to do so, however, in order to ensure complete generality of the formulation for both thin and thick shell cases.

Stress Recovery (Subroutines SQUD41 and SQUD42)

Once the elements are assembled and the system equations solved for the displacements, the user needs to know the element stresses as well. Combining equations (18) and (19) with $\vec{\delta}$ now known, we obtain:

$$\vec{\sigma}' = [D'] [B'] \vec{\delta} \tag{24}$$

Recall however that, in general, [B'] is a function of the curvilinear coordinates (ξ, η, ζ). $\vec{\sigma}'$ is therefore also a function of these coordinates, so we must choose which points we will use for stress evaluation. It is known that the numerical integration points are the best "samples" of the overall element stress field. Unfortunately the values of $\zeta = \pm 0.57735$ do not give the maximum stresses through the thickness if bending is present. We have compromised to select the eight points given by $\xi = \pm 0.57735$; $\eta = \pm 0.57735$, and $\zeta = \pm 1.0$ to allow evaluation of the stresses at the top and bottom surfaces of the element (c.f. diagram in Appendix A). Since the values of $\sigma_{x'x'}$, $\sigma_{y'y'}$ and $\tau_{x'y'}$* are evaluated in the (x', y', z') local system, the stress directions may not be meaningful to the user. Consequently, the principal stresses (σ_1, σ_2, and τ_{max}) are also calculated and form the additional portion of each line of output.

THE CONSISTENT MASS MATRIX (Subroutine MCQUD4)

For simplicity we will neglect the rotational inertias associated with the α and β degrees of freedom. This assumption is particularly

*Notice that $\tau_{x'z'}$ and $\tau_{y'z'}$ are zero on the top and bottom surfaces.

appropriate for thin and moderately thick shells. It allows us to reference everything to the mid-surface ($\zeta = 0$). In particular:

$$[M] = \int_{Vol} \rho\, [\bar{N}]^T\, [\bar{N}]\, dVol \tag{25}$$

Choosing ρ = constant and making use of the above assumption (i.e. $\int_{-1}^{1} d\zeta \equiv t$)

$$[M] = \rho \int_{A} t\, [\bar{N}]^T\, [\bar{N}]\, dA \tag{26}$$

where
$$[\bar{N}] = \left[\begin{array}{ccc:ccc:c:ccc} N_1 & 0 & 0 & N_2 & 0 & 0 & & N_8 & 0 & 0 \\ 0 & N_1 & 0 & 0 & N_2 & 0 & \cdots & 0 & N_8 & 0 \\ 0 & 0 & N_1 & 0 & 0 & N_2 & & 0 & 0 & N_8 \end{array}\right]$$

In general ρ may be allowed to vary quadratically over the element in a manner similar to the thickness. This feature is not required for most cases of interest.

Since $\zeta = 0$ on the midsurface, we must resort to the device of computing the unit area in curvilinear coordinates as (using equations (4) and (5)):

$$dA = dx\, dy = |\vec{s} \times \vec{t}|\, d\xi\, d\eta \tag{26}$$

where $|\vec{s} \times \vec{t}|$ may be interpreted as the projection on the normal vector $\vec{v}_n$ of the normal vector associated with infinitesimal area, $dx \cdot dy$. Thus,

$$[M] = \rho \int_{-1}^{1} \int_{-1}^{1} t\, [\bar{N}]^T\, [\bar{N}]\, |\vec{v}_n|\, d\xi\, d\eta \tag{27}$$

In this case the full three-point Gauss integration must be used to properly evaluate the expression.

THE CONSISTENT LOAD VECTOR (Subroutines PLOAD4 and PWORK)

We derive the expression for a constant pressure (p) normal to the mid-surface of the element. As before, a quadratic variation of the pressure would cause no inherent difficulties. The development is entirely analagous to that used for the consistent mass matrix. Thus,

$$\vec{F} = p \int_{-1}^{1} \int_{-1}^{1} [\bar{N}]^T \vec{v}_n \, d\xi \, d\eta \qquad (28)$$

Again, the three-point Gauss rule is used to evaluate the expression.

SPECIAL NASTRAN CONSIDERATIONS

New Bulk Data Cards

Three new Bulk Data cards have been added to NASTRAN in conjunction with the new element. They are:

CQUAD4 - describing the element connectivity
PLOAD4 - specifying the elements to which constant pressure (p) is applied at the mid-surface
SHLNORM - inputting the direction vector of the normal to the shell surface at each grid point.

A complete description of each of these items is found in Appendix E.

Module to Process Shell Normals*

A new module, GPNORM, has been coded which converts the "external" grid point ID's on a SHLNORM card to the appropriate internal SIL's. The module also transforms the normal vector into the basic coordinate system for the problem and writes the results on the output data block SHLNRM. The DMAP calling sequence for the module is:

```
GPNORM    GEOM1,EQEXIN,BGPDT,CSTM / SHLNRM $
```

GPNORM must be added to the DMAP rigid format immediately prior to the TA1 module. SHLNRM must be added as the final input data block of TA1.

Augmented ECPT and EST Data Blocks*

The make up of the EST (and by analogy the ECPT) for the CQUAD4 element follows the standard format for the first 43 words.

Word	Contents
1	Element ID
2	Material ID
3-10	8 Grid Point SIL's
11-42	8 sets of Grid Point CSID's plus basic x, y, z coordinates
43	Element Temperature

*The idea to use GPNORM to process the shell normals as well as the technique for augmenting the ECPT and EST data blocks is credited to Miles Hurwitz of NSRDC.

The formulation of the element requires the components of the shell normals. These must be appended to the EST by subroutine TA1A.

44-67	8 sets of x, y, z components of the shell normals in basic coordinates

Subroutine TA1B performs a similar augmenting process for the ECPT data block.

VERIFICATION

Consider the limiting case of a square, simply supported flat plate* subjected to two load conditions, 1) a central load normal to the plate and 2) a uniform normal pressure. Figure 2 indicates that excellent convergence to the Timoshenko (ref. 10) result can be obtained with a 1 x 1 or at most a 2 x 2 grid. Note, however, that the usual bound theorems are not available with this particular element due to the use of reduced integration.

The next step in analytical complexity is represented by the problem portrayed in Figure 3, a pinched cylinder with free ends.* According to Timoshenko, the radial deflection at the point of application of the load, for the geometry given, should be -2.76 mm (-0.1087 in.). Timoshenko's result is based on an assumption of inextensional deformation which neglects the middle surface strain of the shell. The CQUAD4 element gives a slightly higher result of -2.89 mm (-0.1139 in.) for a 325 degree of freedom model of one-eighth of the cylinder. Cantin and Clough (ref. 11) predict a deflection of -2.87 mm (-0.1128 in.) using a cylindrical shell element model with 1200 degrees of freedom for one-eighth of the cylinder. Therefore, the CQUAD4 element, although not monotonic in convergence, does give excellent results for a minimum number of degrees of freedom.

An example problem which has become a classic for checking the response of shell-type elements is shown in Figure 4. The example is a cylindrical shell roof loaded by its own weight.* The ends of the shell are supported by diaphragms and the sides are free. It should be noted that two "exact" solutions have been quoted by various researchers. These two solutions may be attributed to Scordelis and Lo (ref. 12) and Cowper, Lindberg, and Olson (ref. 2).

Scordelis and Lo based their calculations on the theory of Gibson (ref. 13) essentially using shallow shell equations. Cowper, Lindberg, and Olson claimed that the shallow shell approximations were not used consistently when particular loadings were considered. They expanded the trigonometric representation of the load variation up to second order within each element by means of a Taylor Series. In addition

*When proper symmetry conditions are applied, only 1/4 or 1/8 of the entire structure need be modeled in each of these cases.

Cowper, et al. performed the integration of both the stiffness and load matrices over the area of the actual shell surface. Hence, the primary difference between the two "exact" solutions is the manner in which the consistent load matrices are formulated. The formulation of the present element follows more closely the method of Scordelis and Lo and hence will be compared to their "exact" solution.

Table 1 gives the computed displacements based on the grids defined in Figure 4. Note that excellent convergence is obtained. Figure 5 compares the predictions of the CQUAD4 element with the CQUAD2 element as well as slightly different formulations of the CQUAD4 element in the MARC (ref. 14) and SUPERB (ref. 15) finite element programs. Based on the results indicated in Figure 5 the CQUAD4 element is judged to be the most accurate.

To demonstrate the applicability of the CQUAD4 element in modeling dynamics problems, consider the rectangular cantilever plate vibration problem reported by Zienkiewicz (ref. 16) (see Figure 6). Compared in Figure 6 are test results by Plunkett (ref. 16) and finite element predictions based on a non-conforming triangle by Zienkiewicz and results from the CQUAD4 element. Note that even the two element idealization with the CQUAD4 element gives excellent results for the first four modes.

POTENTIAL SOURCES OF ELEMENT DEGENERACY

Three potential sources of element degeneracy were investigated. The first, non-rectangularity of the mesh, is illustrated in Figure 7. One quarter of a simply supported flat plate subjected to uniform pressure was modeled as shown with angular "offsets" or variations in the mesh rectangularity of up to 30°. As indicated in Figure 7 by the displacement prediction for the center of the plate, variations of up to 20° resulted in only 2% variation in deflection compared to the regular rectangular grid. The 30° variation resulted in a 7% difference. It would appear from these results that, for most applications, non-rectangularity will not have a significant effect on the results. However, care should be taken to maintain small angle variations of less than 30° as good practice.

The second potential source of degeneracy investigated was the shell thinness ratio, t/R. A pinched cylinder example was once again selected and the t/R ratio varied from 0.1 to 0.0001 as shown in Figure 8. By examining the product of the radial deflection at the point of load application and the flexural rigidity of the shell it is evident that no numerical instability exists even for very thin shells. Notice that for thicker shells (e.g. $t/R \geq 0.1$) Timoshenko's assumption of thin shell behavior is increasingly violated and some deviation of the finite element results from the classical solution is obtained.

The third potential source of element degeneracy to be investigated was similar to the mesh non-rectangularity of the flat plate problem. This example considers the event of a misalignment of the edges of the element with the directions of principal curvature in a shell idealization. Such a discretization may necessarily occur as a result of complex intersections of several shell elements. The pinched cylinder problem discussed previously was chosen as a simple limiting case. A 2 x 2 grid was selected for one-eighth of the cylinder and symmetry conditions were enforced. The element edges in the circumferential direction were allowed to vary from the direction of curvature as shown in Figure 9. The authors found that the radial deflection at the point of load application was virtually unaffected for the cases examined.

It may be concluded that, based upon the previously described investigations regarding element degeneracy which could possibly result from potential misuse, the CQUAD4 element appears to be exceptionally stable. Care should be used, however, in maintaining "relatively" rectangular element configurations.

APPLICATIONS

At least two potential sources of application for the CQUAD4 element exist in the offshore industry. Offshore drilling and production platforms are typically either a space frame of tubular members, commonly called a steel jacket structure, or a reinforced, prestressed concrete structure, commonly called a gravity structure. The welded intersections of tubular members in a steel jacket are called tubular joints and represent sources of potential fatigue problems due to high stress concentrations. The CQUAD4 element represents a significant increase in computational accuracy compared to the CQUAD2 element for conducting stress analyses of these tubular intersections.

The reasons for the improved accuracy are two-fold. The curved surface of the CQUAD4 element is its most obvious advantage. It was often necessary to use excessive CQUAD2 elements in otherwise coarse mesh regions of the joint model just to approximate the cylindrical geometry. An extremely important but less obvious advantage of the CQUAD4 element is its higher-order representation of the displacements, strains, and stresses, without having to expend any additional degrees of freedom. This advantage manifests itself in the degree of mesh refinement required to achieve a given level of accuracy. Whereas a FINE or EXTRA FINE mesh was required to achieve acceptable results using CQUAD2 elements (c.f. reference 17), a COARSE or MEDIUM mesh of CQUAD4 elements is sufficient. Such a typical mesh is shown in Figures 10 and 11 for a T-Joint and a K-Joint respectively. The mesh was automatically generated using the TKJOINT program described in reference (17). That program has recently been recoded to allow generation of the appropriate SHLNORM bulk data cards at each substructure grid point.

It should be pointed out that the CQUAD4 element does not specifically address the problem at the intersection line of the tubular members. Here the question is not whether the local behavior is more closely approximated by thin-shell or thick-shell theory, but how best to provide a transition to the three-dimensional state of stress which exists and how to include the weld geometry. Again the CQUAD4 element has an advantage over the CQUAD2 since it has been derived from a 20-node hexahedron. If a mesh of these 20-node elements is designed for the locality of the intersection, the transitional behavior between the CQUAD4 and the CIHEX2 should be smooth due to the compatibility of the basic interpolation functions. Unfortunately the transition between the two element types will still require a rather complex set of MPC's to be generated and this problem has not been adequately addressed at the time of publication.

The second source of potential application regards the structural modeling of the relatively thick shell cylinders and panels which comprise the base and towers of gravity structures (see Figure 12). Section A-A in Figure 12 illustrates the shell connections where the present element could be used. The individual cells are on the order of 20 meters in diameter and from 0.5 meters to 1.0 meters thick. The CQUAD2 element would be incapable of accurately modeling the structural behavior associated with this geometry. The CQUAD4 element provides the possibility of coupling with the CIHEX2 element to perform global stress analyses of these structures.

APPENDIX A

The biquadratic interpolation functions are well-known throughout the literature. They are repeated here along with their derivative forms only for the sake of completeness.

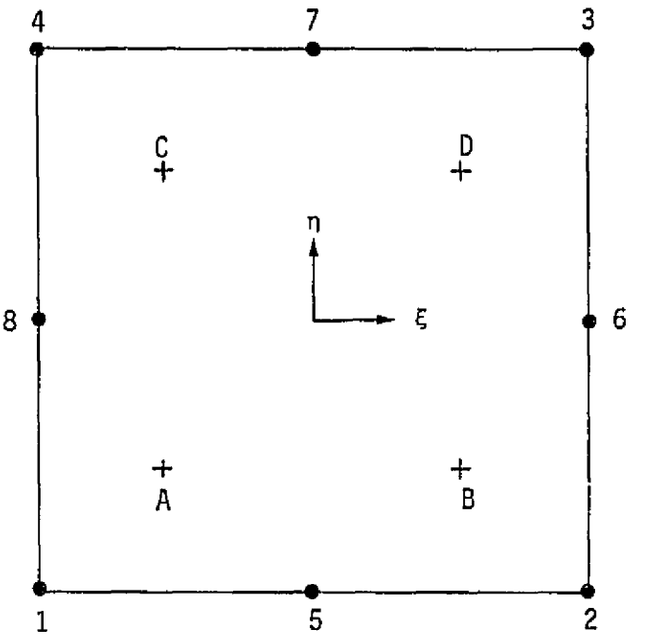

Node	ξ	η	ζ
1	-1	-1	0
2	1	-1	0
3	1	1	0
4	-1	1	0
5	0	-1	0
6	1	0	0
7	0	1	0
8	-1	0	0

Integration Point	ξ	η	ζ
A	-0.57735	-0.57735	±0.57735
B	0.57735	-0.57735	±0.57735
C	-0.57735	0.57735	±0.57735
D	0.57735	0.57735	±0.57735

Corner Nodes ($i = 1, 2, 3, 4$)

$$N_i = \frac{1}{4}(1 + \xi\xi_i)(1 + \eta\eta_i)(\xi\xi_i + \eta\eta_i - 1) \quad \text{(A-1)}$$

$$\partial N_i/\partial\xi = \frac{1}{4}\xi_i(1 + \eta\eta_i)(2\xi\xi_i + \eta\eta_i) \quad \text{(A-2)}$$

$$\partial N_i/\partial\eta = \frac{1}{4}\eta_i(1 + \xi\xi_i)(\xi\xi_i + 2\eta\eta_i) \quad \text{(A-3)}$$

Midside Nodes with $\xi_i = 0$ ($i = 5, 7$)

$$N_i = \frac{1}{2}(1 - \xi^2)(1 + \eta\eta_i) \quad \text{(A-4)}$$

$$\partial N_i/\partial\xi = -\xi(1 + \eta\eta_i) \quad \text{(A-5)}$$

$$\partial N_i/\partial\eta = \frac{1}{2}\eta_i(1 - \xi^2) \quad \text{(A-6)}$$

Midside Nodes with $\eta_i = 0$ ($i = 6, 8$)

$$N_i = \frac{1}{2}(1 + \xi\xi_i)(1 - \eta^2) \quad \text{(A-7)}$$

$$\partial N_i/\partial\xi = \frac{1}{2}\xi_i(1 - \eta^2) \quad \text{(A-8)}$$

$$\partial N_i/\partial\eta = -\eta(1 + \xi\xi_i) \quad \text{(A-9)}$$

APPENDIX B

At each node we are given the vector $\vec{V}_{3i}$ which is normal to the midsurface at that point. With reference to the basic (x, y, z) coordinate system, let $\hat{i}$ = (1 0 0) and $\hat{j}$ = (0 1 0). Choose $\vec{V}_{1i} = \hat{i} \times \vec{V}_{3i}$ which makes $\vec{V}_{1i}$ perpendicular to $\vec{V}_{3i}$ and the x axis. If $\vec{V}_{3i}$ is parallel to $\hat{i}$, then choose $\vec{V}_{1i} = \hat{j} \times \vec{V}_{3i}$ to remove the ambiguity. The third vector of the triad is then $\vec{V}_{2i} = \vec{V}_{3i} \times \vec{V}_{1i}$.

To compute the coordinate system transformation matrix, we normalize the components of each vector by its scalar length and form the set $[\vec{v}_{1i} \quad \vec{v}_{2i} \quad \vec{v}_{3i}]$ where

$$\vec{v}_{1i} = \vec{V}_{1i}/|\vec{V}_{1i}| \quad \text{etc.}$$

APPENDIX C

Equations (3-6) define the components of the Jacobian as:

$$[J] = \begin{Bmatrix} \vec{s}^T \\ \vec{t}^T \\ \vec{n}^T \end{Bmatrix} \tag{C-1}$$

The schematic form of the inverse may be written as:

$$[J]^{-1} = \frac{1}{\det [J]} [(\vec{t} \times \vec{n}) (\vec{n} \times \vec{s}) (\vec{s} \times \vec{t})] \tag{C-2}$$

Equations (7-9) define the local transform [θ] as

$$[\theta] = [\vec{v}_s \ \vec{v}_t \ \vec{v}_n] \tag{C-3}$$

where $\vec{v}_n$ was computed as the normal to the surface ζ = const by taking $\vec{s} \times \vec{t}/|\vec{s} \times \vec{t}|$ and $\vec{v}_s$ as well as $\vec{v}_t$ were defined to be perpendicular to $\vec{v}_n$. It is therefore clear that $\vec{v}_s$ and $\vec{v}_t$ will lie in the same plane as $\vec{s}$ and $\vec{t}$ but that $\vec{v}_n$ may not in general be considered parallel to $\vec{n}$.

Consider the computation of $[\phi] = [\theta]^T [J^{-1}]$

$$[\phi] = \frac{1}{\det [J]} \begin{Bmatrix} \vec{v}_s^T \\ \vec{v}_t^T \\ \vec{v}_n^T \end{Bmatrix} [(\vec{t} \times \vec{n}) (\vec{n} \times \vec{s}) (\vec{s} \times \vec{t})] \tag{C-4}$$

$$= \frac{1}{\det [J]} \begin{bmatrix} \vec{v}_s^T \cdot (\vec{t} \times \vec{n}) & \vec{v}_s^T \cdot (\vec{n} \times \vec{s}) & \vec{v}_s^T \cdot (\vec{s} \times \vec{t}) \\ \vec{v}_t^T \cdot (\vec{t} \times \vec{n}) & \vec{v}_t^T \cdot (\vec{n} \times \vec{s}) & \vec{v}_t^T \cdot (\vec{s} \times \vec{t}) \\ \vec{v}_n^T \cdot (\vec{t} \times \vec{n}) & \vec{v}_n^T \cdot (\vec{n} \times \vec{s}) & \vec{v}_n^T \cdot (\vec{s} \times \vec{t}) \end{bmatrix} \tag{C-5}$$

Now we know that $(\vec{s} \times \vec{t}) = \vec{v}_n = |\vec{v}_n| \cdot \vec{v}_n$. Therefore, since the dot product of perpendicular vectors is zero, we have $\vec{v}_s^T \cdot (\vec{s} \times \vec{t}) \equiv 0$. This completes the derivation of $[\phi]$. Notice that the terms ϕ_{31} and ϕ_{32} are not set to zero as was done in reference (4). The only time that these terms would be zero is when the vector $\vec{n}$ is exactly normal to the surface at the point (ξ, η, ζ). This event will only occur in the case of flat plates. The consequence of neglecting these two terms is to introduce an imbalance in the moment equilibrium of the shell (c.f. ref. 18).

APPENDIX D

We choose to divide the [B'] matrix into the following nodal partitions:

$$\vec{\varepsilon}' = [B_1' \quad B_2' \quad \ldots \quad B_8'] \begin{Bmatrix} \vec{\delta}_1 \\ \vec{\delta}_2 \\ \cdot \\ \cdot \\ \vec{\delta}_8 \end{Bmatrix} \tag{D-1}$$

We shall write out the expression for a typical partition $[B_i']$ by rearranging appropriate terms from equation (17):

$$[B_i'] = \left[[\Omega]\, N_i\, [\theta]^T + [\Omega]\, N_i\, \zeta\, \frac{t_i}{2}\, [\theta]^T \vec{v}_1{}^i \quad - [\Omega]\, N_i\, \zeta\, \frac{t_i}{2}\, [\theta]^T \vec{v}_2{}^i \right] \begin{Bmatrix} u_i \\ v_i \\ w_i \\ \alpha_i \\ \beta_i \end{Bmatrix} \tag{D-2}$$

Define

$$\begin{aligned} g_{1i} &= \phi_{11}\, \partial N_i/\partial\xi + \phi_{12}\, \partial N_i/\partial\eta \\ g_{2i} &= \phi_{21}\, \partial N_i/\partial\xi + \phi_{22}\, \partial N_i/\partial\eta \\ g_{3i} &= \phi_{31}\, \partial N_i/\partial\xi + \phi_{32}\, \partial N_i/\partial\eta \\ h_{3i} &= \phi_{33}\, N_i \end{aligned} \tag{D-3}$$

So

$$[G_i] = [\Omega]\, N_i = \begin{bmatrix} g_{1i} & 0 & 0 \\ 0 & g_{2i} & 0 \\ g_{2i} & g_{1i} & 0 \\ g_{3i} & 0 & g_{1i} \\ 0 & g_{3i} & g_{2i} \end{bmatrix} \tag{D-4}$$

and $[H_i] = \begin{bmatrix} 0 & 0 & 0 \\ 0 & 0 & 0 \\ 0 & 0 & 0 \\ h_{3i} & 0 & 0 \\ 0 & h_{3i} & 0 \end{bmatrix}$ (D-5)

Finally,

$$[B_i'] = [G_i]\,[\theta]^T + \frac{t_i}{2}\,(\zeta\,[G_i] + [H_i])\,[\theta]^T\,\vec{v}_1{}^i - \frac{t_i}{2}\,(\zeta\,[G_i] + [H_i])\,[\theta]^T\,\vec{v}_2{}^i$$

APPENDIX E

BULK DATA DECK

Input Data Card CQUAD4 Quadrilateral Element Connection

Description: Defines a homogeneous quadrilateral membrane and bending element (QUAD4) of the structural model.

Format and Example:

1	2	3	4	5	6	7	8	9	10
CQUAD4	EID	MID	G1	G2	G3	G4	G5	G6	abc
CQUAD4	72	13	13	14	15	16	21	22	ABC
+bc	G7	G8	TH						
+BC	23	24	29.2						

Field	Contents
EID	Element identification number (Integer > 0)
MID	Identification number of a MAT1 material card (Default is EID) (Integer > 0)
G1,G2,G3,G4 G5,G6,G7,G8	Grid point identification numbers of connection points (Integer > 0; G1 ≠ G2 ≠ G3 ≠ G4 ≠ G5 ≠ G6 ≠ G7 ≠ G8)
TH	Material property orientation angle in degrees (Real) The sketch below gives the sign convention for TH.

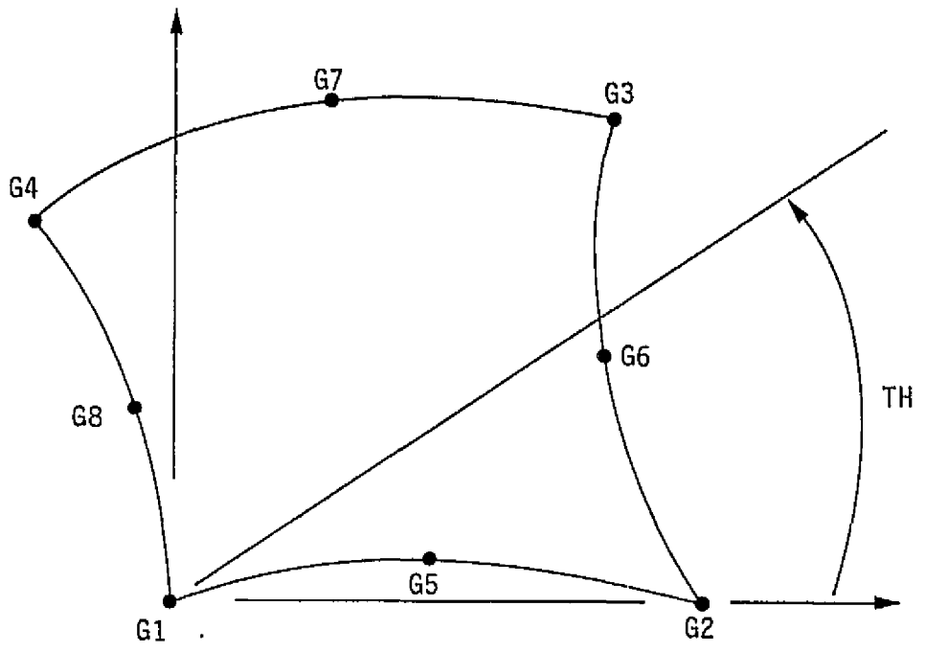

Remarks:

1. Element identification numbers must be unique with respect to all other element identification numbers.

2. Grid points G1 through G4 are corner nodes and must be ordered consecutively around the perimeter of the element in a counter clockwise direction. G5 through G8 are midside nodes and must have similar ordering where:

   G5 lies between G1 and G2
   G6 lies between G2 and G3
   G7 lies between G3 and G4
   G8 lies between G4 and G1

3. The continuation card must be present.

Input Data Card PLØAD4 Pressure Load

Description: Defines a uniform static pressure load applied to two-dimensional elements. Only QUAD4 elements may have a pressure load applied to them via this card.

Format and Example:

1	2	3	4	5	6	7	8	9	10
PLØAD4	SID	P	EID	EID	EID	EID	EID	EID	
PLØAD4	21	-3.6		4	16		2		

Alternate Form

PLØAD4	SID	P	EID1	"THRU"	EID2				
PLØAD4	1	30.4	16	THRU	48				

Field	Contents
SID	Load set identification number (Integer > 0)
P	Pressure value (Real), positive pressure value indicates pressure in the negative normal direction.
EID EID1 EID2	Element identification number (Integer > 0; EID1 < EID2)

Remarks:

1. EID must be 0 or blank for omitted entrys.
2. Load sets must be selected in the Case Control Deck (LØAD=SID) to be used by NASTRAN.
3. At least one positive EID must be present on each PLØAD4 card.
4. If the alternate form is used, all elements in the range EID1 through EID2 must be present.

5. The "work equivalent" load vector is computed for each element using the relation

$$\vec{F} = P \int_{-1}^{1} \int_{-1}^{1} [\bar{N}]^T \vec{v}_n \det [J] \, d\xi \, d\eta$$

6. All elements referenced must exist.

Input Data Card SHLNORM Shell Normal

Description: Defines the direction of a normal to the shell of the structural model.

Format and Example:

1	2	3	4	5	6	7	8	9	10
SHLNORM	ID	CP	X1	X2	X3				
SHLNORM	2	3	1.0	2.0	3.0				

Field	Contents
ID	Grid point identification number (0 < Integer < 999999) at which this normal is located.
CP	Identification number of coordinate system in which the shell normal is defined (Integer ≥ 0 or blank).
X1,X2,X3	Components of the shell normal in coordinate system CP (Real).

Remarks:

1. All grid point identification numbers must be unique with respect to all other structural, scalar, and fluid points.
2. The meaning of X1, X2 and X3 depend on the type of coordinate system, CP, as follows: (see CØRD ___ card descriptions).

Type	X1	X2	X3
Rectangular	X	Y	Z
Cylindrical	R	Θ(degrees)	Z
Spherical	R	Θ(degrees)	Φ(degrees)

REFERENCES

1. Ahmad, S., Irons, B. M. and Zienkiewicz, O. C., "Analysis of Thick and Thin Shell Structures by Curved Finite Elements", Int. J. Num. Meth. Engr., Vol. 2, pp. 419-451, 1970.

2. Cowper, G. R., Lindberg, G. M. and Olson, M. D., "A Shallow Shell Finite Element of Triangular Shape", Int. J. Solids Structures, Vol. 6, 1970, pp. 1133-1156.

3. Dupuis, G. and Goel, J. J., "A Curved Finite Element for Thin Elastic Shells", Brown University Engineering Report N00014-Q007/4, December, 1969.

4. Zienkiewicz, O. C., Taylor, R. L. and Too, J. M., "Reduced Integration Technique in General Analysis of Plates and Shells", Int. J. Num. Meth. Engr., Vol. 3, pp. 275-290, 1971.

5. Pawsey, S. F. and Clough, R. W., "Improved Numerical Integration of Thick Shell Finite Elements", Int. J. Num. Meth. Engr., Vol. 3, pp. 575-586, 1971.

6. Barsoum, R. S., "A Degenerate Solid Element for Linear Fracture Analysis of Plate Bending and General Shells", Int. J. Num. Meth. Engr., Vol. 10, pp. 551-564, 1976.

7. Wergeland, J. H., User's Manual for Program SCQS31 (part of DnV's SESAM program) 31.10.73/01.

8. Hinton, E., Razzaque, A., Zienkiewicz, O. C. and Davies, J. D., "A Simple Finite Element Solution for Plates of Homogeneous, Sandwich and Cellular Construction", Proc. Instn. Civ. Engrs. (London), Part 2, 59, pp. 43-65, March 1975.

9. Irons, B. M. and Hellen, T. K., Short Communication on "On Reduced Integration in Solid Isoparametric Elements When Used in Shells with Membrane Modes", Int. J. Num. Meth. Engr., Vol. 10, pp. 1179-1182, 1975-76.

10. Timoshenko, S. P. and Woinowsky-Krieger, S., Theory of Plates and Shells, 2nd Edition, McGraw-Hill, 1959.

11. Cantin, G. and Clough, R. W., "A Curved, Cylindrical-Shell Finite Element", AIAA Journal, Vol. 6, No. 6, June 1968, pp. 1057-1062.

12. Scordelis, A. C. and Lo, K. S., "Computer Analysis of Cylindrical Shells", Journal of the American Concrete Institute, 61, 1964, pp. 539-561.

13. Gibson, J. E., The Design of Cylindrical Shell Roofs, 2nd Edition, E.&F.N. Spon, 1961.

14. Anon., MARC-CDC User Information Manual, Vol. I-III, Revision J, CDC Publications and Graphics Division, 1977.

15. Nicolos, V. T. and Citipitioglue, E., "SDRC SUPERB, A General Isoparametric Finite Element Program", Paper presented at the Second National Symposium on Computerized Analysis and Design, George Washington University, March 29-31, 1976.

16. Zienkiewicz, O. C., The Finite Element Method in Engineering Science, McGraw-Hill, 1971, p. 353-354.

17. Leick, R. D. and Potvin, A. B., "Automated Mesh Generation for Tubular Joint Stress Analysis," Second National Symposium on Computerized Structural Analysis and Design, George Washington University, March 29-31, 1976.

18. Katnik, R., "A Note on Moment Balance in the Isoparametric Shell Element," Int. J. Num. Meth. Engr., Vol. 11, No. 1, pp. 199-200, 1977.

TABLE 1. DISPLACEMENT CONVERGENCE FOR CYLINDRICAL SHELL ROOF

GRID	V_A	W_B	U_B	W_C	
1 x 1	-0.226	-9.609	-5.413	1.801	cm
	-0.089	-3.783	-2.131	0.709	in.
2 x 2	-0.368	-8.966	-4.752	1.313	cm
	-0.145	-3.530	-1.871	0.517	in.
3 x 3	-0.381	-9.241	-4.879	1.346	cm
	-0.150	-3.638	-1.921	0.530	in.
4 x 4	-0.381	-9.208	-4.854	1.379	cm
	-0.150	-3.625	-1.911	0.543	in.
EXACT	-0.384	-9.406	-4.986	1.334	cm
	-0.150	-3.703	-1.963	0.525	in.

FIGURE 1. ELEMENT GEOMETRY AND LOCAL COORDINATE SYSTEMS

FIGURE 2. CONVERGENCE STUDY FOR SIMPLY-SUPPORTED FLAT PLATE

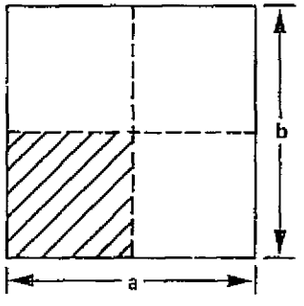

$E = 69.4\ KN/mm^2\ (1.0 \times 10^7\ psi)$

$\nu = 0.3$

a = b = 254 mm (10 in.)

t = 2.54 mm (0.1 in.)

$P = 178.4\ N\ (40\ lb.),\ 6.94\ KN/m^2\ (1.0\ psi)$

GRID	VERTICAL DEFLECTION AT CENTER			
	CENTRAL LOAD		UNIFORM PRESSURE	
	mm	in.	mm	in.
1 x 1	-1.286	-5.062×10^{-2}	-1.214	-4.778×10^{-2}
2 x 2	-1.284	-5.054×10^{-2}	-1.142	-4.498×10^{-2}
3 x 3	-1.294	-5.095×10^{-2}	-1.143	-4.50×10^{-2}
4 x 4	-1.295	-5.098×10^{-2}	-1.139	-4.483×10^{-2}
TIMOSHENKO	-1.287	-5.068×10^{-2}	-1.128	-4.44×10^{-2}

FIGURE 3. CONVERGENCE STUDY FOR PINCHED CYLINDER PROBLEM

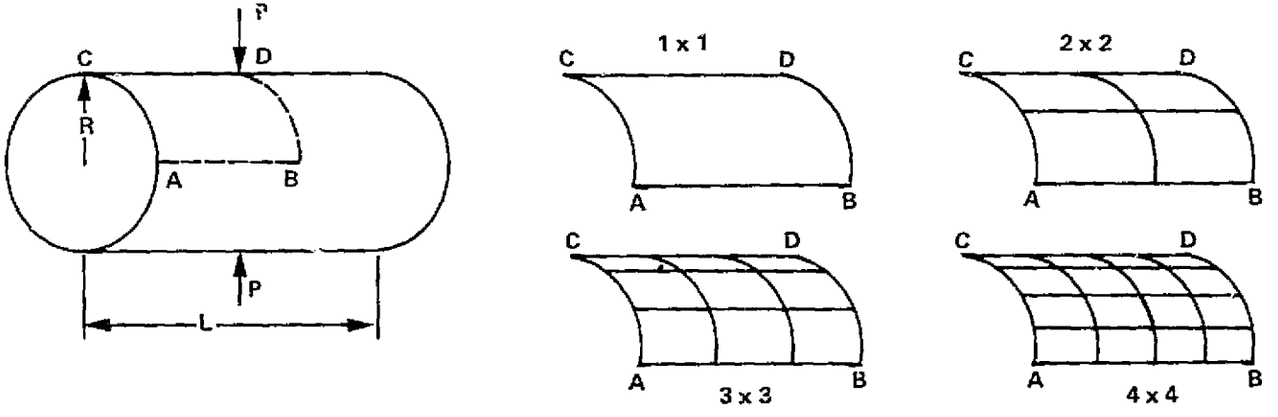

E = 72.9 KN/mm^2 (10.5 x 10^6 psi)

ν = 0.3125

R = 125.8 mm (4.953 in.)

L = 262.9 mm (10.35 in.)

t = 2.39 mm (0.094 in.)

P = 445.9 N (100 lb.)

GRID	DOF (TOTAL)	RADIAL DISPLACEMENT AT POINT D	
		mm	in.
1 x 1	40	-2.517	-0.991×10^{-1}
2 x 2	105	-2.753	-1.084×10^{-1}
3 x 3	200	-2.863	-1.127×10^{-1}
4 x 4	325	-2.893	-1.139×10^{-1}
TIMOSHENKO		-2.761	-1.087×10^{-1}

FIGURE 4. MESH CONFIGURATIONS FOR CYLINDRICAL SHELL ROOF

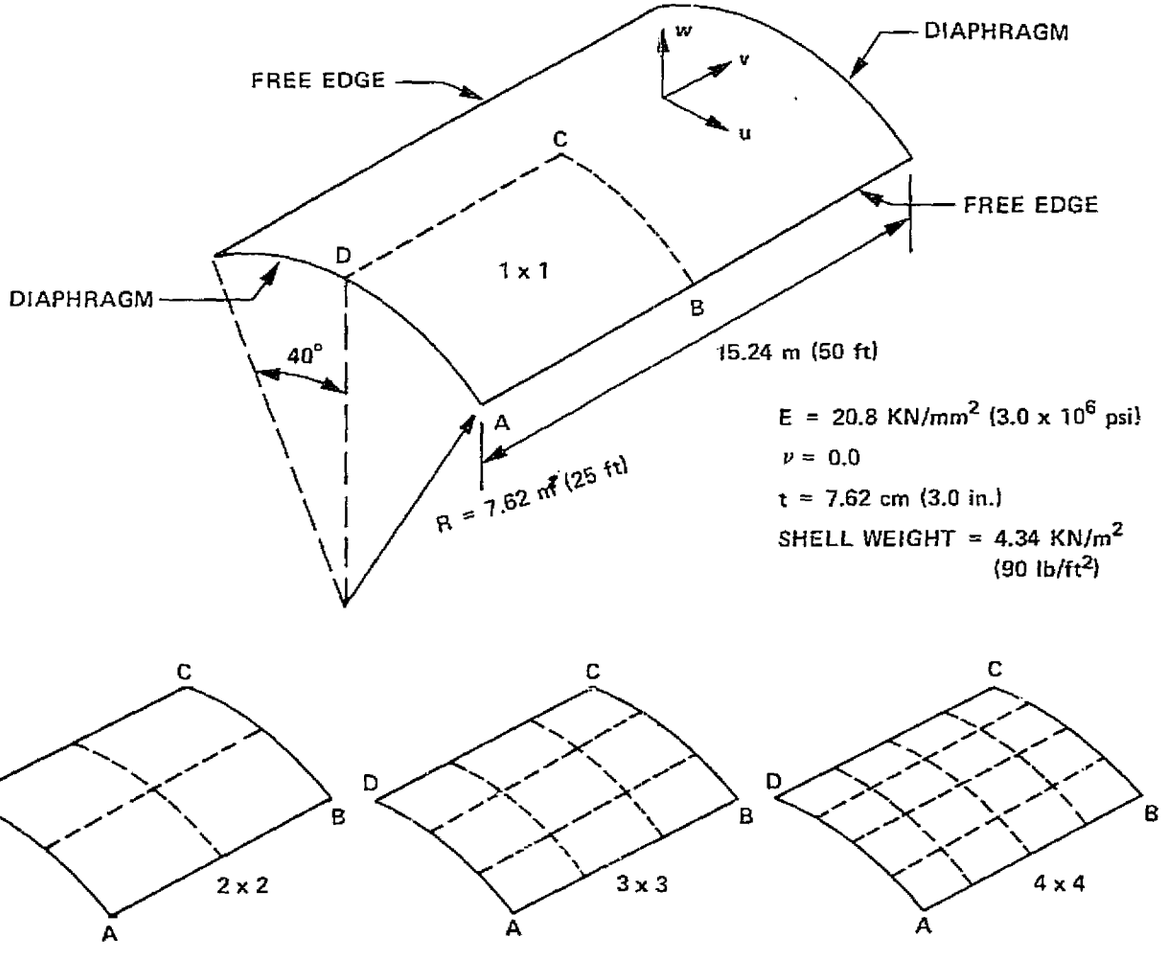

FIGURE 5. ELEMENT CONVERGENCE COMPARISON FOR CYLINDRICAL ROOF PROBLEM

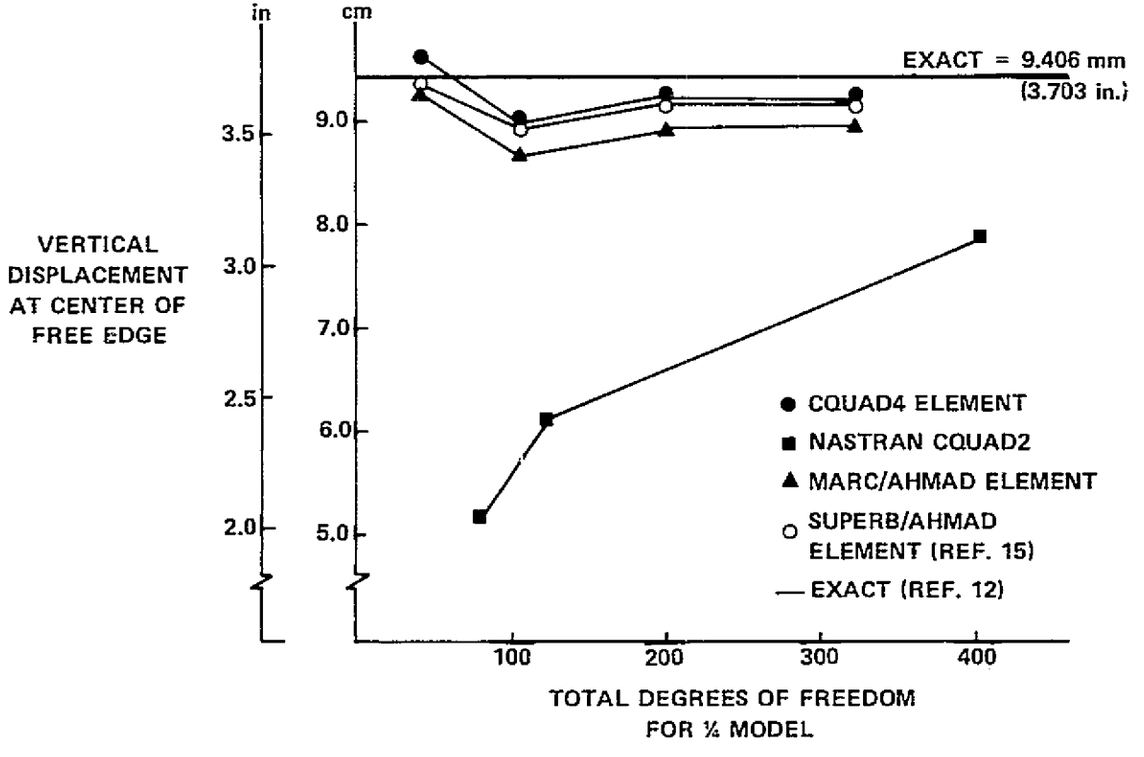

FIGURE 6. FREE VIBRATION OF A CANTILEVER PLATE

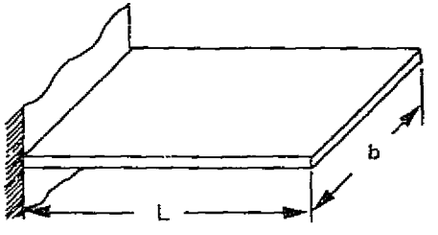

E = 208.3 KN/mm^2 (3.0×10^7 psi)

ν = 0.3

e = 7.85 t/m^3 (0.283 lb/in^3)

L = 50.8 mm (2.0 in.)

b = 25.4 mm (1.0 in.)

t = 2.54 mm (0.1 in.)

MODE	$\omega/\sqrt{D/\rho t L^4}$				
	EXPERIMENTAL (PLUNKETT)	NON-CONFORMING TRIANGLE ZIEN KIEWICZ		CQUAD4 ELEMENT	
		2 x 1	4 x 2	2 x 1	4 x 2
1	3.50	3.39	3.44	3.45	3.43
2	14.50	15.30	14.76	14.64	14.43
3	21.70	21.16	21.60	22.63	21.30
4	48.10	49.47	48.28	49.79	46.82
5	60.50	67.46	60.56		60.55
6	92.30		88.84		90.76
7	92.80		92.24		97.17
8	118.70		117.72		123.05
9	125.10		118.96		130.23
10	154.00				

FIGURE 7. DEGENERACY RESULTING FROM NON-RECTANGULARITY

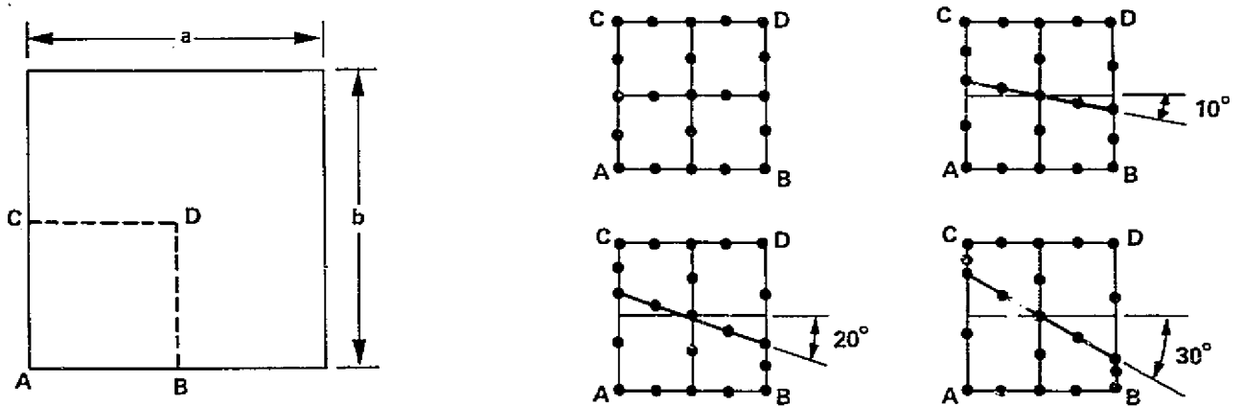

E = 69.4 KN/mm^2 (1.0 x 10^7 psi)

ν = 0.3

a = b = 254 mm (10 in.)

t = 2.54 mm (0.1 in.)

P = 6.94 KN/m^2 (1.0 psi)

GRID	VERTICAL DISPLACEMENT AT POINT D	
	mm	in.
RECTANGULAR	-1.143	-4.498×10^{-2}
10° OFFSET	-1.145	-4.506×10^{-2}
20° OFFSET	-1.118	-4.403×10^{-2}
30° OFFSET	-1.059	-4.169×10^{-2}
TIMOSHENKO	-1.128	-4.44×10^{-2}

FIGURE 8. DEGENERACY DUE TO THINNESS RATIO

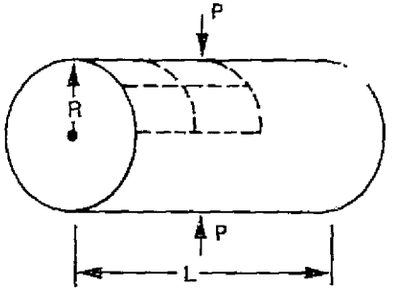

$E = 69.4\ KN/mm^2\ (1.0 \times 10^7\ psi)$

$\nu = 0.3$

R = 25.4 cm (10.0 in.)

L = 50.8 cm (20.0 in.)

P = 445.9 N (100 lb)

$$q_{max} = -\frac{1}{2}(0.149)\frac{P R^3}{2D (L/2)}$$

$$q_{max}\, D = -1.0716 \times 10^6\ N\ mm^2$$

t/R	D (N mm)	q_{max} (mm)	$(q_{max})(D)$
0.1	1.041×10^8	-1.185×10^{-2}	-1.234×10^6
0.01	1.041×10^5	-1.035×10^1	-1.078×10^6
0.001	1.041×10^2	-1.024×10^4	-1.066×10^6
0.0001	1.041×10^{-1}	-1.024×10^7	-1.066×10^6

FIGURE 9. DEGENERACY DUE TO MISALIGNMENT WITH DIRECTIONS OF PRINCIPAL CURVATURE

*NOTE USE OF DEVELOPED SURFACE COORDINATES

FIGURE 10. SUBSTRUCTURE MESHES FOR TYPICAL T-JOINT

NOTE USE OF DEVELOPED SURFACE COORDINATES

FIGURE 11. SUBSTRUCTURE MESHES FOR TYPICAL K-JOINT

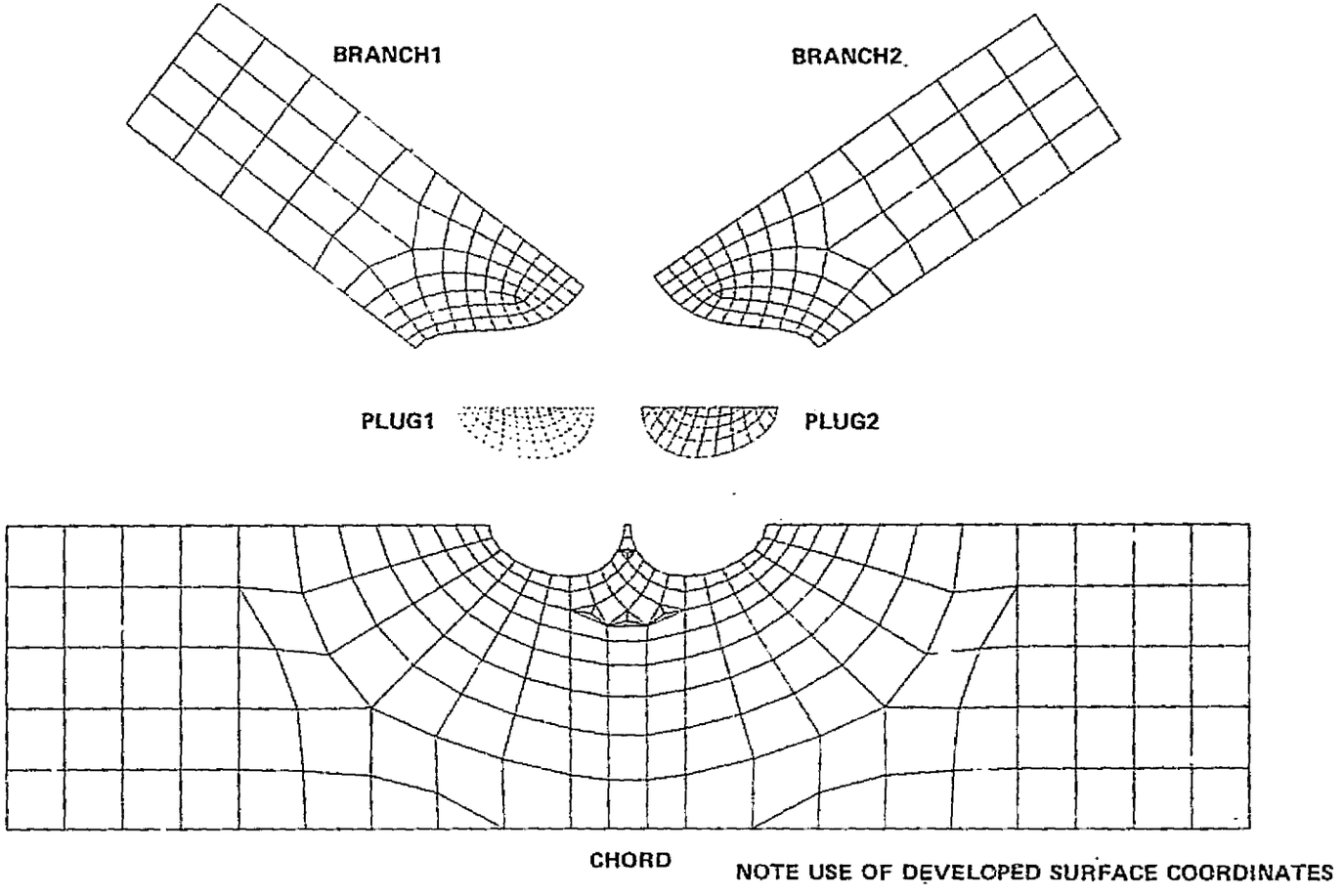

FIGURE 12. TYPICAL CONCRETE GRAVITY STRUCTURE

D12

N78-32478

MODELING STRUCTURAL DAMPING FOR SOLIDS HAVING DISTINCT SHEAR AND DILATATIONAL LOSS FACTORS

A. J. KALINOWSKI
NAVAL UNDERWATER SYSTEMS CENTER

SUMMARY

For steady state time harmonic problems (rigid format 8), the NASTRAN program as currently configured treats internal structural damping through the introduction of a single structural element damping coefficient that typically is viewed as the ratio of the complex to real modulus of elasticity (E^i/E^r). For problems dealing with two or three dimensional dynamic linear viscoelasticity (e.g. a Kelvin-Voigt viscoelastic model), the present NASTRAN capability cannot directly handle this situation wherein two independent damping coefficients are required to properly model the dissipation phenomenon. A technique is presented whereby the user can adapt the standard versions of NASTRAN (without resorting to either DMAP and/or FORTRAN coding changes) for the purpose of treating this class of problem.

INTRODUCTION

This paper is concerned with the solution to 1, 2, or 3 dimensional steady state (time harmonic) structural response problems wherein part or all of the structure is comprised of a linear viscoelastic material. In particular, attention is focused on the representation of the viscoelastic dissipation (or equivalently sound absorption) properties of this class of materials. Typically, rubber-like materials fall into the category of interest. In situations where the driving frequencies of the applied loading is large, the effect of the energy dissipation characteristics on the overall dynamic response (particularly in wave propagation problems) can be significant. Consequently, it is important that the material physical properties are modeled as accurately as possible. In this paper, the Kelvin-Voigt viscoelastic model is selected wherein the corresponding continuous field equations are given by (ref. (1))

$$(1 + \frac{\tilde{\mu}^i}{\mu^r}\frac{\partial}{\partial t})\nabla^2\bar{u} + (\frac{\lambda^r+\mu^r}{\mu^r})(1 + \frac{\tilde{\lambda}^i + \tilde{\mu}^i}{\lambda^r + \mu^r}\frac{\partial}{\partial t})\nabla(\nabla\cdot\bar{u}) = \frac{\rho}{\mu^r}\frac{\partial^2\bar{u}}{\partial t^2} \qquad (1)$$

where λ^r, μ^r are the usual Lame' elastic constants; $\tilde{\lambda}^i$, $\tilde{\mu}^i$ are their viscous counterparts; ρ denotes the mass per unit volume, $\bar{u}$ is the displacement vector; t is time and ∇ is the vector "del" operator $(\partial/\partial x, \partial/\partial y, \partial/\partial z)$. The steady state harmonic version of equation (1) is obtained by substituting $\bar{u} = \bar{u}_o e^{+i\omega t}$ into equation (1) which results in the form

$$\tilde{c}_s^2 \nabla^2\bar{u}_o + \tilde{c}_d^2 \nabla(\nabla\cdot\bar{u}_o) - \tilde{c}_s^2 \nabla(\nabla\cdot\bar{u}_o) = \omega^2\bar{u}_o \qquad (2)$$

where $\tilde{c}_s$ and $\tilde{c}_d$ are the complex wave speeds given by the expressions

$$\tilde{c}_s^2 = c_s^2(1+i\eta_s)$$
$$\tilde{c}_d^2 = c_d^2(1+i\eta_d) \qquad (3)$$

In equations (3), c_s and c_d are the usual elastic shear and dilatational wave speeds, and η_s and η_d are the associated shear and dilatational dissipation constants; these four constants are related to the constants originally employed in equation (1) through the relations:

$$c_s = \sqrt{\mu^r/\rho} \qquad c_d = \sqrt{(\lambda^r + 2\mu^r)/\rho} \qquad (4)$$

$$\eta_s = \mu^i/\mu^r \qquad \eta_d = (\lambda^i + 2\mu^i)/(\lambda^r + 2\mu^r) \qquad (5)$$

where λ^i and μ^i are two independent frequency dependent viscoelastic constants which are determined experimentally. The λ^i, μ^i constants are related to the $\tilde{\lambda}^i$, $\tilde{\mu}^i$ constants of Eq (1) through the relations $\lambda^i = \omega\,\tilde{\lambda}^i$ and $\mu^i = \omega\,\tilde{\mu}^i$. Depending on one's viewpoint, the pair of parameter λ^i, μ^i (or alternatively η_s, η_d) can be viewed as the two independent parameters which describe the dissipation characteristics of the viscoelastic media. Further, the independent constants λ^r, μ^r (or alternatively c_p, c_s) can be viewed as the two independent constants which define the elastic characteristics of the media.

The current version of NASTRAN can treat a solid media governed by equation (2) by using 2 and 3 dimensional elements (e.g. CTRMEM, CQDMEM, CTRAPGR, CTETRA, CTRIARG to name a few) in conjunction with both rigid format 8 and the introduction of a loss factor (e.g. the GE input variable on a MAT1 or MAT2 card; this is referred to as the "structural element damping coefficient" in the NASTRAN manual). Unfortunately, however, the user can introduce only one independent loss factor. A single, rather than two, independent loss factor can properly represent the Kelvin-Voigt model if the relation

$$\frac{\lambda^i}{\lambda^r} = \frac{\mu^i}{\mu^r} = \eta_E \qquad (6)$$

is met. Substituting equation (6) into equations (5) in conjunction with the fact that the Young's modulus, E, is related to μ, λ through $E = \mu(3\lambda+2\mu)/(\lambda+\mu)$ yields the relations

$$\eta_d = \eta_s = \eta_E = E^i/E^r \qquad (7)$$

Thus, the more limited single parameter loss factor case can directly be implementated in NASTRAN by assuming equation (6) holds and setting GE = η_E on a MAT 1 or MAT 2 card as appropriate.

The remainder of this paper is concerned with the situation wherein the viscoelastic physical constants are such that $\eta_d \neq \eta_s$ (i.e. the special case implied by equations (6) are not satisfied). A technique is presented which permits the user to treat this more general case without having to resort to either DMAP instructions and/or modified FORTRAN coding modifications to the original NASTRAN program. Because of this general type "fix", the approach also has applications to other finite element programs having the same one parameter type dissipation limitation found in NASTRAN.

IMPLEMENTATION OF TWO PARAMETER LOSS FACTORS

Here we consider finite elements representing equations (2) for the case $\eta_s \neq \eta_d$. The finite element formulation representing equations (2) leads to a complex set of simultaneous equations to be solved of the form (ref. (2))

$$[\bar{K}]\{U\}=\{P\} \tag{8}$$

where $[\bar{K}]=[-\omega^2[M]+i\omega[B]+[K]]$ (9)

where {U} is the vector of nodal displacement amplitudes, {P} is the vector of applied forces, [M], is the assembled mass matrix, [B] is the assembled damping matrix and [K] is the elastic stiffness matrix. The formation of the mass, stiffness and non-structural damping portion of the matrices in Eq. (8) fol ow exactly the same process used in modeling elasticity type problems, hence will not be commented on here (e.g. see refs. (2,3). Attention is consequently focused on the formation of the structural damping part of the $[\bar{K}]$ matrix; let us define $[\bar{K}]_e^{\eta}$ as the individual element structural damping portion due to the contribution of the e^{th} element. NASTRAN currently forms $[\bar{K}]_e^{\eta}$ from the relation

$$[\bar{K}]_e^{\eta} = i\eta_e[K]_e \equiv i\int_{V_e}\left([C]^T\eta_E[G]_e^r[C]\right)dxdydz \tag{10}$$

where $[K]_e$ is the individual element elastic stiffness matrix, [C] is the corresponding displacement-strain matrix and $[G]_e^r$ is the elastic stress-strain law matrix. For isotropic materials, $[G]_e^r$ is of the form:

$$\begin{Bmatrix} \sigma_{11} \\ \sigma_{22} \\ \sigma_{33} \\ \sigma_{23} \\ \sigma_{31} \\ \sigma_{12} \end{Bmatrix} = \underbrace{\begin{bmatrix} (\lambda^r+2\mu^r) & \lambda^r & \lambda^r & 0 & 0 & 0 \\ \lambda^r & (\lambda^r+2\mu^r) & \lambda^r & 0 & 0 & 0 \\ \lambda^r & \lambda^r & (\lambda^r+2\mu^r) & 0 & 0 & 0 \\ 0 & 0 & 0 & \mu^r & 0 & 0 \\ 0 & 0 & 0 & 0 & \mu^r & 0 \\ 0 & 0 & 0 & 0 & 0 & \mu^r \end{bmatrix}}_{[G]^r_e} \begin{Bmatrix} \varepsilon_{11} \\ \varepsilon_{22} \\ \varepsilon_{33} \\ \varepsilon_{23} \\ \varepsilon_{31} \\ \varepsilon_{12} \end{Bmatrix} \tag{11}$$

where σ_{11}, σ_{22} ... and ε_{11}, ε_{22} ... are the element stresses and strains.

So far we have described, via equations (10) and (11), the form currently in NASTRAN. Next we consider the form of $[\bar{K}]^{\mu}_e$ we would like to have in order to implement the two independent parameter formulation. By comparing what we have to what we would like to have, the "fix" to NASTRAN will become evident. We start by making the important observation that the desired general continuous viscoelastic form of equation (2) can be derived from the usual elastic derivation for the dynamic equations of elasticity (ref. (4)). This is accomplished by following the elastic derivation of ref. (4) with the modification that, in place of the usual isotropic stress-strain law (i.e. Eq. (11)), we use

$$\{\sigma\}=[[G]^r_e + i[G]^i_e]\{\varepsilon\} \tag{12}$$

where $[G]^i_e$ is the same expression as $[G]^r_e$ except all r superscripts are replaced with i superscripts for the λ, μ entries. Similarly, in the finite element formulation, all we need do is replace the usual $[G]^r_e$ matrix in the stiffness derivation with $[G]^r_e+i[G]^i_e$. Thus, the element stiffness becomes

$$[K]_e = \int_{V_e} [C]^T[[G]^r_e+i[G]^i_e][C]dxdydz \tag{12}$$

$$= \underbrace{\int_{V_e} [C]^T[G]^r_e[C]dxdydz}_{\text{Term 1...Usual elastic stiffness contribution to } [\bar{K}] \text{ of Eq. (8).}} + i \underbrace{\int_{V_e} [C]^T[G]^i_e[C]dxdydz}_{\text{Term 2...viscoelastic dissipation contribution to } [\bar{K}] \text{ of equation (8).}} \tag{12b}$$

Now we are in a position to build the desired two independent parameter viscoelastic finite element. The total complex element contribution, $[K]_e$, to the assembled $[\bar{K}]$ matrix in equation (9) is formed in two parts through the creation of an overlapping double viscoelastic element. This double element is shown schematically in Figure (3) (a two dimensional element is shown only for convenience). It consists of two identically shaped element occupying the same physical space and having the same nodal numbers but different element numbers and different material identification cards (MAT1 for 3-d elements and MAT2 for 2-d elements). Our goal is to let one of the overlapping elements form the Term-1 elastic contribution of Eq. (12b) and the other form the Term-2 viscoelastic dissipation contribution. In agreement with the notation of Figure (3), we refer to the first overlapping element as the "elastic element" and the second as the "massless dissipation element". The only part that remains is to define the input constants on the MAT1 (or MAT2) cards so that Term-1 and Term-2 in equations (12b) are properly formed. More specifically, the rationale for the selection of the MAT1 (or MAT2) constants follows from seeking out a set of parameters for the $\eta_E[G]_e^r$ matrix in equation (10), (namely the η_E, and components of the elastic $[G]_e^r$ matrix which are controlled by the user through selection of the input variables on the appropriate MATi cards) that will result in the desired $[G]_e^i$ matrix in Term-2 of equation (12b). The treatment is slightly different for three or two dimensional elements, consequently we treat them one at a time.

Three Dimensional Viscoelastic Elements

- The elastic element contribution is obtained by setting the following parameters on a MAT1 card:

  1) set mass density (RHO) = actual mass density of viscoelastic material

  2) set loss factor (GE) = 0.0 (13)

  3) set $E = \mu^r(3\lambda^r+2\mu^r)/(\lambda^r+\mu^r)$

     $G = \mu^r$

- The massless dissipation element contribution is obtained by setting the following parameters on another MAT1 card specially earmarked for this second overlapping element:

  1) set mass density (RHO) = 0.0 (zero to avoid double counting)

  2) set loss factor $\eta_E \equiv (GE) = \lambda^i/\varepsilon$ (14)

3) set $E = \epsilon R(3+2R)/(1+R)$

$G = \epsilon R$ (14) cont'd)

with $R = \mu^i/\lambda^i$

where ϵ is an arbitrary parameter that is selected small as desired (but not zero). The small ϵ parameter removes the elastic contribution of the massless dissipation element. A suggested value for ϵ is that it is on the order of 10,000 times smaller than the larger of the real components λ^r or μ^r.

The interested reader is invited to back substitute the above values for E, G, and GE (e.g. η_E) into the $\eta_E[G]_e^r$ matrix formed by NASTRAN in conjunction with equation (1) where it can be easily verified that the results reduce (independent of the ϵ choice) exactly to the desired two independent parameter matrix $[G]_e^i$ employed in Eq. (12b). The smallness of ϵ only effects the unwanted elastic stiffness contribution of the massless dissipation element already accounted for in the "elastic element".

Two Dimensional Elements

- The elastic element contribution is obtained by setting the following parameters on a MAT2 card:

1) set mass density (RHO) = actual mass density of viscoelastic material

2) set loss factor (GE) = 0.0

3) set $G11 = \lambda^r+2\mu^r$
$G12 = \lambda^r$
$G13 = 0.0$
$G22 = \lambda^r$
$G23 = 0.0$
$G33 = \mu^r$ (15)

- The massless dissipation element contribution is obtained by setting the following parameters on another MAT2 card specially earmarked for this second overlapping element:

1) set mass density (RHO) = 0.0

2) set loss factor $\eta_E \equiv (GE) = \lambda^i/\epsilon$ (16)

3) set G11 = $\epsilon(1+2\mu^i/\lambda^i)$ (16) cont'd

G12 = ϵ

G13 = 0.0

G22 = ϵ

G23 = 0.0

G33 = $\epsilon\mu^i/\lambda^i$

where as with the three dimensional element, the ϵ is an arbitrary parameter that is selected small as desired (but not zero). See 3-d element write-up for a suggested ϵ value.

DEMONSTRATION PROBLEM

Next we consider a demonstration problem to illustrate the implementation and accuracy of the two independent parameter loss factor viscoelastic elements described in the previous section. The problem is to determine the scattered and transmitted pressures for a water-submerged steel plate, (covered with a constant thickness layer of viscoelastic material), subject to an incident plane wave normal to the plate as illustrated in figure (1). The problem is tractable from a closed form solution point of view, consequently, an independent check on the NASTRAN solution is available. Furthermore, experimental results are also available to further back up the accuracy of the physical representation of the viscoelastic material.

Exact Solution

The exact solution to this problem can initially be treated as an ordinary one dimensional, small deformation wave propagation problem. The effect of viscoelasticity can be introduced by replacing the wave speed c_d with $\tilde{c}_d = c_d\,(1+i\eta_d)^{\frac{1}{2}}$. The solution to the problem illustrated in figure (1) is carried out exactly like the problem given in ref. (5), page 136, except that two finite thick plates (rather than one) is submerged in the fluid. The origin (at x =0) is located at the right face of the viscoelastic layer (+x to the left). The back side fluid is denoted as media (4), steel plate as (3), the viscoelastic layer as (2) and the front side fluid as (1). The thickness of the steel plate is ℓ_3 and the viscoelastic layer is ℓ_2. The following relations define the various waves present in the problem:

$$(p_i)_1 = A_1\, e^{i(\omega t - k_1 x)} \qquad \text{Incident wave in (1)}$$

$$(p_s)_1 = B_1\, e^{i(\omega t + k_1 x)} \qquad \text{Scattered wave in (1)} \qquad (17)$$

$(p_t)_2 = A_2\, e^{i(\omega t - k_2 x)}$ Transmitted wave in (2)

$(p_s)_2 = B_2\, e^{i(\omega t + k_2 x)}$ Scattered wave in (2) (17 cont'd)

$(p_t)_3 = A_3\, e^{i(\omega t - k_3 (x-\ell_2))}$ Transmitted wave in (3)

$(p_s)_3 = B_3\, e^{i(\omega t + k_3 (x-\ell_2))}$ Scattered wave in (3)

$(p_t)_4 = A_4\, e^{i(\omega t - k_4 (x-\ell_2-\ell_3))}$ Transmitted wave in (4)

where in the fluid p is pressure and in the solid, p is the negative of the stress σ_{11} in the x direction. The k quantities are defined as:

$$k_1 = \omega/c_{d1}$$

$$k_2 = \omega/[c_{d2}(1+\eta_{d2})^{\frac{1}{2}}]$$

$$k_3 = \omega/c_{d3}$$

$$k_4 = \omega/c_{d4}$$

where c_{d1}, c_{d2}, c_{d3}, c_{d4} are the real dilatational wave speeds of the four materials and η_{d2} is the dilatational loss factor (equation (5)) of the viscoelastic layer. The six unknown B_1, A_2, B_2, A_3, B_3, A_4 can be determined from equating pressure and particle velocities at the three interfaces, thus providing six equations to balance the six unknowns. All response variables are referred to the incident wave amplitude A_1, thus A_1 is not considered an unknown in the problem.

The quantities of interest are the scattered pressure in the incident side fluid (media 1) and the transmitted pressure in the back side fluid (media 4). After algebraically solving for the constants we obtain

$$\text{Scatter pressure amplitude} \equiv B_1/A_1 = (C_2A_{12}-C_1A_{22})/(A_{21}A_{12}-A_{11}A_{22}) \qquad (19)$$

$$\text{Transmitted pressure amplitude} \equiv A_4/A_1 = (A_{21}A_{32}C_1-A_{32}A_{11}C_2)/(A_{21}A_{12}-A_{11}A_{22})$$

where $C_1 = -\cos(k_2\ell_2)+i\, r_{12}\sin(k_2\ell_2)$; $r_{12}=\rho_2\tilde{c}_{d2}/\rho_1 c_{d1}$; $r_{34}=\rho_4 c_{d4}/\rho_3 c_{d3}$

$C_2 = r_{23} i\, \sin(k_2\ell_2) - r_{23}r_{12}\cos(k_2\ell_2)$; $r_{23}=\rho_3 c_{d3}/\rho_2\tilde{c}_{d2}$; $\tilde{c}_{d2}=c_{d2}(1+i\eta_{d2})^{\frac{1}{2}}$

$$A_{12} = ([1+r_{34}][\cos(2k_3\ell_3)+i\ \mathrm{Sin}(2k_3\ell_3)]/[1-r_{34}])-1$$

$$A_{21} = -r_{23}i\ \mathrm{Sin}(k_2\ell_2)-r_{23}r_{12}\ \cos(k_2\ell_2)$$

$$A_{11} = \cos(k_2\ell_2)+i\ r_{12}\ \mathrm{Sin}(k_2\ell_2)$$

$$A_{22} = 1 + [1+r_{34}][\cos(2k_3\ell_3)+i\ \mathrm{Sin}(2k_3\ell_3)]/[1-r_{34}]$$

$$A_{32} = -2r_{34}[\cos(k_3\ell_3) + i\ \mathrm{Sin}(k_3\ell_3)]/[1-r_{34}]$$

Finite Element Solution

The finite element representation of the figure (1) problem is shown in figure (2). The procedure for representing the infinite domain of fluid on the front and back side of the submerged plate is given in detail in ref. (6). Briefly, it consists of using a plane wave boundary condition at the mesh termination of the form $p=\rho c_d \dot{u}$ where $\dot{u}$ is the normal particle velocity and p is the total pressure at the mesh termination. The nodes along the outer boundaries are constrained to move only in the direction of wave propagation. The figure (2) sketch is drawn to scale and represents the actual number of elements used in the problem. All elements employed in the model are comprised of CQDMEM quadralateral elements. The viscoelastic zone is made up from the overlapping double elements described earlier in the paper (e.g. a typical viscoelastic element is illustrated in figure (3)).

Comparative Results

The demonstration problem (both analytical and finite element) was evaluated with the following set of physical constants

Table 1 - DEMONSTRATION PROBLEM PHYSICAL CONSTANTS

MATERIAL	λ^r psi	μ^r psi	λ^i psi	μ^i psi	ρ lb-sec^2/in^4
Water	345,600.	0.0	0.0	0.0	.000096
Steel	17,307,000.	11,538,000.	0.0	0.0	.000735
Viscoelastic Material	86,703.	115.9	41,736.8	11.6	.0003599

The viscoelastic constants were evaluated by W. Madaigosky at NSWC. For the NASTRAN computer run, the water and steel plate properties were entered on a MAT2 card. The elastic entries G11, G12, etc. correspond to the column and row data in the first, second and sixth (columns and rows) of the $[G]^r_e$ matrix

of equation (11). The viscoelastic data were entered on two separate MAT2 cards corresponding to the procedure described by equations (15) and (16). An ε parameter of $\varepsilon = 4.16$ was used in the actual run. The non-dimensional results are shown in Table 2.

The significance of the added viscoelastic layer on the scattered and transmitted pressure is seen by comparing the results of Tables 2 and 3, wherein the viscoelastic layer has the effect of absorbing a significant amount of the incident energy. The accuracy of the NASTRAN results for both the case with the viscoelastic layer and without the layer are quite good. As expected, the finite element solution accuracy falls off as the incident frequency increases. As pointed out by ref. (7), for problems of this type, at least 8 elements per wave length are needed to accurately model elastic waves in the media. Note in Table 2 that as the incident frequency approaches the 8 elements per wave length limit, the accuracy is starting to deteriorate. The 8 element per wave length limit suggested by ref. (7) was in the absence of structural damping; perhaps the results presented here suggests that more than 8 elements per wave length are required for structural damping (e.g. 12 elements per wave length).

CONCLUDING REMARKS

The procedure outlined here provides the NASTRAN user with an expanded structural damping capability, thus permitting the user to specify two independent loss factors η_s, η_d via the construction of the "overlapping double viscoelastic element" process described in this paper. The demonstration problem shows good accuracy of the procedure relative to the exact solution for the same problem. It is acknowledged that there is some added solution time due to the added calculation time for the formation of the stiffness of the second overlapping element; however, this is a relatively insignificant amount in comparison to the overall solution time of the problem. The double element uses the same node numbers for both the "elastic element" and the superimposed "massless dissipation element", consequently, the matrix size or bandwidth properties are not affected at all.

REFERENCES

1. Gaunaurd, G. C.: "Sonar Cross Section of a Coated Hollow Cylinder In Water". J. Acoustic Soc. Am., Vol. 61, No. 2, February 1977.

2. The NASTRAN Theoretical Manual (Level 16.0), National Aeronautics and Space Administration report NASA-SP-221(03), March 1976.

3. Zienkiewicz, O. C., and Cheung, Y. K.: The Finite Element Method in Structural and Continuum Mechanics, McGraw-Hill Publishing Co., 1968.

4. Sokolnikoff, I. S.: Mathematical Theory of Elasticity, McGraw-Hill Book Co., 2d edition, 1956.

5. Kinsler, L. E. and Frey, A. R.: Fundamentals of Acoustics, 2d edition, John Wiley & Sons, Inc., New York, 1962.

6. Kalinowski, A. J.: "Fluid/Structure Interaction", Shock and Vibration Computer Programs - Reviews and Summaries, edited by W. Pilkey and B. Pilkey, The Shock and Vibration Information Center, 1975.

7. Lysmer, J. and Drake, L.A.: "A Finite Element Method for Seismology", Methods in Computational Physics, edited by B. Bolt, Volume 11 - Seismology; Academic Press, New York, 1972.

Table 2 - COMPARATIVE SOLUTION RESULTS
(with viscoelastic layer present)

Nondimensional frequency; $\omega \ell_3 / c_{d1}$	NASTRAN Scattered Pressure ratio	Exact Scattered Pressure ratio (equation (19))	NASTRAN transmitted pressure ratio	Exact transmitted pressure ratio	Experimental Scattered pressure	Elements per wave length in elastomer
.6545	.401	.398	.273	.273	-	158.
3.272	.191	.190	.028	.028	-	31.6
6.545	.108	.104	.006	.007	-	15.8
9.817	.122	.113	.003	.003	.12	10.5
13.089	.133	.113	.002	.003	.12	7.9

Note that $\ell_3/\ell_2 = 2.2727$ (ratio of steel plate-to-viscoelastic layer thickness)

Table 3 - COMPARATIVE SOLUTION RESULTS
(without viscoelastic layer present)

Nondimensional frequency; $\omega \ell_3 / c_{d1}$	NASTRAN Scattered Pressure ratio	Exact Scattered Pressure ratio (equation (19))	NASTRAN transmitted pressure ratio	Exact transmitted pressure ratio	Experimental Scattered pressure
.654	.930	.928	.374	.373	-
3.27	.995	.996	.090	.090	-
6.54	.998	.998	.067	.067	-
9.82	.996	.994	.113	.113	-
13.09	.957	.952	.306	.307	-

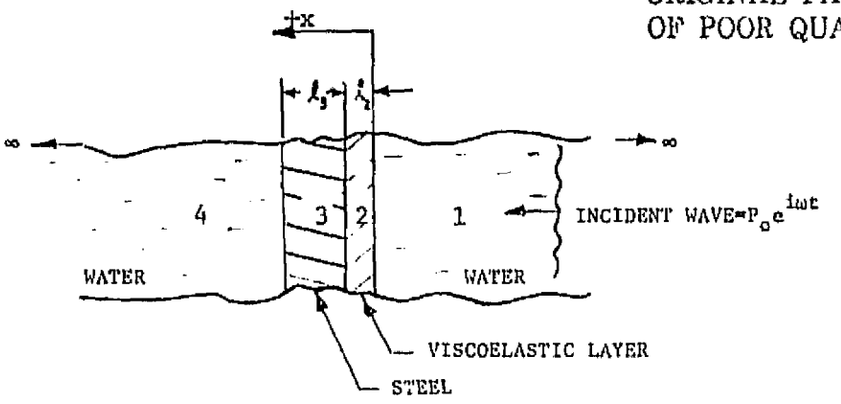

Figure 1. Submerged Plate With Viscoelastic Layer

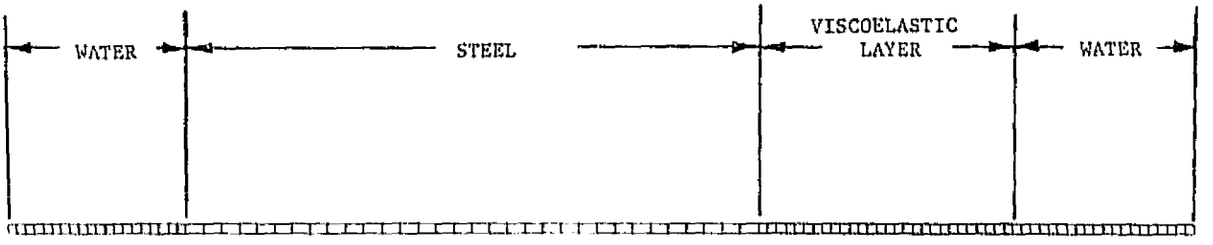

Figure 2. One Dimensional Finite Element Model

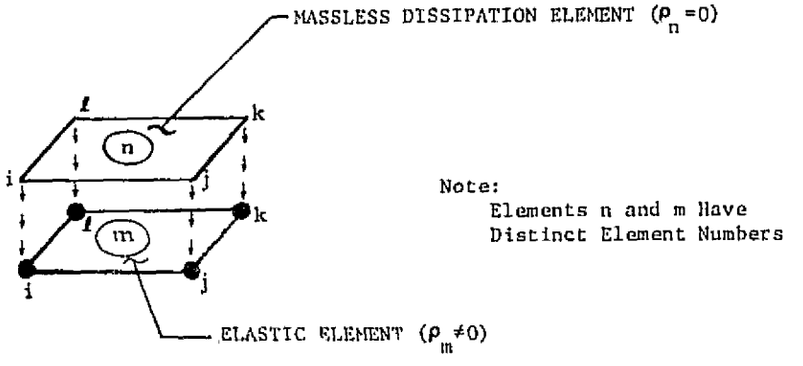

Figure 3. Overlapping Double Viscoelastic Element
(Quadralateral Element Example)

D13

N78-32479

THERMAL STRESS ANALYSIS OF CERAMIC STRUCTURES WITH NASTRAN ISOPARAMETRIC SOLID ELEMENTS

Steven E. Lamberson and Donald B. Paul
Structural Mechanics Division
Air Force Flight Dynamics Laboratory
Wright-Patterson AFB, Ohio

SUMMARY

This paper presents a study of the performance of the NASTRAN level 16.0 twenty node isoparametric bricks (CIHEX2) to thermal loading. A free ceramic plate was modelled using twenty node bricks of varying thicknesses. The thermal loading for this problem was uniform over the surface with an extremely large gradient through the thickness. No mechanical loading was considered. Temperature-dependent mechanical properties were considered in this analysis. The NASTRAN results are compared to one-dimensional stress distributions calculated by direct numerical integration.

INTRODUCTION

In attempting to analyze a ceramic radome no information was available concerning the sensitivity of the twenty node brick to large aspect ratio or large thermal gradients. The free plate was identified as an appropriate problem to examine this sensitivity. The thermal gradient of interest (Fig. 1) is severe and generates significant compressive hoop stress spikes immediately beneath the surface. A model containing sufficient elements near the surface to adequately predict the detailed in-depth response of a full radome model was infeasibly large. Therefore, this study was made to determine the effects of lesser numbers of elements through the thickness on the stress predictions. Also studied was the degradation of the stresses with increase in the ratio of the length of the surface side to the element thickness (aspect ratio).

The basic model used in this study was a 3 in. by 3 in. by 1/4 in. plate modelled with a 4 x 4 x 4 element grid. Various element spacings through the thickness were examined starting with uniform spacing and gradually allowing the surface elements to shrink in-depth while increasing the thickness of the rear elements. Variable Mechanical Properties were used for this analysis (Fig. 2). A total of four cases were examined.

The NASTRAN twenty node bricks showed little sensitivity to high aspect ratios (tests were run to 94:1) for this loading. Stresses, as always with this element, are less uniform than could be desired; but, when averaged in a reasonable fashion the correlation between NASTRAN'S stresses and one-dimensional numerical solutions is good provided any one element does not span more than one inflection point in the stress curve.

SYMBOLS

ρ = mass density

c_p = specific heat at constant pressure

T = temperature field

t = time

z = location through the depth

z+h is the heated surface

k = the thermal conductivity

σ = stress

f = σ_{xx}

E = young's modulus

ν = poisson's ratio

α = thermal expansion coefficient

2h = plate thickness

THERMAL LOADING

The thermal loading is produced by the application of a suddenly applied uniform heat flux over one face of the plate while the other face is maintained adiabatic. The resulting transient temperature distribution is obtained by the implicit finite difference numerical solution of the one dimension variable property heat conduction equation.

$$\rho c_p \frac{\partial T}{\partial t} = \frac{\partial k}{\partial z} \frac{\partial T}{\partial z} + k \frac{\partial^2 T}{\partial z^2} \tag{1}$$

with initial conditions for t<0 T=530°R

and boundary conditions for t>0

$$\begin{aligned} z = +h \qquad & -k \frac{\partial T}{\partial z} = 88 \text{ BTU/in}^2\text{-sec} \\ z = -h \qquad & -k \frac{\partial T}{\partial z} = 0 \end{aligned} \tag{2}$$

Sublimation of the ceramic is modelled with an Arrhenius type function which was derived from test data.

ONE-DIMENSIONAL STRESS DISTRIBUTION

The one-dimensional stress distribution was derived by considering a free plate of arbitrary planform, constant thickness, and with temperature dependent isotropic properties. The plate is thermally loaded with a temperature gradient through the thickness only. It is assumed that the stress field, away from the edges, is also only a function of the thickness coordinate and that all out of plane stresses are zero.

$$\sigma_{xx} = \sigma_{yy} = f(z);\ T = T(z)$$
$$\sigma_{xz} = \sigma_{xy} = \sigma_{yz} = \sigma_{zz} = 0 \tag{3}$$

The boundary conditions are chosen such that the resultant force and moment produced by f(z) are zero over the edges. Under the above assumptions, the equations of equilibrium are satisfied identically. The stress distribution is obtained by direct integration of the compatibility equations and application of the boundary conditions

$$f = \frac{E}{1-\nu}\left[-\alpha T + (D-Bz)\frac{N_T}{H} + (Az-B)\frac{M_T}{H}\right] \tag{4}$$

where

$$A = \int_{-h}^{h} \frac{E}{1-\nu}\,dz \qquad B = \int_{-h}^{h} \frac{E}{1-\nu}\,z\,dz$$

$$D = \int_{-h}^{h} \frac{EZ^2}{1-\nu}\,dz \qquad N_T = \int_{-h}^{h} \frac{\alpha ET}{1-\nu}\,dz \tag{5}$$

$$M_T = \int_{-h}^{h} \frac{\alpha ET}{1-\nu}\,z\,dz \qquad H = AD-B^2$$

The above integrals were numerically evaluated by the trapezoidal method utilizing the predicted temperature distribution and variable thermal properties (Fig. 2).

THREE-DIMENSIONAL NASTRAN ANALYSIS

A 3 in. by 3 in. by 1/4 in. ceramic plate was modelled with a 4 x 4 x 4 element grid (Fig. 4). Surface elements of .0625, .05, .02, and .008 inch thickness were used. The temperature distribution through the thickness (Fig. 1) is applied uniformly over the plate surface. The plate is free-free and mechanical properties that vary with temperature are used (Fig. 2). Four integration points per side were used in all elements.

The stress output from NASTRAN for this element contains a stress value for each node point in each element. These stresses are extrapolated from the values calculated at the integration points and are rarely continuous from one element to the next. The stresses are averaged at each node and these stresses are further averaged for several central locations on the plate.

The stresses for the first two element spacings (Fig. 4) are unacceptable in the first quarter of the structure. The last two spacings adequately describe the stress field (Fig. 5).

CONCLUDING REMARKS

The twenty node brick adequately describes thermal stress fields provided the stress field is sufficiently known to ensure proper element spacing in regions of high stresses. Aspect ratio does not appear to be critical in this element provided the only significant thermal gradient is in the direction of the smallest dimension.

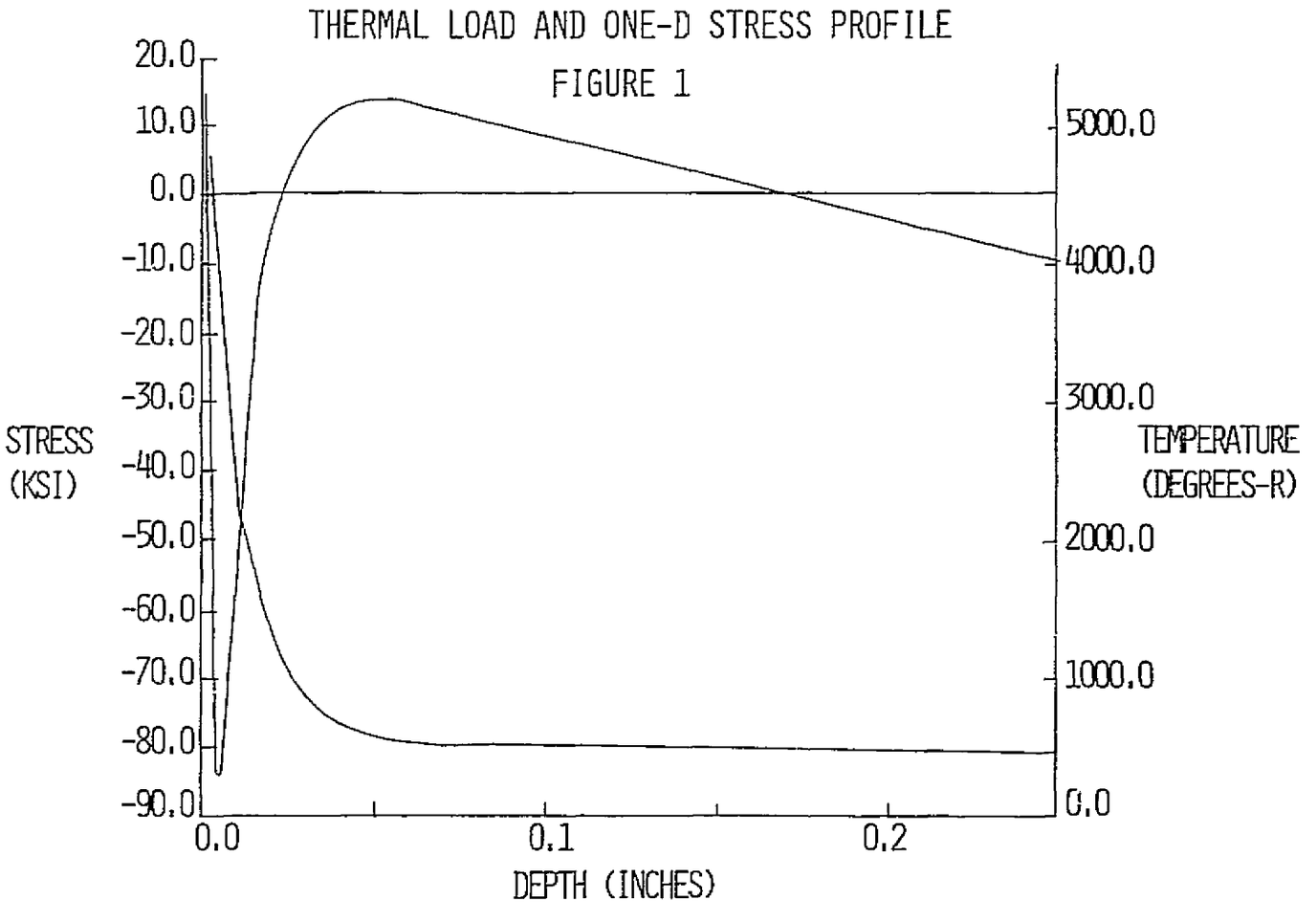
THERMAL LOAD AND ONE-D STRESS PROFILE
FIGURE 1
20.0
10.0
0.0
-10.0
-20.0
-30.0
-40.0
-50.0
-60.0
-70.0
-80.0
-90.0
STRESS
(KSI)
5000.0
4000.0
3000.0
2000.0
1000.0
0.0
TEMPERATURE
(DEGREES-R)
0.0
0.1
0.2
DEPTH (INCHES)

VARIABLE MECHANICAL PROPERTIES

FIGURE 2

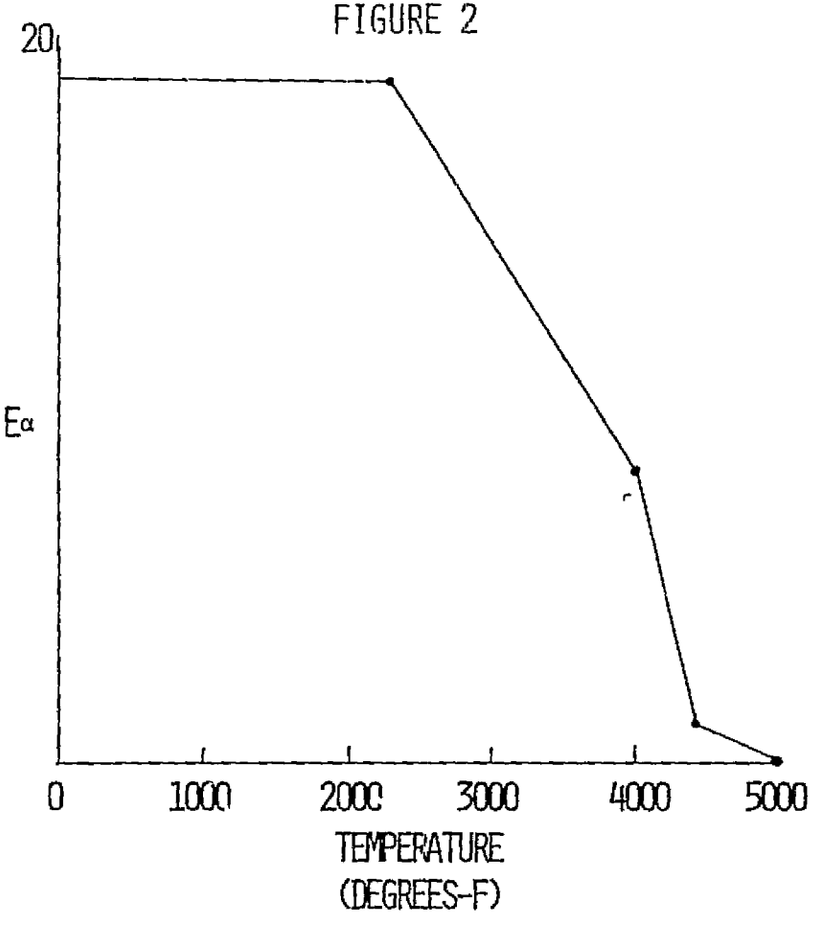

FINITE ELEMENT MODEL

FIGURE 3

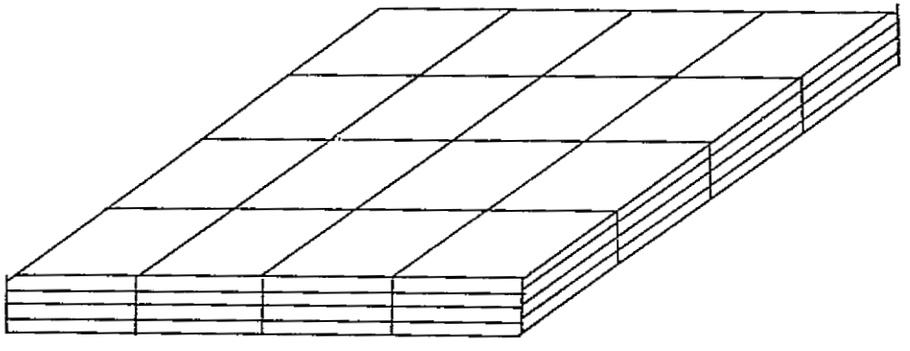

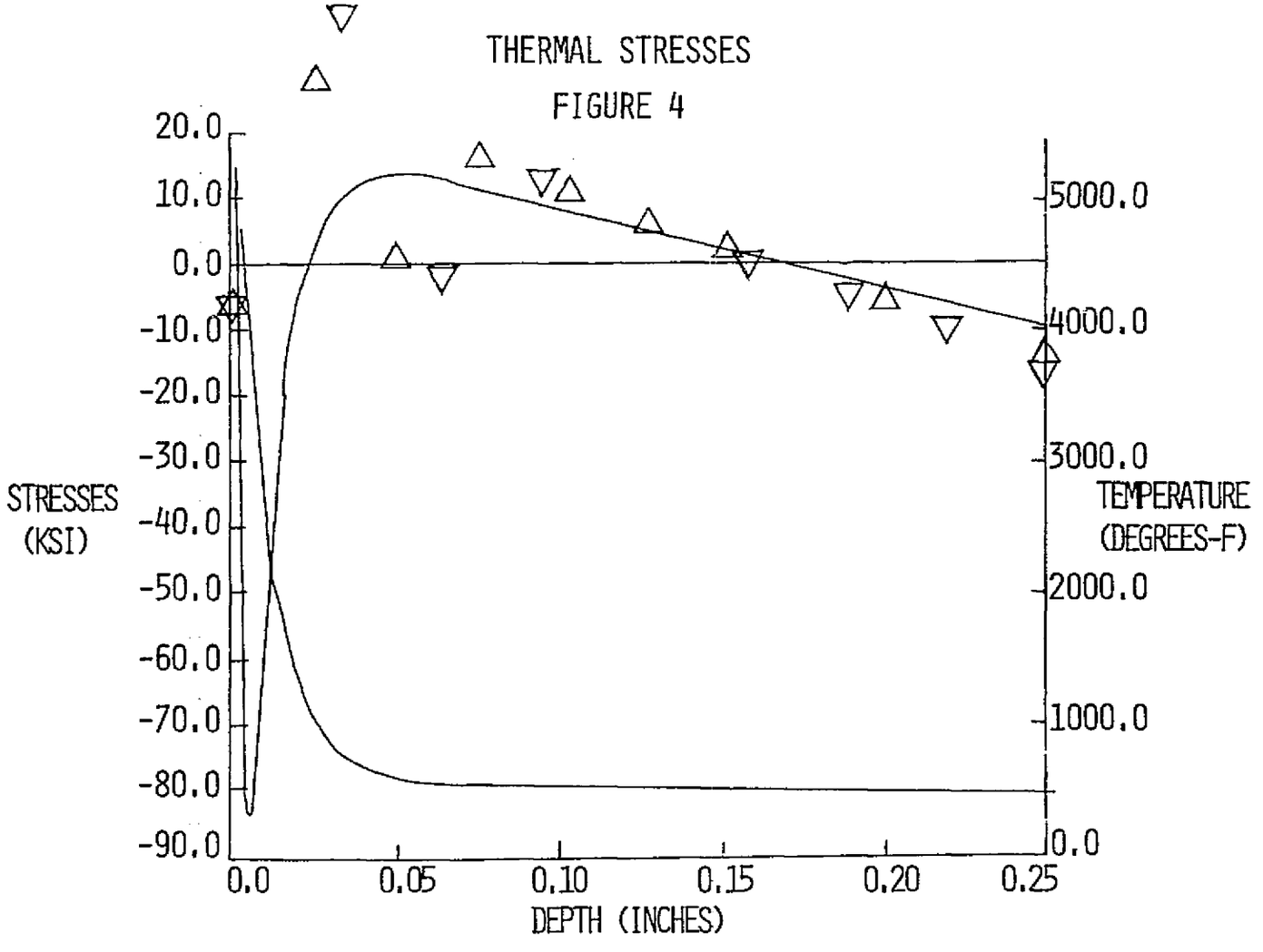

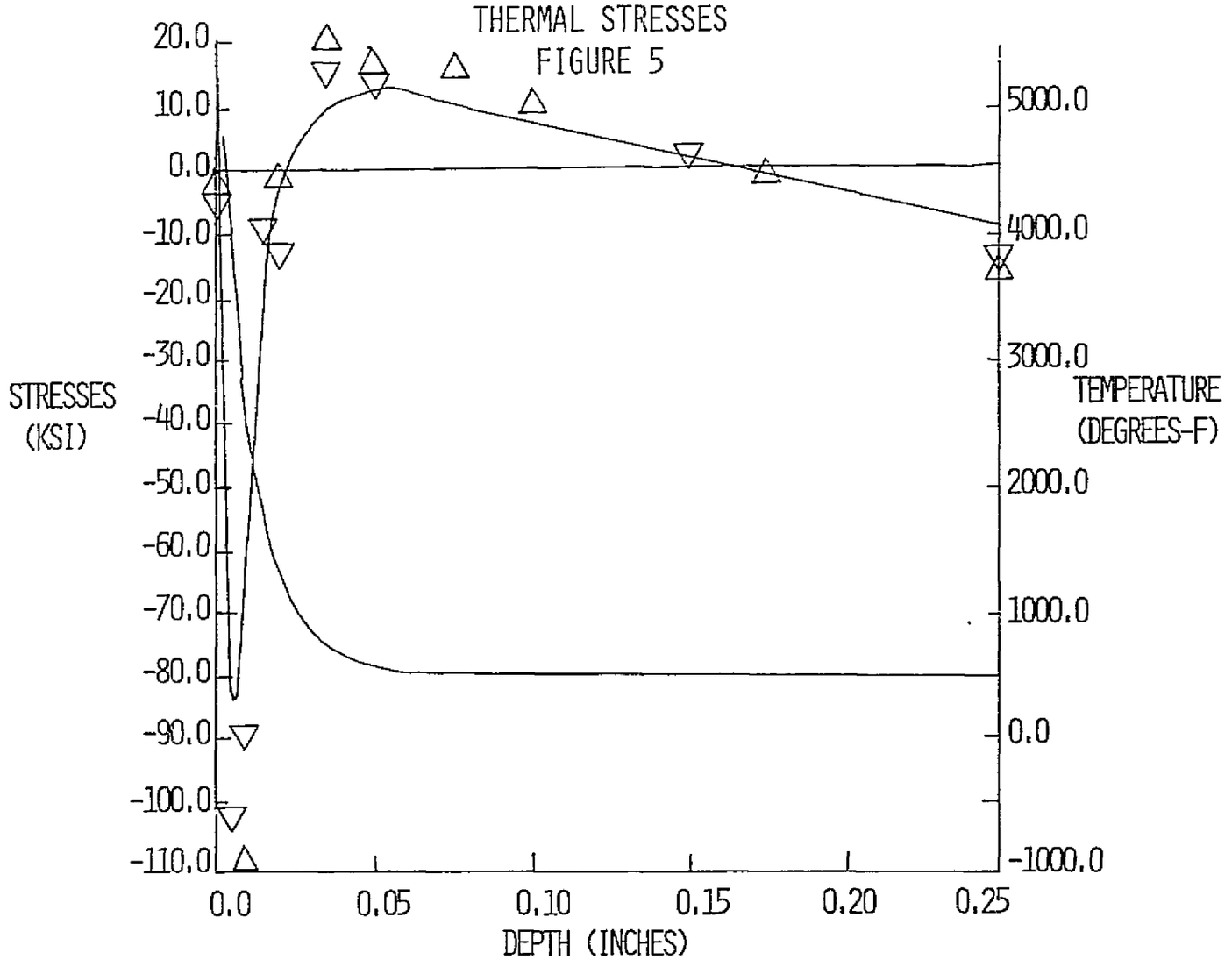
THERMAL STRESSES
FIGURE 5
20.0
10.0
0.0
-10.0
-20.0
-30.0
-40.0
-50.0
-60.0
-70.0
-80.0
-90.0
-100.0
-110.0
STRESSES
(KSI)
5000.0
4000.0
3000.0
2000.0
1000.0
0.0
-1000.0
TEMPERATURE
(DEGREES-F)
0.0
0.05
0.10
0.15
0.20
0.25
DEPTH (INCHES)

D14

N78-32480

A SIMPLE ELEMENT FOR MULTILAYER BEAMS IN NASTRAN THERMAL STRESS ANALYSIS

W.T. Chen and S.K. Wadhwa
International Business Machines Corporation

I. INTRODUCTION

In the study of structural integrity for electronic packages under thermal cycles, an important consideration is the distortion due to the differential thermal expansions of multilayer dissimilar materials. A simple antecedent for such cases is the classical bimetallic beam analysis by S. Timoshenko. In the application of NASTRAN, such structural members are usually represented by bar elements with multi-point constraint cards to enforce the interface conditions. While this is a very powerful method in principle, one finds that in practice the process for specification of constraints becomes tedious and error prone, unless the geometry is simple and the number of grid points low. An alternative approach has been found within the framework of the NASTRAN program. This approach makes use of the idea that a thermal distortion in a multilayer beam may be similar to a homogenous beam with a thermal gradient across the cross section. This paper contains the exact mathematical derivation for the equivalent beam, and all the necessary formulae for the equivalent parameters in NASTRAN analysis. Some numerical examples illustrate the simplicity and ease of this approach for finite element analysis such as NASTRAN.

II. ANALYSIS

Consider an n-layer composite beam of dissimilar materials at constant temperature T, having an external loading N_x as the axial force, and M_y as the bending moment. The cross section is shown in Figure 1.

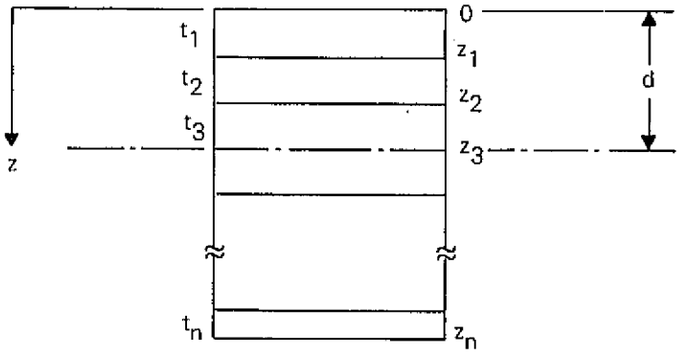

t_i = Thickness of i_{th} layer

z_i = Coordinate of interface

Fig. 1 - Cross Section of n layer Composite Beam

PAGE 216 INTENTIONALLY BLANK

t_1, t_2..t_n are the thicknesses of various layers and z_1..z_{n_i} are the coordinates at the interface. With the coordinates as specified,

$$zi = \sum_{j=1}^{i} t_j$$

Strain at any point can be written as

$$e_{xx} = e + \frac{z-d}{r} - \alpha T \qquad (1)$$

where e_{xx} = elastic strain

e = average axial strain of composite
z = coordinate of the point
d = composites neutral axis
r = radius of curvature
αT = thermal strain
α = thermal coefficient of expansion of the layer

$$\sigma_{xx} = E\, e_{xx}$$

The axial force N_x and bending moment M_y are given by

$$N_x = \int \sigma_{xx}\, dA$$

$$M_y = \int (z-d)\, \sigma_{xx}\, dA \qquad (2)$$

Let E_i, α_i, t_i be the Young's modulus, thermal coefficient of expansion and thickness of ith layer with uniform width b.

Define $z_o = 0$ and,

$$\beta = \int EdA = b \int_{o}^{zn} Edz$$

$$= b \sum_{i=1}^{n} E_i \ (z_i - z_{i-1})$$

$$= b \sum_{i=1}^{n} E_i \ t_i \qquad (3)$$

$$\gamma = \int EzdA = b \int_{o}^{zn} Ezdz$$

$$= \frac{b}{2} \sum_{i=1}^{n} E_i \ (z_i^2 - z_{i-1}^2 \qquad (4)$$

$$\delta = \int Ez^2 dA = b \int_{o}^{zn} Ez^2 dz$$

$$= \frac{b}{3} \sum_{i=1}^{n} E_i \ (z_i^3 - z_{i-1}^3 \qquad (5)$$

$$N_T = \int E \ \alpha \ T \cdot dA = bT \int_{o}^{zn} E \ \alpha \ dz$$

$$= bT \sum_{i=1}^{n} E_i \ t_i \ \alpha_i \qquad (6)$$

$$M_T = \int E \ \alpha \ Tz \cdot dA = bT \int_{o}^{zn} E \ \alpha \ zdz$$

$$= \frac{bT}{2} \sum_{i=1}^{n} E_i \ \alpha_i \ (z_i^2 - z_{i-1}^2 \qquad (7)$$

then

$$N_x = \int_{zn} \sigma_{xx} dA$$

$$= b \int_o \left(Ee + E \frac{(z-d)}{r} - \alpha T \right) dz$$

$$= \beta e + \frac{\gamma - \beta d}{r} - N_T \qquad (8)$$

Similarly M_y can be shown as

$$M_y = \gamma e + \frac{\delta - \gamma d}{r} - M_T - d\left(\beta e + \frac{\gamma - \beta d}{r} - N_T \right) \qquad (9)$$

From Equation (3), since N_x should be independent of r,

therefore

$$\beta d - \gamma = o$$

$$d = \frac{\gamma}{\beta} = \text{distance of neutral axis,}$$

substituting this in Equations (8) and (9) we get

$$N_x = \beta e - Nt \qquad (10)$$

$$M_y = \left(\delta - \frac{\gamma^2}{\beta} \right) \frac{1}{r} - \left(M_T - \frac{\gamma}{\beta} N_T \right) \qquad (11)$$

Thus the external force and moment have been derived for n layer structure. Expression $\delta - \frac{\gamma^2}{\beta}$ is simply area stiffness [in which E is included] moment of inertia about centroid, and can be proved as follows.

δ = Area Stiffness M.I. about coordinate axis [as defined by Equation 5].

MI about centroid [using parallel axis theorem] =

$$= \delta - \text{Area Stiffness} \times d^2$$
$$= \delta - \beta \cdot \frac{\gamma^2}{\beta^2}$$
$$= \delta - \frac{\gamma^2}{\beta}$$

Consider now an equivalent homogenous beam of area A, centroid moment of inertia I, Young's modulus E, thermal coefficient of expansion having thermal gradient $\frac{dT}{dz}$.

Then

$$e_{xx} = e + \left(\frac{z}{r} - z\,\frac{dT}{dz}\,.\alpha\right) - \alpha T$$

where the coordinate axes are the neutral axes of the beam. By using the previous formulation it can be derived that

$$N_x = AEe - AE\alpha T \tag{12}$$

$$M_y = \frac{I}{r} - I\alpha\,\frac{dT}{dz} \tag{13}$$

Comparing Equation 10 to 12 and 11 to 13, the following parametric relationships can be written for equivalency.

$$AE = \beta \tag{14}$$

$$AE\alpha T = N_T \tag{15}$$

$$I = \delta - \frac{\gamma^2}{\beta} \tag{16}$$

$$I\alpha\,\frac{dT}{dz} = P_T - \frac{\gamma}{\beta}\,N_T \tag{17}$$

Thus assuming E for the equivalent beam, Area A, α, I, $\frac{dT}{dz}$ can be calculated from Equations 14 through 17.

Thus a nonhomogenous beam [specified as a finite element in NASTRAN] at constant temperature can be solved by a mathematical equivalent homogenous beam with temperature gradient at the cross section.

III. TIMOSHENKO'S BIMETALLIC BEAM

It can further be proved that for two layer structure, in the absence of external forces, Equation 9 degenerates to Timoshenko bimetallic beam.

Consider now a bimetallic beam of thickness $t_1 = t_2 = t$, and therefore

$z_1 = t$, $z_2 = 2t$.

From Equations 3, 4, 5, 6 and 7

$$\beta = \frac{bt}{2}(E_1 + E_2)$$

$$\gamma = \frac{bt^2}{8}\left[E_1 + 3E_2\right]$$

$$\delta = \frac{b}{24}t^3\left[E_1 + 7E_2\right]$$

$$N_T = bT\frac{t}{2}(E_1\alpha_1 + E_2\alpha_2)$$

$$M_T = \frac{bt}{8}t^2(E_1\alpha_1 + 3E_2\alpha_2)$$

$$M_T - \frac{\gamma}{\beta}N_T$$

$$= \frac{bt^2}{8}T\left[E_1\alpha_1 + 3E_2\alpha_2\right] - \frac{bt^2}{8}T\left[E_1\alpha_1 + E_2\alpha_2\right]\left[\frac{E_1+3E_2}{E_1+E_2}\right]$$

$$= \frac{bt^2}{4}T\left[\alpha_2 - \alpha_1\right]\frac{E_1E_2}{E_1+E_2}$$

$$\delta - \frac{\gamma^2}{\beta}$$

$$= \frac{b}{24}t^3\left[E_1 + 7E_2\right] - \frac{bt^3}{32}\frac{(E_1+3E_2)^2}{E_1+E_2}$$

$$= \frac{bt^3}{96}(E_1+E_2) + \frac{bt^3}{8}\left(\frac{E_1E_2}{E_1+E_2}\right)$$

Substituting in Equation 11, we get

$$M_y = \frac{1}{r}\left\{\frac{bt^3}{96}(E_1+E_2) + \frac{bt^3}{8}\left(\frac{E_1E_2}{E_1+E_2}\right)\right\} - \frac{bt^2}{4}T(\alpha_2-\alpha_1)\frac{E_1E_2}{E_1+E_2}$$

$$= \frac{bt^2}{4}\frac{E_1E_2}{E_1+E_2}\left[\frac{\frac{4}{bt^2}I(E_1+E_2)\left(\frac{1}{E_1}+\frac{1}{E_2}\right) - \frac{t}{2}}{r} - (\alpha_2-\alpha_1)T\right]$$

In the absence of external force, the expression in parentheses is zero, which is identical to Timoshenko's bimetallic beam.

IV. EXAMPLE

For the purpose of illustration, the example in Strength of Materials Part I by Timoshenko [1] will be discussed. To model a bimetallic beam section, one defines four grid points and two bar elements. For each pair of grid points, continuity of the interface displacements must be specified. Multipoint constraints or MPC cards must be used to relate the displacements and rotation of one bar element to the other of the following form

$$u_1 + h_1 \theta_1 = u_2 + h_2 \theta_2$$

It should be noted that this could become quite complicated when many elements are used to represent a curved beam in space.

An equivalent beam with the same mechanical response will now be constructed. The bending curvature of the bimetallic beam will now be induced by the TEMPRB Bulk Data card. The bending stress in the original bimetallic beam due to differential expansion will now be replaced by the thermal moment thermal gradient defined by the TEMPRB card for each bar element. In the example in reference [1], page 219, we shall use

$$b = h = 1,\ E_1 = 1 \times 10^7,\ E_2 = 1.15 \times 10^7,\ \alpha_1 = 1 \times 10^{-4},\ \alpha_2 = 2 \times 10^{-4}$$

Then it turns out that the equivalent beam should be

$$A = 1.8695,\ I = .62091,\ E = 1.15 \times 107,\ \alpha = 1.5348 \times 10^{-4};$$

with 100 degree rise in temperature, the gradient should be 48.8.

V. DISCUSSION

The method proposed in this paper has been found to be very useful in analysis dealing with deformation associated with multi-layered curved beam structures undergoing thermal loads. The main advantages are (1) elimination of the time-consuming task in specifying multipoint constraints, and (2) reduction in number of grid points.

VI. REFERENCES

1. S. Timoshenko, Strength of Materials Part I, D. Van Nostrand, Inc., 1940

D15

N78-32481

ALIGNMENT DISPLACEMENTS OF THE SOLAR OPTICAL TELESCOPE PRIMARY MIRROR

Walter V. Medenica
NASA/Goddard Space Flight Center

SUMMARY

Solar Optical Telescope (SOT) is a Space Shuttle payload which is at the present time (1978) being planned at Goddard Space Flight Center (GSFC). The selected alignment method for the telescope's primary mirror is such that the six inclined legs supporting the mirror are at the same time motorized alignment actuators, changing their own length according to the alignment requirement and command. This paper describes the alignment displacements, including circumvention of some apparent NASTRAN "limitations".

INTRODUCTION

According to Reference 1," the basic scientific justification for SOT is the need to achieve the very high spatial resolution required to determine the density, temperature, magnetic field, and non-thermal velocity field in a large number of solar features, on the scale of which the various physical processes of interest are occuring. These processes include changes in magnetic field strength, waves, single pulses, and systematic mass flows. To study them, it is necessary to resolve regions over which significant gradients occur in the local magnetic and velocity fields, as well as in the local densities and temperatures.

"The SOT is a '1-m telescope'. Its aperture is 125 cm diameter, which will give it a resolution of 0.1 arc sec at 5500 Å (72 km on the sun). It operates from 1100 Å into the infrared and so can observe solar phenomena from the photosphere up through the chromosphere and transition zone to the base of the corona. It will be possible to obtain long sequences of observations that will have uniformly high resolution over the field of view.

"The basic SOT is a large, high resolution space telescope system which will accomodate numerous experiment instruments."

The SOT is one of the Spacelab payloads and its first launch, on the Space Shuttle, is tentatively scheduled for early 1983.

The Space Shuttle Orbiter with the SOT is shown in Figure 1, and the SOT alone is shown in Figure 2. As a Spacelab payload, the SOT remains attached to the Orbiter throughout the launch, flight, and landing. Typical mission would be of several days duration during which time solar observations are made. After return to earth, the SOT is refurbished and prepared for the next flight, typically with a different set of instruments.

The SOT consists of a 3.81 m diameter, 7.31 m long truss structure at the after end of which is mounted the primary mirror (Figure 2). The primary mirror assembly provides active alignment, including focusing, offsetting, rastering, image motion compensation, and sub-arc-second pointing, while the secondary (Gregorian) mirror is fixed (Figure 3). The estimated mass of the first flight SOT is approximately 3000 kg.

ALIGNMENT DISPLACEMENTS

The objective of this paper is to describe the use of NASTRAN for determining the alignment displacements of the SOT primary mirror.

The alignment system has been proposed by Dr. Richard B. Dunn of the Sacramento Peak Observatory in New Mexico. This displacement system is such that the 6 inclined legs supporting the primary mirror are at the same time motorized displacement actuators, changing their own length in response to alignment requirement and command. Figures 4, 5 and 6 show the geometric configuration of the actuator system and the NASTRAN model.

The command system for the displacements consists mainly of three alignment telescopes located around the primary mirror and an annular alignment mirror attached to the secondary mirror. The alignment command system is not part of this paper.

According to References 1 and 2, the following motions of the primary mirror are anticipated as required for alignment:

1. Rotation of the mirror about its focus (Figure 3 and grid point 15 in Figure 6). This motion will be used to offset, to correct the line-of-sight, to raster, and to provide the internal motion compensation. The expected range of this motion $\pm$ 0.5° which corresponds to a translation or decentering of the mirror of approximately $\pm$ 4cm.

2. Tilting of the mirror about its vertex (grid point 14 in Figures 5 and 6). This motion will be used to bring the conic foci of the primary and secondary mirrors (Figure 3) into coincidence. The expected range of this motion is $\pm$30 arc seconds which corresponds to a translation of the focus of approximately $\pm$ 0.65 mm.

3. Focusing, which is the translation of the mirror along the Z axis (Figure 6). The expected range of this motion is $\pm$1 cm.

4. Translations of the focus along the X and Y axes (Figures 4 and 6). The expected range of this motion is not known at the present time.

The specified tolerances are $\pm$ 38 microns "across the prime focal plane", as well as across all planes parallel to it, and $\pm$ 5 microns in focusing, motion No. 3 above. The "prime focal plane" is the X-Y plane at grid point 15.

The fundamental problem to be solved is a geometric one. That is, given the rotations and translations of the focus and the tilt of the vertex, determine the change in length of the actuators.

The displacement problem on hand is a complex and tedious geometric problem, unless it is modeled appropriately, and unless several "tricks" are used in order to permit the application of NASTRAN Rigid Format 1 for solution without resorting to the use of ALTERS.

First, in order to be able to rotate the mirror about the focus, a fictitious rigid element, the Mac Neal-Schwendler's RBE2 (Figure 6), has been introduced as part of the analytical model. The lines connecting the grid point 15 with the grid points 1 through 6, 13, and 14 are merely figurative representations of this element.

The element RBE2 and other features of the indicated analytical model (Figures 4, 5, and 6) make this an over-constrained rigid body problem with no "free point" to start inverting the matrices. This obstacle has been circumvented by the introduction of another fictitious elastic element into the system, CROD 8, between grid points 8 and 16, with the grid point 16 providing the free point (one degree of freedom on the GRID card). This element is theoretically connected to the actual structure at grid point 8. But in order to make it quite obvious that this fictitious element and free point can be entirely independent of the structure, another, alternate, element was placed arbitrarly somewhere in space. The second version of the solution for "Rotations and Translations" uses the fictitious element CBAR 9 (instead of CROD 8) located between fictitious grid points 100 and 101, away from, and unconnected to, the mirror and the fictitious element RBE2 7. The grid point 100 is constrained and the grid point 101 is free in all six degrees of freedom on its GRID card. The results were identical to those obtained with the element CROD 8.

The explanation for this phenomenon lies in the fact that NASTRAN needs at least one elastic element, no matter how fictitious, anywhere in space, with at least one "free point" to start inverting the matrices. One could compare it with priming a water pump.

Secondly, there are no loads, no forces, and no stresses involved in this problem, only displacements. But the element force recovery feature of NASTRAN has been utilized to determine the fundamental unknown: the change in length of the actuators (mirror's legs, Figure 5). This is an important parameter in the displacement system. In order to get these changes in length calculated directly and printed in the output, the original length of the actuators (336.1547 mm) has been substituted for the Young's modulus of elasticity on the material card (MAT1, Table 2). This is based on the following rearragement of the equation for elongation:

$$\delta = \frac{PL}{AE}$$

For A = 1.0 and E = L

$$\delta = \frac{PL}{L} = P$$

Consequently, the NASTRAN output under FORCES IN ROD ELEMENTS contains actually the changes in length of the actuators (in millimeters, Table 4).

After the above fictitious elements are introduced into the model, and the actuators' lengths substituted for the modulus of elasticity, the analyses become very simple.

The following basic analyses were performed:

1. Rotations about the focus and translations of the focus (grid point 15) along the three orthogonal axes using the fictitious element CROD 8.

2. The same as under 1. above using the fictitious element CBAR 9, instead of CROD 8 (Tables 1, 2, 3 and 4).

3. Tilting about the vertex (grid point 14) using the fictitious element CROD 8.

The following aspects are common to all three basic analyses:

1. Rigid Format 1 of the Mac Neal-Schwendler version of NASTRAN has been used. The reason for using this version instead of the NASA/ Cosmic Level 16 version was the fact that the Cosmic rigid elements CRIGD 1 and 2 each require two ALTER replacements while the Mac Neal-Schwendler rigid element RBE2 does not require any ALTER cards. Reportedly, the Cosmic limitation has been removed in the Level 17 version.

2. One-third of the mirror's circle (Figure 4) was covered in 5°-steps, from 0° to 120°, beginning at the + X axes, using two SUBCASES, rotation about the X axis and rotation about the Y axis, and then the combinations of the cosine and sine functions, respectively, of SUBCASE 1 and SUBCASE 2 as SUBCOMS (Table 1). In other words, the X axis is first rotated 5° about the Z axis and then the mirror is rotated about that new axis at the focus (by the selected unit of rotation of one arc second). The remaining two-thirds of the mirror's circle are repetitions of the covered one-third with some changes in sign.

3. The displacements are initiated by a combination of SPC and SPC1 constraints (Table 2).

4. The dimensions used are millimeters and radians, unless otherwise noted.

Examples of the output are shown in Tables 3 and 4.

A NASTRAN Rigid Format 1 limitation is that it will readily solve linear problems only. The problem on hand is geometrically non-linear, but NASTRAN can still be used for small displacements, depending on the required accuracy. Figure 7 presents geometric correction factors to be used with the NASTRAN output for the case of rotation about the focus, i. e. for the motion which produces the largest errors.

It was determined by inspection and comparison that the displacements as produced in the original output (Tables 3 and 4) do not exceed the indicated tolerances, therefore no corrections were required for any of the four basic motions.

A greater accuracy, had it been required, could have been achieved using NASTRAN Rigid Format 1. Assuming, for instance, that the given accuracy beyond a rotation angle of 10 minutes (of the focus, about the X axis, see Figure 4 and 6) is not satisfactory the correction could have been achieved in the following piece-wise linear manner:

1. On the basis of the original location of the grid points and the original length of the actuators, induce a 10-minutes-rotation. Add the increments to the original values.

2. The results of Step 1 provide the locations of the grid points and the lengths of the actuators after a 10-minutes-rotation. On that basis, induce another 10-minutes-rotation. Add the increments to results of Step 1.

3. The results of Step 2 provide the locations of the grid points and the lengths of the actuators for the second 10-minutes-rotation. On that basis induce another 10-minutes-rotation.

4. The addition of increments from steps 1, 2 and 3 offer the grid point displacements and actuator lengths for a 30-minutes-rotation.

   This process is illustrated in Figure 8.

   Table 5 lists the results of such a correction. By comparing the table in Figure 7 with Table 5, one may notice that the accurate correction in Figure 7 for the dimension "a" is 181.0 microns while the approximate correction in Table 5 is 120.7 mircons (Z coordinate). This correction process would be rather voluminous and tedious for the problem on hand because it would have to be repeated for each of the 26 SUBCASES and SUBCOMS of rotation about the focus. Depending on the required accuracy, more or less than three steps would have to be included, and possibly the process repeated for translations and tilt as well. Moreover, a separate MAT1 card would have to be used for each CROD, except the fictitious CROD 8. Without this correction process, one MAT1 card suffices (Table 1).

A correction program along these lines could be developed using NASTRAN.

CONCLUDING REMARKS

This problem and its solution illustrate the importance of proper modeling in the application of NASTRAN, which may mean the difference between a complex, tedious, and time-consuming job on one side and a simple and short job on the other without any sacrifice in accuracy.

It also points at the wide application possibilities of NASTRAN Rigid Format 1, without ALTERS, indicating that this Rigid Format can be used beyond statics, with no forces and stresses and elastic deformations.

REFERENCES

1. NASA/Goddard Space Flight Center/SSPP Office: Executive Summary Solar Optical Telescope Program Plan, May 1978.

2. Dunn, R. B., Sacramento Peak Observatory: Preliminary Design Analysis for the Solar Optical Telescope Main Mirror Actuator, August 1977. NASA CR 156701.

3. The Mac Neal-Schwendler Corporation: MSR-39 MSC/NASTRAN User's Manual, May 1976 (Revised January 1977).

4. NASA/Cosmic: The NASTRAN User's Manual (Level 16.0), March 1976. NASA SP-222 (03).

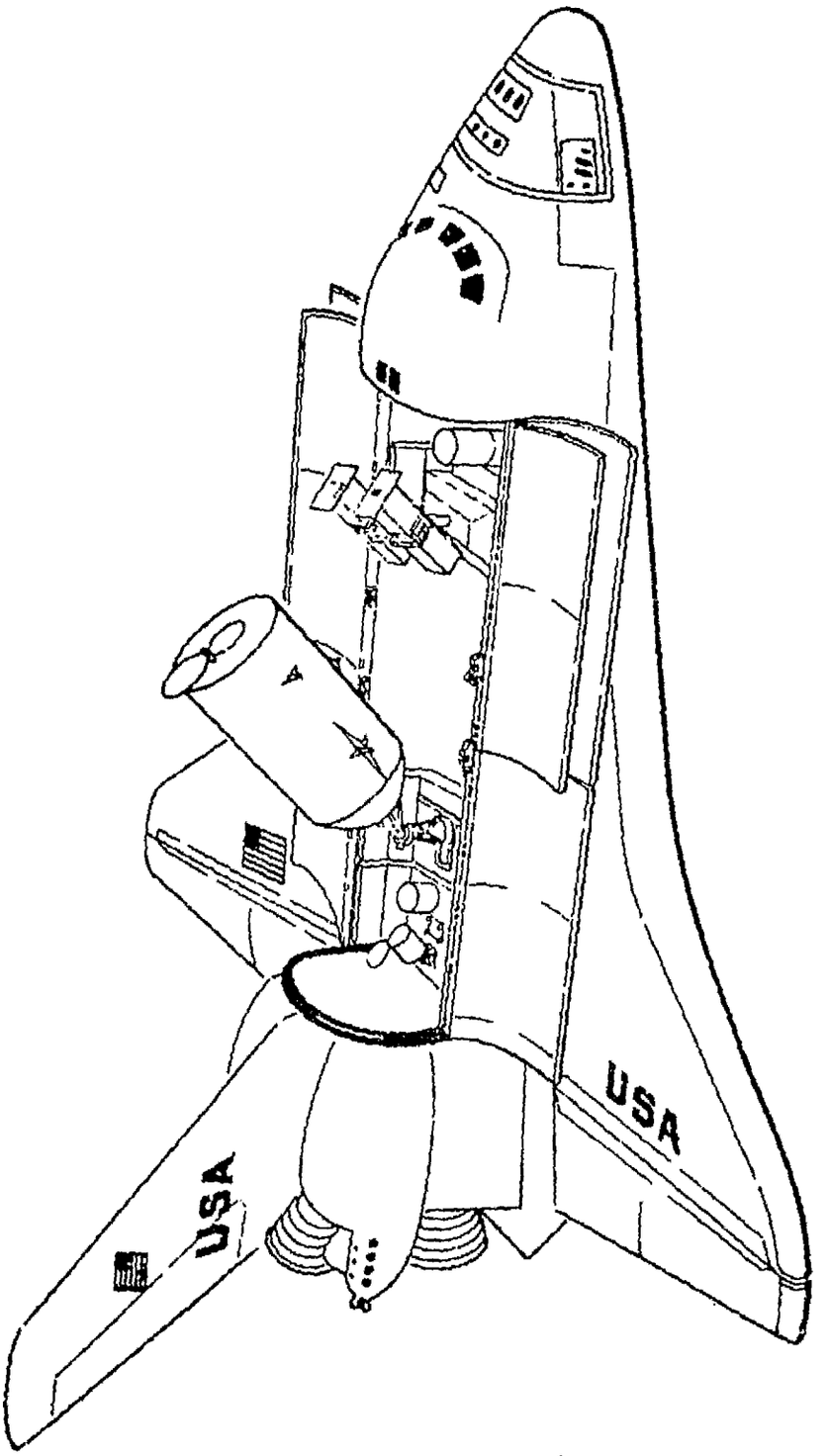

FIGURE 1: ORBITER WITH SOT

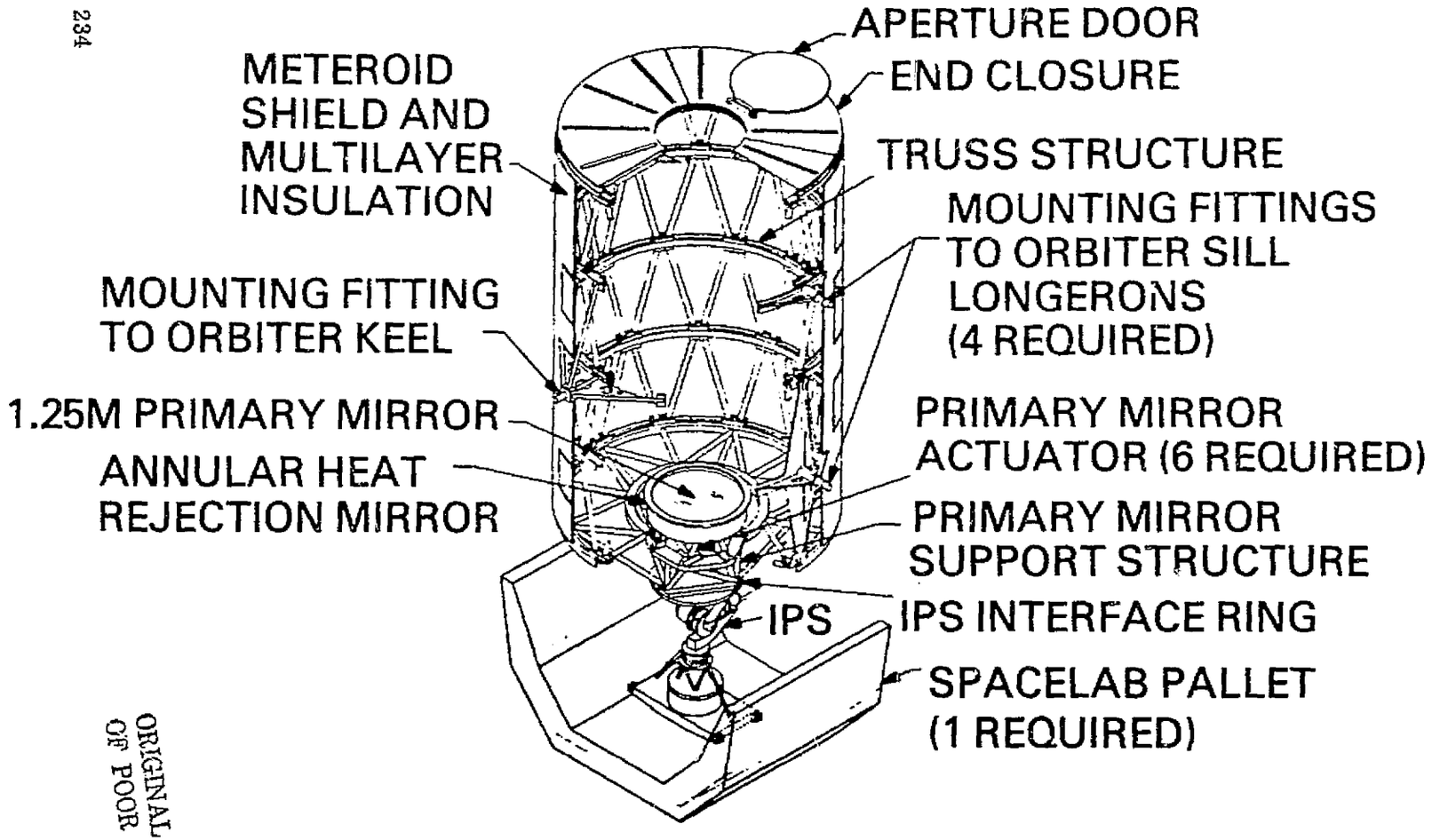

FIGURE 2: BASIC SOT

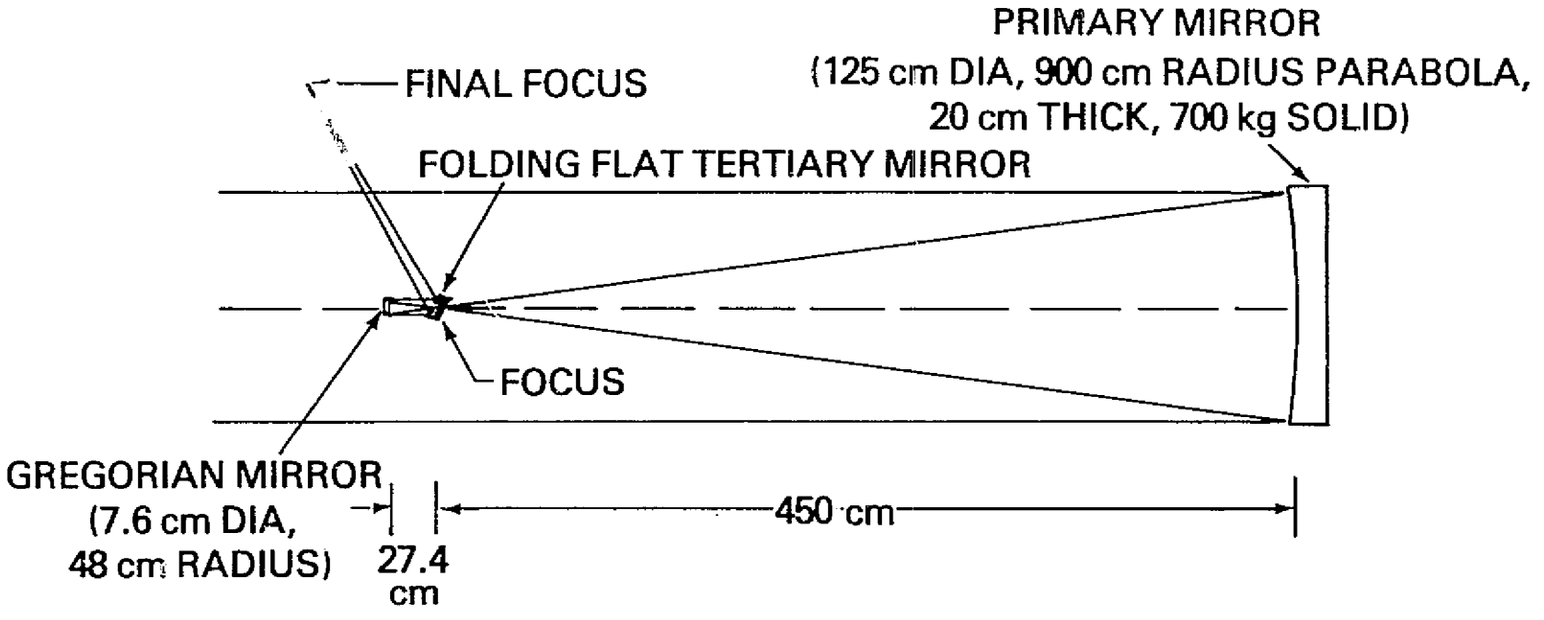

FIGURE 3: TELESCOPE CONFIGURATION

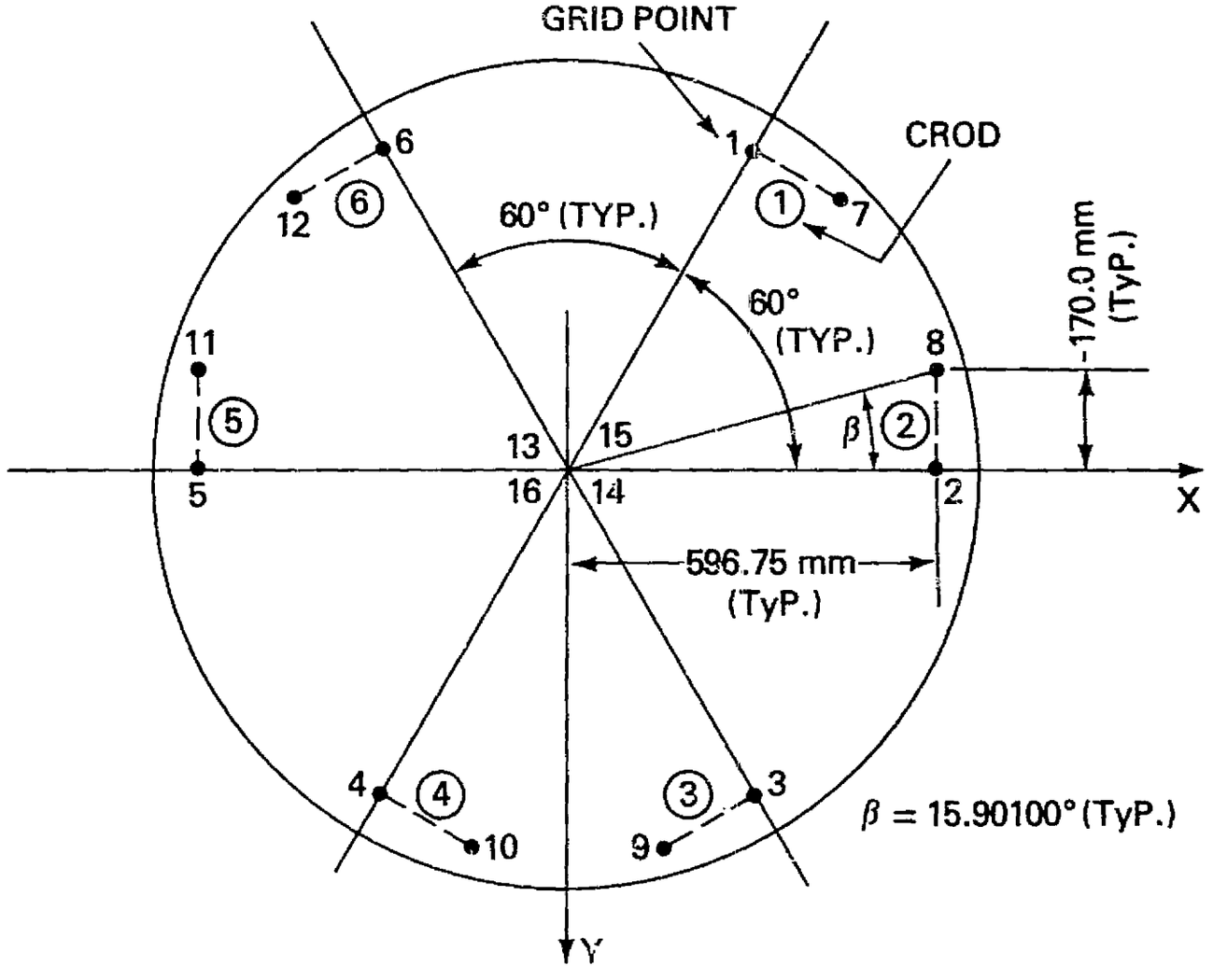

FIGURE 4: PLAN VIEW OF MIRROR & PARTIAL MODEL

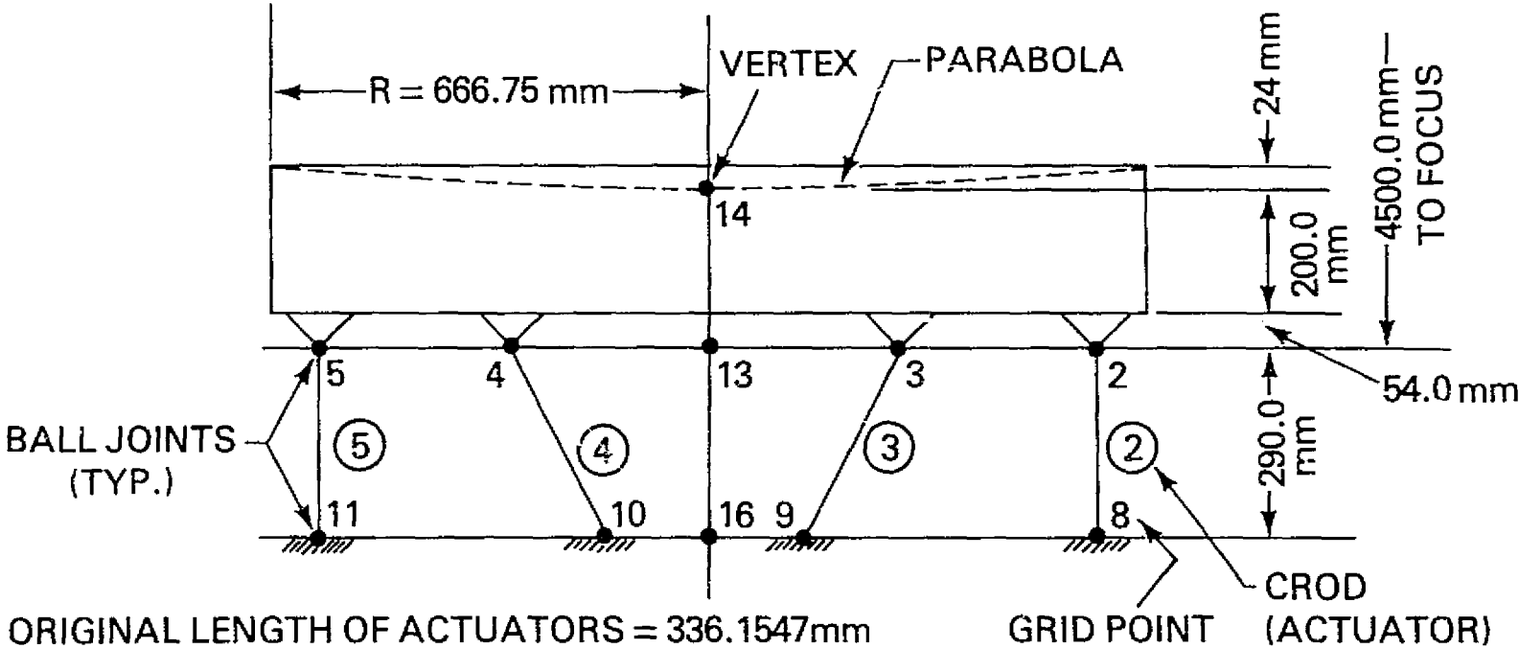

FIGURE 5: SIDE VIEW OF MIRROR & PARTIAL MODEL

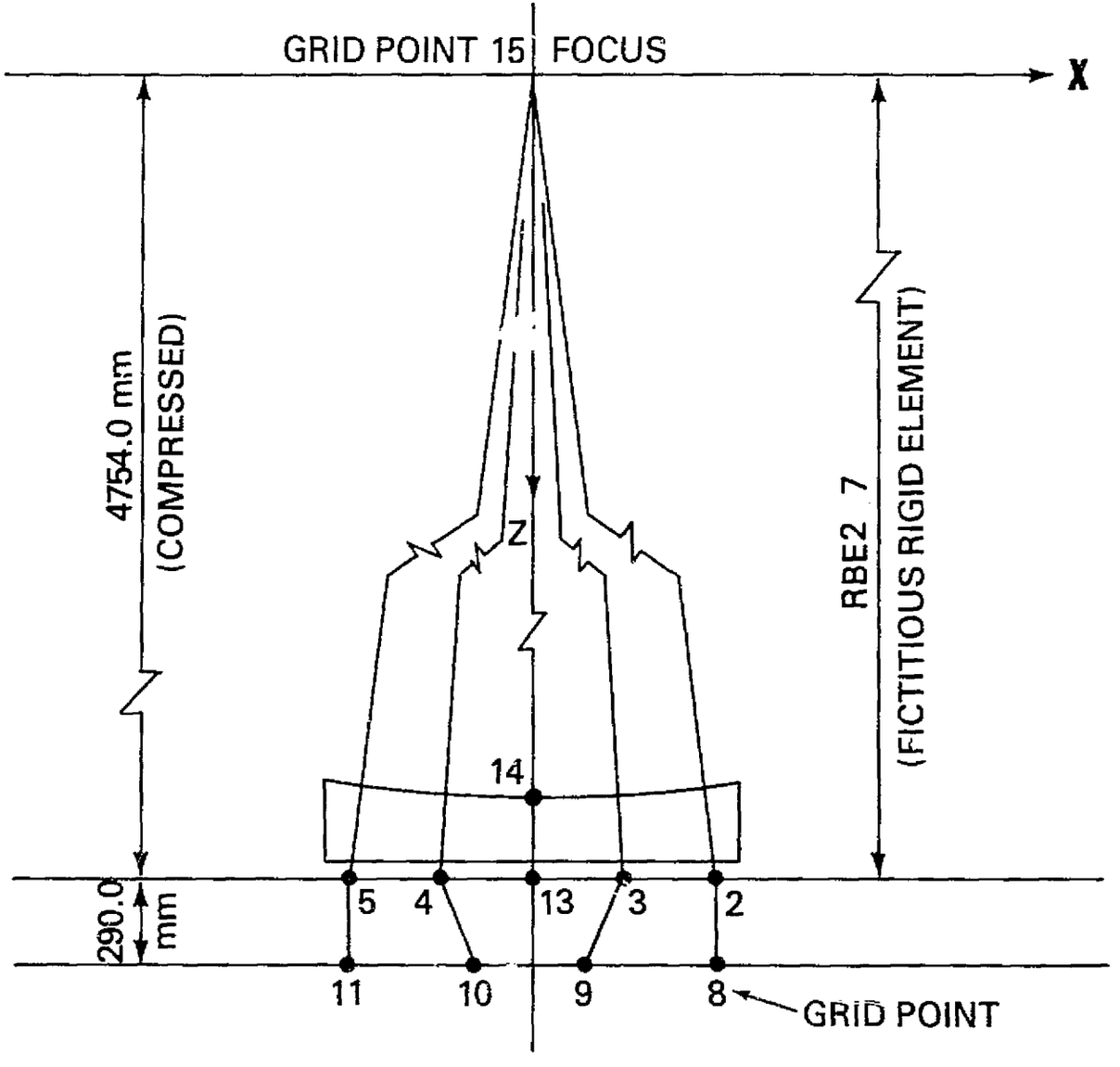

FIGURE 6: SIDE VIEW OF PARTIAL MODEL

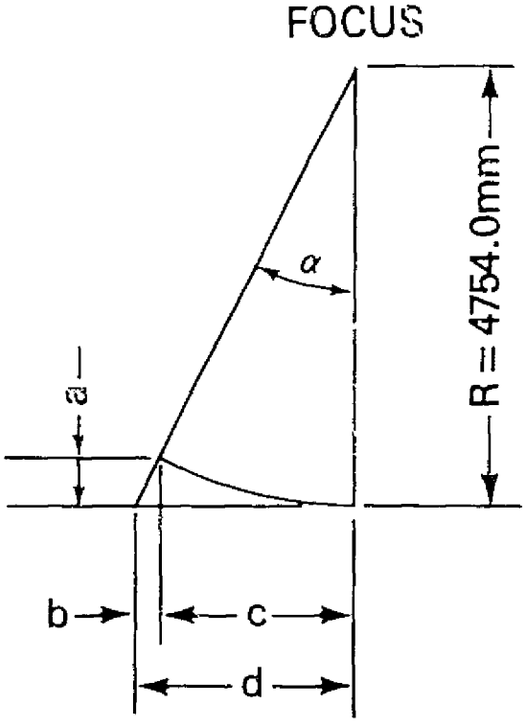

α	a	b
	MICRONS	
1″	0.0001	0.0000
30″	0.0503	0.0000
1′	0.2011	0.0001
10′	20.1132	0.0585
20′	80.4526	0.4681
30′	181.0178	1.5797

$a = R(1\text{-}COS\ \alpha) = C\ TAN\ (\frac{\alpha}{2})$ $\quad d = R\ TAN\ \alpha$

$c = R\ SIN\ \alpha$ $\quad b = d - c = R\ (TAN\ \alpha - SIN\ \alpha)$

a = b = o IN NASTRAN OUTPUT, I.E. d = TRANSLATION VALUE FOR ROTATION α

FIGURE 7: ACCURATE CORRECTION SAMPLE

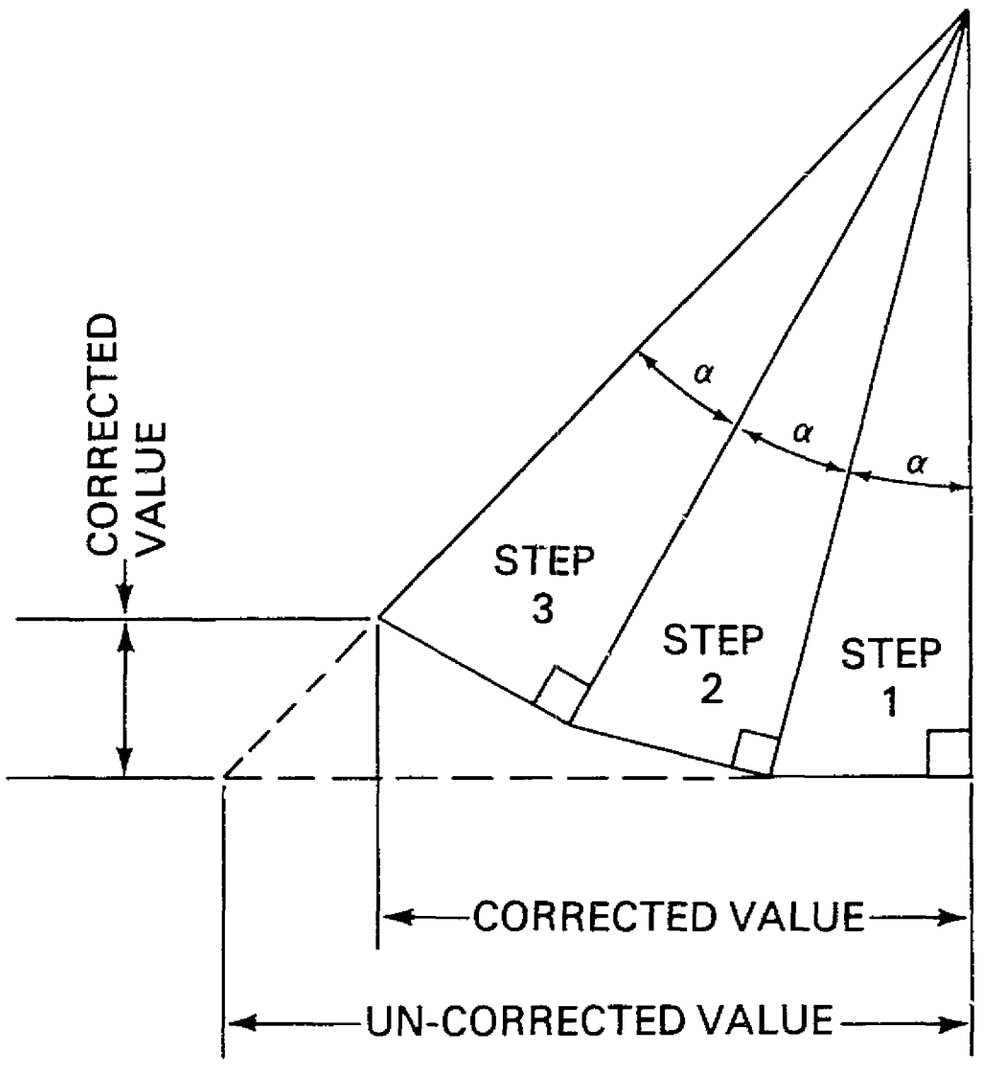

FIGURE 8: APPROXIMATE CORRECTION METHOD

TABLE 1:

SOT PRIMARY MIRROR WITH FICTITIOUS G.P. 100 + 101
ROTATION + TRANSLATION DISPLACEMENTS

C A S E C O N T R O L D E C K E C H O

```
CARD
COUNT
 1      TITLE = SOT PRIMARY MIRROR WITH FICTITIOUS G.P. 100 + 101
 2      SUBTITLE = ROTATION + TRANSLATION DISPLACEMENTS
 3      LINE = 70
 4      OUTPUT
 5         SET 1 = 1 THRU 6
 6         DISPLACEMENT = ALL
 7         ELFORCE = 1
 8         SUBCASE 1
 9           LABEL = 1 ARC SEC ROTATION ABOUT X AXIS
10           SPC = 1
11         SUBCASE 2
12           LABEL = 1 ARC SEC ROTATION ABOUT Y AXIS
13           SPC = 2
14         SUBCOM 3
15           LABEL = 1 ARC SEC ROTATION AT 5 ARC DEGREES FROM X AXIS
16           SUBSEQ = 0.9961946981, 0.0871557427
17         SUBCOM 4
18           LABEL = 1 ARC SEC ROTATION AT 10 ARC DEGREES FROM X AXIS
19           SUBSEQ = 0.984807753, 0.1736481777
-.             . . . .

83         SUBCOM 26
84           LABEL = 1 ARC SEC ROTATION AT 120 ARC DEGREES FROM X AXIS
85           SUBSEQ = -0.5, 0.8660254038
86         SUBCASE 27
87           LABEL = 1 ARC SEC ROTATION ABOUT Z AXIS
88           SPC = 27
89         SUBCASE 28
90           LABEL = 1 MICRON TRANSLATION OF FOCUS IN X DIRECTION
91           SPC = 28
92         SUBCASE 29
93           LABEL = 1 MICRON TRANSLATION OF FOCUS IN Y DIRECTION
94           SPC = 29
95         SUBCASE 30
96           LABEL = 1 MICRON TRANSLATION OF FOCUS IN Z DIRECTION (FOCUSING)
97           SPC = 30
98      BEGIN BULK
```

TABLE 2:

SOT PRIMARY MIRROR WITH FICTITIOUS G.P. 100 + 101
ROTATION + TRANSLATION DISPLACEMENTS

S O R T E D B U L K D A T A E C H O

CARD COUNT	. 1	.. 2	.. 3	.. 4	.. 5	.. 6	.. 7	.. 8	.. 9	.. 10	.
1-	CBAR	9	1	100	101	1.	0.0	1.	1		
2-	CROD	1	1	1	7						
3-	CROD	2	1	2	8						
4-	CROD	3	1	3	9						
5-	CROD	4	1	4	10						
6-	CROD	5	1	5	11						
7-	CROD	6	1	6	12						
8-	GRID	1		298.375	-516.801	4754.					
9-	GRID	2		596.75	0.0	4754.0					
10-	GRID	3		298.375	516.8007	4754.0					
11-	GRID	4		-298.375	516.8007	4754.0					
12-	GRID	5		-596.75	0.0	4754.0					
13-	GRID	6		-298.375	-516.801	4754.0					
14-	GRID	7		445.5993	-431.801	5044.		123456			
15-	GRID	8		596.75	-170.	5044.		123456			
16-	GRID	9		151.1507	601.8007	5044.		123456			
17-	GRID	10		-151.151	601.8007	5044.		123456			
18-	GRID	11		-596.75	-170.	5044.		123456			
19-	GRID	12		-445.599	-431.801	5044.		123456			
20-	GRID	13		0.0	0.0	4754.0					
21-	GRID	14		0.0	0.0	4500.0					
22-	GRID	15		0.0	0.0	0.0					
23-	GRID	100		0.0	0.0	10.		123456			
24-	GRID	101		10.	0.0	10.					
25-	MAT1	.	336.1547		.3						
26-	PBAR	1	1	1.	.083	.083	.141				
27-	PROD	1	1	1.0							
28-	RBE2	7	15	123456	1	2	3	4	5	+RB7	
29-	+RB7	6	13	14							
30-	SPC	1	15	4	4.8481-6						
31-	SPC	2	15	5	4.8481-6						
32-	SPC	27	15	6	4.8481-6						
33-	SPC	28	15	1	1.0-3						
34-	SPC	29	15	2	1.0-3						
35-	SPC	30	15	3	1.0-3						
36-	SPC1	1	12356	15							
37-	SPC1	2	12346	15							
38-	SPC1	27	12345	15							
39-	SPC1	28	23	15							
40-	SPC1	29	13	15							
41-	SPC1	30	12	15							
	ENDDATA										

TABLE 3:

SOT PRIMARY MIRROR WITH FICTITIOUS G.P. 100 + 101
ROTATION + TRANSLATION DISPLACEMENTS

1 ARC SEC ROTATION ABOUT X AXIS

SUBCASE 1

D I S P L A C E M E N T V E C T O R

POINT ID.	TYPE	T1	T2	T3	R1
1	G	0.0	-2.304786E-02	-2.505501E-03	4.848100E-06
2	G	0.0	-2.304785E-02	0.0	4.848100E-06
3	G	0.0	-2.304785E-02	2.505500E-03	4.848100E-06
4	G	0.0	-2.304785E-02	2.505500E-03	4.848100E-06
5	G	0.0	-2.304785E-02	0.0	4.848100E-06
6	G	0.0	-2.304785E-02	-2.505501E-03	4.848100E-06
7	G	0.0	0.0	0.0	0.0
8	G	0.0	0.0	0.0	0.0
9	G	0.0	0.0	0.0	0.0
10	G	0.0	0.0	0.0	0.0
11	G	0.0	0.0	0.0	0.0
12	G	0.0	0.0	0.0	0.0
13	G	0.0	-2.304785E-02	0.0	4.848100E-06
14	G	0.0	-2.181643E-02	0.0	4.848100E-06
15	G	0.0	0.0	0.0	4.848100E-06
100	G	0.0	0.0	0.0	0.0
101	G	0.0	0.0	0.0	0.0

ALL R2 AND R3 DISPLACEMENTS ARE ZERO.

TABLE 4:

SOT PRIMARY MIRROR WITH FICTITIOUS G.P. 100 + 101
ROTATION + TRANSLATION DISPLACEMENTS

1 ARC SEC ROTATION ABOUT X AXIS SUBCASE 1

F O R C E S (N R O D E L E M E N T S (C R O D)

ELEMENT ID.	AXIAL FORCE	ELEMENT ID.	AXIAL FORCE
1	7.989358E-03	2	-1.165550E-02
3	3.666280E-03	4	3.666283E-03
5	-1.165550E-02	6	7.989228E-03

TABLE 5: EFFECT OF APPROXIMATE CORRECTION ON ROTATION OF 30 MINUTES (IN 10-MIN-STEPS) ABOUT X AXIS AT FOCUS

ACTU-ATORS	CHANGE IN LENGTH (mm)		DIFFERENCE
	CORRECTED	UN-CORRECTED	(mm)
1 & 6	15.9327	14.3806	– 1.5521
2 & 5	– 19.5224	– 20.9800	– 1.4526
3 & 4	8.3499	6.5993	– 1.7506
GRID POINTS	CHANGE IN Y COORDINATE (mm)		
	CORRECTED	UN-CORRECTED	
1 & 6	– 41.4735	– 41.4861	– 0.0126
2 & 5	– 41.4866	– 41.4861	0.0005
3 & 4	– 41.4997	– 41.4861	0.0136
GRID POINTS	CHANGE IN Z COORDINATE (mm)		
	CORRECTED	UN-CORRECTED	
1 & 6	– 4.6306	– 4.5099	0.1207
2 & 5	– .1207	0.0	0.1207
3 & 4	4.3893	4.5099	0.1206

D16

N78-32482

APPLICATION OF NASTRAN TO TFTR TOROIDAL FIELD COIL STRUCTURES*

S.J. Chen
EBASCO Services, Incorporated

E. Lee
Grumman Aerospace Corporation

SUMMARY

The application of NASTRAN to the structural analysis of the Tokamak Fusion Test Reactor (TFTR) Toroidal Field (TF) magnetic coils and their supporting structures are described in this paper. The primary applied loads on the TF coils are electromagnetic and thermal. The complex structure and the tremendous applied loads necessitated computer type of solutions for the design problems. In the early stage of the TF coil design, many simplified finite element models were developed for the purpose of investigating the effects of material properties, supporting schemes, and coil case material on the stress levels in the case and in the copper coil. In the more sophisticated models that followed the parametric and scoping studies, the isoparametric elements, such as QUAD4, HEX8 and HEXA, were used. The analysis results from using these finite element models and the NASTRAN System were considered accurate enough to provide timely design information. These analytical results were further confirmed by using the EBASCO developed isoparametric composite element.

INTRODUCTION

The TFTR, now under construction and expected to be operational by 1981, will be the first Tokamak in the world to produce 14 MeV fusion neutrons and 3.5 MeV fusion alpha particles in a break-even experiment involving a deuterium-tritium plasma. The information to be obtained from the TFTR project will contribute to the effort aimed at the construction of demonstration fusion power reactors in the early 1990s. This would help meet our nation's energy demands.

The main components of the TFTR are the large doughnut-shaped vacuum vessel (or torus) which contains the plasma and the TF coils which generate the magnetic field for plasma confinement (see Figure 1). There are 20 TF coils (see Figure 2); each coil has 44 turns of copper winding which are insulated from one another. The coils are wrapped in epoxy and placed in a structural

---

*The work described herein was performed pursuant to Princeton Plasma Physics Laboratory's Subcontract No. 258, under ERDA Contract No. EY76-C-02-3093 with Princeton University.

246

case (see Figure 3). These coils are supported near the machine's center (see Figure 1) by an inner ring and column system and outboard of the coils by outer shear-compression members (see Figure 4).

The coils are operated in a pulsed mode with the current increased from zero until the desired magnetic field strength is reached. The field is held constant (flat top) for approximately 3 seconds before decreasing. The minimum time between pulses is 300 seconds; the coils are required to sustain 300,000 full-power pulses. Heat generated by the electric current in the copper coils is removed by cooling water flowing through the coils at an inlet temperature of 10°C (50°F) and an outlet temperature not more than 68.3°C (155°F).

The primary applied loads on the TF coils are electromagnetic and thermal. There are two electromagnetic loads; one is due to the interaction of the toroidal current and its field which results in a net centering force of 27 076 kN (6087 kips). The other electromagnetic load is due to the interaction of the toroidal current and the Equilibrium Field (EF) which results in a lateral moment of 11 890.0 kNm (105 240 inch-kips) (see Figure 5). The thermally-induced load is mainly due to temperature difference between the copper winding and the coil case.

The complex structure and large applied loads necessitated computer-based analysis for solutions to various design problems. In order to investigate the effects of material properties, supporting schemes, coil case material and manufacturing tolerances on the stress levels in the case and in the coil, simplified finite element models were developed and analyzed using NASTRAN. In the more sophisticated models that followed the parametric and scoping studies, isoparametric elements such as QUAD4, HEX8 and HEXA were used.

This paper will describe the various finite element models that were used in support of the coil design. In addition, the element types, size of each model, multi-point constraints and cyclic symmetry features of NASTRAN are discussed. The analytical results and correlations among the various models are also presented. A comparison of the results obtained using the common NASTRAN isoparametric elements with results obtained using the EBASCO-developed composite isoparametric element will be included.

FINITE ELEMENT MODELS

The finite element method was employed in the structural analysis of the TF coils. Several models of the TF coil were generated during the preliminary and the detailed design phases of the Tokamak Project. They can be categorized as follows:

- Simplified 2-D and 3-D Models
- Detailed 3-D Model
- Detailed Local Models
- Detailed 3-D EBASCO developed Composite Element Model.

The first group of finite element models (FEM) was used primarily during the preliminary design phase, where numerous studies were conducted to achieve an optimum TF coil design with respect to coil shape and coil support schemes. Since the preliminary design phase is characterized by fast design changes, the FEMs must be simple enough for modifications to be accomplished in a short time and the results generated must meet the design objectives. The first three FEMs, summarized in Table I, are considered as Simplified 2-D and 3-D models. TF1G3D was later modified to include dynamic, fault and seismic analyses.

Following the completion of the design studies using the Simplified Models, a preliminary design configuration of the TF coil assembly was subjected to a more detailed stress analysis. The second generation 3-D model (TF2G3D in Table I) was developed for this effort. This model includes the TF coil, outboard inter-coil shear compression box and the inner rings attached to the central column. Analytical results from this model had shown that the stresses in the epoxy and the copper winding in the vicinity of the ring supports were high, but this model was not fine enough to provide accurate results required. Since the demand for design information in the epoxy, copper, coil case bolts and the bolts in the yoke were of such a detailed nature, Detailed Local Models were developed. These models are summarized in Table I as TF3G2D, TF3G3D, 90° Yoke Segment, and Local Stress Concentration.

These models provided timely information for the TF coil design effort from the preliminary design to a final design phase of the Tokamak Program. In the meantime, a more sophisticated isoparametric composite element was being developed. A model using the composite element was generated to confirm the results produced by previous models using available NASTRAN elements, as well as to verify the structural integrity of the TF coil.

A more detailed description of the above mentioned FEMs are presented in the following paragraphs.

First Generation 2-D Model (TF1G2D)

The purpose of this model was to study the different coil shapes and to investigate various support conditions.

The first generation 2-D model consisted of three different models: the circular shape, the dee shape and the tear drop shape, which was basically the dee shape turned around. Due to the symmetric condition of the geometry, as well as the loading (TF force), only one-half the coil was considered in this model, along with its supports.

The coil was represented by a one-line model consisting of beam elements, with the nose and outboard supports simulated by spring elements (see Figure 6). All of the beam elements had six degrees of freedom per element, while the springs had two degrees of freedom per element.

For all analyses, both homogeneous and composite section properties were considered, along with the change of the cross section due to the wedge at the

nose. These properties were calculated at the center of each member, while also applying a factor of the ratios of the Young's moduli of the steel and copper, in order to compensate for the different materials.

The model had support points along the horizontal line of symmetry. These points were assumed to only have the freedom of horizontal displacement. The supports at the outboard inter-coil connections were simulated as horizontal springs whose stiffnesses were calculated based upon the resistance capability of the connections in the horizontal direction. At the nose, the coil originally had a wedge support where the side plates of the steel casing actually came in contact with the adjacent coils, providing resistance to horizontal displacement. In later design, this was replaced by support rings coming from a center column. All three models were considered with the wedge support, and in addition, the circular shape model was analyzed with the support rings. The values of these spring constants depended on the stiffness of such support.

Second Generation 2-D Model (TF2G2D)

The purpose of this model was to understand the force and moment transmitted from the copper winding, through the epoxy, to the steel case, as the coil was subjected to the toroidal field force. This study included the effects of shear modulus in epoxy, the Young's modulus of the copper winding, and the failure of the epoxy in shear.

Due to the symmetric condition of the geometry, as well as the loading (TF force), one-half of the coil with the supports was considered in this model.

The model consisted of three radii, with the inner and outer ones containing the steel casing grid points and the middle one for the copper grid points. When the constant copper cross-section design was introduced, another radius, coincident with the copper grid point radius, was added for additional steel casing grid points. This was needed in order to create a finer mesh to handle the varying thickness of the side plates.

In the model, the steel casing, including outer and inner flanges, and the side plates were modeled as BAR (beam) and QDMEM2 (quadrilateral membrane) elements, respectively. The copper winding was modeled as BAR elements which connected the copper nodal points located in the middle of the coil. The epoxy between steel casing and the copper winding were represented by ROD (beam with pin connections) and SHEAR elements. The cross-sectional areas of ROD and SHEAR elements were calculated based on the equivalent stiffness of the epoxy in resisting the relative movement of the steel casing and the copper winding in radial and tangential directions, respectively. The supports at the nose and the outboard box of the coil basically resisted the movement of the steel casing in the horizontal direction and were modeled as horizontal springs (ELAS2).

Many cases have been investigated with this model and various support schemes have been analyzed. The bond in the epoxy between the copper bundle and the casing have been considered, as well as the case of no bond in epoxy.

Analysis has also been performed to determine the redistribution of stresses, moments, and forces with varying material and cross-sectional properties. This model has also been used to determine the effect of having a gap between the coil and support rings. In addition, various analyses have been performed using the constant copper cross-section design.

The results obtained from these analyses included displacements of grid points, loads in the copper, forces at the supports, and the forces and stresses in the steel casing, copper, and epoxy. All of these results were obtained for both toroidal field (TF) loads and for thermal loads.

First Generation 3-D Model (TF1G3D)

This model, shown in Figure 7, was originally generated to investigate support schemes for the TF coil subjected to out-of-plane loading. It was later modified for dynamic (EF out-of-plane), faulted (TF coil short circuits) and seismic analyses. This coarse type model was selected to avoid the expensive computer cost usually incurred in analyses for dynamic and nonsymmetric static loads. It was estimated that the effects of these loads are minor on the stress in the critical region of the TF coils and the inner support structure (ISS) compared with the normal operating electromagnetic static loads. This model can give a qualitative comparison of TF coil and ISS stress results, and reasonably accurate results for reaction forces at the support pedestals and floor system. This section first describes the finite element model used in the nonlinear dynamic analysis performed for the out-of-plane TF coil pulse loading induced by the interaction of the EF coil magnetic field with the TF coil electrical current field, and then describes the modifications made to this model in the seismic and faulted load analyses.

Dynamic Analysis Model - This model has taken into account the geometric nonlinearity associated with the TF coil pedestal supports, which prevent horizontal lateral displacement of the TF coil in only one direction. Structural damping was also included.

Because of the geometric rotational symmetry of the TF coils, ISS and floor system, a three-dimensional finite element model of a 36° segment of the structure, composed of one-dimensional and two-dimensional finite elements, was used in the analysis (see Figure 7). The model was sufficiently detailed so that the effects of the TF coil pulse loading, seismic loads and fault loads could be determined, but local structural details, such as keyed and bolted splices and cutouts, were not incorporated into the model. A total of 262 nodal points and 248 finite elements (114QUAD4, 76BAR, 44RBAR, 12ROD, 2CELAS2) were used.

The TF coils, represented by BAR elements, were connected to the support pedestals by means of RBAR elements and CELAS2 spring elements which take into account the coil base pedestal stiffness. These connections provide horizontal lateral load transfer from the TF coils to the pedestals. At these connection points between coil base and pedestal top, a nonlinear transient force-displacement relationship was defined to represent the nonlinear behavior of the pedestal support system. This geometric nonlinearity is such that

the restraint imposed on the coil base is a function of the direction of the relative horizontal lateral displacement between the coil base and the pedestal. Physically, this restraint is provided by a snubber plate against which one side of the coil base initially rests. The snubber plate location alternates from side to side, from coil to coil. Under load, when the coil base tends to displace such that it bears against the snubber, resistance to that displacement is provided. When the coil base displaces away from the snubber, it can do so freely and without restraint.

The floor structure was modelled as a system of QUAD4 elements and BAR elements. Connection of the pedestals to the midheight of the floor were made with REAR elements.

The TFTR structure is externally supported at the machine floor level by connection of the outer edge of the machine floor to vertical columns and the building floor system, and by connection of the inner edge of the floor system to vertical columns. These external boundary conditions were incorporated into the finite element model by fully restraining all degrees of freedom at the outer edge of the machine floor (3 displacements and 3 rotations). The vertical floor columns were not incorporated into the model because their effect on the analyses performed is negligible.

To simulate the symmetric behavior of the structure, boundary condition relationships equating displacements and rotations at boundary grid points were imposed.

Model Modifications for Seismic and Faulted Load Analyses - The primary modifications made to the model for the seismic and faulted load analyses were related to the boundary conditions. Since these loads were not rotationally symmetric like the dynamic load, the symmetric boundary condition used in the dynamic analysis was not valid. NASTRAN's cyclic symmetry features were used to represent the entire 360° structure, including 20 TF coils. In order to use the cyclic symmetric features, the non-linear connections between the TF coils and the tops of the pedestals were removed. It was assumed that only one out of every pair of coils was connected to the support pedestal. The floor system, which has a minor effect on these analyses, was totally restrained to reduce the problem size.

Second Generation 3-D Model (TF2G3D)

The first generation finite element models described in previous paragraphs were used mainly in the preliminary design of the TF coil, in the selection of coil shapes, and finally in the baseline design. Having designed a baseline TF coil, the next step was to perform more detailed stress analyses. In order to support the detailed design phase of the TF coil, a more sophisticated finite element model was required. The second generation 3-D model was developed for this effort. This model is a three-dimensional finite element model which includes the TF coil, outboard inter-coil support box and the inner rings attached to the central column support. The second generation 3-D finite element model represents an 18° sector which includes part of the ring and column support, one coil, and two half shear-compression supports from

each side of the coil (see Figure 8). The coil case is simulated by plate elements (QUAD2, TRIA2) with inplane and bending stiffnesses.

There are 44 copper windings in each coil; they are electrically isolated from each other and the coil case. The copper windings are represented by four solid elements (HEX8), and they are separated from the coil case by the epoxy and the electrical insulating material.

The center column and ring supports and the outboard inter-coil shear-compression boxes are represented by plate elements. The TF coil finite element model is supported at the bottom of the coil. This pedestal support allows the coil to move in the upward direction (no hold-down) but supports the weight and loads in the downward direction. In addition, the coil is allowed to move laterally (perpendicular to the coil plane), but is restrained by a key in the opposite direction. Radially from the device center, the coil is unrestrained. The coil nose area is connected in three directions to a 4-ring system. The two outer rings are in turn attached to the central cylinder only in the tangential direction, normal to the coil plane. The inner rings, however, are rigidly connected to the central cylinders.

The cyclic symmetry capability of NASTRAN was used to effect the remaining 19 sections of the TF coil system. The boundary points are defined as input to the program. The computer time was excessive when cyclic symmetry was used. Since the structural analysis of the baseline configuration was mainly using symmetric load, the multipoint constraints (MPC) can be used on the boundary points and, therefore, one coil model is needed. The computer time has been reduced considerably by using the MPCs. However, for unsymmetric loading, the cyclic symmetry must be used.

The epoxy bond between the copper and the coil case may have been separated during the curing process. In order to simulate this condition in the finite element model, the epoxy can have only compressive strength. When the result showed any epoxy spring element that was in tension, the spring element was eliminated from the model. After several iterations, all spring elements that were in tension were eliminated from the model. The results were representative of the no epoxy bond case.

The second generation 3-D TF coil finite element model has 1006 grid points, 1274 elements (46 TRIA2, 524 QUAD2, 176 HEX8, 528 ELAS2), and 4239 degrees of freedom. A typical run of this model, employing MPC boundary conditions, had used approximately 3000 system resource units (SRU) of computer time, whereas a run using cyclic symmetry had used three times as much time.

There were several NASTRAN runs made using the 3-D model in direct support of the TF coil design effort. The effect of different materials (e.g., titanium or steel) for the coil case and the inner support structure was investigated. Studies were done to vary the location and number of rings for the central column support. Varying thicknesses of the coil outer flange was also analyzed using the 3-D model.

The grid point forces and displacements, element forces, and stresses are printed output from the NASTRAN run. Some of the results are usually summa-

rized manually to provide immediate design information. However, the amount of data remaining to be summarized was massive; therefore, it was imperative that a computer aided post-processing program be developed. The output of these FORTRAN programs was in both tabulated and plotted formats. Plots of shear load per unit length for the inner and outer flanges were made. These plots provided the designer with the necessary information for sizing the bolts required for fastening the coil sideplate to the inner and outer flanges. These plots and tabulated data were subsequently used for fatigue analysis. In addition to these plots, copper hoop stress, epoxy normal stress, and casing membrane stress intensity were also plotted.

The copper stresses were printed in the basic rectangular coordinate system; however, this was not convenient for evaluation. The latest version of NASTRAN with the HEXA element has rectified this shortcoming. However, the corner stress "jump" for the solid element was very disturbing. Fortunately, the copper hoop stress was reasonably accurate when the 4-corner HEXA stresses were arithmetically averaged. This was perhaps due to the fact that there was no applied load in that direction. In the radial direction, the HEXA stresses cannot be simply "averaged". It was estimated using the grid point force output. More experience is required for the interpretation of the solid element stress output.

Third Generation 2-D Model (TF3G2D)

Since the inter-laminar epoxy stresses from the second generation 3-D model were obtained from a relatively crude epoxy/copper simulation, a more detailed third generation 2-D model (TF3G2D in Table I) was developed. Symmetry required only half of the coil in the model (see Figure 9). Bar elements were used for copper layers and inner and outer flanges of the case. A shear panel provided only shearing strength for the copper-to-copper and copper-to-case interfaces. A rod element provided two degrees of freedom which gave direct relative motion of the interfaces. An energy equivalence was made to obtain a spring constant for the rod and a shear strength for the shear panel. In addition to the elements in the bar-shear-spring model, a membrane element was applied in TF3G2D. This type of element was used to simulate the in-plane deformation and strength of the case side plates.

Local bending and tangential extension of all grid points at both ends of the half coil were restrained due to symmetry. Rod elements provided horizontal elastic supports at center column ring supports and connecting box supports. An energy equivalent was made for those rod elements to obtain the proper stiffness constants.

The number of nodal points for a representative model of this kind was 612, which resulted in 1604 degrees of freedom. The two-dimensional elements included 900 bars, 480 rods, 120 membranes, and 390 shear panels. Total number of force units applied to the system, for magnetic force in static analysis alone, was 434. Number of variable temperature grids was 588. Average computing time for each run was 648 system seconds on a CDC-6600 for three loading cases.

Third Generation 3-D Local Model (TF3G3D)

The third generation 2-D model described in the previous paragraphs was used to investigate shear stress distribution in epoxy due to in-plane loads (TF and thermal). The third generation 3-D local model (see Figure 10) was used primarily for the study of the shear stress in the epoxy and copper stress due to in-plane and out-of-plane (EF) loads at the critical area.

To keep the model small enough to be analyzed in the current computer and still render good critical stress data, a portion of the TF coil was analyzed. This local model consisted of the coil cut from horizontal zero degree plane and approximately 54-degree plane from the horizontal. By applying a symmetric and an anti-symmetric boundary condition to the model, a cut was made to the middle plane which was the separation of the reverse copper winding by a barrier strip. The barrier strip retained full capability of bonding; however, the bonding between the copper bundle and the case was removed except where the compression was developed by the combined loads. The nose supporting ring was simulated by springs in all directions. Boundary forces were applied to the 54-degree cross section. These forces were obtained through global 3-D model. Magnetic loads and thermal data were carefully distributed to all grid points of the model. It was the thinner copper layer and the flexibility of the layer in the other direction that made the usage of plate elements in 3-D model. TF load applied to the model included a radial in-plane load and a transverse out-of-plane load which squeezed the copper to the barrier strip.

The differences between this model and the third generation 2-D model were that plate elements were used in the 3-D model to represent copper layers, whereas bar elements were used in the 2-D model. In addition, solid elements were used in the 3-D model for the outer flange, whereas bar elements were used in the 2-D model. Due to the geometric complexity and the thickness variation of the outer flange, the solid element was used. Two types of solid elements were used in the 3-D model. A HEXA element had eight nodal points at the corners. Each corner had three translational degrees of freedom. Two HEXA elements used in the model had extra points along the edges for the proper modeling of wedge transition. A WEDGE element had six nodal points at the corners. Each corner had three translational degrees of freedom. HEXA elements were used also for the barrier strip. Plate elements used for copper, side wall, and inner flange were QUAD4s. A QUAD4 element had four nodal points at the corners and each nodal point had five degrees of freedom. The cooling hole stiffness was reduced by using offset capability of QUAD4. Shear panels used in the model were SHEAR's which were obtained from energy equivalent. The shear panels had only shear capability and each panel had four degrees of freedom. These panels connected the copper layers in two ways. A series of shear panels took the resistance of slip between copper layers in tangential direction and the other series of shear panels prevented copper from relative movement in the transverse out-of-plane direction. Finally, a set of two degrees of freedom rod elements provided compressibility of copper layers and epoxy which wrapped copper layers and copper bundle. The connection between the outer flange and the side wall was accomplished with bars and rods.

The number of grid points in the system was 2,347. It had 10,761 degrees of freedom for symmetric load condition and 11,231 degrees of freedom for anti-symmetric load condition. The number of total bulk data lines (or cards) was 14,894. Total execution time in SRU was 14,610 on a CDC-6600 for three subcases and two subcombs by NASTRAN code.

TF Coil Yoke Finite Element Model

The yoke finite element model is a 90° segment (90° - 180°) taken from the second generation 3-D model. The boundary loads were based on the TF2G3D model. The main objective of the 90° segment yoke model was to ascertain the bolt loads between the yoke and the coil case, and between the yoke and the shear-compression box (see Figure 11). Revisions to the yoke model required fewer manhours and computer usage time compared to the full coil model. Therefore, this model was used for yoke design support and parametric studies. The yoke model includes all elements associated with the second quadrant (90° - 180°) of the second generation 3-D TF coil model. The coil case is simulated by plate elements (QUAD4, TRIA3) with inplane and bending stiffnesses. The copper windings are represented by 6 solid elements (HEXA); they are separated from the coil case by the epoxy and the electrical insulating material. Due to design considerations, the epoxy material between the copper winding and the casing is assumed to take compression loads only, and has no shear or tension capabilities. The spring element (ELAS2), which has two degrees of freedom, is used to simulate these compression forces.

The bolt shear and contact stiffnesses are simulated by using the spring element (ELAS2). The yoke and shear-compression box are simulated by plate elements. A typical section is shown in Figure 11. The bolt shear stiffnesses were calculated by assuming that the parent material had yielded to 2% of the bolt diameter, and these stiffnesses were beamed to the nearest grid points.

The coil case is made of steel; the gages at the side wall, outer and inner flanges are 2.9 cm (1 1/8 in.), 14.6 cm (5 3/4 in.), 6.9 cm (2 3/4 in.), respectively. The shear-compression box and yoke assembly are shown in Figure 11.

The yoke model uses the NASTRAN multipoint constraints (MPC) at the shear-compression box boundary points. The boundary loads at both 90° and 180° are calculated using the TF2G3D model.

The contact stiffness between the shear-compression box and the yoke and the bolt axial stiffness are simulated by using spring elements. When the contact spring elements are in tension, they are eliminated from the input data set. When the bolt is in tension, the tensile stiffness is used.

The yoke finite element model has 616 grid points, 922 elements and 3,696 degrees of freedom. The computer time usage is 1,500 seconds (SRU).

Local Stress Concentration Model

The fatigue life requirement is one of the critical items in the TF coil design. A better understanding of the peak stress (including stress concentration) distribution around the bolt hole of the coil casing is essential to the estimation of the fatigue life. The primary contributors to the peak stress around the bolt hole are the bypassing stress (hoop tension) and the pin loads (both tangential and radial directions). Because of the complicated nature of the casing geometry, the effects of the by-passing stress and the pin loads are coupled. It implies that without knowing the load path around the bolt hole, it is difficult to predict how much of the peak stress is contributed by the by-passing stress or by the pin loads. Therefore, a finite element analysis was initiated to study the load path in the critical bolt hole and predict the critical peak stress. The finite element model included a segment of side plate with the critical bolt holes connecting the inner flange.

The "Multilevel Superelements" approach available in the NASTRAN program was chosen in this analysis. The advantage of the superelement approach is to allow a fine mesh model near the critical bolt holes, but a coarse mesh away from the critical area without losing the accuracy. Moreover, it is only required to have one fine mesh bolt hole model which can be repeated as many times as desired to simulate a series of bolt holes.

Two mesh generators were written to automatically generate two separate models. One is the coarse mesh model, designated as the residual superelement (see Figure 12), which included a segment of the side plate, including the bolt holes away from the critical area. The other is the fine mesh model of a typical bolt hole, designated as the primary superelement (see Figure 13). Then any number of the secondary superelement, which is similar to the primary superelement, can be automatically generated. Figure 14 shows the combined geometry of the residual and primary superelements, and indicates the location of two secondary superelements. The mesh generators were programed to include the parameters, such as diameter of bolt hole, pitch of bolt hole, numbers of bolt holes and the dimensions of the side plate segment.

The model is two-dimensional. The quadrilateral (QUAD4) and triangular (TRMEN) plate elements were used in the residual superelement, while the TRMEN element was used in the primary superelement. The QUAD4 element has eight degrees of freedom, while TRMEN has six degrees of freedom.

The force boundary condition was used to describe the boundary at the edges of the side plate segment and the pin loads acting on the bolt hole. These data were obtained from the result of 3-D analysis (TF2G3D model). The residual superelement model was used to check these applied forces for the static equilibrium. The stresses in the side plate resulting from the equilibrium check run were also compared with the 3-D result. The uniform radial pressure distribution was assumed for the pin loads acting at the primary and secondary superelements.

Three different loading conditions were considered for each model: pin loads in both tangential and radial conditions, pin load in tangential direc-

tion only (shear key to take radial shear), and no pin load. The "no pin load" condition was not the real design option being considered. However, it was included to approximately simulate the condition if the friction took all the shear loads. For all loading cases, the stress printouts plus the stress contour plots for the maximum principal stress were obtained directly from NASTRAN runs.

Composite Element 3-D Model

This model uses the EBASCO developed 3-D solid composite elements for heterogeneous material. These elements simulate the composite action of the copper and epoxy bundle and also give detail stress information in both copper and epoxy. The composite element is defined by 8 to 20 nodes.

The coil case was represented by composite elements with homogeneous isotropic properties. There were two radial layers to represent the 5 3/4 inch thick outer flange. The yoke, inter-coil shear compression boxes, pedestal support, and support rings at the nose were also modeled using the composite element. The composite element TF coil model has 2567 grid points, 740 composite elements, and 736 non-linear spring elements. Further discussion and theoretical presentation of the composite element can be obtained from references 1 and 2, respectively.

DISCUSSION OF MODEL RESULTS

Representative results from the previously described finite element models are discussed in the following paragraphs.

Figure 6 shows the various coil shapes represented by the TF1G2D models. The high energy requirements for the dee shape had eliminated it from further consideration. The practical design difficulties of the inclined spring support for the tear-drop shape with T1 = T2 (see Figure 6), and the large tension jump which exists in the tear-drop shape with T1 $\neq$ T2 have also eliminated it from consideration. Manufacturing simplicity of the circular coil and its low-energy requirements were the important points for the selection of the circular configuration.

Figure 15 shows the casing stress versus location and stiffness of the double ring supports for the circular coil. This was obtained by using the TF2G2D model.

Using the TF1G3D model, a NASTRAN non-linear dynamic transient analysis was performed for the 0.42 Tesla Strong Compression plasma off run 41 EF load condition. This out-of-plane TF coil loading was applied to TF coil nodes as concentrated time dependent nodal forces. The load-time profile used is shown in the normalized strong compression EF current of Figure 16. Both dynamic and static analyses were made using the TF1G3D model. Comparisons of

the stresses obtained from the dynamic and static analyses were made to determine the dynamic effect of the operational EF loading. Typical stress multiplication factors for various parts of the TF coil structure were less than 1.09 except in the area near the pedestal support. The factor is 1.18 at the pedestal support. The tangential load transmitted to the floor at the pedestal increases from 0 (static loads) to 60 kips (dynamic load). This is due to the inertia load induced by the restraint at the pedestal. Similar results were obtained for the faulted load (one or more coil short-circuited) and seismic analyses. Both the faulted and seismic loads have little effect on the coil, whereas the pedestal receives a significant amount of loads.

A plot of maximum shear stress in the epoxy due to the TF and thermal loads from the TF3G2D model is shown in Figure 17. Since the model is 2-D, epoxy shear stress due to EF load is not available; it can be obtained from the 3-D model TF2G3D (see Figure 18).

The design criteria used for the coil case is basically derived from the ASME Boiler and Pressure Vessel Code. This code uses stress intensity, which is defined as the largest algebraic difference between any two of the three principal stresses. In order to facilitate the evaluation of coil case stress, all NASTRAN output for the TF2G3D model were post-processed and presented in both tabulated and plotted formats. A typical plot of membrane stress intensity is shown in Figure 19. A plot shown in Figure 20 was used by the designer in the determination of bolt requirement (the bolts fasten the coil side plate to the flange).

Stress distributions in various parts of the TF3G3D local model are shown in Figure 21. These results are for the early TF coil, with titanium as casing material. This model was not re-run for the latest configuration, since at that time the composite element was available for model development. However, the results from the early coil configuration served as a benchmark for the TF2G3D model.

The yoke load distribution calculated by using the yoke model is shown in Figure 22.

The major principal stress and the maximum stress intensity (twice of maximum shear) are presented in Table II. In general, the maximum principal stress is the tensile stress in the tangential direction of the TF coil. The stress level was mostly due to the by-passing stress; the radial pin load contributed about 15% to 18% and the tangential pin load contributed about 7%. The difference between the principal stress and the stress intensity was primarily due to the bearing (compressive) stress of the pin loads. In load cases 2 and 3, there were minor or no differences between the maximum principal stress and stress intensity, since no radial pin loads were directly applied at the edge of the bolt holes.

The stress levels in the coil components from the Composite Element model and the second generation 3-D model are compared in Table III. Despite the number of different model techniques used in these models, the stress levels were fairly close.

CONCLUDING REMARKS

There were sufficient NASTRAN diagnostics used in all models described in this paper such that good numerical results were obtained. Force balance at the inner support structure and selected coil nodal force balances were performed so that the confidence in these models was ascertained. Furthermore, the stress outputs from these models were compared and were found to be relatively close. The analysis results from these finite element models and the NASTRAN System were considered accurate enough to provide timely design information.

The application of available NASTRAN elements to the Tokamak toroidal field coil finite element models was considered very effective and the analysis results were acceptable. However, care should be taken in using the spring and isoparametric elements. Some of the comments pertaining to these elements are listed below:

- The plate element has no inplane rotational stiffness. Special care should be taken when it is connected to one-dimensional elements.
- The spring element used for non-colinear connection will induce unbalance moment.
- The nodal force balance output does not include the "lock-in" force induced by the thermal load.
- In a coarse model, the corner stresses for solid elements HEX8 and HEXA are not reliable.

The effect of the local detail design, such as the bolt joint connection between the sideplate and the flange, was neglected in the TF2G3D and other simplified models described in this paper. This effect will be analyzed separately when design detail is available.

REFERENCES

1. Chen, S.J., Heifetz, J., "The Toroidal Field Coil Stress Analysis - As Planned and Executed for the TFTR," Seventh Symposium on Engineering Problems of Fusion Research, Knoxville, Tennessee, October 1977.

2. Chang, H., Huang, N.S., "A 3-D Solid Finite Element for Heterogeneous Materials," Seventh Symposium on Engineering Problems of Fusion Research, Knoxville, Tennessee, October 1977.

Table I Finite Element Models

MODEL	OBJECTIVES	MODEL DESCRIPTION	LOADS
TF1G2D	• COIL SHAPE SELECTION • COIL SUPPORT SCHEME	• BAR, ELAS2 ELEMENTS • ONE-HALF OF COIL WITH SYMMETRIC BOUNDARY CONDITION	TF
TF2G2D	• COIL SUPPORT SCHEME • EFFECT OF INSULATION	• BAR, QDMEM2, ROD, SHEAR, ELAS2 ELEMENTS • ONE-HALF OF COIL WITH SYMMETRIC BOUNDARY CONDITION	TF
TF1G3D	• COIL SUPPORT SCHEME • DYNAMIC, SEISMIC, FAULT LOADS ANALYSES	• BAR, QUAD2, (QUAD4, ROD, ELAS2) ELEMENTS • TWO COILS WITH ROTATIONAL SYMMETRIC BOUNDARY CONDITION OR CYCLIC SYMMETRIC FEATURE	TF, EF, DYNAMIC, SEISMIC, FAULT
TF2G3D	• LOAD AND STRESS IN CASING • UPDATE DESIGNS • PROVIDE BOUNDARY COND FOR LOCAL MODELS • ESTIMATE STRESS INSIDE COIL	• QUAD2, HEX8, TRIA2, ELAS2 ELEMENTS • ONE COIL WITH ROTATIONAL SYMMETRIC BOUNDARY CONDITION OR CYCLIC SYMMETRIC FEATURE	TF, EF, THERMAL, DEAD
TF3G2D	• STRESS IN THE COPPER AND EPOXY • UPDATE DESIGNS	• BAR, SHEAR, ROD, QDMEM2 ELEMENTS • ONE-HALF OF COIL WITH SYMMETRIC BOUNDARY CONDITION • INCLUDE TWENTY-TWO LAYERS OF COPPER AND EPOXY INSULATION	TF, THERMAL
TF3G3D	• DETAILED STRESS IN THE CASING, COPPER, AND INSULATION AT THE CRITICAL NOSE AREA	• QUAD4, HEXA, WEDGE, SHEAR, ROD, BAR ELEMENTS • ONE-HALF OF 54.7° SEGMENT WITH SYMMETRIC AND ANTI-SYMMETRIC BOUNDARY CONDITIONS AND BOUNDARY FORCE FROM TF2G3D MODEL	TF, EF, THERMAL
90° YOKE SEGMENT	• BOLT LOADS AT THE OUTBOARD SUPPORT (YOKE)	• QUAD4, TRIA3, HEXA, ELAS2 ELEMENTS • 90° SEGMENT WITH THE BOUNDARY FORCE FROM TF2G3D MODEL	TF, EF, THERMAL
LOCAL STRESS CONCENTRATION	• PEAK STRESS AT THE BOLT HOLE OF SIDE WALL	• QUAD4, TRMEN ELEMENTS • APPROX 30° SEGMENT OF SIDE WALL WITH BOLT HOLES MODELED • MULTIPLE LEVEL SUPERELEMENT APPROACH USED	TF, EF, THERMAL
EBASCO COMPOSITE ELEMENT	• CONFIRMS PREVIOUS MODEL RESULTS • VERIFICATION OF COIL STRUCTURAL INTEGRITY	• EBASCO DEVELOPED COMPOSITE, SPRING AND PLATE ELEMENTS	TF, EF, THERMAL

Table II Peak Stress Near Bolt Hole

STRESS IN MPa (KSI)

CONFIG / STRESS / LOAD	8 IN. OUTER FLANGE		5¾ IN. OUTER FLANGE	
	MAXIMUM PRINCIPAL STRESS	MAXIMUM STRESS INTENSITY	MAXIMUM PRINCIPAL STRESS	MAXIMUM STRESS INTENSITY
LOAD CASE 1 (PIN LOAD IN TWO DIRECTION)	1036.3 (150.3)	1170.0 (169.7)	706.0 (102.4)	917.0 (133.0)
LOAD CASE 2 (PIN LOAD IN TANG DIRECTION)	872.2 (126.5)	872.2 (126.5)	578.5 (83.9)	637.1 (92.4)
LOAD CASE 3 (NO PIN LOAD)	807.4 (117.1)	807.4 (117.1)	526.8 (76.4)	526.8 (76.4)

NOTE: BOUNDARY FORCES WERE DERIVED FOR 3-D (TF2G3D MODEL) RUNS 2C26 AND 2C33B FOR TF + EF + THERMAL LOAD.

Table III TFTR Coil Comparison of Maximum Stresses (Toroidal Field, Equilibrium Field and Thermal Loads)

STRESS IN MPa (KSI)

MODEL NAME		COMPOSITE ELEMENT MODEL RUN CA-12A-2	TF2G3D MODEL RUN 2C33B
MODEL CHARACTERISTICS		1) ALL SOLID COMPOSITE ELEMENTS 2) COIL CONFIGURATION 12A 3) FINE GRID MODEL 4) 4-RING SOLID ELEMENT SUPPORTS 5) UNBONDED CASING AND CORE (NON-LINEAR SPRING)	1) PLATE ELEMENT FOR CASING, SOLID ELEMENTS FOR CORE 2) COIL CONFIGURATION 12A 3) FINE GRID MODEL 4) 4-RING PLATE ELEMENT SUPPORTS 5) UNBONDED CASING AND CORE (LINEAR SPRING WITH ITERATION)
CASING STRESS INTENSITY (MEMBRANE & BENDING)	INNER	252.3 (36.6)	250.3 (36.3)
	OUTER	292.3 (42.4)	289.6 (42.0)
	SIDE	283.4 (41.1)	262.7 (38.1)
COPPER HOOP STRESS		-137.9 (-20.0)	-101.4 (-14.7)
EPOXY SHEAR STRESS (R_ϕ)		20.0 (2.9)	23.4 (3.4) FROM TF2G3D AND TF3G2D

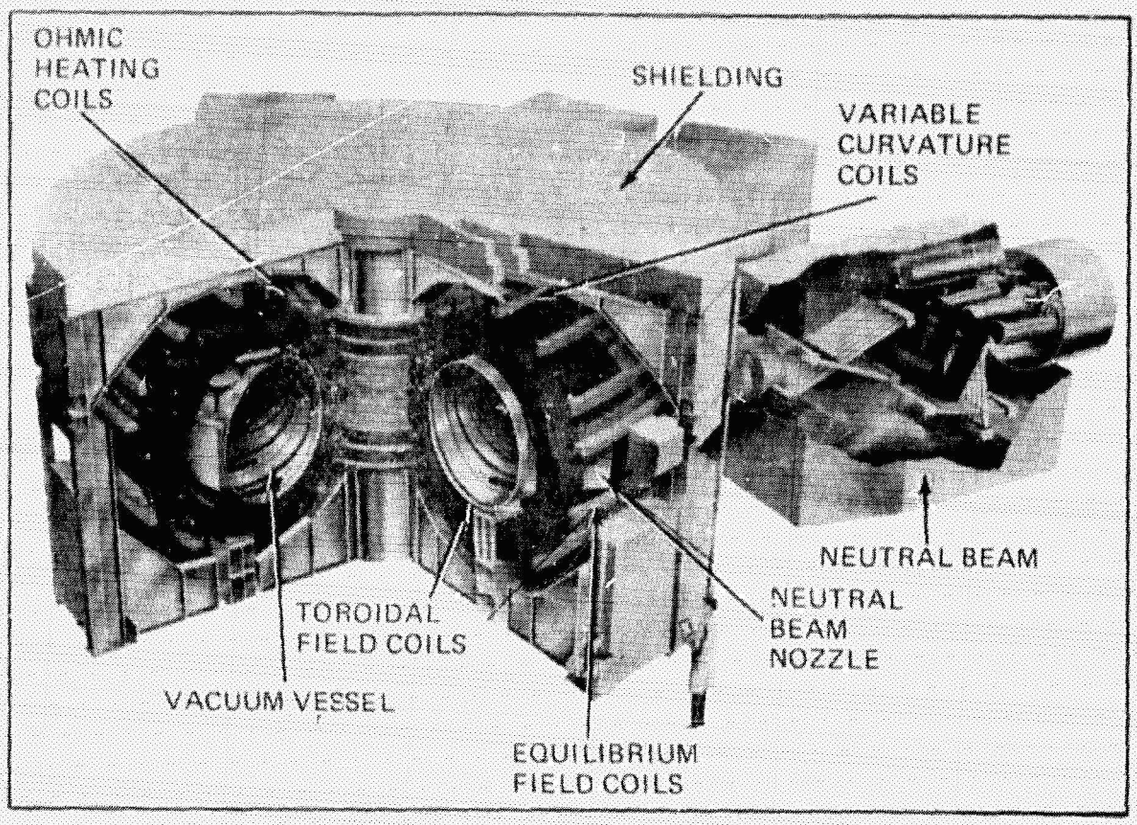

Figure 1 Tokamak Fusion Test Reactor

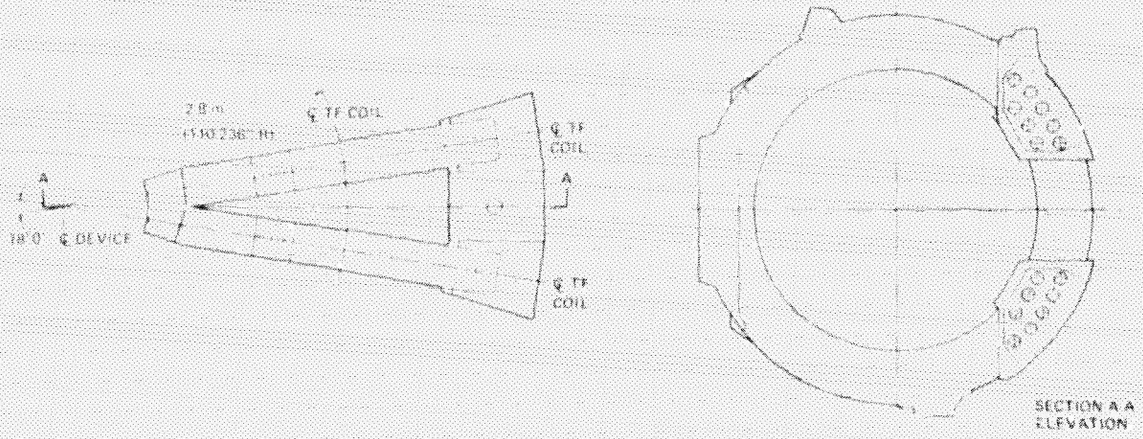

Figure 2 TF Coil Sector Assembly

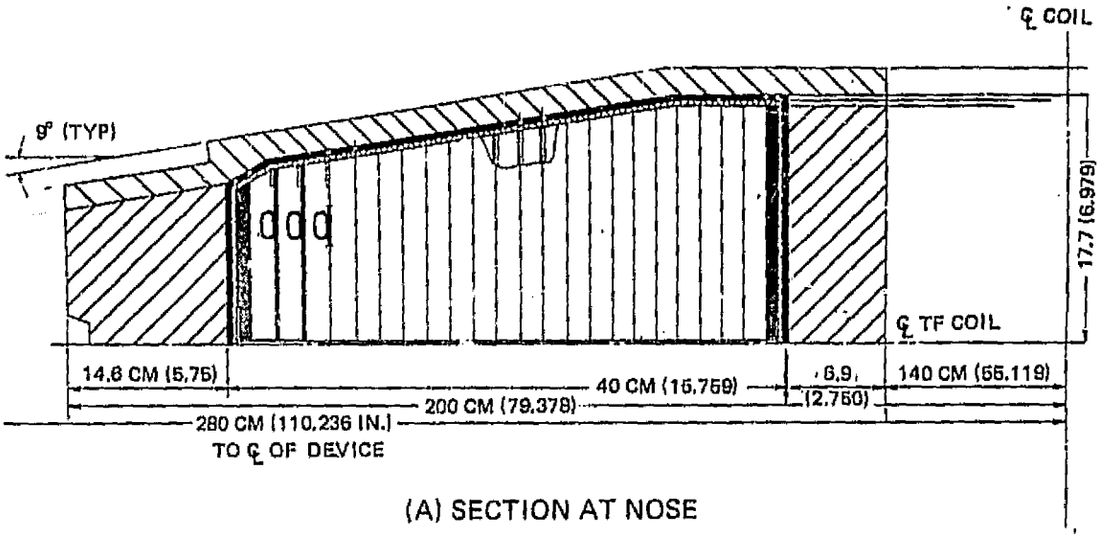

(A) SECTION AT NOSE

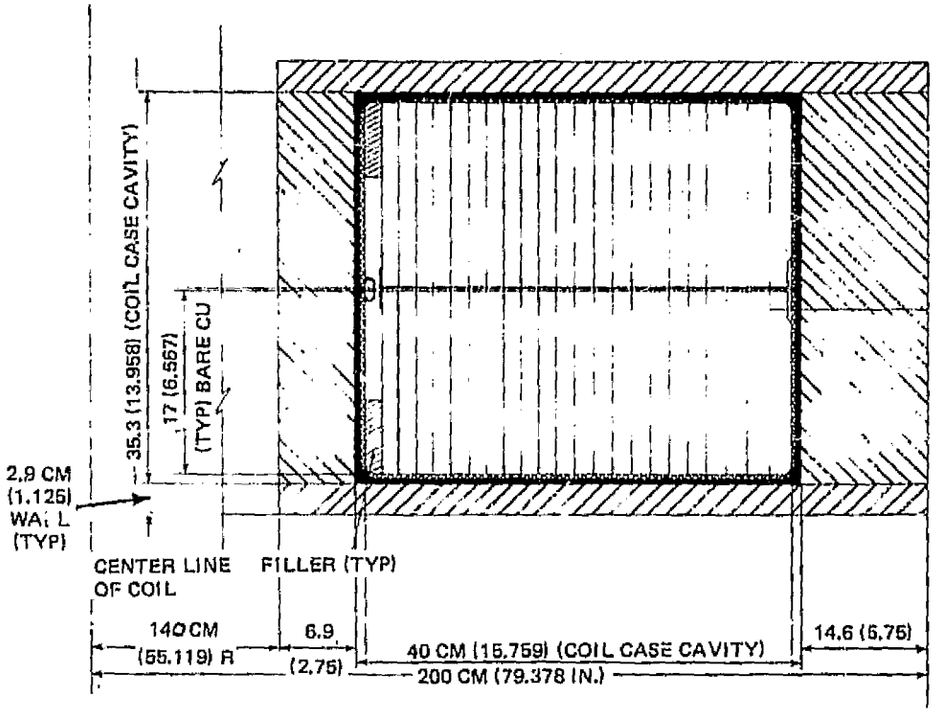

(B) TYPICAL SECTION

Figure 3 Typical Section of Coil Configuration

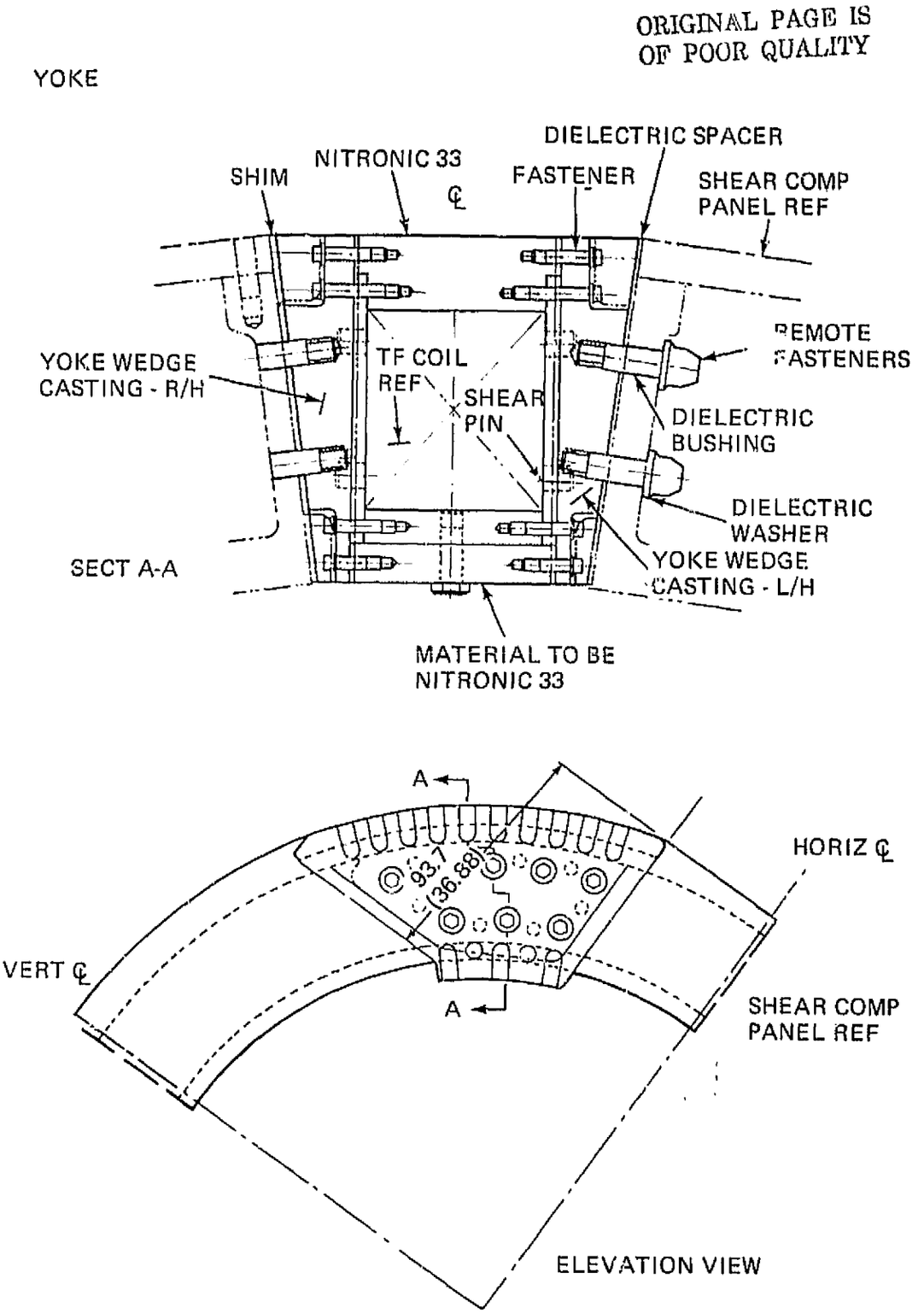

Figure 4 Shear-Compression Box and Yoke

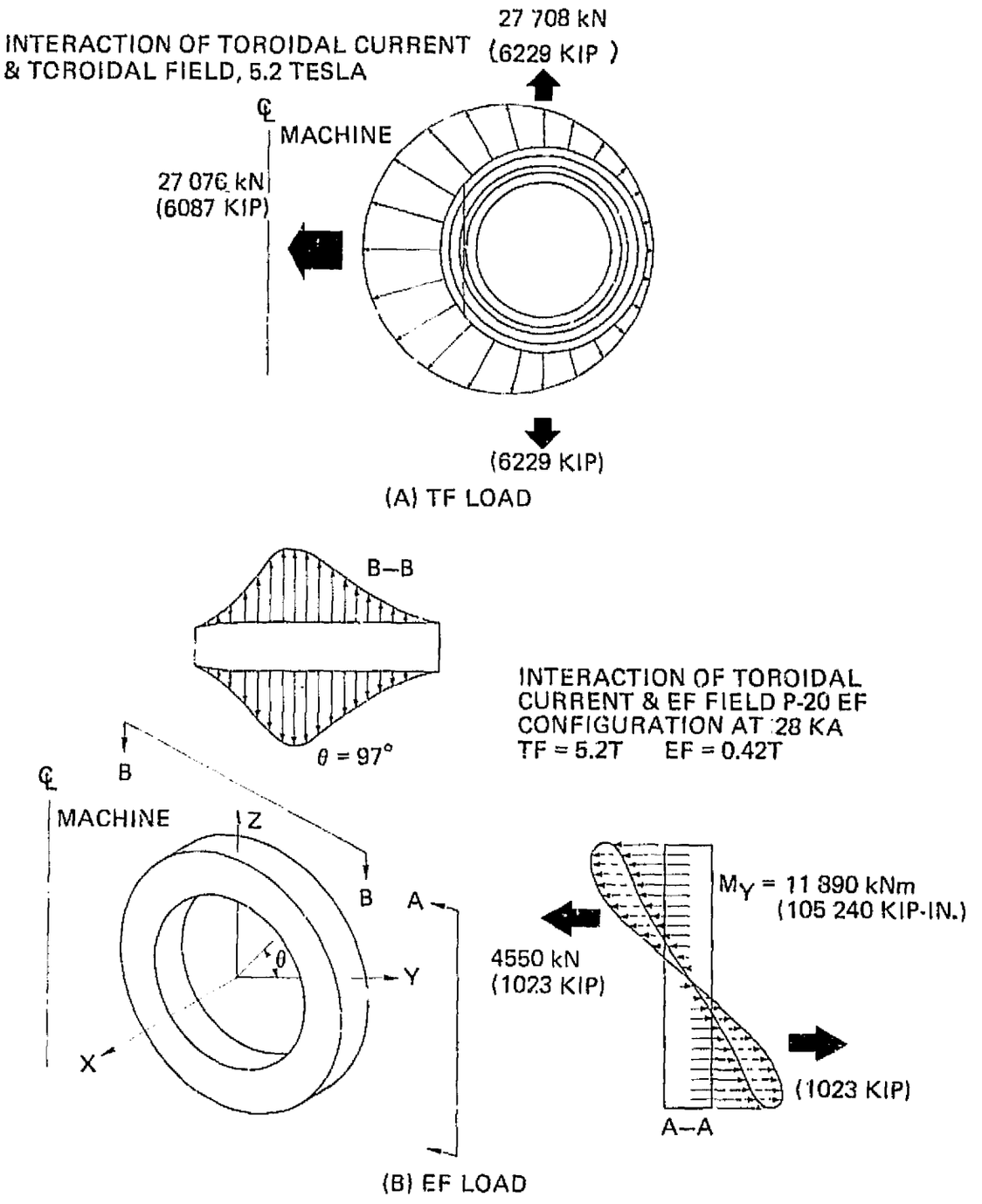

Figure 5 TF and EF Loads

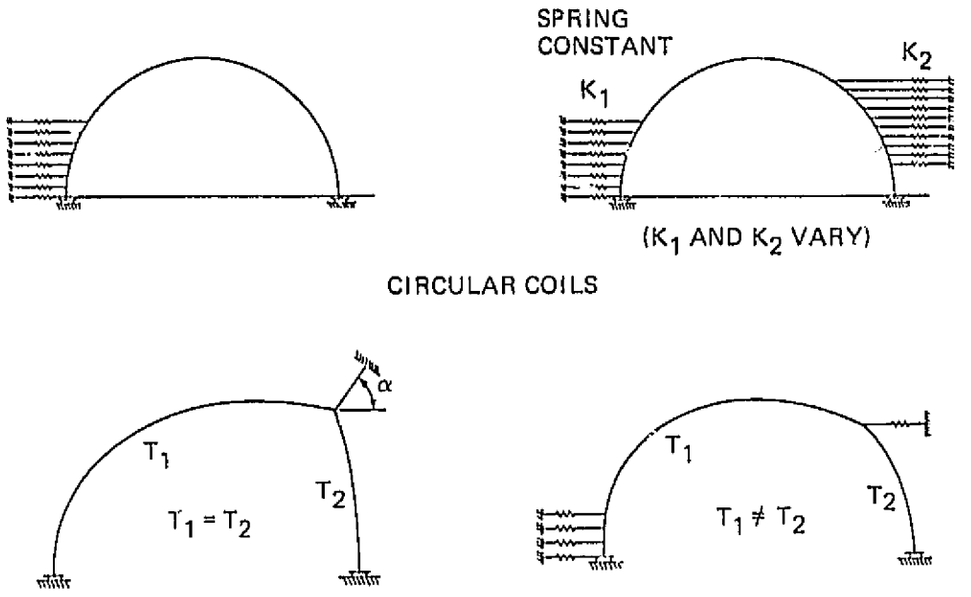

Figure 6 Configuration and Support of Coils (TF1G2D)

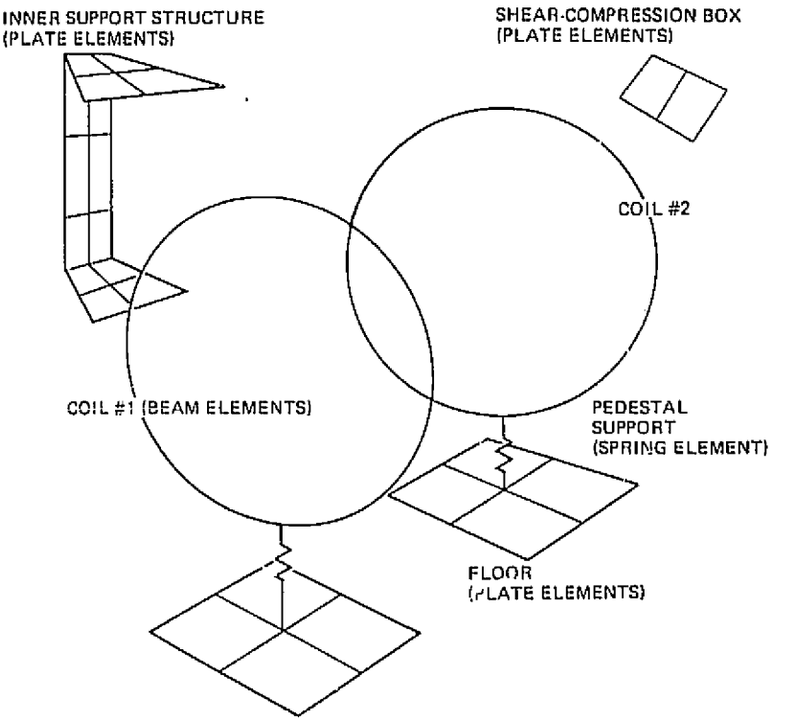

Figure 7 First Generation 3-D Model (TF1G3D)

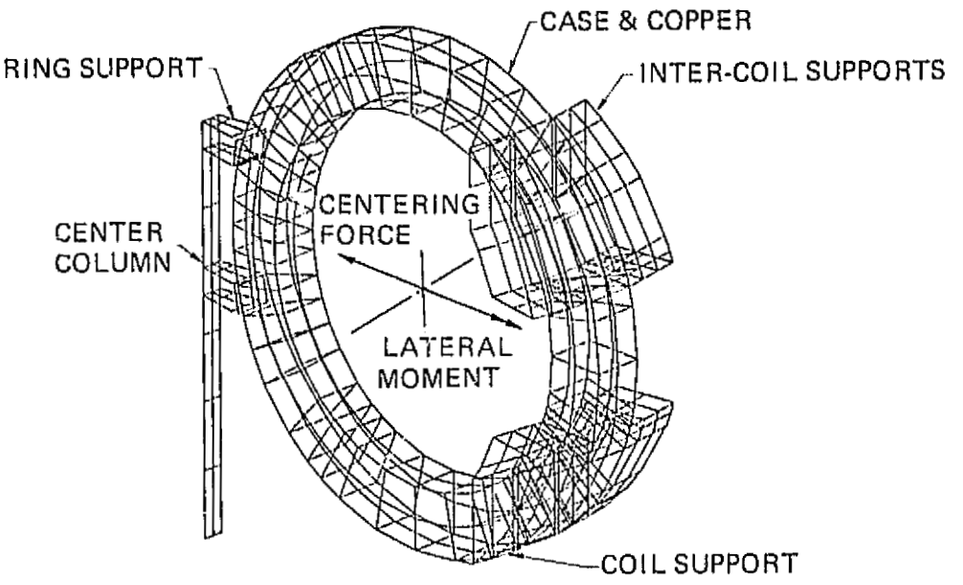

(A) TF COIL 3-D FINITE ELEMENT MODEL

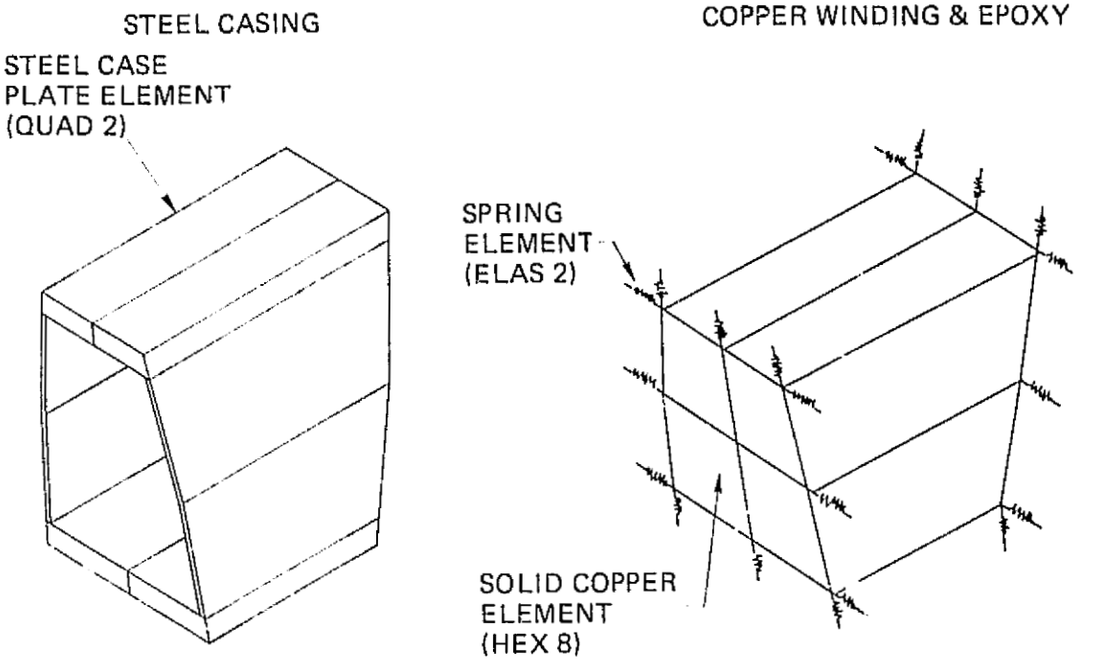

(B) COIL SEGMENT OF 3-D MODEL

Figure 8 Second Generation 3-D Model (TF2G3D)

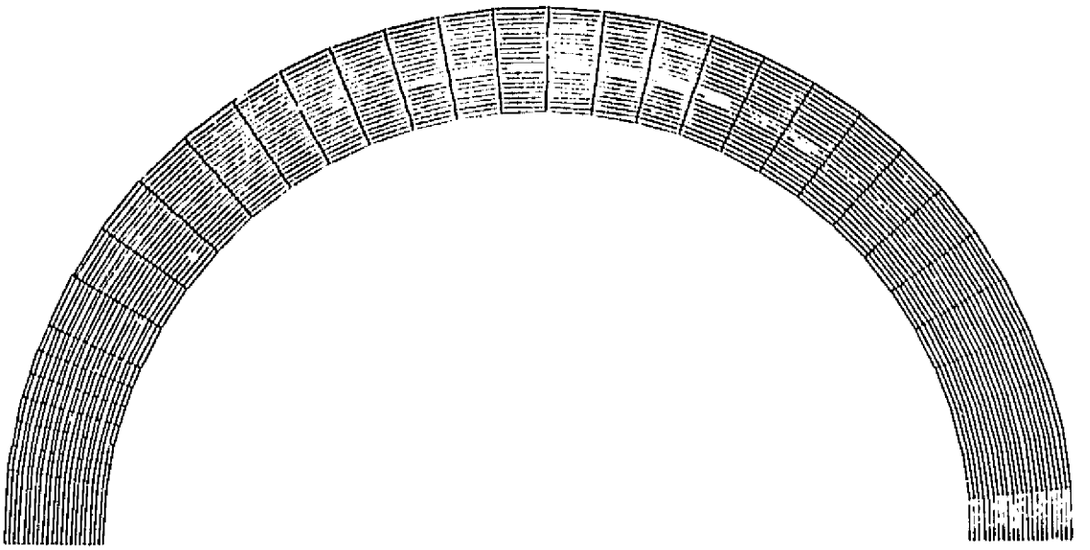

(A) SHEAR ELEMENTS

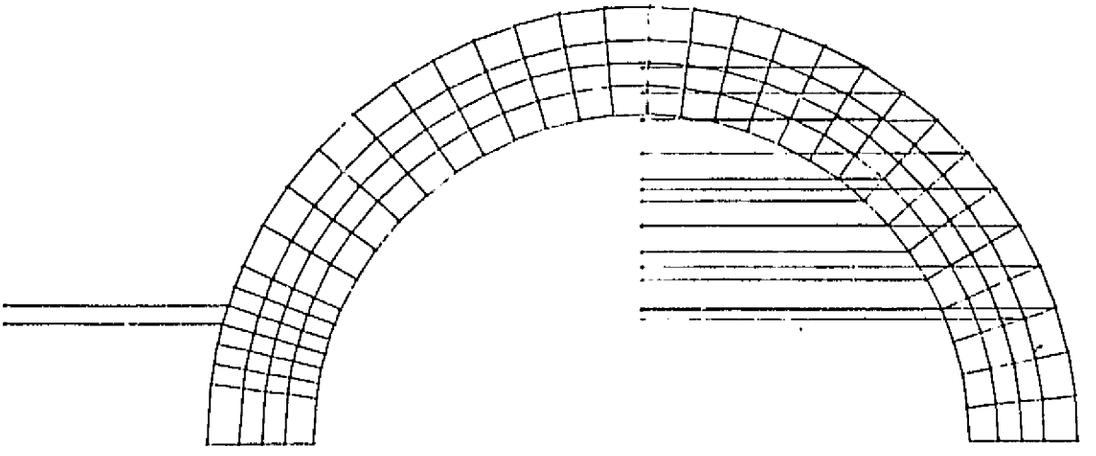

(B) QDMEM2 AND CONROD ELEMENTS AT SUPPORTS

Figure 9 Third Generation 2-D Model (TF3G2D)

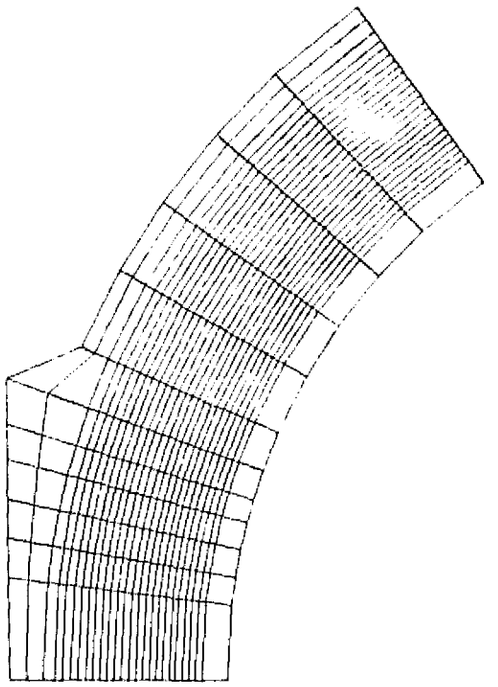

Figure 10 TF Coil 3-D Local FEA Model (TF3G3D)

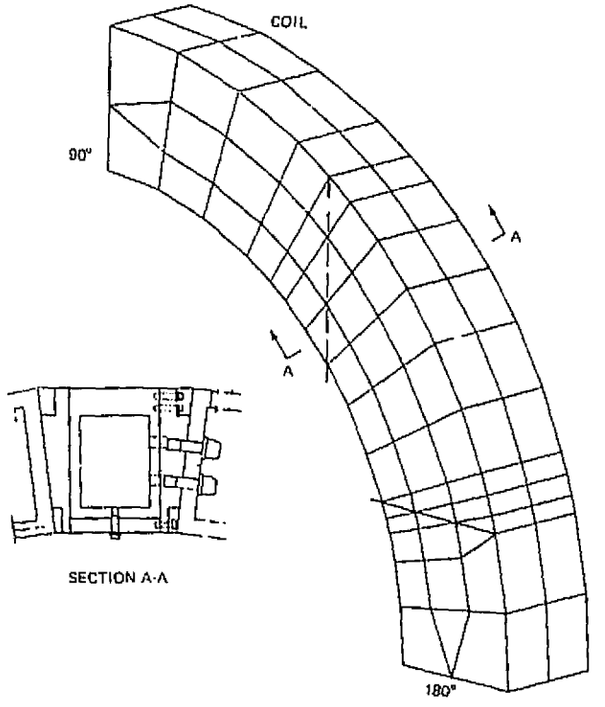

Figure 11 90^{o} Yoke Segment Model

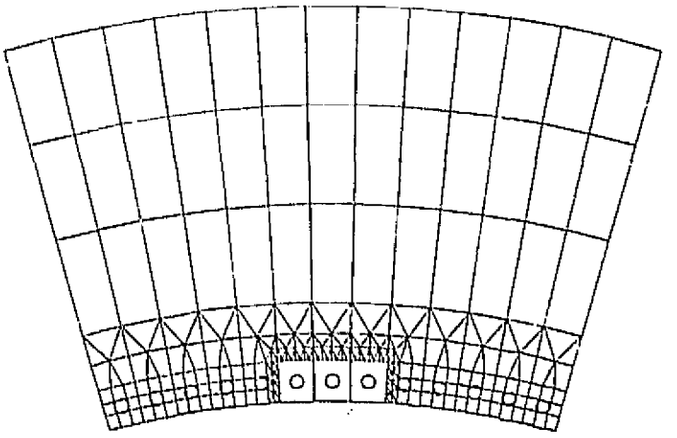

Figure 12 Residual Superelement

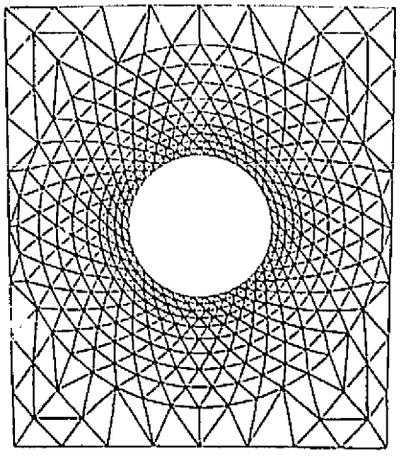

Figure 13 Primary Superelement

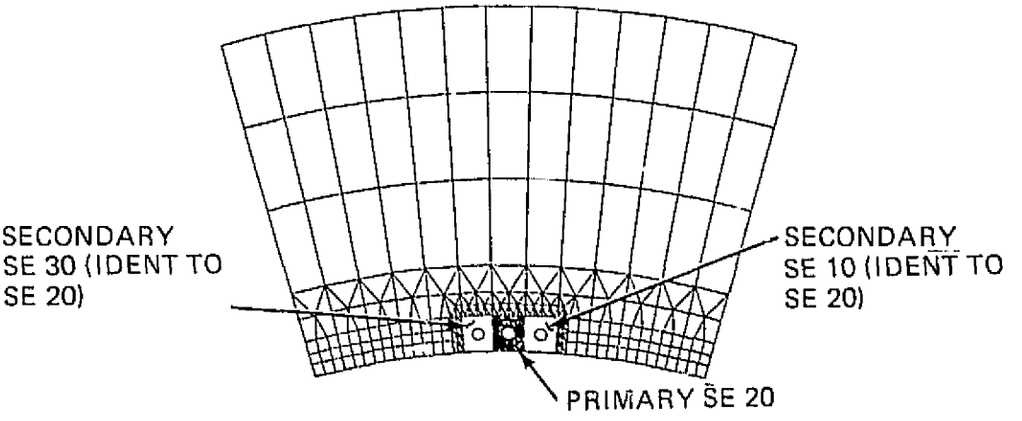

Figure 14 Remainder of Structure Considered SE 0 or Residual Structure

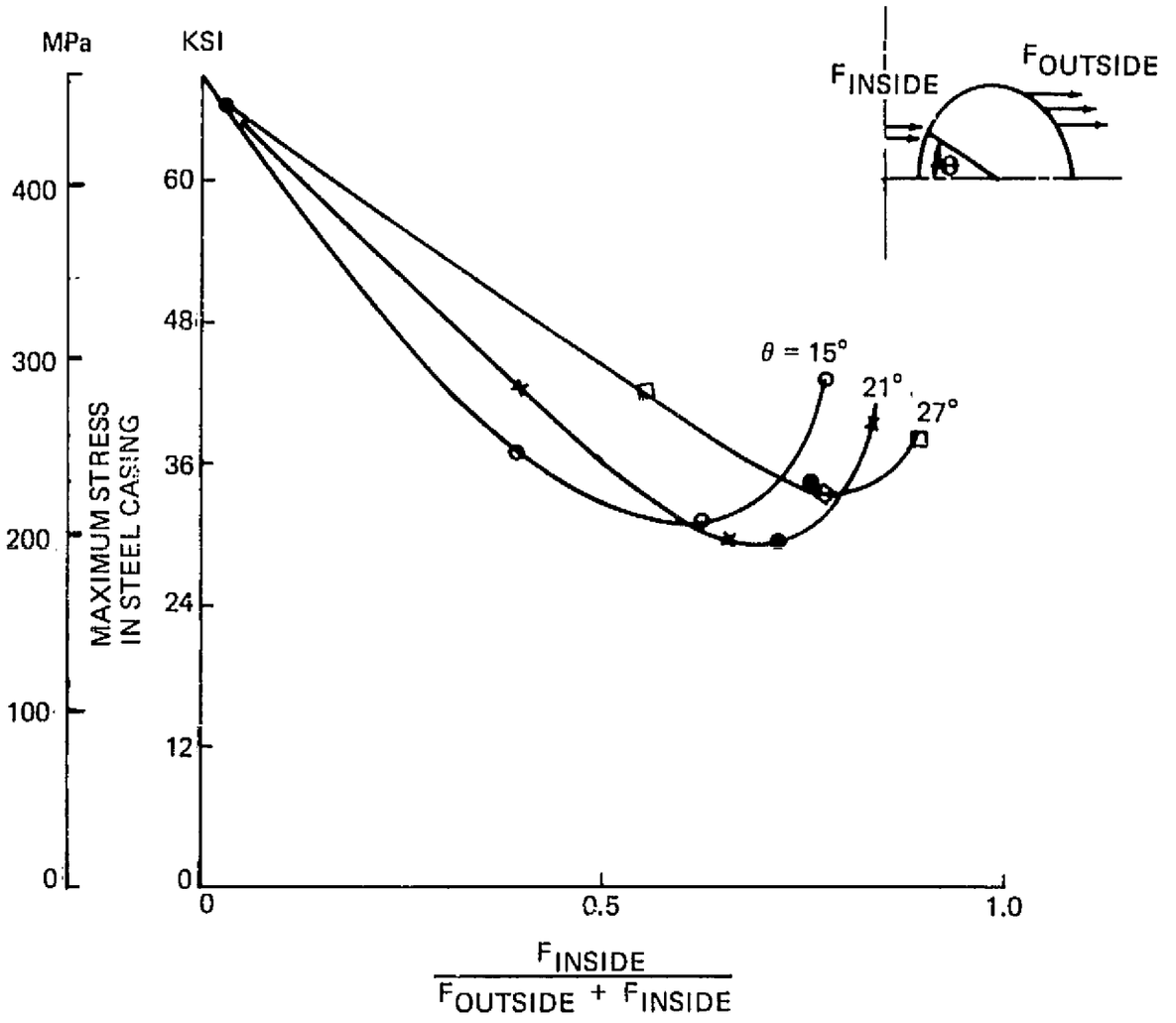

Figure 15 Maximum Stress in Steel Casing vs Stiffness and Location of Support (Represented by Force Ratio)

(A) TOROIDAL FIELD COIL FORCE – TIME SCENARIO FOR INPLANE LOADS

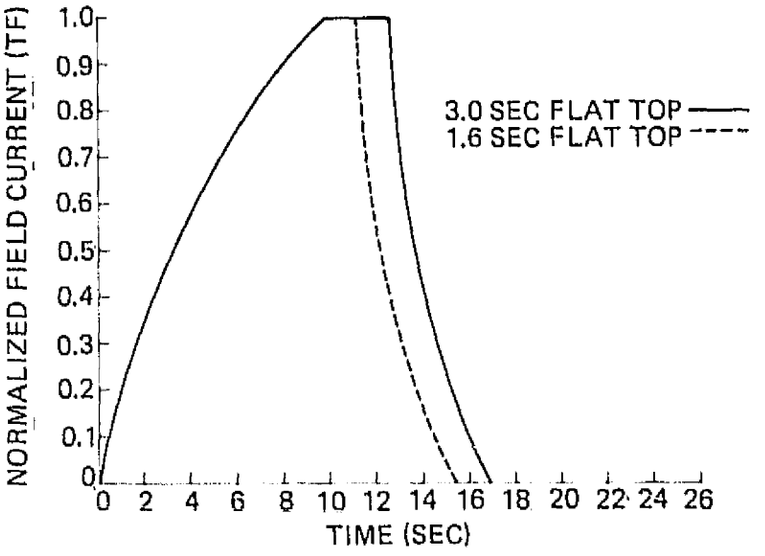

(B) TOROIDAL FIELD COIL FORCE – TIME SCENARIO FOR OUT-OF-PLANE LOADS

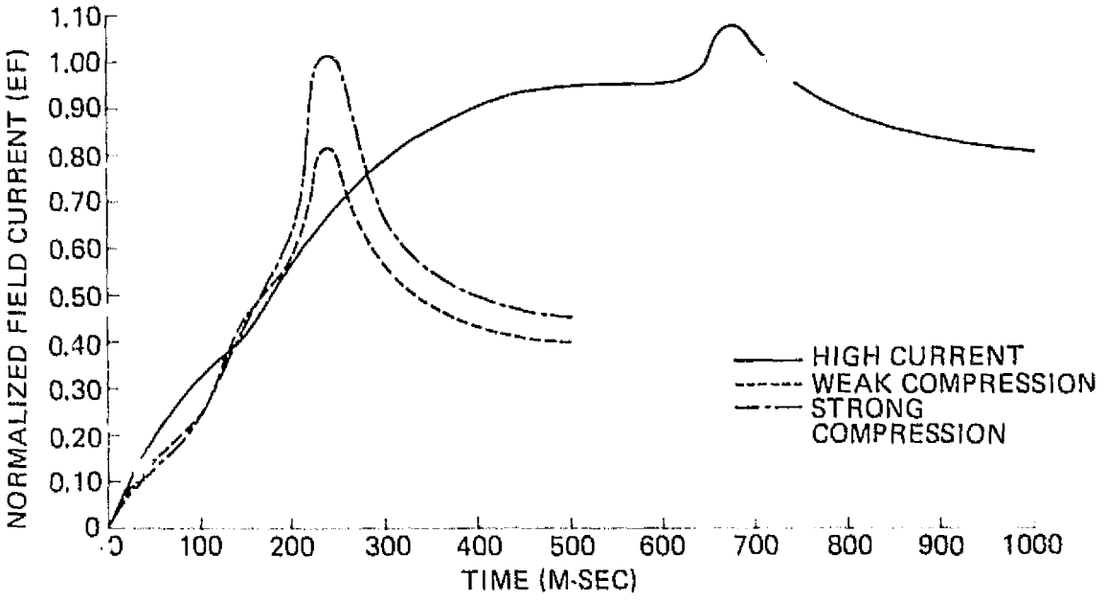

Figure 16 TF and EF Scenarios

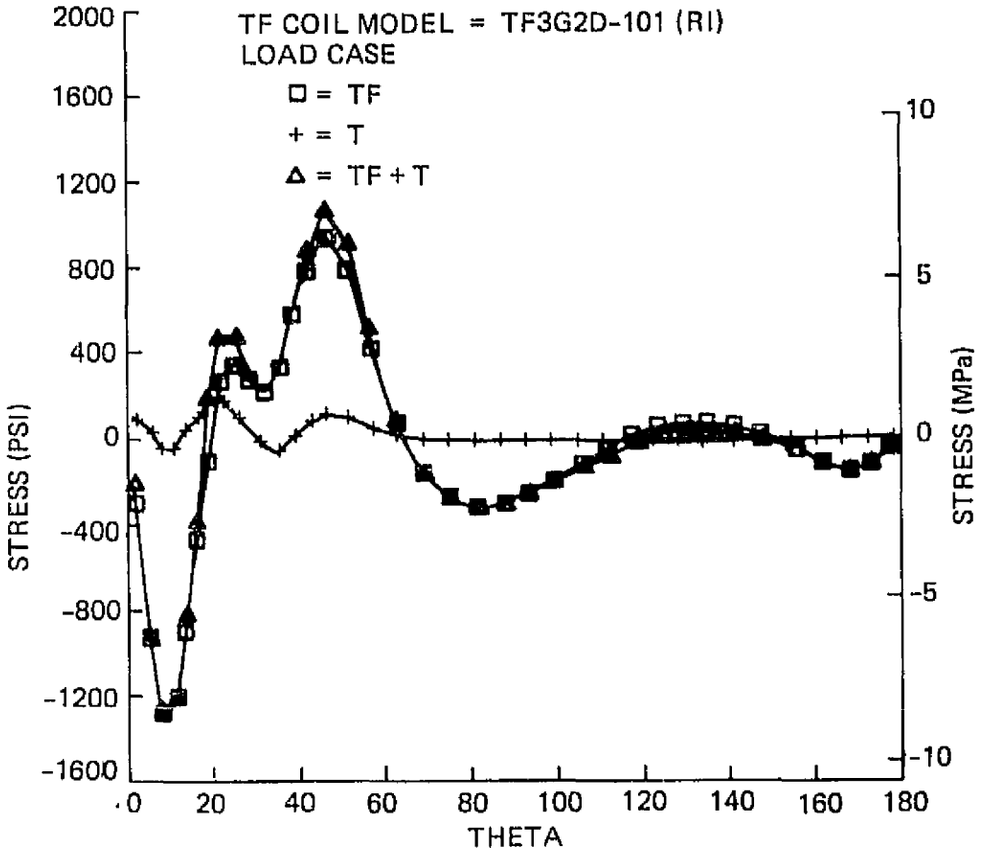

Figure 17 Epoxy Max Shear Stress

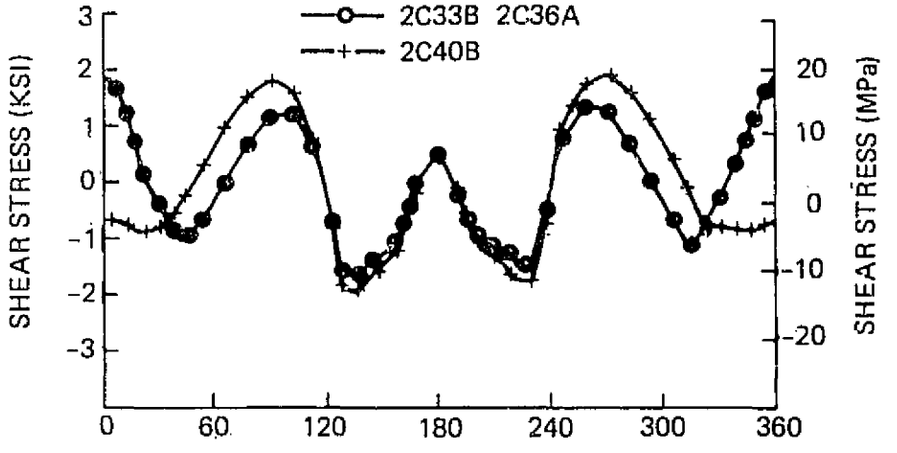

Figure 18 Estimated Shear Stress of Epoxy Due to Torque Induced by EF Load

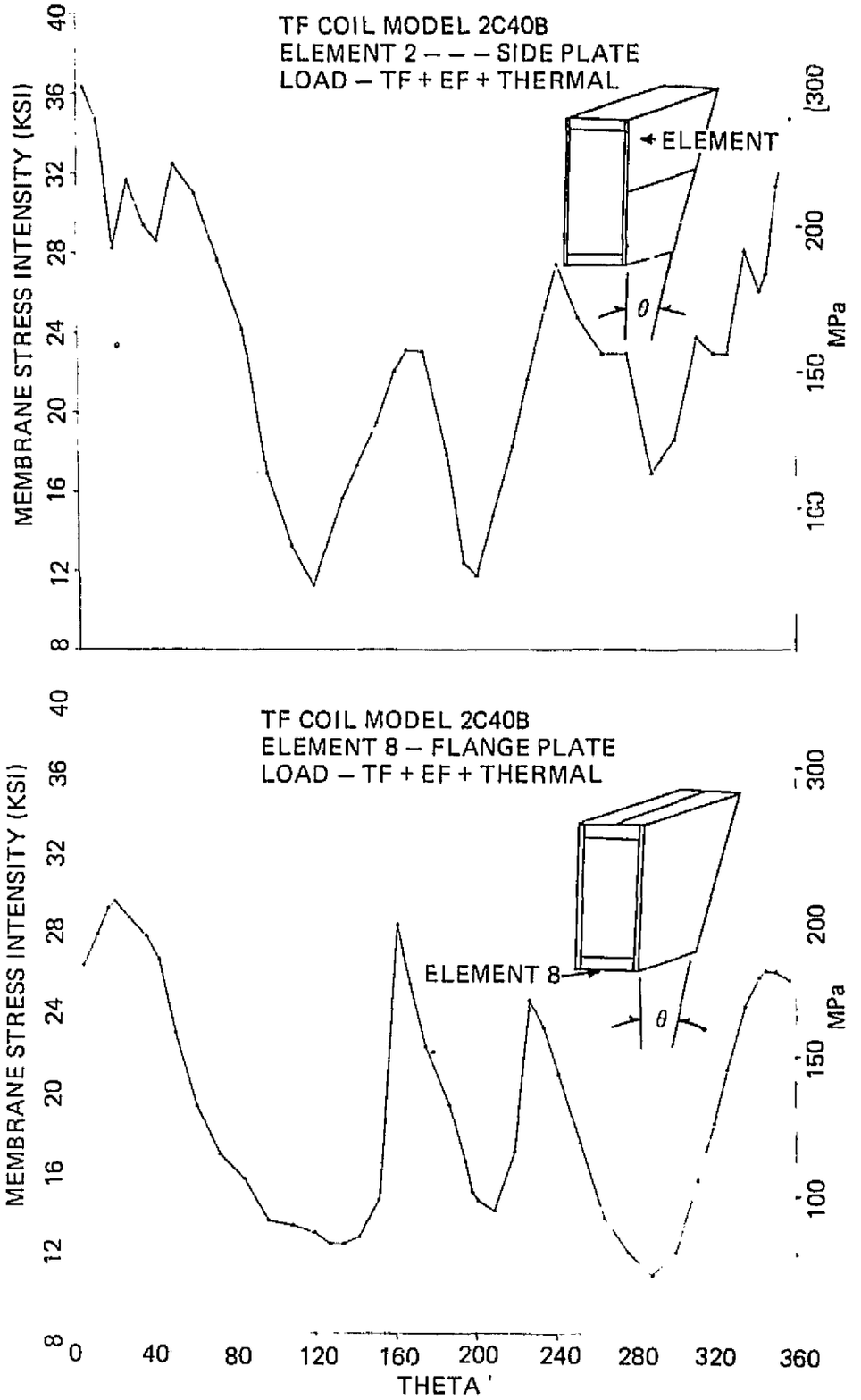

Figure 19 Typcial Membrane Stress Intensity

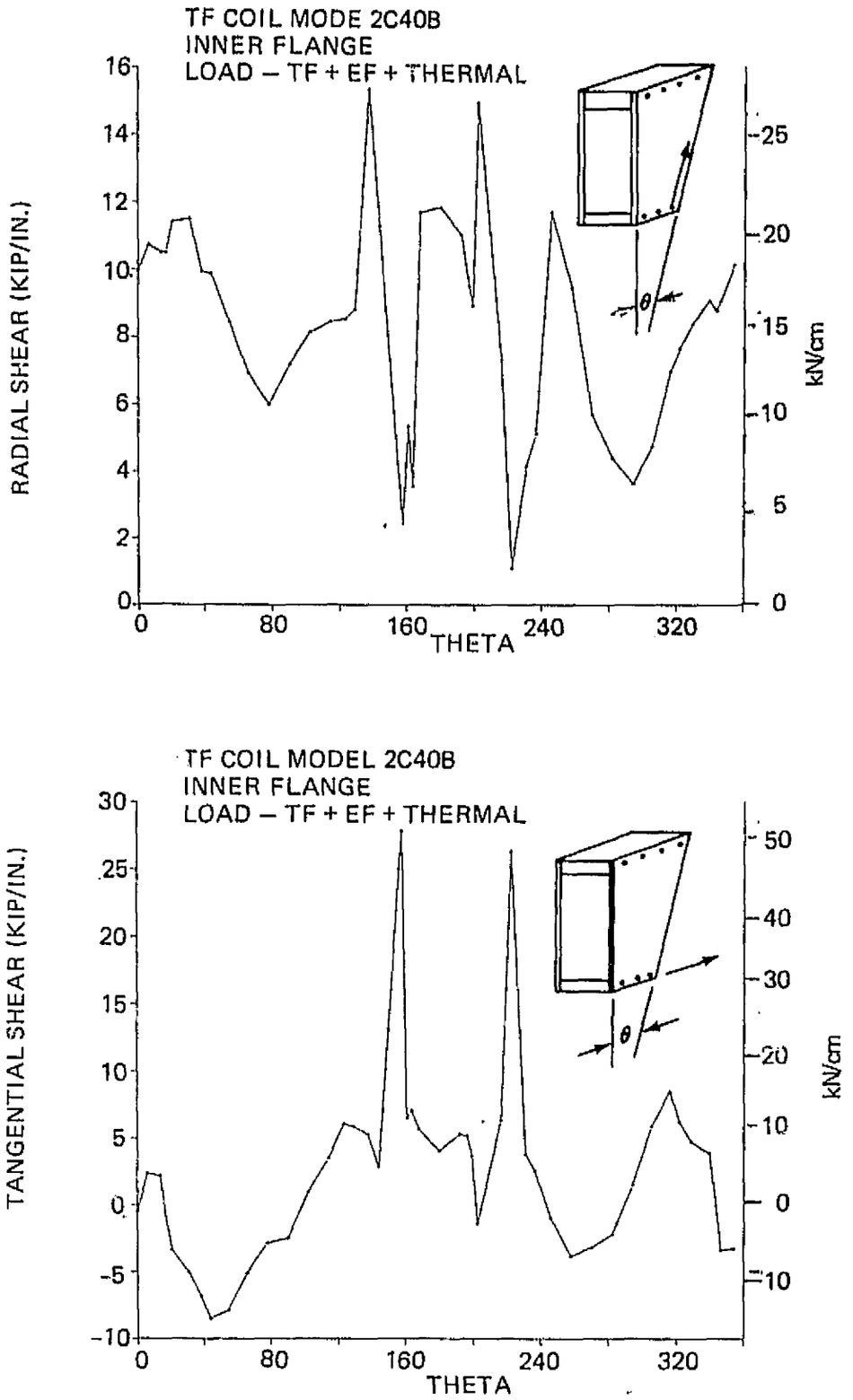

Figure 20 Typical Radial and Tangential Shear

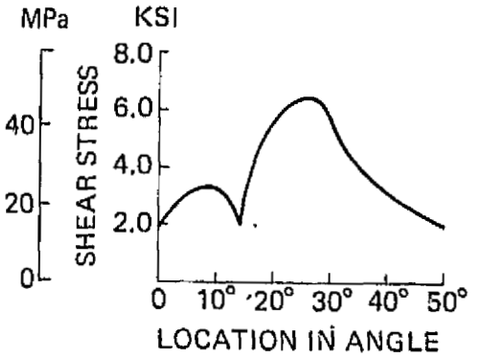

(A) MAXIMUM INTERLAMINAR SHEAR STRESS

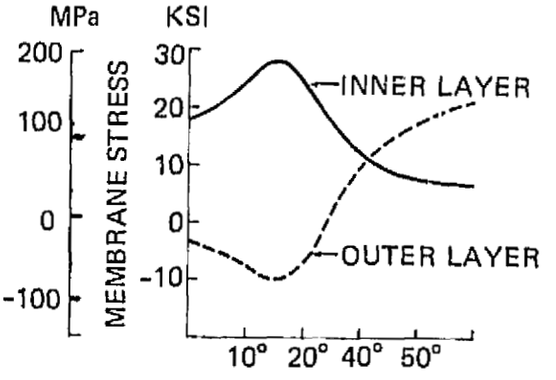

(B) COPPER STRESS IN HOOP DIRECTION

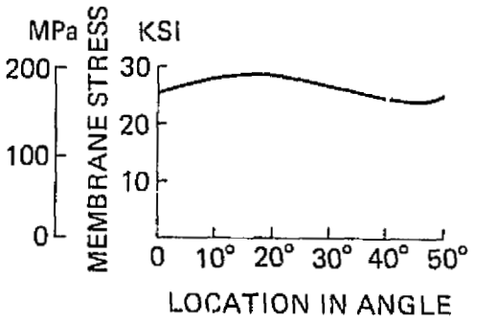

(C) INNER FLANGE STRESS IN HOOP DIRECTION

Figure 21 Stress Plots from Third Generation 3-D Local Model

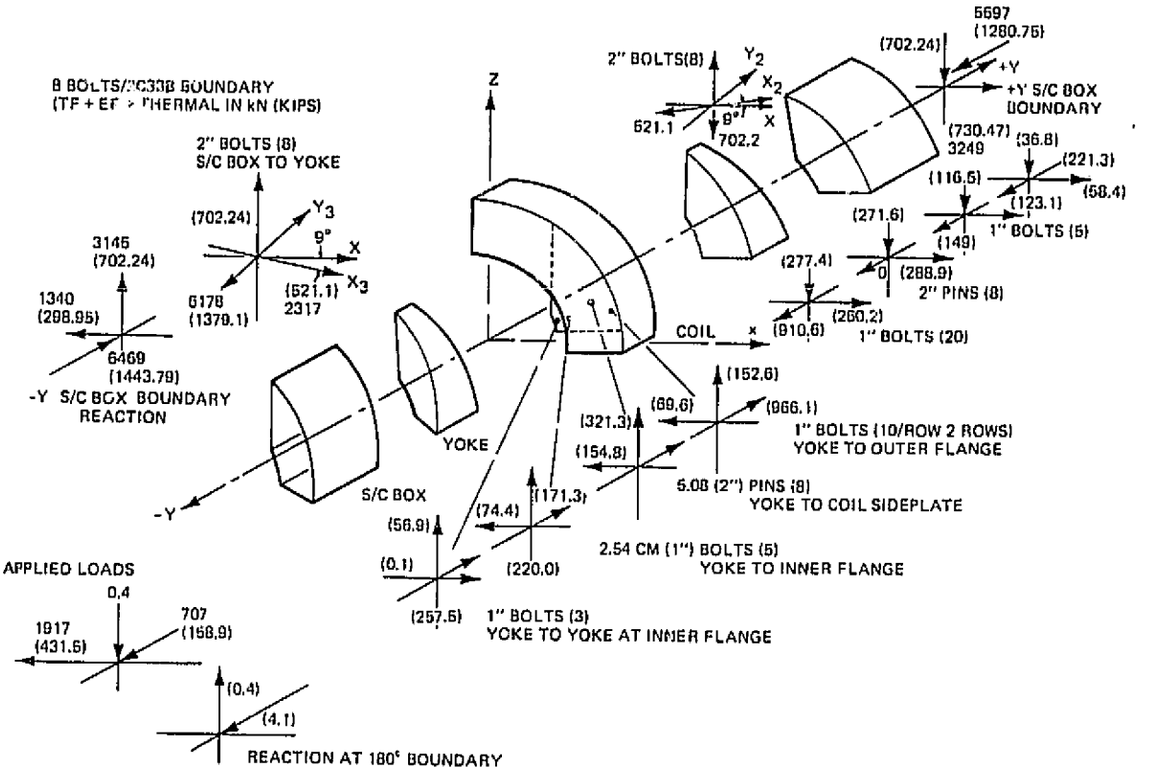

ORIGINAL PAGE IS
OF POOR QUALITY

Figure 22 Load Distribution Yoke Finite Element Model

D17

N78-32483

STATIC ANALYSIS OF A SONAR DOME RUBBER WINDOW

J. L. Lai
BFGoodrich Company

SUMMARY

The application of NASTRAN (level 16.0.1) to the static analysis of a sonar dome rubber window (SDRW) is demonstrated. The assessment of the conventional model (neglecting the enclosed fluid) for the stress analysis of the SDRW is made by comparing its results to those based on a sophisticated model (including the enclosed fluid). The fluid is modeled with isoparametric linear hexahedron elements with approximate material properties whose shear modulus is much smaller than its bulk modulus. The effect of the chosen material property for the fluid on the results obtained is also discussed.

INTRODUCTION

The SDRW (or window) of a ship (fig. 1) is a rubber composite structure. It is used for protecting the sonar device inside it and giving a small amount of the transmission loss to the acoustic wave. The rubber composite used for the SDRW has steel wires of cross-ply construction as its structural reinforcing members (fig. 2). The maximum amount of the reinforcements used in the window is subject to the specification of its acoustic performance requirement.

The internal pressurization of the window from its enclosed fluid (sea water) becomes necessary to generate its additional structural stiffness and rigidity. Designers prefer to have the internal pressure being greater than the external pressure induced from a ship's operation. However, the maximum allowable internal pressure depends on the amount of the steel wires used in the window. Under some severe loading conditions such as slamming and impact, external pressures on some areas of the window exceed its internal pressure. The enclosed fluid is, therefore, expected to play an important role on sustaining its structural integrity.

The conventional model, in which the enclosed fluid is not included, is adequate for analyzing the window of a ship under a normal operation. It does not give us satisfactory results as the window is subject to severe loads. So, more reliable results are only available for this severe loading situation, if a sophisticated model which includes the internal fluid of the window, is used. In this paper, simple models instead of complete and complicated models will be presented for demonstrating the application of NASTRAN to the static analysis of a SDRW.

CONVENTIONAL MODEL

The complete model for a type of a SDRW is shown in figure 3. This model is for a complete window structure which is attached to the ship structure. The enclosed fluid is not included in the model. It has been used for the preliminary evaluation on the structural integrity of the SDRW subject to various static loads. They are: hydrostatic forces, internal pressure, forces induced from the weight of the window, the enclosed fluid and other hardwares, steady state hydrodynamic forces, the equivalent static forces induced from the slamming and impact on the window, and the combinations of some loads as mentioned.

The window is modeled with quadrilateral and triangular plate elements (CQUAD2 and CTRIA2). Their anisotropic material properties (MAT2) are obtained based on the rubber composite theory (ref. 1 and 2). Some properties are obtained with the use of Halpin-Tsai equations (ref. 3). The appropriate boundary conditions are implemented with SPC or SPC1. The loads on the window can easily be input with GRAV, PLOAD2 and FORCE.

The results, obtained from the conventional model for the case of the window under normal operational loads, are satisfactory. However, excessive and unreasonable deformations compared to the observed are obtained if the window is under severe loads. Thus, the external loads on some areas of the window are greater than its internal loads. Its maximum displacements are greater than the thickness of the window. A better model is, therefore, required for obtaining more realistic solutions. After some consideration, a feasibility study of the model which includes the enclosed fluid, was made.

SOPHISTICATED MODEL

It was developed by adding isoparametric linear hexahedron elements (CIHEX1) for the enclosed fluid to the conventional model. These elements are considered as a special isotropic solid whose shear modulus being much smaller than its bulk modulus. Because of NASTRAN's limitation on MAT1, its approximate Poisson's ratio chosen to be very close to .5 (ref. 4) and Young's modulus, which is determined with the chosen Poisson's ratio and its exact bulk modulus, are used. The continuity of the translational displacements of the corresponding grid points at the fluid-structure interfaces are constrained with MPC. The fluid boundaries are constrained with SPC.

A demonstrated model has been developed for evaluating the feasibility of using a complete sophisticated model for the static analysis of the SDRW structure. This demonstrated model is shown in figure 4. Two loading cases on this model are considered in this paper. They are: (1) a uniform internal pressure, and (2) a combined load of an internal pressure and a non-uniform external pressure induced from the slamming.

SAMPLED PROBLEM

The simplified sophisticated model used for the demonstration of NASTRAN's capability on the SDRW analysis is shown in figure 4. Two circular arcs are for the window structure. Their dimensions are given in figure 4. The internal pressure is 22.4 (27.1 for the combined load case) N/cm^2. The maximum external pressure is 40.3 N/cm^2 exerting on one side of the window. The minimum thickness of the window model is 1.27 cm.

The results obtained from the sophisticated model will be compared to those from a simplified conventional model. They will also be compared to those from the same model with air as the enclosed fluid. The Young's modulus and the Poisson's ratio used for sea water is .1368 N/cm^2 and .4999999. Those for air is .844-4 N/cm^2 and .4999999.

RESULTS AND DISCUSSION

Only the critical results obtained will be discussed in this section. They are: displacements, reaction forces and moments, and membrane stresses (more important information than element stresses for designing rubber composite structures). The membrane stresses are obtained thru a post-processor excluding the bending stresses in element stresses. The effect of the approximate Poisson's ratio used for the fluid (sea water) on the results from the sophisticated model will also be discussed.

From the results given in table 1, we can find that the enclosed water, which has a relatively high compressibility, can sustain the window shape under the severe load. Due to the low compressibility of air, the window filled with air from the sophisticated model yields results about the same as those from the conventional one under both loading cases. As the window is under an internal pressure which gives a small deformation, the conventional model should be good enough for analyzing the window. Under the severe load, the sophisticated model should be used. Its enclosed fluid can: (1) decrease critical displacements, reaction forces and membrane stresses on the loading side and increase those on the non-loading side, (2) decrease critical reaction moments substantially on the loading side, (3) move the maximum displacement and membrane stress to the non-loading side of the window.

The effect of the approximate Poisson's ratio chosen for the enclosed fluid on the critical results are given in table 2. A small increment in the Poisson's ratio for sea water inside the window can: (1) increase critical displacements, (2) change reaction forces and moments negligibly, and (3) increase membrane stresses slightly.

FINAL REMARKS

NASTRAN has been used as a design/analysis tool for the SDRW. Satisfactory results can be obtained if a proper model is used. For time and cost-saving

purposes, a conventional model which only includes the window structure can be used. If the displacements of the window exceeds its wall thickness, a sophisticated model which includes the enclosed fluid should be used for obtaining better solutions. The method as demonstrated in this paper gives us reasonably good results compaired to those from engineering experience. The approximate Poisson's ratio of the enclosed fluid is recommended to be .4999999. With this approach, a costly differential stiffness or other approaches may be avoided.

The method developed by Everstine et al. (ref. 5) has been considered. This method can assure the continuity of normal displacements and pressures at the interface of the window and the enclosed fluid from the structure and the fluid elements. The technique implementing this method for the titled subject is being developed.

REFERENCES

1. Brewer, H.K.: Stress and Deformations in Multi-Ply Aircraft Tires Subject to Inflation Pressure Loading, Technical Report AFFDL-TR-70-62, June 1970.

2. Brewer, H.K.: Prediction of Tire Stresses and Deformations from Composite Theory, Tire Science and Technology, TSTCA, Vol. 1, No. 1, February 1973, pp. 47-76.

3. Halpin, J.C.; and Tsai, S.W.: Environmental Factors in Composite Material Design, AFML-TR-67-423, Air Force Materials Laboratory, Wright-Patterson Air Force Base, Ohio, 1968.

4. Fung, Y.C.: Foundations of Solid Mechanics, Prentice-Hall, Inc., Englewood Cliffs, N. J., 1965, pp. 129-130.

5. Everstine, G.C., et al.: The Dynamic Analysis of Submerged Structures, NASTRAN: User's Experiences, NASA TM X-3278, September 1975, pp. 419-429.

TABLE 1. CRITICAL RESULTS

Loading Cases	1	2	
Displacements (cm)			
A	.463	12.81	-13.38
B	.463	12.70	-13.27
C (loading side)	.446	.379	-.26
C (non-loading side)	.446	.605	
Reaction Forces (N) and Moments (N-cm)	(F)	(F)	(M)
A	2.22+4	1.35+4	2.97+5
B	2.22+4	1.35+4	2.95+5
C (loading side)	1.73+4	1.66+4	8.14+3
C (non-loading side)	1.73+4	2.26+4	2.81+3
Membrane Stresses (N/cm^2)			
A	2,454	1,344	
B	2,454	1,342	
C (loading side)	1,703	1,253	
C (non-loading side)	2,454	2,566	

where A is for the window model, B is for the window-air model, and C is for the window-sea water model.

TABLE 2. EFFECT OF POISSON'S RATIO ON CRITICAL RESULTS

Loading Cases	1	2
Displacements (cm)		
D	.376	.505
E	.432	.595
F	.446	.605
Reaction Forces (N)		
D	1.7 +4	2.24+4
E	1.71+4	2.24+4
F	1.73+4	2.26+4
Membrane Stresses (N/cm^2)		
D	1,642	2,419
E	1,673	2,534
F	1,703	2,566

where D, E and F are for Poisson's ratio being equal to .4999, .499999 and .999999 respectively.

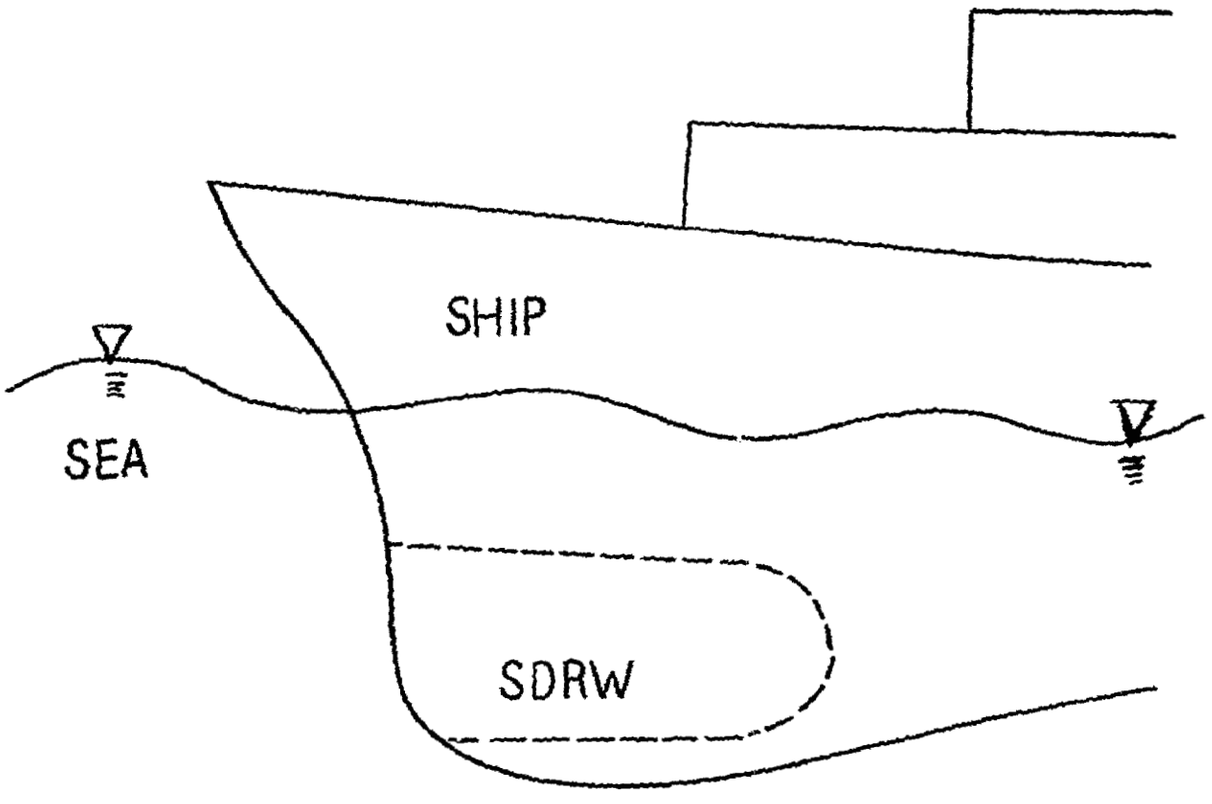

Figure 1. A Sonar Dome Rubber Window

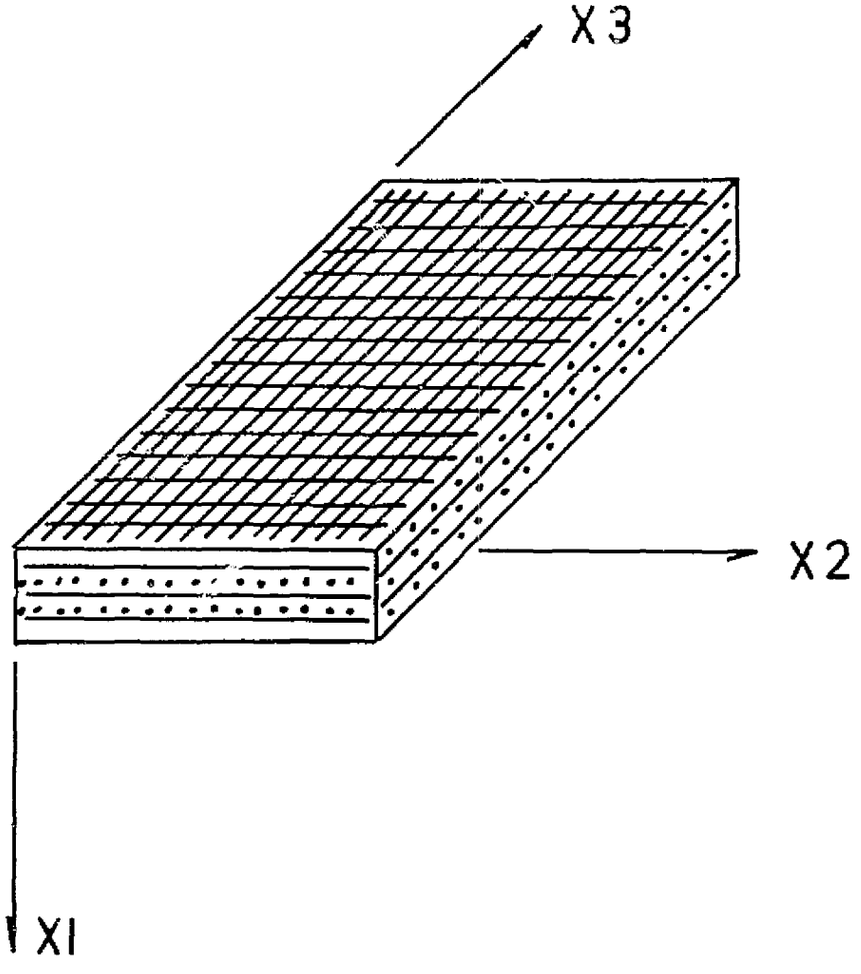

Figure 2. Cross-Ply Construction of Rubber Composite

Figure 3. NASTRAN Model of A Sonar Dome Rubber Window

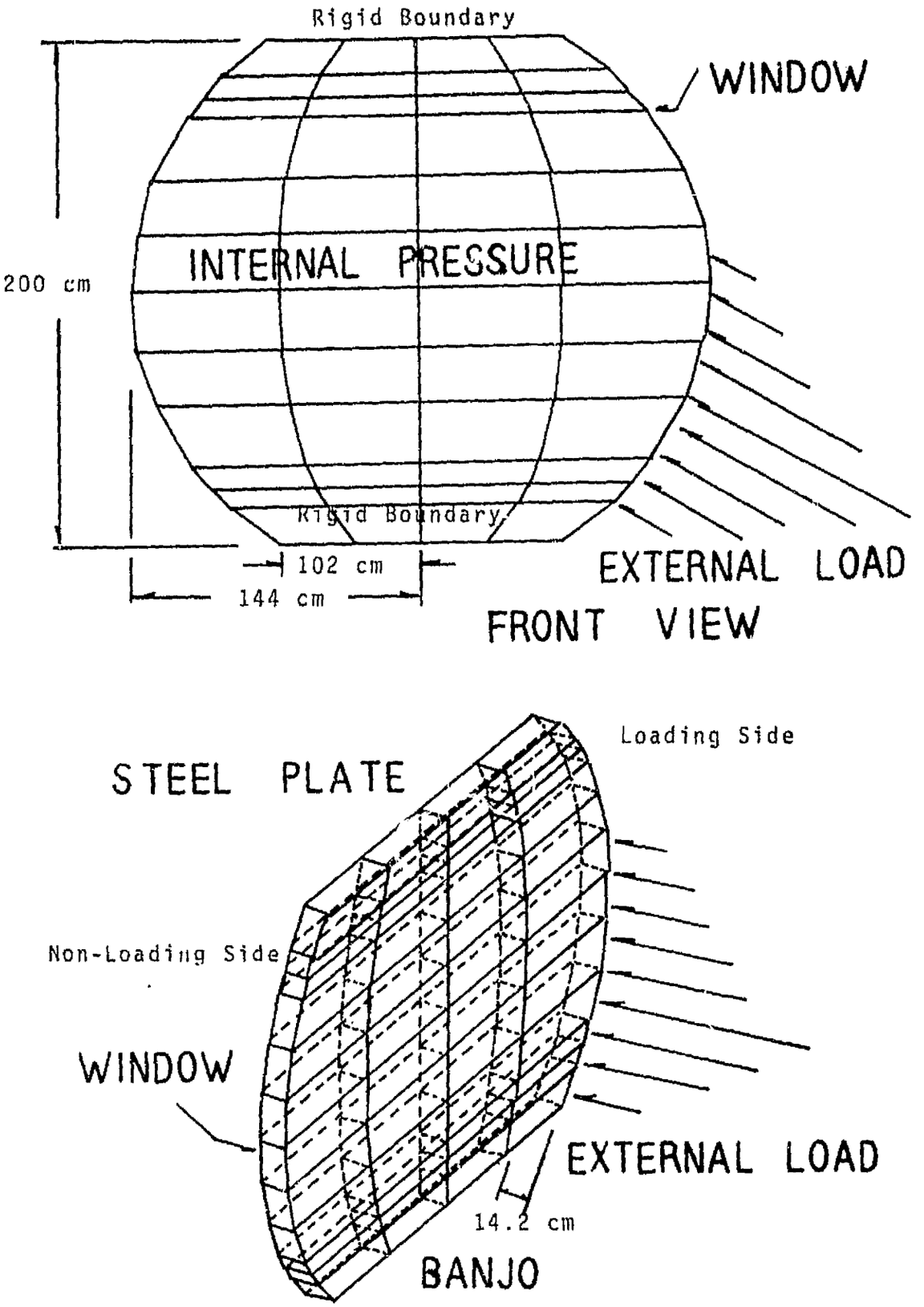

Figure 4. A Simplified Sophisticated Model for A Sonar Dome Rubber Window

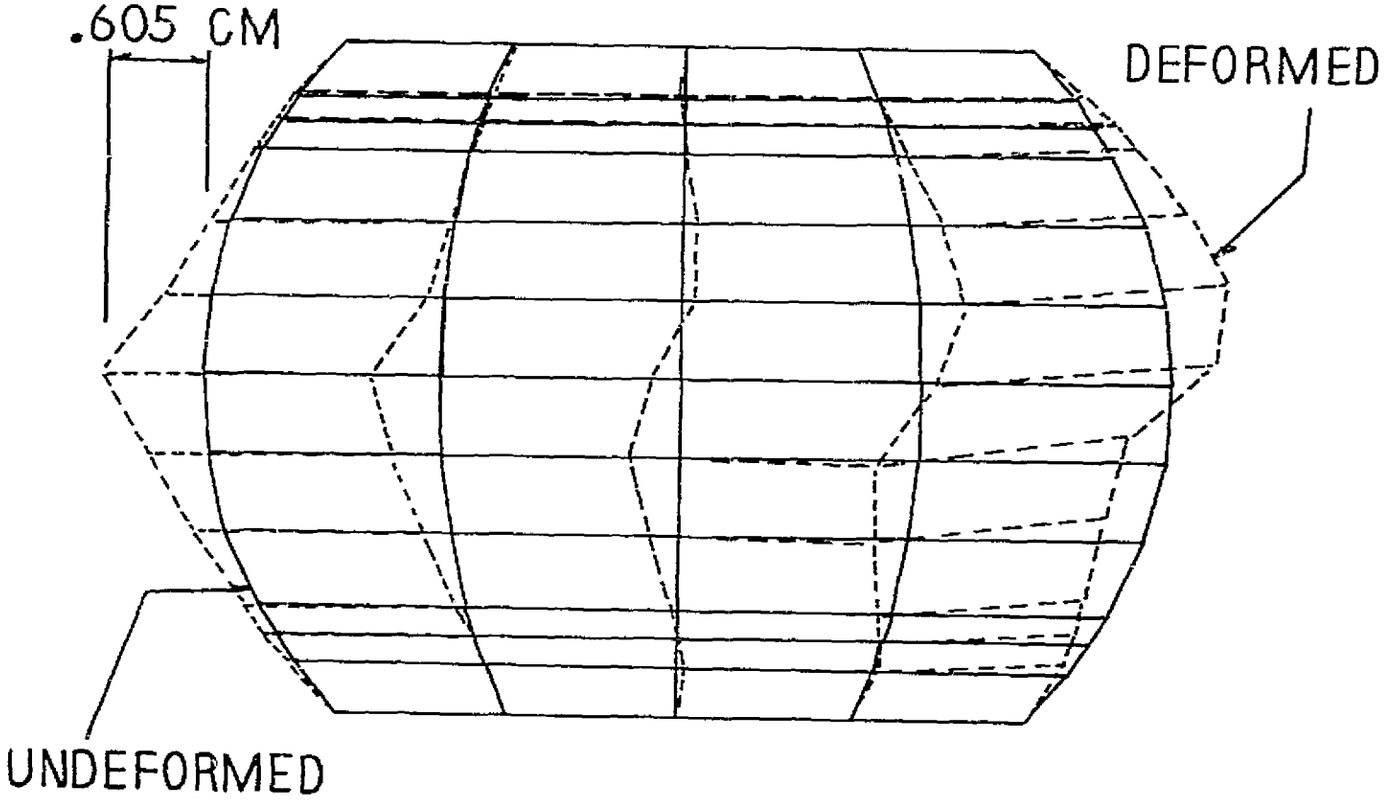

Figure 5. Deformed Shape of The Window Filled with Sea Water

Figure 6. Deformed Shape of The Window Filled with Air

D18

N78-32484

SOLVING MAGNETOSTATIC FIELD PROBLEMS WITH NASTRAN

Myles M. Hurwitz and Erwin A. Schroeder
David W. Taylor Naval Ship Research and Development Center

SUMMARY

Determining the three-dimensional magnetostatic field in current-induced situations has usually involved vector potentials, which can lead to excessive computational times. A recent paper shows how such magnetic fields may be determined using scalar potentials. The present paper shows how the heat transfer capability of NASTRAN Level 17 has been modified to take advantage of the new method.

INTRODUCTION

All classical electromagnetic phenomena are governed by the four Maxwell equations:

$$\nabla \times H = J + \frac{\partial D}{\partial t} \tag{1}$$

$$\nabla \times E + \frac{\partial B}{\partial t} = 0 \tag{2}$$

$$\nabla \cdot D = \rho \tag{3}$$

$$\nabla \cdot B = 0 \tag{4}$$

where the vector quantities are defined as follows:

H	Magnetic field strength or intensity
B	Magnetic induction or flux density
J	Current density
E	Electric field strength
D	Electric displacement

and the scalar quantities are defined as follows:

ρ	Charge density
t	Time

There is also a constitutive relation between B and H, given by

$$B = \mu H \tag{5}$$

where μ is the magnetic permeability.

Electromagnetic problems are often solved by introducing and solving for the magnetic vector potential A, where

$$B = \nabla \times A \tag{6}$$

Spreeuw and Reefman (ref. 1) used this method with NASTRAN in solving for harmonically oscillating electromagnetic fields in the presence of conductors carrying alternating currents. However, in order to use the existing structural and heat transfer capabilities in NASTRAN, simplifying assumptions had to be made. In particular, the magnetic vector potential A and the source current densities J were allowed to have components in only one direction, and those components were invariant in that direction. These assumptions effectively reduce the problem to one of solving for a scalar potential, which can be handled by NASTRAN's heat transfer analyses.

In the same paper, Spreeuw and Reefman also considered a problem in which A was not unidirectional and were able to use NASTRAN's structural analysis capability only because the governing equations uncoupled for the components of A.

Another problem with this formulation is the requirement that

$$\nabla \cdot A = -\varepsilon\mu\frac{\partial\phi}{\partial t} \tag{7}$$

where ε is the electric permittivity.
Spreeuw and Reefman used a separate post-processor to handle this condition. Frye and Kasper (ref. 2), in solving magnetostatic problems using the vector potential, use a Lagrange multiplier method (similar to multi-point constraints) to satisfy constraint (7). They also point out that special boundary conditions are required at boundaries where the permeability μ changes.

In reference 3, Zienkiewicz, Lyness, and Owen have developed a method for solving general, three-dimensional magnetostatic problems using scalar potentials, so that standard heat transfer analyses may be used and constraint equation (7) is not required. They also indicate that special boundary conditions, such as those mentioned in reference 2, are not needed.

The present paper shows how this new method has been implemented in NASTRAN Level 17.

BASIC EQUATIONS AND ASSUMPTIONS

The problem to be solved is the determination of the magnetostatic field due to a body placed in an existing magnetic field produced, for example, by direct current-carrying loops. The materials are assumed to be linear, but may be anisotropic. The governing equations are:

$$\nabla \times H = J \tag{8}$$

$$B = \mu H \tag{9}$$

$$\nabla \cdot B = 0 \tag{10}$$

Zienkiewicz separates H into two parts,

$$H = H_c + H_m \tag{11}$$

H_c is the field in a homogeneous region due to current J, satisfies

$$\nabla \times H_c = J \tag{12}$$

and is computed using the Biot-Savart law. H_m is the unknown magnetic field strength and satisfies

$$\nabla \times H_m = 0 \tag{13}$$

so that

$$H_m = \nabla \phi \tag{14}$$

and

$$\nabla \cdot \mu \nabla \phi + \nabla \cdot \mu H_c = 0 \tag{14a}$$

where ϕ is the scalar potential. Zienkiewicz then uses standard variational principles, with equations (9) and (10), to arrive at the standard finite element form

$$K\phi = F \tag{15}$$

where K is the "stiffness" matrix,

F is the "load" vector, and

$$k_{ij} = \int_V (\nabla N_i)^T \mu \nabla N_j dV \tag{16}$$

$$f_i = \int_V (\nabla N_i)^T \mu H_c dV \tag{17}$$

where

N_i is the finite element shape function for the i^{th} grid point, and

V is the volume of the finite element.

The formulation (16) for k_{ij} is exactly that of the standard heat transfer conductivity matrix with magnetic permeability μ playing the role of thermal conductivity. The formulation (17) for f_i, however, is not a standard heat transfer quantity and must be computed either in a separate program and input to NASTRAN or in a new NASTRAN capability. Also, note that f_i is element-dependent, as evidenced by the shape function gradient in equation (17).

Equation (15) is solved for ϕ subject to standard natural or forced boundary conditions. H_m can then be computed from equation (14), and the final results can be obtained using equations (11) and (9).

NASTRAN IMPLEMENTATION

To solve magnetostatic problems with NASTRAN Level 17 using the methods of the previous section, we select rigid format 1, HEAT approach. However, we have modified the program to

1) compute the H_c field due to circular, direct current-carrying loops;
2) accept a specified H_c field;
3) compute f_i (equation (17)) for the axisymmetric solid ring elements TRAPRG and TRIARG;
4) perform the addition specified in equation (11), where H_m is a transformation of the "temperature" gradients; and
5) output B (equation (9)) for subsequent NASTRAN plotting.

The implementation thus far has been limited to solid axisymmetric problems using TRAPRG and TRIARG finite elements and is running on the DTNSRDC CDC 6000 computers.

NEW BULK DATA CARDS

Two new bulk data cards have been introduced into the program for computing H_c fields. They are CEMLOOP, for computing the H_c fields due to circular current loops, and SPCFLD, for specifying H_c at selected grid points. (See figures 1 and 2 for detailed descriptions of these cards.)

MODIFIED NASTRAN ROUTINES

Nineteen existing NASTRAN routines have been modified to accommodate the new capability. The routines and the nature of the modifications are as follows:

Routine	Reason for Change
IFP,IFS4P,IFX1BD-IFX7BD	Recognize and check new bulk data cards CEMLOOP and SPCFLD.
LD21	Restart with CEMLOOP and SPCFLD in Static Heat Transfer Analysis.
GP3A,GP3BD	Recognize CEMLOOP and SPCFLD as "heat transfer" load specifications and place on HSLT (Heat Static Load Table).

Routine	Reason for Change
SSGSLT	Retrieve CEMLOOP and SPCFLD specifications from HSLT. CEMLOOP cards are copied directly to data block NEWSLT for later processing. All SPCFLD specifications are combined into one vector giving total H_c at all grid points. This vector is placed on NEWSLT.
EXTERN	Call new routine EANDM, which retrieves CEMLOOP and SPCFLD specifications from NEWSLT and computes f as given in equation (17).
XBSBD, XMPLBD	Specify table updates so that NASTRAN will recognize new functional module EMFLD.
XSEM14	Call new functional module EMFLD.
OFP1A	Specify new headings to output new data block HOEH1 giving magnetic field strength and induction.
OFPZZZZ	Call for new headings from OFP1A when HOEH1 is recognized.

NEW ROUTINES

Three new routines have been developed. Subroutine EANDM reads into open core CEMLOOP and SPCFLD data from data block NEWSLT, reads information for an element from the Element Summary Table (EST), and calls an element-dependent routine to compute the load as given in equation (17).

Subroutine EMRING is called by EANDM and computes the load due to CEMLOOP and SPCFLD specifications for solid axisymmetric trapezoidal (TRAPRG) and triangular (TRIARG) rings. We assume that H_c is constant over an element. Therefore, for TRIARG elements, H_c is computed at the centroid due to all CEMLOOP's using an elliptic integral formulation. If SPCFLD's are given, H_c is computed to be the average of the H_c's at the three vertices. Each TRAPRG element is divided into four overlapping triangles, and each triangle is treated as a TRIARG element. Once H_c has been computed for a triangle, equation (17) is used to compute the load at each grid point forming the triangle. Subroutine EMRING also outputs to Fortran file 11 certain element information, including H_c, for later processing by functional module EMFLD. This is a temporary method for passing information from EMRING to EMFLD. The normal method, of course, is to use data blocks. However, subroutine EMRING resides in functional module SSG1, and adding a new output data block to that existing module would require a change to every rigid format in the program. These changes will be made at a later time.

Subroutine EMFLD, which is also a new functional module, computes the magnetic field strength and induction, according to equations (11) and (9), for each finite element in the model. EMFLD retrieves from data block HOEF1 the

"temperature" gradient for an element. Since the gradient H_m was computed in an element coordinate system, EMFLD transforms it into basic coordinates. Then Fortran file 11 is searched to match the element identification number, and, on a match, H_c for the element is retrieved, added to the transformed H_m, and put out to data block HOEH1. Also computed and output to HOEH1 is the magnetic induction B. HOEH1 is later output using normal Output File Processor (OFP) execution. EMFLD also computes and outputs other information for plotting purposes, as explained in the next section.

PLOTTING MAGNETOSTATIC RESULTS

Normal NASTRAN plot processing allows for deformed plots based on grid point displacements or contour plots of stresses. In the present analysis, however, the "displacements" (the scalar potentials) are of little use by themselves. The "stresses" (H or B fields coming from EMFLD) are more useful, but what we would really like to see for "nice" plots are the lines of induction. The lines of induction indicate the direction of the magnetic induction B, and the number of lines per unit area indicates the magnitude of B. While we do not presently plot these lines of induction, we do plot the actual induction, magnitude and direction, for each element. Therefore, functional module EMFLD outputs other quantities as follows. For each element, two coincident grid points are created at the centroid of the element, and the corresponding GRID cards are punched. Also punched is a PLOTEL card connecting the two grid points. (The length of the PLOTEL element is zero.) Then a "displacement" vector is created by assigning zero values to each of the original grid points in the model and assigning the magnetic induction value for an element to each of the two coincident grid points created for the element. (The "displacement" vector uses six degrees of freedom per grid point since B is a vector, not a scalar.) This vector is packed in EMFLD and output in DMAP using module OUTPUT1. On a subsequent NASTRAN run, the new GRID and PLOTEL cards are merged with the original data, the "displacement" vector is retrieved using DMAP module INPUTT1 as data block UGV, and a deformed plot is requested with the VECTOR R option. This NASTRAN run is performed with rigid format 1, DISP approach, and ALTERs are used to execute only those modules required for deformed plots. The plots show the original structure as an underlay, and a vector is drawn at each element centroid indicating the magnitude and direction of B in that element.

SAMPLE PROBLEMS

At the time that this paper was being prepared, the only axisymmetric problems run with NASTRAN for which analytical results were readily available were problems with uniform permeability. The comparison between the NASTRAN and analytical results was very good. Although problems with nonuniform permeability have been run with NASTRAN and "reasonable-looking" results have been obtained, analytical results, required for verification, are still forthcoming.

REFERENCES

1. Spreeuw, E.; and Reefman, R.J.B.: Rigid Format Alter Packets for the Analysis of Electromagnetic Field Problems. Fourth NASTRAN Users' Colloquium, NASTRAN: Users' Experiences, NASA TM X-3278, September 1975, pp. 557-570.

2. Frye, J.W.; and Kasper, R.G.: Analysis of Magnetic Fields Using Variational Principles and CELAS2 Elements. Sixth NASTRAN Users' Colloquium, NASA Conference Publication 2018, October 1977, pp. 175-192.

3. Zienkiewicz, O.C.; Lyness, John; and Owen, D.R.J.: Three-Dimensional Magnetic Field Determination Using a Scalar Potential - A Finite Element Solution. IEEE Transactions on Magnetics, Vol. MAG-13, No. 5, September 1977, pp. 1649-1656.

Input Data Card CEMLOOP Circular Current Loop

Description: Defines a circular current loop in magnetic field problems.

Format and Example:

1	2	3	4	5	6	7	8	9	10
CEMLOOP	SID	J	AXI	X1	Y1	Z1	X2	Y2	+A
+A	Z2	XC	YC	ZC	CID				
CEMLOOP	3	2.5	1	5.2	0.	2.25			

Field	Contents
SID	Load set identification number (integer > 0).
J	Current through loop (units of positive charge/sec)(real ≥ 0).
AXI	= 0 nonaxisymmetric problem (not yet implemented) = 1 axisymmetric problem; TRAPRG and TRIARG elements are implied (integer).
X1,Y1,Z1 X2,Y2,Z2	Coordinates of two points through which the loop passes (given in coordinate system CID)(real).
XC,YC,ZC	Coordinates of center of loop (given in coordinate system CID) (real).
CID	Coordinate system identification number (integer ≥ 0).

Remarks:

1. Load sets must be selected in the Case Control Deck (LOAD=SID) to be used by NASTRAN.

2. If AXI=1, Y1 must be 0. or blank, and all data fields after Z1 must be 0. or blank. (Continuation card need not be present.)

Figure 1. Bulk Data Description of CEMLOOP

Input Data Card SPCFLD Specified Magnetic Field

Description: Specifies magnetic field at selected grid points.

Format and Example:

1	2	3	4	5	6	7	8	9	10
SPCFLD	SID	HCX	HCY	HCZ	G1	G2	G3	G4	
SPCFLD	18	12.25	0.	62.	8	17	103	1	

or

SPCFLD	SID	HCX	HCY	HCZ	GID1	THRU	GID2		
SPCFLD	18	12.25	0.	62.	9	THRU	27		

or

SPCFLD	SID	HCX	HCY	HCZ	-1				
SPCFLD	18	12.25	0.	62.	-1				

Field	Contents
SID	Load set identification number (integer > 0).
HCX,HCY,HCZ	Components of specified H_c field (real).
Gi,GIDi	Grid point identification numbers (integer > 0).
-1	Implies the H_c field applies at all grid points.

Remarks:

1. Load sets must be selected in the Case Control Deck (LOAD=SID) to be used by NASTRAN.

2. All grid points referenced by GID1 THRU GID2 must exist.

Figure 2. Bulk Data Description of SPCFLD

TRANSIENTS BY SUBSTRUCTURING WITH DMAP

Thomas G. Butler
BUTLER ANALYSES

SUMMARY

Automated substructuring in level 16 of NASTRAN was employed as a preface to the solution of a direct transient analysis. The DMAP ALTER statements written to adapt the substructuring for transient purposes are explained. Data recovery was accomplished with transfer functions. Proof of the success of the method is presented with an application to a missile structure.

INTRODUCTION

Substructure analysis capability in NASTRAN has been automated for rigid formats 1, 2, and 3 only. Rather than wait for the extension of automation to rigid format 9, it was found advantageous to use as much of automated substructuring as is now available. Considerable effort was needed to couple the substructure data to the transient analysis and then recover the transient responses of individual substructures.

The two principle features of substructuring that made this effort worth while were the ability to condense small pieces of the matrices at a time and the ability to combine component substructures in different ways. The structure under investigation was liable to damage, and the attraction of substructuring was its ability to substitute damaged components for the hapless predecessors. Many additional advantages of substructuring became evident during the progress of the analysis, but the most notable was the necessity of the analyst to organize thoroughly.

The method presented in this paper could be characterized as a five phased analysis as opposed to the usual three in automated substructuring. Dave Herting of Universal Analytics was extremely helpful in planning the solution path and other substructuring items. Phase one defines the basic substructures without load. Phase two combines components and reduces them to a final pseudostructure but applies deformations for a loading. Phase three recovers influence coefficient matrices for the responses of individual component substructures to the deformations of the pseudostructure. The next phase is the direct transient analysis of the scalar model of the pseudostructure, but is not called phase four. Phase four recovers the response of individual component substructures to the transient excitation using modified static rigid format. A post-processor was written to scan the stress data for the times and locations of parts exceeding a threshold value.

SOLUTION STRATEGY

Answers need to be found to some important questions when one proposes to use substructuring with transients. For instance,

What can and what can't automated substructuring do?
How is the transfer of matrix data from phase two to rigid format 9 accomplished?
What has to be done to get the transient rigid format to recognize the matrices offered to it by substructuring?
How is damping introduced?
How is transient data to be recovered in the component substructures?
How are plots to be obtained?

Outline of Solution

As with any investigation, answers to questions beget more questions. The answers will therefore not be clear-cut until a chain is satisfied. In short, automated substructuring can organize the characteristics of the pseudostructure, as it is modeled for transients, into its stiffness and mass matrices, but will yield neither a damping matrix nor loading. At first blush, it seemed feasible to represent this pseudostructure in scalar form for rigid format 9. Knowing the retained degrees of freedom in the pseudostructure, one then calls for an equivalent number of scalar points for transients. During transients the matrices from phase two substructuring can be introduced by a DMAP ALTER. All matrix generating modules can be by-passed and all matrix partitioning can be circumvented because all SPC's, MPC's, and OMIT's were incorporated during the formation of the pseudostructure stiffness matrix. Taking the response output from the TRD module one can process it by influence coefficient matrices to recover the component responses. This sounds fairly straight forward, so one is encouraged to tangle with the detailed problems.

Data Recovery

Looking first at the data recovery problem using influence coefficent matrices, it helps to think in terms of a super stiffness matrix. In phase two if a unit displacement were imposed in one degree of freedom while holding all others to zero and this is done for each degree of freedom in the pseudostructure, it amounts to an enforced displacement in the form of a unit diagonal matrix. Translating this notion to specifics means that a unit diagonal matrix is needed for substitution as the UGV matrix after module SDR1. Now the SOLVE and RECOVER modules can process the results onto the SOF (Substructure Operating File).

Appendix A contains the details of how these ideas were implemented. The Operations that are important are the DMI input of the unit diagonal matrix, the substitution of the unity matrix for UGV with an EQUIV, the use of a SOLVE command to name the pseudostructure for which the solution chain is intended,

and the use of a RECOVER command to get the solution data out on to the SOF in an orderly fashion so that phase three executions can readily partition the data from the internal substructuring book-keeping scheme.

A rare thing was uncovered that almost shattered this plan. A non-open-endedness, which is quite contrary to the original design philosophy of NASTRAN, was encountered. Only 100 subcases were provided for in any one execution in level 16. But this pseudostructure was of order 916. To impose a unit displacement in each of the 916 degrees of freedom one at a time, meant the assignment of a static subcase for each of the 916 enforced deformations. It was a rare looking Case Control packet that was as large as the Bulk Data deck. In discussing this unhappy event with John McDonough of Computer Sciences, he said that relief of this limitation was already worked out by extending the allowance to 300 subcases. This was small comfort in view of the need for 3 times that amount of relief before this job could execute. The good news was that John had determined, during his investigation preparatory to increasing the allowance to 300, no table restriction or other kind of overflow condition would be confronted if a further extension were attempted. It took two tries to dilate both the standard solution and the automated substructuring section to order 1,000. This has not been generalized yet, but a scheme is believed to be under consideration which will allow the analyst to communicate his needs to the OSCAR and the FIAT by either a DIAG or NASTRAN card entry giving the size of his non-standard subcase array.

The second step in data recovery is to create a set of influence coefficient matrices using automated substructuring phase three. The dimension of the i,j^{th} term of the influence coefficient matrix is

"Displacement in the i^{th} degree of freedom of a Basic S/S per Unit displacement in the j^{th} degree of freedom of the P/S."

where S/S means substructure and P/S means pseudostructure. Any such matrix will designated $[INFL]_{xxx}$, where INFL represents the matrix of terms with dimension u/U=1 and xxx is the subscript to denote the basic S/S by name. This influence coefficient matrix will be used in a post-transient operation to perform the matrix multiplication

$$[INFL]_{xxx}\ [U(t)] = [u(t)]_{xxx},$$

to obtain time varying displacements in a component S/S, where U(t) is a matrix of the P/S response displacement vectors at each of the transient output times, and u(t) is a matrix of the response displacment vectors of component S/S, xxx, at corresponding transient output times.

In computing these influence coefficient matrices during phase three, the number of subcases are required to match the phase two array. This means that in the particular problem, the phase three runs for each component substructure contained 916 subcases. Once again this plan was almost shattered by a bug. For economy purposes the phase three runs were submitted as restarts of the phase one checkpointed runs. Each phase one solution was R. F. 2, and each phase three solution was R. F. 1. The phase three restarts aborted. Only by the chanciest strokes of good fortune did John McDonough happen to have faintly

remembered that somewhere he heard that some difficulty with restarts were overcome by using option 9 on the SOL card, i.e. SOL 1,9. It worked! In effect option 9 avoids the consideration of the optimization features of R. F. 1. This bug appeared during restarts involving change of rigid formats only.

This phase three operation is not out of the woods yet, because a needed data block from the phase one run did not get checkpointed. Appendix B gives the details of how to remedy this defect. Appendix B also explains how the INFL matrix is equated to the UGV matrix and is then written to disc files for the final solution recovery.

Before taking up the problems with transients, the third and last step in data recovery will be completed. Assuming that the matrix of pseudostructure response displacement vectors, U(t), has been successfully written to a disk file, and assuming that the INFL matrices for the several basic substructures have been written to disk files, the task of recovering basic substructure time varying responses in displacements, stresses, and forces is at hand. These jobs will be outside the realm of automated substructuring except that they will be restarted from phase one checkpointed runs. The first task to be performed is to set up the case control such that the vector of response displacements at each output time slice shall be considered as a static solution case. The labelling of each subcase with the output time proves to be a great convenience. Next, the restart data has to be fetched in order to re-establish the internal book-keeping scheme so that the OFP (Output File Processor) module can function in an orderly fashion. Since the product [INFL] [U(t)] will produce a matrix that can be considered the static solution matrix [UGV], no matrix generators or matrix partitioning is needed. The first module needed after the undeformed plot routines is SDR2 so the ALTER packet to bring in the matrices and do the matrix multiply, can start just before SDR2. The outputs from SDR2 are then delivered to OFP to satisfy the output requests in case control. The stress table is output for scanning by a post processor. A normal termination turns control over to the PLOT routine and exits. Details of how these tasks were implemented are given in Appendix C.

Transient Solution

Problems for transient solution begin in phase two of substructuring. Due to a bug in the command "REDUCE" the mass matrix which is produced is designated as square not symmetric. If this were allowed to go uncorrected transient solutions would be 4 times more expensive than expected, because the trailers would telegraph to the DCOMP and FBS modules that unsymmetric routines would have to be called. A scheme was devised, which after much streamlining turns out to be disarmingly simple, using MERGE to change this trailer from square to symmetric. It was no small task to discover how simple it could be to output the pseudostructure stiffness and mass matrices. It was a matter of discovering that there was a module within the substructuring lexicon that was available for addressing explicitly but which was not individually featured. The name of the module is SØFØ. It is incorporated frequently in the listings of DMAP ALTER packets for major commands, so by studying these commands listings it finally registered that if "they" can do it then I can do it. The two complimentary

modules SØFØ and SØFI deserve to be given individual billing in the documentation. Listings of their use for the trailer change to symmetry and for the output of stiffness and mass matrices are contained in Appendix D.

As a preface to the tasks relating to transients, it would be well to ponder what the aims are. At the very least the output result for the pseudostructure should be a matrix of displacement response vectors at a sequence of time slices. Possibly velocity and acceleration outputs may be needed. Plots of the pseudostructure are certainly desireable. It is mandatory that the transients be able to be restarted at a time earlier than the latest time of the preceding run. Restarting the problem with an old set of initial conditions on a new configuration must include acceleration. The model is to be scalar with matrices to be delivered from the phase two pseudostructure. Loads are to be applied to this scalar model. Damping needs to be introduced.

Strange to say, the damping problem will be discussed first. The reason for this order is to settle the question as to whether all matrix generation modules can be by-passed. If uniform structural damping is an acceptable representation of the way the structure behaves, then the damping matrix can be generated by a scalar multiplication of the stiffness matrix, which already exists. This was decided on. Consequently, all matrix generation modules could be by-passed and an ALTER packet could be added which would do the matrix multiplication and whatever related parameter manipulation that would be needed. The Bulk Data of course must contain a PARAM card for the W3 frequency. Myles Hurwitz of David Taylor NSRDC was of inestimable value in helping with parameter manipulations and other system problems.

Now the operation of bringing in the stiffness and mass matrices from phase two is simply a matter of using INPUTT1 and renaming them with an EQUIV statement so that transients can proceed along the normal chain of the rigid format. The Bulk Data of course must contain an SPOINT card containing the number of points equal to the degrees of freedom in the pseudostructure.

The problem of load definition is mainly a matter of book-keeping. Whether the model is geometric or scalar, the nature of the load is such that each component of load has a separate amplification time history so the TABLED1 input data is the same in either case. The DLOAD cards must refer to scalar points, so it is necessary to consult a table to determine which scalar point corresponds to a loaded component of a geometric point. Fortunately, the automated substructuring output items anticipate this need very nicely. The name of the table which tabulates the correspondence between an internal degree of freedom number and the physical point component is "SUMMARY OF PSEUDOSTRUCTURE CONNECTIVITIES." This table is printed in response to the analyst's selection of subcommand "OUTPUT Option 12" during a COMBINE operation. Of course, in this case the table to be used is that associated with the final COMBINE operation which produced the final pseudo-structure. If however, the operation which produced the final pseudostructure configuration were a REDUCE operation, then one needs to consult a pair of tables: the EQSS set of tables and the last PSEUDOSTRUCTURE CONNECTIVITIES table. The EQSS is printed in response to the analyst's selection of option 5 of the subcommand OUTPUT during a REDUCE operation.

The problem of restarting the transient integration at a time earlier than the last of the preceding run is complex. The reason for imposing this requirement is that damage is expected to occur to the structure, but the time of damage won't be known until the results of a previous run are examined. If a stress level is found to be exceeded, the flexibility is provided to substitute a replacement substructure in a damaged configuration. The reconfigured structure will then be restarted at the instant at which the stress level was found to be exceeded. This capability to restart at an earlier time meant that a change in the code of the TRD module had to be made. Simultaneously, a provision in the DMAP listings had to be made to allow for the modification of two book-keeping items. The value of the parameter NCOL had to be set to tell the TRD module at what column in the matrix of the displacements, velocities, and accelerations the data is to be fetched to represent the initial conditions at the time of restart. The table TOL (Transient Output List) has to be enabled so that additions can be made to the table. The changes to the code and to the DMAP were all generously provided by P. R. Pamidi of Computer Sciences.

The problem of initial conditions on a changed configuration could now be handled as a restart at a time specified by the NCOL and a revised TSTEP card without having to go into an external definition using an IC card. Such a restart also provides for initial accelerations to be imposed as well as initial velocities and displacements. Such gymnastics are possible under two conditions. First, the changed configuration must have matrices of the same size (order N), and in the same sequence as the original model. Secondly, the analyst has to be content with the approximate values of the initial conditions on the changed configuration being the same as the terminal values of its predecessor. Under certain conditions this reconfiguring with substructuring allows an analyst to get valuable information about a nonlinear problem using linear analysis.

The final transient task arises because of the particular nature of the UDVT matrix. The CFP arranges a triplet of values for every time. Consequently, UDVT consists of U, $\dot{U}$, & $\ddot{U}$ at t_0, followed by U, $\dot{U}$, & $\ddot{U}$ at t_1, and so forth through time t_N. Only the matrix of time varying displacements is needed for the data recovery phase; therefore the displacements will have to be stripped from UDVT by use of the DMAP utility PARTN. Of course, a partitioning vector will have to be defined by DMI in the Bulk Data to which PARTN can refer. Having the matrix of displacements only, it just remains to use OUTPUT1 to read them onto an external disk file.

Unfortunately, plots of the pseudostructure cannot be obtained because it was defined in R. F. 9 by scalars which have no geometric properties. However, plots of each individual basic substructure can be obtained in the data recovery phase. A listing along with explanations of the ALTER packet for R. F. 9 to implement these tasks are given in Appendix E.

APPLICATION

The technique of combining automated substructuring with direct transients was applied to the analysis of a current missile. Figure 1 shows a picture of the hardware. Figures 2 through 7 depict the undeformed plots of the substruc-

tures. Figure 8 shows a chart giving the evolution of the analysis from the definition of individual substructures, the combining into pseudostructures, through transient analysis and finally data recovery. This chart is usually called a substructure analysis tree or simply a tree. In this case, however, there are five phases instead of three. Figure 9 displays the variations in the tree under different configurations with a minimal of annotation.

The technique proved to be quite successful in that the analytical results compared quite favorably with two full scale tests.

HINDSIGHT

Naturally, when one achieves a certain measure of success with a task, the thinking process does not end abruptly. It has occured to me that some things could have been done differently. One is in the area of dynamic loads. Allow me to retrogress for a moment. During the analysis great care was taken to control the band and the density of the K matrix. Banding was performed on each substructure. Condensations were performed on matrices whenever possible when they were of small order; e.g. OMIT's were introduced in phase 1 as deeply as possible without interfering with connections or loads; reducing was used in phase two at connection interfaces without interfering with loads. Condensations, after loads were defined in transients, were considered but abandoned, because the pay-off among trade-offs was not immediately evident. Parallel condensations would have to be performed in phase two and in R. F. 9, because matrices would have to be delivered to R. F. 9 in uncondensed form, then a phase two condensation would have to follow the matrix transfer to match the condensation that would take place in transients, because data recovery of necessity is based upon the matrices in "SDISPLACEMENT" form from transients. This penalty of double condensation plus the increased density may outweigh the advantage of order reduction in transient DCOMP and FBS. A way of omitting the double condensation penalty has surfaced after the analysis. The DAREA loading could have been represented as "unity" static loading in phases one and two with condensations including some of the loaded points. The "static load matrix" could be examined after phase two and before transients to arrive at the weighting functions different than 1 for the DAREA cards. Time amplifications would have to be adjusted accordingly.

Another post hoc idea occurred in the area of plotting. After the transient analysis of the scalar model was complete, another grid point model could be assembled with a grid point for every scalar point wherein the other 5 degrees of freedom would be constrained. An ALTER packet to admit the static and deformed PLOT modules and substitute the scalar UDVT for the "SDISPLACEMENT" input to the VDR module would allow the plots to be obtained for the pseudostructure transient response at a small cost.

CONCLUDING REMARKS

A technique for combining automated substructure analysis with transient analysis has been devised and successfully applied. The technique can be summarized in the form of a recipe to assist an analyst, who may want to try this technique, as to what factors have to be taken into account.

Recipe

1. Run S/S through Ø2. Combine & reduce to produce the transient P/S model.
2. Run Ø2 SOLVE & RECOVER operations with ALTER packet to read [I] matrix into UGV data block and supply subcases for each of the N degrees of freedom.$
3. Run Ø2 to change MMTX from sq. to sym. using MERGE* packet. Read KMTX & MMTX onto external disk file using SØFØ command and OUTPUT1 packet.
4. Set up transients as a scalar problem. Read KMTX & MMTX in from external file. Supply loading data to scalar degrees of freedom.
5. Apply ALTER packet to jump around matrix generators, to build damping matrix, to set transient parameters, to partition displacements from UDVT, and to provide for restart @ earlier time than last.**
6. Run Ø3 as SØL 1,9* with ALTER packet to correct SDR1* and output INFL.
7. Run Ø4 as SØL 1,9* with ALTER packet to jump around matrix generators, to multiply for basic S/S transient displacement response, and output stress table.

$ N is limited to 300 in standard level 17.
* These steps will not be necessary in an operating version with these bugs corrected.
** Level 17 has this feature incorporated in the code.

Figure 1
MISSILE HARDWARE

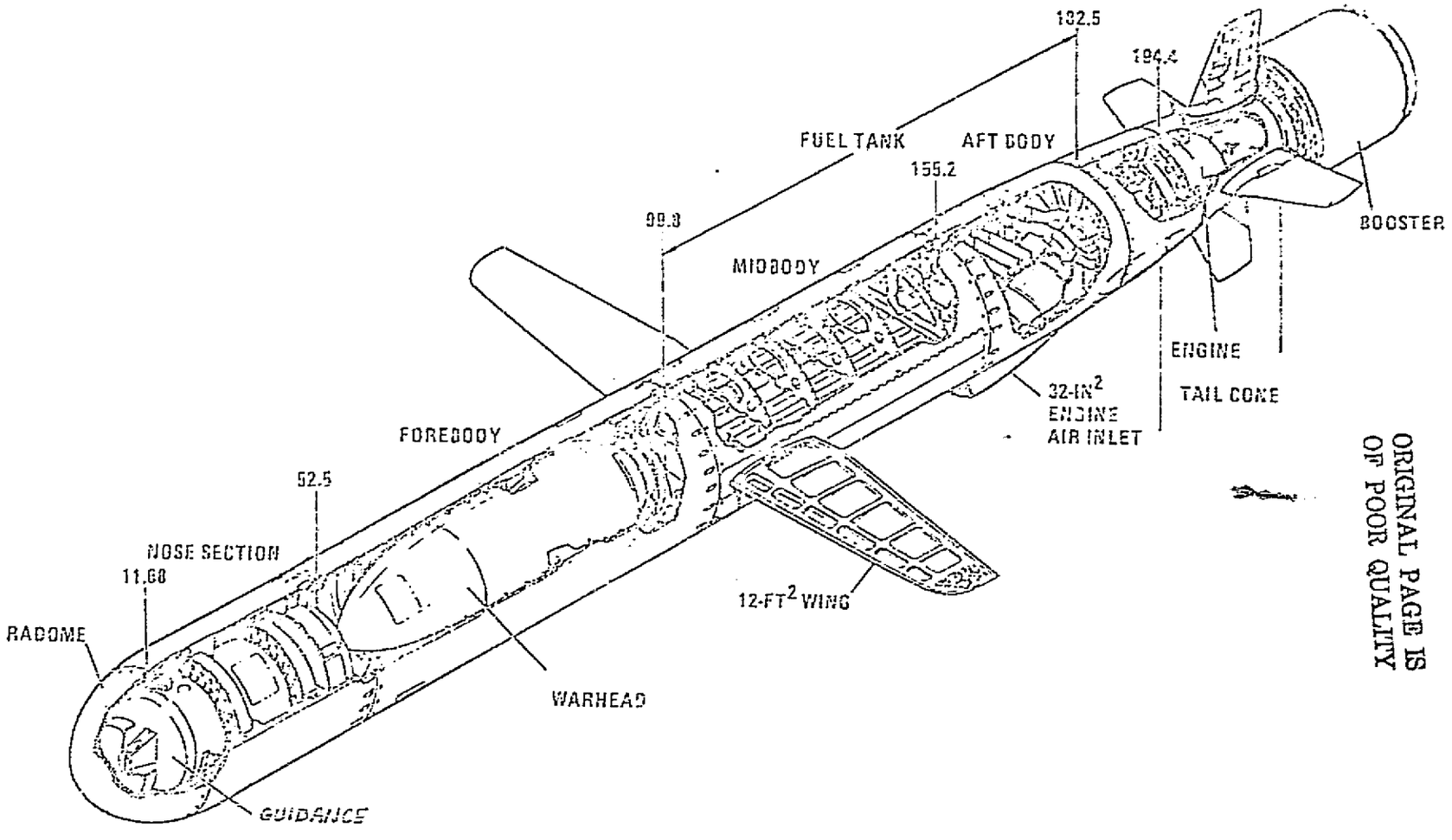

Figure 2

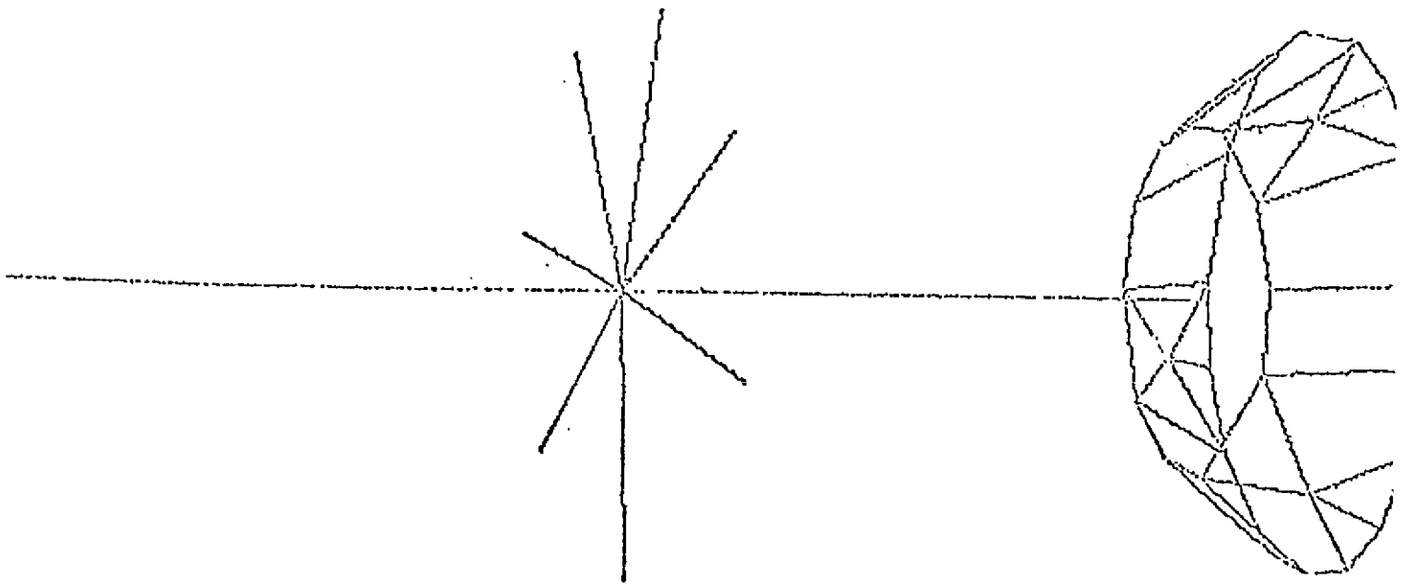

BUL

Figure 3

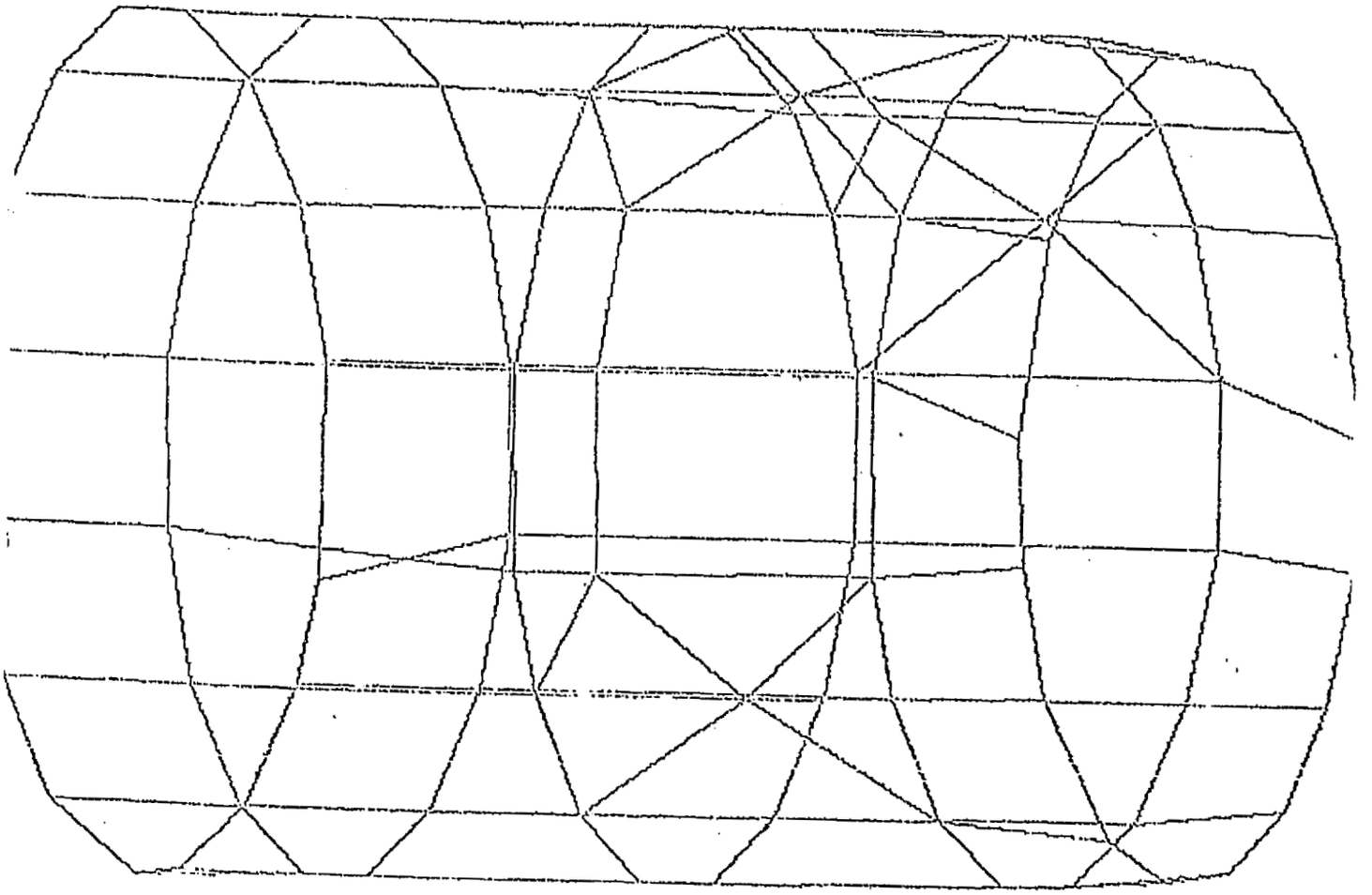

SHL

Figure 4

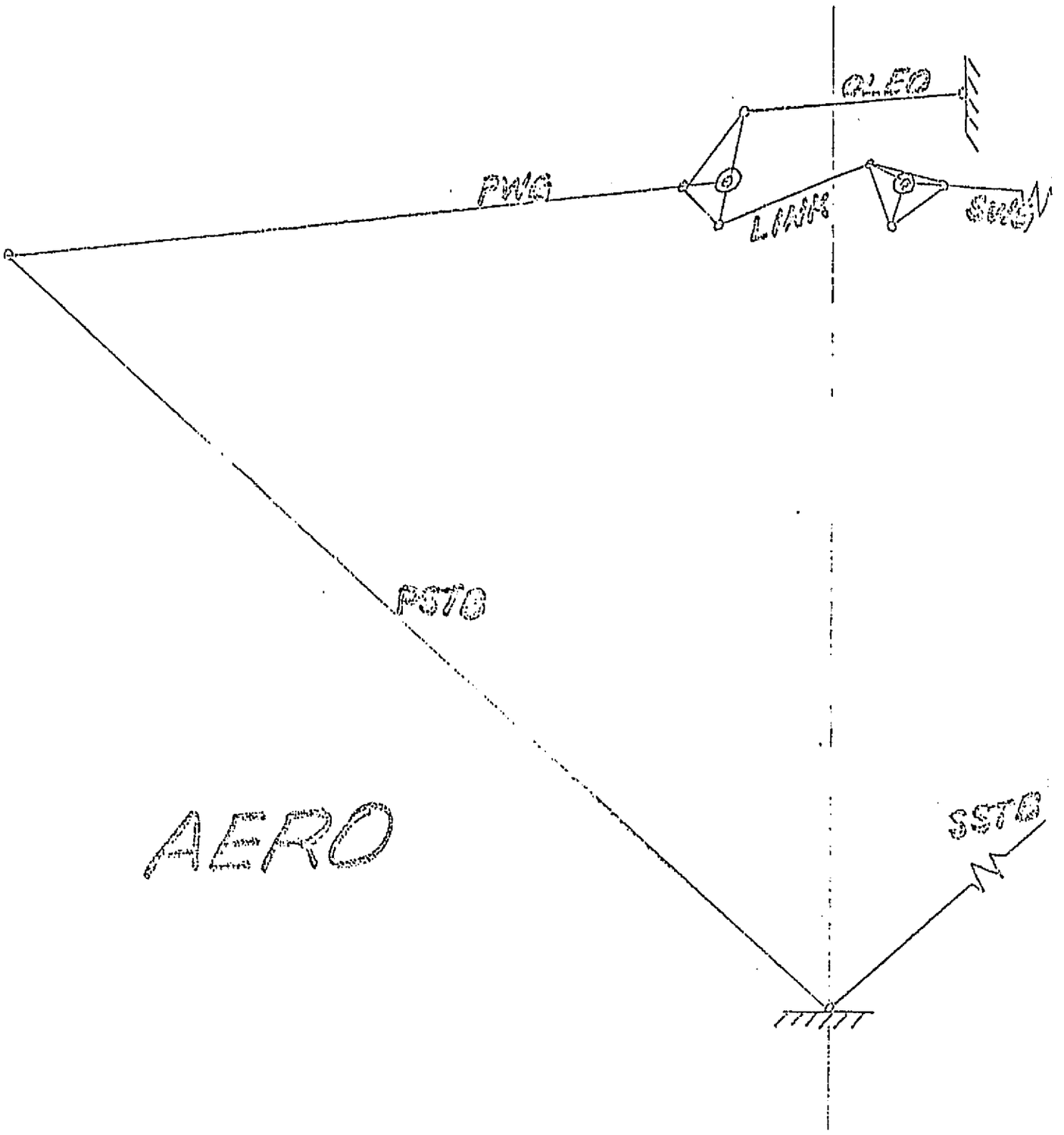

Figure 5

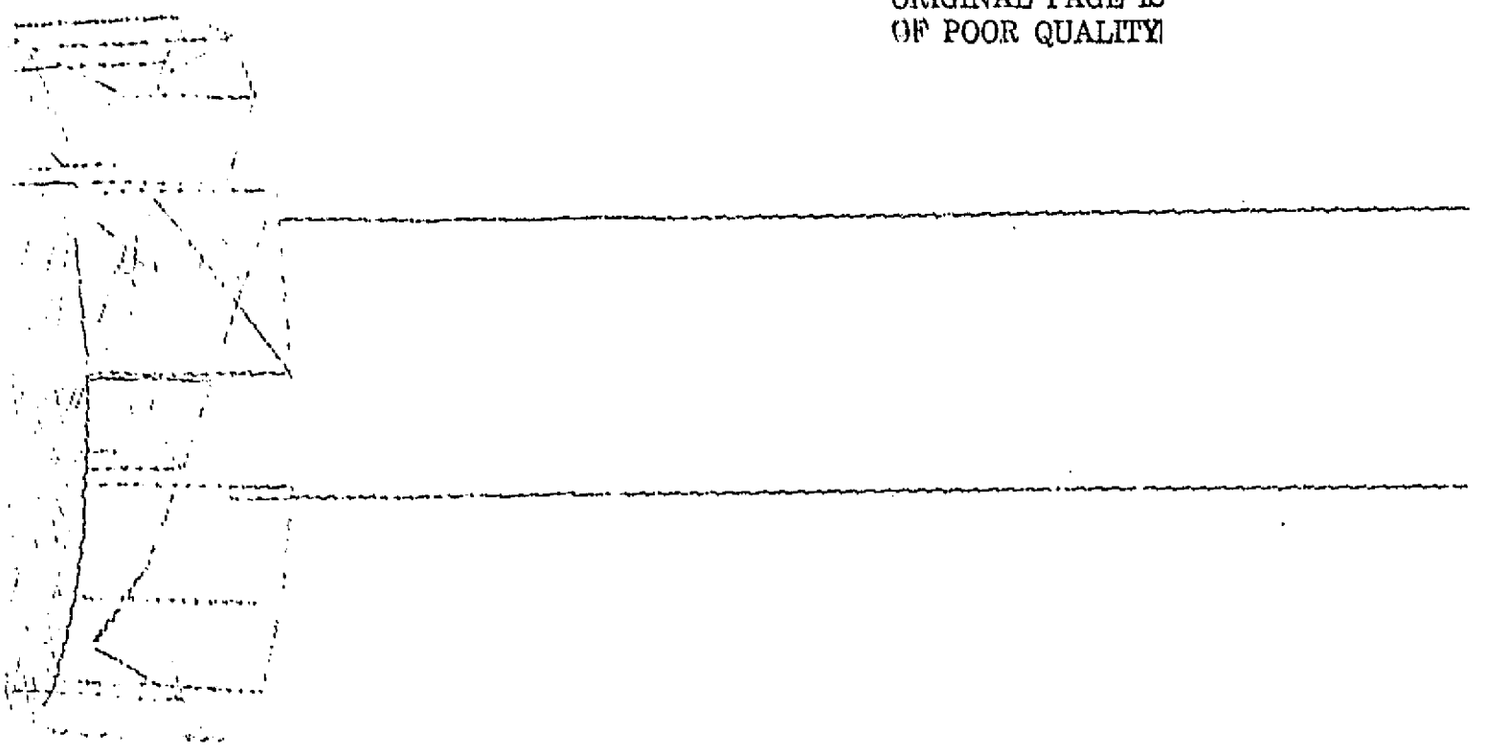

Figure 6

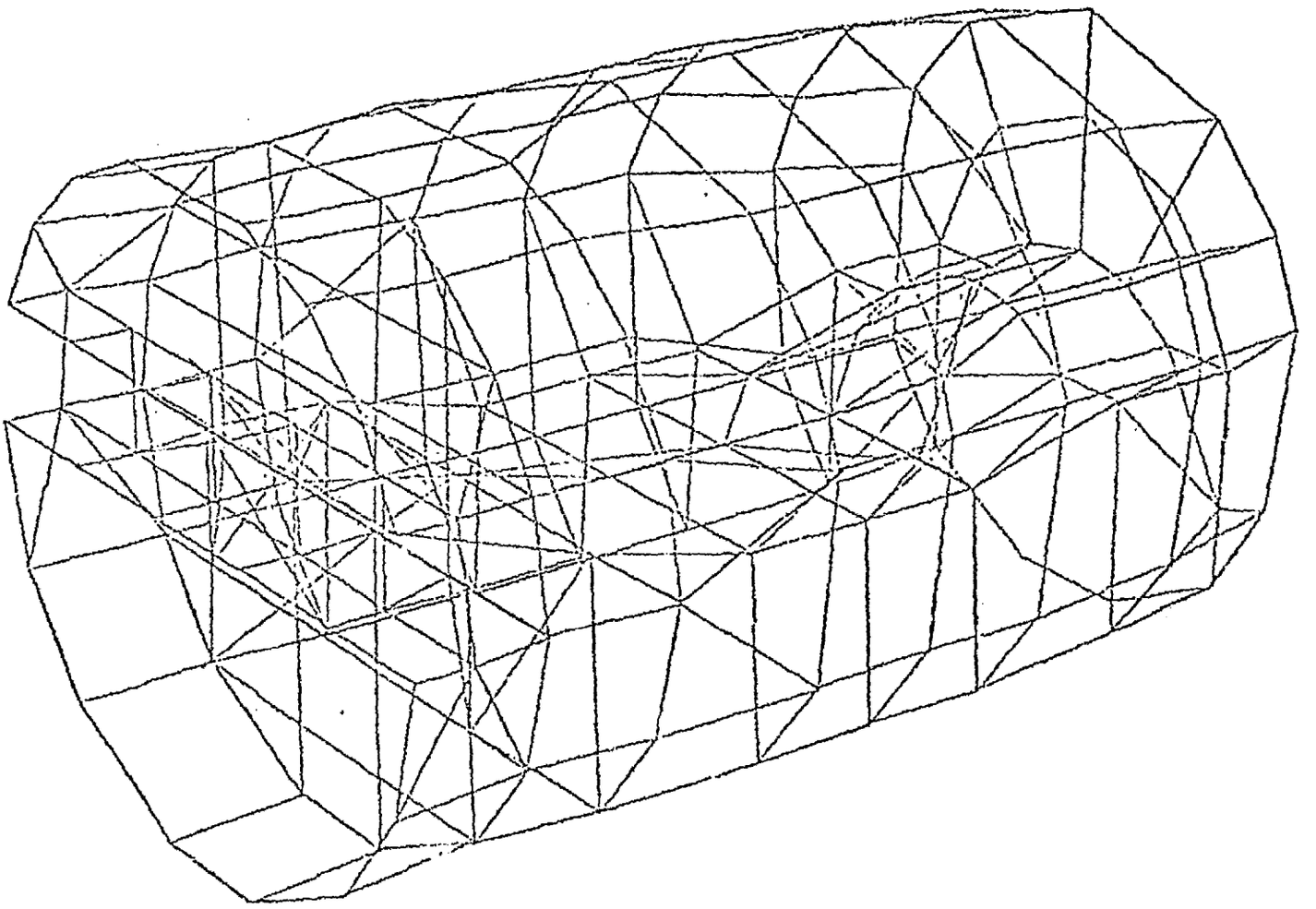

Figure 7

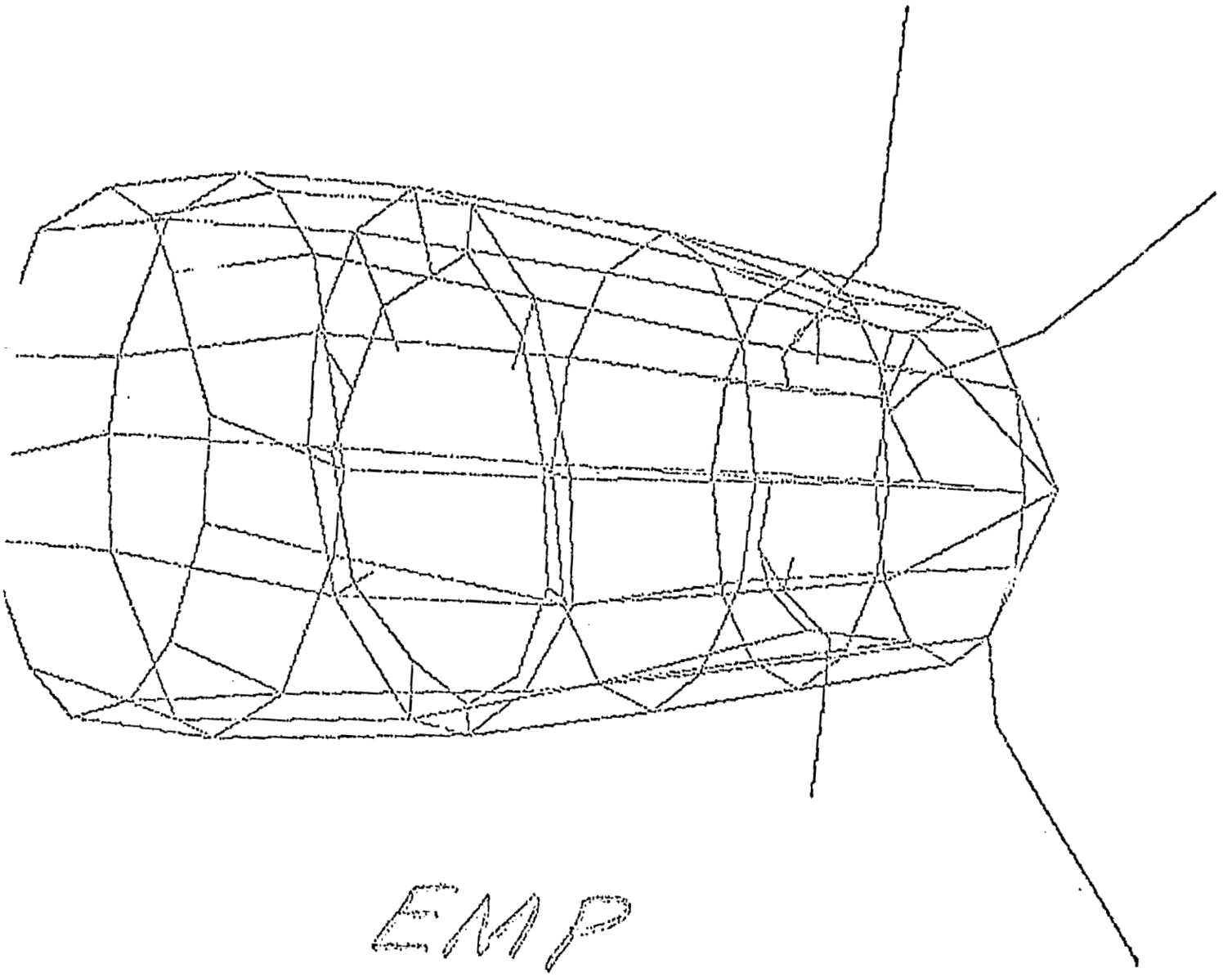

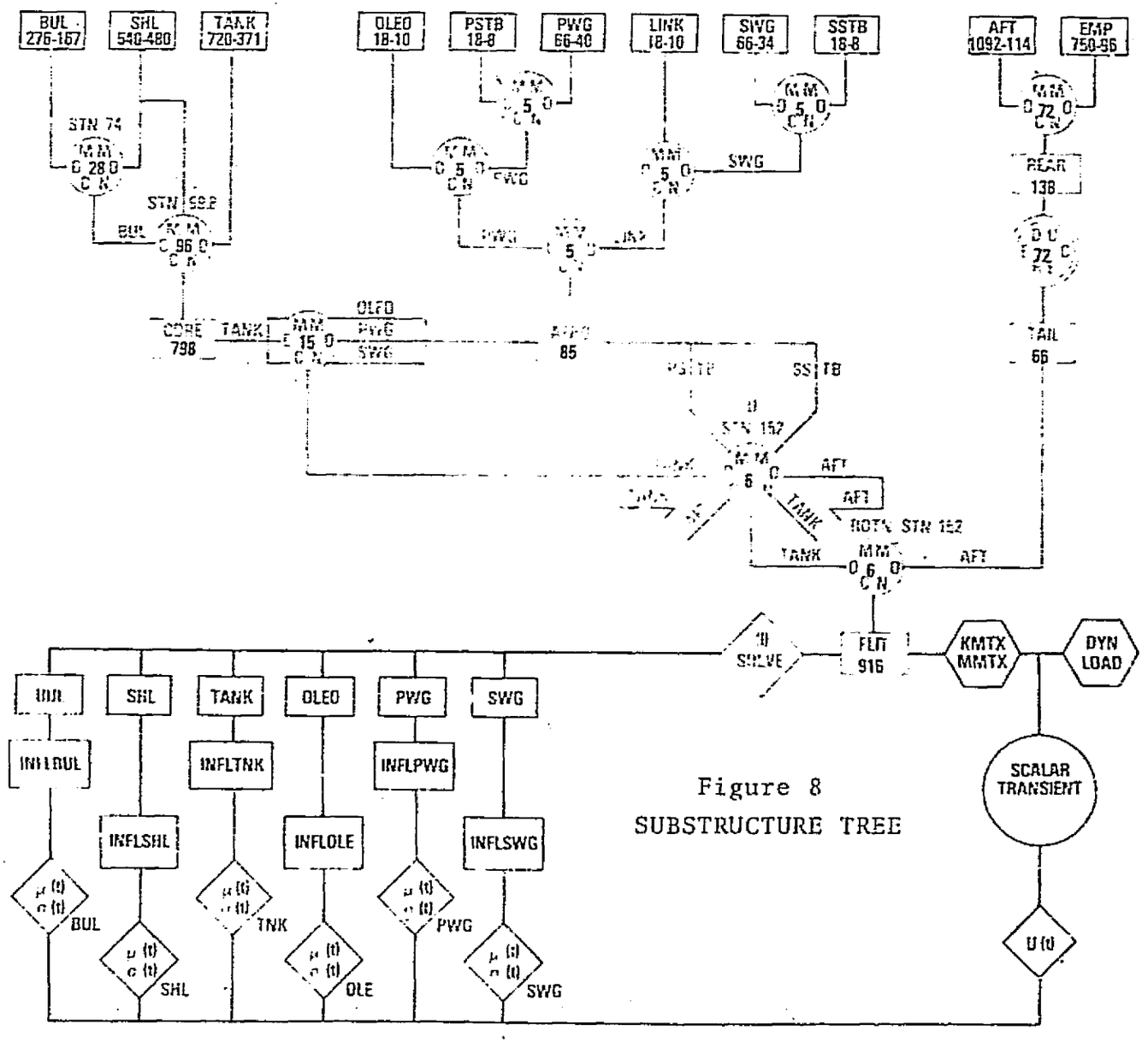

Figure 8
SUBSTRUCTURE TREE

Figure 9

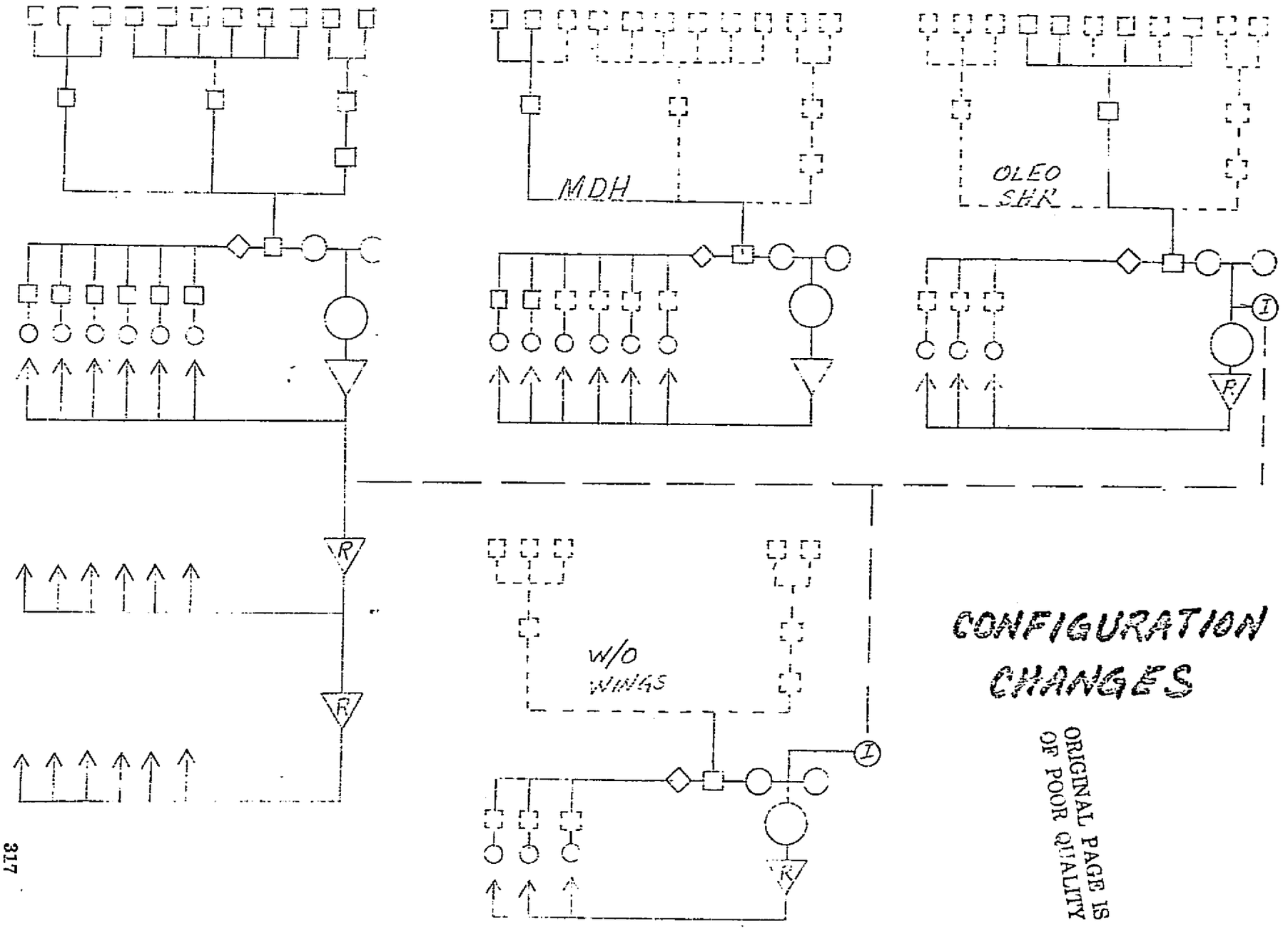

APPENDIX A

DMAP ALTER TO R.F.I. FOR UNITARY MATRIX LOADING WITH S/S SOLVE

This appendix supplements the description of SUBSTRUCTURE Phase II Solution Strategy. The Phase II DMAP ALTER statements are given first, followed by explanations according to statement number.

```
1.  ALTER 100
2.  JUMP TGB $
3.  ALTER 126
4.  LABEL TGB $
5.  EQUIV PARTUGV, UGV/ALWAYS $
6.  ENDALTER
```

Statement Explanations:

1. Since these ALTER statements are used in conjunction with S/S commands SOLVE and RECOVER, this ALTER must not interfere with the automated ALTER's associated with these commands, i.e. these must be avoided 2, 4 to 5, 9 to 22, 29 to 30, 41, 58 to 61, 73 to 78, and 134 to 164. The ordinary preparation of matrices such as constraints and omits will in general be needed. The operations to be eschewed as unnecessary and costly are decompositions, load assembly, FBS (Forward Backward Substitution), and SDR1 (Stress Data Recovery). Begin the ALTER at statement 100 in R.F.1 because constraints and omits have been completed by this point, and it precedes the decomposition.

2,3,4. Start the avoidance of unwanted operations with a JUMP command to a label located after the recovery of UGV in module SDR1.

5. The name o the unitary matrix input via DMI cards is PARTUGV. Since it is desired to have NASTRAN recognize this unitary matrix as the displacement solution, it must be labeled UGV for succeeding modules to so recognize it. There PARTUGV is equivalent to UGV. The parameter ALWAYS was used to make this EQUIV "take" because it was established earlier in the automatic ALTER's with a value of negative one.

APPENDIX B

DMAP ALTER FOR CORRECTING SDR1 AND OUTPUTTING INFLUENCE COEFFICIENT MATRIX

This appendix supplements the description of SUBSTRUCTURE Phase III Solution Strategy. The Phase III DMAP ALTER statements are given first, followed by explanations according to statement number.

```
1.  ALTER 126, 126
2.  COND      NOUOOV, OMIT $
3.  FBS       LOO,,PO/UODK/C,N,1/C,N,1/C,N,1/C,N,1 $
4.  CHKPNT    UODK $
5.  EQUIV     UODK, UOOV/ALWAYS $
6.  CHKPNT    UOOV $
7.  LABEL     NOUOOV $
8.  SDR1      USET, PG, ULV, UOOV, YS, GO, GM, PS, KFS,
              KSS,/UGV, PGG, QG/V,N,NSKIP/C,N, STATICS $
9.  OUTPUT 1, ,,,,//C,N,-1/C,N,3 $
10. OUTPUT 1 UGV,,,,//C,N/O/C,N,3 $
11. EXIT $
12. ENDALTER
```

Statement Explanations:

1. This is a restart of a SUBSTRUCTURE Phase 1 checkpoint. A required input data block UOOV for module SDR1 did not get checkpointed in the Phase I run because SSG3 was automatically ALTERed out, so therefore is not available for restart and its absence would cause an abort because UOOV is not allowed to be absent as an input data block if an OMIT occurred.

Since the SDR1 module in R.F. 1 is statement number 126, the patch for remedying this defect must be inserted either ahead of or in place of 126. In this case it is inserted in place of 126, because constraint forces QR were not checkpointed in the Phase I run either, necessitating the removal of QR as an input data block to SDR1.

2 thru 7. These six statements are intended to provide for both the presence and absence of a Phase I OMIT. If there were a Phase I OMIT, the parameter named OMIT would be given a positive value when output from GP4 and the COND conditional jump to label NOUOOV would not take; thus causing the operation sequence to pass to statement 3, FBS. If there were no Phase I OMIT, the parameter named OMIT would have retained its negative one default value, and the COND conditional jump to label NOUOOV would "take" and the FBS module would be by-passed.

The reason that it is desired to cause this conditional jump is that UOOV would have existed albeit as a purged data block, and would satisfy the input requirements of SDR1. The EQUIV of data block UODK to UOOV uses parameter ALWAYS because ALWAYS was defined to be negative one by automated substructuring. Data blocks UODK and UOOV are checkpointed before and after the EQUIV because the DMAP compiler is very particular about tidiness in specifying the precedents and antecedents in EQUIV.

3. Data block PO is required to be supplied by the analyst as DMI input. It is of order "A" rows and "0" columns and is null. This will create a null UOOV. The reason that UOOV

should be null is that no load has been put on any omitted points.

8. The call statement for SDR1 must be written without an input data block appearing after KSS. It is not necessary to remove output data block QG even though QR is absent, because SDR1 will generate QG as purged in the absence of QR.

Output data block UGV will now be the basic substructure influence coefficient matrix.

9,10. These modules will output the influence coefficients to a NASTRAN file INP3. If the JCL is written to make a disk file of INP3 it should be named INFLxxx for ready identification.

11. An exit is taken after outputting the INFLxxx data because no more processing is needed.

Statements 4, 5, 6 could have been omitted and UODK could have been used in place of UOOV as an input data block to SDR 1, because USET would have sensed that UOOV was purged during execution of DMAP #71 of R,F, 1 in the event of no OMIT, and would have relieved SDR1 from requiring UOOV as input to SDR1.

APPENDIX C

DMAP ALTER TO R.F.1 FOR POST-TRANSIENT DATA RECOVERY

This appendix supplements the description of STATIC DATA RECOVERY PHASE IV. The Phase IV DMAP ALTER statements are given first, followed by explanations according to statement number.

```
1.  ALTER       39, 155
2.  INPUTT1     /,,,,/C,N,-1/C,N,3 $
3.  INPUTT1     /INFLxxx,,,,/C,N,O,/C,N,3 $
4.  INPUTT1     /,,,,/C,N,-1/C,N,4 $
5.  INPUTT1     /FLIT#U,,,,/C,N,O/C,N,4 $
6.  MPYAD       INFLxxx, FLIT#U,/TRANxxx/C,N,)/C,N,1/
                C,N,O/C,N,1 $
7.  PARAM       //C,N,MPY/V,N,ALWAYS/C,N,-1/C,N,L $
8.  EQUIV       TRANxxx, UGV/ALWAYS $
9.  CHKPNT      UGV $
10. SDR2        CASECC, CSTM, MPT, DIT, EQEXIN, SIL,
                GPTT, EDT, BGPDT,,,UGV, EST,,/,,OUGVI
                OES1, OEF1, PUGV1/C,N,STATICS/
                V,N,NOSORT2=-1 $
11. SAVE        NOSORT2 $
12. OFP         OUGV1,,,OEF1, OES1, //V,N, CARDNO $
13. SAVE        CARDNO $
14. OUTPUT2,    ,,,,//C,N,-1/C,N,11 $
15. OUTPUT2     OES1,,,,//C,N,O/C,N,11 $
16. OUTPUT2,    ,,,,//C,N,-9/C,N,11 $
17. ENDALTER
```

1. The operations that are needed in this step are fetching of restart data, forming of basic time varying displacement matrix, exercising of SDR2 and OFP, plotting of deformed responses, and outputting of stress data to the post-processor. Call statements for SDR2 and OFP in standard form process more than is needed here, hence their input and output data blocks are destined to be rewritten consequently everything from before matrix generators to just before structure plots can be by-passed. Hence, the ALTER control causes a jump from statement 39 to statement 155.

2,3,4, and 5. Influence coefficient matrix [INFLxxx] is read in from disc file via INP3. Transient response FLIT#U is read in from disc file via INP4.

6. The matrix multiply operation [INFLxxx] x [FLIT#U] = [TRANxxx] gives the Basic Substructure time varying response TRANxxx.

7,8, and 9. A control parameter ALWAYS is assigned the value -1 to make the succeeding EQUIV operation "take" so that the Basic Substructure time varying response TRANxxx is equivalenced to the static solution matrix UGV. Then UGV is checkpointed.

10 and 11. Basic Substructure time varying displacements, element forces and element stresses are recovered according to the specifications stated in Case Control. The output parameter NOSORT2 is saved.

12 and 13. The displacements, forces, and stresses from SDR2 are formatted for printing. The output parameter CARDNO

is saved.

14, 15 and 16. The table of stresses OES1 are output to a FORTRAN file and stored on a disc with dataset name STRSxxx. This is now in a form that the post processor scan program can access it.

APPENDIX D

MMTX TRAILER CHANGE AND MATRIX TRANSFER FROM SOF TO EXTERNAL

This appendix supplements the description of TRANSIENT SOLUTION STRATEGY. The DMAP listing is given first, followed by an image of the partitioning vector, then the explanations according to statement number.

```
1.   BEGIN  $
2.   SOFI       /K1,M1,,,/C,N,+1/C,N,MFLT/C,N,KMTX/C,N,MMTX  $
3.   MERGE      M1,,,,BLNKVEC,/SQRSYM/C,N,2/C,N,1/C,N,6  $
4.   PARAM      //C,N,ADD/V,N,TRALR/C,N,0/C,N,-1 $
5.   EQUIV      SQRSYM,M2/TRALR $
6.   SOFUT      //C,N,+1/C,N,MFLT/C,N,EDIT/C,N,2/V,N,ZXX/V,N,ZXX/
                C,N,DUMPARAM/V,N,ZXX/V,N,ZXX/V,N,ZXX/V,N,ZXX/
                V,N,ZXX $
7.   SØFØ       ,M2,,,,//C,N,+1/C,N,MFLT/C,N,MMTX $
8.   SOFUT      //C,N,+1/C,N,TOC/C,N,SOFP/C,N,0/V,N,ZXX/V,N,ZXX/
                C,N,DUMPARAM/V,N,ZXX/V,N,ZXX/V,N,ZXX/V,N,ZXX/
                V,N,ZXX $
9.   OUTPUT1,   ,,,,//C,N,-1/C,N,0 $
10.  OUTPUT1    K1,M2,,,//C,N,0/C,N,0 $
11.  END        $

DMI  BLNKVEC  0    2    1    1        916    1    +PART
DMI  BLNKVEC  1    1
```

2. The utility SOFI brings information form the SOF into the current execution. The name of the P/S is MFLT and the two data blocks belonging to MFLT, KMTX and MMTX are being requested and being given temporary temporary data set names K1 and M1 respectively.

3. A merge operation of the mass matrix M1 with a null matrix is performed by using a 916th order null partitioning vector. The partitioning vector is easy to specify as shown on the example DMI card. Ablank entry is given for the first row of the first column and implied blanks for all others. The output matrix is named SQRSYM. The 3rd parameter states that the trailer of the output matrix is to be symmetric.

4,5. A parameter is defined for use in the EQUIV statement so that the output mass matrix can conform to the substructuring format for naming.

6,7,8. SOFUT is used to purge the old MFLT square mass matrix M1 from the SOF. SOFO is used to output the summetric mass matrix M2 from the current execution to the SOF record of P/S MFLT. SOFUT is used to get a listing of the SOF table of contents to verify that the mass matrix was read onto the SOF.

9,10. The utility OUTPUT1 reads K1 & M2 onto the NASTRAN file INPT.

APPENDIX E

DMAP MODIFICATIONS TO DIRECT TRANSIENTS

This appendix supplements the description of DIRECT TRANSIENT ANALYSIS Solution Strategy. The Rigid Format 9 DMAP ALTER statements are given first, followed by explanations according to statement number.

```
 1.  ALTER     2,2
 2.  FILE      KGGX = TAPE/KGG = TAPE/UDVT = APPEND/
               TOL=APPEND $
 3.  ALTER     30,30
 4.  ALTER     33,33
 5.  PARAM         //C,N,ADD/V,N,NOBGG=-1/C,N-1/C,N,O $
 6.  ALTER     34
 7.  COND      LBL1, NOSIMP $
 8.  ALTER 67
 9.  INPUTT1       /,,,,/C,N,-1/C,N,O $
10.  INPUTT1       /K1,M1,,,/C,N,O/C,N,O $
11.  EQUIV         K1, KGG/NOBGG/M1, MGG/NOBGG $
12.  ALTER         102
13.  PURGE         MAA/NOKGGX $
14.  ALTER         110
15.  JUMP          LBL5 $
16.  ALTER         113
17.  PURGE         K4AA/NOKGGX $
18.  ADD           KAA,/K4AA/C,N,(0.03, 0.0)$
19.  CHKPNT        K4AA $
20.  ALTER         139
```

```
21.  PARAM       //C,N,ADD/V,N,NOSIMP/C,N,1/C,N,0 $
22.  ALTER       163,163
23.  EQUIV       PPT, PDT/NOSET $
24.  EQUIV       PDT, PD/PDEPDO $
25.  ALTER       167
26.  PARTN       UDVT, USTRIP,/,,FLITOU,/C,N,7/C,N,1/C,N,2/C,N,2/
                 C,N,2/C,N,2 $
27.  OUTPUT1     ,,,,//C,N,-1/C,N,4 $
28.  OUTPUT1     FLITOU,,,,//C,N,0/C,N,4 $
29.  SDR2        CASEXX, CSTM, MPT, DIT, EQDYN, SILD,,, BGDT, TOL,,,
                 EST,, PPT/OPP1,,,, C,N,TRANRESP $
30.  SDR3        OPP1,,,,,/OPP2,,,,, $
31.  CHKPNT      OPP2 $
32.  OFP         OPP2,,,,,//V,N, CARDNO $
33.  SAVE        CARDNO $
34.  EXIT        $
35.  ENDALTER
```

Statement Explanations:

1,2. The TOL (TRANSIENT OUTPUT LIST) must be enabled to that it can be appended for any continuation of integration. Initially, when there is no restart, the TOL need not be appended, but for all subsequent restarts it needs to be appended, so it is enabled here to be ready for all runs. Instead of inserting a separate APPEND statement, it becomes more concise to add the APPEND to the existing FILE statement. Consequently, the existing file statement was removed and put back with the added APPEND statement.

4.5 Subsequently it is desired to incorporate a structural damping matrix and no other kind of damping, but to equip the code via a DMAP ALTER and not through a matrix generator module. Ordinarily the EMG module would sense the absence of viscous damping and automatically set the parameter NOBGG to negative one so that the viscous damping matrix, BGG, would not be generated. But in this solution path EMG will be bypassed by the conditional jump of statement 7 (because stiffness and mass matrices are input via statements 9, 10, 11). Something must be done about parameter NOBGG so the OSCAR can do a proper job in providing storage space for input data blocks. NOBGG must be preset to -1, so the parameter entry C,N,1 must be changed to C,N,-1. The original PARAM statement must be replaced by this revised statement therefore the ALTER 33,33 was used.

3 thru 7. All matrix data is being read in from disc and no matrix generator will be called upon. The compiler recognizes this and sets NOSIMP to -1 during execution of TA1. This is all very well but if the sequence of operations were left unchanged NOSIMP would cause the conditional jump of statement 30 to engage statement #62 next and would completely bypass the PARAM statement #33 in spite of all the modifications discussed above. Consequently, the conditional jump based on NOSIMP was taken out (position 30 with the ALTER 30,30, and restored after the PARAM executes in position 33 and needs to have a value of +1 later on.

8 thru 11. Stiffness and mass matrices from Phase II need to be introduced into the DMAP stream after the matrix operators and before the matrix partitioners implying after statement #6.5,

SMA3, and before statement #75, GSPS. Here, ALTER 67 brings it in just before GP4.

The matrices on file FLITKM from Phase II can be internally subscripted to any variety of numbers from K1, M1 to K9, M9 and higher depending on the execution order of commands in Phase II. In anticipation of this, statements 10 and 11 use subscript one followed by equivalences to KGG and MGG which will always "take" because parameter NOBGG was preset to -1. If K & M are written out with other than subscript one, the acting values should be written into statements 10 and 11.

12 and 13. If there were OMIT's the SFA (Segment File Allocator) could not provide for MAA, because it was purged back in statement #28. This purge at #28 took place in this instance, because NOSIMP is negative as explained above. In order to equip SFA to provide for SMP2, MAA has to be unpurged before statement #103 when SMP2 goes into operation; therefore the unpurge is introduced at #102 with the control parameter NOKGGX which was set equal to +1 at statement #31.

14 and 15. It is the intention to provide for the damping matrix K4AA by a DMAP ALTER subsequently, besides which K4FF does not exist to act as an input data block for SMP2; therefore SMP2 and CHKPNT are jumped around.

16, 17, 18 and 19. Now the damping will be generated. The output data block name will be K4AA. But this was purged along with MAA at statement #28 so it also has to be unpurged; again the choice of control parameter is NOKGGX Spatially

uniform structural damping is proportional to stiffness so a simple scalar multiply will serve. The ADD statement performs $\alpha A + \beta B = c$. If B=0, then C=αA. The coefficient α on A is a complex number, demanding that the real and imaginary parts be supplied. In this instance, the real part is 0.03 and the imaginary part is 0.0.

20 and 21. KDEK2 is a parameter which indicates to module GKAD whether or not matrices KAA and MAA are present according to its value of +1 or -1. Its value is computed in statement #140 by a logical AND operation on the values of NEGENL and NOSIMP from their most recent update according to the VPS table. Unless something is changed at this point NOGENL and NOSIMP are both = -1 so their AND result = -1 and KEDK2 will be negative. This negative value would indicate that KAA and MAA do not exist, but they do exist, because matrices were read in without benefit of general elements or from element matrix generators. A non-negative value reflects the condition of these matrices. By changing NOSIMP to +1, the computed value of KDEK2 is +1, satisfying the non-negative requirement.

23 and 24. EQUIV statement #163 has a bug in it. To correct this bug, the two EQUIV statements are written in place of the defective statement.

26, 27, and 28. These statements provide for stripping velocity and acceleration vectors from the UDVT matrix. The partitioning vector USTRIP is supplied by the analyst via DMI card data. The displacement vectors in UDVT occur in columns 1, 4, 7, ... , the last output displacement. The last output

displacement is calculated to be:

$$\frac{160\left(\begin{array}{l}\text{the number of integration}\\ \text{time steps selected on}\\ \text{the T STEP card}\end{array}\right)\times 3\left(\begin{array}{l}\text{the number of vec-}\\ \text{tors per time step}\\ U,\ \dot{U},\ \ddot{U}\end{array}\right)}{8\left(\begin{array}{l}\text{the output interval}\\ \text{selected on the T STEP card}\end{array}\right)}+3\left(\begin{array}{l}\text{3 vectors}\\ \text{for the}\\ \text{zeroeth}\\ \text{time step}\end{array}\right)$$

$= \frac{160\times 3}{8} + 3 = 63$. This value is put in field 8 of the DMI card indicating that the DMI vector for controlling the columns partitioning will have 63 rows. The matrix of displacement vectors will be named FLIT #U, where # indicates the restart number starting with the zeroeth.

29 thru 35. The call to SDR2 allows the modules to respond to the Case Control Card OLOAD. Modules are limited to the input and output data blocks necessary to process only the loads. Exit after OFP because no plots are requested.

D20

N78-32486

DYNAMIC ANALYSIS USING SUPERELEMENTS FOR A LARGE HELICOPTER MODEL

Magan P. Patel
Hughes Helicopters

Lalit C. Shah
Multiple Access Inc.

SUMMARY

Using superelements (substructures), modal and frequency response analysis was performed for a large model of the Advanced Attack Helicopter (AAH) developed for the U. S. Army. Whiffletree concept was employed so that the residual structure along with the various superelements could be represented as beam-like structures for economical and accurate dynamic analysis. A very large DMAP alter to the rigid format was developed so that the modal analysis, the frequency response, and the strain energy in each component could be computed in the same run.

INTRODUCTION

The helicopter model shown in figure 1 consists of 13 substructures having 1000 grid points and 4000 structural elements. The dynamic analysis was performed using the residual structure, which represented a beam-like structure along the centerline of the aircraft at its nominal elastic axis, with appendages in the form of other beams. The residual structure was connected to the superelements by rigid elements in a sort of "whiffletree" form. This is an interesting, newly developed concept in that it allows dynamic analysis with the efficiency of a "stick" model, resulting in significant cost saving while at the same time retaining more involved effects accounted for in the detailed finite element model.

In order that normal mode analysis as well as frequency response computations could be executed in the same run, a special alter to the rigid format was developed. The alter was extended to further include calculations of strain energies in each component, so that the critical parts of the structure for each model could be easily identified. To determine the most sensitive mode to the rotor excitation, rotor impedance factors were calculated using eigenvectors generated from NASTRAN run.

The structural contributions due to the different subsystems, designed by other companies, were incorporated into the main helicopter model by employing the NASTRAN general elements (GENEL). To better evaluate the interaction between the basic structure and the subsystem, transient response analysis due to gun firing forces and frequency response analysis due to the rotor excitation were conducted by utilizing the results computed by the normal mode analysis.

Separate set of values obtained from the analytical approach were found to be in very good agreement. Harmonic analysis is being currently performed using the time history output from the transient response analysis to determine the frequency content.

DESCRIPTION OF THE MODEL

The Advanced Attack Helicopter consists of the fuselage, the wing and the vertical tail, all composed of typical skin-stringer construction. The horizontal stabilizer is a semimonocoque structure utilizing beaded skin construction. The complete finite element model is shown in figure 1. This consists primarily of simpler elements in NASTRAN library. This model was divided into 10 primary superelements and three secondary (image) superelements. Advantages of substructuring and its limitations were fully considered in selecting this particular scheme of dividing up the model. Figures 2 and 3 show a more detailed definition of a typical superelement representation. Table I provides the element breakdown for each of the superelements in the model. As can be seen, this is definitely not a small model for dynamics. For the convenience of the users, table II shows the various set sizes for each superelement.

The dynamic analysis is performed using the a-set points, which in the superelement concept is defined as the residual structure or superelement 0. This structural model is a beam-like structure along the centerline of the vehicle with appendages in the form of other beams and/or GENEL elements. This residual structure is not a normal structure consisting of a-set points but is connected to the other superelements by means of a unique set of rigid

elements. This concept is given the name of "whiffletree," further described in the next section.

WHIFFLETREE CONCEPT

Dynamics analysis involves some form of technique to reduce the size of problem from the statics analysis model. Most people are very familiar with the "stick" or beam or EI/GJ models and even today are quite content using those models. With NASTRAN users, Guyan reduction has become quite a popular technique for achieving the smaller model. Whiffletree concept uses rigid elements or, more appropriately, MPCs for the same goal; namely, the smaller model. MPC or the multipoint constraints can be used such that the behavior of several grid/mass points is represented by one single grid/mass or a scalar point.

Figure 4 shows a typical whiffletree arrangement for one of the bulkheads in the AAH model. As can be seen, the point in the middle (does not have to be located there) is "connected" to the more important grid points on the bulkhead using a general rigid element RBE3. This single point now represents the average behavior of that complete bulkhead without any matrix reduction. Continuing in this fashion the end product is a pseudo stick model that would predict the dynamic characteristics of the complete structure. Figure 5 shows this model.

These points were all left in the residual or boundary structure and thus they were in the a-set of each superelement. As a matter of fact, the residual structure consists of this kind of points only. Because of this technique it was possible to keep the size of a-set points well within control for high efficiency while retaining in the solution the more complex behavior of the total structure. Certainly MCE1 and MCE2 modules are not that inexpensive but, compared to the exponential cost increase of SMP1 and SMP2 modules, this approach was found to be more cost-effective.

ALTERS FOR CONVENIENCE

One of the major tasks undertaken to complete this project consisted of formulating an Alter to the Rigid Format so that the following three analyses could be performed in the same run:

(a) Normal modes analysis with frequency response,

(b) Rotor impedance factors computation,

(c) Modal strain energy distribution.

All three alters are merged into one large alter to make it a production tool. Although it is not easy to keep up the alter compatible with the newer versions of MSC/NASTRAN, successful transition was made from CDC 6600 Version 32 to IBM Version 38; and, presently, efforts are in progress for adopting the alter to the latest IBM Version 46.

Natural Frequencies and Modes

As shown in table II, the total dynamic degrees of freedom (a-set) add up to the matrix size of 177. Grid points with dynamic degrees of freedom (a-set) are shown in table II. The modes are identified in somewhat arbitrary manner by looking at the deformed shape of the structure in a particular mode in conjunction with the computed mode shapes and strain energy distribution. The isometric views of the deformed structure are shown in figures 6 and 7.

Rotor Impedance Factors

The rotor impedances are calculated from the relation

$$\frac{1}{\text{rotor impedance}} \alpha \ \phi_i^{\,2}$$

where ϕ_i is the eigenvector at the main rotor head in the i^{th} direction, and are plotted in figure 8 as $\phi_i^{\,2}$ versus the significant modes in their relative order of modal strength. The modes with the lowest impedance (i. e., the highest inverse ratio) are most sensitive to rotor excitation.

Modal Strain Energy Distribution

The MSC/NASTRAN computer program with this alter has the capability to compute and print out strain energy distribution in each flexible mode. This is very helpful in identifying the critical parts of the structure for each mode.

The program computes the strain energy in percentage form in each superelement for the desired modes.

The results are shown by MATRIX SPT in figure 9. The column number identifies the mode number (e.g., col 7 means mode 7) and the rows 1 through 10 denote the corresponding superelements 1 through 10. The strain energy in superelement number zero is computed separately under MATRIX RPT; however, it is included in figure 9 for convenience.

FREQUENCY AND TRANSIENT RESPONSE

Frequency Response

Alternating aerodynamic forces acting on rotor blades and on the fuselage and nonrotating parts of the vehicle are the major source of vibrations. Variations in these forces are periodic and all the steady alternating force inputs to the rotor hub occur in even multiples of the rotating speed such as 1/rev (1P), 2/rev (2P), 3/rev (3P), etc. However, only alternating forces and moments which are integral multiples of the number of blades are transmitted to the rotor hub. This helicopter has four-bladed rotor, therefore 4/rev, 8/rev, etc., are the only input to the hub. The 4/rev (4P) excitation forces which are the major contributor to the input at the hub were considered for this analysis. These excitation forces are obtained from DART (Dynamic Analysis Research Tool) program for various forward speeds of the helicopter and are multiplied by 4/rev response loads per unit excitation at rotor hub (computed by NASTRAN PROGRAM) to obtain total response at crew, stabilized sight and various other desired locations.

The effect of rotor speed variation on pilot and copilot station vibrations assuming no change in rotor forces is shown in figures 10 and 11.

Transient Response

Transient response due to gun firing is computed at several locations, such as crew stations, stabilized sight and gun center of gravity. The input impulse time history is shown in figure 12, and a typical response time history in figure 13.

CONCLUSIONS

A large model for dynamic analysis has been successfully used for the AAH project. Once again it is clear that NASTRAN is capable of solving a rather complex analysis scheme in a production manner provided proper

resources are put into planning and writing some interesting DMAPs. The concept of MPCs and/or rigid elements is a very powerful tool that seems to provide new answers to several old problems.

TABLE I – VARIOUS ELEMENTS IN THE MODEL

Element Type \ Superelement No.	1	2	3	4	5	6	7	8	9	10	0
Bar	158	84	76	4	4	38	6	25	25	29	36
Con Rod	660	372	6	1	1	-	1	1	1	-	31
Rod	122	108	224	44	44	-	-	-	-	221	16
Shear	202	165	100	10	10	-	-	-	-	119	-
TRMEM	26	-	8	5	5	-	-	-	-	2	-
QDMEMI	64	24	-	-	-	-	-	9	9	32	-
Con M1	-	-	-	-	-	-	-	-	-	-	3
Con M2	-		-	-	-	-	-	-	-	-	123

TABLE II – VARIOUS MATRICES IN THE MODEL

Matrix Size \ Superelement No.	1	2	3	4	5	6	7	8	9	10	0
Grid	363	211	140	37	37	50	7	27	27	145	145
n-set	2178	1266	840	222	222	300	42	162	162	870	870
m-set	215	42	54	30	30	60	0	68	68	134	36
f-set	1210	774	511	95	95	240	36	68	68	430	648
o-set	940	492	197	59	59	186	24	56	56	382	471
a-set	270	282	114	36	36	54	12	12	12	48	177

Figure 1. Advanced Attack Helicopter Model

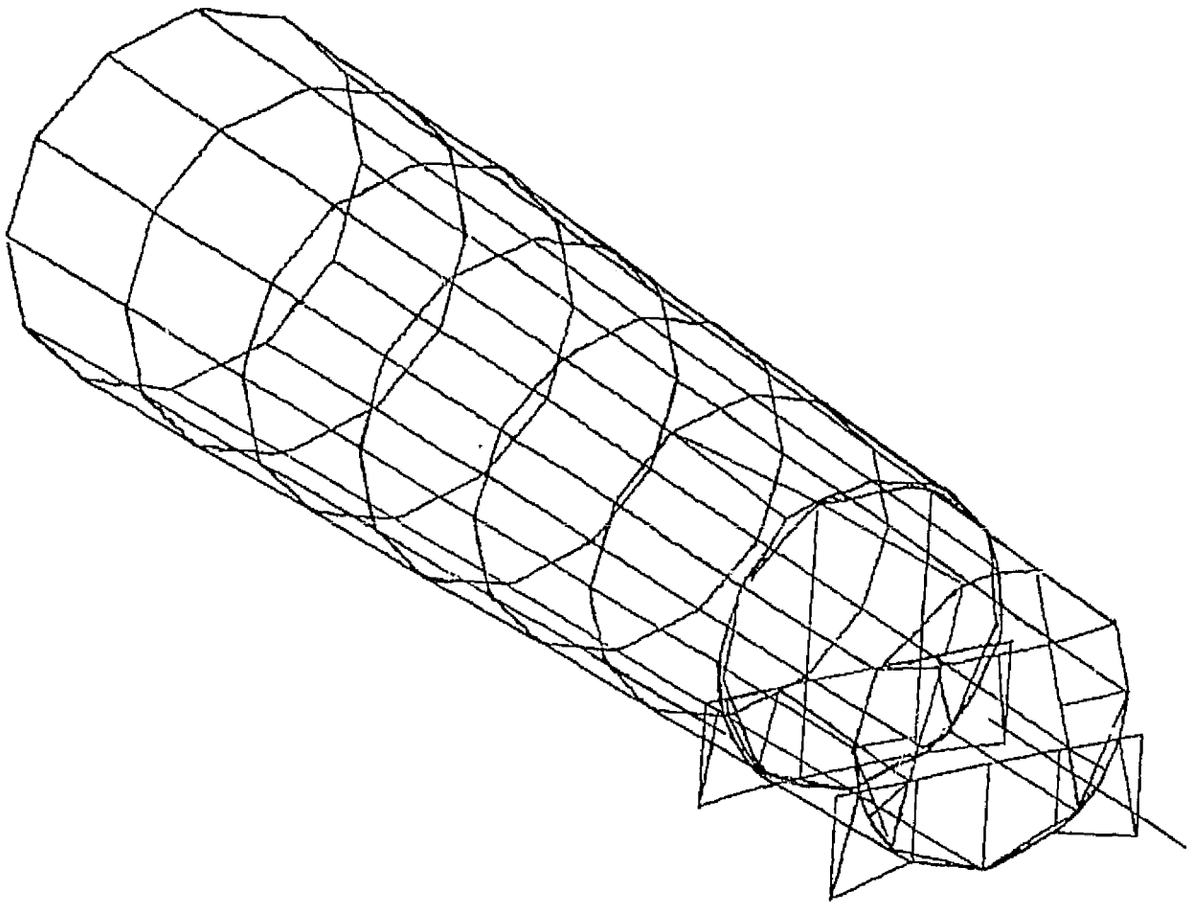

Figure 2. Advanced Attack Helicopter Tail Cone (Superelement 3) Model

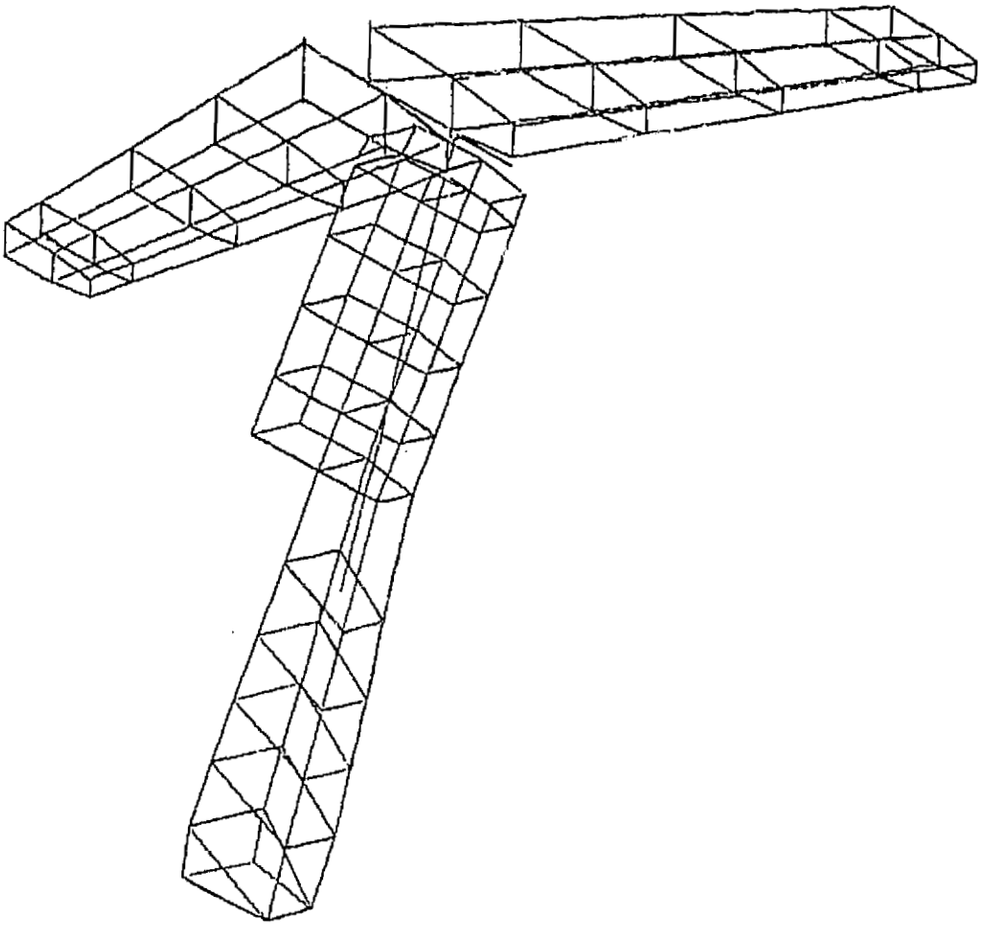

Figure 3. Advanced Attack Helicopter Model Empennage (Superelement 10)

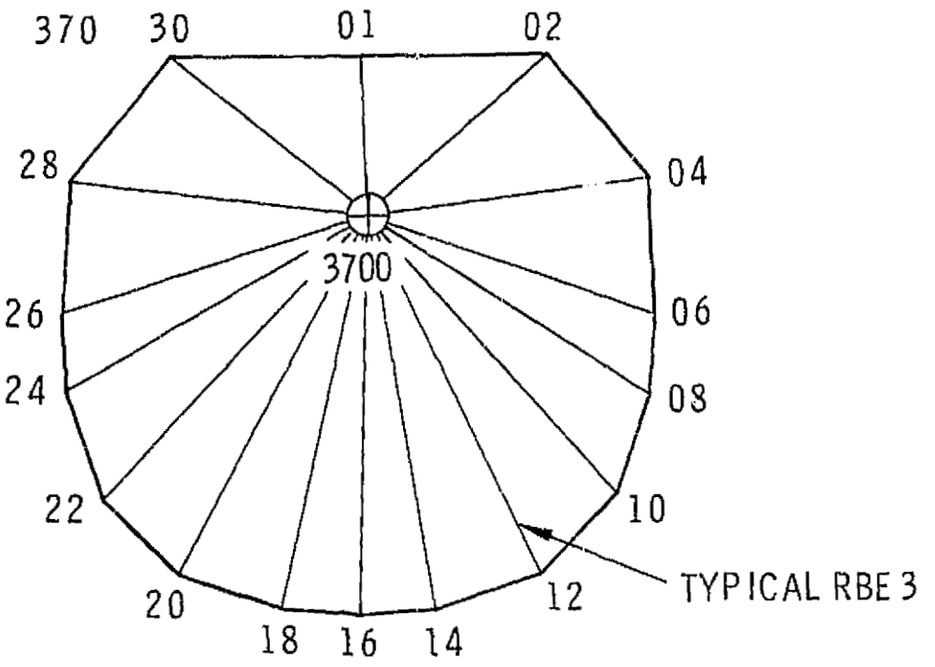

Figure 4. Typical Whiffletree Arrangement

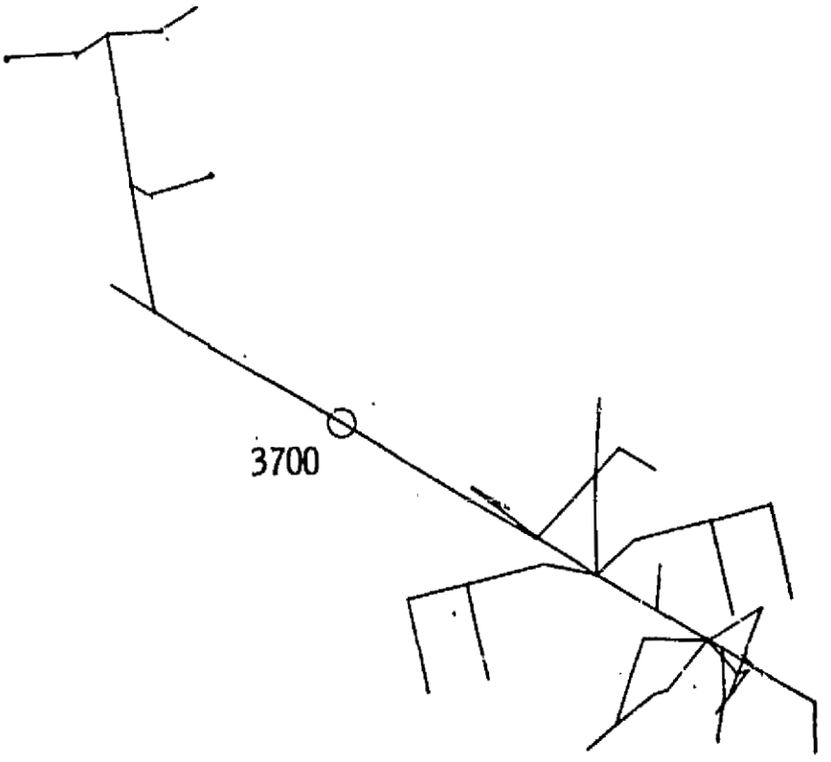

Figure 5. Complete Whiffletree Model

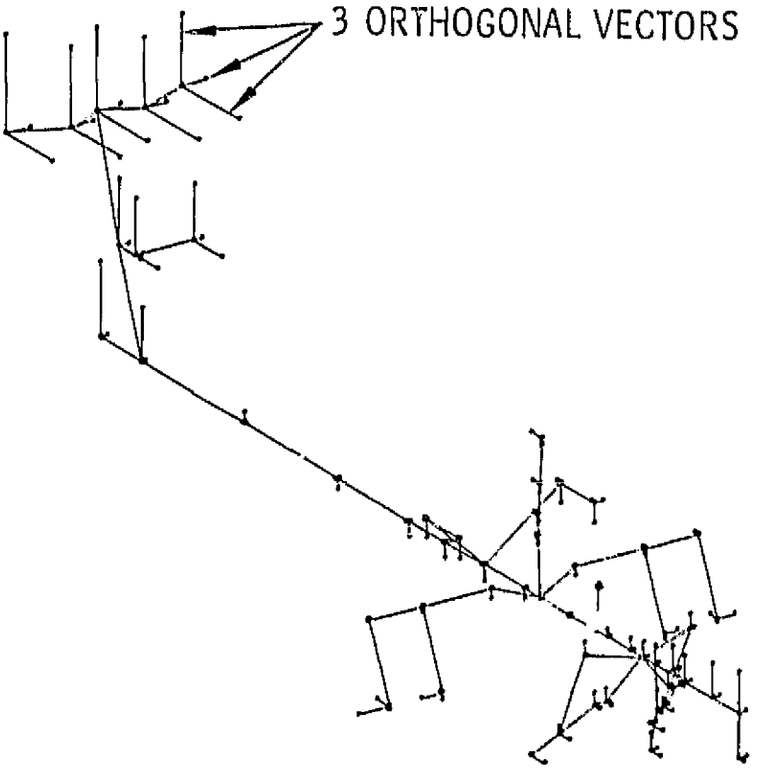

Figure 6. First Vertical Mode

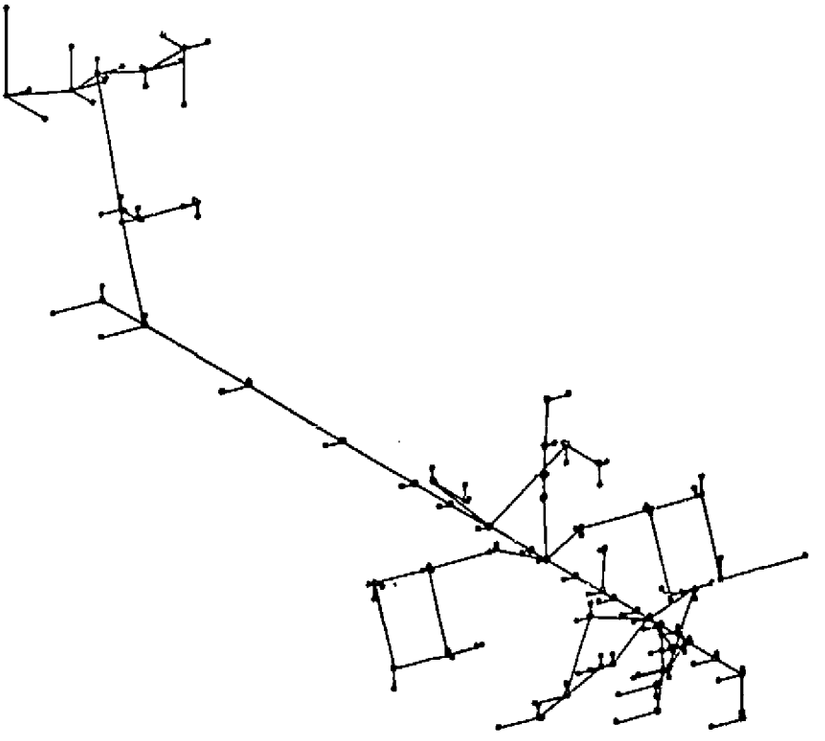

Figure 7. First Lateral Mode

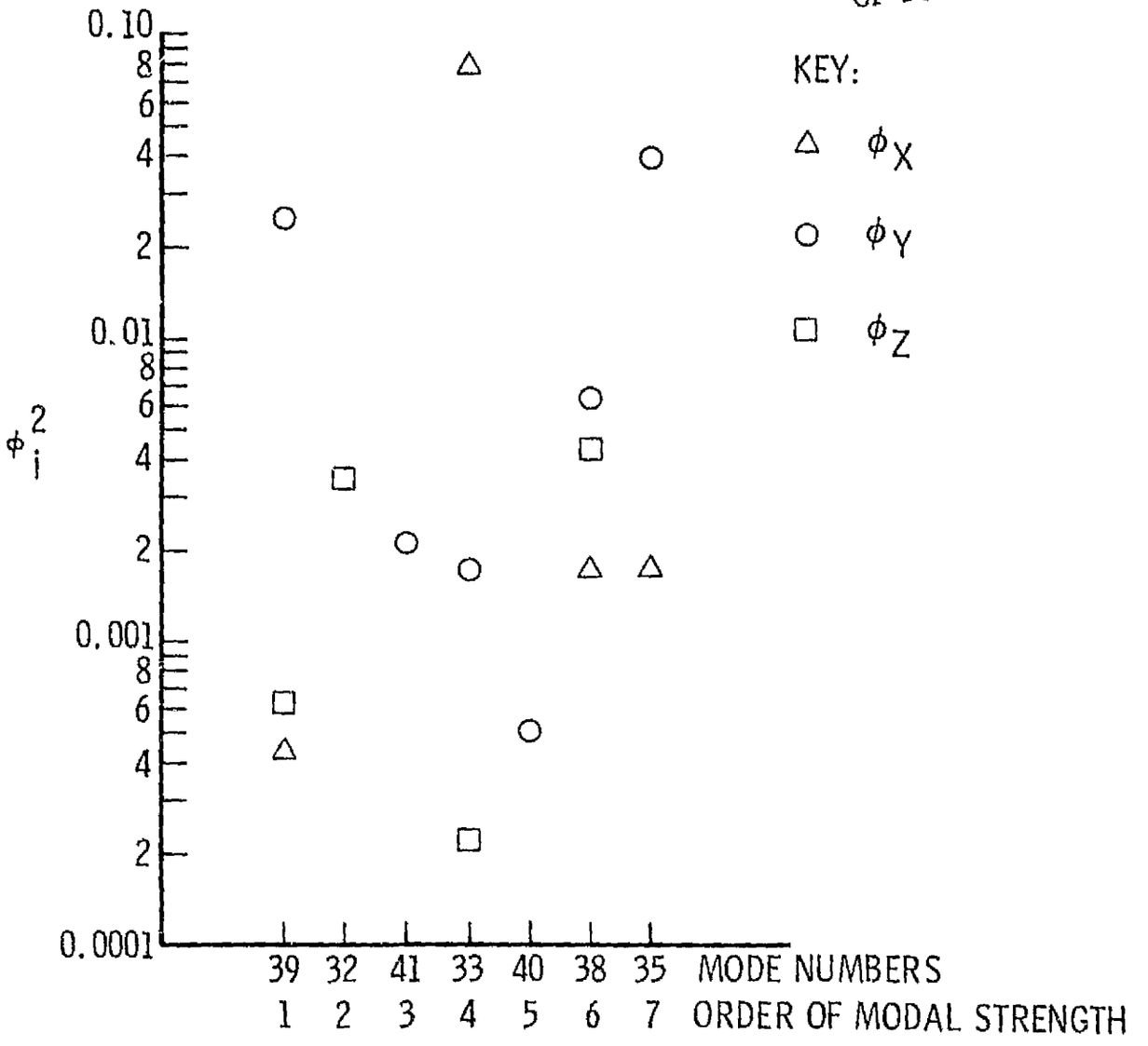

Figure 8. Rotor Impedance Factors

ADVANCED ATTACK HELICOPTER,
MODEL 41, 4 ROCKET PODS

APRIL 28, 1978

SAME AS MOD. 40 EXCEPT WITH 4 ROCKET STORES

MATRIX SPT (GTNO NAME 101) IS A REAL 50 COLUMN X 11 ROW RECTANG MATRIX.

1 FOREBODY	2 MIDBODY	3 TAIL BOOM	4 RH ENGINE	5 LH ENGINE	6 MAST	7 GUN	8 RH PYLON	9 LH PYLON	10 EMPENNAGE	0 RESIDUAL
COLUMN 7	ROWS 1 THRU 10									
1.08505E+01	3.78566E+01	1.61150E+01	1.19587E-02	2.31849E-02	1.36959E-01	7.94538E-03	2.58542E+00	2.96324E+00	1.03065E+01	1.56900E+01
COLUMN 8	ROWS 1 THRU 10									
3.64225E+01	7.24255E-01	9.60606E-02	9.39502E-03	1.88068E-02	1.40263E-02	4.77110E-04	3.00968E+00	2.97164E+00	3.50264E-02	8.13727E+01
COLUMN 9	ROWS 1 THRU 10									
5.46679E+00	9.38937E-01	1.31929E-01	2.16397E-02	1.90812E-02	2.71306E-02	3.55040E-04	2.50160E+01	1.74856E+01	1.73573E-02	1.98235E+01
COLUMN 10	ROWS 1 THRU 10									
2.16722E+00	3.78037E+00	2.08015E+00	3.61191E-03	1.43733E-02	8.50601F-02	6.28391E-03	3.02564E+01	4.77730E+01	1.77607E+00	2.42154E+00
COLUMN 11	ROWS 1 THRU 10									
2.31511E-01	3.01653E-01	1.20460E-01	2.81355E-03	2.29848E-03	8.33319E-03	3.61482AE-04	3.71927E+01	6.70512E+00	9.52429E-02	1.46903E+00
COLUMN 12	ROWS 1 THRU 10									
1.50201E+00	1.31389E+00	7.88849E-01	2.46119E-03	6.34529E-03	1.80286E-02	5.40990E-03	5.12660F-01	2.37786E+01	7.03844E-01	8.22361E+00
COLUMN 13	ROWS 1 THRU 10									
8.47383E+00	1.05215E+01	5.34165E+00	1.32769F-01	4.38991E-03	2.39782F-01	7.80420E-03	7.22833E+00	9.52037E-01	5.49466E+00	3.60770E+01
COLUMN 14	ROWS 1 THRU 10									
8.92168E+00	7.55696E+00	2.66655E+00	1.90300E-02	1.32307E-01	1.87329E-01	2.33965E-03	3.71012E+00	6.86447E+00	2.15255E+00	3.02318E+01
COLUMN 15	ROWS 1 THRU 10									
1.78278E+01	4.56231F+01	1.23314E+01	3.52700E-01	3.84216E-01	6.30589E-01	1.86693E-02	1.52411E+00	7.89611F+01	2.50942E+00	1.09513E+01
COLUMN 16	ROWS 1 THRU 10									
1.73978E+01	3.68366E+00	6.98647E-01	1.25266E-01	2.51980E-01	7.91287E-01	1.56678E-01	3.00305E+00	5.04201E+00	2.17450E+00	3.56372F+01
COLUMN 17	ROWS 1 THRU 10									
9.15962E-01	3.26315E-01	8.56976E-02	7.45369E-03	7.08367E-03	3.67268E-02	1.83568E-03	3.44550E+01	2.97451E+01	1.88741E-01	1.56726F+01
COLUMN 18	ROWS 1 THRU 10									
8.25085E-01	2.11533E-01	7.95934E-02	6.56889E-03	9.43121E-03	3.45208E-03	7.04527E-04	3.02618E+01	3.51790E+01	4.63029E-02	1.55963E+01

Figure 9. Typical Strain Energy Output

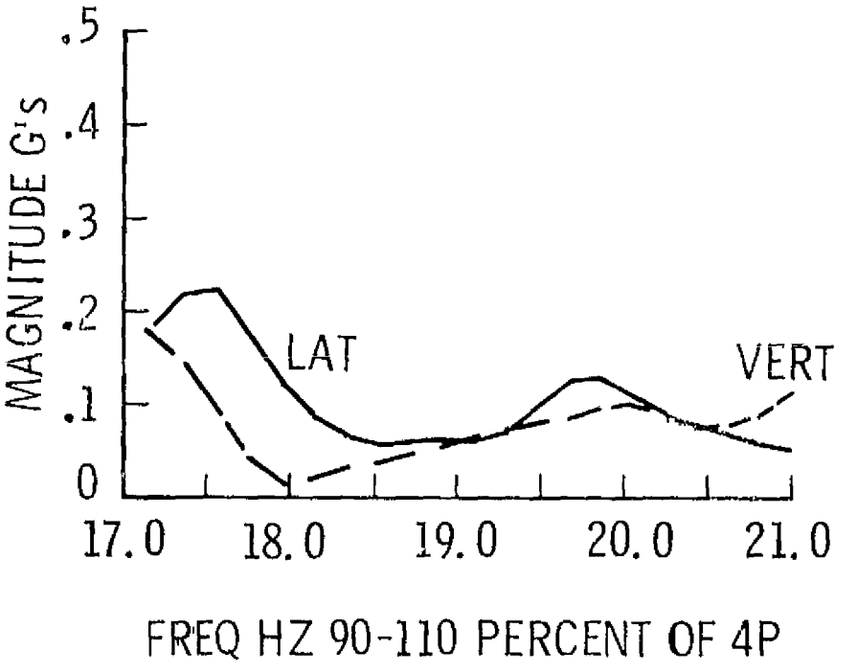

Figure 10. Frequency Response at Pilot Seat

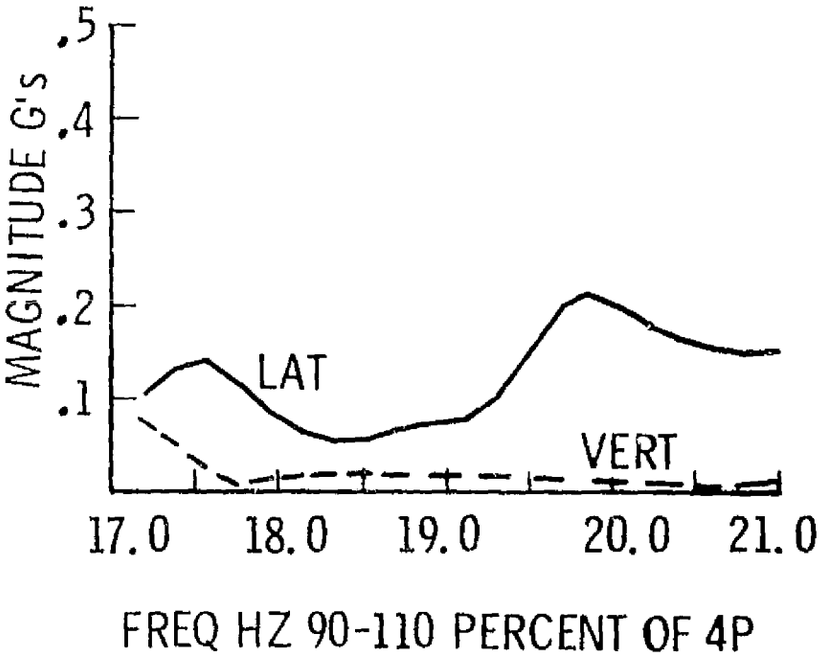

Figure 11. Frequency Response at Copilot Seat

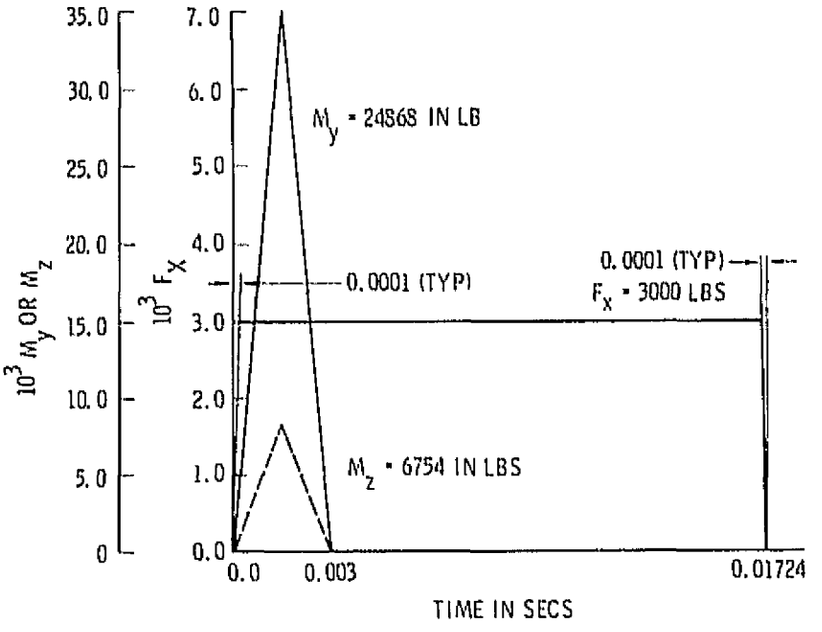

Figure 12. Input Impulse Due to Gun Firing

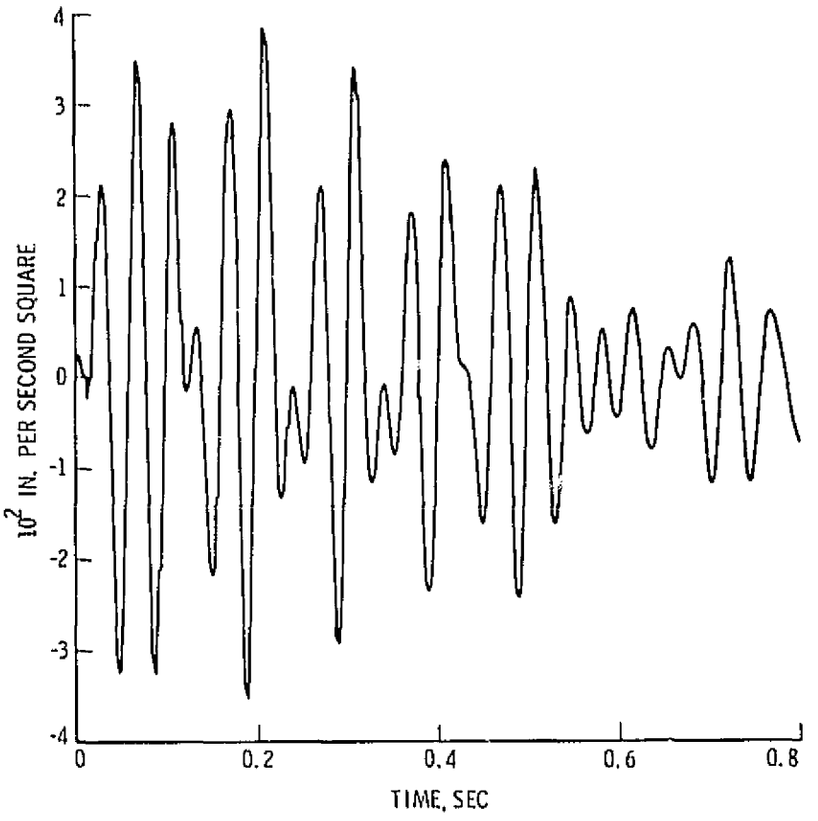

Figure 13. Transient Response at Gun Stabilized Sight

N78-32487

D21

COMPARISON OF SEVERAL NASTRAN ANALYTICAL TECHNIQUES FOR LARGE STRUCTURES

David T. Zemer
Northrop Corporation

SUMMARY

In order to plan for the finite element structural analysis of future aircraft at Northrop, five static analysis techniques using the MacNeal-Schwendler Corporation version of NASTRAN are evaluated. The structure is analyzed as:

1. A single model with a symmetric loading condition.
2. A single model with symmetric/unsymmetric loading conditions.
3. Three substructures in three phases using tape storage with a symmetric loading condition.
4. Three superelements using data base storage with a symmetric loading condition.
5. Three superelements using data base storage with cyclic symmetry for symmetric/unsymmetric loading conditions.

The superelement techniques prove superior to the single model approaches by reducing computer time for redesign work by as much as 70 percent.

Job control errors are also substantially reduced by using the NASTRAN data base in place of the tapes necessary in substructuring. The evaluation indicates that the superelement methods are more productive than the single model and substructure methods when a large amount of computer resources for a stress analysis are required.

INTRODUCTION

Before scheduling a large project using finite element analysis, the specific solution methods chosen must be thoroughly tested. This is true not only for the analysis flow, which in the case of NASTRAN is the Direct Matrix Abstraction Program (DMAP), but also for internal software restrictions and data center hardware constraints.

Too often the analysis method selected is based upon small prototype testing. This, coupled with an incomplete understanding of both the finite element program being used and the peculiarities of the computer system in a

large solution environment, frequently leads to:

(a) Deadlines consistently missed.

(b) Complaints against the finite element program being used.

(c) The computer system "crashing" during excessively long computer residency.

(d) Computer runs terminated due to insufficient core or data base space.

An effort was started in 1977 within the NASTRAN group at Northrop to evaluate these problem areas prior to selecting a method of analysis for a new aircraft project. A small prototype model (Figure 1) and an actual production model containing 9500 degrees of freedom (Figure 2) were selected for evaluating the MSC superelement capability. The results are compared here with previous results using a single model and substructure approaches. Five criteria for this comparison are:

(1) NASTRAN software behavior.

(2) Hardware limitations.

(3) CPU time for a preliminary analysis.

(4) CPU time for a redesign analysis.

(5) Total calendar time.

TESTING PROCEDURE

Realistic evaluation of the MSC/NASTRAN superelement analysis method is made using a finite element model of the T-38 structure (wing, center and forward fuselages only). A comparison of the program response and the computer system billing for this model was possible using results from previous single structure and substructure analyses.

Five different analyses over a one year period were made, then rerun with a redesigned wing simulating a realistic production situation (Figure 3).

TESTS

(1-1a) Single Structure Analysis With One Set of Boundary Conditions

Rigid Format 24 was used without any alters. Because this model, as with all others, was symmetric about the x-axis, only the left hand side was idealized.

Only symmetric loads were used for this analysis which required one set of boundary conditions along the x-axis. A redesigned wing was run from a cold start.

(2-2a) Single Structure Analysis With Two Sets of Boundary Conditions

Rigid Format 24 with RF alter 24$13 allowed two sets of boundary conditions to be stored. The redesigned wing was run as a cold start.

(3-3a) Substructure Analysis With One Set of Boundary Conditions

Rigid Format 24 with RF alter 24$37 allows only one set of boundary conditions. Therefore, only a symmetric load case was run. DMAP's have been written to work with two sets of boundary conditions by Sodha, Reference 1. However, due to anticipation of the superelement cyclic symmetry capability, no attempt was made to duplicate this effort. The redesign was limited to and required only reanalysis of the wing.

(4-4a) Superelement Analysis With One Set of Boundary Conditions

Rigid Format 48 was used in Version 38, but was replaced with DMAP1 in Version 46. As in the substructure analysis, symmetric loads were used and the redesign test required only reanalysis of the wing and the residual structure.

(5-5a) Superelement Analysis Using Cyclic Symmetry

DMAP1C, Version 46, was used to allow the left hand side to be duplicated into a right hand side, Reference 2. Symmetric and unsymmetric loadings were then applied. Redesign of the wing necessitated only the reanalysis of that particular structure.

TEST RESULTS

Figures 4 and 5 show that the superelement/substructure methods for a large analysis are comparable to the single structure if only one solution is required. However, the first analysis is usually not sufficient and requires many iterations before a satisfactory solution is obtained. Under these circumstances the substructure/superelement method proves itself far superior, requiring only one-third of the CPU time for a reanalysis using a new wing. Not only does this reduce the billing time, but even more important, this increases the chances that the job will run before the computer malfunctions.

The superelement method uses a disk pack data base which reduces the multitude of Job Control Language (JCL) cards necessary to run the substructure analysis. This, in turn, reduces chances of making errors when a large group of engineers works on the same project. No NASTRAN errors were encountered when using the superelement method; only a minor problem was found in the estimation of space needed on the data base.

CONCLUSIONS

The superelement method will substantially lower computer run times for a large finite element analysis. This will decrease the job execution wall-clock time, which will decrease the chances that the computer system will malfunction before an analysis is finished. For structures which require a large amount of computer resources and long execution time, the calendar time to finish an analysis will also be reduced.

Simplification in Job Control Language, use of disk pack storage, and future resource commitment to the superelement method strongly recommend this technique to replace the single structure and substructure methods for any future project.

REFERENCES

1. Sodha, R.: Substructure Analysis in MSC NASTRAN of Symmetric Structures Subject to Asymmetric Loading. British Aircraft Corporation, Warton Aerodrome, Tornado Unified Analysis Project Report, 25 January 1977.

2. Joseph, Jerrard A: Cyclic Symmetry in MSC/NASTRAN. MSC/NASTRAN Application Manual, November 1972.

FIGURE 1 - NORTHROP T-38 FINITE ELEMENT MODEL

PROTOTYPE - 36 DEGREES OF FREEDOM

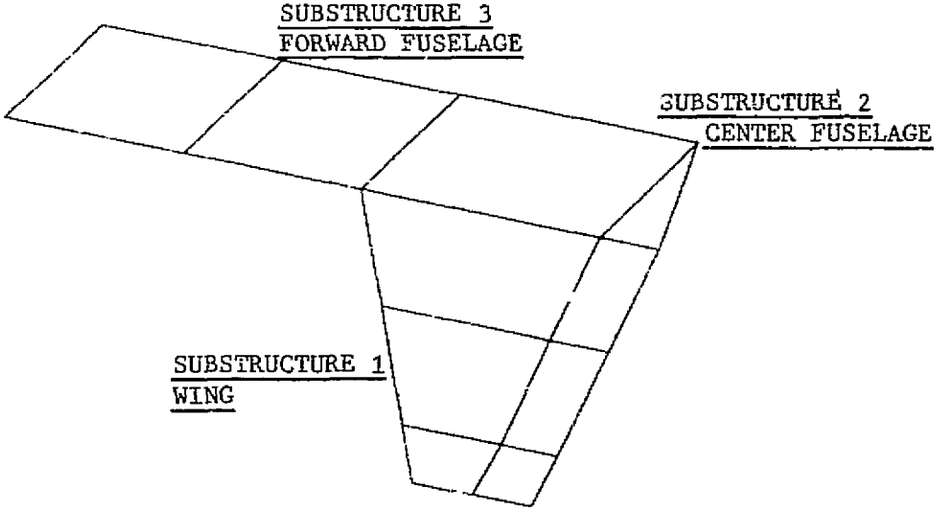

FIGURE 2 - NORTHROP T-38 FINITE ELEMENT MODEL
PRODUCTION MODEL - 9500 DEGREES OF FREEDOM

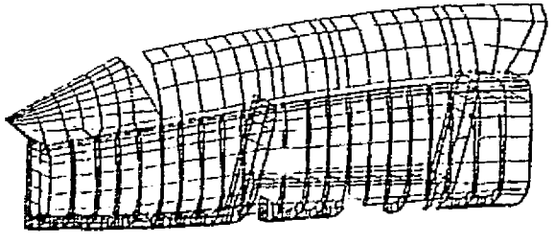

SUBSTRUCTURE 3

FORWARD FUSELAGE

(3000 dof)

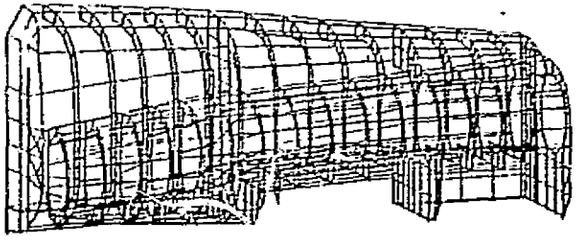

SUBSTRUCTURE 2

CENTER FUSELAGE

(2500 dof)

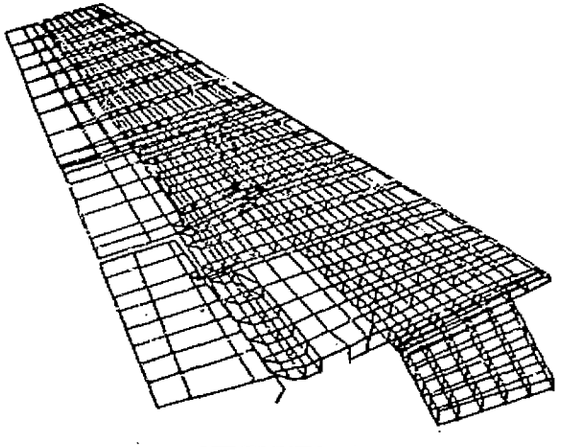

SUBSTRUCTURE 1

WING

(4000 dof)

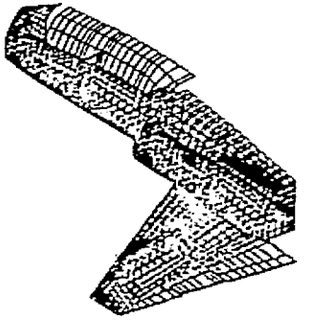

COMBINED STRUCTURE

(9500 dof)

FIGURE 3 - NASTRAN MODEL TEST SCHEDULE

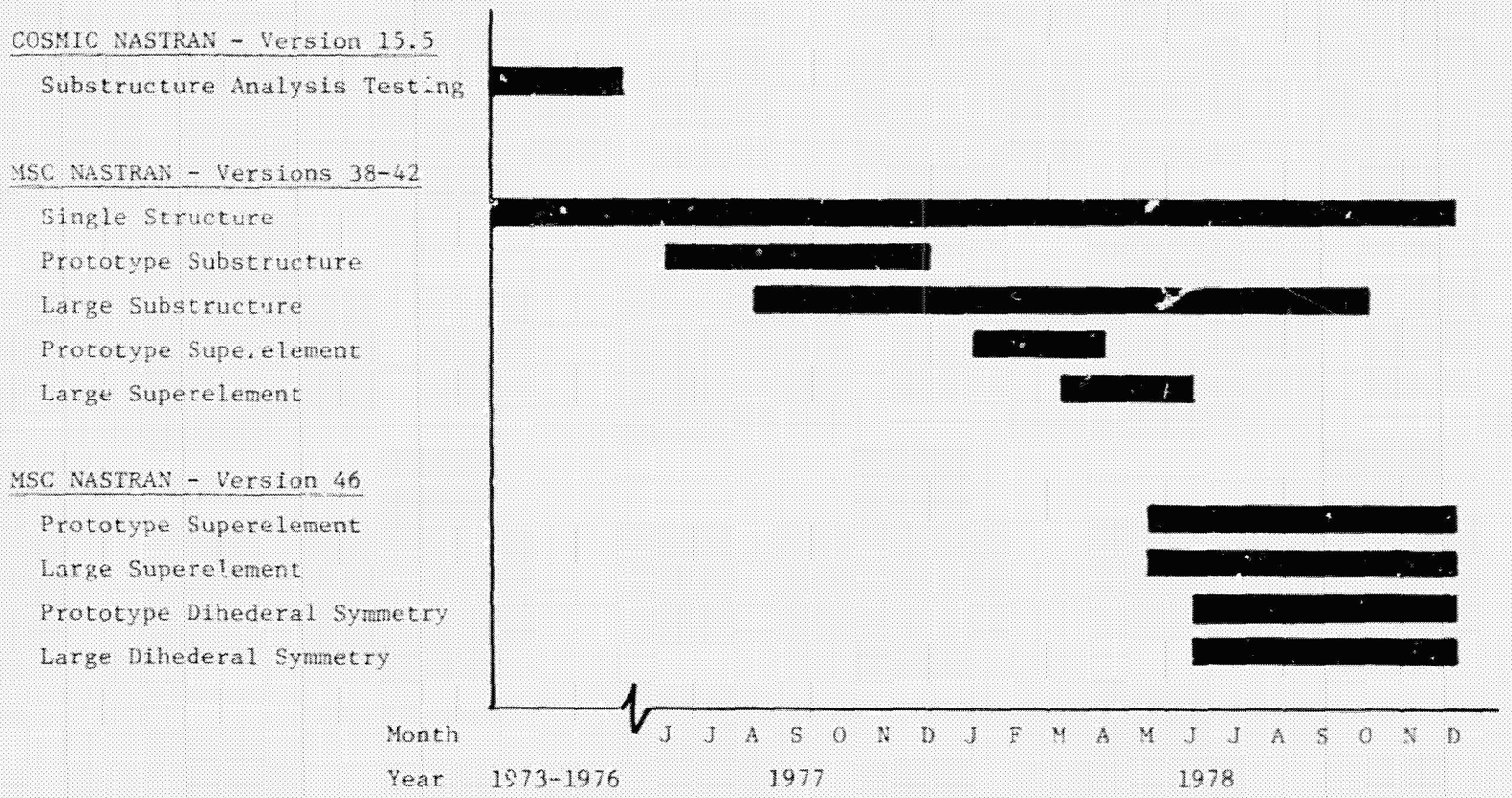

FIGURE 4 - T-38 NASTRAN ANALYSIS USING FIVE DIFFERENT METHODS

9500 ANALYSIS DEGREES OF FREEDOM

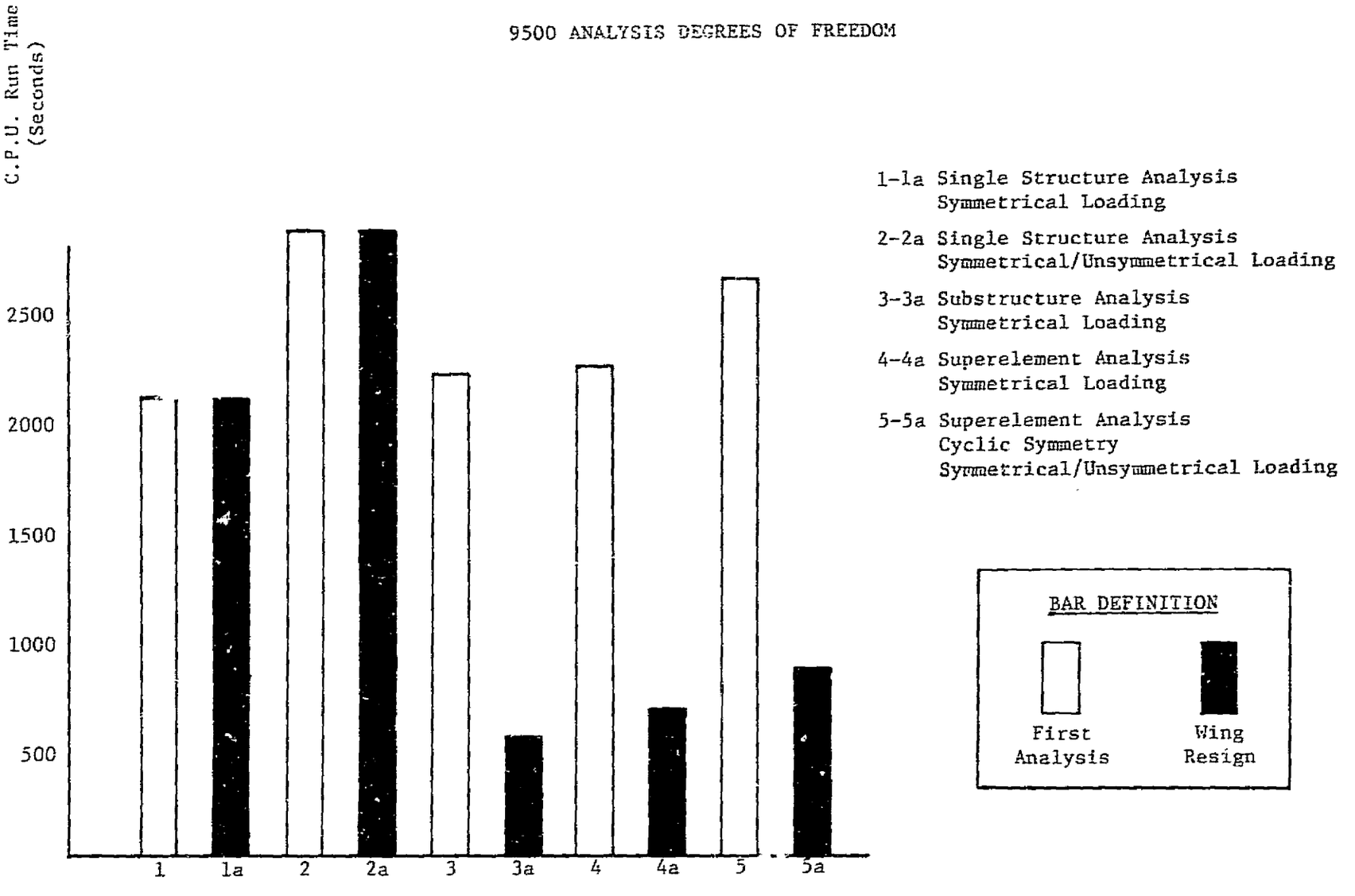

FIGURE 5 - COMPARISON OF NASTRAN COMPUTER RUNS FOR T-38

	1-1a	2-2a	3-3a		4-4a		5-5a	
	Single Structure (L.H. Side)	Single Structure (Both Sides)	Substructure (L.H. Side)		Superelement (L.H. Side)		Superelement Cyclic Symmetry (Both Sides)	
MATRIX SIZE	KAA	KAA	KAA	KOO	KAA	KOO	KAA	KOO
Substructure I	9575	9575	30	3944	30	3938	104	3914
II			156	2500	138	2497	606	2373
III			126	3031	114	3039	504	2899
Total Size			312	9475	282	9474	1214	9186
EMG (Sec.)								
Substructure I	281	296	33		35		33	
II			131		133		140	
III			129		130		138	
Total Time			293		298		311	
EMA (Sec.)								
Substructure I	90	90	39		40		34	
II			39		35		31	
III			26		24		26	
Total Time			104		99		91	
Decomp (Sec.)								
Substructure I	317	689	137		139		93	
II			86		85		51	
III			78		77		50	
Total Time			301		301		194	
FBS (Sec.)								
Substructure I			66		59		221	
II	--	--	152		129		283	
III			132		98		347	
Total Time			350		286		851	
Total Elapsed CPU (Sec.)	1588	2190	1682		1700		2025	
Redesign CPU (Sec.)	1588	2190	413		518		662	
Restart Storage	Tape	Tape	Tape		2470 Trks		3183 Trks	

Computer Used: IBM 370/168 - MVS

Disk Pack: 3330 - Mod. II

ORIGINAL PAGE IS
OF POOR QUALITY

D22

N78-32488

A NASTRAN ANALYSIS OF A TOKAMAK VACUUM VESSEL USING INTERACTIVE GRAPHICS

by
Arthur Miller
Grumman Aerospace Corp.
and
Morris Badrian
EBASCO Services, Inc.

SUMMARY

A TAKOMAK Vacuum Vessel was analyzed using MSC/NASTRAN. Isoparametric quadrilateral and triangular elements were used to represent the Vacuum Vessel shell structure. For toroidally symmetric loadings, MPCs were employed across model boundaries and Rigid Format 24 was invoked. Un-symmetric loadings required the use of the cyclic symmetry analysis available with Rigid Format 49. NASTRAN served as an important analysis tool in the TOKAMAK design effort by providing a reliable means for assessing structural integrity. Interactive graphics were employed in the finite element model generation and in the post-processing of results. The authors feel that model generation and checkout with interactive graphics reduced the modelling effort and debugging man-hours significantly.

INTRODUCTION

This paper presents the structural modelling method, analysis procedures and results of a TOKAMAK Vacuum Vessel finite element analysis. The analysis described herein was required for the design-verification of the TOKAMAK FUSION TEST REACTOR (TFTR) Vacuum Vessel. The TOKAMAK is a toroidal device through which magnetic fields permeate to confine a plasma. The magnetic fields are produced by strong electric currents on the order of 40,000 amperes passing through both copper coils and the plasma. In the TOKAMAK, there are two major magnetic fields: a toroidal field generated by current flowing in the coils enveloping the torus, and a poloidal field generated by current flowing through both the plasma and an equilibrium field coil. By combining toroidal and poloidal magnetic fields, the TOKAMAK achieves a higher level of plasma stability than has been realized in any previous magnetic-confinement

system. The increased plasma stability permits longer confinement times of higher temperature plasmas. The TFTR will therefore come closer to meeting all necessary conditions for a net production of fusion energy than any previous magnetic fusion device. A basic function of the Vacuum Vessel is to provide containment of the hot (100 million degrees Celsius) Deuterium-Tritium plasma while excluding the atmosphere.

SYMBOLS

Values are given in both SI and US Customary Units. Calculations were made in US Customary Units.

f_b	Bending stress, psi (MPa)
f_{max}	Maximum combined stress, psi (MPa)
f_m	Membrane stress, psi (MPa)
f_{xy}	In-plane shear stress, psi (MPa)
F_x	Circumferential (toroidal) membrane load, lb/in. (N/m)
F_y	Meridional membrane load, lb/in. (N/m)
F_{xy}	In-plane membrane shear load, lb/in. (N/m)
Q_x	Transverse shear load (causing M_x bending), lb/in. (N/m)
M_x	Circumferential (toroidal) bending load, in lb/in. (N-m/m)
M_y	Meridional bending load, in. lb/in. (N-m/m)
q_x	Transverse shear stress, psi (MPa)
t	Material Thickness, in. (m)

THE TOKAMAK VACUUM VESSEL

The Vacuum Vessel (Fig. 1) is essentially a large doughnut-shaped vessel (or torus) composed of ten stainless steel segments joined at ten parting planes. Each segment contains five intersecting cylinders (three pie sections and two bellows cases) as shown in the plan view (Fig. 2). The diametral centerline of each cylindrical section intersects the vertical axis of symmetry of the machine. Six of the segments include a Neutral Beam Injection Duct, as shown in Figure 1. (The purpose of the Neutral Beam Injection Duct is to produce high-energy Deuterium atoms and to inject them into a magnetically-confined Tritium

plasma causing Deuterium-Tritium fusion reactions to occur.) Each segment is supported at both a radially inboard and a radially outboard location. Inboard supports supply essentially vertical restraint, supporting approximately 1/3 of the deadweight of the Vacuum Vessel. Outboard supports allow free radially inward displacement while restraining radially outward, toroidal and vertical motion.

FINITE ELEMENT IDEALIZATION

Two models of Vacuum Vessel segments have been developed which span from parting plane to parting plane. A derivative of the non-Neutral Beam Injection Duct model was also created for analysis of anti-symmetric loading. The first model, shown in Figure 3, contains detailed features such as diagnostic and access port extensions, non-structural port covers, the parting plane (P/P) weld thickness with its stiffening rings, the plasma limiter support structure, pie bellows-case (P/B) stiffening rings, and the inboard and outboard supports. QUAD4 and TRIA3 isoparametric plate bending elements were used for the shell idealization. (These elements were chosen because they provide superior results with fewer elements. The results of element test problems carried out by MSC (Ref. 1) has shown that the accuracy of the QUAD4 element is effectively independent of the aspect ratio.) Beam elements were used to simulate the stiffening rings at the P/B intersections, and those adjacent to the parting plane. These element types were also used to idealize the Vacuum Vessel supports and flanges at the ends of the port extensions. Rod elements were used to model the protrusions at the port-shell intersections. Continuity of the finite element model across structural interfaces (viz. at the P/B intersections, parting plane/ring intersections and at the vessel support connections) was achieved by means of rigid-bar and rigid-triangular elements. The second model as shown in Figures 4 and 5, is essentially the same as the first except for the inclusion of a Neutral Beam Injection Duct. Each model consisted of approximately 1900 nodes with 6 DOF at each node.

MODEL GENERATION WITH INTERACTIVE GRAPHICS

The interactive display feature of Control Data's UNISTRUC program facilitated the modelling of the numerous penetrations, eccentricities and extensions which comprise more than 60% of the total model. In order to develop this geometrically complex finite element idealization it was necessary to employ several pre-processors. (The sequence of steps employed in the model generation which are described below are schematically depicted in Figure 6.) First, a FORTRAN program was written to geometrically outline the boundaries of major individual structural components. The results of this program were input into UNISTRUC in terms of "lines" and "points". The boundary interiors were then meshed by employing UNISTRUC's generic element library (Ref. 2).

In addition to nodes and elements, loads, material properties and physical properties were defined and graphically reviewed through UNISTRUC. This information was written to a "Neutral Input File" in an application-independent format. Inputting this file to the "NASTRAN Input-File Translator" resulted in a file containing properly formatted Executive Control, Case Control and Bulk Data card images. To take advantage of more recent NASTRAN features which are not currently compatible with UNISTRUC (e.g. rigid elements) it was necessary to edit the card images. This was accomplished through the use of the INTERCOM interactive editing feature of Control Data's Scope 3.4 Operating System (Ref. 3). Model bandwidth optimization and SEQGP card generation was accomplished by a stand-alone optimizer residing on a linked mainframe, and subsequently merged, through INTERCOM, with the NASTRAN Bulk Data.

LOADINGS

The TFTR is subjected to several different loading combinations. These combinations include the Normal Operating Condition, Bakeout, Discharge Cleaning, Plasma Disruption, Seismic and Coil Short-circuiting. As of this writing the Vacuum Vessel has been analyzed for the severe conditions associated with a Plasma Disruption. A Plasma Disruption loading consists of electromagnetic centering forces, electromagnetic pressure and electromagnetically-induced toroidal and racking forces on the bellows case rings in addition to the

deadweight of the Vessel, and external pressurization. For the sake of brevity, this paper will only present results related to the gravity and pressurization subcase.

ANALYSIS PROCEDURE

Due to budgetary constraints it was decided early in the program not to model the entire torus structure. Instead, individual models consisted of a single segment type with boundary conditions selected so as to simulate a complete torus. Analysis with smaller models had shown that results of sufficient accuracy would be obtained with this idealization. For torcidally symmetric loadings, the most efficient analysis technique was to employ MPCs across the boundaries of the selected segment type and invoke Rigid Format 24. Unsymmetric loadings required the use of the more expensive Cyclic Symmetry Analysis available in Rigid Format 49. (A Cyclic Symmetric run with a harmonic index of five was found to require twice the CPU time and 3.5 times the I/O as compared to the MPC'd boundary model.) Based on the economic and technical resources available, it was decided to perform the analyses on a second mainframe containing the MSC/NASTRAN Version 40 operating under the Network Operating System/Batch Environment.

ANALYSIS RESULTS

The resulting significant internal membrane and bending force distributions are depicted in Figures 7 through 10. Continuity of the curves was obtained by smoothing the computer-output values at element centroids. In regions of load and/or structural discontinuity, the results were extrapolated to the edges of the finite elements under consideration. These results were checked, where feasible, by utilizing equilibrium and compatibility relationships, thus maximizing the information yielded by the analysis. Post processing of the results would have been more expeditious had an option been available in NASTRAN to print out element internal load intensities (Mx, My, Nx, Ny, Nxy, Qx, Qy) at the element corners in addition to the element centroid. This feature would more clearly define internal load gradients. Had this option been available, much of the time expended in manually smoothing and extrapolating the

results would have been saved. Figures 7 and 8 present the critical internal loads below the torus' horizontal axis of symmetry, specifically at the following critical locations: the maximum pie/bellows interface eccentricities and at the connection of the outboard supports to the torus. Figures 9 and 10 each present the internal loads along a meridian. Figure 9 depicts the axial and bending loads along the centerline of pie 2, while Figure 10 depicts the loads in the parting plane weld.

The relationship between the internal loads and the resulting stresses is as follows:

$$f_{max} = f_m \pm f_b = \frac{F_x}{t} \pm \frac{6M_x}{t^2}$$

$$\text{or } \frac{F_y}{t} \pm \frac{6M_y}{t^2}$$

} combined membrane and bending stresses

$$f_{xy} = \frac{F_{xy}}{t}$$ In-plane shear stress

$$q_x = \frac{Q_x}{t}$$ Transverse shear stress

where t = .5 inches (.0127 meters) applicable to Figures 7 thru 9
t = .312 inches (.00792 meters) applicable to Figure 10, parting plane weld

An inspection of the results indicates that the critical stresses occur in the following Vacuum Vessel locations:

-In Pies 1 and 2, at the maximum pie/bellows interface eccentricities, Figure 7.

$$fx_{max} = \frac{F_x}{t} + \frac{6M_x}{t^2} = \frac{-900}{.5} - \frac{6 \times 450}{(.5)^2} = \begin{matrix}-12,600 \text{ psi} \\ (-86.874 \text{ MPa})\end{matrix}$$

-In Pie 2, at the diagnostic port-shell intersection, Section A-A, Figure 8.

$$fx_{max} = \frac{Fx}{t} + \frac{6M_x}{t^2} = \frac{-4500}{.5} - \frac{6 \times 100}{(.5)^2} = \begin{matrix}-11,400 \text{ psi} \\ (-78.6 \text{ MPa})\end{matrix}$$

- In Pie 2, at the diagnostic port-shell intersection, Figure 9.

$$fy_{max} = \frac{Fy}{t} + \frac{6M_y}{t^2} = \frac{-2500}{.5} - \frac{6 \times 130}{(.5)^2} = \begin{matrix} -8120 \text{ psi} \\ (-55.9 \text{ MPa}) \end{matrix}$$

In the parting plane weld region, Figure 10, the Mx bending results are increased by 20% to account for moment peaking at the intersection of the 5/16 inch (.00794 meters) weld with the P/P stiffening ring:

$$fx_{max} = \frac{Fx}{t} + 1.2\,\frac{6M_x}{t^2} = \frac{-750}{.312} - 1.2\,\frac{6 \times 100}{(.312)^2} = \begin{matrix} -9800 \text{ psi} \\ (-67.57 \text{ MPa}) \end{matrix}$$

DEFLECTIONS

Grid point displacements, element forces and stress were output to the NASTRAN UT1 file by appropriate DMAP instructions generated by UNISTRUC. The contents of the UT1 file were transformed by means of the UNISTRUC file translator for compatibility with the UNISTRUC system, thus making interactive display of the results possible. Displays of the deflected shapes of major structural components appear in Figures 11 thru 16. A maximum deflection of .037 inches (0.00094 meters) occured at the intersection of the outside edge of the diagnostic port and the shell on Pie 2 as shown in Figure 14.

CONCLUSIONS

NASTRAN proved to be a valuable analysis tool for the design-verification of a TFTR Vacuum Vessel. Furthermore, it was found that analysis of a 1/10 segment of a structure with Rotational Cyclic Symmetry (K = 5) and non-symmetrical loading was approximately 2 1/2 times more costly than for a symmetrically loaded model of the same fundamental region with MPCs across the boundaries.

The use of interactive graphics in both the pre and post-processing modes was found to be an indispensible tool when dealing with complex three-dimensional models.

REFERENCES

1. MacNeal-Schwendler Corporation, MSC/NASTRAN Application Manual For CDC 6000 Series, Los Angeles, California.

2. Control Data Corporation, Unified Structural Design System (UNISTRUC), Version 1.2, Publication No. 76079600, Publications and Graphics Division, St. Paul, Minnesota.

3. Control Data Corporation, CYBERNET Service INTERCOM 4 Reference Manual, Publication No. 84000024, Publications and Graphics Division, Data Services Publications, Minneapolis, Minnesota.

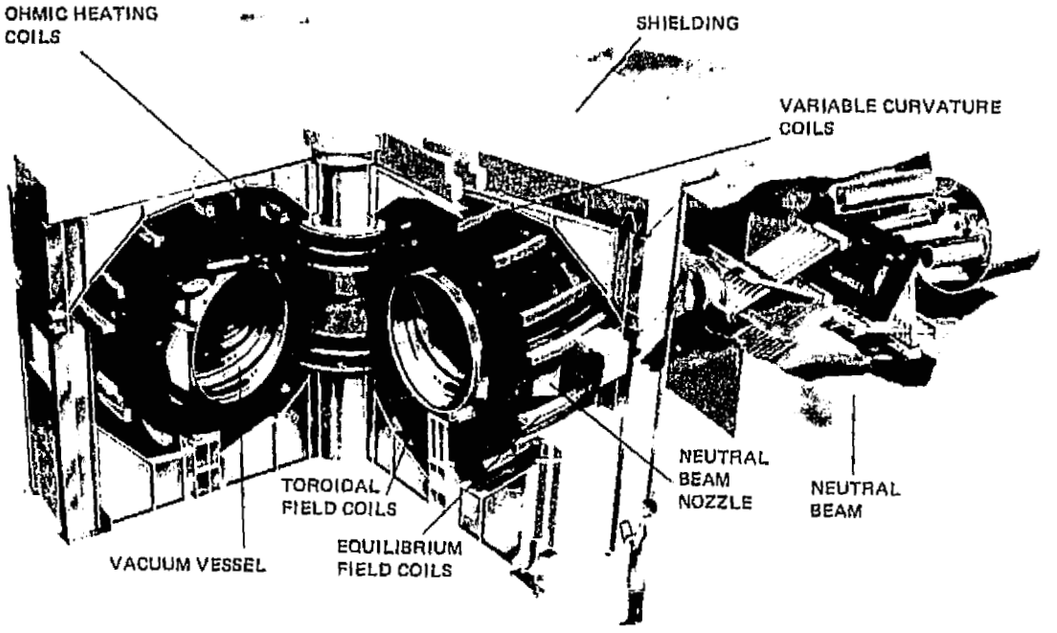

(a) Tokamak Fusion Test Reactor

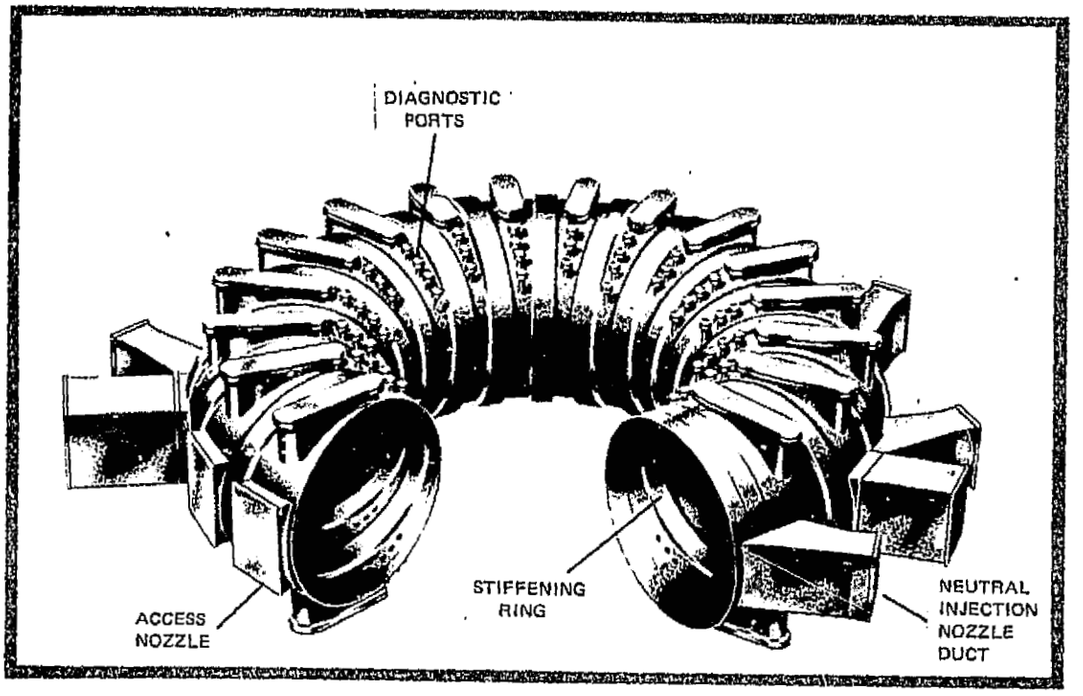

(b) Vacuum Vessel

2036-001

Figure 1 Tokamak Fusion Test Reactor – Vacuum Vessel

C-5

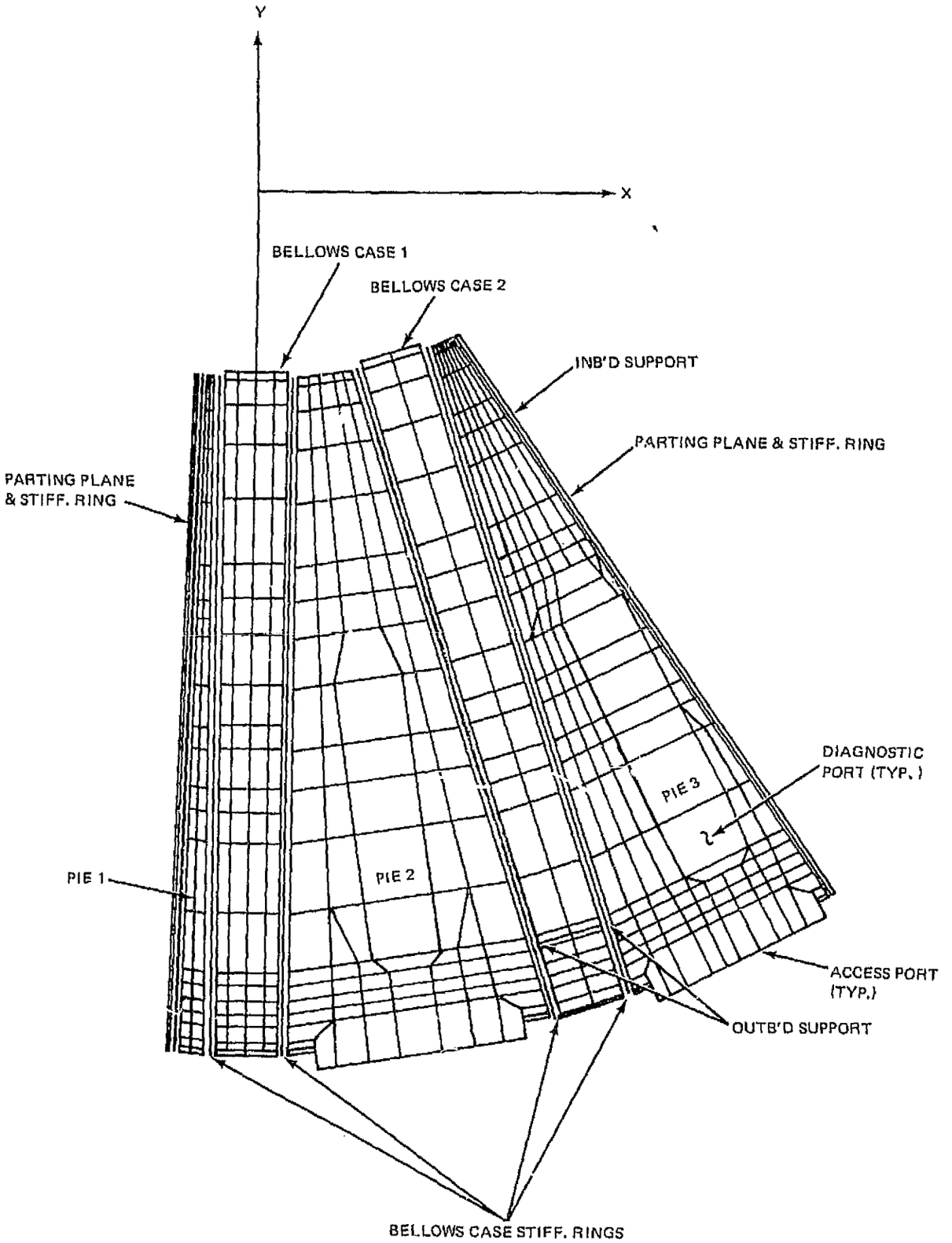

Figure 2 TFTR Vacuum Vessel – Finite Element Model, Plan View

ORIGINAL PAGE IS
OF POOR QUALITY

2036-003

Figure 3 TFTR Vacuum Vessel - Finite Element Model, Isometric View

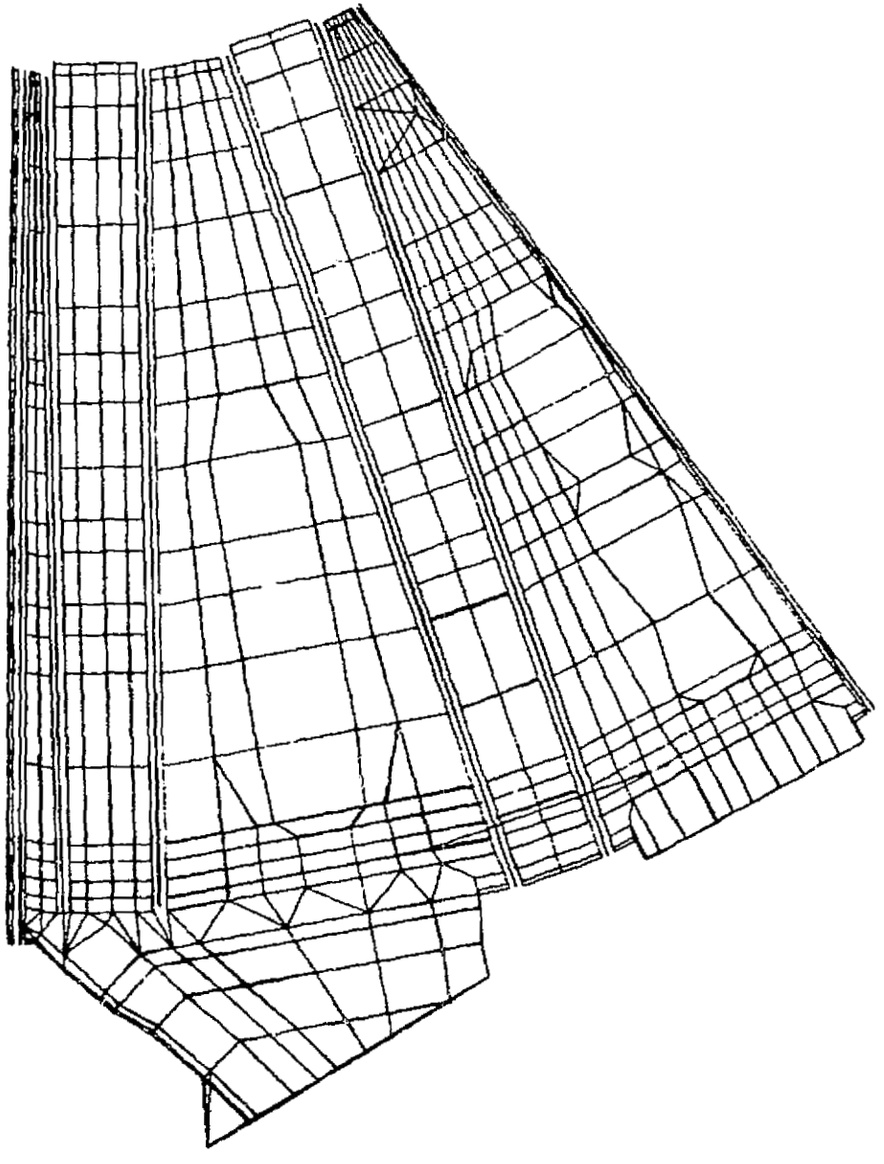

2036-004

Figure 4 Neutral Beam Duct Segment - Finite Element Model, Plan View

Figure 5 Neutral Beam Duct Segment - Finite Element Model, Isometric View

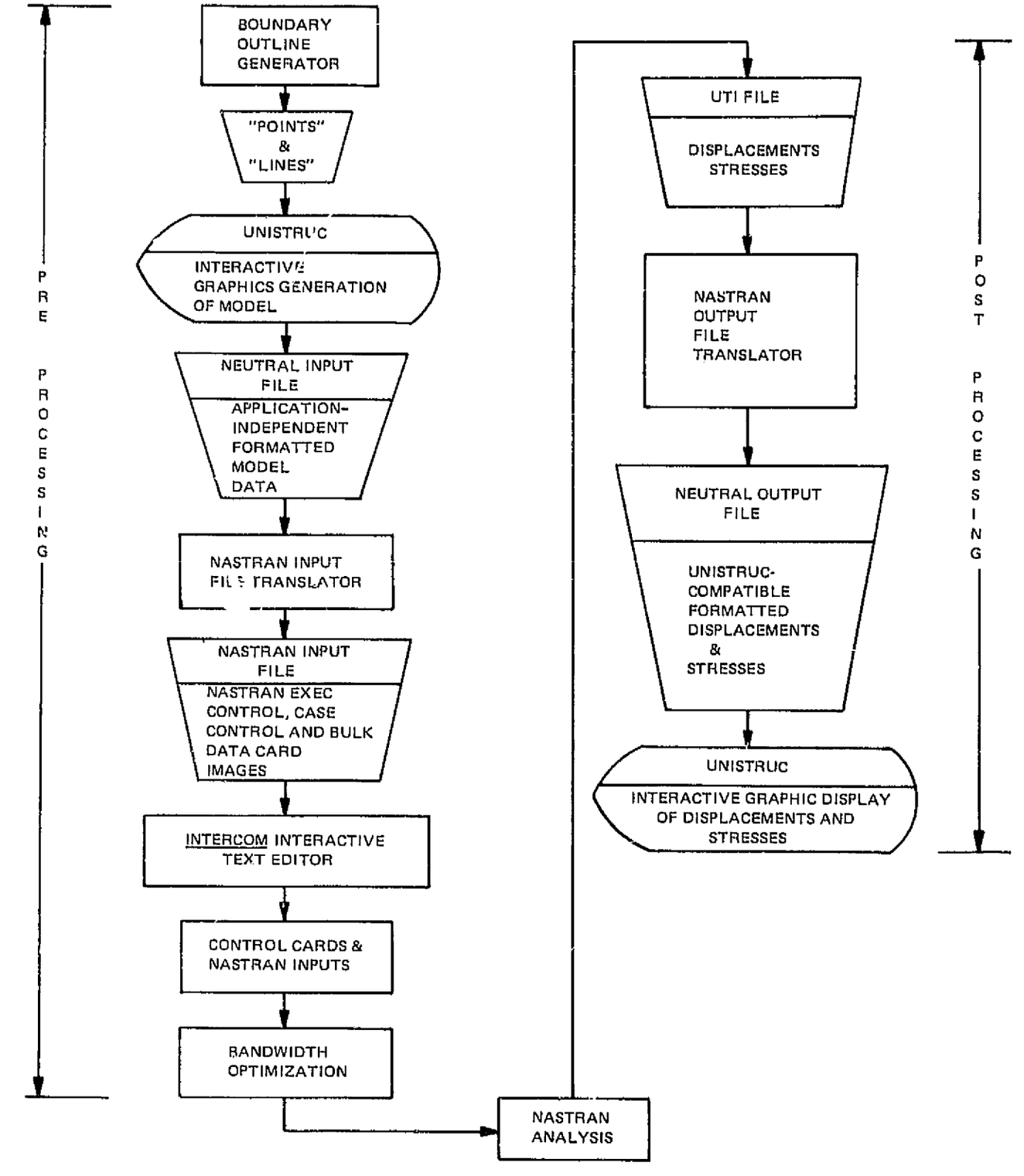

Figure 6 Pre and Post Processing with Interactive Graphics

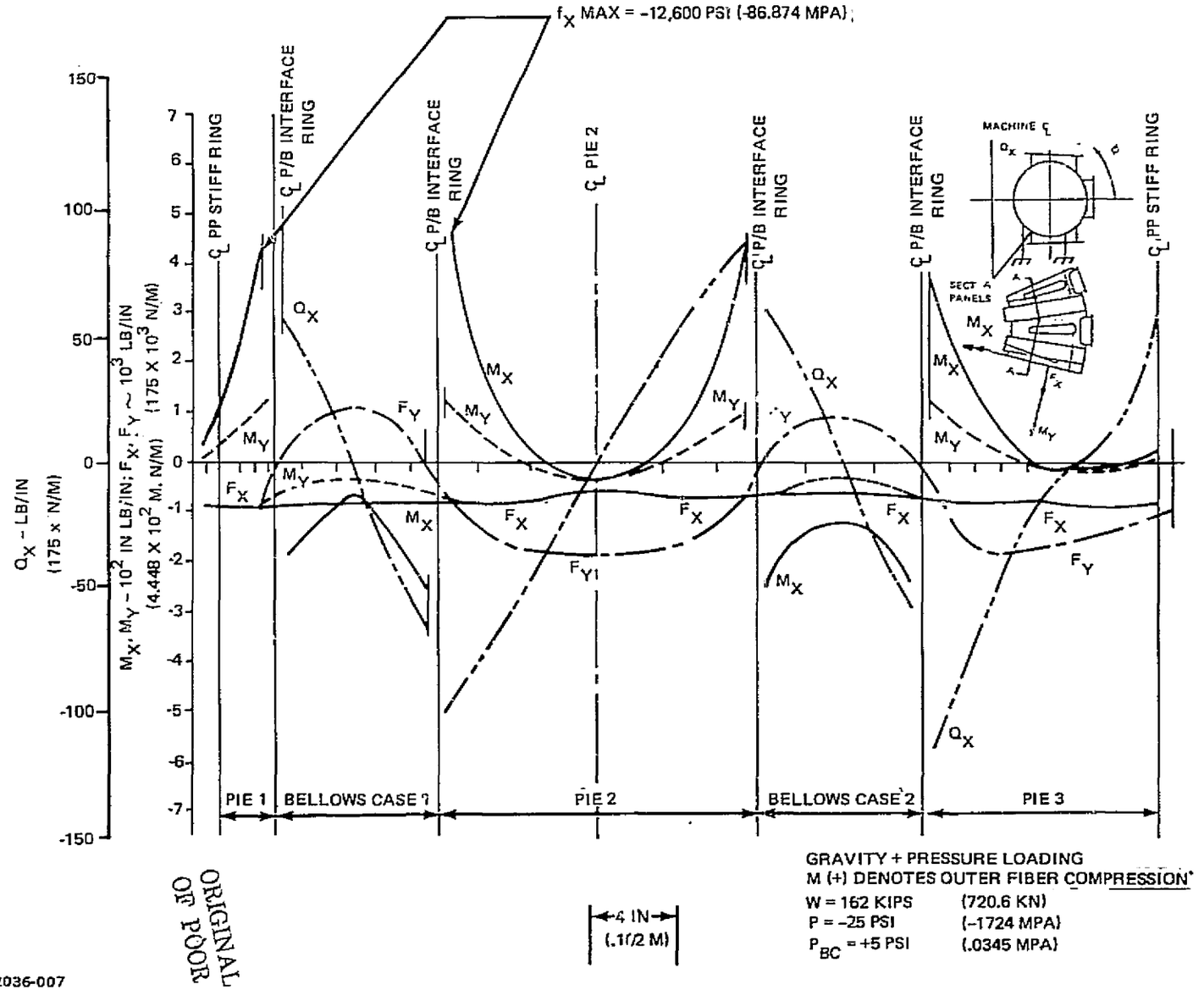

Figure 7 Loads at Maximum Pie/Bellows Case Interface Eccentricity

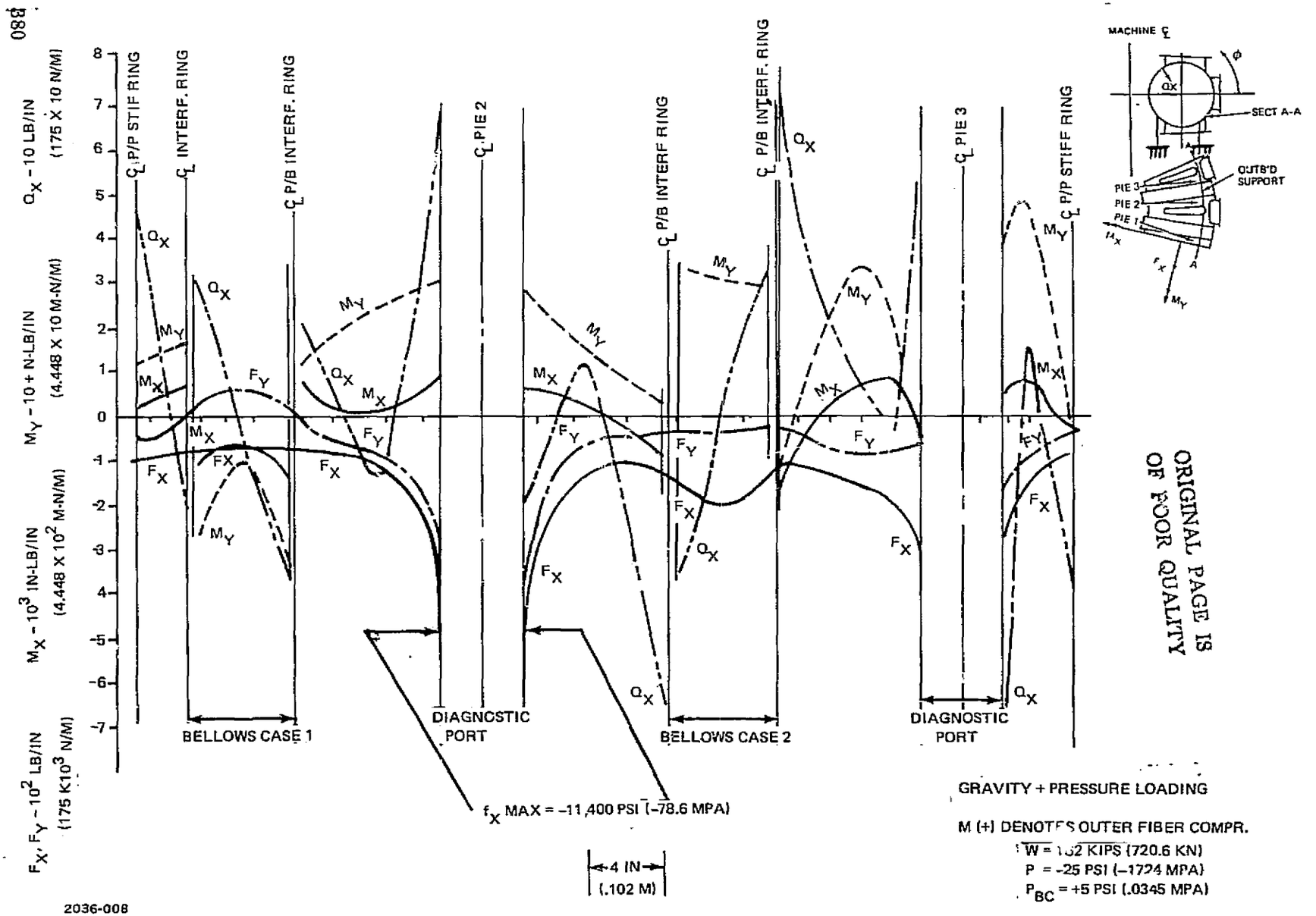

Figure 8 Loads at the Connection of the Outboard Supports to the Torus

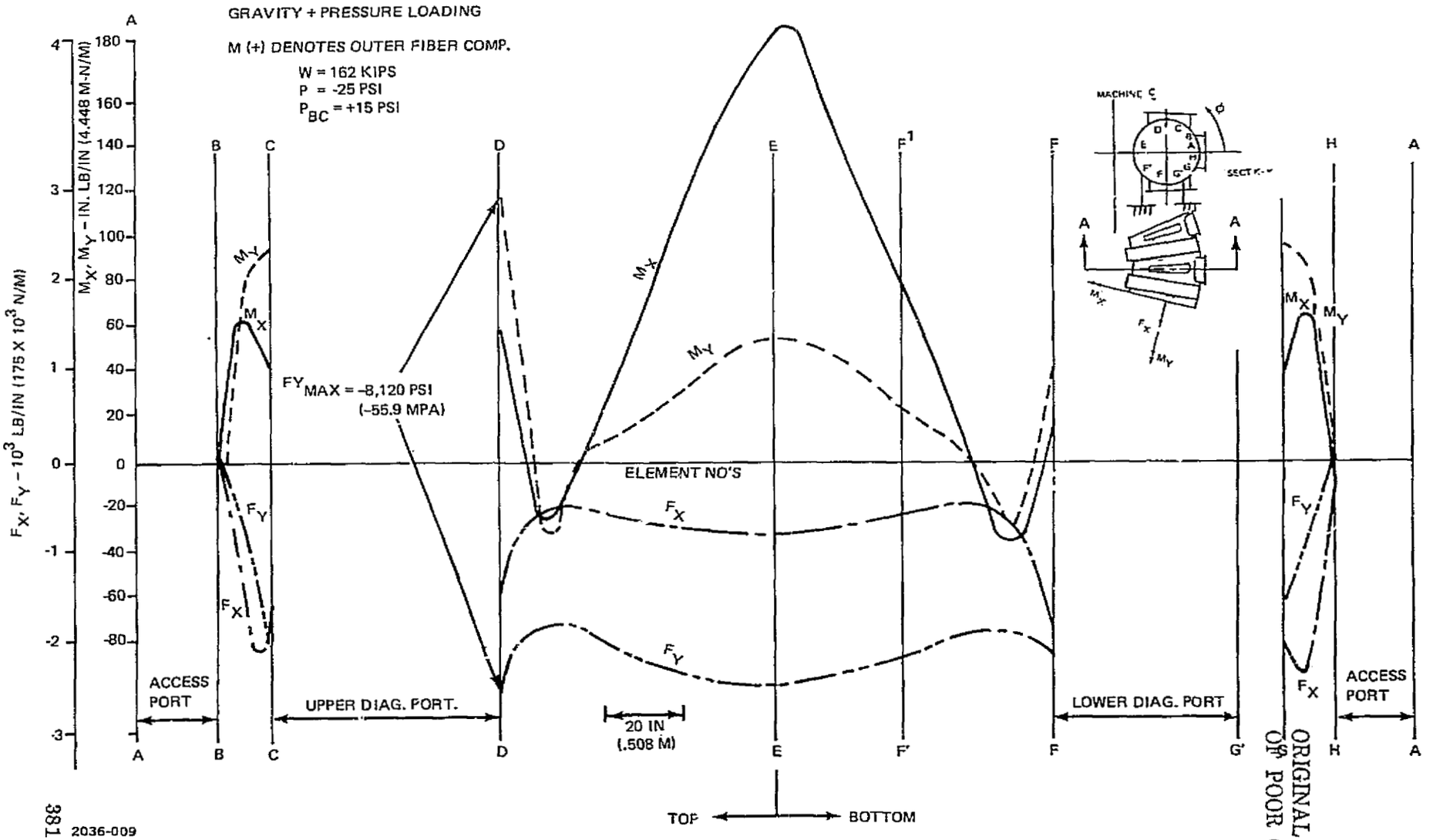

Figure 9 Loads Along the Centerline of Pie 2

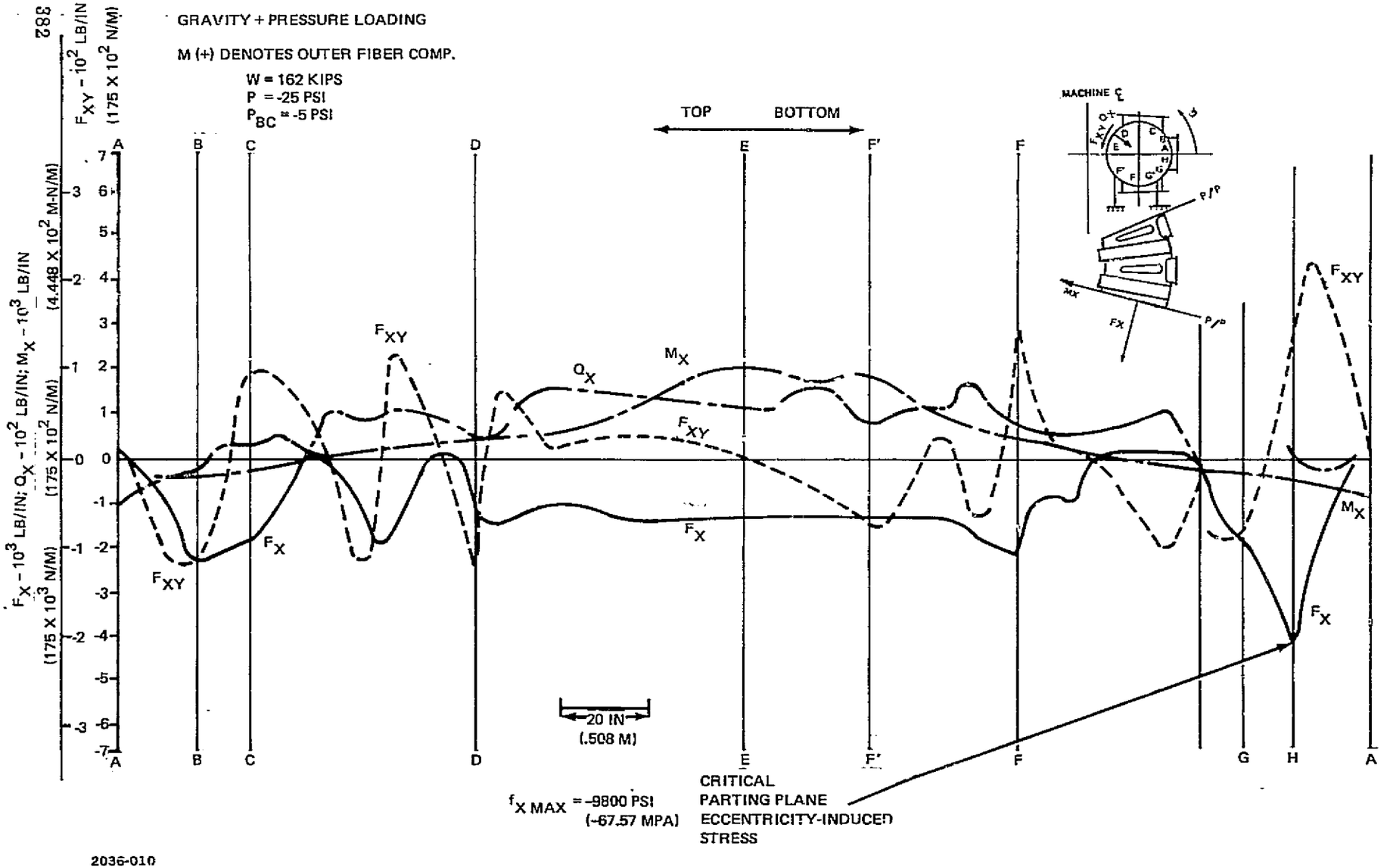

Figure 10 Loads in the Parting Plane Weld

LOAD CONDITION:
PRESSURE & GRAVITY

P_{SHELL} = -25 PSI (-.1724 MPa)

$P_{BELLOWS\ CASE}$ = + 5 PSI (.0345 MPa)

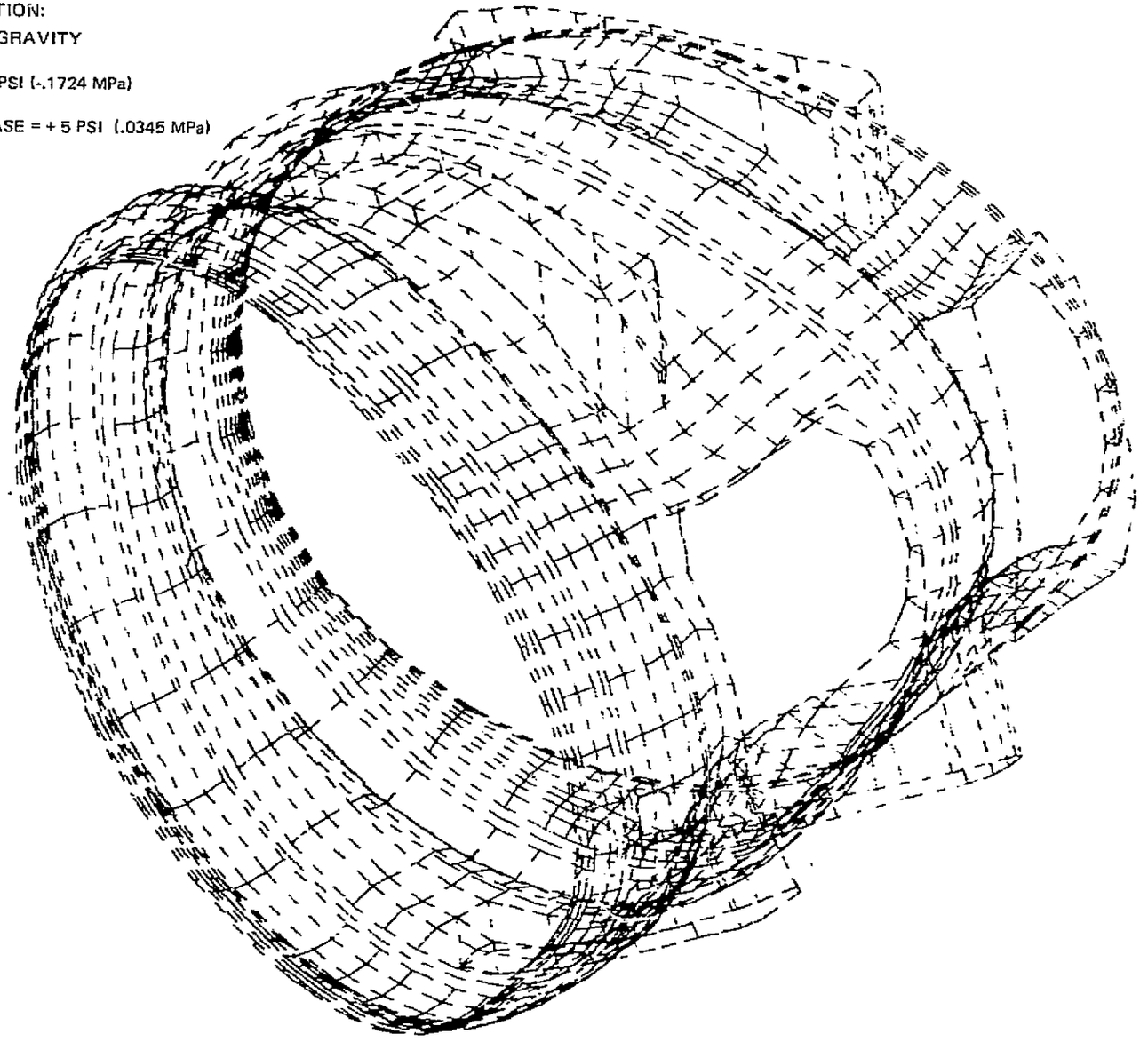

2036-011

Figure 11 Deformed Shape of TFTR Vacuum Vessel Finite Element Model, Isometric View

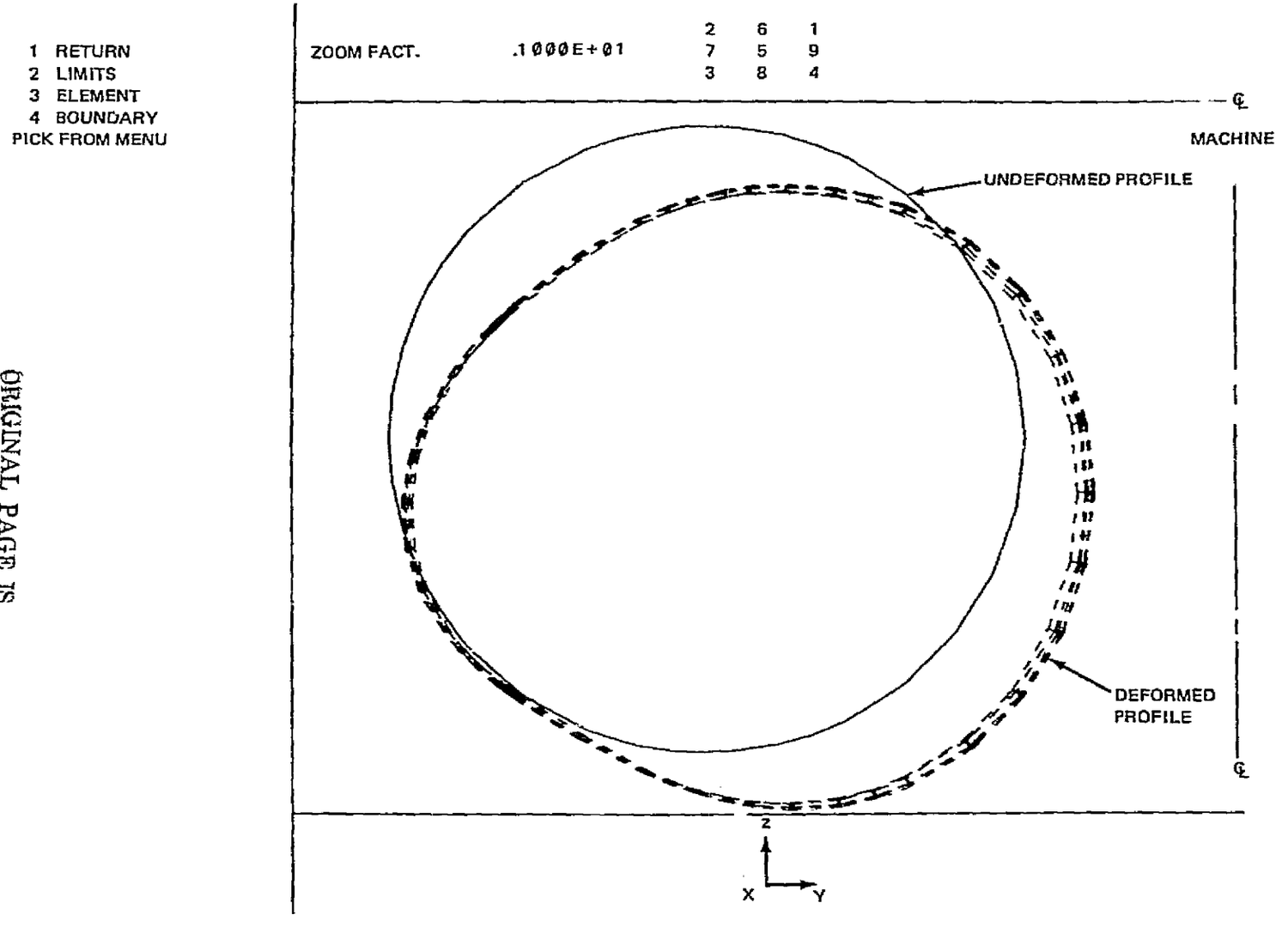

2036-012

Figure 12 Deformed and Undeformed Profiles of Bellows Case 1

2036-013

Figure 13 Deformed and Undeformed Profiles of Bellows Case 2

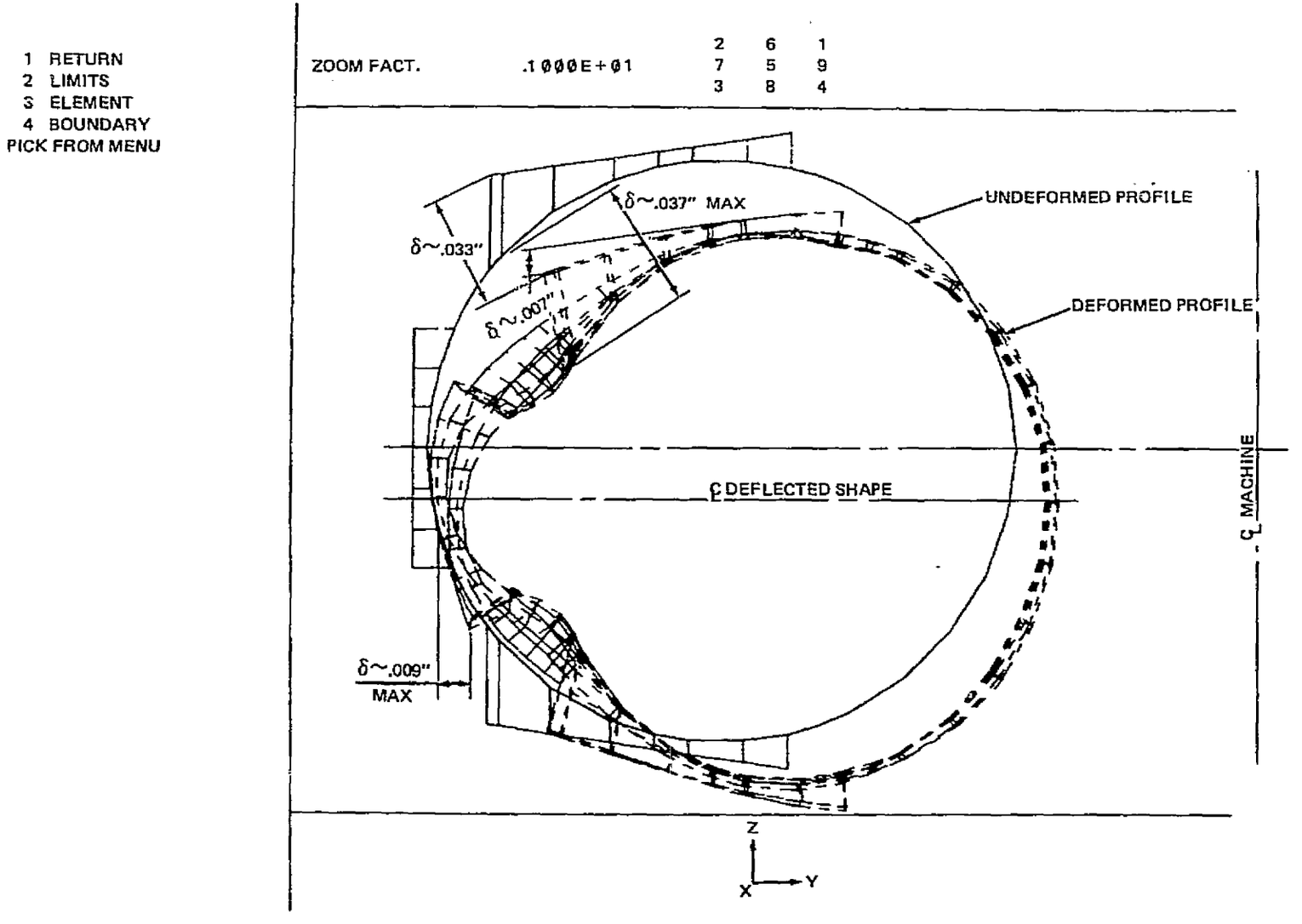

Figure 14 Deformed and Undeformed Profiles of Pie 2

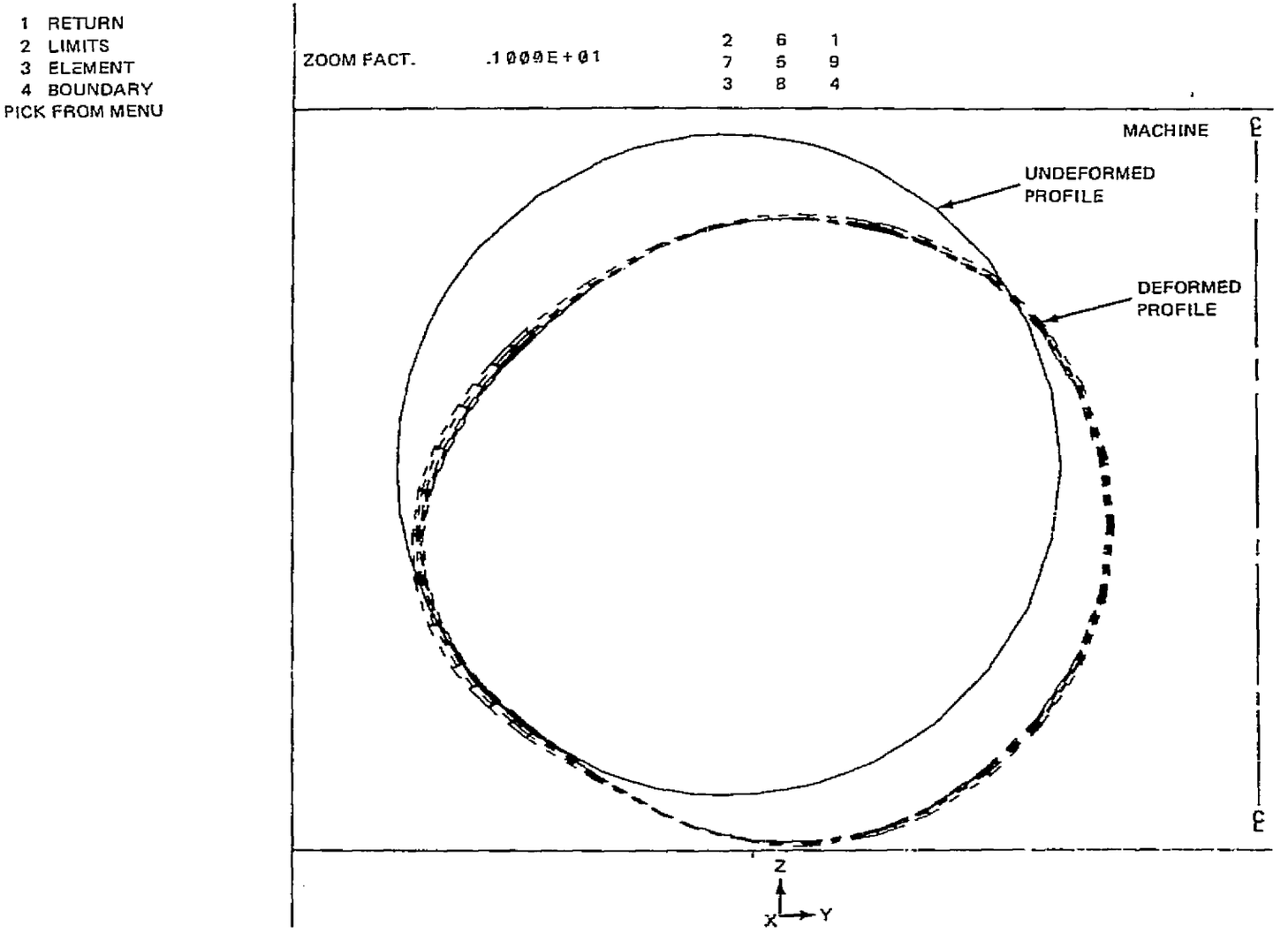

2036-015

Figure 15 Deformed and Undeformed Profiles of Pie 1 and the Parting Plane

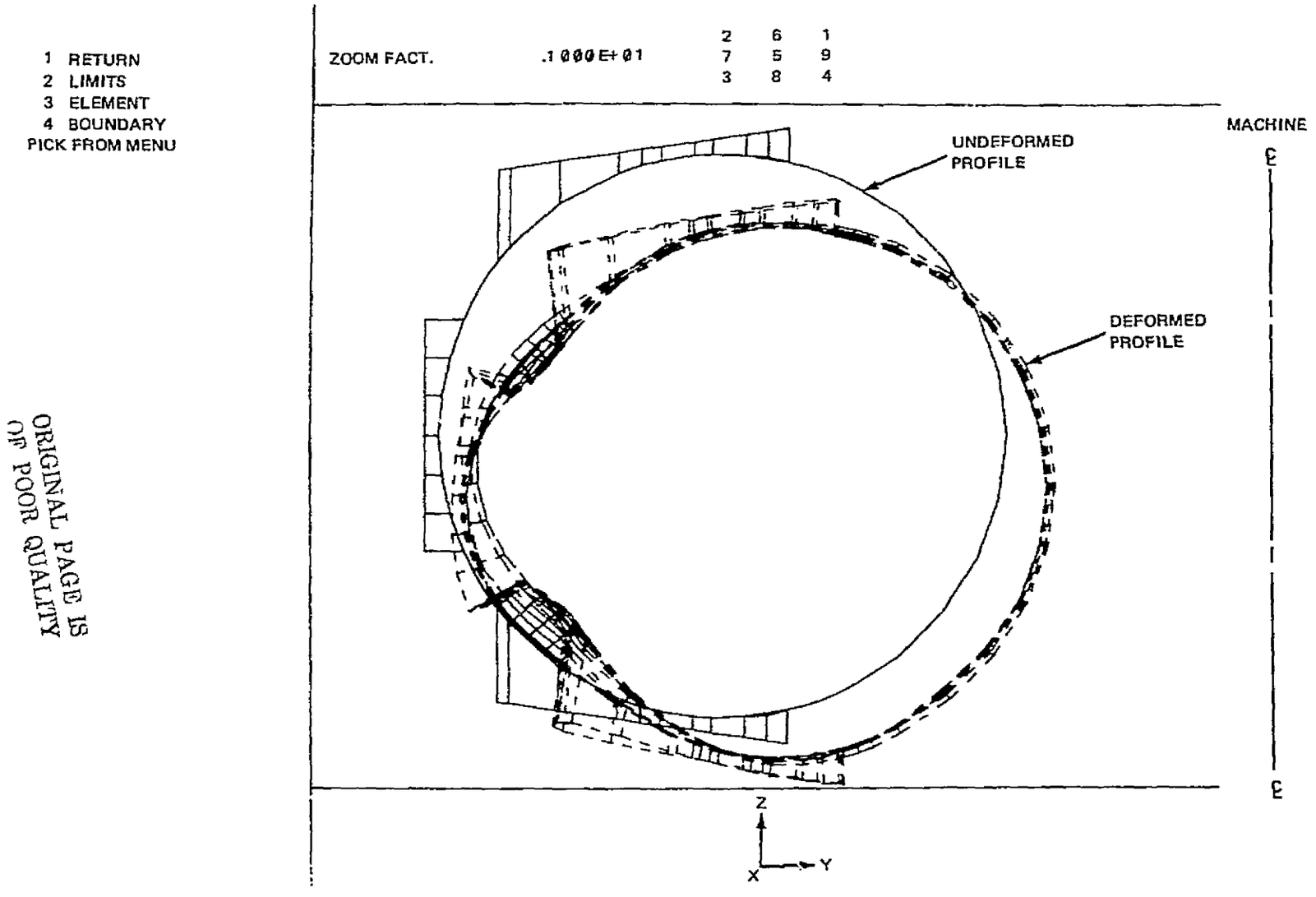

Figure 16 Deformed and Undeformed Profiles of Pie 3

D23

N78-32489

ACCURACY OF RESULTS WITH NASTRAN MODAL SYNTHESIS

D. N. Herting
Universal Analytics, Inc.

SUMMARY

A new method for component mode synthesis has been developed for installation in NASTRAN Level 17.5. An introduction and summary of the method was presented at the 1977 NASTRAN Colloquium [Ref. 1], but actual results were unavailable at that time. This paper serves as a continuation to Reference 1 by presenting results obtained from the new method and comparing these results with existing modal synthesis methods.

INTRODUCTION

The modal synthesis system developed by Universal Analytics, Inc. (UAI) for NASTRAN is a new development which provides for the benefits inherent in existing methods but eliminates the restrictions and computational drawbacks associated with other methods. In Reference 1 it was postulated that the new method was sufficiently general to duplicate the results of other, more restricted, methods simply by choosing different types of normal modes or vector recovery procedures. The test problems described herein have been selected for direct comparison with other published results. The goal of this effort was to determine the relative accuracy of the UAI method with its different options.

The use of structural modes as generalized degrees of freedom in dynamic models originated in the analog computer field where structures were combined with aeroelastic and control system models. The first applications to digital computers were simple extensions of the analog techniques. This so-called classical approach proved both highly restrictive and limited in accuracy. Many different approaches have been developed in recent years having increased accuracy and more generality in solving large-order structure dynamics problems.

Although the previous methods used in component mode synthesis vary considerably in both approach and application, they may be grouped into two distinct categories. The first category contains all of the methods using a Rayleigh-Ritz approach in which the component degrees of freedom represent the deflections of normal modes and static deflection shapes. The second category contains methods in which the component degrees of freedom are actual physical displacements plus a set of modal coordinates. Here, the classical

method has been improved by adding flexibility coefficients to the matrices to account for the effects of a truncated set of modes.

The theoretical development of the NASTRAN modal synthesis system is being issued in Reference 2, the Level 17.5 Theoretical Manual. In this development the "residual flexibility" approach is used as a starting point but the end results become very similar to the Rayleigh-Ritz approach. The new method, in effect, is related to both categories of modal synthesis and shows that the differences between them are more related to computational procedures than in theoretical basis.

The two test problems described below were selected for comparison with several advanced mode synthesis methods. The problems also provide a comparison of the various options that will be available in the NASTRAN system which are summarized below:

1. The boundary conditions used to obtain component modes are not restricted. Free, constrained, and partially free modes may be used.

2. Inertia relief displacement shape functions may be included as degrees of freedom as a user option. These provide for exact static response of free bodies and more accuracy for low frequency response.

3. In the vector recovery process, after a system solution has been obtained, a "mode acceleration" procedure which calculates "improved" displacements is available.

4. A full set of error check procedures are available to assess the accuracy of the results. These include printout of the equilibrium forces, energy checks of truncated modes, and direct evaluation of the participation of the modal coordinates.

The test problems and their results are summarized below, followed by a summary of the conclusions which follow from the evaluation of the tests.

NOMENCLATURE

u - Physical Displacement

G - Guyan Reduction Transformation Matrix

K - Stiffness Matrix

M - Mass Matrix

ℓ - Length

x - Spacial Coordinates

T - Kinetic Energy

V - Potential Energy

ε - Error Ratio

ξ - Generalized Displacement of a Mode

ρ - Density

ϕ - Eigenvector

ω - Radian Frequency

EXACT ROD PROBLEM

A convenient test problem for modal synthesis evaluation was used by Rubin [Ref. 3] to compare various methods, including his own new method. The problem, illustrated in Figure 1 consists of a single rod with extensional motion. Rather than solve the problem with finite elements, a set of closed form integral solutions may be used to obtain the modal synthesis matrix coefficients. In effect, the results will simulate a problem with an infinite number of elements. This procedure will elminate the finite element errors and will allow analysis of errors resulting only from the modal synthesis formulation.

The problem solved by Rubin uses the free-free modes of the rod to fomulate a component mode substructure. The solution matrix is then constrained to obtain cantilever modes. If the end degree of freedom were included in the normal formulation it could be attached to another structure directly. The errors in the results will occur because the sine wave solutions for the cantilever rod must be approximated by the dissimilar cosine waves of the free rod.

In the UAI method, the displacement shapes are

Static Displacements

$$u_1^i(x) = \left[-\frac{I}{G}-\right]\{u_b\} = u_1 \tag{1}$$

Inertial Relief:

$$u_2^i(x) = k_{ii}^{-1}\left[M_{ib} + M_{ii}G\right]\phi_o\xi_o$$

$$= \frac{\rho\ell^2}{E}\left(x - \frac{x^2}{2\ell}\right)\xi_o \tag{2}$$

Normal Modes:

$$u_k(x) = \{\phi_{1k} - G\phi_{bk}\}\xi_k$$

$$= \left(\cos \frac{\pi k x}{\ell} - 1 \right) \xi_k \qquad k = 1,2,\ldots\infty \tag{3}$$

After normalizing the units, the total displacement at any point on the rod is:

$$u(x) = u_1 + \frac{1}{\ell}\left(x - \frac{x^2}{2\ell} \right) \xi_o + \sum_k \left(\cos \frac{\pi k x}{\ell} - 1 \right) \xi_k \tag{4}$$

Instead of performing matrix transformations the stiffness, [K], and mass, [M], matrices are obtained using the La Grange formulation which states:

$$M_{ij} = \frac{d}{dt} \frac{\partial^2 T}{\partial \dot{q}_i \partial \dot{q}_j} \tag{5}$$

and

$$K_{ij} = \frac{\partial^2 V}{\partial q_i \partial q_j} \qquad , q_1 = u_1, \xi_o, \xi_1 \cdots , \tag{6}$$

where the potential energy, V, and the kinetic energy, T, are:

$$V = \int_o^\ell \frac{EA}{2} \left(\frac{\partial u}{\partial x} \right)^2 dx \tag{7}$$

$$T = \int_o^\ell \frac{PA}{2} \dot{u}^2 dx \tag{8}$$

After evaluating the integrals, the stiffness matrix produced by the new method is:

$$[K] = \frac{EA}{\ell}\begin{bmatrix} 0 & 0 & 0 & 0 & 0 & \\ & \frac{1}{3} & \frac{-1}{3} & \frac{-1}{3} & \frac{-1}{3} & \cdots \\ & & \frac{\pi^2}{2} & 0 & 0 & \cdots \\ & & & \frac{4\pi^2}{2} & 0 & \cdots \\ & \text{sym} & & & \frac{9\pi^2}{2} & \cdots \\ & & & & & \frac{(k\pi)^2}{2} \end{bmatrix} \tag{9}$$

The mass matrix is:

$$[M] = PA\ell\begin{bmatrix} 1 & \frac{-1}{3} & -1 & -1 & \cdots & -1 \\ \frac{-1}{3} & \frac{2}{15} & -\left(\frac{1}{3}+\frac{1}{\pi^2}\right) & -\left(\frac{1}{3}+\frac{1}{4\pi^2}\right) & \cdots & -\left(\frac{1}{3}+\frac{1}{(k\pi)^2}\right) \\ & & \frac{3}{2} & 1 & \cdots & 1 \\ & & & \frac{3}{2} & 1 & 1 \\ & (\text{sym}) & & & & \frac{3}{2} \end{bmatrix} \tag{10}$$

Since the first row corresponds to the displacement at x = 0, the boundary constraint, $u_1 = 0$, requires that the first row and column be deleted for calculation of the cantilever modes.

The results of the modal solution are the frequencies ω_i and generalized displacements ξ_{oi}, ξ_{ki}, k = 1, 2 ... . The actual mode shapes may be obtained from equation (4). However, a mode acceleration method (UIMPROVE) available in NASTRAN and also used by Rubin will enhance the vectors. Transforming the matrix equations into equivalent integrals results in the equation:

$$\phi_2(x) = u(0) + \int_0^x \left[\frac{\rho}{E}\int_x^{\ell} - \ddot{u}(x)dx\right] dx \tag{11}$$

where $\ddot{u}(x)$ is obtained by multiplying the displacement $u(x)$ in Equation (4) by $-\omega^2$. This results in the mode shape:

$$\phi_2 = \frac{\omega_1^2\rho\ell^2}{E}\left\{\left(\frac{\bar{x}}{3} - \frac{\bar{x}^3}{6} + \frac{\bar{x}^4}{24}\right)\xi_o - \sum_k \left[\bar{x} - \frac{\bar{x}^2}{2} + \frac{1}{(\pi k)^2}(1 - \cos\pi k\bar{x})\right]\xi_k\right\} \tag{12}$$

where $\bar{x} = x/\ell$ is used for simplicity.

The exact solutions for the cantilever rod problem modal frequencies are:

$$\omega_{ex} = \frac{(2n - 1)\pi}{2\ell}\sqrt{\frac{E}{\rho}} \tag{13}$$

The exact mode shapes are:

$$\phi_{ex} = \text{sine}\ \frac{(2n - 1)\pi x}{2\ell} \tag{14}$$

The calculated natural frequencies for the synthesized system produce an error ratio ε_ω, defined by the equation:

$$\varepsilon_\omega = \frac{\omega - \omega_{ex}}{\omega_{ex}} \tag{15}$$

The resulting errors in natural frequency are tabulated in Table 1. These errors match Rubins results for his method exactly. Note that, except for the single degree of freedom problem, the error in the last mode for any matrix size is nearly constant and that the convergence rate for a given order matrix is nearly uniform.

An order of magnitude fit of the frequency errors is produced by the equation:

$$\varepsilon_{\omega n} \sim 0.01\frac{\omega_n^4}{\omega_k^2(\omega_k^2 - \omega_n^2)} \tag{16}$$

where ω_k is the frequency of the lowest truncated mode shape. The equation is not accurate for the lower modes of the large order matrices due to computer round-off. Single precision arithmetic produced numerical errors of the order 10^{-7}.

The RMS errors for the calculated eigenvectors are shown in Table 2 for the same order synthesized matrices. Both first and second methods for calculating the vectors were used. The equations used for the vector errors are:

$$\varepsilon_\phi^1 = \frac{1}{\phi_{max}} \sqrt{\frac{1}{\ell} \int_o^\ell (\phi_1 - \phi_{ex})^2 dx} \tag{17}$$

and

$$\varepsilon_\phi^2 = \frac{1}{\phi_{max}} \sqrt{\frac{1}{\ell} \int_o^\ell (\phi_2 - \phi_{ex})^2 dx} \tag{18}$$

Both vectors were normalized to unit modal mass.

Note that the improved displacement calculations (ϕ_2) produce much better results when the first order errors are between 10^{-2} and 10^{-6}.

In other words, a good first approximation will produce a better improved solution. A poor first solution, such as the last mode in a set, will result in little improvement. A nearly exact first solution will not improve due to numerical round-off.

The results of this test are nearly identical to Rubin's [Ref. 3] results for his method. The frequency errors fall exactly on the published curves. The displacement errors for the UAI method appear to be better than Rubin's results. However it is suspected that differences in numerical procedures produced these changes. Also the first order displacement results compare with the referenced results for the modified Bamford method used in Reference 3.

TWO COMPONENT TRUSS PROBLEM

This problem has nearly become a standard for the evaluation of modal synthesis methods. It has been used in References 4, 5, and others for comparison between different formulations and procedures. A large quantity of data is available for validation of any new method. The basic problem, shown in Figure 2, consists of two truss substructures. Each substructure is reduced to its normal modes plus any additional shape functions used by a particular method. The trusses are combined at the three common grid points and the unconstrained modes of the combination are obtained.

This problem was solved directly on the UAI modal synthesis system implemented on L16 NASTRAN. Several different options and matrix sizes were tested. The parameters of the test cases are shown in Table 3. The matrix sizes were chosen to provide direct comparison with the results in Reference 4.

The results were compared with a single-structure NASTRAN execution to obtain the percentage errors of the frequencies. These errors are shown in Tables 4 and 5 along with results from Hintz [Ref. 4]. In all cases an excellent correlation was obtained between the NASTRAN results and the results of the equivalent formulations used by Hintz The only deviation occurred when the errors became too small to calculate when the NASTRAN printout truncated the difference in results. In each case the results are not shown where the eigenvector became unrecognizable and/or the natural frequencies changed in sequence.

It is important to note that the cases using free component modes, with no inertia relief effects, produced very poor results. This is due to the fact that the free modes approximate half waves while the cantilever modes approximate quarter waves. The shapes of the first modes of the combination apparently are difficult to approximate by a set of higher order shapes. The inertia relief shapes supply these smooth functions. Their contribution is most significant in the lower frequency modes.

Also indicated in the tables, by dashed lines, are the lowest truncated frequencies for the component modes used in the analysis. The results indicate that in the inertia relief cases, this frequency is a good indication of the limit for valid results. When only normal and constraining modes are used, this frequency has some significance, but does not indicate possible errors due to poor approximation of the actual mode shapes.

As a further check the problem was executed using 36 elastic degrees of freedom (case 9). This case also correlated with the Reference 4 results, having 29 modes with a frequency error of less than 5%. Nearly all of the first 15 modes were calculated to values exact to the last digit of the printout. However this case should not be considered as a typical example since only 60 degrees of freedom existed in the original structure. The typical application of modal synthesis would result in a matrix size with a much smaller fraction of the original matrix size.

CONCLUSIONS

As was postulated in Reference 1, the new modal synthesis method to be available in NASTRAN is capable of simulating the results and accuracy of any of the current state-of-the-art modal synthesis methods. The differences in the results occur from selecting different types of component modes and types of solution vector recovery processing. Furthermore, it was observed from these tests that the frequencies of the truncated component normal modes are a significant indicator of the upper limit of valid combination modes.

Although the new system provides accuracies equal to or better than any other advanced method, it also eliminates the restrictions that are imposed by the other formulations. The UAI method does not require unconstrained modes required by the Rubin and McNeal [Ref. 6] formulations. The method conveniently uses the actual boundary grid points as degrees of freedom (as in the Rubin and MacNeal methods) as opposed to the conventional Rayleigh-Ritz methods, in which an actual boundary displacement coordinate must be expressed as a combination of mode displacements. Furthermore, it allows any choice of mode shapes, including modes fixed at non-boundary points, partially free modes, and user supplied vectors.

The results for both test problems indicate that the inertia relief option is recommended for most cases. The number of calculations to obtain these shape functions is small relative to the modal calculations. A maximum of six extra degrees of freedom per component are added to the system. Results from the second test problem indicate that one should not replace modal coordinates with the inertia relief components since this will lower the effective frequency range.

The use of the "improved displacement" options in the solution vector recovery process appears to be less dramatic in its effectiveness. This option will be most effective when the first order vectors are reasonably valid and accurate stress data are required.

REFERENCES

1. Herting, D.N. and Hoesley, R. L., "Development of an Automated Multi-Stage Modal Synthesis System for NASTRAN", Sixth NASTRAN User's Colloquium Papers, NASA Conference Publication 2018, October, 1977.
2. Herting, D.N. and Morgan, M. J., "Analysis of Structures Using Component Modes", Chapter 18, NASTRAN Theoretical Manual, Level 17.5 Updates.
3. Rubin, S., "Improved Component-Mode Representation for Structural Dynamic Analysis", AIAA Journal, Vol. 12, August 1975, pp. 995-1006.
4. Hintz, R.M., "Analytical Methods in Component Modal Synthesis", AIAA Journal, Vol. 13, Aug. 1975, pp. 1007-1016.
5. Benfield, W.A. and Hruda, F.R., "Vibration Analysis of Structures by Component Substitution", AIAA Journal, Vol. 9, July 1971, pp. 1255-1261.
6. MacNeal, R.H., "A Hybrid Method of Component Mode Synthesis", Computers and Structures, Vol. 1, Dec. 1971, pp. 581-601.

TABLE 1. MODE FREQUENCY ERRORS, $\varepsilon\omega$, VERSUS MATRIX ORDER - FREE ROD PROBLEM

MODE NO.	MATRIX ORDER						
	1	2	3	4	6	8	12
1	6.6-3	9.5-5	8.5-6	1.21-6	6.1 -7	5.5 -6	3.0-6
2		3.1-2	1.1-3	1.88-4	1.78-5	-1.21-6	-2.1-5
3			4.4-2	2.4 -3	1.73-4	3.4 -5	-2.1-5
4				5.2 -2	8.9 -4	1.5 -4	-3.3-5
5					4.1 -3	5.1 -4	-2.9-5
6					5.9 -2	1.5 -3	-4.4-6
7						4.9 -3	7.4-5
8						6.2 -2	2.8-4
9							7.5-4
10							1.8-3
11							4.8-3
12							5.9-2

TABLE 2. EIGENVECTOR RMS ERRORS VERSUS
MATRIX ORDER - FREE ROD PROBLEM

MODE NO.	MATRIX ORDER						
	1	2	3	4	6	8	12
1	1.31-2 (2.69-2)*	3.18-5 (4.70-4)	3.06-6 (9.76-5)	6.16-7 (3.25-5)	1.81-7 (6.97-6)	1.35-7 (2.32-6)	2.23-7 (6.52-7)
2		9.81-3 (2.78-2)	1.03-3 (3.79-3)	1.66-5 (1.05-3)	1.87-5 (2.01-4)	9.71-6 (6.72-5)	5.00-6 (1.25-5)
3			2.15-2 (4.30-2)	3.36-3 (7.81-3)	2.16-4 (1.11-3)	5.44-5 (3.27-4)	5.50-5 (6.00-5)
4				3.19-2 (5.37-2)	1.65-3 (4.10-3)	2.77-4 (1.039-3)	1.11-4 (1.73-4)
5					9.19-3 (1.51-2)	1.12-3 (2.76-3)	2.04-4 (4.05-4)
6					4.79-2 (6.79-2)	4.06-3 (8.91-3)	5.46-4 (8.34-4)
7						1.56-2 (2.12-2	9.35-4 (1.62-3)
8	$\varepsilon\hat{\phi}$ $(\varepsilon\phi)$					6.01-2 (1.34-2)	2.01-3 (3.06-2)
9							3.96-3 (5.96-3)
10							9.12-3 (1.21-2)
11							2.46-2 (2.93-2)
12							7.57-2 (8.20-2)

*( ) without UIMPROVE

TABLE 3. TEST CASE PARAMETERS
FOR THE TWO COMPONENT TRUSS PROBLEMS

CASE	NUMBER OF MODAL COORDINATES	NUMBER OF INERTIA RELIEF COORDINATES	TYPE OF COMPONENT MODE	TOTAL ELASTIC DOF
1	9	0	Free	12
2	3	6	Free	12
3	17	0	Free	20
4	11	6	Free	20
5	9	0	Cantilever	12
6	3	6	Cantilever	12
7	17	0	Cantilever	20
8	11	6	Cantilever	20
9	27	6	Cantilever	36

TABLE 4. PERCENT FREQUENCY ERRORS WITH 12 ELASTIC DEGREES OF FREEDOM TWO COMPONENT TRUSS PROBLEM

ELASTIC MODE NO.	NASTRAN CASE				REF. 4 RESULTS		
	1 Free Modes	2 Free w/I.R.	5 Cant. Modes	6 Cant. w/I.R.	Free w/I.R.	Hurty	Cant. w/I.R.
1	24.27	.006	.011	.00039	.006	.011	.00067
2	3.28	.021	.013	.194	.019	.013	.187
3	10.41	.737	.031	.737	.074*	.031	.743
4	4.51	.147	.150	2.93	.150	.155	2.94
5	2.47	1.82	.197	10.83	1.68	.190	10.3
6	4.50	6.45	.184	17.06	6.55	.184	16.9
7	1.00	16.02	6.49		16.8	7.39	
8	4.87		6.44				
9	0.75						
10		indicates freq. of first truncated mode					
11							
- - -			- - -				

*Suspected typo error

TABLE 5. PERCENT FREQUENCY ERRORS WITH 20 ELASTIC DEGREES OF FREEDOM
TWO COMPONENT TRUSS PROBLEM

ELASTIC MODE NO.	NASTRAN CASE				REF. 4 RESULTS		
	3 Free Modes	4 Free w/I.R.	7 Cant. Modes	8 Cant. w/I.R.	Free w/I.R.	Hurty (Cant. Modes)	Cant. w/I.R.
1	8.92	.00034	.00043	.00034	.000017	.00074	9×10^{-9}
2	1.21	.00902	.0017	0	.000061	.0018	3×10^{-6}
3	7.67	.0135	.0098	.0061	.0138	.0096	.00584
4	1.08	.00023	.0096	.00002	.00024	.0092	.00002
5	6.00	.00083	.033	0	.00081	.034	.0014
6	0.85	.0020	.0098	.00060	.0020	.0103	.00054
7	0.61	.080	.947	.268	.083	.941	.264
8	1.58	.0071	.122	.021	.0068	.117	.018
9	.084	.00098	.59	.54	.00093	.80	.69
10	.030	.0041	.36	.40	.0045	.20	.25
11	.90	.021	.33	.98	.022	.30	1.03
12	3.30	.428	.49	12.3	.134	.28	11.1
13	4.01	5.35	.16		5.33	.14	
14	.244	7.87	.77		7.15	.72	
15	1.10		2.37			2.63	
16	-.59		12.15			11.4	
17	6.69						

indicates freq. of first truncated mode

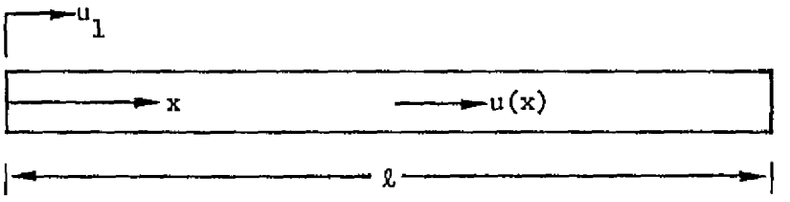

(a) Basic Definition

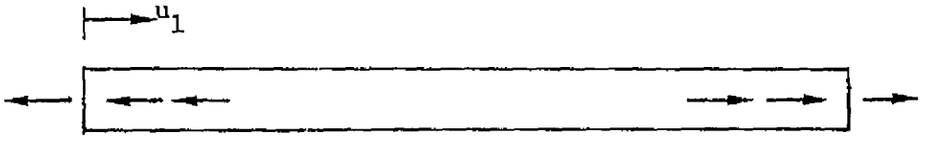

(b) Component Modes (Free) $\phi = \cos \frac{n\pi x}{\ell}$

(c) Solution Modes $\phi = \sin \frac{(2n - 1)\pi x}{2\ell}$

FIGURE 1. EXACT ROD PROBLEM

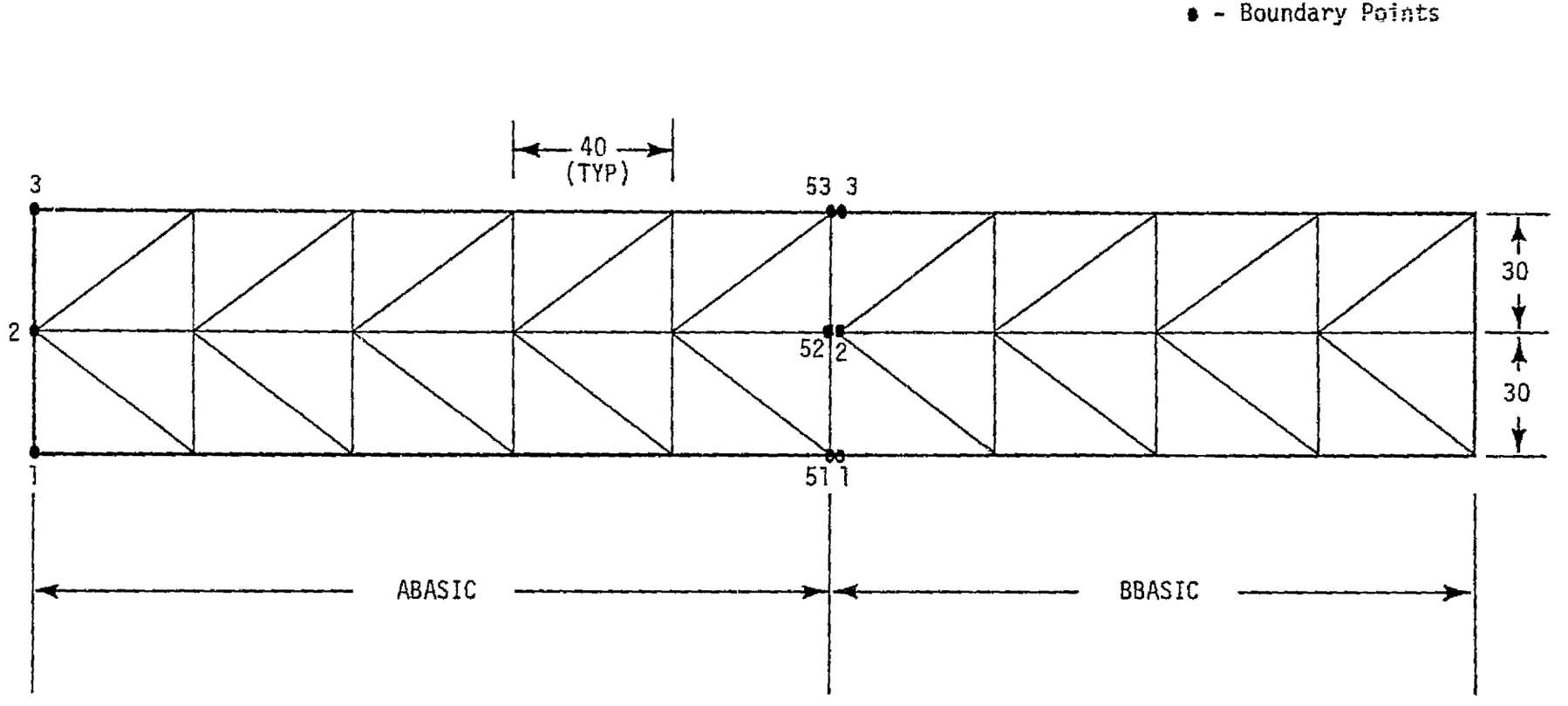

Figure 2. Nine-cell truss basic substructures.

D24

N78-32490

ON THE APPEND AND CONTINUE FEATURES IN NASTRAN

P. R. Pamidi
Computer Sciences Corporation

SUMMARY

This paper describes two very important and useful features available in Level 17.0 version of NASTRAN. The first one is the APPEND feature which is applicable in the case of real eigenvalue analysis. This feature permits the addition of new eigenvalues and eigenvectors to those already computed in a previously checkpointed run without re-executing the entire problem. The second feature is the CONTINUE feature which is applicable in the case of transient analysis of coupled equations. This feature enables the integration of coupled equations to be continued beyond the last (or from any earlier intermediate) output time for which the solution was obtained in a previously checkpointed run (without re-executing the entire problem). The paper illustrates the use of these two features by suitable examples.

INTRODUCTION

The checkpoint/restart feature available in NASTRAN is a very useful capability that permits the restarting of previously checkpointed runs without re-executing the entire problem. The modules that need to be executed on restart are determined by the nature of modifications made to the checkpointed data by the user upon restart. Depending on these modifications, four types of restarts may be identified. These are the Unmodified Restart, Modified Restart, Rigid Format Switch and Pseudo Modified Restart. The details of these restarts are discussed in Reference 1. It is to be noted, however, that the user does not explicitly specify the type of restart. It is implied and automatically determined by the changes made to the NASTRAN data deck upon restart.

It is important to note that a restart only determines the modules that need to be executed during the current run. A restart does not, in general, affect the logic of execution within a given module. There are, however, two important exceptions to this. These are the APPEND and CONTINUE features available in Level 17.0 version of NASTRAN. These are discussed in detail in the following sections.

THE APPEND FEATURE

In real eigenvalue analysis, it is frequently necessary to add new eigenvalues and eigenvectors to those already computed in a previous run. The APPEND feature available in Level 17.0 version of NASTRAN makes it possible to do this

without re-executing the entire problem. It is available only when using the Inverse Power, Determinant and Tridiagonal Reduction (FEER) methods of eigenvalue extraction in Rigid Formats 3, 10, 11, 12, 13 and 15 (Displacement approach) and in Rigids Formats 10 and 11 (Aeroelastic approach). This feature is particularly valuable in the case of large order eigenvalue problems.

In order to use the APPEND feature, the user first requests a checkpoint of an eigenvalue problem employing one of the three above-mentioned methods of eigenvalue extraction. This run can terminate for any reason so long as the READ (Real Eigenvalue Analysis-Displacement approach) module finds at least one eigenvalue and one eigenvector and the LAMA (eigenvalue) and PHIA (eigenvector) files are successfully checkpointed. The READ module also sets the parameter NEIGV to be equal to the number of eigenvalues and eigenvectors found on this checkpoint run.

The user then restarts and activates the APPEND feature by changing either the METHØD card in the Case Control Deck and/or the EIGR card in the Bulk Data Deck so as to force the re-execution of the READ module. The method of eigenvalue extraction used in the restart need not be the same as that used in the checkpoint run, but the structural model and the constraint data must be the same. Also, the user must ensure that the range of eigenvalues specified on the EIGR Bulk Data card for the restart does not include the eigenvalues that have previously been found and checkpointed. It is left to the user to satisfy this requirement. The program does not check for this condition.

The APPEND feature causes the READ module to retrieve the eigenvalues and eigenvectors from the previously checkpointed LAMA and PHIA files, respectively, (this retrieval is done in subroutine READ7 within the READ module; the number of eigenvalues and eigenvectors retrieved is indicated by a user information message) and to subsequently combine them with the newly computed results. This is shown schematically by the flow diagram in Figure 1. The eigenvalues and eigenvectors output by the restart include those previously checkpointed. Also, the resulting eigenvectors are normalized according to the method of normalization specified in the restart.

In certain cases of restart, the user may not be interested in retrieving all the NEIGV eigenvalues and eigenvectors found on a checkpoint run. In such cases, the user may retrieve only the first n (n < NEIGV) eigenvalues and eigenvectors from the LAMA and PHIA files, respectively, by resetting the parameter NEIGV in the restart to be equal to n (this capability is not available in Level 17.0, but will be in Level 17.5.) by means of a PARAM statement just before the READ module in the DMAP sequence. This is done by means of a DMAP alter in the Executive Control Deck of the restart.

THE CONTINUE FEATURE

In transient analysis, it is frequently necessary to continue the integration of the coupled equations beyond the last (or from any earlier intermediate) output time for which the solution was obtained in a previous run. Thus, the initial time for the new run is to be a specified output time of the previous

run. Also, the displacements, velocities and accelerations corresponding to the specified output time of the previous run are to be used as the initial conditions for the new run. The CONTINUE feature available in Level 17.0 version of NASTRAN makes it possible to do this without re-executing the entire problem. It is available in both Rigid Formats 9 and 12 (Displacement approach). This feature can be particularly valuable in the case of large order transient analysis problems involving extended integrations.

In order to use the CONTINUE feature, the user first requests a checkpoint of a coupled transient analysis problem in the normal manner. This run can terminate for any reason so long as the TRD (Transient Analysis-Displacement approach) module computes the solution for at least one output time and the UDVT (displacement-velocity-acceleration) file is successfully checkpointed. The TØL (list of output times) file would have been previously checkpointed subsequent to the execution of the TRLG (Transient Load Generator) module. The TRD module also sets the parameter NCØL to be equal to the number of output time steps (which is also equal to one-third the number of columns in the UDVT matrix) in the checkpoint run.

The user then restarts and activates the CONTINUE feature by changing any one or more of several cards either in the Case Control Deck (DLØAD, NØNLINEAR, TSTEP cards) and/or in the Bulk Data Deck (TSTEP, DAREA, DLØAD, FØRCE, etc.) that define either the dynamic loading and/or the time step selection. This forces the re-execution of both the TRLG and TRD modules. The dynamic loading and/or the time step selection in the restart need <u>not</u> be the same as that used in the checkpoint run, but the structural model and the constraint data <u>must</u> be the same.

The CONTINUE feature causes the integration of the coupled equations to continue from a specific initial time. For normal restarts (in which the checkpointed value of the parameter NCØL is automatically used), this initial time is the last output time of the checkpoint run. However, in certain cases, the user may wish to restart the integration from an intermediate (rather than from the last) output time of the checkpoint run. In such cases, the user should reset the parameter NCØL to correspond to the desired intermediate output time by means of a PARAM statement just before the TRLG module in the DMAP sequence. This is done by means of a DMAP alter in the Executive Control Deck of the restart.

The output of the restart does <u>not</u> include the solutions of the checkpoint run, but <u>only</u> those solutions that are computed by the restart. Also, any initial conditions specified in the restart data are ignored since the solution is continued by using the displacements, velocities and accelerations corresponding to the specified output time of the checkpoint run as initial conditions for the restart.

The first displacement $\{u_1\}$ of the restart (or CONTINUEd run) is given by

$$[D]\{u_1\} = \frac{1}{3}\{P_{-1} + P_0 + P_1\} + \{N_0\} + [C]\{u_n\} + [E]\{u_{-1}\} \quad , \quad (1)$$

where the matrices [D], [C] and [E] are given by

$$[D] = \left(\frac{1}{\Delta t^2}[M] + \frac{1}{2\Delta t}[B] + \frac{1}{3}[K]\right) \quad , \tag{2}$$

$$[C] = \left(\frac{2}{\Delta t^2}[M] - \frac{1}{3}[K]\right) \quad , \tag{3}$$

and

$$[E] = \left[\frac{-1}{\Delta t^2}[M] + \frac{1}{2\Delta t}[B] - \frac{1}{3}[K]\right] \quad , \tag{4}$$

and

$$\{P_0\} = [K]\{u_n\} + [B]\{\dot{u}_n\} + [M]\{\ddot{u}_n\} \quad , \tag{5}$$

$$\{u_{-1}\} = \{u_n\} - \Delta t\{\dot{u}_n\} + \frac{\Delta t^2}{2}\{U_n\} \quad , \tag{6}$$

$$\{\dot{u}_{-1}\} = \{\dot{u}_n\} - \{\ddot{u}_n\}\Delta t \quad , \tag{7}$$

$$\{P_{-1}\} = [M]\{\ddot{u}_n\} + [B]\{\dot{u}_{-1}\} + [K]\{u_{-1}\} \quad . \tag{8}$$

In the above equations, [M], [B] and [K] are the mass, damping and stiffness matrices, respectively; $\{u_n\}$, $\{\dot{u}_n\}$ and $\{U_n\}$ are the displacements, velocities and accelerations, respectively, at the specified output time t_n of the checkpoint run, and Δt is the initial time step for the restart. $\{P_1\}$ is the load at time $t = t_n + \Delta t$ and $\{N_0\}$ is the initial non-linear load.

The assumptions represented by Equations (6) through (8) introduce errors in the restart. These inherent errors may be minimized by selecting the initial time step in the restart to be the same as the time step used in the checkpoint run just before the restart.

EXAMPLES

In order to illustrate the use of the APPEND and CONTINUE features discussed above, two examples were selected. Example 1 is the analysis of the transverse vibrations of a 10-cell beam. The finite element model used is shown in Figure 2. Example 2 is the transient analysis of a 1000-cell string (travelling wave problem). This is the same as NASTRAN Demonstration Problem No. 9-2-1 (Reference 2). The finite element model used is shown in Figure 3. Both these problems were run on the CDC CYBER computer using a post-Level 17.0 version of NASTRAN.

Discussion of Example 1

All the twenty (20) natural frequencies of the model of Example 1 were first computed. These are listed in Table 1 to facilitate comparison with subsequent results. In order to illustrate the use of the APPEND feature, a checkpoint run was then made using the Inverse Power method and the first eight modes were computed. These are presented in Table 2. Using the results of this checkpoint run, restarts were then made under various conditions using different extraction methods. The results obtained are presented in Table 3. As can be seen, all these restarts involve the retrieval of the eight modes of the checkpoint run of Table 2.

Discussion of Example 2

A transient analysis of the model of Example 2 was first made using twenty (20) time steps. (All runs for this example were made on Rigid Format 9 using time steps of 0.0005 seconds.) The displacements for point 10 are listed in Table 4 to facilitate comparison with subsequent results. In order to illustrate the CONTINUE feature, a checkpoint run was then made using only ten (10) time steps. The displacements for point 10 obtained in this run are presented in Table 5. As can be seen, these results are merely a subset of those in Table 4. The integration of Table 5 was then CONTINUEd for ten (10) more time steps by restarting from the last output time in Table 5 (0.005 second). The results are presented in Table 6. In order to illustrate the resetting of the parameter NCØL, an additional restart was made by changing the value of NCØL to 6 (from its original value of 11) and the integration of Table 5 was CONTINUEd for fifteen (15) more time steps. This thus involved starting from an initial time of 0.0025 second. The results of this run are shown in Table 7. A comparison of the results of Tables 6 and 7 with the corresponding results in Table 4 reveals the inherent errors caused by the CONTINUE feature.

SUMMARY AND CONCLUSIONS

Two very important and useful features available in Level 17.0 version of NASTRAN have been described. The first one is the APPEND feature which is applicable in the case of real eigenvalue analysis. This feature permits the addition of new eigenvalues and eigenvectors to those already computed in a previously checkpointed run without re-executing the entire problem. The second feature is the CONTINUE feature which is applicable in the case of transient analysis of coupled equations. This enables the integration of coupled equations to be continued beyond the last (or from any earlier intermediate) output time for which the solution was obtained in a previously checkpointed run (without re-executing the entire problem). The use of these two features has been illustrated by means of two suitable examples.

REFERENCES

1. The NASTRAN User's Manual, (Level 16.0), NASA SP-222(03), March 1976.

2. The NASTRAN Demonstration Problem Manual, (Level 16.0), NASA SP-224(03), March 1976.

Table 1. Results for Example 1
(using Givens method)

Mode no.	Natural frequency (Hz)
1	1.591560E-02
2	6.366879E-02
3	1.433160E-01
4	2.550698E-01
5	3.994578E-01
6	5.775080E-01
7	7.909161E-01
8	1.042057E+00
9	1.332764E+00
10	1.766489E+00
11	2.091890E+00
12	2.549921E+00
13	3.086530E+00
14	3.712652E+00
15	4.440216E+00
16	5.273030E+00
17	6.187597E+00
18	7.097013E+00
19	7.814544E+00
20	8.095071E+00

Table 2. Results of Checkpoint Run of Example 1
(using Inverse Power method)

Mode no. in Table 1	Natural frequency (Hz)
1	1.591560E-02
2	6.366879E-02
3	1.433160E-01
4	2.550698E-01
5	3.994578E-01
6	5.775080E-01
7	7.909161E-01
8	1.042057E+00
Eigenvalue extraction data	
F1 = 0.0 Hz	NE = 8
F2 = 1.2 Hz	ND = 8

Table 3. Results of Restart Runs of Example 1 Using Checkpoint Run of Table 2

Inverse Power method		Determinant method		Tridiagonal Reduction (FEER) method		Remarks
Mode no. in Table 1	Natural frequency (Hz)	Mode no. in Table 1	Natural frequency (Hz)	Mode no. in Table 1	Natural frequency (Hz)	
1	1.591560E-02	1	1.591560E-02	1	1.591560E-02	Results retrieved from the checkpoint run of Table 2
2	6.366879E-02	2	6.366879E-02	2	6.366879E-02	
3	1.433160E-01	3	1.433160E-01	3	1.433160E-01	
4	2.550698E-01	4	2.550698E-01	4	2.550698E-01	
5	3.994578E-01	5	3.994578E-01	5	3.994578E-01	
6	5.775080E-01	6	5.775080E-01	6	5.775080E-01	
7	7.909161E-01	7	7.909161E-01	7	7.909161E-01	
8	1.042057E+00	8	1.042057E+00	8	1.042057E+00	
12	2.549921E+00	10	1.766489E+00	9	1.332764E+00	Results computed by the method selected
13	3.086530E+00	11	2.091890E+00	10	1.766489E+00	
14	3.712652E+00	12	2.549921E+00	11	2.091890E+00	
15	4.440216E+00	13	3.086530E+00	12	2.549921E+00	
16	5.273030E+00	14	3.712652E+00	13	3.086530E+00	
17	6.187597E+00	15	4.440216E+00	14	3.712652E+00	
18	7.097013E+00			15	4.440216E+00	
19	7.814544E+00			16	5.273030E+00	
				17	6.187597E+00	
				18	7.097013E+00	
				19	7.814544E+00	
				20	8.095071E+00	
Eigenvalue extraction data						
F1 = 3.0 Hz NE = 8 F2 = 9.0 Hz ND = 16		F1 = 2.0 Hz NE = 6 F2 = 6.0 Hz ND = 14		F1 = 5.0 Hz ND = 11		

Table 4. Results for Example 2

Time (sec.)	Time step no.	Displacement of Point 10
0.0	1	1.800000E+00
0.0005	2	1.797927E+00
0.0010	3	1.787102E+00
0.0015	4	1.755303E+00
0.0020	5	1.690605E+00
0.0025	6	1.589987E+00
0.0030	7	1.464497E+00
0.0035	8	1.334881E+00
0.0040	9	1.220342E+00
0.0045	10	1.127921E+00
0.0050	11	1.049639E+00
0.0055	12	9.691645E-01
0.0060	13	8.733444E-01
0.0065	14	7.607323E-01
0.0070	15	6.416159E-01
0.0075	16	5.300468E-01
0.0080	17	4.338371E-01
0.0085	18	3.495874E-01
0.0090	19	2.659541E-01
0.0095	20	1.724413E-01
0.0100	21	6.725148E-02

Table 5. Results of Checkpoint Run of Example 2

Time (sec.)	Time step no. of Table 4	Displacement of Point 10
0.0	1	1.800000E+00
0.0005	2	1.797927E+00
0.0010	3	1.787102E+00
0.0015	4	1.755303E+00
0.0020	5	1.690605E+00
0.0025	6	1.589987E+00
0.0030	7	1.464497E+00
0.0035	8	1.334881E+00
0.0040	9	1.220342E+00
0.00	10	1.127921E+00
0.00	11	1.049639E+00

Table 6. Results of Restart Run of Example 2 Using Checkpoint Run of Table 5

Time (sec.)	Time step no. of Table 4	Displacement of Point 10
0.0050	11	1.049639E+00
0.0055	12	9.644270E-01
0.0060	13	8.673986E-01
0.0065	14	7.575025E-01
0.0070	15	6.432689E-01
0.0075	16	5.357538E-01
0.0080	17	4.405755E-01
0.0085	18	3.543471E-01
0.0090	19	2.677839E-01
0.0095	20	1.729413E-01
0.0100	21	6.924284E-02

Table 7. Results of Restart Run of Example 2 Using Checkpoint Run of Table 5 and With Parameter NCØL Reset to 6

Time (sec.)	Time step no. of Table 4	Displacement of Point 10
0.0025	6	1.589987E+00
0.0030	7	1.470335E+00
0.0035	8	1.344651E+00
0.0040	9	1.229273E+00
0.0045	10	1.132560E+00
0.0050	11	1.049933E+00
0.0055	12	9.681384E-01
0.0060	13	8.746610E-01
0.0065	14	7.659208E-01
0.0070	15	6.489350E-01
0.0075	16	5.357538E-01
0.0080	17	4.349093E-01
0.0085	18	3.459289E-01
0.0090	19	2.605215E-01
0.0095	20	1.692299E-01
0.0100	21	6.859591E-02

ORGANIZATION OF DYNAMIC ANALYSIS

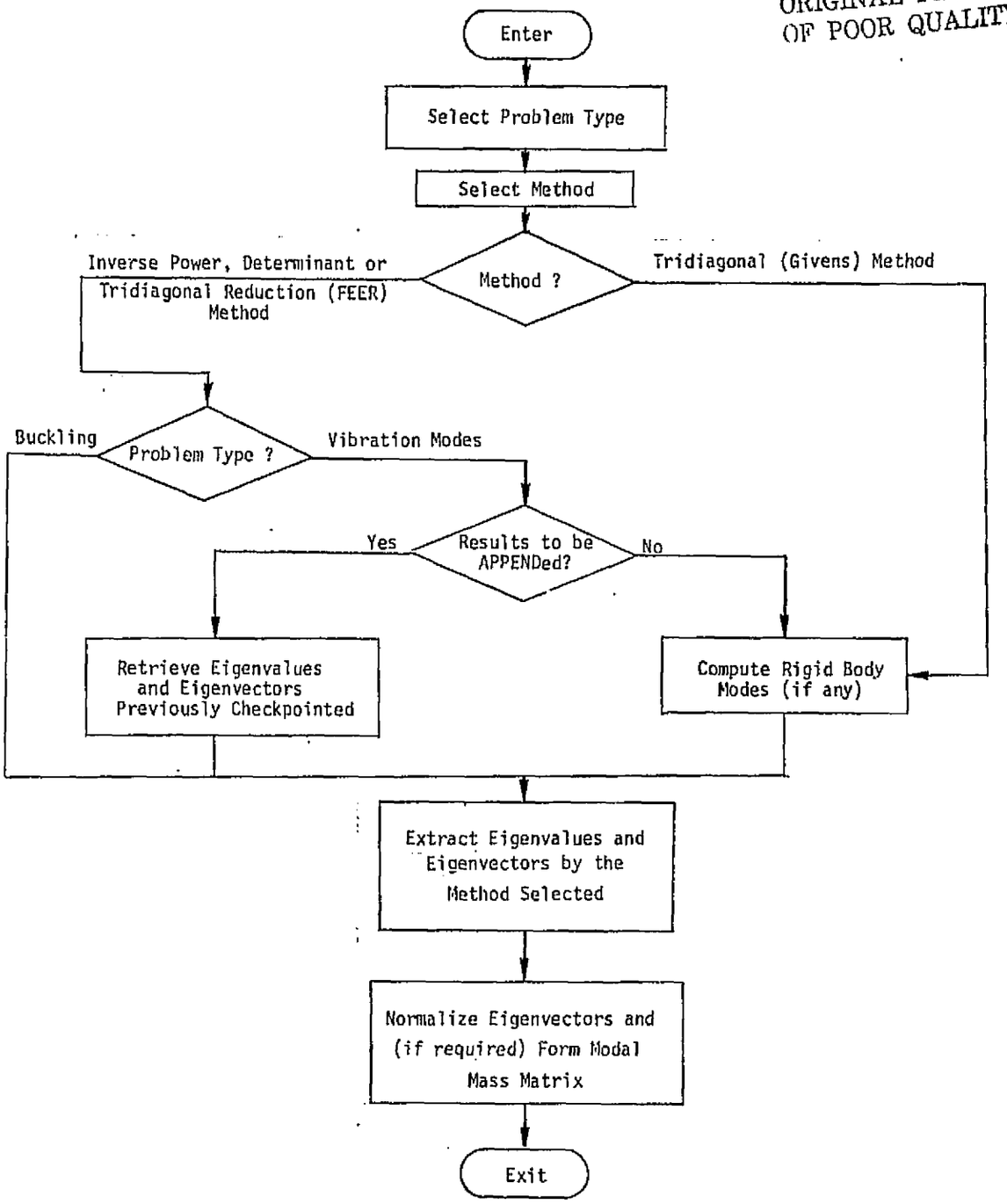

Figure 1. Flow Diagram for the Real Eigenvalue Analysis Module, READ.

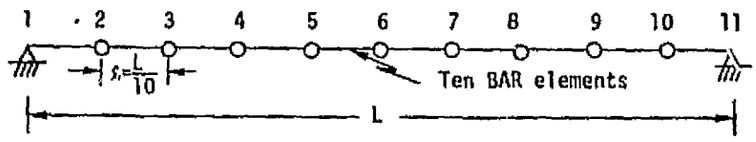

Parameters:

Length of each BAR element = $\ell = \frac{L}{10}$ = 1000.0 in. (25.4 m)

Young's modulus = Shear modulus = 1.0×10^7 psi (6.89477×10^{10} N/m^2)

Mass density = 0.9869604 lb.-sec^2/in.^{4} (1.05475×10^7 Kg/m^3)

Area of cross section of each BAR element = 9.869604 in.^{2}
= 6.36747×10^{-3} m^2

Area moments of inertia = 1.0×10^6 in.^{4}
= 0.41623 m^4

Figure 2. Representation of 10-Cell Beam of Example 1

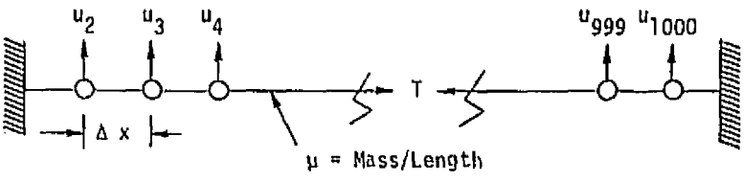

1000-Cell String

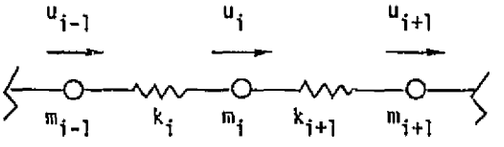

Finite Element Model

Parameters:

$k_i = \frac{T}{\Delta x} = 10^7$ (stiffness units) for all i

$m_i = \mu \Delta x = 10$ (mass units) for all i

Loading:

The initial displacements are given by:

$u_i = 0.2\ (i-1)$ for $2 \leq i \leq 11$

$u_i = 0.2\ (21-i)$ for $11 \leq i \leq 21$

and

$u_i = 0.0$ for $i \geq 21$

Figure 3. Representation of 1000-Cell String of Example 2

D25

N78-32491

EXTENSION OF THE TRIDIAGONAL REDUCTION (FEER) METHOD FOR COMPLEX EIGENVALUE PROBLEMS IN NASTRAN

Malcolm Newman*
Inter-City Testing & Consulting Corp.

and

Frederick I. Mann*
Business and Technological Systems, Inc.

SUMMARY

An extension of the Tridiagonal Reduction (FEER) method in Level 17 of NASTRAN for complex eigenvalue analysis is described. As in the case of real eigenvalue analysis, the eigensolutions closest to a selected point in the eigenspectrum are extracted from a reduced, symmetric, tridiagonal eigenmatrix whose order is much lower than that of the full-size problem. The reduction process is effected automatically, and thus avoids the arbitrary lumping of masses and other physical quantities at selected grid points. The statement of the algebraic eigenvalue problem admits mass, damping and stiffness matrices which are unrestricted in character, i.e., they may be real, symmetric or unsymmetric, singular or nonsingular.

The basic concepts underlying the method are summarized and special features, such as the estimation of errors and default modes of operation are discussed. In addition, the new user-information and error messages, and optional diagnostic output relating to the complex Tridiagonal Reduction method, are presented.

Some numerical results and initial experiences relating to usage in the NASTRAN environment are provided, including comparisons with other existing NASTRAN methods for complex eigenvalue extraction.

INTRODUCTION

The complex Tridiagonal Reduction method is an extension of the FEER algorithm (Fast Eigenvalue Extraction Routine) for real eigenvalue analysis to

---

*Formerly with Analytical Mechanics Associates, Inc.

H18

PAGE 17 INTENTIONALLY BLANK

complex, algebraic eigenproblem formulations. A specified number of eigenvalues lying closest to a selected point in the complex plane are sought, as well as the associated eigenvectors. As in the case of real eigenvalue analysis (ref. 1), these eigensolutions are extracted from a symmetric, tridiagonal eigenmatrix whose order is much lower than that of the full-size problem. In fact, the size of this canonical, reduced matrix is of the same order of magnitude as the number of desired roots, even if the discretized system model possesses thousands of degrees of freedom. The reduction process is carried out via an automatic algorithm requiring a finite number of steps. Thus, a basic weakness of methods requiring the lumping of masses and other physical quantities at arbitrarily selected degrees of freedom (refs. 2-4) is avoided in reducing the problem size.

With regard to computational speed, the complex Tridiagonal Reduction method is somewhat slower than the Hessenberg method (refs. 5 and 6) for small problems (on the order of one hundred or less degrees of freedom), if all the existing eigensolutions are to be calculated. However, it becomes more efficient than the Hessenberg method when the number of requested eigensolutions is much less than the full problem size. Moreover, for much larger problems, the central memory requirement of the Hessenberg method exceeds the capabilities of most large computers, so that it becomes unavailable as a solution option. This limitation does not exist in the case of the Tridiagonal Reduction Method.

The complex Tridiagonal Reduction method employs a single initial shift point, and hence only one matrix decomposition is required for each neighborhood chosen in the complex plane. It therefore is more efficient than the complex Inverse Power method, which typically performs many shifts and decompositions for each region selected. In addition, both the complex Inverse Power method and the complex Determinant method require that the user supply the length and width of rectangular regions in the complex plane, within which the eigenvalues are desired, as well as the number of estimated roots in each region. This can be burdensome to the user, who usually does not have enough advance insight to select these parameters intelligently. An improper choice (e.g., a strip too wide, or too small an estimate on the number of roots within the strip) can lead to an inordinately large number of computations or failure to extract any roots at all within the allotted machine time. These disadvantages are eliminated in the complex FEER method, where the user is only required to select points, closest to which a specified number of eigensolutions are desired.

The theory and computational procedures for complex analysis depart from those of real analysis in the following major respects:

1. Both left and right bi-orthogonal vectors must be created in the process of constructing the reduced tridiagonal matrix.

2. The reduced tridiagonal matrix, while symmetric in form, is, in general, complex rather than real.

3. The calculated theoretical errors in the computed eigenvalues are estimates rather than upper bounds.

4. Eigensolutions closest to one or more specified points (shift points) in the complex plane are found. All eigensolutions obtained for previous shift points are swept out of the problem to prevent their regeneration when dealing with the current shift point.

AN OVERVIEW OF THE COMPLEX TRIDIAGONAL REDUCTION METHOD

A detailed development of the analytical and computational procedures, including programming aspects and flow charts can be found in the NASTRAN Level 17 Theoretical and Programmer's Manuals. The following is a summary of the basic features of the complex Tridiagonal Reduction Scheme.

The general complex eigenvalue problem is stated in the form

$$[Mp^2 + Bp + K]\{u\} = 0 \ , \tag{1}$$

where [M], [B], and [K] may be real, complex, symmetric or unsymmetric, singular or non-singular. A specified number of eigenvalues, p , lying closest to a specified point, λ_o , (called a shift point) in the complex plane are to be found, as well as the associated eigenvectors {u} . The eigenvalues may include multiplicities. By a suitable transformation, the above can be expressed in the standard inverse form,

$$[A]\{x\} = \Lambda\{x\} \ , \tag{2}$$

where [A] is double the size of the stiffness, mass and damping matrices, and

$$\Lambda = \frac{1}{p-\lambda_o} \ . \tag{3}$$

In the special case where [B] is null (e.g., no damping), the double-size eigenvalue problem can be avoided by considering the mathematical eigenvalues to be p^2 and defining

$$\Lambda = \frac{1}{p^2-\lambda_o^2} \tag{4}$$

in equation (2).

Since the eigenmatrix, [A] , is, in general, unsymmetric, the eigenvectors, {x} , are orthogonal to the eigenvectors, $\{\bar{x}\}$, of the transpose eigenproblem

$$[A]^T\{\bar{x}\} = \Lambda\{\bar{x}\} \ , \tag{5}$$

so that for $\Lambda_i \neq \Lambda_j$,

$$\{\bar{x}_j\}^T\{x_i\} = 0; \ i \neq j \ . \tag{6}$$

The above relationship is a biorthogonality condition and the associated eigenvectors, $\{x_i\}$ and $\{\bar{x}_j\}$, are called right and left eigenvectors, respectively.

A reduction of the order of the eigenvalue problem, equation (2), is effected through the transformation

$$\underset{nx1}{\{\hat{x}\}} = \underset{nxm}{[V]} \underset{mx1}{\{y\}} , \tag{7a}$$

and

$$\underset{nx1}{\{\hat{\bar{x}}\}} = \underset{nxm}{[\bar{\bar{V}}]} \underset{mx1}{\{\bar{\bar{y}}\}} , \tag{7b}$$

where $\{\hat{x}\}$ and $\{\hat{\bar{x}}\}$ are approximations of $\{x\}$ and $\{\bar{\bar{x}}\}$, respectively, n is the order of the unreduced problem, and $m \leq n$. The above transformation matrices are chosen to be biorthonormal, so that

$$[\bar{\bar{V}}]^T[V] = [I] . \tag{8}$$

From equations (2), (7), and (8), it is seen that

$$[H]\{y\} = \bar{\Lambda}\{y\} , \tag{9}$$

where

$$\underset{mxm}{[H]} = [\bar{\bar{V}}]^T[A][V] , \tag{10}$$

and $\bar{\Lambda}$ is an approximation of the eigenvalue, Λ.

Thus, equation (9) is an mth order eigenvalue problem, where $m \leq n$. The value of m is established according to the criteria given later.

As in the case of real eigenvalue analysis (ref. 1), the Lanczos algorithm is used to construct the transformation matrices vector by vector, i.e.,

$$\underset{nxm}{[V]} = [\{v_1\}, \{v_2\}, \ldots, \{v_m\}] , \tag{11a}$$

$$\underset{nxm}{[\bar{\bar{V}}]} = [\{\bar{\bar{v}}_1\}, \{\bar{\bar{v}}_2\}, \ldots, \{\bar{\bar{v}}_m\}] , \tag{11b}$$

such that the reduced mxm matrix, $[H]$, is tridiagonal and its eigenvalues accurately approximate the roots of equation (2) having the largest magnitude (or, equivalently, the physical roots, p, closest to the specified point of interest, λ_o, in the complex plane). Using symmetry arguments similar to those employed for real eigenvalue analysis, it can be shown that the transformed, reduced eigenmatrix in equation (9) is tridiagonal and symmetric, having the form,

$$[H] = [\bar{\bar{V}}]^T[A][V] = \begin{bmatrix} a_{11} & d_2 & & & \\ d_2 & a_{22} & d_3 & & \\ & d_3 & a_{33} & d_4 & \\ & & \ddots & \ddots & d_m \\ & & & d_m & a_{mm} \end{bmatrix} \tag{12}$$

The matrix coefficients are theoretically given by the simplified recurrence formulas

$$\left.\begin{aligned} a_{i,i} &= \{\bar{\bar{v}}_i\}^T[A]\{v_i\} \\ \{w_{i+1}\} &= [A]\{v_i\} - a_{i,i}\{v_i\} - d_i\{v_{i-1}\} \\ \{\bar{\bar{w}}_{i+1}\} &= [A]^T\{\bar{\bar{v}}_i\} - a_{i,i}\{\bar{\bar{v}}_i\} - d_i\{\bar{\bar{v}}_{i-1}\} \\ d_{i+1} &= [\{\bar{\bar{w}}_{i+1}\}^T\{w_{i+1}\}]^{1/2} \end{aligned}\right\} \quad i = 1,m \tag{13a}$$

$$\left.\begin{aligned} \{v_{i+1}\} &= \frac{1}{d_{i+1}}\{w_{i+1}\} \\ \{\bar{\bar{v}}_{i+1}\} &= \frac{1}{d_{i+1}}\{\bar{\bar{w}}_{i+1}\} \end{aligned}\right\} \quad i = 1, m-1 \tag{13b}$$

where the sequence is initialized by choosing random, biorthonormal starting vectors for $\{v_1\}$, $\{\bar{\bar{v}}_1\}$ and by setting $d_1=0; \{v_o\}=\{\bar{\bar{v}}_o\}=\{0\}$.

The final off-diagonal term, d_{m+1} , given by equations (13) is used in establishing error estimates for the computed eigenvalues, as described below. In addition, the above algorithm is modified in the computational scheme as follows:

1. Each pair of vectors $\{v_{i+1}\}$, $\{\bar{\bar{v}}_{i+1}\}$, calculated in equations (13b), is reorthogonalized to all previously computed pairs, before re-entering equations (13a).

2. The size, m , of the reduced problem is a function of the number of accurate eigenvalues requested by the user and is limited to the number of finite physical eigenvalues available.

The eigenvalues, $\bar{\lambda}$, and eigenvectors, $\{y\}$, of equation (9) are extracted using the Q-R iteration algorithm and eigenvector computational scheme described in connection with the Upper Hessenberg method in NASTRAN (ref. 5). They are then converted to physical form.

CRITERIA FOR THE SIZE OF THE REDUCED EIGENVALUE PROBLEM

The maximum number of finite eigensolutions, including any existing rigid body modes, is equal to the rank, r, of the eigenmatrix, [A], in equation (2). Thus, for example, massless degrees of freedom, appearing as zero diagonal terms in the [M] matrix, will result in singularities (rank reduction), which imply infinite physical eigenvalues. These spurious roots are swept out of the problem in the complex FEER process, with a consequent reduction in the available eigensolutions.

A further consideration in limiting the maximum problem size is that the user has the option of requesting eigensolutions in the neighborhood of several shift points $(\lambda_{01},\lambda_{02},\ldots)$ in the complex plane. In the Tridiagonal Reduction method, all eigensolutions, f, obtained for previous shift points are swept out of the problem to prevent their re-genera ion when dealing with the current shift point. This implies that the maximum possible size, m, of the reduced problem is further limited to

$$m_{max} = r - f \quad . \tag{14}$$

On the basis of numerical experiments, similar to those cited in reference 1 for real eigenvalue analysis, it has been found that when $m << m_{max}$, a first grouping of more than $m/2$ computed eigenvalues closest to the shift point are in accurate agreement with the corresponding number of exact eigenvalues, provided that $7 \leq m \leq m_{max}$. The remaining reduced-system roots are spread across the remaining exact eigenspectrum. To enhance the accuracy of the associated eigenvectors, the minimum problem size is further increased to twelve, again assuming that $m << m_{max}$.

Thus, if the user requests a total of $\bar{q}$ eigenvalues closest to a specified point in the complex plane, the order of the reduced problem is initially set to

$$m \begin{cases} = \min[(2\bar{q}+10),(2n-f)]; & [B] \neq [0] \quad , \qquad (15a) \\ = \min[(2\bar{q}+10),(n-f)]; & [B] = [0] \quad . \qquad (15b) \end{cases}$$

Although the total number of eigensolutions requested should not exceed m_{max}, there is usually no simple way to discern this upper limit in complex eigenvalue problems. However, the reorthogonalization tests are designed to automatically establish this upper limit. If the latter tests fail for some vector pair $\{v_{i+1}\}$, $\{\bar{v}_{i+1}\}$, this is an indication that a null vector has

been generated because m_{max} linearly independent vectors have already been obtained. The recurrence algorithm, equations (13), is then terminated and the order of the eigenproblem is further reduced to $m = i$.

ERROR ESTIMATES FOR THE COMPUTED EIGENVALUES

Following a development similar to that of reference 1 for real eigenvalue analysis, it can be shown that

$$||\Lambda_i| - |\bar{\Lambda}_i|| \approx |d_{m+1} y_{mi}| \quad . \tag{16}$$

The above shows that the absolute value of the difference between the computed and true eigenvalue magnitudes is proportional to the magnitude of d_{m+1} (which is the next off-diagonal term that would be generated had the reduced tridiagonal matrix, [H] , been increased from order m to order $m+1$) and y_{mi} , (which is the last term in the reduced-system eigenvector associated with $\bar{\Lambda}$) .

Converting equation (16) to physical eigenvalue form, using equations (3) and (4), yields,

$$\xi_i = \left| \frac{|\bar{p}_i - \lambda_o|}{|p_i - \lambda_o|} - 1 \right| \approx \frac{|d_{m+1} y_{mi}|}{|\bar{\Lambda}_i|} \quad ; \; [B] \neq [0] \quad , \tag{17a}$$

$$\xi_i = \left| \frac{|\bar{p}_i^2 - \lambda_o^2|}{|p_i^2 - \lambda_o^2|} - 1 \right| \approx \frac{|d_{m+1} y_{mi}|}{|\bar{\Lambda}_i|} \quad ; \; [B] = [0] \quad . \tag{17b}$$

The use of the above error estimates as criteria for acceptable eigensolutions is as follows:

(a) If the physical eigenvalue, $\bar{p}_i$, corresponds to a zero root (e.g., a rigid body mode), the above computational scheme is invalid and therefore bypassed. Denoting t as the number of digits carried in the computations, a zero root is assumed to occur whenever

$$\frac{|\bar{p}_i|}{RMS} < 10^{-t/3} \quad , \tag{18}$$

where

$$RMS = \frac{1}{m} \left[|\bar{p}_1^2| + |\bar{p}_2^2| + \ldots\ldots + |\bar{p}_m^2| \right]^{1/2} \quad , \tag{19}$$

and is denoted by setting the error ξ_i to zero.

(b) The eigenvalues are listed in order of increasing distance from the shift point, λ_o , to determine whether their associated estimated errors, ξ_i , meet an acceptable relative error tolerance set by the user on the EIGC bulk data card (the default value is 0.10/n, where n is the order of the stiffness matrix). The first eigenvalue not meeting the tolerance test, as well as all subsequent eigenvalues further removed from the center of interest, are considered to lack sufficient accuracy and are therefore discarded.

(c) Acceptable eigenvalues obtained in the above manner are reordered according to the magnitude of the imaginary part, with positive values considered as a group ahead of all negative values.

NASTRAN USER'S INSTRUCTIONS

Figure 1 shows modifications of the EIGC card in the NASTRAN bulk data deck which accommodate user implementation of the Tridiagonal Reduction method for complex eigenvalue analysis. The modifications consist of additions to the standard user instructions and are underscored for ease in identification.

When the complex Tridiagonal Reduction method is invoked, the E parameter on this card represents the maximum allowable value of the computed absolute relative error in a physical eigenvalue. If this value is exceeded, the associated eigensolution is not accepted for further processing by NASTRAN. A detailed list of the maximum relative errors computed by complex FEER can be obtained by requesting DIAG 12 in the NASTRAN Executive Control Deck.

USER MESSAGES AND OPTIONAL DIAGNOSTICS

Functional Module User Messages

The following is a description of the NASTRAN user messages which may be generated by NASTRAN during the execution of the Complex Tridiagonal Reduction method and which are unique to this method. Explanatory information is provided following the text of each message and, in the case of a fatal message, corrective action is indicated. Refer to the NASTRAN Users' Manual, Section 6 for a complete listing of other system and user messages.

Fatal messages cause the termination of the execution following the printing of the message text. These messages will always appear at the end of the NASTRAN output. Warning and information messages will appear at various places in the output stream. Such messages convey only warnings or information to the user. Consequently, the execution continues in a normal manner following the printing of the message text.

3149 *** USER WARNING MESSAGE 3149, USER SPECIFIED NEIGHBØRHØØD CENTERED AT ØRIGIN NØT ALLØWED, CENTER SHIFTED TØ THE RIGHT .001.

Point of interest in the complex plane $(\alpha_{ai},\omega_{ai})$, closest to which the eigenvalues will be computed, was input as (0.0, 0.0) on an EIGC bulk data continuation card. Since this is an inadmissible choice, the point automatically used was (.001, 0.0).

3150 *** USER WARNING MESSAGE 3150, DESIRED NUMBER ØF EIGENVALUES *** INVALID. SET = 1.

Number of accurate roots desired N_{d1} , was omitted, input as zero or negative on an EIGC bulk data continuation card. The number automatically used was 1.

3151 *** USER WARNING MESSAGE 3151, DYNAMIC MATRIX IS SINGULAR (ØCCURRENCE ****) IN NEIGHBØRHØØD CENTERED AT **** ****

Point of interest in the complex plane $(\alpha_{ai},\omega_{ai})$, closest to which the eigenvalues will be computed, was input too close to an eigenvalue on an EIGC bulk data continuation card. The point is automatically shifted by adding .02 to both the real and imaginary parts. If the dynamic matrix is still singular, the next neighborhood, if any, is searched.

3152 *** USER INFØRMATIØN MESSAGE 3152, SUBRØUTINE ALLMAT ØUTPUT EIGENVALUE **** IS NULL.

When an eigenvalue output from subroutine ALLMAT is exactly zero, the formula for computing the associated theoretical error test fails. The magnitude of the eigenvalue is considered to be 10^{-10} for use in that formula.

3153 *** USER WARNING MESSAGE 3153, ATTEMPT TØ NØRMALIZE NULL VECTØR IN SUBRØUTINE CFEER4. NØ ACTION TAKEN.

An eigenvector output from subroutine ALLMAT is a zero-vector.

3154 *** USER WARNING MESSAGE 3154, SIZE ØF REDUCED PRØBLEM DECREMENTED ØNCE (NØW ****) DUE TØ NULL ERRØR ELEMENT.

If subroutine CFEER4 receives a reduced tridiagonal matrix having error element d_{m+1} exactly (0,0), it is impossible to compute meaningful theoretical error estimates for any of the eigenvalues. The size of the reduced problem is reduced by one, so that d_m becomes the new error element.

3155 *** USER WARNING MESSAGE 3155, REDUCED PRØBLEM HAS VANISHED. NØ RØØTS FØUND.

If decrementing the size of the reduced problem (see message 3154) causes the size to become zero, the program continues to the next neighborhood, if any.

3156 *** USER WARNING MESSAGE 3156, SIZE ØF REDUCED PRØBLEM RESTØRED TØ **** BECAUSE NEXT ERRØR ELEMENT WAS ALSØ NULL. ERRØR ELEMENT SET = **** ****

This message follows message 3154. If d_m is also exactly zero (in addition to d_{m+1} being exactly zero), then the original reduced problem size is restored and d_{m+1} is set to $(\varepsilon,0)$ where $\varepsilon = E/100$ and E is the error tolerance on acceptable eigenvalues input on the EIGC bulk data card.

3157 *** USER WARNING MESSAGE 3157, FEER PRØCESS MAY HAVE CALCULATED FEWER ACCURATE MØDES **** THAN REQUESTED IN THE NEIGHBØRHØØD ØF **** ****

The desired number of eigenvalues specified on the EIGC bulk data continuation card exceeds the additional number that can be calculated by the Complex Tridiagonal Reduction (Complex FEER) method in the current neighborhood.

3158 *** USER WARNING MESSAGE 3158, NØ ADDITIØNAL MØDES CAN BE FØUND BY FEER IN THE NEIGHBØRHØØD ØF **** ****

An initial pseudo-random vector cannot be made orthogonal to the existing set of orthogonal vectors (which come from Restart and from all prior-neighborhood sets of eigensolutions).

3159 *** USER INFØRMATIØN MESSAGE 3159, ALL SØLUTIØNS HAVE BEEN FØUND.

The FEER method has solved the entire problem. Any additional neighborhoods (as specified by the presence of EIGC bulk data continuation cards) are ignored.

3160 *** USER INFØRMATION MESSAGE 3160, MINIMUM ØPEN CØRE NØT USED BY FEER **** WØRDS (**** K BYTES).

This message indicates the amount of open core, in both bytes and words, not used by FEER.

3161 *** USER WARNING MESSAGE 3161, DESIRED NUMBER ØF EIGENSØLUTIØNS **** FØR NEIGHBØRHØØD **** ØF **** CENTERED AT **** **** EXCEEDS THE EXISTING NUMBER ****, ALL EIGENSØLUTIØNS WILL BE SØUGHT.

The desired number of eigenvalues specified on the EIGC bulk data continuation card exceeds the size of the eigenmatrix, which is the maximum possible number of existing eigenvalues.

3162 *** USER WARNING MESSAGE 3162, ATTEMPT TØ NØRMALIZE NULL VECTØR. NØ ACTIØN TAKEN.

The general vector normalization routine (CFNØR1 or CFNØR2) has a zero-vector input to it.

3163 *** USER WARNING MESSAGE 3163, ALL **** SØLUTIØNS HAVE FAILED ACCURACY TEST. NØ RØØTS FØUND.

The number of eigensolutions passing the relative error test is zero. The maximum allowable error for the relative error test is specified in field 7 of the EIGC bulk data card. A detailed list of the computed error bounds could have been obtained by requesting DIAG 12 in the Executive Control Deck.

3164 *** USER INFØRMATIØN MESSAGE 3164, ALL **** SØLUTIONS ARE ACCEPTABLE.

All the eigensolutions obtained in the reduced problem corresponding to the point of interest pass the relative error test. The maximum allowable error for the relative error test is specified in field 7 of the EIGC bulk data card. A detailed list of the computed error estimates could have been obtained by requesting DIAG 12 in the Executive Control Deck.

3165 *** USER INFØRMATIØN MESSAGE 3165, **** SØLUTIØNS HAVE BEEN ACCEPTED AND **** SØLUTIØNS HAVE BEEN REJECTED.

Some eigensolutions passed the relative error test and some did not.

3166 *** USER INFØRMATIØN MESSAGE 3166, **** MØRE ACCURATE EIGENSØLUTIØNS THAN THE **** REQUESTED HAVE BEEN FØUND FØR NEIGHBØRHØØD **** ØF **** CENTERED AT **** ****. USE DIAG 12 TØ DETERMINE ERRØR ESTIMATES.

The number of eigensolutions passing the relative error test is greater than the number requested on the corresponding EIGC bulk data continuation card. The maximum allowable error for the relative error test is specified in field 7 of the EIGC bulk data card. A detailed list of the computed error estimates could have been obtained by requesting DIAG 12 in the Executive Control Deck.

The Eigenvalue Summary Table

The following summary of the eigenvalue analysis performed, using the complex Tridiagonal Reduction (FEER) method, is automatically printed:

1. Number of eigenvalues extracted.

2. Number of starting points used.

   This corresponds to the total number of random starting and restart vectors used by the complex FEER process for all neighborhoods.

3. Number of starting point moves.

   Not used in FEER (set equal to zero).

4. Number of triangular decompositions.

   Always equal to the number of points of interest (neighborhoods) in the complex plane processed by FEER, since ordinarily only one triangular decomposition is required by FEER for each point of interest, unless the dynamic matrix is singular at a given point of interest, in which case an additional decomposition is required (obtained by moving the point of interest slightly).

5. Total number of vector iterations.

   The total number of reorthogonalizations of all the trial vectors employed.

6. Reason for termination.

   (0) All, or more solutions than the number requested by the user, have been determined (normal termination).

   (1) All neighborhoods have been processed, but FEER has not obtained the desired number of roots in each neighborhood, possibly because they have already been found in other neighborhoods.

   (2) Abnormal termination - either no roots found or none pass the FEER error test.

Optional Diagnostic Output

The user can obtain special detailed information relating to the generation of the reduced problem size, the elements of the reduced tridiagonal matrix, vector reorthogonalization iterations, computed error estimates, order of eigenvalue extraction, and distance of extracted

eigenvalue from the center of interest by requesting DIAG 12 in the NASTRAN executive control deck.

The meaning of this information is explained below in the order in which it appears in the DIAG 12 output.

****FEER**** (FAST EIGENVALUE EXTRACTIØN RØUTINE)****

This header is always printed first.

****SINGLE PRECISIØN WØRDS ØF ØPEN CØRE NØT USED (SUBRØUTINE XXXX)

**** - Open core not used by subroutine XXXX, in single-precision words.
XXXX - Either CFCNTL, CFEER3, or CFEER4. This message appears three times.

CFCNTL ACCURACY CRITERIØN * (INPUT VALUE**)

* - Accuracy criterion, used for rejecting eigensolutions (expressed as a percentage).
** - Value of accuracy criterion input by the user on the EIGC bulk data card.

CFCNTL NEICHBØRHØØD * CENTER = ** ** NØ.DES.RTS. = *** NØNSYM = ****

* - Positive integer indicating which neighborhood, or center of interest, is currently being processed.
** ** - Center of interest in the complex plane.
*** - Number of desired roots for the current neighborhood, input by the user on the corresponding EIGC bulk data continuation card.
**** - Indicator which, when nonzero, forces the program to consider the matrices as non-symmetric, even though they may actually be symmetric. This is input by the user in field 7 of each EIGC bulk data continuation card. This input was used during program checkout of the complex FEER process, and it should have no affect on the solution. However, the user should leave field 7 blank on each EIGC continuation card.

REØRTHØGØNALIZATIØN ITERATIØN * TARGET VALUE = **
ERRORS = *** *** *** ***

* - The reorthogonalization iteration-number. This message will appear many times, as the FEER process "cleans up" each trial vector by forcing it to be as orthogonal as possible to the set of vectors already computed.
** - Convergence tolerance, such that the errors must be smaller than this value. In order to avoid taking square roots, the tolerance and errors are all squared.
*** *** *** *** - Four reorthogonalization errors, the first two of which correspond to the orthogonality of the current right and left handed trial vectors, respectively, with respect to all

previously computed vectors in the current neighborhood, and the latter two of which correspond to the orthogonality of the same vectors with respect to all eigenvectors previously computed (restart and prior neighborhoods).

```
REDUCED TRIDIAGØNAL MATRIX ELEMENTS RØW *
ØFF DIAGØNAL = ** **
    DIAGØNAL = *** ***
```

*	-	The row number of the (reduced) tridiagonal matrix.
** **	-	Value of the off-diagonal element for that row.
*** ***	-	Value of the diagonal element for that row.

Following the printing of several lines containing reorthogonalization information and reduced tridiagonal matrix elements, when the FEER process has finished its computations for the current point of interest, the header (see above) is printed once again, followed by a table which summarizes all the eigensolutions found by FEER. This table has seven columns, as follows:

(1) Solution number. This is simply a positive integer 1,2,3,... .

(2) Order of extraction. These numbers indicate the order in which the tridiagonal matrix was constructed.

(3) Distance from center. This is the distance from the extracted eigenvalue to the neighborhood center (which is printed above the table) in the complex plane. The tabular values are sorted according to increasing distance from the center.

(4) Real part of the extracted eigenvalue.

(5) Imaginary part of the extracted eigenvalue.

(6) Theoretical error estimate. This value must be smaller than the Accuracy Criterion (see above) for the eigensolution to be acceptable.

(7) Status. A single word, "accept" or "reject", to indicate the result of the accuracy test. A minus sign (-) is added to "reject" so that the eye can more rapidly distinguish between the two words.

Finally, this table is printed a second time, but with the rejected eigensolutions deleted.

For very small problems, there is a Very Detailed Printout (VDP) option. This option was originally used to debug the complex FEER logic, and is no longer required. DIAG 12 must be specified in the executive control deck to invoke the VDP option, and furthermore, field 6 of a given EIGC bulk data continuation card must have a (floating point) value equal to or greater than the size of the stiffness matrix. Thus, field 6 of each EIGC continuation

card should ordinarily be left blank, so that the VDP option will be suppressed. The actual printed output of this option consists of all vectors for each step of the complex FEER process, which is too extensive and detailed for normal user purposes.

NUMERICAL RESULTS AND COMPARISON WITH EXISTING NASTRAN EIGENVALUE METHODS

Test Problem

During the developmental stages of the complex Tridiagonal Reduction method, a simple three degree of freedom model consisting of the rod and dashpot system shown in figure 2, was employed for experimental and check-out purposes. The eigenvalues of this system consist of one complex-conjugate pair, one pure imaginary and three zero roots., the latter corresponding to rigid-body modes.

A comparison of the performance of the complex Tridiagonal Reduction method, the complex Determinant method and the complex Inverse Power method, is summarized for this example in table I. In run 1, all six eigensolutions were successfully found using complex FEER and a single shift point in the second quadrant of the complex plane; only one triangular decomposition of the dynamic matrix was required. In run 2, using the complex Determinant method, 29 triangular decompositions were performed and only two, non-zero, eigenvalues were found, in spite of the fact that multiple search regions were used, including one region encompassing the origin. The reason given for termination in the eigenvalue summary table was that "all predictions for eigenvalues are outside the regions specified", even though this was not the case.

Runs 3-5 were with the complex Inverse Power method, which did not fare too well in this exercise. A large number of iterations were performed, resulting in relatively high CPU and I/O times. In addition, the first run yielded only two roots and the remaining two, none at all, even though the search regions selected, while differing from run to run, encompassed the known eigenvalues.

All the above runs, and those reported below, were performed on the NASA/GSFC IBM 360/95 computer.

Tidal Frequencies and Modes in Closed, Shallow Basins

Concurrent with the complex FEER development, an independent study was conducted (ref. 7) to estimate the tidal frequencies and mode shapes in two of the Great Lakes, namely, Lake Erie and Lake Superior. It was decided to use a finite-element displacement formulation and the complex eigenvalue extraction capabilities in NASTRAN for this purpose. The mathematical modeling was based on the following assumptions:

(a) Negligible convective accelerations and other nonlinear effects.

(b) Inviscid, incompressible flow.

(c) Negligible vertical velocity compared to lateral velocities.

(d) The Boussinesq hypothesis of hydrostatic pressure variations.

(e) Sufficient shallowness to permit integration-averaging through the depth.

As a consequence of the above simplifications, the Navier-Stokes equations reduce to the two-dimensional form,

$$\frac{\partial \bar{u}}{\partial t} + g \frac{\partial \zeta}{\partial x} - f\bar{v} = 0 \tag{20a}$$

$$\frac{\partial \bar{v}}{\partial t} + g \frac{\partial \zeta}{\partial y} + f\bar{u} = 0 \tag{20b}$$

$$\frac{\partial \zeta}{\partial t} + \frac{\partial}{\partial x}(h\bar{u}) + \frac{\partial}{\partial y}(h\bar{v}) = 0 \quad , \tag{20c}$$

where

$\bar{u}, \bar{v}$ = integrated average velocities in the x and y (horizontal) directions
ζ = local water height, measured from the mean surface
h = local depth of water, measured from the mean surface
f = the Coriolis parameter, $2\Omega sin\phi$, with ϕ the latitude, and Ω the earth's rotational rate
g = acceleration due to gravity.

Using the Galerkin method, a finite element representation of the above equations was developed, in which the nodal variables are $\bar{u}$, $\bar{v}$ and ζ . A data-generator code was then written, which generated DMIG card images for use as NASTRAN input.

The two lakes are shown in figures 3 and 4 and their finite-element meshes are given in figures 5 and 6. The mesh of Lake Erie contains 81 nodes and 204 unconstrained degrees of freedom, while the representation of Lake Superior involves 124 nodes and 299 unconstrained degrees of freedom. These selections were based on numerical convergence studies with successively finer meshes, and represent the fineness needed to obtain two or three accurate modes.

In the early stages of the study, the complex Inverse Power method was used, but had to be abandoned because of inconsistencies in the results; the roots obtained seemed to depend on the search region selected and false roots were almost always calculated very close to the starting point in the region. A tightening of the convergence criterion "E" on the EIGC bulk data card was attempted, but this did not resolve the difficulties.

Some limited success was achieved using the complex Determinant method, but here again, difficulties were encountered. Unless the search region could be rather carefully and precisely defined, the chances of finding roots was somewhat remote. The method is apparently quite sensitive in its search pattern, and does not home-in on a root if there is an extensive search area to work on.

At some point approximately mid-way in the study the complex FEER capability was completed and integrated into NASTRAN, whereupon it was applied to the tidal mode problem for the lakes. The results obtained were consistently good. To check their accuracy, changes were made in the shift points, mathematical scaling and the number of requested eigensolutions (i.e., the truncated size of the problem). These variations had only a negligible effect on the calculated frequencies and mode shapes.

Some timing results for Lake Erie, using complex FEER and the Determinant method are given in table II. As noted above, the Determinant method was viable only if the search regions were made very small, implying that the locations of the roots were rather well known in advance.

The Upper Hessenberg method could not be used for these models, since the maximum region available on the IBM 360/95 was 900K, which would only permit a 43 node mesh with this method.

CONCLUDING REMARKS

Initial experiences with the complex Tridiagonal Reduction (FEER) method indicate that it is very effective in extracting any desired number of accurate complex eigensolutions in the neighborhood of a selected shift point on the complex plane. The method automatically computes complex roots at increasing distances from the selected point until the requisite number, specified by the user, is obtained. In this respect, a disadvantage of the complex Determinant and complex Inverse Power methods, namely, a very careful delineation of search regions, is eliminated. In the case of multiple shift points, it has been found that complex FEER successfully sweeps-out eigensolutions obtained for previous shift points and prevents their regeneration when dealing with the current shift point.

Since the mathematical properties and characteristics of complex eigenvalue problems are very broad and varied, it should be recognized that the results reported herein with regard to computational efficiency and timing, are only indicative of a small class of problems. A fuller assessment of the capabilities of this new method can only be obtained following extensive application experiences within the user community.

REFERENCES

1. Newman, M.; and Flanagan, P. F.: Eigenvalue Extraction in NASTRAN by the Tridiagonal Reduction (FEER) Method. NASA CR-2731, Aug. 1976.

2. Guyan, R. J.: Reduction of Stiffness and Mass Matrices. AIAA J., Vol. 3, No. 2, 1965, p. 380.

3. Kaufman, S.; and Hall, D. B.: Reduction of Mass and Loading Matrices. AIAA J., Vol. 6, No. 3, 1968, pp. 550-551.

4. Ramsden, R. N.; and Stoker, R. J.: Mass Condensation: A Semi-automatic Method for Reducing the Size of Vibration Problems. Int. J. Num. Meth. Eng., Vol. 1, 1969, pp. 333-349.

5. The NASTRAN Theoretical Manual (Level 17), NASA SP-221, National Aeronautics and Space Administration, 1978, Section 10.5.

6. Wilkinson, J. H.: The Algebraic Eigenvalue Problem. Clarendon Press, Oxford, 1965.

7. Eades, J. B., Jr.: Tidal Frequency Estimation for Closed Basins. AMA Report No. 78-11, NASA Contract NAS5-22927, Feb. 1978.

TABLE I. COMPARISON OF EIGENVALUE METHODS FOR ROD-AND-DASHPOT TEST PROBLEM

Run	Method	Time, minutes CPU	Time, minutes I/O	Region (K)	Comments
1	Complex FEER	0.151	2.262	300	Eigensolutions Found: All 6 No. of Triangular Decompositions: 1 Search Regions: One point in 2nd quadrant of complex plane Reason for Termination: All solutions found.
2	Complex Determinant	0.174	2.858	320	Eigensolutions Found: 2 (3 rigid body modes at origin missed) No. of Triangular Decompositions: 29 Search Regions: 3, around known roots, including origin Reason Given for Termination: All predictions are outside regions specified
3	Complex Inverse Power	0.271	8.997	320	Eigensolutions Found: 2 (3 rigid body modes missed) No. of Triangular Decompositions: 1 in last search region Search Regions: 3, around known roots, including origin Reason Given for Termination: Number of desired roots have been found
4	Complex Inverse Power	0.238	4.100	320	Eigensolutions Found: None No. of Triangular Decompositions: 4 in last search region Search Regions: 1, encompassing all 5 existing roots on and above real axis Reason Given for Termination: Four starting point moves while tracking a single root
5	Complex Inverse Power	0.149	1.566	320	Eigensolutions Found: None No. of Triangular Decompositions: 2 Search Regions: Around origin, in attempt to find rigid-body modes Reason Given for Termination: Two successive singularities found while performing triangular decomposition

TABLE II. TIMING RESULTS FOR LAKE ERIE TIDAL MODE CALCULATIONS - 81 NODE MODEL

Run	Method	Time, minutes CPU	Time, minutes I/O	Region (K)	Comments
1	Complex FEER	2.164	5.886	700	6 accurate modes requested 4 obtained
2		2.425	8.593	350	15 accurate modes requested 12 obtained
3		7.576	27.751	560	50 accurate modes requested 54 obtained
4	Complex Determinant	6.572	8.618	700	3 modes obtained; insufficient time for more
5		5.315*	7.489	700	6 modes obtained; insufficient time for more

*Less time used due to a more careful choice of the search region.

BULK DATA DECK

Input Data Card EIGC Complex Eigenvalue Extraction Data

Description: Defines data needed to perform complex eigenvalue analysis

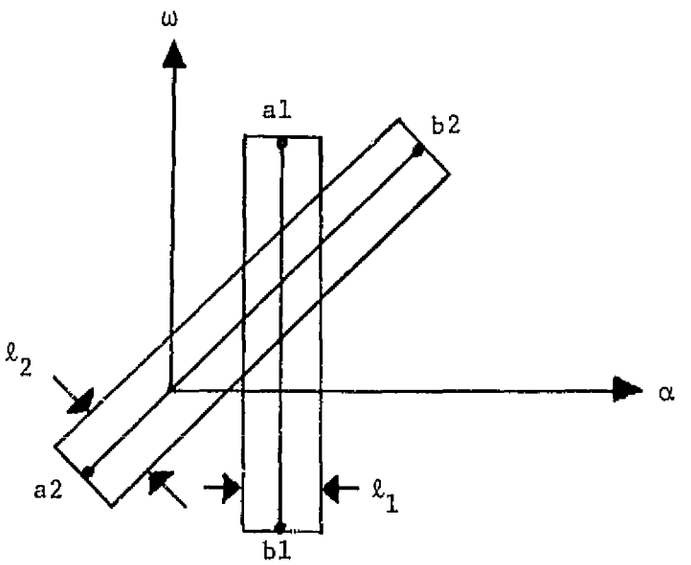

Format and Example:

1	2	3	4	5	6	7	8	9	10
EIGC	SID	METHØD	NØRM	G	C	E			+abc
EIGC	14	DET	PØINT	27		1.-8			ABC
+abc	α_{a1}	ω_{a1}	α_{b1}	ω_{b1}	ℓ_1	N_{e1}	N_{d1}		+def
+BC	2.0	5.6	2.0	-3.4	2.0	4	4		DEF
+def	α_{a2}	ω_{a2}	α_{b2}	ω_{b2}	ℓ_2	N_{e2}	N_{d2}		
+EF	-5.5	-5.5	5.6	5.6	1.5	6	3		

(etc.)

Figure 1. Modifications to the EIGC bulk data card for the Tridiagonal Reduction Method.

Field	Contents
SID	Set identification number (unique integer > 0)
METHØD	Method of complex eigenvalue extraction, one of the BCD values, "INV", "DET", "HESS" or "FEER" INV - Inverse power method DET - Determinant method HESS - Upper Hessenberg method FEER - Tridiagonal Reduction Method
NØRM	Method for normalizing eigenvectors, one of the BCD values "MAX" or "PØINT" MAX - Normalize to a unit value for the real part and a zero value for the imaginary part, the component having the largest magnitude PØINT - Normalize to a unit value for the real part and a zero value for the imaginary part the component defined in fields 5 and 6 - defaults to "MAX" if the magnitude of the defined component is zero.
G	Grid or scalar point identification number (Required if and only if NØRM=PØINT)(Integer>0)
C	Component number (Required if and only if NØRM="PØINT" and G is a geometric grid point)(0≤integer≥6)
E	Convergence criterion (optional)(Real≥0.0) For method = "FEER", error-tolerance on acceptable eigenvalues in percent (default value is .10/n, where n is the order of the stiffness matrix)
$(\alpha_{aj}, \omega_{aj})$ $(\alpha_{bj}, \omega_{bj})$	Two complex points defining a line in the complex plane (Real) For method = "FEER", $(\alpha_{aj}, \omega_{aj})$ is a point of interest in the complex plane, closest to which the eigenvalues are computed; $\lvert\alpha_{aj}\rvert + \lvert\omega_{aj}\rvert > 0$. The point $(\alpha_{bj}, \omega_{bj})$ is ignored.
ℓ_j	Width of region in complex plane (Real>0.0) Blank for method = "FEER".
N_{ej}	Estimated number of roots in each region (Integer>0) Ignored for method = "FEER".

Figure 1. Continued

N_{dj} Desired number of roots in each region (Default is $3N_{ej}$) (Integer>0) Desired number of accurate roots for method = "FEER" (Default is 1).

Remarks:

1. Each continuation card defines a rectangular search region. For method = "FEER", the card defines a circular search region, centered at $(\alpha_{aj}, \omega_{aj})$ and of sufficient radius to encompass N_{dj} roots. Any number of regions may be used and they may overlap. Roots in overlapping regions will not be extracted more than once.

2. Complex eigenvalue extraction data sets must be selected in the Case Control Deck (CMETHØD=SID) to be used by NASTRAN.

3. The units of α, ω and ℓ are radians per unit time.

4. At least one continuation card is required.

5. For the determinant method with no damping matrix, complex conjugates of the roots found are not printed.

6. See Section 10.4.4.5 of the Theoretical Manual for a discussion of convergence criteria.

7. For the Upper Hessenberg method, N_{d1} controls the number of vectors computed. Only one continuation card is considered and the (α, ω) pairs, along with the parameters ℓ_1 and N_{e1}, are ignored. Insufficient storage for HESS will cause the program to switch to INV.

8. The error tolerance, E, for the "FEER" method is with regard to

$$\left| \frac{|\tilde{p}_i-(\alpha_{aj}, \omega_{aj})|}{|p_i-(\alpha_{aj}, \omega_{aj})|} - 1 \right| \quad \text{for } [B] \neq [0] \quad \text{and}$$

$$\left| \frac{|\tilde{p}_i^2-(\alpha_{aj}, \omega_{aj})^2|}{|p_i^2-(\alpha_{aj}, \omega_{aj})^2|} - 1 \right| \quad \text{for } [B] = [0] \quad ,$$

where $\tilde{p}_i$ is a computed eigenvalue and p_i an exact eigenvalue.

Figure 1. Concluded.

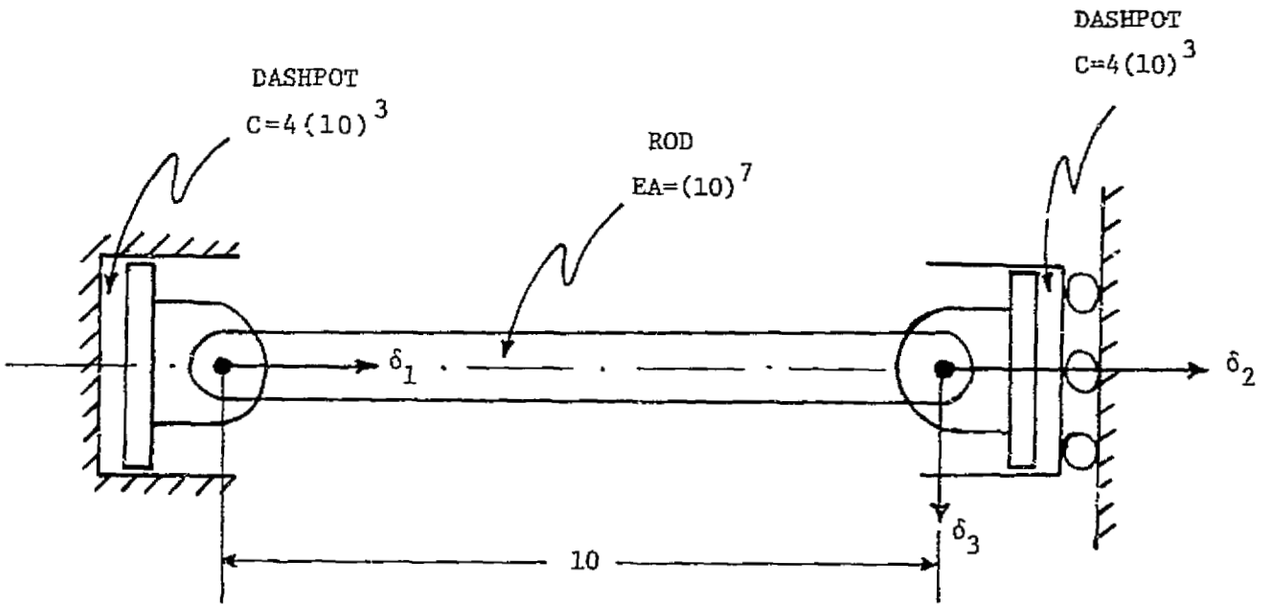

Figure 2. Test Problem -- Rod and Dashpots with 3 Degrees of Freedom

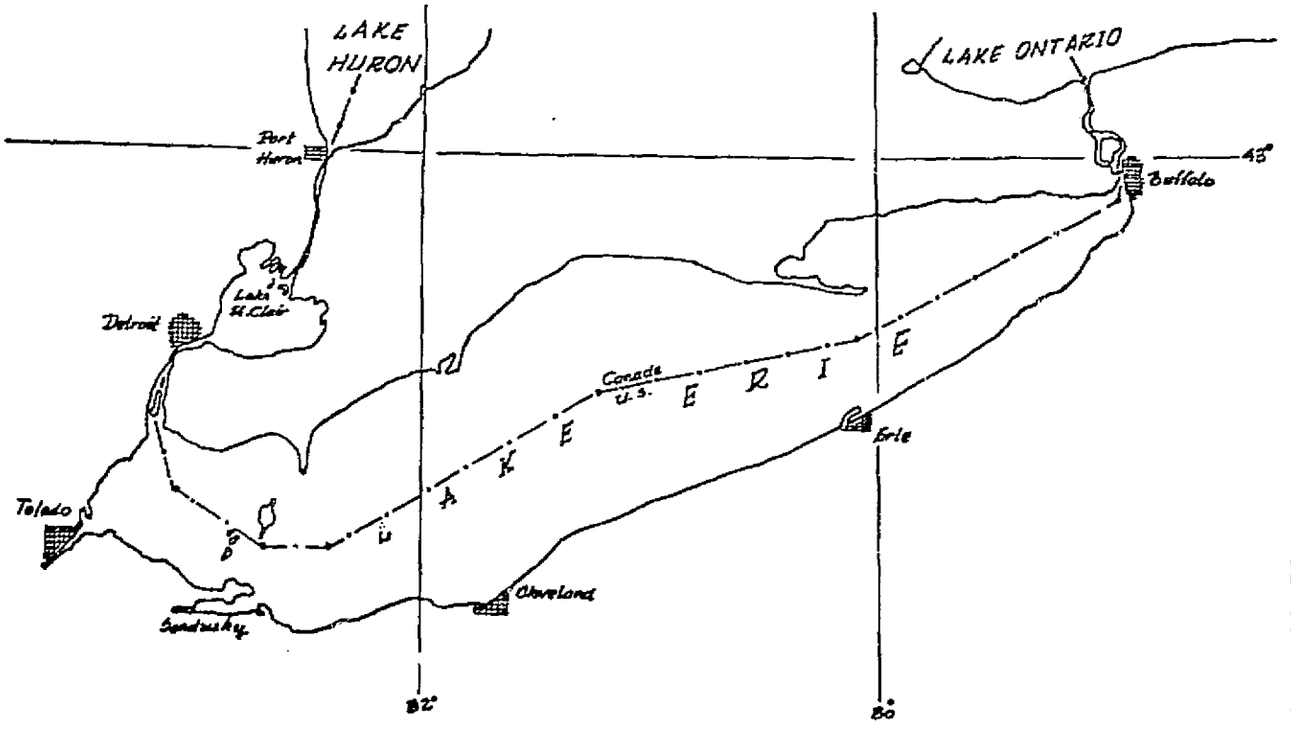

Figure 3. Illustration of Lake Erie and the adjacent geography.

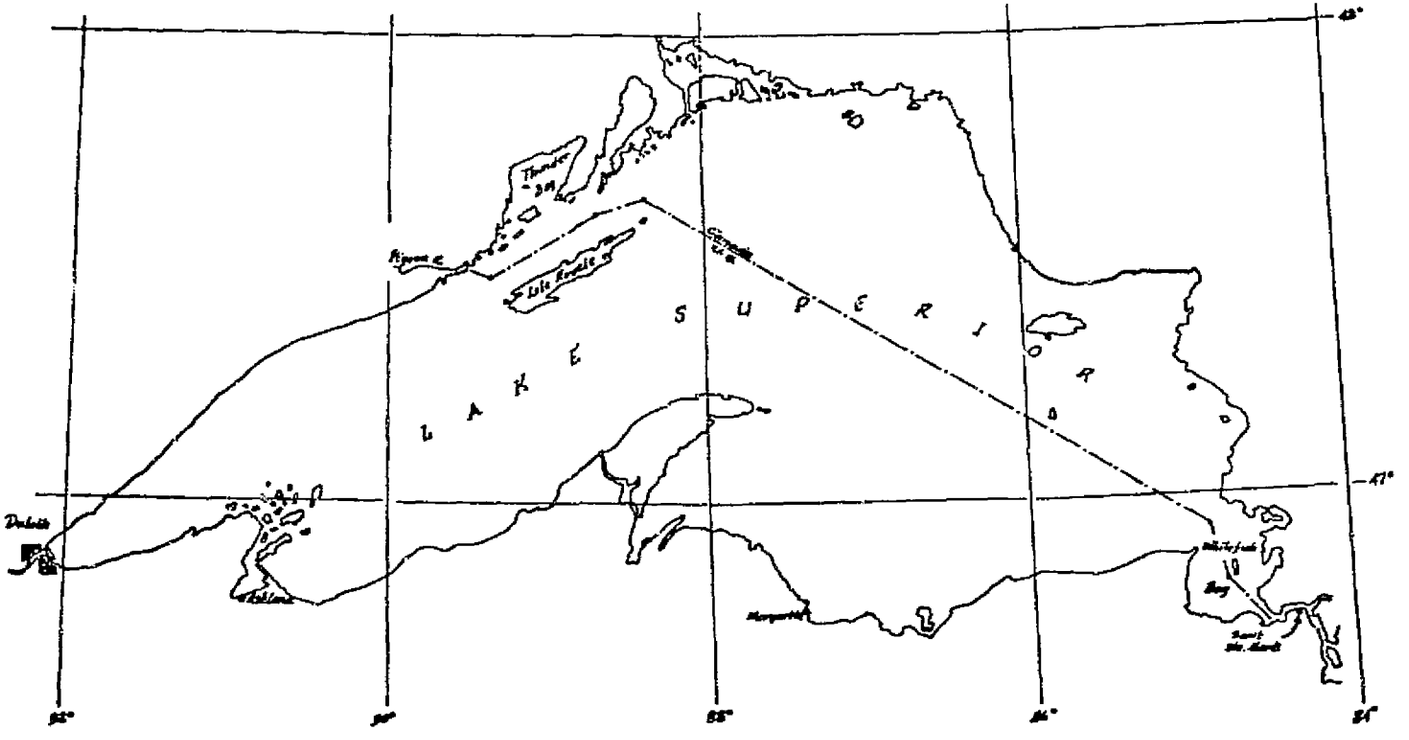

Figure 4. Illustration of Lake Superior and its local geography.

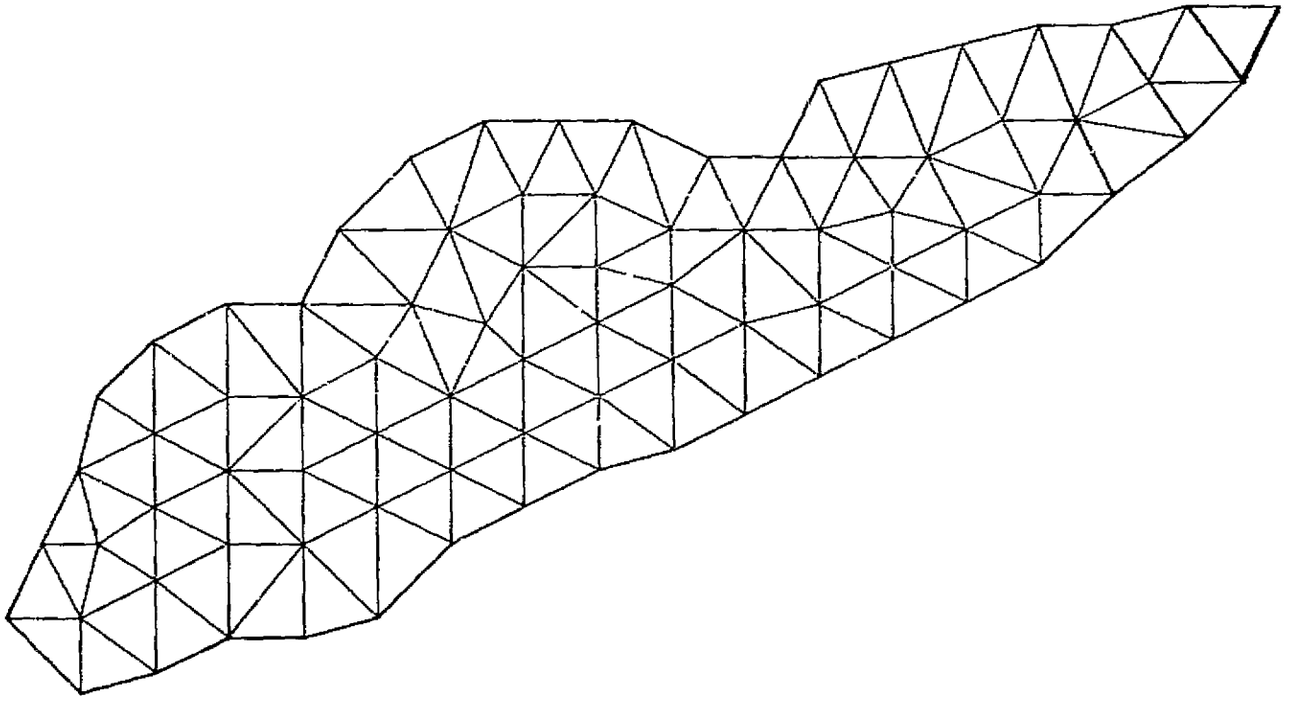

Figure 5. 81 Node Finite Element Model for Lake Erie.

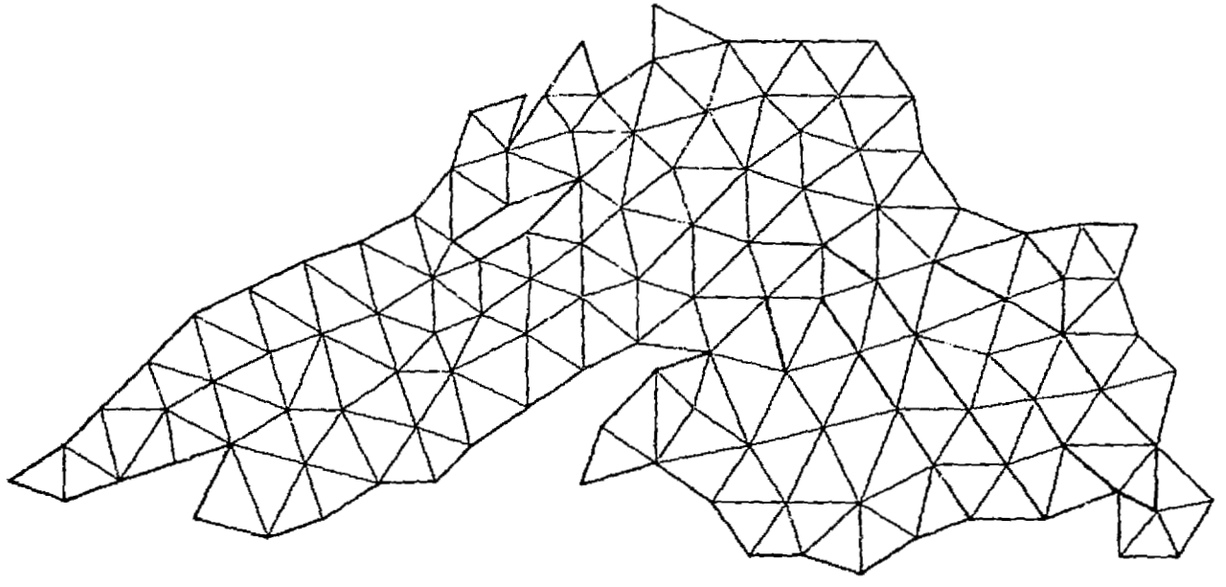

Figure 6. 124 node finite element model for Lake Superior.